University of Alberta

Numerical Investigation of Stiffened Steel Plates

by

Ming Jin

A thesis submitted to the Faculty of Graduate Studies and Research
in partial fulfillment of the requirements for the degree of

Doctor of Philosophy
in
Structural Engineering

Department of Civil and Environmental Engineering

Fall 2010
Edmonton, Alberta

Examining Committee

Dr. Gilbert Grondin, Civil and Environmental Engineering

Dr. Vivek Bindiganavile, Civil and Environmental Engineering

Dr. Samer Adeeb, Civil and Environmental Engineering

Dr. Jozef Szymanski, Civil and Environmental Engineering

Dr. Chong-Qing Ru, Mechanical Engineering

Dr. Magdi Mohareb, Civil Engineering, University of Ottawa

ABSTRACT

Because of their high strength to weight ratio, stiffened steel plates are often used in light structures where plates are placed into compression. The stability of steel plates stiffened with longitudinal tee-shaped stiffeners and subjected to uniaxial compression or combined axial compression and out-of-plane bending formed the basis for this research project. The research was conducted to develop a simple approach to assess the post-buckling behaviour of stiffened steel plates and provide a limit states design procedure that accounts for the post-buckling stability in the assessment of the resistance factor.

The behaviour of stiffened plates was investigated using a finite element model that had been validated through comparison with test results. An exhaustive parametric study, including 1440 finite element analyses, was conducted to investigate the strength and behaviour of stiffened steel plates. A virtual work model was developed to explain the effect of the formation of a plastic hinge mechanism on the post-buckling strength and behaviour. Combined with the numerical results, the theoretical model confirms that the plastic hinge mechanism can cause a sudden loss of capacity. The required lateral deflection for a plastic hinge development can be calculated using the virtual work model for prediction of the unstable behaviour.

Based on a better understanding of the behaviour of stiffened steel plates, a set of design equations were developed to calculate the strength of stiffened steel plate subjected to compression in the direction of the stiffener and out-of-plane bending.

The proposed design equations were compared with current design guidelines through a comparison of the design approaches with the finite element analysis results. The proposed method showed much better accuracy than the current design approaches.

A reliability analysis was conducted to provide appropriate resistance factors for limit states design. Due to the complexity of the design formulas, the Monte Carlo simulation technique was used to generate the statistical distributions of the predicted strength. The second-moment method was used to calculate the resistance factors for different values of safety index. The resistance factor varied from 0.90 to 0.65 for values of safety index from 2.5 to 4.5, respectively.

ACKNOWLEGEMENTS

This study received invaluable help from other graduate students at the University of Alberta. Especially, Ian MacPhedran provided consistent technical support in application of the numerical software and made very useful suggestions in the thesis writing.

Professor Gilbert Y. Grondin has been giving insights into the methodology throughout the research. His contributions to this thesis are invaluable and gratefully acknowledged.

Special thanks go to my wife. Her patience and understanding constitutes the solid support for me to accomplish this PhD study.

Scholarship support from the F. S. Chia Scholarship at the University of Alberta, and Natural Sciences and Engineering Research Council, is gratefully acknowledged.

TABLE OF CONTENTS

LIST OF TABLES

LIST OF FIGURES

LIST OF SYMBOLS

a	=	chord length of half of the deformed panel
A	=	area of the full cross-section of the stiffened plate
A_e	=	area of the effective cross-section of the stiffened plate
A_p	=	plate area
A_s	=	stiffener area
b	=	plate width
b_e	=	reduced plate width
b_f	=	stiffener flange width
d	=	center to center distance between the plate and flange
d_c	=	distance between the centroid and the pure bending plastic neutral axis of the full section
e	=	distance between centroid of the full section and reduced section
h_w	=	web height
L	=	length of the stiffened plate
E	=	elastic modulus of stiffened plate
F_{Ee}	=	Euler buckling stress of the effective stiffened plate
F_k	=	characteristic buckling stress of the side being checked
F_r	=	maximum residual stress
F_y	=	yield stress of the stiffened plate
F_{yp}	=	yield stress of the plate
F_{ys}	=	yield stress of the stiffener
G	=	actual geometric properties
$\hat{G}$	=	nominal geometric properties

I	=	the moment of inertia of the full cross-section
I_e	=	the moment of inertia of the effective cross-section
I_s	=	the moment of inertia of the stiffener about an axis parallel to the plate and taken at the base of the stiffener
KL	=	effective length depending on the boundary condition
M	=	internal bending moment
M_a	=	the applied moment (positive if making stiffener in compression)
M_{ae}	=	the end moment about the centroid of the effective cross-section (positive if making stiffener in compression)
M_i	=	internal bending moment about the centroid of the full section
M_{ie}	=	internal bending moment about the centroid of the effective section
M_{ir}	=	internal bending moment resistance about the centroid of the full cross-section
M_p	=	plastic moment capacity
M_{pe}	=	plastic moment capacity of the effective cross-section
M_p'	=	reduced plastic moment capacity due to the interaction of axial load
M_{ye2}	=	yield moment capacity of the second effective cross-section for bending in the ABS guide
$M_{ye,\mathrm{c}}$	=	yield moment capacity of the effective cross-section at the concave side
$M_{ye,\mathrm{p}}$	=	yield moment capacity of the effective cross-section at the plate surface

$M_{ye,\mathrm{t}}$ = yield moment capacity of the effective cross-section at the convex side

m = number of stiffeners

$\hat{M}$ = nominal material properties

$\hat{M}_P$ = the plastic moment capacity of the nominal panel

n = a coefficient in column buckling equation

P = axial load

P_c = critical axial load

P_{Ee} = elastic column buckling load of the effective specimen

P_i = internal load

P_y = yield force

P_{ye} = yield force of the effective cross-section

P_{ue} = column buckling load capacity of the effective specimen

p_r = proportional limit of steel

R_{FEA} = resistance of the actual member predicted by finite element analysis

R_n = resistance of the actual member predicted by the proposed design method

R_{Test} = resistance of the actual member from tests

r_e = the radius of gyration of the effective cross-section about the axis through the centroid and parallel to the plate

r_{yz} = the torsional radius of gyration of the stiffener about its centroid

$\hat{R}_n$	=	resistance of the nominal member predicted by the proposed design method
t	=	plate thickness
t_1	=	thickness of the plate compression block for plate induced plastic hinge
t_2	=	height of the web tension block for plate induced plastic hinge
t_3	=	thickness of the flange tension block for plate induced plastic hinge
t_4	=	thickness of the plate tension block for stiffener induced plastic hinge
t_c	=	thickness of the area of the midspan cross-section to resist axial load
t_f	=	stiffener flange thickness
t_w	=	web thickness
u_1	=	the longitudinal shortening
u_3	=	midspan out-of plane deflection
V	=	coefficient of variation, with subscripts
V_G	=	geometry coefficient of variation
V_M	=	material coefficient of variation
V_{MG}	=	overall material and geometric coefficient of variation
V_P	=	overall professional coefficient of variation
V_{P1}	=	professional coefficient of variation associated with ρ_{P1}
V_{P2}	=	professional coefficient of variation associated with ρ_{P2}
V_R	=	resistance coefficient of variation

x	=	a general variable (mean $\overline{x}$, standard deviation σ_x)
$X_{0.001}$	=	the 0.1% fractile
$X_{0.05}$	=	the 5% fractile
z_p	=	distance between the centroid and the plate bottom face
z_s	=	distance between the centroid and the stiffener top face
α	=	aspect ratio
α_R	=	the separation factor for resistance
β	=	safety index
β_1	=	plate slenderness ratio
β_2	=	stiffener web slenderness ratio
β_3	=	stiffener flange slenderness ratio
β_4	=	ratio of stiffener torsional slenderness to plate slenderness
β_5	=	stiffener to plate area ratio
β_6	=	plate imperfection ratio
β_7	=	stiffener imperfection ratio
β_8	=	residual stress ratio
β_9	=	applied to plastic moment ratio
β^*	=	compound parameter
δ	=	eccentricity of internal load, *P*, to the centroid at midspan cross-section
δ_i	=	stiffened plate imperfection
δp	=	maximum plate imperfection
δs	=	maximum web imperfection

δu_1	=	virtual displacement of u_1
$\delta\theta$	=	virtual displacement of θ
θ	=	end rotation angle
ϕ	=	resistance factor
λ_e	=	column slenderness parameter of the effective specimen
ν	=	Poisson's ratio, taken as 0.3 for steel
ρ_G	=	geometric mean-to-nominal ratio
ρ_M	=	material mean-to-nominal ratio
ρ_{MG}	=	overall material and geometric mean-to-nominal ratio
ρ_P	=	professional mean test-to-predicted ratio
ρ_{P1}	=	professional mean FEA-to-predicted ratio
ρ_{P2}	=	professional mean test-to-FEA ratio
ρ_R	=	resistance mean-to-nominal ratio
σ	=	standard deviation with subscripts x, $\ln(x)$
Ψ	=	actual-to-nominal ratio of a variable
ω_1	=	the moment adjustment coefficient

CHAPTER 1

INTRODUCTION

1.1 GENERAL

Steel plates stiffened with welded stiffeners are important components of many structural systems such as ship hulls, offshore structures, and bottom flanges of box-girders. Although local failure of individual panels will not cause widespread collapse of the overall structure, each stiffened panel should be well designed to ensure sufficient capacity.

Overall flexure of the structure can introduce dominant longitudinal compressive stresses in the stiffened plates. This may be coupled with local bending moments arising from transverse loads applied directly on the stiffened plate. Due to the large width-to-thickness ratio of the plate and the predominantly in-plane compressive load, stiffened plates are susceptible to buckling.

A common design approach to estimate the buckling capacity of stiffened plates is to treat one stiffener with the corresponding plate as a simply supported beam-column as seen in DNV-RP-C201 [Det Norske Veritas (DNV), 2002], API bulletin 2V [American Petroleum Institute (API), 2000] and the ABS guide [American Bureau of Shipping (ABS), 2007],, where the effective width concept is used to account for buckling of the plate between the stiffeners (Faulkner, 1975). Various interaction formulas have been adopted in design documents when stiffened plates are subjected to a combination of axial and flexural loads. A number of researchers (Ghavami, 1994; Balaz and Murray, 1992; Sheikh *et al.*, 2002, 2003; Wang *et al.*, 2006; Sun and Wang, 2005) have assessed various design methods against test results and numerical analysis results, and the agreements were not quite satisfactory. Their work has identified areas where more research effort is required to improve the accuracy of the design methods. As part of the study presented in the following chapters, behaviour of the stiffened plates needs further investigation, especially the instability observed in recent research (Sheikh *et al.* 2002, 2003; Wang *et al.* 2006) where tripping failure of the stiffener may be involved as part of the failure process. Since a major goal of this investigation is to propose a design method for stiffened plates, further understanding of the behaviour is necessary to provide a rational approach.

With the development of the limit states design, resistance and load factors were introduced in design to obtain a design that provides a consistent level of safety against failure for the various possible failure modes. This design philosophy has not been thoroughly applied in design documents for the design of stiffened steel plate. Some design specifications such as API bulletin 2V (API, 2000), and the ABS guide (ABS, 2007), are still based on allowable stress design. To address a complete design approach, it is necessary to develop a statistical description of the strength of stiffened steel plates and to derive the appropriate resistance factors for given probabilities of failure.

1.2 OBJECTIVES

The main objectives of this study are as follows:

1. Establish a comprehensive database of stiffened steel plate configurations under various load conditions. The database should include information about loading history, stress distribution, strain distribution, deformed shape, and yield pattern for each stiffened steel plate.

2. Gain further understanding of the behaviour of stiffened plates, especially the cause of the sudden loss of capacity observed under certain loading conditions and plate geometries.

3. Propose a more accurate approach to estimate the capacity of the stiffened plates and predict the occurrence of sudden instability.

4. Assess the proposed approach and evaluate some current design guidelines with the numerical results in the database.

5. Derive appropriate resistance factors for the selected design approach by using a reliability analysis.

1.3 ORGANISATION

Chapter 2 mainly focuses on interpreting the behaviour of the stiffened plates and proposes a method to predict the occurrence of sudden loss of capacity. It describes the finite element model and the parameter values selected for a factorial design of the database. A theoretical virtual work model is then established to help interpret the instability behaviour. A number of representative panels are selected as examples to describe the behaviour of stiffened steel plates under combined in-plane compression and out-of-plane bending. Based on analysis of the database, a simple method to predict the failure mode for stiffened steel plates is proposed.

The information obtained in Chapter 2 is used to investigate the strength of stiffened plates presented in Chapter 3. A design method is proposed to predict the load carrying capacity of stiffened plate panels. The results of the database introduced in Chapter 2 are used to assess this proposed method, and to evaluate the current design guidelines.

Chapter 4 describes a reliability analysis associated with the proposed design formulas in Chapter 3. Monte Carlo simulations are used in Chapter 4 to obtain the statistical description of the capacity of the designed panels. Resistance factors are recommended for safety indices varying from 2.5 to 4.5.

Finally, Chapter 5 presents a summary, conclusions, and suggestions for further investigations.

1.4 THESIS FORMAT

This thesis is written in accordance with the regulations for a Paper Format Thesis as set by the Faculty of Graduate Studies and Research at the University of Alberta (FGSR, 2009). The introductory chapter and final chapter have their own reference. Each of the other chapters is presented in a paper format without an abstract, but with its own list of references. Tables and figures are grouped at the end of each chapter. List of tables, figures and symbols are placed in the prefatory pages. The definitions of the symbols are consistent throughout the thesis. A large amount of data, including a sample input file of the finite element model, tables of raw data, analysis results, load vs. deformation figures, virtual work model development and Monte Carlo simulation results are presented in the appendices. In the thesis, cross references to other chapters or appendices take the simple form such as Chapter 2 or Appendix A.

References:

American Bureau of Shipping (ABS) (2007). *Guide for buckling and ultimate strength assessment for offshore structures*. Houston, Texas

American Petroleum Institute (API) (2000). *API Bulletin 2V: Design of flat plate structures*, Washington, D. C., U.S.

Balaz, I., and Murray, N. W.(1992)."A Comparison of Some Design Rules with Results from Tests on Longitudinally Stiffened Deck Plates of Box-Girders." *Journal of Constructional Steel Research*, 23(1), 31–54

Det Norske Veritas (DNV) (1995). Classification Notes No. 30.1: Buckling Strength Analysis, Norway.

Faulkner, D. (1975). "A review of effective plating for use in the analysis of stiffened plating in bending and compression" *Journal of Ship Research*, 19 (1), 1–17.

Faculty of Graduate Studies and Research (2009), *FGSR Thesis Format Specifications*, Faculty of Graduate Studies and Research, University of Alberta

Ghavami, K.(1994)."Experimental Study of Stiffened Plates in Compression up to Collapse." *Journal of Construction Steel Research*, 28(2), 197–221

Sheikh, I. A., Grondin, G. Y., Elwi, A. E. (2002). "Stiffened steel plates under uniaxial compression" *Journal of Constructional Steel Research*, 58(5), 1061-1080.

Sheikh, I. A., Elwi, A. E., Grondin, G. Y. (2003). "Stiffened steel plates under combined compression and bending." *Journal of Constructional Steel Research*, 59(7), 911- 930.

Sun, H. and Wang, X.(2005)."Buckling and Ultimate Strength Assessment of FPSO Structures." *2005 SNAME Marine Technology Conference & Expo*., Oct. 2005, Houston, Texas

Wang, E. C. L., Grondin, G. Y., Elwi, A. E. (2006), "Interaction Buckling Failure of Stiffened Steel Plates", *Structural Engineering Report No. 264*, Department of Civil and Environmental Engineering, University of Alberta, Canada.

CHAPTER 2

BEHAVIOUR OF STIFFENED STEEL PLATES UNDER COMPRESSION AND BENDING

2.1 INTRODUCTION

Because of their high strength to weight ratio, steel plates stiffened with longitudinal stiffeners and transverse beams are extensively used in ship decks, offshore structures and box girder bridges. Stiffened steel plates are often subjected to compressive stresses in the direction of the stiffeners. These stresses are commonly due to overall bending of the entire hull of a ship or negative moments developed at the supports of steel box girders with a stiffened bottom flange. They may also have to carry local bending moments arising from the transverse water pressure on a ship hull, for example. Owing to the presence of the axial compression, these panels are susceptible to overall flexural buckling, with the plate either on the concave side of the stiffened plate or on the convex side. The former mode is referred to as plate induced overall buckling and the latter is referred to as stiffener induced overall buckling.

Since stiffeners are attached only to one side of a plate, overall buckling behaviour of the panel differs in the two bending directions. For plate induced overall buckling of stiffened panels with slender plates, the plate buckling failure mode is often coupled with overall flexural buckling. Plate buckling itself does not usually represent the limit of the capacity since stiffened plates can develop significant post-buckling strength and, therefore, can reach the overall buckling capacity of the panel (Faulkner, 1975). Due to the large in-plane stiffness of the plate, plate induced overall buckling generally shows a stable post-buckling behaviour. However, the interaction between plate induced overall buckling and the formation of a plastic hinge may lead to a sudden loss of load-carrying capacity. Such interaction has been identified in experimental and analytical work (Aalberg *et al*., 2001; Sheikh *et al*., 2002, 2003; Chen *et al*., 2004; Hughes *et al.*, 2004; Wang *et al*., 2006).

Aalberg *et al*. (2001) conducted 21 tests on stiffened aluminium panels under axial compression. A test specimen with trapezoid stiffeners showed a sharp drop in capacity after a period of stable post-buckling behaviour. The ends of the specimen were observed to rotate rapidly after the sharp reduction in capacity, indicating the formation of a plastic collapse mechanism.

Sheikh *et al.* (2002, 2003) observed the same kind of behaviour in finite element models of steel plates stiffened with tee stiffeners and subjected to axial loading (load in the direction of the stiffeners) or combined out-of-plane bending and axial loading. A few of the stiffened plate panels analysed showed a rapid loss of capacity after overall buckling and some stable post-buckling behaviour. Some of the models that displayed this instability had failed by plate induced overall buckling. This behaviour was interpreted as the interaction of two failure modes, namely, plate buckling followed by plate induced overall buckling. An examination of the yield progression indicated the formation of a plastic hinge at midspan when the post-buckling regime showed a sudden loss of capacity. Some finite element models that failed by stiffener induced overall buckling also showed a sudden loss of capacity. In this case the post-buckling behaviour was unstable and loss of load carrying capacity was observed immediately after the peak load. This failure mode was interpreted as stiffener tripping since the loss of capacity lead to failure of the stiffener by tripping.

Unstable plate behaviour was also observed by Hughes *et al.* (2004) who noticed the formation of a plastic hinge at midspan under the action of an axial compression force. Since the stiffened plates modeled in their work simulated a three-span panel under axial compression, both plate induced failure and stiffener induced failure modes were involved in the failure mode. This led to the conclusion that a multi-span stiffened plate panel fails only by stiffener induced failure. In reality, plate induced failure may be the governing mode for some cases, for example, local bending moments favour plate induced failure. In all cases examined, Hughes *et al.* (2004) observed yielding of the stiffener web and, in some cases, yielding of the plate. It should be noted that Hughes *et al*. (2004)

based their observation on the calculated stress at the plate mid-thickness, which may give the impression that the plate does not yield when the neutral axis is located in the plate, which is often not the case as will be seen later in this chapter.

Using the analysis results presented by Sheikh *et al.* (2002, 2003), Wang *et al*. (2006) designed test specimens to examine the stiffener tripping behaviour experimentally. Four stiffened plate panels were tested under eccentric axial loading; three specimens with an eccentricity of 5 mm or 10 mm towards the plate, and one specimen with an eccentricity of 3 mm towards the stiffener flange. The load versus displacement curves for two of the test specimens that failed by plate induced modes showed a plateau between the peak load and the sudden reduction of axial load carrying capacity.

Stiffener induced overall buckling results in a more sudden loss of capacity than plate induced overall buckling because overall buckling places the stiffener flange under increased compression, which can lead to instability of the stiffener (stiffener tripping). Most panels failing by stiffener induced overall buckling show a rapid loss of load carrying capacity due to the loss of stiffness resulting from tripping of the stiffener. Although this mode of instability has received considerable attention (Sheikh *et al*., 2003; Danielson, 1995; Hu *et al*., 2000; Zheng and Hu, 2005), it is still not thoroughly understood. Given that the formation of a plastic hinge causes severe instability in plate induced failure, it should also have undesirable influence on stiffener induced failure.

The severe instability observed for certain stiffened plates in the post-buckling regime does not affect the design load carrying capacity, but it directly determines the consequence of failure and thus the selection of an appropriate safety index for limit states design. An extensive investigation of this unstable behaviour will be conducted using finite element analysis and earlier test results (Grondin *et al.*, 1998; Chen *et al.*, 1997). A method will be proposed to predict this unstable post-buckling behaviour. The analysis presented in the following is limited to plates stiffened with longitudinal tee stiffeners, simply supported at the loaded ends, and subjected to uniaxial compression or combined axial compression and out-of-plane bending.

2.2 FINITE ELEMENT ANALYSIS

2.2.1 Description of Model

Multiple longitudinal stiffeners are typically welded to the plate at equal spacing and span between girders. Because of the symmetry of loading, geometry and deformation, the behaviour can be investigated using only one stiffener with the attached plate (Figure 2-1 (a)).

The finite element model of a stiffened plate panel was developed using the commercial finite element code ABAQUS (2003). A stiffened plate panel was modeled with 768 rectangular shell elements of type S4R; 512 elements for the plate and 128 elements each for the web and the flange of a tee shape stiffener. The S4R shell element is a 3-dimensional, 4-node, quadrilateral shell element with reduced integration. The model incorporated initial imperfections, residual stresses, and inelastic material properties, and used large deformation theory. A similar model was developed and validated by Grondin *et al*. (1998) through comparison with the results of tests on full-scale plates.

Initial imperfections were incorporated directly in the node coordinates definition. From field measurements on 196 plates, Carlsen and Czujko (1978) determined that the deformed shape of welded stiffened plates used in ship structures can be expressed by a double trigonometric series. One half sine wave across the width of the plate and four half sine waves along the length of the plate was recommended by Grondin *et al*. (1999) as a shape that lead to conservative estimate of stiffened plate capacity. This shape was adopted in this study. The shape of the initial imperfections, depicted in Figure 2-1 (b), is expressed as

$$\delta_i(x,y) = \delta_p \sin\left(\frac{4\pi x}{L}\right)\sin\left(\frac{\pi y}{b}\right) \qquad [2\text{-}1]$$

where x is the coordinate along the length L of the plate, y is the coordinate across the width b, and δ_p is the maximum out-of-plane imperfection magnitude.

The initial imperfections in the web of the stiffener were defined by a half sine wave along the length, with a parabolic variation over the web height, as recommended by Sheikh *et al.* (2001). The shape of the initial imperfections of the web is shown in Figure 2-1 (c) and is expressed as:

$$\delta_i(x,z) = \delta_s\left(\frac{z}{d}\right)^2 \sin\left(\frac{\pi x}{L}\right) \qquad [2\text{-}2]$$

where z is the distance perpendicular to the plate surface and is equal to 0.0 at the plate to web junction, and d is the distance between the flange and plate centerlines. Initial imperfections in the flange were introduced by forcing the flange plate to remain at right angle to the web along its centreline. This conferred a half sine wave imperfection in the plane of the flange and a half sine wave out-of-plane imperfection along the length.

Residual strains were introduced into the model in the form of nodal temperature changes, which were a function of the desired residual strain magnitude and the coefficient of thermal expansion used for the analysis. The resulting residual stress distribution, expressed as a fraction of the nominal yield strength, F_y, is shown in Figure 2-1 (d). The magnitude of the residual stresses varies from F_y in tension at the stiffener to plate welded junction, to 0.3 F_y in compression in the plate and at the flange tips. The adopted compressive residual stresses in the plate are considered to be severe (Smith *et al.*, 1992), although higher compressive residual stresses have been adopted for design, such as 0.4 F_y for stiffened box girders in the AASHTO LRFD bridge design specifications (AASHTO, 2007). The residual stress pattern shown in Figure 2-1 (d) satisfies self equilibrium of moments and forces.

A bi-linear, elastic–hardening, material model consisting of an elastic range with a modulus of elasticity of 200 000 MPa, followed by a hardening range with a modulus of 100 MPa, was implemented for the analysis. The hardening material model was selected to model the yield plateau typical of mild steel while providing some stiffness to facilitate convergence of the solution during the analysis. The von Mises yield criterion and isotropic hardening rule were used beyond the elastic range.

It is expected that in actual practice the stiffened plates would be welded to massive transverse beams or girders that are stiff in their own planes but flexible in the out-of-plane direction. An ideal boundary condition in analysis would allow the ends of the stiffened plates to rotate locally but maintain the shape of the cross-section which could be accurately simulated by a one-bay stiffened plate model. In the finite element model of this study, the nodes of the loaded end cross-sections were connected to corresponding nodes of rigid end plates. The rigid plate was pinned at each loaded end at a point located at the centroid of the stiffened plate.

An axial load was applied directly to the rigid end plates. Only one of the loaded ends of the stiffened plate panel is allowed to move longitudinally and both loaded ends are allowed to rotate about the transverse axis (y-axis). In order to simulate plate continuity at the plate model edges, the unloaded edges are only restrained from rotation about the longitudinal axis (x-axis) and in-plane twist (rotation about the z-axis). The transverse in-plane translation degree of freedom in structures with multiple stiffeners is in an intermediate state between free and restrained. Both restraint conditions were investigated and the results will be presented in section 2.2.2.

The loading procedure consists of up to three different load steps, namely, application of the temperature change to introduce the desired residual strains, application of the bending moment for the panels loaded under combined out-of-plane bending and axial loading, and, in the last step, application of axial load until a nominal strain (change in length of the panel divided by the initial length) of 1% in the longitudinal direction was reached. The solution strategy makes use of the Newton-Raphson procedure in the first load step and the moment application step. A modified Riks procedure is used in the last step (application of the axial force) to trace the post-buckling behaviour through the softening regime.

The finite element model used for this investigation was validated by comparison with full-scale test results as presented by Grondin *et al.* (1998). It was demonstrated that the model provides accurate predictions of both the capacity and the behaviour of stiffened steel plates subjected to axial compression or combined axial compression and out-of-plane bending.

2.2.2 Parametric Study

A parametric study was conducted using the finite element model described above. A set of dimensionless parameters that describe uniquely the behaviour of stiffened steel plates was proposed and validated by Sheikh *et al.* (2002, 2003), and will be used in this work. The nine input parameters (β_1 to β_9) are defined as:

Plate slenderness ratio, $\beta_1 = \dfrac{b}{t}\sqrt{\dfrac{F_{yp}}{E}}$;

Web slenderness ratio, $\beta_2 = \dfrac{h_w}{t_w}\sqrt{\dfrac{F_{ys}}{E}}$;

Flange slenderness ratio, $\beta_3 = \dfrac{b_f}{t_f}\sqrt{\dfrac{F_{ys}}{E}}$;

Ratio of stiffener torsional slenderness to plate slenderness, $\beta_4 = \left(\dfrac{L}{r_{yz}}\sqrt{\dfrac{F_{ys}}{E}}\right)\Big/\beta_1$;

Stiffener to plate area ratio, $\beta_5 = \dfrac{A_s}{A_p}$;

Plate imperfection ratio, $\beta_6 = \dfrac{\delta_p}{t}$;

Stiffener imperfection ratio, $\beta_7 = \dfrac{\delta_s}{L}$;

Residual stress to yield strength ratio, $\beta_8 = \dfrac{F_r}{F_{yp}}$;

Applied to plastic moment ratio, $\beta_9 = \dfrac{M_a}{M_p}$.

In the above dimensionless parameters, t is the plate thickness, F_{yp} is the plate yield strength, E is the elastic modulus, h_w and t_w are the web height and thickness, respectively, F_{ys} is the stiffener yield strength, b_f and t_f are the flange width and thickness, respectively, r_{yz} is the polar radius of gyration of the stiffener about its centroid, A_s and A_p are the stiffener area and plate area, respectively, F_r is the maximum compressive residual stress, M_a is the applied end moments and is positive if putting the stiffener flange in flexural compression, and M_p is the plastic moment capacity of the full cross-section. The parameters β_1, β_2, β_3, β_4 and β_5 define the basic geometry and material properties, β_6 and β_7 define the level of initial imperfections for the plate and the stiffener, respectively, β_8 defines the magnitude of residual stresses, and β_9 defines the magnitude of the end moments. The virtue of these dimensionless parameters is that they are scale independent (both geometry and material) (Sheikh *et al*., 2002).

Plate slenderness is well known to have a significant influence on the strength and behaviour of stiffened plates (Faulkner, 1975; Smith *et al*., 1992; Grondin *et al*., 1999). Faulkner (1975) indicated that practical values of β_1 are less than 3.0. Sheikh *et al*. (2002) investigated four values of β_1, namely, 0.7, 1.28, 2.0, and 2.7 where the minimum value represents a stocky plate for which full yielding is expected to take place before buckling. The values of 1.28 and 2.7 represent the limit of inelastic and elastic plate buckling, respectively. The same four values of β_1 as those used by Sheikh *et al*. (2002) are used in this work.

Selection of the tee cross-section is limited by the availability of standard rolled sections. Inspection of the available rolled tee sections in the CISC Handbook of Steel Construction [CISC, 2006] indicated that β_2 is in the range of 0.13 to 1.40 and β_3 from 0.17 to 1.06. An examination of the available European rolled tee sections [British Standards Institution (BSI), 2005] indicated that β_2 ranges 0.71 to 1.39 and β_3 ranges from 0.38 to 0.81. Hughes and Ma (1996) indicated that the typical range of β_2 is 0.76 to 1.53. Generally, an upper bound for stiffener slenderness is set to prevent local buckling of the flange or the web before yielding under uniaxial compression. These limits are 1.5 for β_2 and 0.89 for β_3 according to the requirements for compression members in the North American steel design standards [Canadian Standards Association (CSA), 2009; AISC, 2005].

For elements in flexural compression, CSA-S16-09 (CSA, 2009) recognizes four classes of sections. In the four classes, classes 1 (plastic design), 2 (compact), and 3 (non-compact) sections allow either full or partial yielding of the cross-section before local buckling. The web of a T-shape stiffener can be either fully or partially in flexural compression when the stiffened plate is subjected to bending. In the worst case scenario, the web may be in full compression when a plastic hinge is developed and the neutral axis is not in the web. Thus the classifications for flanges of rectangular hollow sections (web-type plates under uniform compression) are used as a conservative approximation to reflect this worst case scenario for the web. This gives the limits for the web slenderness of class 1, 2 and 3 sections as β_2 = 0.94, 1.17, 1.50, respectively. The classifications in CSA-S16-09 (2009) for flanges of I-sections or T-sections gives the flange slenderness limits for classes 1, 2 and 3 sections as β_3 = 0.65, 0.76, 0.89, respectively.

When $\beta_2 \leq 1.50$ and $\beta_3 \leq 0.89$ the stiffener is at least a class 3 section. These slenderness limits are consistent with the three design guidelines that specifically include stiffened plate design, namely, DNV-RP-C201 [Det Norske Veritas (DNV), 2002], API bulletin 2V [American Petroleum Institute (API), 2000], and the ABS guide [American Bureau of Shipping (ABS), 2007], as presented in Table 2-1. Based on the above review of availability and section classification, β_2 is taken as 0.17, 0.8 and 1.5, and β_3 is taken as 0.17, 0.6, and 0.9 in this study, where the middle value is approximately the average of the upper and lower bounds.

The stiffener to plate area ratio, β_5, does not affect the strength of the panels failing by plate buckling (Grondin *et al*., 1999; Timoshenko and Gere, 1961), but it has an impact when the panels fail by stiffener induced overall buckling (Sheikh *et al*., 2003). The area ratio commonly used in ship construction is 0.2 (Smith *et al*., 1992). A value of the ratio less than 0.3 was found to trigger stiffener tripping if the out-of-plane loading places the stiffener flange in flexural compression (Grondin *et al*., 1999). Therefore, Sheikh *et al*. (2003) selected values of 0.075, 0.15 and 0.3 to study the panel behaviour especially for stiffener induced failure. The same three values are adopted in this work.

The parameters β_1, β_2, β_3 and β_5 define the cross-section configuration, while β_4 incorporates the panel length. When the values of β_1, β_2, β_3 and β_5 are set, i.e. the cross-section is set, a change in β_4 is achieved by varying the panel length. A full factorial design (four values for β_1, three values each for β_2, β_3 and β_5) results in 108 different cross-section configurations. If four values of β_4 and five load cases are introduced, the number of analysis cases reaches 2160 (108 × 4 × 5). In order to reduce the number of cases to a more manageable size, a fractional factorial design will be conducted with β_2 and β_3 taken as only three pairs, namely, (0.17, 0.17), (0.8, 0.6), and (1.5, 0.9). This fractional factorial design (four values for β_1, three pairs for β_2 and β_3, and three values for β_5) leads to

36 different cross-section configurations. For five load cases and four values of β_4, the total number of analysis cases is 720.

The four values of β_4 selected by Sheikh *et al*. (2002, 2003) were 0.5, 1.0, 1.5, and 2.0. Using these four values with each of the 36 cross-section configurations results in 144 panel configurations, as shown by the 144 data points presented in Figure 2-2. In the figure, each vertical line corresponds to one cross-section configuration with varying lengths. The four data points presented on one vertical line, from bottom to top, represent the four panel aspect ratios corresponding to values of β_4 of 0.5, 1.0, 1.5, and 2.0. The common range of aspect ratio (L/b) varies from 1.5 to 6 for ship structures (Smith *et al*., 1987), and 1 to 5 for bridges (Yoo *et al*., 2001). In this study the aspect ratio varies from 0.32 to 13 and most panels have an aspect ratio ranging from 1 to 7, as shown by the shaded area in Figure 2-3. In order to have a better control on the aspect ratio in the factorial design, a new parameter, β^*, is introduced. It is defined as $\beta^* = \beta_1^{0.5}\beta_2^{0.4}\beta_3^{0.1}\beta_4\beta_5^{0.5}$.

As β^* takes the values of 0.15, 0.4, 0.7 and 1.0, the plate aspect ratio varies from 0.93 to 6.85 as shown in Figure 2-3. β^* is therefore selected as one of the parameters for the fractional factorial design. The values of β_1, β_2, β_3, β_5 and β^* selected for the factorial design are listed in Table 2-2. Table 2-3 presents the fractional factorial design adopted for this study, where each row represents four configurations with identical cross-section but different lengths. The values of β_4 resulting from each value of β^* are listed in the last column of Table 2-3.

As described in section 2.2.1, Carlsen and Czujko (1978) showed that sinusoidal imperfection shapes are representative of ship plating. Timoshenko and Gere (1961) demonstrated that this imperfection shape is the critical shape for buckling of stiffened plates. The magnitude of the plate imperfection has been found to be proportional to β_1^2 based on extensive surveys and the average magnitude corresponds to $\beta_6 = 0.1\beta_1^2$ (Smith *et al*., 1992). This average magnitude is adopted in the current study.

The stiffener imperfection ratio, β_7 , reflects the out-of-straightness of the stiffener. The magnitude of $\delta_s = 0.0015L$ is considered by Smith *et al*. (1992) as the average level. A fabrication tolerance of $\delta_s = 0.0015L$ or $\delta_s = 0.001L$ is also quite common in design standards and guidelines such as DNV Classification Notes No. 30.1 (DNV, 1995), CAN/CSA-S6-06 (CSA, 2006), CSA-S16-09 (CSA, 2009) and CSA G40.20-04 (CSA, 2004). Thus the stiffener imperfection ratio, β_7, is taken as 0.0015.

The parameter β_8 represents the level of residual stresses. The presence of residual stresses is mainly due to welding of the stiffeners to the plate. According to residual stress measurements presented by Thimmhardy (1988) and Grondin *et al*. (1998), the residual stress distribution shown in Figure 2-1 (d) is representative of the actual residual stresses in stiffened steel plates. The magnitude of the compressive residual stress is around 0.2 F_y for the plating in box-girder bridges and 0.15 F_y for plating in ship elements (Thimmhardy, 1988; Grondin *et al*., 1998). The AASHTO LRFD bridge design specifications (AASHTO, 2007) have adopted a much higher value of 0.4 F_y for design purpose. As reported by Smith *et al*. (1992), 0.15 F_y and 0.3 F_y are classified as the average and severe residual stress magnitudes for ship construction representing mean and 97% fractile of the survey results, respectively. In this study, the severe magnitude, i.e. 0.3 F_y or β_8 = 0.3, is used for the analysis.

The parameter β_9 defines the load condition rather than the panel configuration. β_9 = 0 corresponds to a concentric axial load. A value of β_9 = 0.2 indicates that a moment of 0.2 M_p is applied to the panel prior to the application of the axial load. Positive values of β_9 indicate that the end moment creates flexural compression in the stiffener flange. Five values of β_9 are investigated in this study, namely, –0.4, –0.2, 0, 0.2 and 0.4.

The fractional factorial design used in this study leads to 720 separate cases (144 configurations described in Table 2-3 and five loading conditions) to be analyzed. As mentioned in section 2.2.1, the real boundary condition along the unloaded edges of the plate is such that the plate is neither completely free to expand nor completely restrained transversely. In order to establish the error caused by an ideal boundary condition in a model of a single stiffener panel both restraint conditions have been applied in the finite element analysis for the 720 different panel configurations. Two of the models had convergence problems when the unloaded edges were fully restrained in the transverse direction. The remaining 718 configurations that converged are compared in Figure 2-4 where the plate capacity ratio, P_c/P_y, for plates with unloaded edges fully restrained, is plotted against the plate capacity ratio for the plates free to expand and contract. A small number of cases show noticeable difference in capacity due to the difference of failure mode. The data point farthest from the diagonal line, which lies above the diagonal line, represents a normalized capacity of 0.665 when the unloaded edges are free to expand and a normalized capacity of 1.103 when the unloaded edges are fully restrained from in-plane translation. For a similar reason (failure mode change), a limited number of points are observed below the diagonal line. For the panel with the unloaded edges free to expand, failure took the form of plate induced overall buckling whereas the panel with restrained unloaded edges failed by stiffener induced overall buckling. In general, the mean value of the ratio of capacities with plates restrained in the transverse direction to the capacities with plate free in the transverse direction, $\left(P_c/P_y\right)_{\text{restrained}} / \left(P_c/P_y\right)_{\text{free}}$, is 1.043 and the associated coefficient of variation is 0.073. Less than 2% of the cases investigated have a ratio less than 0.95. In order to control the number of analysis cases to a manageable size, only the conservative condition, the edges free to expand, will be used in the current work to form a database from which the strength and behaviour of stiffened steel plates can be investigated.

A typical input file for the finite element analysis for the boundary condition with the plate free in the transverse in-plane direction is presented in Appendix A as an example. The detailed analysis results for this boundary condition and the dimensions and material properties for these panels are presented in Appendix B. The capacity comparisons of the 718 panels shown in Figure 2-4 are also presented in Appendix C for various load cases.

2.3 VIRTUAL WORK MODEL FOR PLASTIC HINGE

Although the post-buckling behaviour of stiffened plates was analyzed using finite element analysis, a simple theoretical model describing post-bucking behaviour of stiffened plates is desirable to provide a design tool to evaluate the post-buckling stability of panels. The behaviour of primary interest is the sudden loss of load carrying capacity observed in the post-buckling range because such panels should be designed with a higher safety index.

In the presence of an in-span plastic hinge, the increasing lateral deflection at the plastic hinge directly affects the moment equilibrium due to the second-order effects resulting from the axial load. Since the moment resistance remains constant at the plastic moment, the axial load cannot remain constant as the deflection increases after the development of the plastic hinge. In current steel design standards such as CAN/CSA–S16–09 (CSA, 2009), the plastic moment capacity of a beam-column is estimated by using a cross-section strength interaction equation for bending moment and axial force, where the P–δ effect is accounted for by applying an amplification factor to the first-order moment. Although this simplified approach provides a reasonable estimate of the member capacity at full yielding of the cross-section, it does not predict the behaviour of the member beyond the peak load.

Another problem is that the interaction equation is dependent on the cross-section shape. The interaction equations in some design standards, including the Canadian design standards CSA-S16-09 and CSA-S6-06, are a linear approximation of the actual nonlinear interaction curves of doubly symmetric I sections. The only variable affecting the nonlinear interaction curves of I sections is the area ratio of the web to the full cross-section because the flanges are equal. This is obviously not applicable for monosymmetric stiffened plates as the stiffener flange is much smaller than the plate. Although the stiffened plate is not a doubly symmetric section, API bulletin 2V (2000) uses the interaction curve derived by Soreide (1981) based on I sections for stiffened plates. Other design guides for stiffened plates such as DNV-RP-C201 (DNV, 2002) and the ABS guide (ABS, 2007) do not consider the plastic behaviour. In this section, a theoretical model will be derived to predict the load versus deformation characteristic of a stiffened plate panel beyond the peak load.

2.3.1 Virtual Work Model

The proposed model is based on the principle of virtual work. Detailed derivation of this model is provided in Appendix D. The plastic hinge mechanism is defined as plate induced plastic hinge when the plate outer surface is in flexural compression, or stiffener induced plastic hinge if the stiffener flange is in flexural compression. For most commonly used stiffened plates the plate area is usually larger than the stiffener area. In fact, the investigation presented in this report used a range of stiffener to plate area ratio (β_5) of 0.075 to 0.3. Thus the pure bending plastic neutral axis (P.N.A.) is always located in the plate. For a plate induced plastic hinge the part of the cross-section in compression would be from the plate outer surface to the pure bending P.N.A. If an axial compression force is superimposed to the bending moment, the portion of the cross-section in compression will spread towards the flange outer surface, and the P.N.A. can be anywhere between the pure bending P.N.A. and the flange outer surface. Three equations are therefore required depending on the location of the P.N.A.

For the P.N.A. in the plate,

$$\frac{u_3}{L} = \frac{\beta_9 M_p}{PL} + \left(\frac{P_y}{P} + 1\right)\left(\frac{z_p}{L} - \frac{P_y + P}{4F_y bL}\right), \qquad \frac{P}{P_y} \le 1 - \frac{2A_s}{A} \qquad [2\text{-}3]$$

For the P.N.A in the web,

$$\frac{u_3}{L} = \frac{\beta_9 M_p}{PL} + \frac{2F_y A_f}{P}\left(\frac{z_s}{L} - \frac{t_f}{2L}\right) + \left(\frac{P_y - 2F_y A_f}{P} - 1\right)\left(\frac{z_s}{L} - \frac{t_f}{L} - \frac{P_y - P}{4F_y t_w L} + \frac{A_f}{2t_w L}\right),$$
$$1 - \frac{2A_s}{A} \le \frac{P}{P_y} \le 1 - \frac{2A_f}{A}$$

[2-4]

For the P.N.A. in the flange,

$$\frac{u_3}{L} = \frac{\beta_9 M_p}{PL} + \left(\frac{P_y}{P} - 1\right)\left(\frac{z_s}{L} - \frac{P_y - P}{4F_y b_f L}\right), \qquad \frac{P}{P_y} \ge 1 - \frac{2A_f}{A} \qquad [2\text{-}5]$$

where u_3 is the out-of-plane deflection at the centre of the stiffened plate, A_f is the flange area, z_p is the distance between the centroid of the full section to the plate outer surface (see Figure D-1), z_s is the distance between the centroid of the full section and the flange outer surface, and P_y is the yield force of the full section.

Since β_5 is less than 1.0, the P.N.A. for a stiffener induced plastic hinge under bending only lies in the plate, with the stiffener and part of the plate in compression. As an axial compression force is superimposed to the bending moment, a larger portion of the cross-section goes into compression, thus forcing the neutral axis to remain in the plate or move outside of the cross-section for all combinations of axial compression and bending moment. Therefore, only one equation is required for stiffener induced plastic hinge, that is:

$$\frac{u_3}{L} = \frac{\beta_9 M_p}{PL} - \left(\frac{P_y}{P} - 1\right)\left(\frac{z_p}{L} - \frac{P_y - P}{4F_y bL}\right) \qquad [2\text{-}6]$$

Equations [2-3] and [2-6] can also be expressed in a simplified form, as shown by Equations [2-7] and [2-8], respectively.

For plate induced buckling with the P.N.A. in the plate,

$$\frac{u_3}{L}=\frac{d_c}{L}+\frac{(1+\beta_9)M_p}{PL}-\frac{P}{4F_y bL}, \qquad \frac{P}{P_y}\leq 1-\frac{2A_s}{A} \qquad [2\text{-}7]$$

For stiffener induced buckling,

$$\frac{u_3}{L}=\frac{d_c}{L}-\frac{(1-\beta_9)M_p}{PL}+\frac{P}{4F_y bL} \qquad [2\text{-}8]$$

where d_c is the distance between the pure bending P.N.A. and the centroid of the full cross-section.

When plate buckling takes place, the plate cannot yield fully due to unloading of the plate that takes place after the plate has buckled (the plate stresses decreases where it is more flexible, half way between the stiffeners, and it increases near the supporting stiffeners). In order to account for the loss of plate effectiveness when plate buckling occurs, the plate can be replaced by a plate of effective width, smaller than or equal to the plate actual width (Faulkner, 1975). The reduced plate width and the attached stiffener can be considered as an effective cross-section that can fully yield. The use of the effective cross-section with the virtual work model gives rise to Equations [2-9] to [2-11] for plate induced plastic hinge and Equation [2-12] for stiffener induced plastic hinge.

For plate induced plastic hinge and the P.N.A. in the plate,

$$\frac{u_3}{L}=\frac{\beta_9 M_p}{PL}+\left(\frac{P_{ye}}{P}+1\right)\left(\frac{z_{pe}}{L}-\frac{P_{ye}+P}{4F_y b_e L}\right)-\frac{z_{pe}}{L}+\frac{z_p}{L}, \qquad \frac{P}{P_{ye}}\leq 1-\frac{2A_s}{A_e} \quad [2\text{-}9]$$

For plate induced plastic hinge and the P.N.A. in the web,

$$\frac{u_3}{L}=\frac{\beta_9 M_p}{PL}+\frac{2F_yA_f}{P}\left(\frac{z_{se}}{L}-\frac{t_f}{2L}\right)+\left(\frac{P_{ye}-2F_yA_f}{P}-1\right)\left(\frac{z_{se}}{L}-\frac{t_f}{L}-\frac{P_{ye}-P}{4F_yt_wL}+\frac{A_f}{2t_wL}\right)-\frac{z_{pe}}{L}+\frac{z_p}{L}, \qquad 1-\frac{2A_s}{A_e}\le\frac{P}{P_{ye}}\le 1-\frac{2A_f}{A_e} \tag{2-10}$$

For plate induced plastic hinge and the P.N.A. in the flange,

$$\frac{u_3}{L}=\frac{\beta_9 M_p}{PL}+\left(\frac{P_{ye}}{P}-1\right)\left(\frac{z_{se}}{L}-\frac{P_{ye}-P}{4F_yb_fL}\right)-\frac{z_{pe}}{L}+\frac{z_p}{L}, \qquad \frac{P}{P_{ye}}\ge 1-\frac{2A_f}{A_e} \tag{2-11}$$

For stiffener induced plastic hinge,

$$\frac{u_3}{L}=\frac{\beta_9 M_p}{PL}-\left(\frac{P_{ye}}{P}-1\right)\left(\frac{z_{pe}}{L}-\frac{P_{ye}-P}{4F_yb_eL}\right)+\frac{z_{pe}}{L}-\frac{z_p}{L} \tag{2-12}$$

where P_{ye} is the yield capacity of the effective cross-section, z_{pe} is the distance between the plate outer surface and the centroid of the effective cross-section (see Figure D-8), A_e is the area of the effective cross-section, and z_{se} is the distance between the flange outer surface and the centroid of the effective cross-section. A number of effective width equations are available in the literature for the calculation of the effective cross-section. In this study, the effective plate width, b_e, is obtained using the equation proposed by Faulkner (1975) as follows:

$$\left.\begin{aligned}\frac{b_e}{b}&=1 && \text{if } \beta_1\le 1\\ \frac{b_e}{b}&=\frac{2}{\beta_1}-\frac{1}{\beta_1^2} && \text{if } \beta_1>1\end{aligned}\right\} \tag{2-13}$$

The values of P and u_3 can be substituted into Equation [2-14] to obtain the internal moment about the centroid at the midspan cross-section, M_i, which is equal to the applied end moment plus a second order moment due to the P-δ

effect. This equation is valid regardless of the stress distribution in the cross-section.

For plate induced failure,

$$\frac{M_i}{M_p} = \frac{Pu_3}{M_p} - \beta_9 \tag{2-14a}$$

For stiffener induced failure,

$$\frac{M_i}{M_p} = -\frac{Pu_3}{M_p} + \beta_9 \tag{2-14b}$$

2.3.2 Additional Considerations

Some factors are not accounted for in the virtual work model directly. However, the finite element analysis shows that these factors have insignificant impact on the stiffened plate behaviour, which will be presented in the following sections. The factors are given as below:

1. Partial yielding at the plastic hinge cross-section, spread of plasticity along the length of the panel, and strain-hardening behaviour;

2. Local buckling of the stiffener and stiffener tripping;

3. Presence of residual stresses and initial imperfections.

Partial yielding, spread of plasticity and strain-hardening effects

When the neutral axis lies in the cross-section, full cross-section yielding can never be attained because the material near the neutral axis remains at low stresses throughout the loading process. Partial yielding at the plastic hinge cross-section and spread of plasticity cause a reduction in capacity and stiffness that are not accounted for in the virtual work model.

Material strain-hardening causes an increase in the plastic moment capacity. Since it tends to offset the effect of partial yielding and spread of plasticity, these effects are often neglected (ASCE, 1971; Neal, 1977; Chen and Han, 1988). The strain at which strain-hardening starts in mild steel is generally in the order of 0.01 to 0.02 (Neal, 1977). The steel used in the finite element analysis was given a modulus of 100 MPa from the yield point to a plastic strain of 1.0 mainly to prevent numerical convergence difficulties that may arise with a modulus of 0.0. This material model is conservative because it underestimates the strain-hardening effect.

The finite element analysis results that will be presented in section 2.4 indicates that a plastic hinge behaviour can be developed in spite of partial yielding and spread of plasticity. A good agreement always occurs between the virtual work model and the finite element analysis results, although the deflection at which it occurs is sometimes large when stiffened plates are proportioned such that overall buckling occurs before the reduced plastic moment is developed as will be described in section 2.4. Section 2.5 will demonstrate that, even for these configurations, the virtual work model can be used to assess the level of stability in the post-peak range.

Stiffener local buckling and stiffener tripping

Stiffener local buckling and stiffener tripping can result in a significant loss of effectiveness of the stiffener. Given that premature local buckling was prevented by limiting the width-to-thickness ratio of the stiffener flange and web, local buckling of the stiffener was observed only in the post-buckling range; in the late post-buckling range if the flange and web met the requirements of class 1 or 2 sections. In the 720 FEA models examined in this research, no instance of stiffener tripping was observed prior to overall buckling of the stiffened plate as well. The load carrying capacity, based on the observations in section 2.4, is not affected by stiffener tripping and stiffener local buckling. As will be demonstrated in section 2.5, although the virtual work model cannot provide accurate prediction for the entire post-buckling range, it provides a good prediction for the part of most interest; the early post-buckling range. Since the design process would only need to identify the severity of the loss of capacity, the prediction of the early post-buckling behaviour provides sufficient information for design.

Residual stresses and initial imperfections

Although residual stresses will cause gradual yielding during loading process, the plastic moment capacity of stiffened plates can be attained regardless of the presence of residual stresses.

The out-of-straightness tolerance is generally in the order of 0.001 L to 0.0015 L in most design guidelines and standards such as DNV Classification Notes No. 30.1 (1995), CAN/CSA-S6-06 (2006), CSA-S16-09 (2009) and CSA G40.20-04 (2004). The effect of initial imperfection can be captured if this tolerance is superimposed to the u_3 term in the virtual work model equations. Since the post-peak deflection investigated in this research is one order of magnitude larger than the tolerance, the effect of initial out-of-straightness is not significant.

2.4 RESULTS OF ANALYSIS

2.4.1 Plate Induced Failure Mode

The main purpose of this section is to gain more insight into the panel behaviour in both the pre-buckling and post-buckling ranges, based on stress and strain distributions, deformed shapes, load history from the finite element analysis, and theoretical verification of the overall stiffened plate behaviour. A number of stiffened panels governed by plate induced failure will be selected from the database of analysis results. Based on the practical range of values of the parameters discussed in section 2.2.2, a typical panel is selected as the reference panel to illustrate the plate induced failure mode behaviour of stiffened steel plates. A parametric analysis will then be conducted based on this reference panel. The parameters to be examined in this section are the plate slenderness ratio, β_1, and the plate aspect ratio, *L/b*, which are known to have a significant impact on plate induced mode (Grondin *et al*.,1999; Sheikh *et al*., 2003).

The selected reference panel has the following properties: 500 mm × 17.90 mm plate, 115.0 mm × 6.59 mm web, 87.5 mm × 6.69 mm flange, 1249 mm length, and 420 MPa yield strength. These dimensions result in the following non-dimensional parameter values: β_1 = 1.28, β_2 = 0.8, β_3 = 0.6, β_4 = 1.05, β_5 = 0.15, β^* = 0.4, L/b = 2.50. It is designated as panel 222_22. Each digit in the designation indicates the sequence number, from Table 2-2, for the dimensionless parameters, β_1, β_2, β_3, β_5, and β^*, in that order. The number 2 for the first digit indicates that the β_1 takes the second value tabulated in Table 2-2, namely 1.28, and so on. An underscore is inserted after the third digit to indicate that β_4 is not specified in the specimen designation since it is defined through β^*. Therefore, the digit following the underscore refers to the value of β_5 as tabulated in Table 2-2. This panel designation convention is illustrated in Figure 2-5. The values of the imperfection and residual stress parameters, β_6 to β_8, are not varied in this parametric study. The loading case for the reference panel is taken as β_9 = –0.4, namely, 40 percent of the plastic moment capacity is applied to place the plate outer surface initially in flexural compression. The conclusions drawn for this load case also apply for the other three load cases under which plate induced failure was observed, namely, β_9 = –0.2, 0, and 0.2. At β_9 = 0.4 only stiffener induced failure was observed.

Effect of Plate Slenderness Ratio, β_1

As previously discussed, β_1 is one of the major parameters affecting the panel strength and behaviour. Three plate slenderness ratios are investigated in this section, namely, 0.7, 1.28, and 2.7. The plate slenderness ratio is varied by changing the thickness of the plate. The other dimensionless parameters of the parameter group were selected as β_2 = 0.8, β_3 = 0.6, β^* = 0.4, β_5 = 0.15, $\beta_6 = 0.1\beta_1^2$, β_7 = 0.0015, β_8 = 0.3, β_9 = –0.4. The plate specimens selected for this analysis are panels 122_22, 222_22 (the reference panel), and 422_22 and *L/b* = 2.50 for all the three.

Figures 2-6 to 2-8 present a detailed representation of the behaviour of panels with values of β_1 varying from 0.7 to 2.7, respectively. The behaviour is illustrated in terms of axial load versus deformation (axial deformation and lateral deflection at the centre of the panel) and moment versus lateral deflection. The deflection along the plate edge and the extent of yielding at various load stages are also presented. Figure 2-6, for the plate with the smallest slenderness, shows that from the peak axial load at A to the point of instability (between points B and C) the internal moment increased to the point where at point B the stiffener flange and the plate had both yielded, and the web had completely yielded by the time point C was reached where a plastic hinge had formed at midspan. It is noted that the plates with higher slenderness ratios (β_1 = 1.28 in Figure 2-7 and β_1 = 2.7 in Figure 2-8) were not able to yield by the time the peak load was reached at point A. The deformed shape of the plate edge presented in figures (d) indicates that for β_1 = 0.7 the plate yielded before overall buckling took place at point A, for β_1 = 1.28 the plate buckled, but only after substantial yielding (see Figure 2-7 (f) and (g)), and for β_1 = 2.7 the plate buckled elastically (see Figure 2-8 (d) and (g) for the extent of yielding at point B). An examination of figures (c) indicate that for all three values of β_1, point B is either very close to the formation of the reduced plastic moment or has already reached the reduced plastic moment capacity. It is seen that at point C, the internal moment has reached its full value, which, according to figures (h), corresponds to full yielding of the cross-section. The region A-B in all figures (a) for the three values of β_1 corresponds to the zone of stable post-peak capacity behaviour where a plastic hinge forms. It is noted that as β_1 increases, the stable post-peak zone shortens, and at β_1 = 2.7, the stiffened plate becomes unstable right at the peak, where the internal moment has reached almost the full reduced moment capacity (Figure 2-8 (c)).

A comparison of the virtual work model presented in section 2.3 with the finite element analysis results is shown in figures (b) and (c). For the two cases with the largest β_1 values (panels 222_22 and 422_22), two curves are shown for the virtual work model, namely, the top curve corresponding to the full plate width, and the lower curve corresponding to the effective plate width to account for the plate buckling phenomenon observed for these two cases. Figure 2-6 shows that the virtual work model provides an excellent prediction of the observed behaviour past the peak load for a stiffened plate with β_1 = 0.7. For β_1 = 1.28, both the calculations with the full cross-section and with the reduced section provide similar predictions. This is expected since plate buckling took place in the inelastic range, making the plate section almost fully effective. This is not the case, however, for the specimen with the largest plate slenderness where a significant discrepancy between the full section and the reduced section prediction is observed, although as a plastic collapse mechanism sets in with the formation of a plastic hinge at point C both models converge to the behaviour predicted by the finite element analysis.

Effect of Plate Aspect Ratio, L/b

As previously discussed, length is one of the major parameters affecting the panel strength and behaviour. Three stiffened plate panels with identical cross-section but various lengths will be examined in this section. The plate specimens selected for this analysis are panels 222_21, reference panel 222_22 described previously, and 222_24. The values of L/b for the three panels are 0.94, 2.50 and 6.50, and

β^* are 0.15, 0.40 and 1.00, respectively, in that order. The other dimensionless parameters of the parameter group (β_1 to β_3, β_5 to β_9) are kept at the reference panel values, namely, β_1 = 1.28, β_2 = 0.8, β_3 = 0.6, β_5 = 0.15, $\beta_6 = 0.1\beta_1^2$, β_7 = 0.0015, β_8 = 0.3, β_9 = –0.4. The behaviour of the three panels is illustrated in Figures 2-7, 2-9, and 2-10.

The shortest of the three panels, 222_21 (*L/b* = 0.94), shows significantly smaller out-of-plane deflection (u_3) than the longer panels (maximum u_3/L of less than 0.01 compared to values of over 0.07 for the other two panels). This reduced out-of-plane response is due to the fact that the panel failed by plate buckling rather than overall buckling as evidenced by a comparison of Figures 2-7, 2-9 and 2-10 (d). Because plate buckling is a relatively stable failure mode, Figure 2-9 (a) shows a long stable post-peak behaviour. Figure 2-9 (d) indicates that plate buckling was imminent at point A where the peak load was reached and almost the full cross-section yielded in compression after point A with little bending action. Panel 222_24, with the largest aspect ratio, failed by elastic overall buckling. Overall buckling was triggered at point A on the load versus deformation curves and a plastic hinge, resulting from the P-δ effects, was almost entirely developed by the time point B on the load vs. deflection curves was reached. The behaviour of panel 222_22, with an intermediate aspect ratio is found to be one where plate buckling started at point A (see Figure 2-7 (d)), but overall buckling, or the formation of a plastic hinge, took place between points B and C, which resulted in a sudden loss of load carrying capacity. Because the virtual work model is based on the formation of a plastic hinge, the predicted behaviour based on this model for panels 222_22 and 222_24 is accurate only once a plastic hinge has formed. Since panel 222_21 failed by plate buckling and behave as an axial hinge rather than a flexural hinge on which the virtual work model is based, the virtual work model did not predict the behaviour of this model accurately.

2.4.2 Stiffener Induced Failure Mode

While a stable post-buckling behaviour has been observed before a sudden loss of capacity for some of the stiffened plates failing in the plate induced overall buckling mode, a review of the literature indicates that the unstable behaviour of stiffener induced failure is characterized by a sudden loss of load carrying capacity immediately after the peak load. This failure mode has been designated as stiffener tripping because the stiffener has been observed to fail by lateral torsional buckling some time after the sudden loss of capacity. However, in the case of plate induced failure mode investigated in section 2.4.1 the sudden loss of capacity was found to result from a plastic hinge mechanism. Therefore, the effect of plastic hinge mechanism on stiffener induced failure will be investigated in this section.

Panel 222_22 will once again be used as the reference panel. The load case is taken as β_9 = 0.4, namely, 40 percent of the plastic moment capacity is applied to place the stiffener flange initially in flexural compression. The parameters to be examined in this section are the stiffener slenderness ratios (β_2 and β_3) and the plate aspect ratio, *L/b*. It was found that these three parameters have a significant impact on the behaviour for stiffener induced failure.

Effect of Plate Aspect Ratio, L/b

The stiffened plates selected for this analysis are panels 222_21, the reference panel 222_22, and 222_24. The values of L/b for the three panels are 0.94, 2.50 and 6.50, and the values of β^* are 0.15, 0.4 and 1, respectively. The other dimensionless parameters of the parameter group (β_1 to β_3, β_5 to β_9) are kept at the reference panel values, namely, β_1 = 1.28, β_2 = 0.8, β_3 = 0.6, β_5 = 0.15, $\beta_6 = 0.1\beta_1^2$, $\beta_7 = 0.0015$, $\beta_8 = 0.3$, $\beta_9 = +0.4$.

Figures 2-11 to 2-13 summarize the behaviour of panels with L/b varying from 0.94 to 6.50. Figure 2-11(e), for the shortest of the three panels, 222_21, shows that at point A (see figures (a) and (b)) the flange and 75% of the web have yielded along most of the plate length. On the other hand, the two longer panels (L/b = 2.50 in Figure 2-12 and L/b = 6.50 in Figure 2-13), show less extensive yielding at point A. A closer examination of the shortest panel (Figure 2-11b) indicates that the out-of-plane deflection u_3 at point A (about 0.001 L) is considerably smaller than the plate thickness (t = 0.038 L), and is in the same order of magnitude as the panel edge deflection due to local buckling (Figure 2-11 (d)), meaning that the compression stresses in the plate are not insignificant. Because the out-of-plane deflections in region A-B shown in Figure 2-11(b) (u_3 = 0.001~0.007 L) are small relative to the plate thickness(t = 0.038 L), the behaviour of the stiffened plate in Figure 2-11 (a) shows stable behaviour between A and B. The two longer panels (L/b = 2.50 in Figure 2-12 (a) and L/b = 6.50 in Figure 2-13(a)), however, become unstable at the peak load (point A). An examination of figures (c) indicates that at this point of instability, the rate of change of the internal moment reduces significantly, indicating a plastic hinge action. The yield patterns shown in Figures 2-12 and 2-13 indicate that the plastic hinge is partially developed at point B and entirely developed at point C. However, local buckling in the flange and web and tripping in the stiffener are also observed in the deformed shape. It is therefore difficult to identify the failure mode at point A.

In order to decouple the effects of plastic hinge and stiffener tripping, the finite element models were re-analyzed with a laterally supported stiffener to prevent tripping. The lateral support to the stiffener was provided by applying transverse restraints along the flange tip at y = +0.5 b_f. The behaviour of the three panels in the restrained models are compared to the behaviour of the unrestrained models as shown in Figures 2-14 to 2-16. An examination of figures (a) to (c) indicates that for all three values of L/b, the restrained models display identical behaviour to their unrestrained counterpart up to the peak load at A. This indicates that stiffener tripping has no effect on the axial load capacity and the failure mode at that point. It is noted that the two longer panels (L/b = 2.50 and 6.50), for which instability was observed at the peak load when unrestrained (Figures 2-12 (a) and 2-13 (a)), still become unstable at the same peak load level when restrained. Since tripping is effectively prevented in the restrained models, the instability is believed to be the result of the accelerated P-δ effect due to the plastic hinge action. Both the restrained and the unrestrained finite element models showed little to no increase of internal moment resistance with a significant increase in curvature (see Figures 2-15 (c) and 2-16 (c)).

Because stiffener tripping has not taken place for the shortest panel with L/b = 0.94 as illustrated in Figure 2-14, it is deduced that the formation of a plastic hinge is the primary failure mode observed in Figure 2-11(c). For this failure mode the virtual work model is found to predict the internal moment accurately up to point C where local buckling of the stiffener was observed (Figure 2-11 (g)).

For L/b = 2.50 (Figure 2-12 (c)) and L/b = 6.50 (Figure 2-13(c)), the internal moment ratio, M_i/M_p , obtained from the finite element analysis is significantly lower than predicted by the virtual work model due to failure of the stiffener by a combination of tripping and local buckling. When stiffener tripping is prevented by providing lateral restraint to the edge of the stiffener flange the virtual work model provides a good prediction of the internal moment ratio in region B-C for the panel with L/b = 2.50 (Figure 2-15 (c)), indicating that a plastic hinge can form when stiffener tripping is prevented. This observation is also made for the plate with L/b = 6.50 as demonstrated in Figure 2-16 (c).

It is noted that good agreement between the finite element model and the virtual work model starts before point B when stiffener tripping is restrained for the panel with L/b = 2.50 (Figure 2-15 (c)), which is before the plastic hinge is fully developed at point C. In order to check if the panel can develop most of the plastic moment capacity without yielding the entire section, the analysis of the panel with L/b = 2.50 was repeated with pure end moments, with and without lateral flange restraint, as shown in Figures 2-17 and 2-18, respectively. Figure 2-17, which shows the results for the restrained model, indicates that 90.4% of the plastic moment capacity is developed by the time the flange and 75% of the web have yielded. This is expected because about 75% of the plastic section modulus of this panel is contributed by the stiffener. The results of the analysis on the unrestrained model presented in Figure 2-18 show that stiffener tripping reduces the moment capacity to 80.8% of the plastic moment capacity, most of which is achieved when the flange and only 75% of the web have yielded.

Two sets of virtual work model curves are shown in Figures 2-11 and 2-12, namely, one for the cross-section with the full plate width, and one with an effective plate width to account for plate buckling. The behaviour predicted based on the effective plate width (95% of the full width if using Equation [2-13]) is almost identical to that based on the full plate width, indicating that the ineffective portion of the plate does not contribute much to the plastic section modulus. In fact, the effective width is even larger than the predicted value using the effective width equation because the neutral axis resides in the plate. Since the axial force reduces in the post-buckling range, the effective plate width calculated based on the peak load is not strictly applicable past the peak load. Therefore, only the full plate width was used for the panels in the following analysis for stiffener induced failure.

Effect of stiffener local buckling (β_2 and β_3)

This section investigates the effect of stiffener local buckling on the strength and behaviour of stiffened steel plates. Therefore, panel 233_32 will be investigated as a comparison to the reference panel 222_22. The web and flange slenderness ratios (β_2 and β_3) of panel 233_32 are set to 1.5 and 0.9, respectively, and the maximum value of stiffener to plate area ratio ($\beta_5 = 0.3$) is used to maximize the effect of stiffener failure on the stiffened panel behaviour. The flange slenderness ratio makes the section a class 3 section. The other dimensionless parameters for panel 233_32 are as follows: β_1 = 1.28, β_4 = 0.55, β^* = 0.4, L/b = 2.49, β_9 = +0.4. The behaviour of this panel is illustrated in Figure 2-19.

For an applied moment ratio of $\beta_9 = 0.4$, which places the stiffener initially in compression, and an area ratio significantly smaller than 1.0 (β_5 = 0.3) the neutral axis is expected to remain in the plate for all values of axial force. This was confirmed by the analysis results. Therefore, the full web is in compression and its slenderness ratio should be calculated based on twice the web height when compared to the classification limits. Based on CSA-S16-09 the slenderness limits for webs of I-section beams subjected to flexural moment only are $2\beta_2 \leq 2.46$, 3.80, and 4.25 (or $\beta_2 \leq 1.23$, 1.90, and 2.13) for classes 1, 2 and 3 sections, respectively. These limits will be reduced if an axial force is applied with the moment. As for panel 233_32 being investigated, the web therefore could be in class 2 or 3 depending on the axial force (it is at least a class 3 web as presented in section 2.2.2).

Figures 2-19 (g) and (h) show large local buckling deformations of the flange and web with the flange to web junction remaining virtually straight during the local buckling process, indicating no stiffener tripping. The model with the stiffener restrained for this panel (Figure 2-20) further confirms that there is no stiffener tripping. Therefore, the discrepancy between the virtual work model curve and the FEA curve in Figure 2-19 (c) is caused by deformation of the cross-section due to stiffener local buckling. The virtual work model provides a good prediction of the internal moment up to the point of stiffener local buckling (Figure 2-19 (c)).

In order to investigate the effect of stiffener local buckling without interference of stiffener tripping, the restrained panel 233_32 (β_2 = 1.5, β_3 = 0.9) in Figure 2-20(c) is compared to the restrained reference panel 222_22 (β_2 = 0.8, β_3 = 0.6) in Figure 2-15(c). It is observed that the stiffened plate cannot develop its plastic moment capacity when the stiffener local buckling sets in. This behaviour is also observed for the restrained panel 222_21 in Figure 2-14 (c), although the effect of stiffener local buckling is less severe.

Extremely slender panels due to combined effects of all parameters

Low axial load carrying capacity and stable post-peak performance has been observed for some panels in stiffener induced failure. This is believed to be a combined effect of all the parameters making the stiffened panel slender against overall buckling. Some examples are described below.

A representative panel 122_14 has the following parameters: β_1 = 0.7, β_2 = 0.8, β_3 = 0.6, β_5 = 0.075, β^* = 1, $\beta_9 = 0.4$, L/b = 6.25. This panel is made of a compact plate (β_1 = 0.7) and a small stiffener (β_5 = 0.075). With the largest L/b, the slenderness of the panel becomes large. As a result, the axial load capacity of the panel is small. Therefore, the P-δ effect is small and no sudden loss of capacity is expected. As shown in Figure 2-21, the load carrying capacity of panel 122_14 is limited by overall buckling and then decreases very slowly. This observation is not affected by stiffener tripping because tripping is observed only at the late post-buckling range based on the comparison between the restrained and unrestrained models in Figure 2-21 (c). The virtual work model was not able to predict the behaviour accurately until the formation of the plastic hinge. This behaviour, however, can be predicted in design as will be presented in section 2.5. Three more panels are shown in Figure 2-22 and the observations for panel 122_14 apply to them as well.

Stiffener induced failure observed in tests

Some experimental data have been presented in the literature for stiffener induced failure. The behaviour observed in the tests was similar to the behaviour observed in the FEA and will be briefly presented here.

Chen *et al.* (1997) reported the results of a series of tests on stiffened steel plate panels where the results of three specimens of interest are described in the following. The three specimens, designated as SP 1.4, SP 1.5, and SP 1.6, had identical nominal dimensions and material properties. The averages of the measured properties are: 500.4 mm × 9.67 mm plate, 119.1 mm × 6.22 mm web, 103.9 mm × 8.06 mm flange, 2000 mm length. The measured yield strength was 425 MPa for the plate, 411 MPa for the stiffener web and 395 MPa for the stiffener flange. The corresponding dimensionless parameters are: β_1 = 2.39, β_2 = 0.86, β_3 = 0.58, β_4 = 0.85, β_5 = 0.326, and L/b = 4.10. The tee stiffener for the three test specimens met CSA-S16-09(CSA, 2009) requirements for class 1 sections. Rotational restraints were applied along the unloaded edges for SP 1.4 and SP 1.6, but not for SP 1.5. The three specimens were intentionally designed to fail by stiffener induced failure by applying third-point lateral loads to place the stiffener flange in initial flexural compression. The magnitude of the third-point out-of-plane loads was 25 kN for SP 1.4 and SP 1.5, and 10 kN for SP 1.6, creating a constant moment region in the middle of the panel. The ratio of the applied constant moment to plastic moment capacity (equivalent to β_9 [1]) is 0.307 for SP 1.4 and SP 1.5, and 0.123 for SP 1.6.

These test results are presented in Figure 2-23 with the prediction from the virtual work model. The three test specimens displayed the same post-buckling behaviour, namely, a significant loss of capacity after the peak load, similar to the behaviour of the FEA specimens discussed earlier. Figure 2-23 shows excellent agreement between the test results and the predicted plastic hinge curve using

[1] The term equivalent is used to indicate the fact that the moment distribution used in the tests was different from the moment distribution used in the parametric study.

Equations [2-6] and [2-14b]. SP 1.4 and SP 1.5 have the same virtual work load versus deformation behaviour because the virtual work model does not account for the difference in boundary conditions along the unloaded edges.

Stiffener tripping was observed in the three specimens within the constant moment region. However, Figure 2-23 indicates that more than 90 % the moment capacity of the critical cross-section was developed at the peak axial load and it is the subsequent plastic hinge action that caused the sudden loss of capacity.

The FEA results in the parametric study indicated that for the wide range of practical configurations of tee stiffeners in this work the stiffeners have sufficient torsional stiffness so that tripping occurs only in the post-buckling range. Compared to panel 222_24 in the parametric study (see section 2.4.2), the three test panels have similar web slenderness β_2 (0.86 vs. 0.80) and flange slenderness β_3 (0.58 vs. 0.60). With a smaller aspect ratio (4.10 vs. 6.25) and smaller ratio of stiffener torsional slenderness to plate slenderness, β_4 (0.85 vs. 2.63), the test specimens are less likely to have early stiffener tripping. Therefore, stiffener tripping of these three specimens is believed to occur in the post-buckling range as for panel 222_24 (β_9 = 0.4) presented in section 2.4.2.

2.5 PROPOSED DESIGN APPROACH TO PREDICT SUDDEN CAPACITY LOSS

Section 2.4 indicated that the abrupt loss of capacity observed after the peak load is caused by a large increase in curvature while the internal moment resistance, M_{ir}, remains constant or decreases. The purpose of this section is to propose a design approach to identify the stiffened plates that will experience such a sudden loss of capacity. It was observed that the peak load can be maintained over some deformation. Since the behaviour far beyond the peak load is not of practical design interest, in the following discussion an unstable failure will be limited to cases where the sudden loss of capacity occurs within an axial strain of 0.01. The value of 0.01 is approximately five times of the yield strain of an axially loaded stiffened plate with no initial imperfections. Both the current research and earlier work by Sheikh *et al*. (2001) have indicated that sudden failure occurs within the axial strain of 0.008. An abrupt loss of capacity will be considered to have taken place when an increase in u_1 / L of 0.0001 causes a reduction of P / P_y of at least 0.02.

2.5.1 Stiffener induced failure

Stiffener induced plastic hinge behaviour is described by Equation [2-6] when the P.N.A. lies in the plate. The out-of-plane deflection at the peak axial load as predicted by the virtual work model indicates the midspan displacement in the plane of bending required to initiate a plastic hinge mechanism. It is designated as $(u_3/L)_H$ and shown in Figure 2-24 (a). Since the virtual work model provides an upper bound curve, the out-of-plane deflection predicted by the FEA is smaller than or equal to the deflection predicted by the virtual work model. When the magnitude of $(u_3/L)_H$ is smaller than 0.015, the stiffened plate is expected to follow the plastic hinge behaviour shortly after the peak axial load with an abrupt loss of capacity, as illustrated in Figure 2-12. When the magnitude of $(u_3/L)_H$ is large (greater than 0.015 or so), the stiffened plate is expected to deform considerably before the formation of a plastic hinge. This is illustrated by the stable post-buckling range in Figures 2-21 and 2-22. The configurations of the panels in the figures are presented in Appendix B.

The value of $(u_3/L)_H$ can be obtained by substituting the stiffened plate capacity, P_c, for P in Equation [2-6]. In 10 out of the 720 finite element analysis cases, the peak load is greater than the yield load due to strain-hardening, where the maximum peak load observed is 1.025 times of the yield load. Since Equation [2-6] is valid with the axial load within the nominal yield strength, the plate capacity, P_c, for calculation of $(u_3/L)_H$ is the minimum of the peak load or the yield load. Although P_c has been obtained so far from finite element analysis, closed formed solutions for its determination are presented in Chapter 3.

Stiffener induced failures were observed in the FEA for three load conditions, namely, β_9 = 0, 0.2, 0.4. Figure 2-25 shows plots of normalized critical load, P_c/P_y, from the FEA results versus $(u_3/L)_H$, calculated using Equation [2-6] for a value of P equal to the FEA peak load. The data points are divided between stable and unstable post-buckling behaviour depending on the FEA axial load vs. axial deformation curves. Although the data set for β_9 = 0 (see Figure 2-25 (a)) is too small to draw any conclusion, Figures 2-25 (b) and (c) show that unstable behaviour is observed mostly in the range of $-0.015 < (u_3/L)_H < 0$. A limited number of cases with stable post-peak behaviour are also observed in this range. They generally represent short panels, such as panel 222_21 (β_9 = 0.4) shown in Figure 2-11, for which a plastic hinge doesn't result in a large out-of-plane deflection. Since the points of stable and unstable post-peak response presented in Figures 2-25 (b) and (c) are clustered in the range of most interest (P_c/P_y > 0.2) and stiffener local buckling and tripping are likely to take place after overall buckling, all the stiffener induced failures should be treated as unstable failure as a simple and conservative approach.

2.5.2 Plate induced failure

When considering plate induced failure, the value of $(u_3/L)_H$ is calculated using the minimum of P_c and P_{cH} (the load at which the P.N.A. is at the centroid, see Figures 2-24 (b) and (c)). Because plate induced plastic hinge behaviour is described by three equations, depending on the behaviour range (Equations [2-3], [2-4] and [2-5]), the appropriate range must first be determined.

Plate induced failures were observed in the FEA in four loading conditions, namely, β_9 = –0.4, –0.2, 0, 0.2. Figure 2-26 shows plots of normalized critical load, P_c/P_y, versus $(u_3/L)_H$ for the four levels of applied moment. Unlike stiffener induced failure, some data points that have a large value of $(u_3/L)_H$ show stable post-peak behaviour above P_c/P_y = 0.4. A clear boundary between stable and unstable post-peak behaviour exists at $(u_3/L)_H$ = 0.025. In total, 93% (183/197) of the data points having unstable failure and 18% (49/271) of the data points having stable failure lie on the left of $(u_3/L)_H$ = 0.025.

The $(u_3/L)_H$ approach for plate induced failure is more difficult to apply than that for stiffener induced failures since it makes use of three equations rather than a single equation to describe the plate behaviour. It also introduces an extra variable, P_{cH}. In order to find a simplified method, the above $(u_3/L)_H$ approach for plate induced failure is further investigated.

Since the axial load used to calculate $(u_3/L)_H$ is either less than or equal to P_{cH}, $(u_3/L)_H$ can be evaluated using the part of the virtual work model curve for which the P.N.A. lies below the centroid (see Figures 2-24 (b) and (c)). Due to the large area of the plate relative to that of the stiffener, the centroid of a stiffened plate is either in the plate or in the web, close to the plate. Therefore, $(u_3/L)_H$ is calculated using either Equation [2-3] (P.N.A. in the plate) or Equation [2-4] (P.N.A. in the web). For the wide range of panel configurations investigated in this research, the centroid of the stiffened plates was always close to the plate, even when it was in the web. For this case, Equation [2-4] can be accurately approximated by Equation [2-3] with the extended domain as follows.

$$\frac{u_3}{L} = \frac{\beta_9 M_p}{PL} + \left(\frac{P_y}{P} + 1\right)\left(\frac{z_p}{L} - \frac{P_y + P}{4F_y bL}\right), \quad \frac{P}{P_y} \le 1 \qquad [2\text{-}15]$$

The results of $(u_3/L)_H$ calculated using the minimum of P_c and P_{cH} in Equation [2-15] are shown in Figure 2-27. The difference between $(u_3/L)_H$ calculated using Equations [2-3] to [2-5] and that using Equation [2-15] alone is smaller than

1.21%. Using Equations [2-15] alone, 92% (182/197) of the data points experiencing unstable failure and 18% (49/271) of the data points experiencing stable failure lie on the left of $(u_3/L)_H$ = 0.025. This is the same limit as the limit obtained using Equations [2-3] to [2-5]. Equation [2-15] is therefore a good substitute for Equations [2-3] to [2-5].

A further simplification of this procedure to identify cases of sudden loss of capacity for plate induced failure consists of using P_c in Equation [2-15], thus avoiding the need to calculate P_{cH}. The result of this approach is presented in Figure 2-28. It should be noted that only the points that were calculated using P_{cH} are affected by this simplified approach, that is, only the points for which $P_c > P_{cH}$ are affected. For all the other points ($P_c \le P_{cH}$) the values of $(u_3/L)_H$ remain unchanged because they were originally obtained based on P_c. Using this simplified approach with Equation [2-15] and $P = P_c$, 98% (193/197) of the data points having unstable failure and 23% (61/271) of the data points having stable failure lie on the left of $(u_3/L)_H$ = 0.025. Although being conservative because more panels actually experiencing stable failure are predicted to be unstable (23% in this simplified approach compared to 18% in the original approach), the 2.5% limit still stands. Therefore, calculation of $(u_3/L)_H$ with Equation [2-15] and $P = P_c$ is recommended.

2.6 SUMMARY AND CONCLUSIONS

Recent experimental and analytical research of stiffened steel plates has identified a phenomenon of sudden loss of load carrying capacity in the post-buckling range. For some plate induced failure the sudden loss of load carrying capacity may be preceded by a stable post-buckling range. The sudden loss of capacity occurs as a result of the formation of a plastic hinge mechanism, which causes a large increase in curvature and decrease or little increase of internal moment resistance.

A theoretical model using the principle of virtual work is proposed to describe stiffened plate behaviour once a plastic hinge has formed. The model is described by Equations [2-3] to [2-5] for plate induced plastic hinge mechanism, and Equation [2-6] for stiffener induced plastic hinge mechanism. Comparisons between the proposed plastic hinge model and non-linear finite element analyses showed that the plastic hinge model can predict the post-buckling behaviour accurately unless an axial hinge takes place instead of a flexural plastic hinge. In either case, however, the virtual work model can be used to predict the occurrence of the sudden loss of capacity.

For the range of plate geometries and loading conditions used in this research and presented in section 2.2, it can be concluded that all stiffened plates in stiffener induced failure and stiffened plates with $(u_3/L)_H$ less than 0.025 as calculated from Equation [2-15] for plate induced failure are susceptible to a sudden loss of capacity within an axial strain of 1%. These plates should therefore be designed for a lower probability of failure since the consequence of failure is more severe. A proposed limit states design approach, which account for all possible stiffened plate and the consequence of failure is presented in Chapter 3.

References:

Aalberg, A., Langseth, M., Larsen, P. L. (2001). "Stiffened aluminum panels subjected to axial compression." *Thin-Walled Structures*, 39 (10), 861–885.

ABAQUS Inc. (2003). *ABAQUS/Standard Version 6.4-1*, Pawtucket, U.S.

American Association of State Highway Transportation Officials (AASHTO) (2007). *AASHTO LRFD bridge design specifications*, 4ed, Washington, D.C.

American Bureau of Shipping (ABS) (2007). Guide for buckling and ultimate strength assessment for offshore structures. Houston, Texas.

American Institute of Steel Construction (AISC) (2005), *ANSI/AISC 360-05: Specifications for Structural Steel Buildings*, Chicago, IL, U.S.

American Petroleum Institute (API) (2000). *API Bulletin 2V: Design of flat plate structures*, Washington, D. C., U.S.

American Society of Civil Engineers (ASCE) and Welding Research Council (WRC) (1971), *Plastic Design in Steel: A guide and Commentary*, 2ed, New York,

British Standards Institution (BSI) (2005), *BS 4-1: 2005: Structural steel sections. Specification for hot-rolled sections*, London, British.

Canadian Institute of Steel Construction (CISC) (2006). *Handbook of Steel Construction*, 9ed., Toronto, Ontario, Canada.

Canadian Standards Association (CSA) (2004). *CAN/CSA G40.20-04: General Requirements for Rolled or Welded Structural Quality Steel*, Toronto, Ontario, Canada.

Canadian Standards Association (CSA). (2006). *CAN/CSA-S6-06: Canadian Highway Bridge Design Code*, Toronto, Ontario, Canada.

Canadian Standards Association (CSA). (2009). *CSA-S16-09: Design of Steel Structures*, Toronto, Ontario, Canada.

Carlsen, C. A. and Czujko, J. (1978). "The specification of post-welding distortion tolerances for stiffened plates in compression." *The Structural Engineer*, 56A (5), 133–141.

Chen, Q., Hanson, R. S., Grondin, G. Y. (2004). "Interactive Buckling Testing of Stiffened Steel Plate Panels" *Ship structure committee report 433*, Washington, D.C., U.S.

Chen,Q., Zimmerman,T.J.E., Degeer, D.D., Kennedy, B.W.(1997)."Strength and stability testing of stiffened plate components." *Ship structure committee report 399*, Washington, D.C., U.S.

Chen, W.F. and Han, D.J. (1988), Plasticity for structural engineers, Springer-Verlag, New York.

Danielson, D. A. (1995)."Analytical tripping loads for stiffened plates." *International journal of solids and structures*, 32(8/9), 1319-1328.

Det Norske Veritas (DNV) (1995). Classification Notes No. 30.1: Buckling Strength Analysis, Norway.

Det Norske Veritas (DNV) (2002). Recommended Practice DNV-RP-C201: Buckling Strength of Plated Structures, Norway.

Faulkner, D. (1975). "A review of effective plating for use in the analysis of stiffened plating in bending and compression" *Journal of Ship Research*, 19 (1), 1–17.

Grondin, G. Y., Chen, Q., Elwi, A. E., Cheng, J. J. R. (1998). "Stiffened plates under compression and bending." *Journal of Constructional Steel Research*, 45(2), 125–148.

Grondin, G. Y., Elwi, A.E., Cheng, J.J.R. (1999). "Buckling of Stiffened Steel Plates -A Parametric Study." *Journal of Constructional Steel Research*, 50(2), 151-175.

Hu, Y., Chen, B., and Sun, J.(2000). "Tripping of thin-walled stiffeners in the axially compressed stiffened panel with lateral pressure." *Thin-Walled Structures*, 37, 1–26.

Hughes, O. F., Ghosh, B., Chen, Y. (2004). "Improved prediction of simultaneous local and overall buckling of stiffened panels." *Thin-Walled Structures*, 42(6), 827-856.

Hughes, O.F. and Ma, M. (1996). "Inelastic analysis of panel collapse by stiffener buckling." *Computers and structures*, 61(1), 107-117.

Neal, B.G. (1977), The plastic methods of structural analysis, 3ed, John Wiley & Sons, New York.

Sheikh, I. A., Elwi, A. E., Grondin, G. Y. (2003). "Stiffened steel plates under combined compression and bending." *Journal of Constructional Steel Research*, 59 (7), 911–930.

Sheikh, I. A., Grondin, G. Y., Elwi, A. E. (2001). "Stiffener tripping in stiffened steel plates", *Structural Engineering Report No. 236*, Department of Civil and Environmental Engineering, University of Alberta, Canada.

Sheikh, I. A., Grondin, G. Y., Elwi, A. E. (2002). "Stiffened steel plates under uniaxial compression" *Journal of Constructional Steel Research*, 58 (5-8), 1061-1080.

Smith, C. S., Anderson, N., Chapman, J. C., Davidson, P. C., Dowling, P. J. (1992). "Strength of stiffened plating under combined compression and lateral pressure." *Transactions of the royal institute of naval architects*, 134, 131-147.

Smith, C.S., Davidson, P.C., Chapman, J.C., Dowling, P.J.(1987)."Strength and stiffness of ships' plating under in-plane compression and tension." *Transactions of the royal institute of naval architects*, 130, 277-296.

Soreide, T. H.(1981). *Ultimate load analysis of marine structures*, 5.61–5.78, Tapir Press, Trondheim. Norway

Thimmhardy, E. G.(1988). Influence of residual stresses and geometric imperfections on buckling strength of stiffened compression flanges of steel box girder bridges, Ph.D dissertation, Concordia University, Canada.

Timoshenko, S.P., and Gere, J.M.(1961), *Theory of elastic stability*, McGraw-Hill, 2ed, New York.

Wang, E. C. L., Grondin, G. Y., Elwi, A. E. (2006), "Interaction Buckling Failure of Stiffened Steel Plates", *Structural Engineering Report No. 264*, Department of Civil and Environmental Engineering, University of Alberta, Canada.

Yoo, Chai H., Choi, Byung H., and Ford, Elizabeth M.(2001)."Stiffness requirements for longitudinally stiffened box-girder flanges." *ASCE Journal of Structural Engineering*, 127(6), 705-711.

Zheng, G., and Hu, Y.(2005)."Tripping of thin-walled stiffeners in the axially compressed stiffened panel with lateral pressure and end moment." *Thin-Walled Structures*, 43 (5), 789–799.

Table 2-1 Local buckling requirements for stiffeners

	Web, β_2	Flange, β_3
API	1.48 [1]	0.75 [1]
	1.49 [2]	0.56 [2]
DNV	1.440	0.960 [3]
		1.028 [4]
ABS	1.5	0.8

[1] for compact sections

[2] for non-compact sections

[3] for welded stiffeners

[4] for rolled stiffeners

Table 2-2 Values selected for the factorial design

β_1	β_2	β_3	β_5	β^*
0.7	0.17	0.17	0.075	0.15
1.28	0.8	0.6	0.15	0.4
2.0	1.5	0.9	0.3	0.7
2.7				1.0

Table 2-3 Fractional factorial design

β_1	β_2	β_3	β_5	β^*	β_4
0.70	0.17	0.17	0.075	0.15/ 0.4/ 0.7/ 1	1.59/ 4.23/ 7.41/ 10.59
1.28	0.17	0.17	0.075	0.15/ 0.4/ 0.7/ 1	1.17/ 3.13/ 5.48/ 7.83
2.00	0.17	0.17	0.075	0.15/ 0.4/ 0.7/ 1	0.94/ 2.5/ 4.38/ 6.26
2.70	0.17	0.17	0.075	0.15/ 0.4/ 0.7/ 1	0.81/ 2.16/ 3.77/ 5.39
0.70	0.17	0.17	0.150	0.15/ 0.4/ 0.7/ 1	1.12/ 2.99/ 5.24/ 7.48
1.28	0.17	0.17	0.150	0.15/ 0.4/ 0.7/ 1	0.83/ 2.21/ 3.87/ 5.54
2.00	0.17	0.17	0.150	0.15/ 0.4/ 0.7/ 1	0.66/ 1.77/ 3.1/ 4.43
2.70	0.17	0.17	0.150	0.15/ 0.4/ 0.7/ 1	0.57/ 1.52/ 2.67/ 3.81
0.70	0.17	0.17	0.300	0.15/ 0.4/ 0.7/ 1	0.79/ 2.12/ 3.7/ 5.29
1.28	0.17	0.17	0.300	0.15/ 0.4/ 0.7/ 1	0.59/ 1.57/ 2.74/ 3.91
2.00	0.17	0.17	0.300	0.15/ 0.4/ 0.7/ 1	0.47/ 1.25/ 2.19/ 3.13
2.70	0.17	0.17	0.300	0.15/ 0.4/ 0.7/ 1	0.4/ 1.08/ 1.89/ 2.69
0.70	0.80	0.60	0.075	0.15/ 0.4/ 0.7/ 1	0.75/ 2.01/ 3.52/ 5.02
1.28	0.80	0.60	0.075	0.15/ 0.4/ 0.7/ 1	0.56/ 1.49/ 2.6/ 3.71
2.00	0.80	0.60	0.075	0.15/ 0.4/ 0.7/ 1	0.45/ 1.19/ 2.08/ 2.97
2.70	0.80	0.60	0.075	0.15/ 0.4/ 0.7/ 1	0.38/ 1.02/ 1.79/ 2.56
0.70	0.80	0.60	0.150	0.15/ 0.4/ 0.7/ 1	0.53/ 1.42/ 2.49/ 3.55
1.28	0.80	0.60	0.150	0.15/ 0.4/ 0.7/ 1	0.39/ 1.05/ 1.84/ 2.63
2.00	0.80	0.60	0.150	0.15/ 0.4/ 0.7/ 1	0.32/ 0.84/ 1.47/ 2.1
2.70	0.80	0.60	0.150	0.15/ 0.4/ 0.7/ 1	0.27/ 0.72/ 1.27/ 1.81
0.70	0.80	0.60	0.300	0.15/ 0.4/ 0.7/ 1	0.38/ 1/ 1.76/ 2.51
1.28	0.80	0.60	0.300	0.15/ 0.4/ 0.7/ 1	0.28/ 0.74/ 1.3/ 1.86

Table 2-3 Fractional factorial design (continued)

β_1	β_2	β_3	β_5	β^*	β_4
2.00	0.80	0.60	0.300	0.15/ 0.4/ 0.7/ 1	0.22/ 0.59/ 1.04/ 1.49
2.70	0.80	0.60	0.300	0.15/ 0.4/ 0.7/ 1	0.19/ 0.51/ 0.89/ 1.28
0.70	1.50	0.90	0.075	0.15/ 0.4/ 0.7/ 1	0.56/ 1.5/ 2.63/ 3.75
1.28	1.50	0.90	0.075	0.15/ 0.4/ 0.7/ 1	0.42/ 1.11/ 1.94/ 2.77
2.00	1.50	0.90	0.075	0.15/ 0.4/ 0.7/ 1	0.33/ 0.89/ 1.55/ 2.22
2.70	1.50	0.90	0.075	0.15/ 0.4/ 0.7/ 1	0.29/ 0.76/ 1.34/ 1.91
0.70	1.50	0.90	0.150	0.15/ 0.4/ 0.7/ 1	0.4/ 1.06/ 1.86/ 2.65
1.28	1.50	0.90	0.150	0.15/ 0.4/ 0.7/ 1	0.29/ 0.78/ 1.37/ 1.96
2.00	1.50	0.90	0.150	0.15/ 0.4/ 0.7/ 1	0.24/ 0.63/ 1.1/ 1.57
2.70	1.50	0.90	0.150	0.15/ 0.4/ 0.7/ 1	0.2/ 0.54/ 0.95/ 1.35
0.70	1.50	0.90	0.300	0.15/ 0.4/ 0.7/ 1	0.28/ 0.75/ 1.31/ 1.88
1.28	1.50	0.90	0.300	0.15/ 0.4/ 0.7/ 1	0.21/ 0.55/ 0.97/ 1.39
2.00	1.50	0.90	0.300	0.15/ 0.4/ 0.7/ 1	0.17/ 0.44/ 0.78/ 1.11
2.70	1.50	0.90	0.300	0.15/ 0.4/ 0.7/ 1	0.14/ 0.38/ 0.67/ 0.95

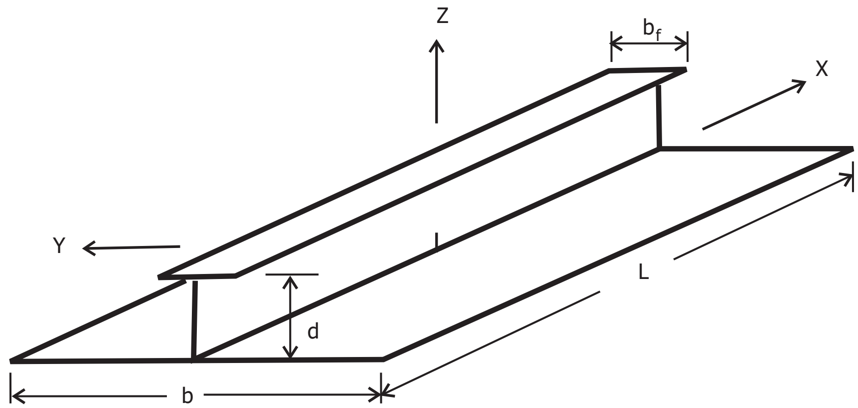

(a) Panel configuration

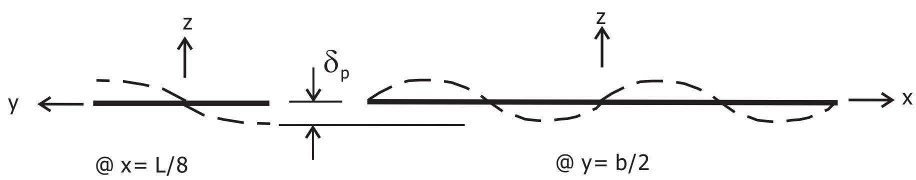

(b) Plate imperfection

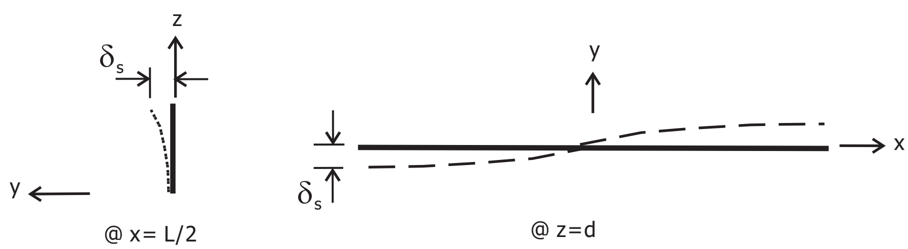

(c) Web imperfections

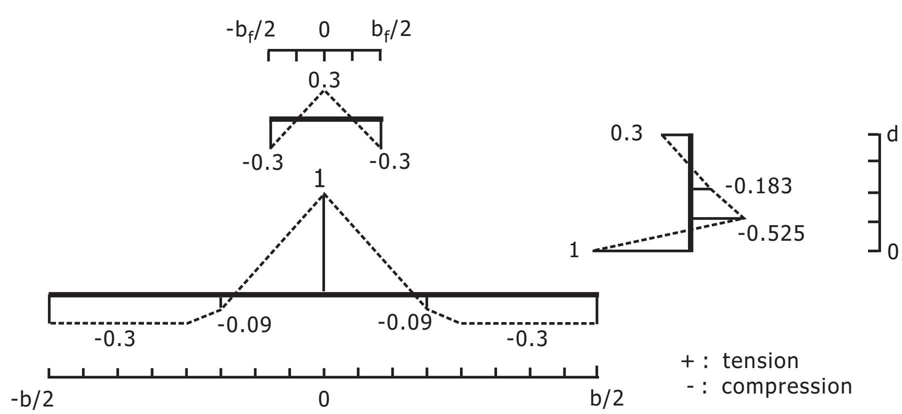

(d) Ratio of residual to yield stress

Figure 2-1 Imperfections and residual stresses

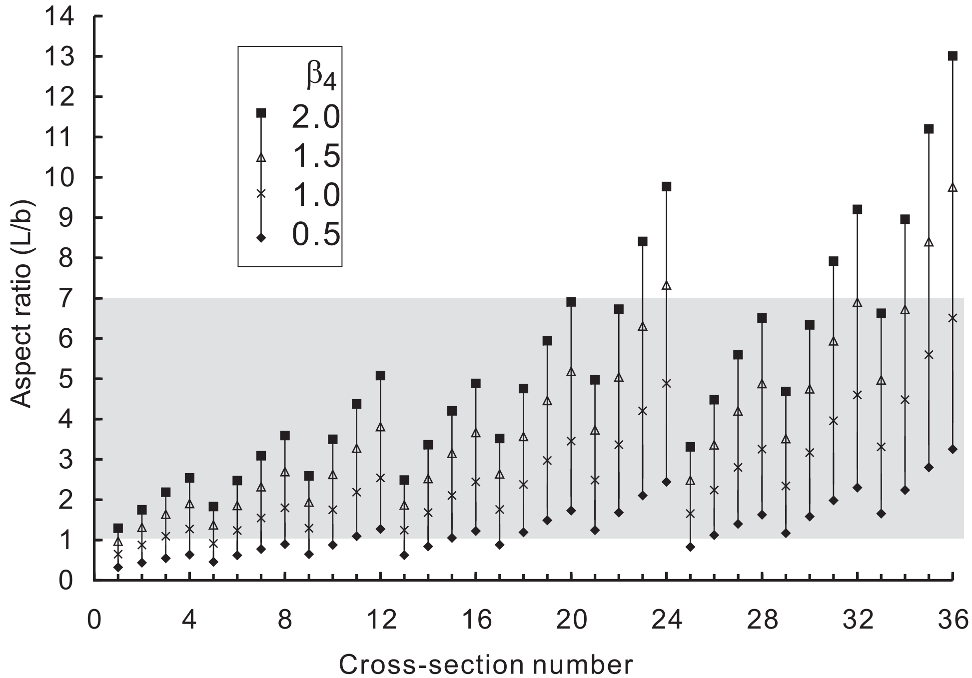

Figure 2-2 Aspect ratios of panels with the 36 cross-section configurations

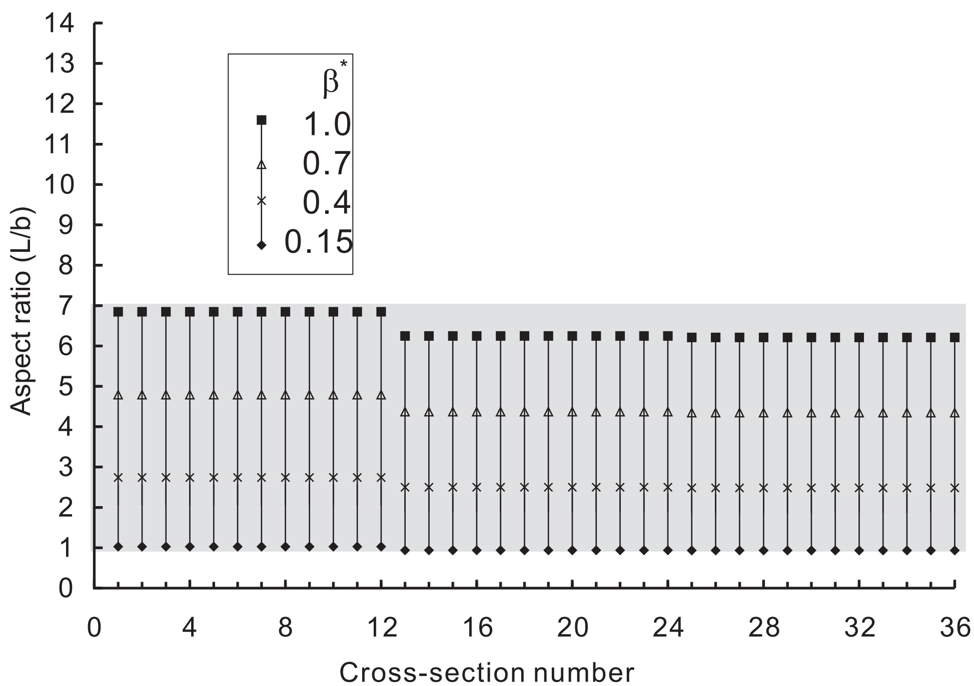

Figure 2-3 Aspect ratios of panels with the 36 cross-section configurations
(controlled in practical range)

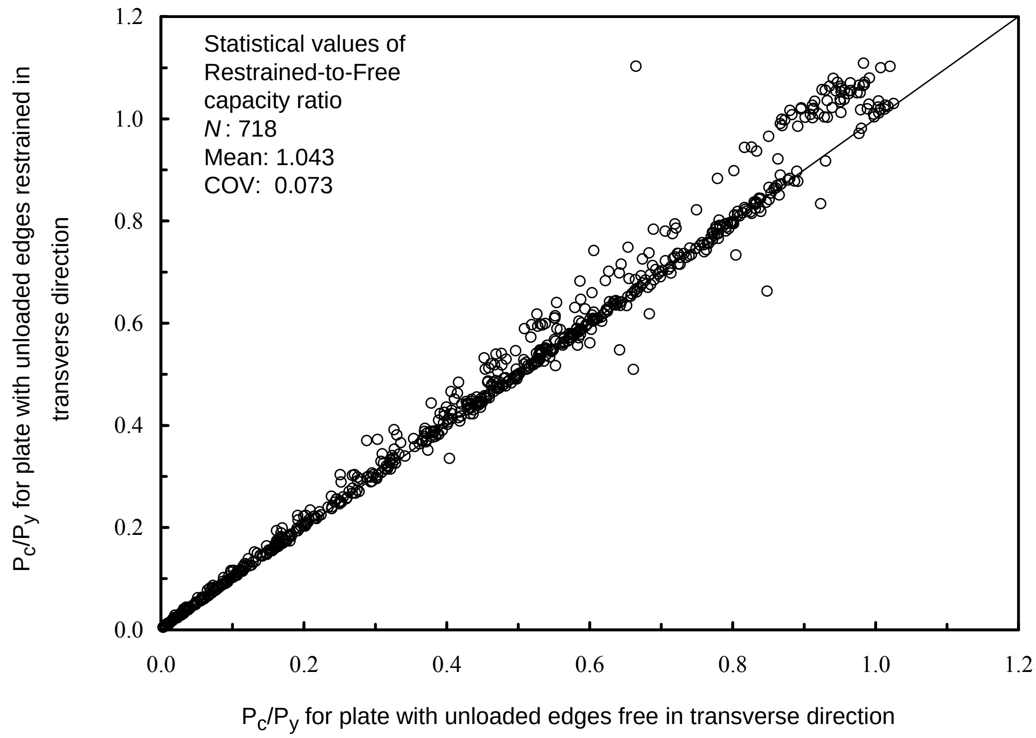

Figure 2-4 Effect of the unloaded edges' boundary conditions

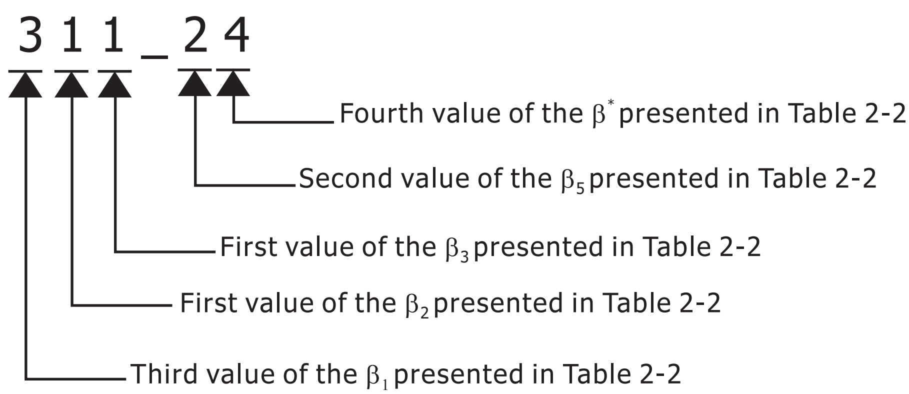

Examples:

Name	β_1	β_2	β_3	β_5	β^*
311_24	2.0	0.17	0.17	0.15	1.0
233_12	1.28	1.5	0.9	0.075	0.4

Figure 2-5 Panel designation convention

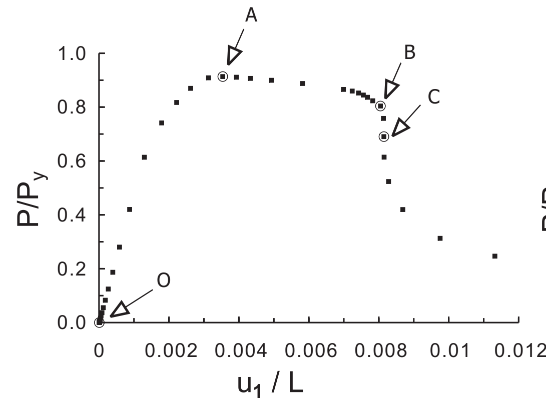

(a) Axial load vs. axial deformation

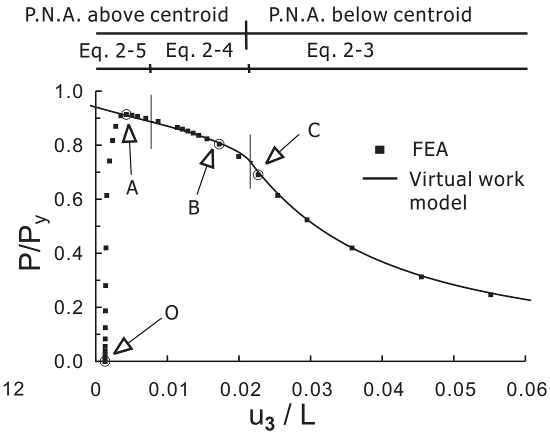

(b) Axial load vs. lateral deflection at centre of the stiffened panel

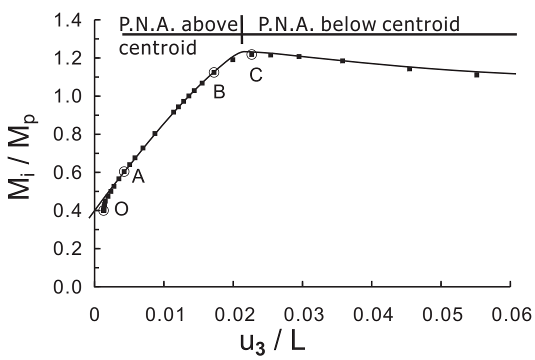

(c) Internal moment vs. lateral deflection

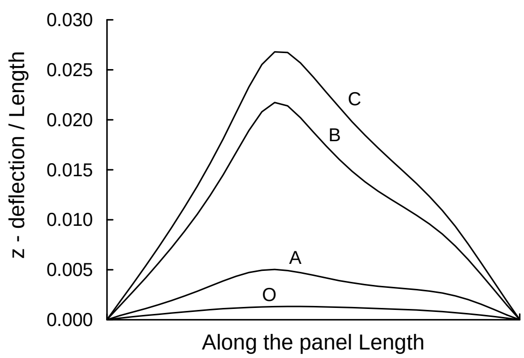

(d) Deflection of plate edge (y = –b/2)

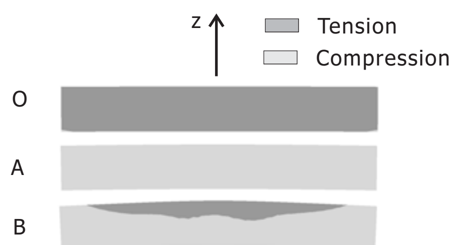

(e) Strain in the web

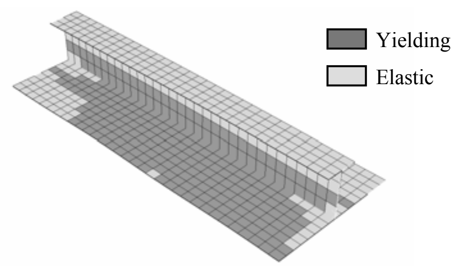

(f) Extent of yielding at A

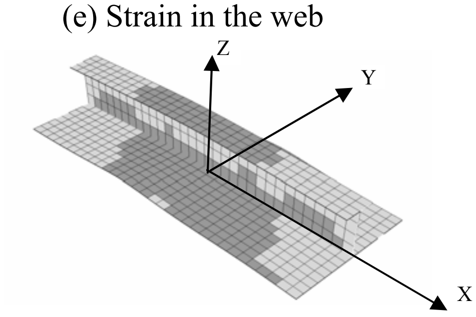

(g) Extent of yielding at B

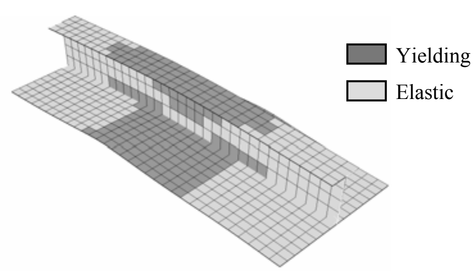

(h) Extent of yielding at C

Figure 2-6 Behaviour of panel 122_22 (β_1 = 0.7, β_9 = –0.4)

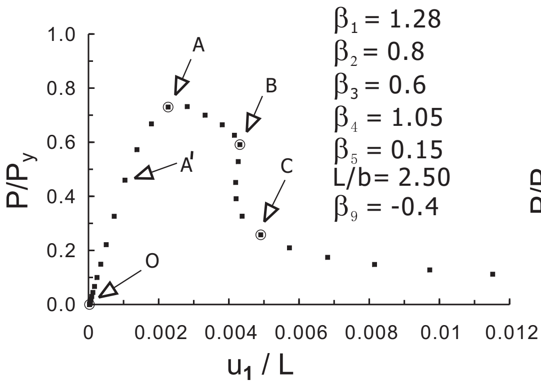

(a) Axial load vs. axial deformation

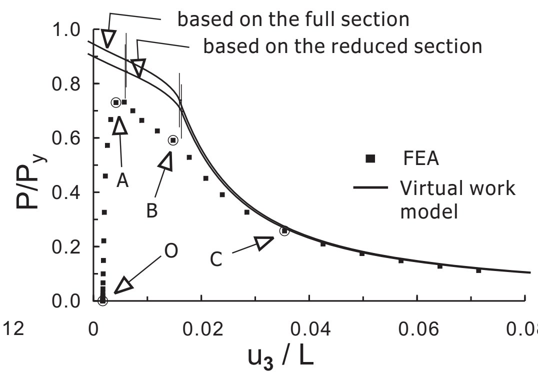

(b) Axial load vs. lateral deflection at centre of the stiffened panel

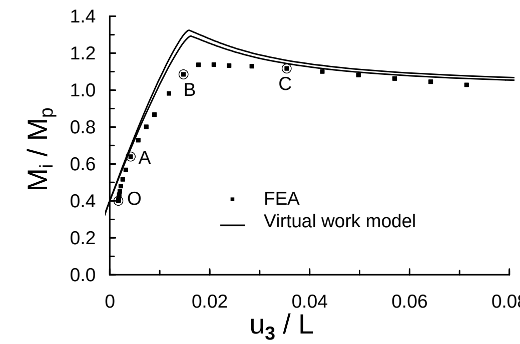

(c) Internal moment vs. lateral deflection

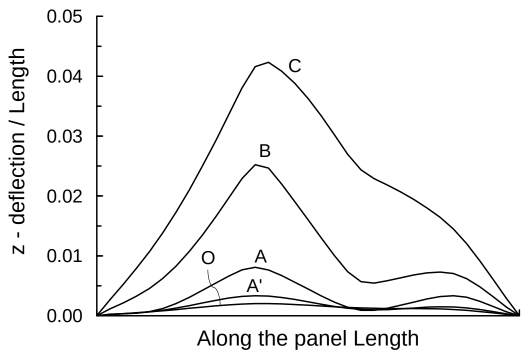

(d) Deflection of plate edge (y = –b/2)

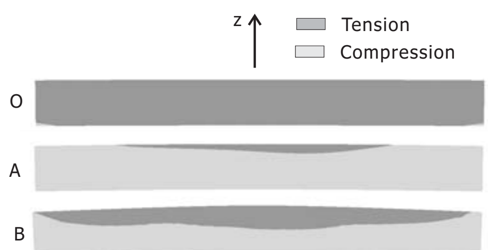

(e) Strain in the web

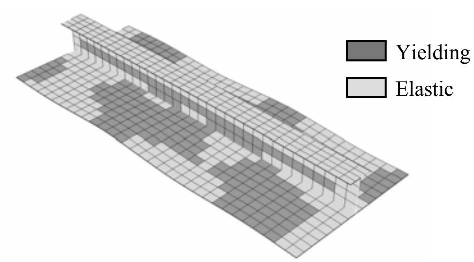

(f) Extent of yielding at A

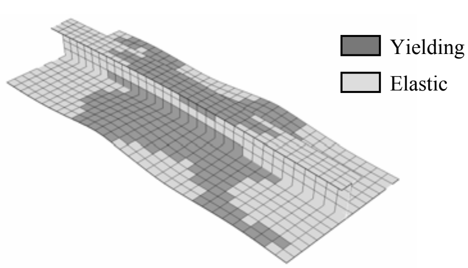

(g) Extent of yielding at B

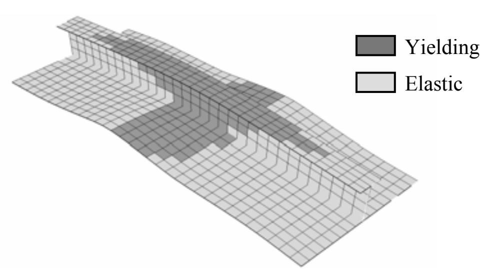

(h) Extent of yielding at C

Figure 2-7 Behaviour of panel 222_22 (β_1 = 1.28, β_9 = –0.4, L/b = 2.50)

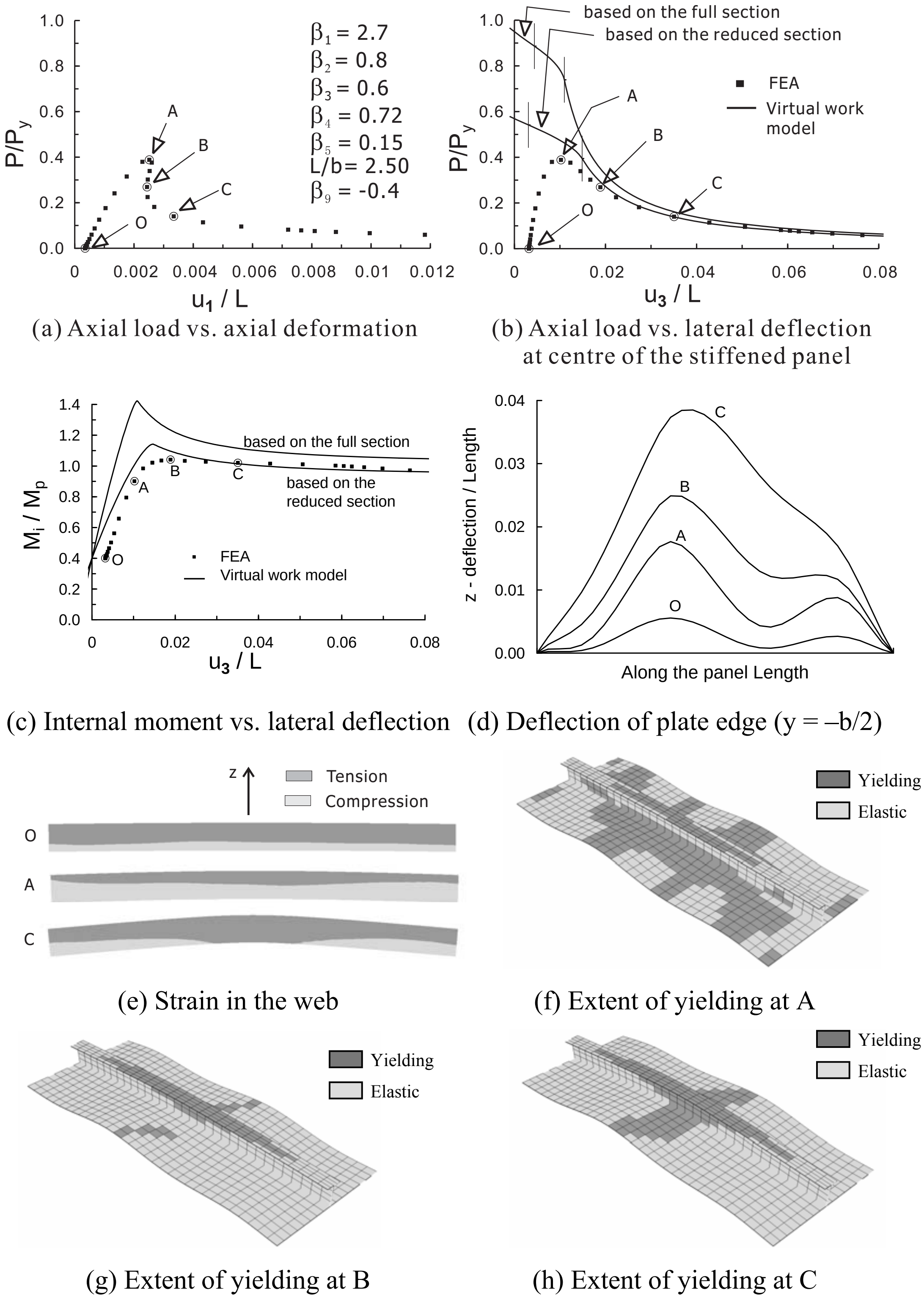

(a) Axial load vs. axial deformation

(b) Axial load vs. lateral deflection at centre of the stiffened panel

(c) Internal moment vs. lateral deflection

(d) Deflection of plate edge (y = –b/2)

(e) Strain in the web

(f) Extent of yielding at A

(g) Extent of yielding at B

(h) Extent of yielding at C

Figure 2-8 Behaviour of panel 422_22 ($\beta_1 = 2.7$, $\beta_9 = -0.4$)

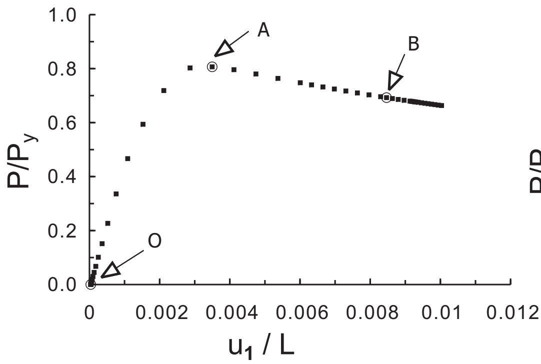

(a) Axial load vs. axial deformation

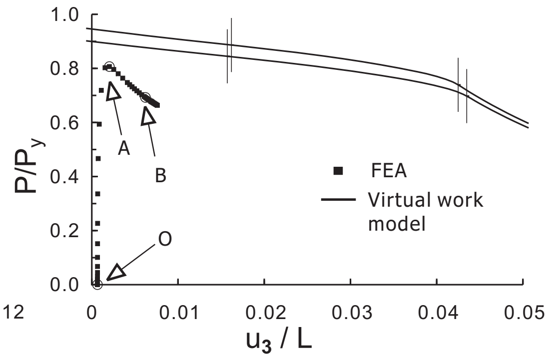

(b) Axial load vs. lateral deflection at centre of the stiffened panel

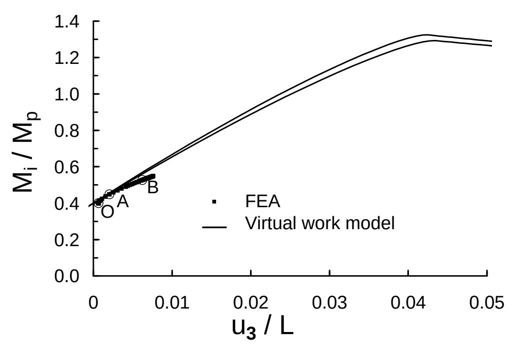

(c) Internal moment vs. lateral deflection

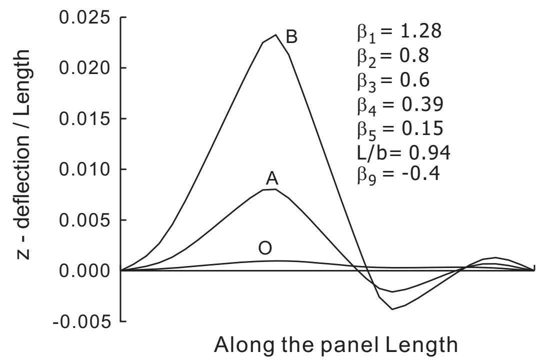

(d) Deflection of plate edge (y = –b/2)

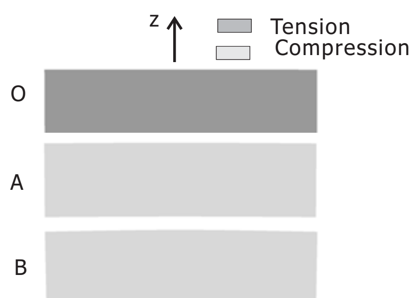

(e) Strain in the web

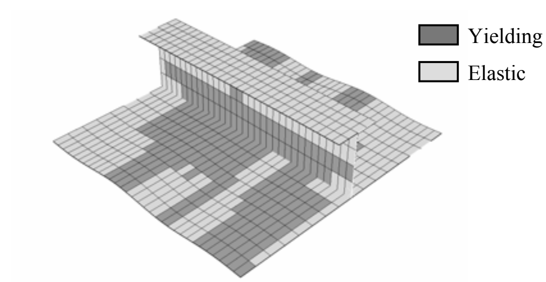

(f) Extent of yielding at A

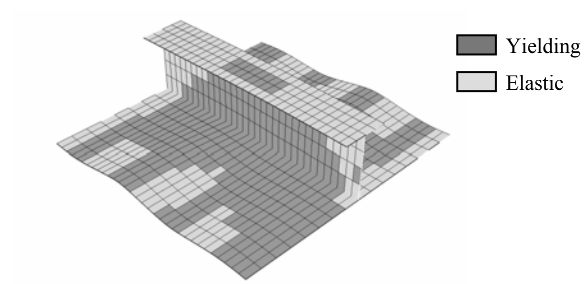

(g) Extent of yielding at B

Figure 2-9 Behaviour of panel 222_21 (β_9 = –0.4, L/b = 0.94)

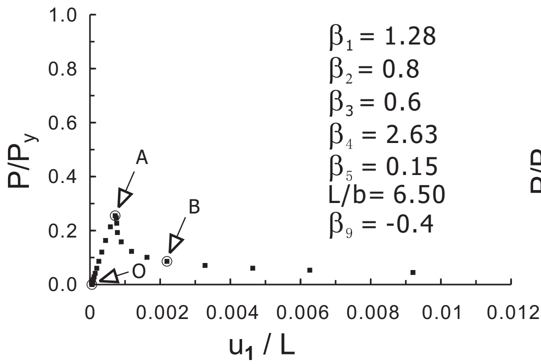

(a) Axial load vs. axial deformation

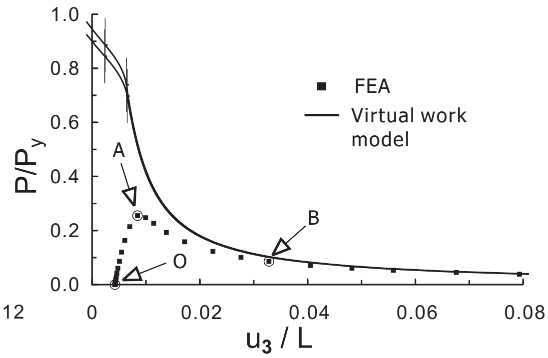

(b) Axial load vs. lateral deflection at centre of the stiffened panel

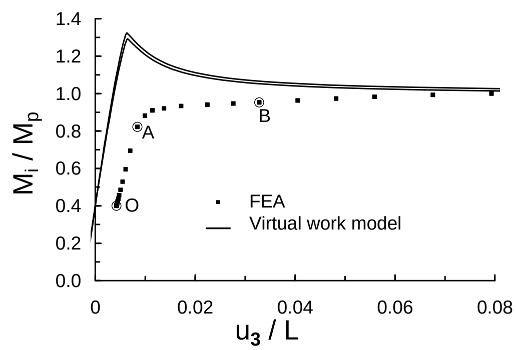

(c) Internal moment vs. lateral deflection

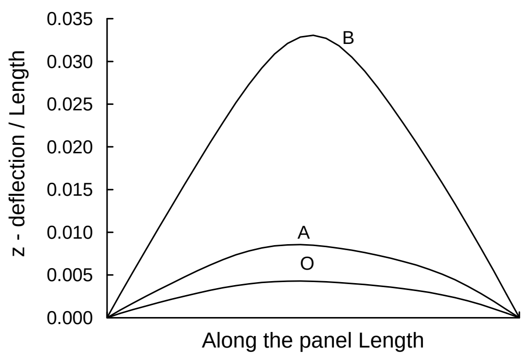

(d) Deflection of plate edge (y = –b/2)

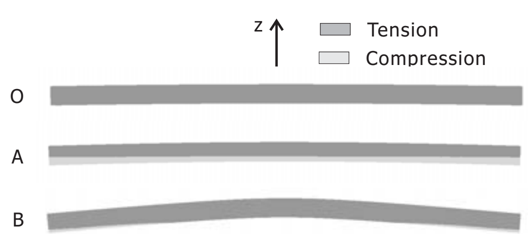

(e) Strain in the web

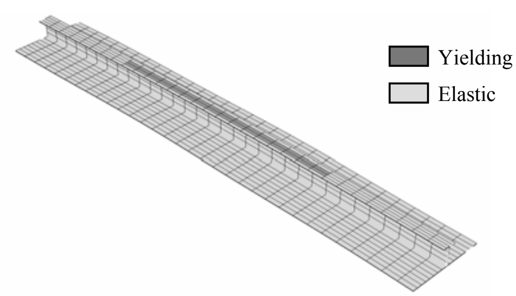

(f) Extent of yielding at A

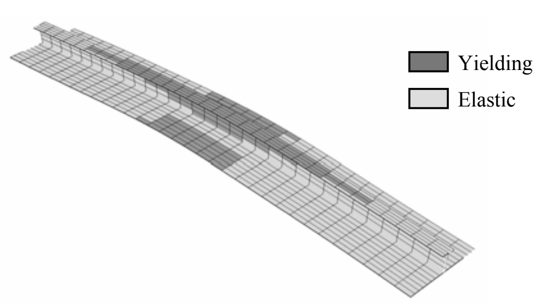

(g) Extent of yielding at B

Figure 2-10 Behaviour of panel 222_24 (β_9 = –0.4, *L/b* = 6.50)

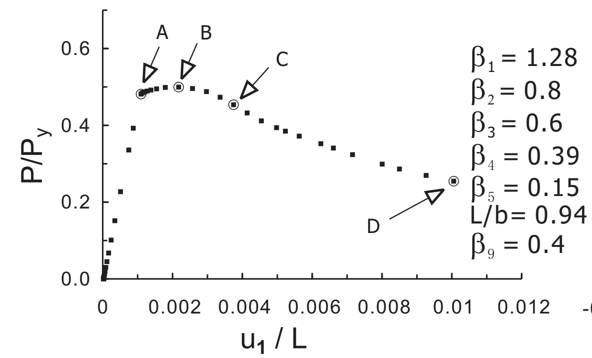

(a) Axial load vs. axial deformation

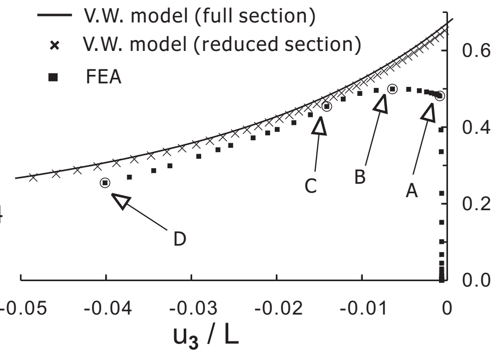

(b) Axial load vs. lateral deflection at centre of the stiffened panel

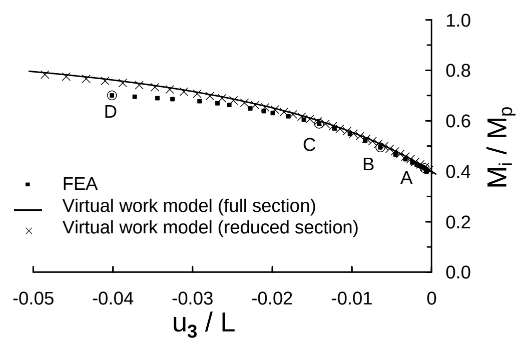

(c) Internal moment vs. lateral deflection

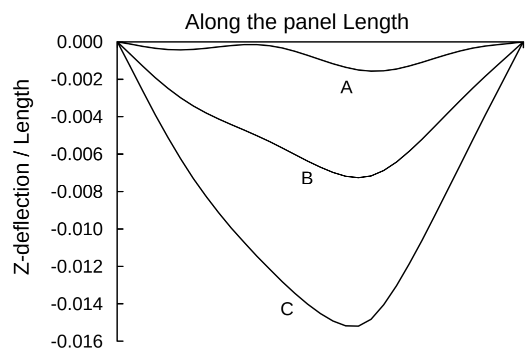

(d) Deflection of plate at y= -b/2

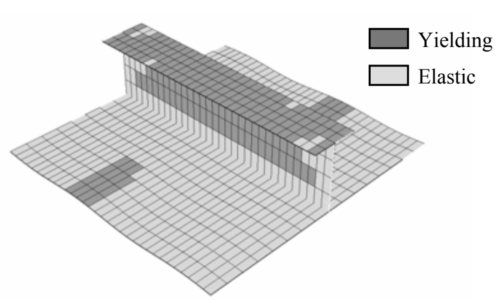

(e) Extent of yielding at A

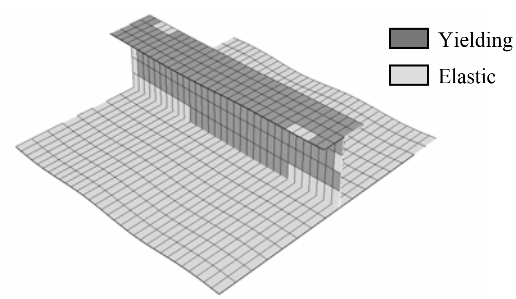

(f) Extent of yielding at B

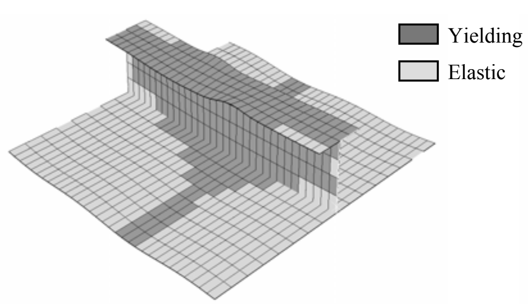

(g) Extent of yielding at C

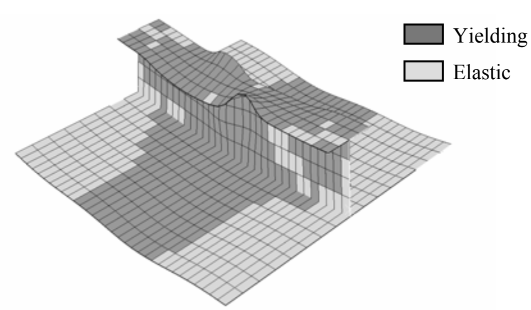

(h) Extent of yielding at D

Figure 2-11 Behaviour of panel 222_21 (L/b = 0.94, β_9 = 0.4)

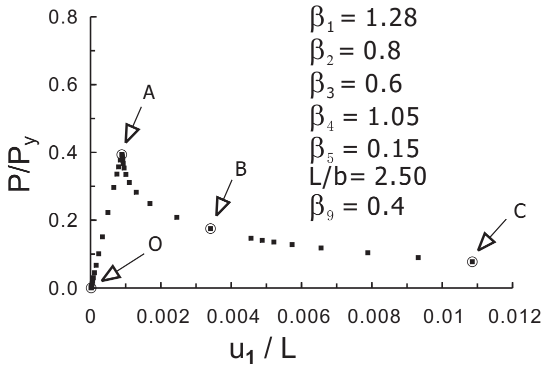

(a) Axial load vs. axial deformation

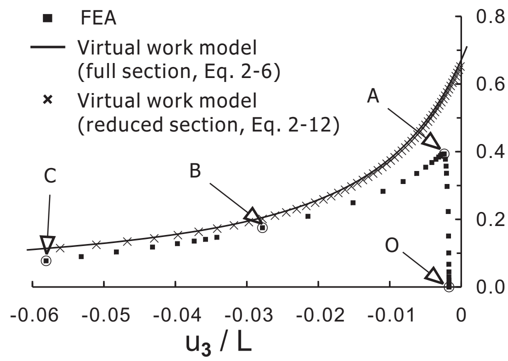

(b) Axial load vs. lateral deflection at centre of the stiffened panel

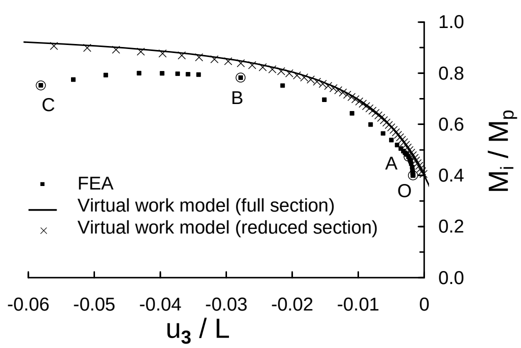

(c) Internal moment vs. lateral deflection

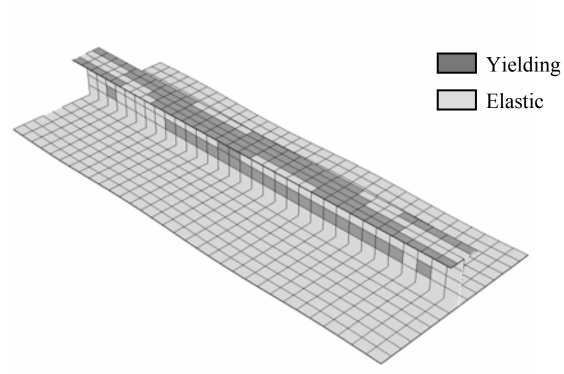

(d) Extent of yielding at A

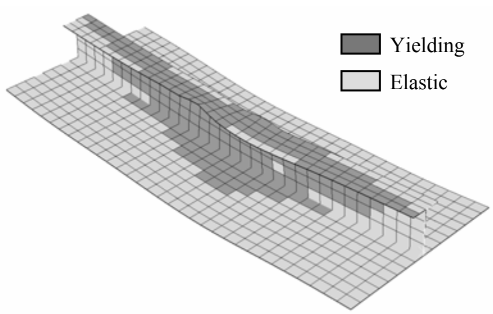

(e) Extent of yielding at B

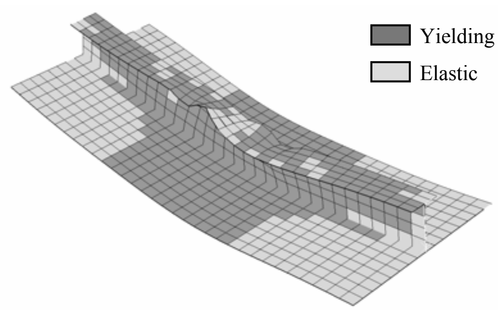

(f) Extent of yielding at C

Figure 2-12 Behaviour of panel 222_22 (L/b = 2.50, β_9 = 0.4)

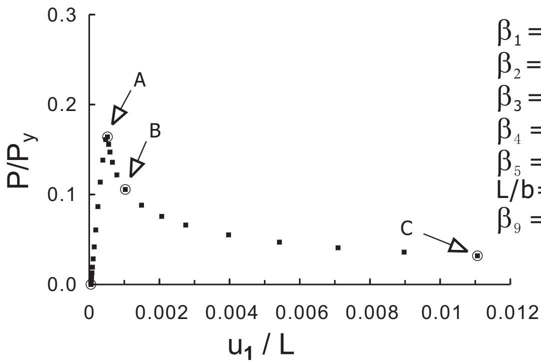

(a) Axial load vs. axial deformation

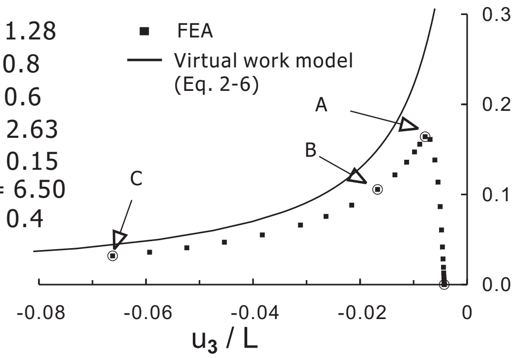

(b) Axial load vs. lateral deflection at centre of the stiffened panel

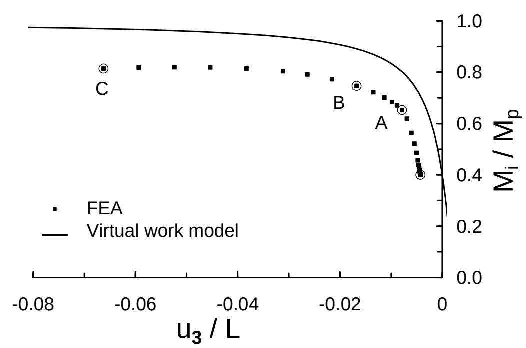

(c) Internal moment vs. lateral deflection

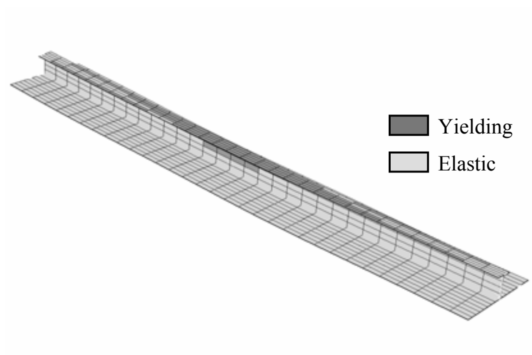

(d) Extent of yielding at A

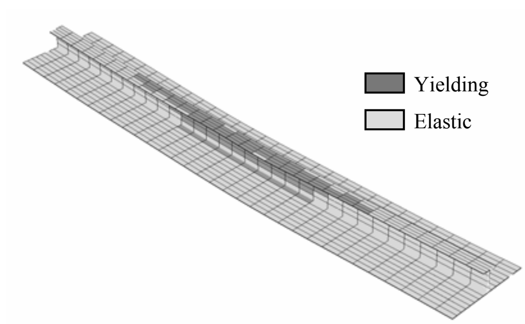

(e) Extent of yielding at B

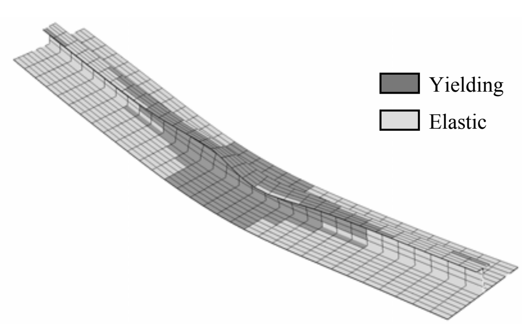

(f) Extent of yielding at C

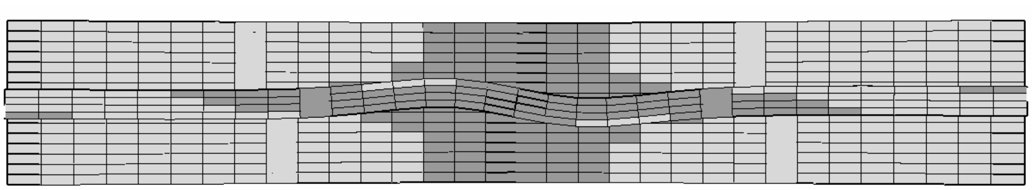

(g) Extent of yielding at C (plan view)

Figure 2-13 Behaviour of panel 222_24 (L/b = 6.50, β_9 = 0.4)

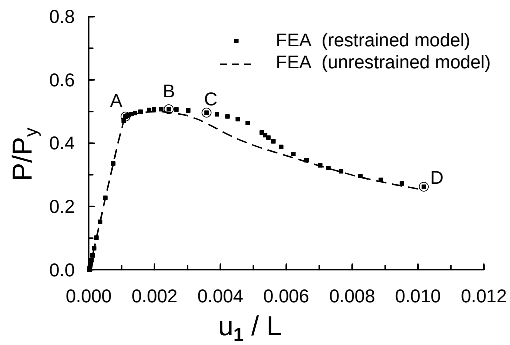

(a) Axial load vs. axial deformation

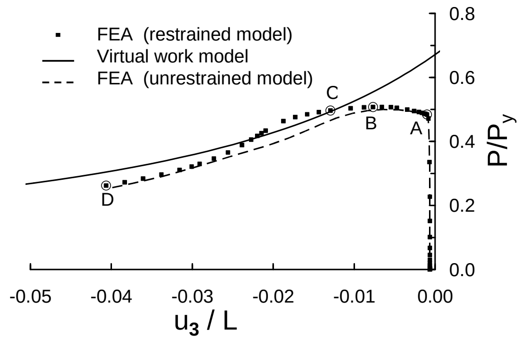

(b) Axial load vs. lateral deflection at centre of the stiffened panel

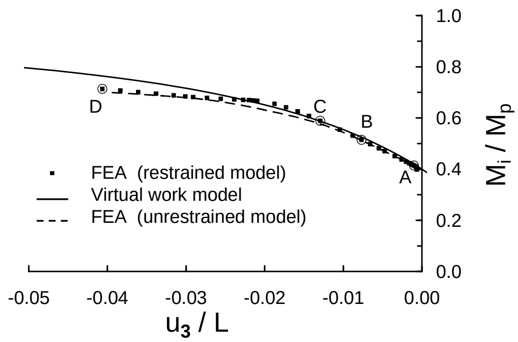

(c) Internal moment vs. lateral deflection

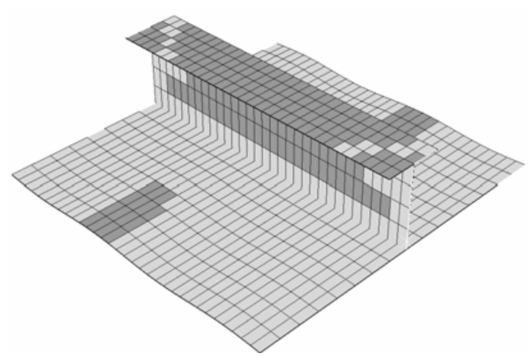

(d) Extent of yielding at A

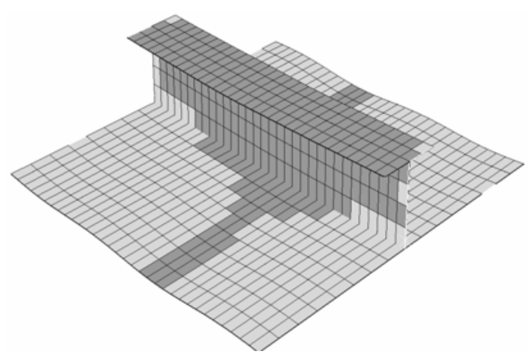

(e) Extent of yielding at C

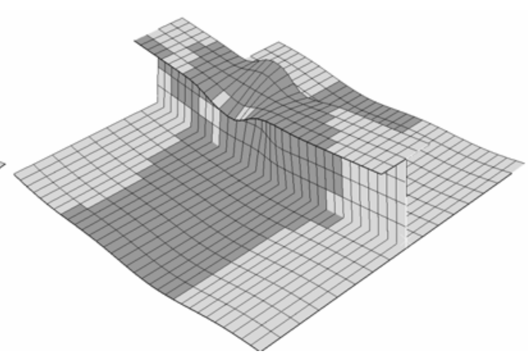

(f) Extent of yielding at D

Figure 2-14 Behaviour of panel 222_21 (β_9 = 0.4) (one flange tip at y = +0.5 b_f is restrained in y-direction to prevent stiffener tripping)

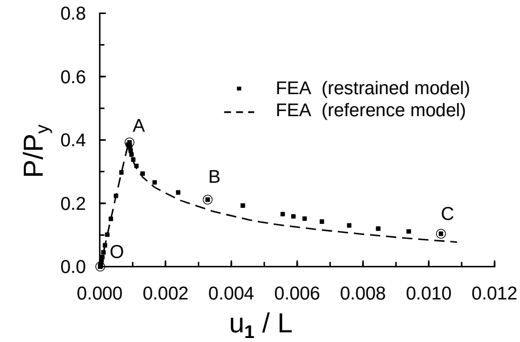

(a) Axial load vs. axial deformation

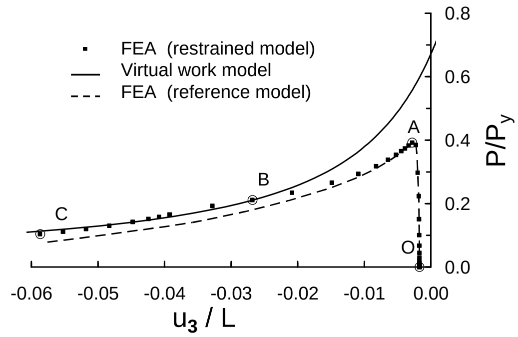

(b) Axial load vs. lateral deflection at centre of the stiffened panel

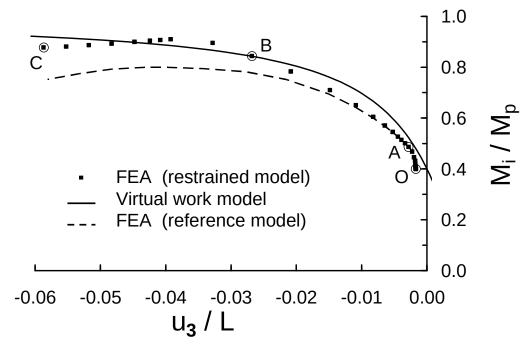

(c) Internal moment vs. lateral deflection

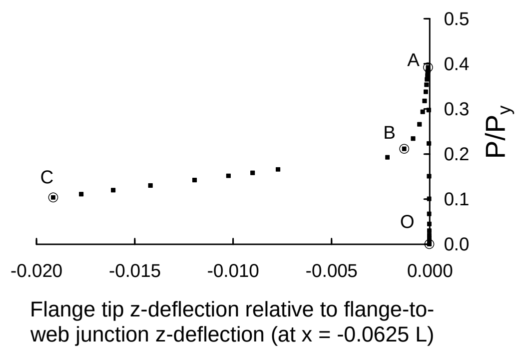

(d) Axial load vs. relative z-deflection

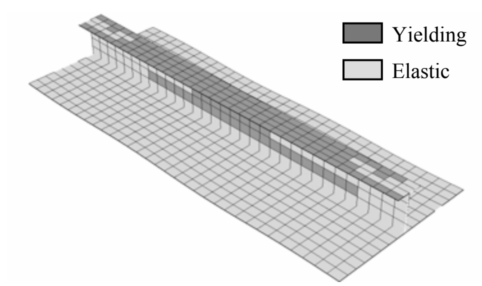

(e) Extent of yielding at A

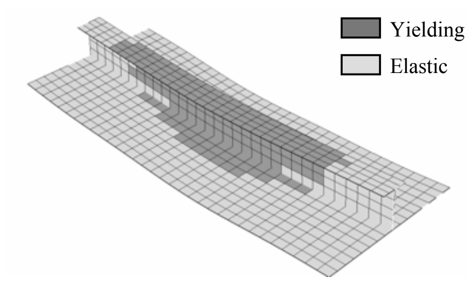

(f) Extent of yielding at B

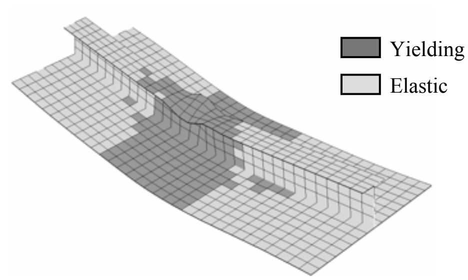

(g) Extent of yielding at C

Figure 2-15 Behaviour of panel 222_22 (β_9 = 0.4) (one flange tip at y = +0.5 b_f is restrained in y-direction to prevent stiffener tripping)

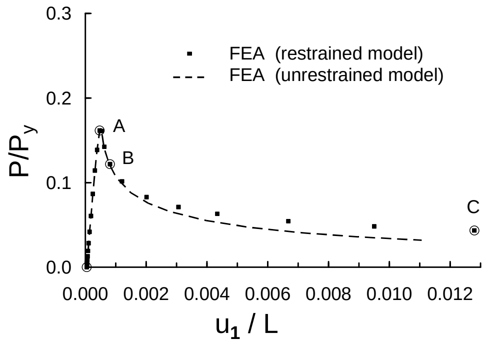

(a) Axial load vs. axial deformation

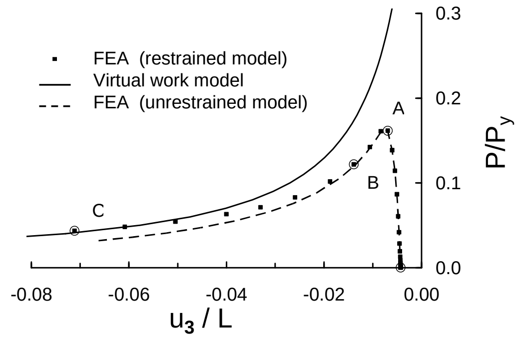

(b) Axial load vs. lateral deflection at centre of the stiffened panel

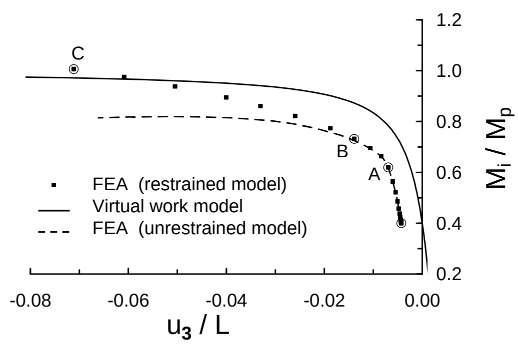

(c) Internal moment vs. lateral deflection

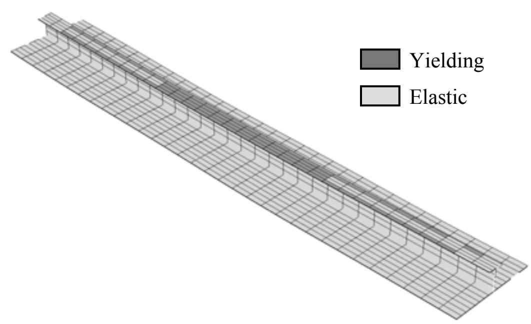

(d) Extent of yielding at A

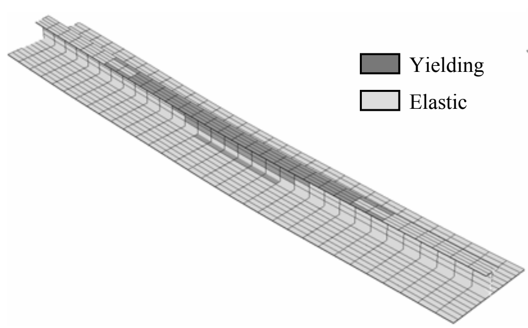

(e) Extent of yielding at B

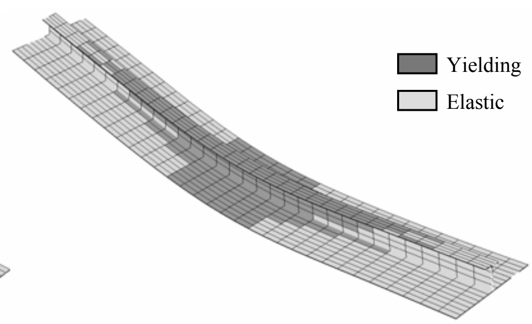

(f) Extent of yielding at C

Figure 2-16 Behaviour of panel 222_24 (β_9 = 0.4) (one flange tip at y = +0.5 b_f is restrained in y-direction to prevent stiffener tripping)

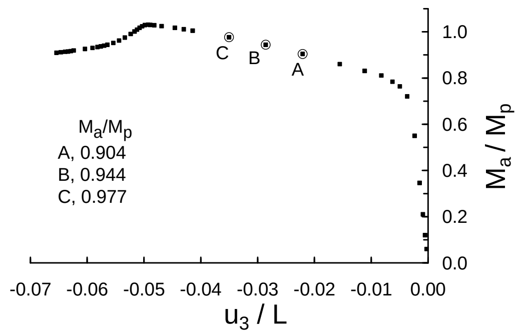

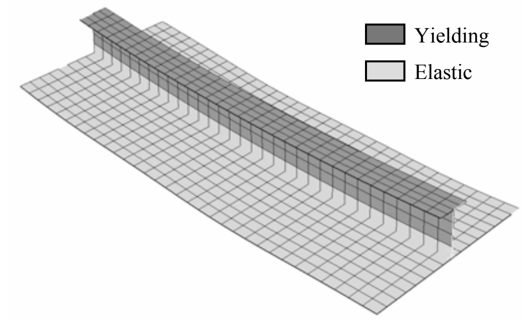

(a) Applied moment vs. lateral deflection at centre of the stiffened panel

(b) Extent of yielding at A

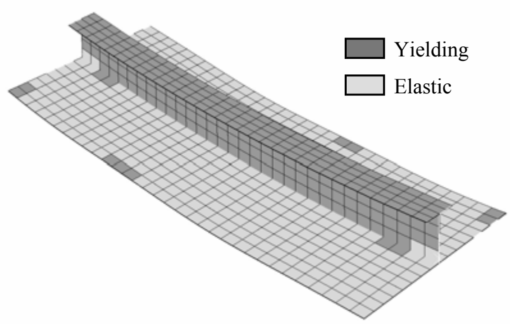

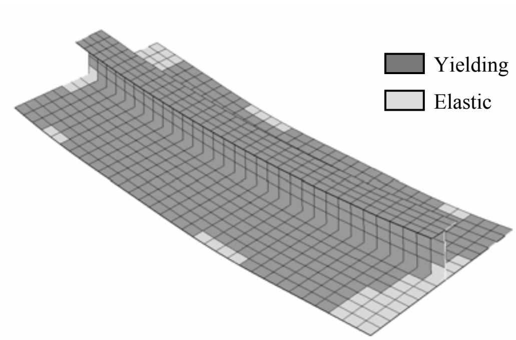

(c) Extent of yielding at B

(d) Extent of yielding at C

Figure 2-17 Behaviour of panel 222_22 (pure bending loading condition) (one flange tip at y = +0.5 b_f is restrained in y-direction to prevent stiffener tripping)

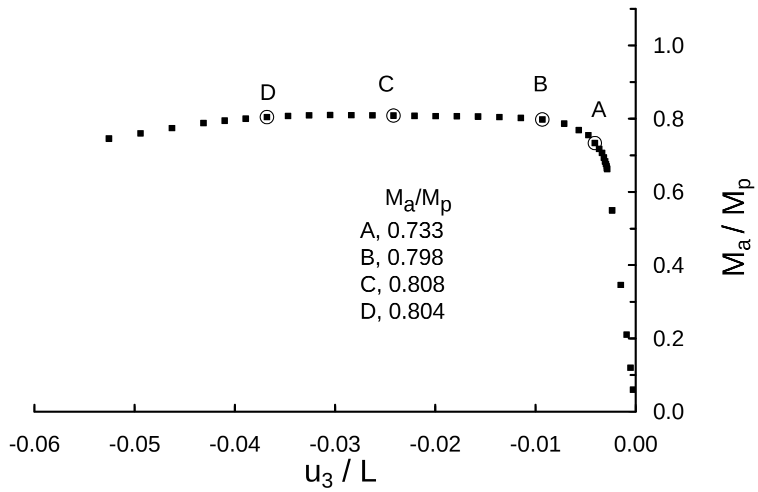

(a) Applied moment vs. lateral deflection at centre of the stiffened panel

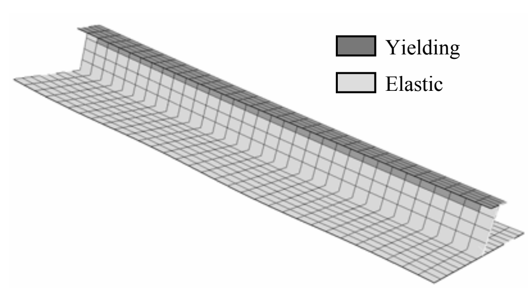

(b) Extent of yielding at A

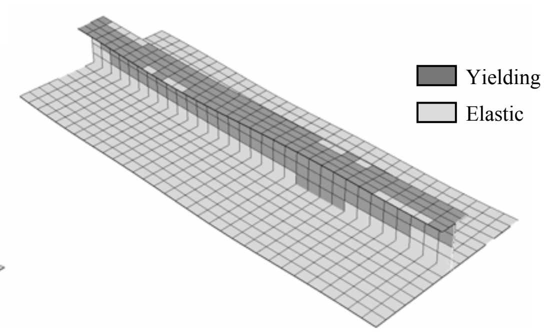

(c) Extent of yielding at B

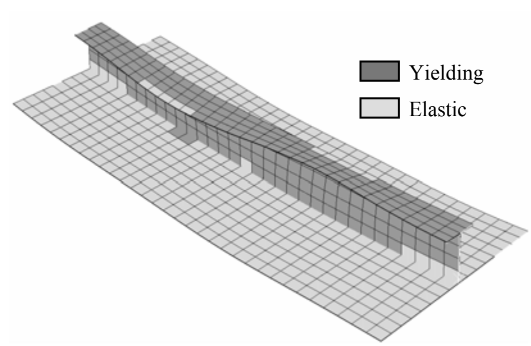

(d) Extent of yielding at C

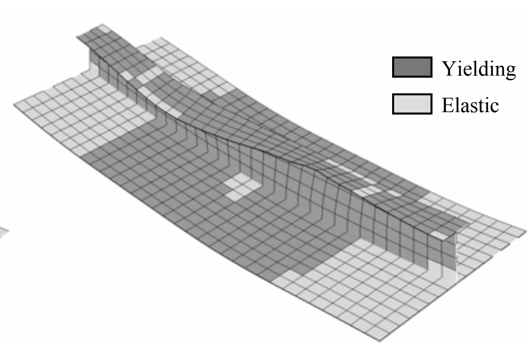

(e) Extent of yielding at D

Figure 2-18 Behaviour of panel 222_22 (pure bending load condition)

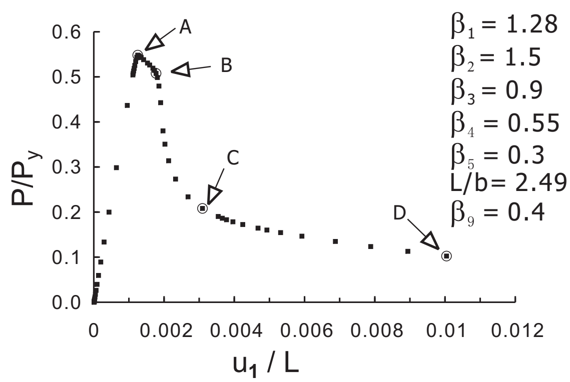

(a) Axial load vs. axial deformation

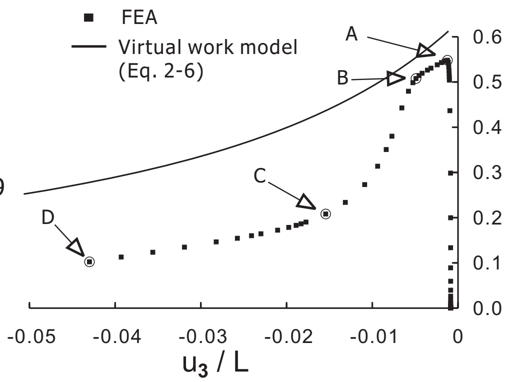

(b) Axial load vs. lateral deflection at centre of the stiffened panel

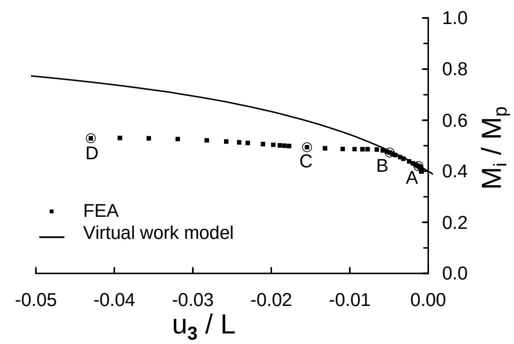

(c) Internal moment vs. lateral deflection

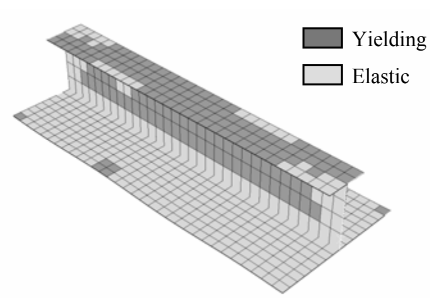

(d) Extent of yielding at A

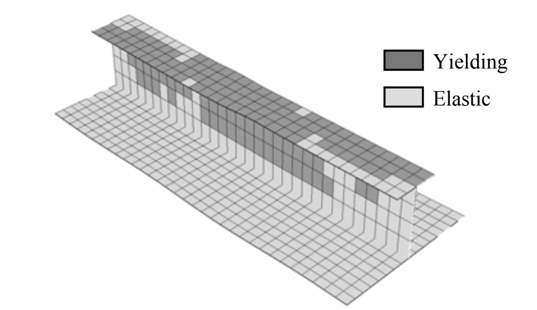

(e) Extent of yielding at B

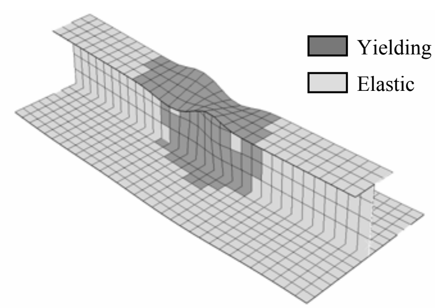

(f) Extent of yielding at C

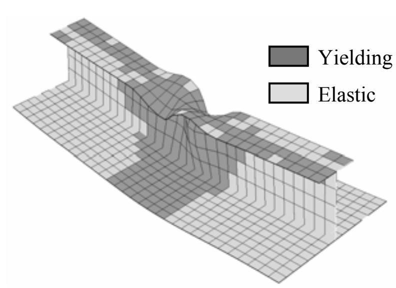

(g) Extent of yielding at D

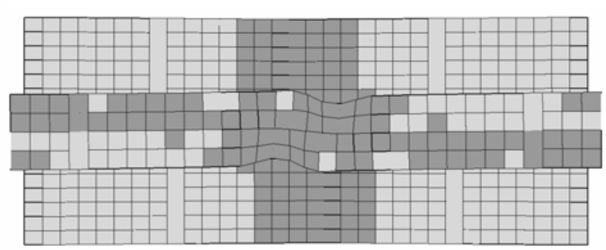

(h) Extent of yielding at D (plan view)

Figure 2-19 Behaviour of panel 233_32 (β_2 = 1.5, β_3 = 0.9, β_9 = 0.4)

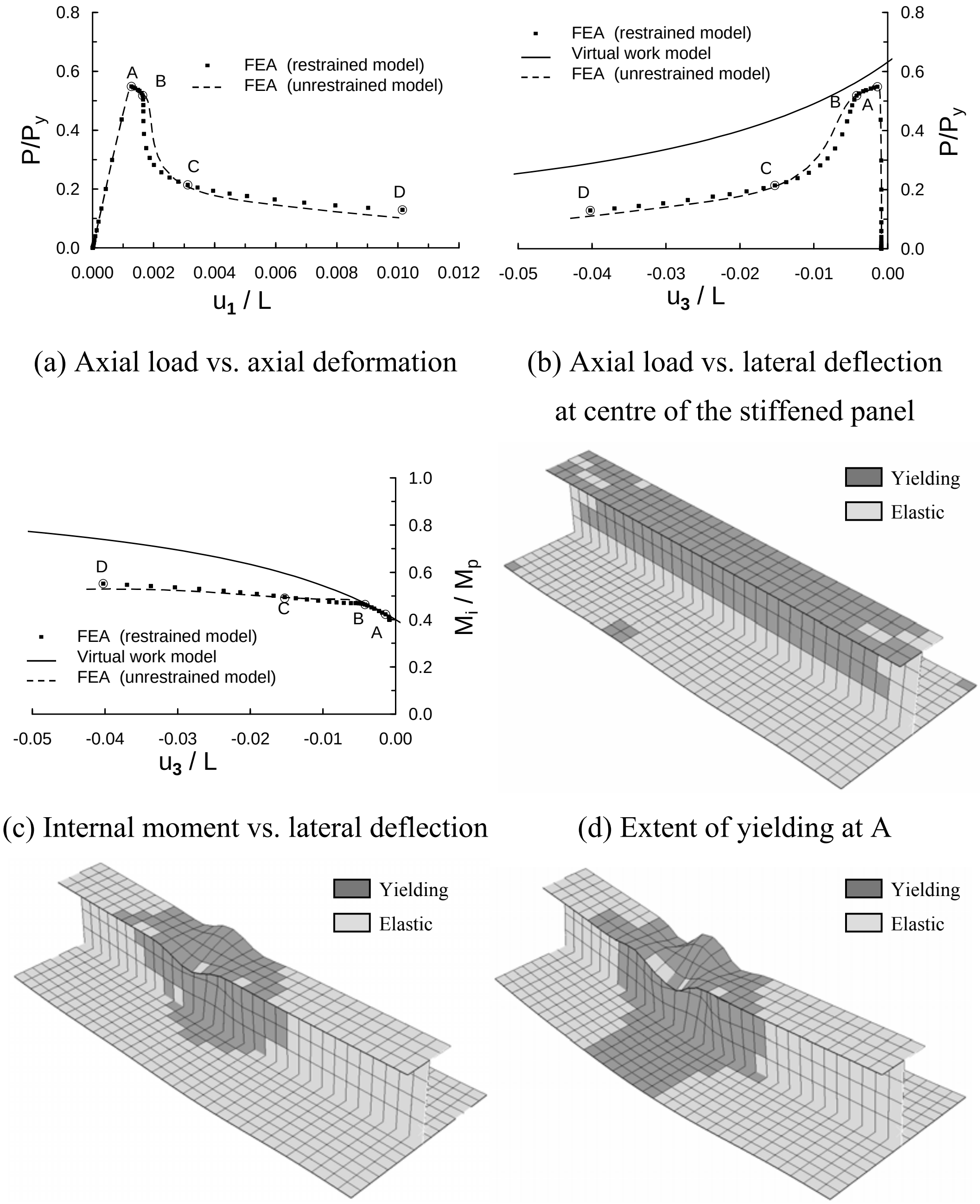

(a) Axial load vs. axial deformation

(b) Axial load vs. lateral deflection at centre of the stiffened panel

(c) Internal moment vs. lateral deflection

(d) Extent of yielding at A

(e) Extent of yielding at C

(f) Extent of yielding at D

Figure 2-20 Behaviour of panel 233_32 (β_9 = 0.4) (one flange tip at y = +0.5 b_f is restrained in y-direction to prevent stiffener tripping)

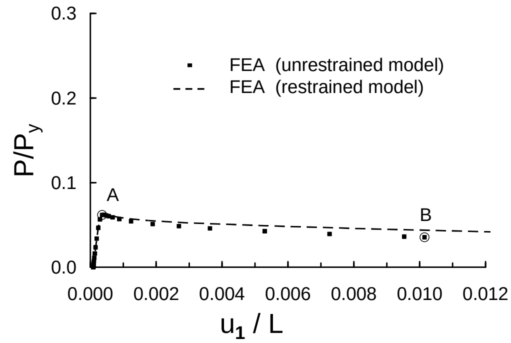

(a) Axial load vs. axial deformation

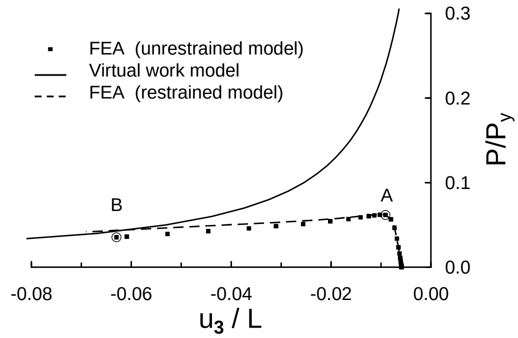

(b) Axial load vs. lateral deflection at centre of the stiffened panel

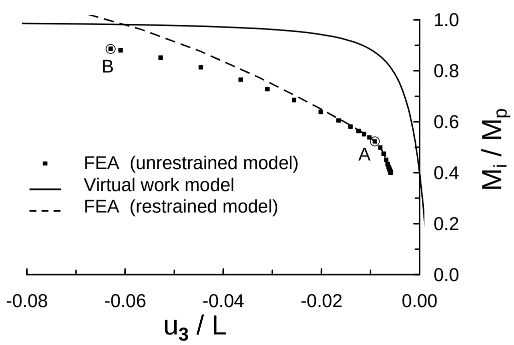

(c) Internal moment vs. lateral deflection

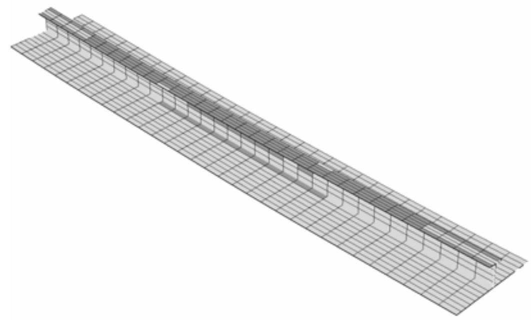

(d) Extent of yielding at A (unrestrained model)

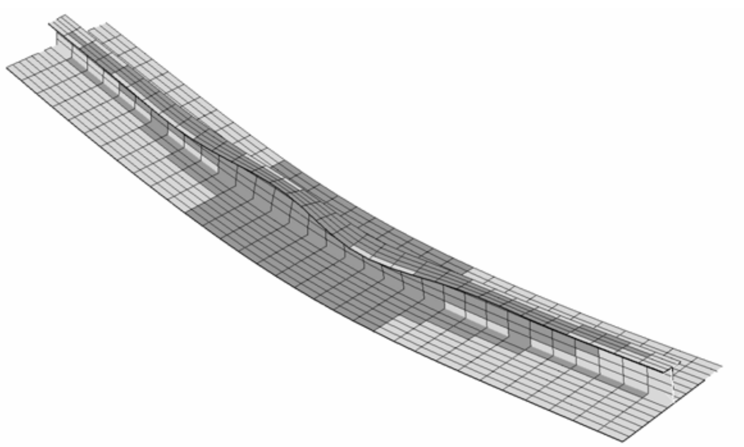

(e) Extent of yielding at B (unrestrained model)

Figure 2-21 Behaviour of panel 122_14 (β_9 = 0.4) (unrestrained and restrained model (one flange tip at y = +0.5 b_f is restrained in y-direction to prevent stiffener tripping))

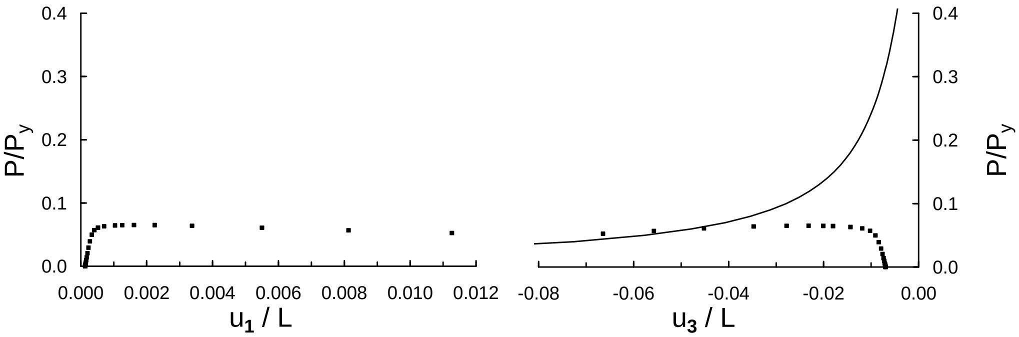

(a) Panel 211_12 (β_9 = 0.4)

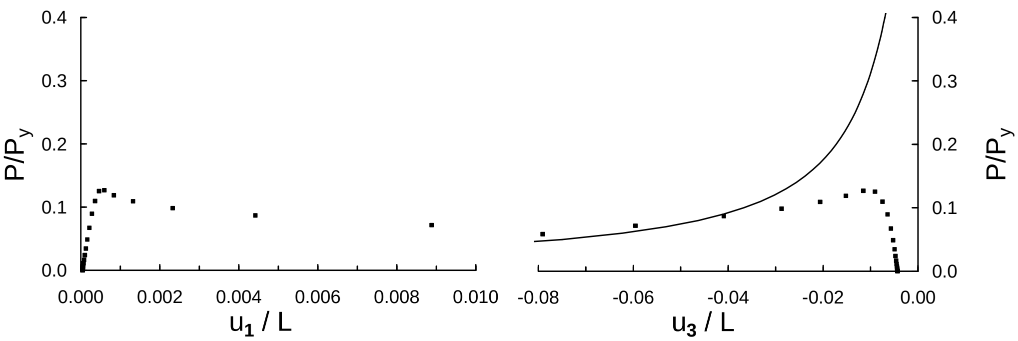

(b) Panel 111_13 (β_9 = 0.2)

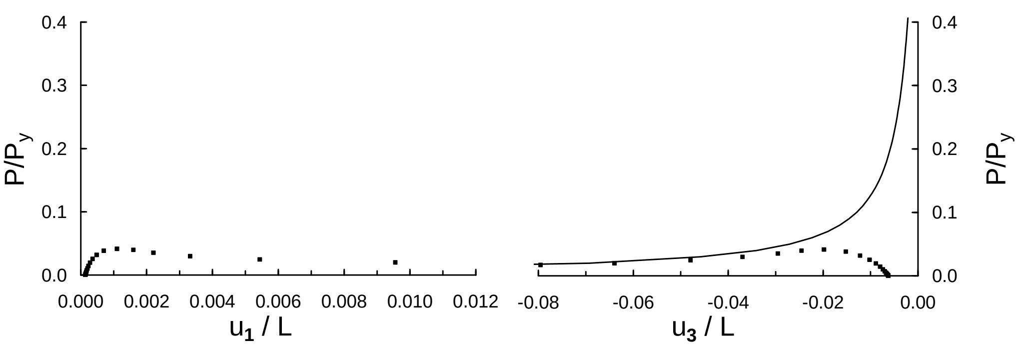

(c) Panel 411_24 (β_9 = 0.2)

Figure 2-22 Examples of stiffener induced failure for which large deformation is required before the formation of a plastic hinge

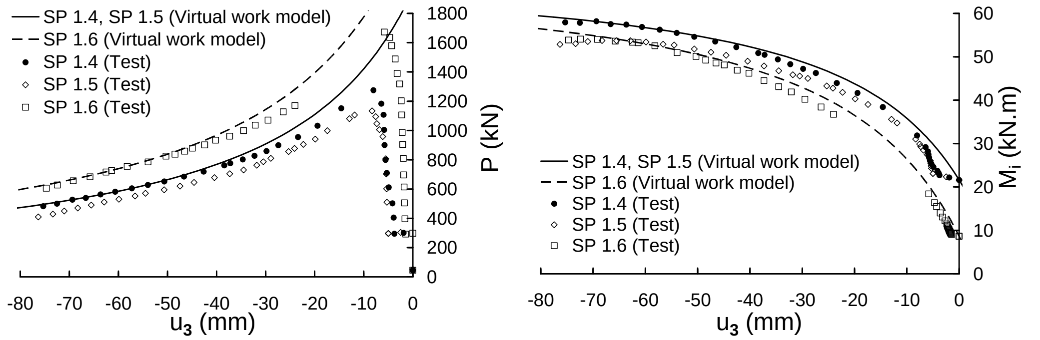

(a) Axial load vs. lateral deflection at centre of the stiffened panel

(b) Internal moment at midspan vs. lateral deflection at centre of the stiffened panel

Figure 2-23 Comparison between test results (Chen *et al.*, 1997) and theoretical plastic hinge curves

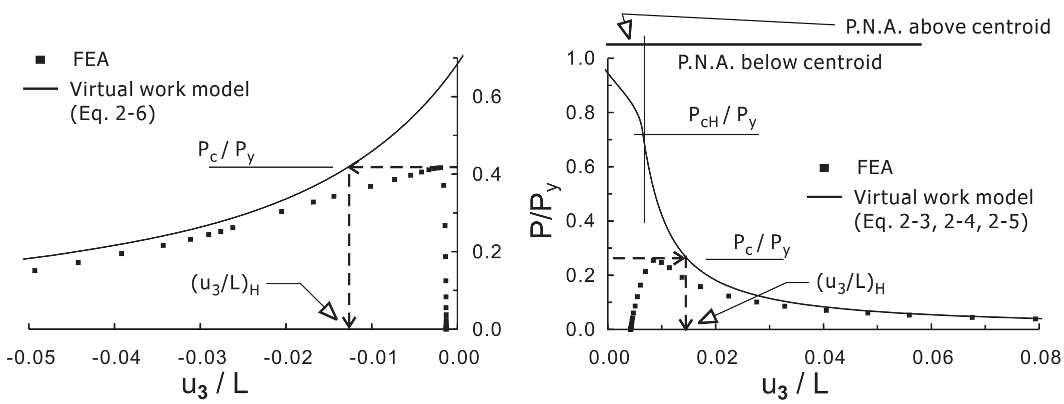

(a) Stiffener induced failure (Panel 122_22, $\beta_9 = 0.4$)

(b) Plate induced failure (Panel 222_24, $\beta_9 = -0.4$)

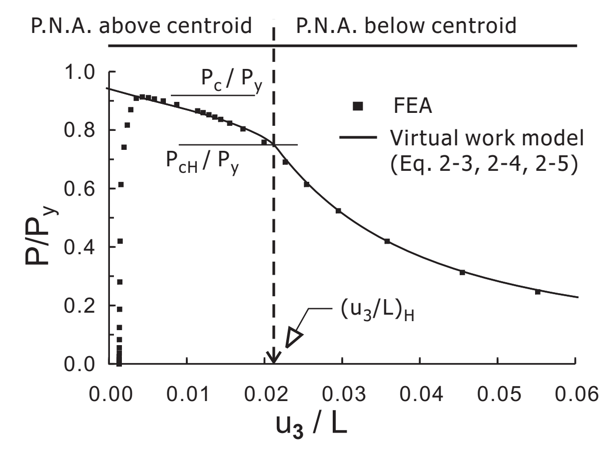

(c) Plate induced failure (Panel 122_22, $\beta_9 = -0.4$)

Figure 2-24 Illustration of $\left(u_3/L\right)_H$

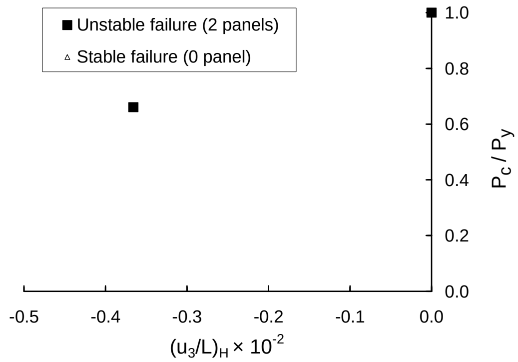

(a) $\beta_9 = 0$

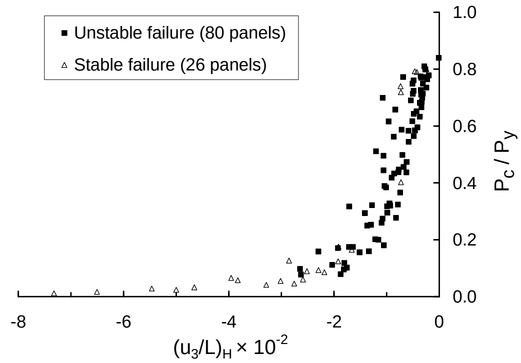

(b) $\beta_9 = 0.2$

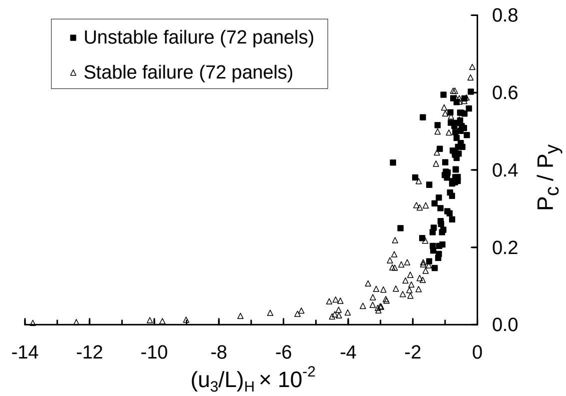

(c) $\beta_9 = 0.4$

Figure 2-25 Distribution of unstable and stable stiffener induced failures

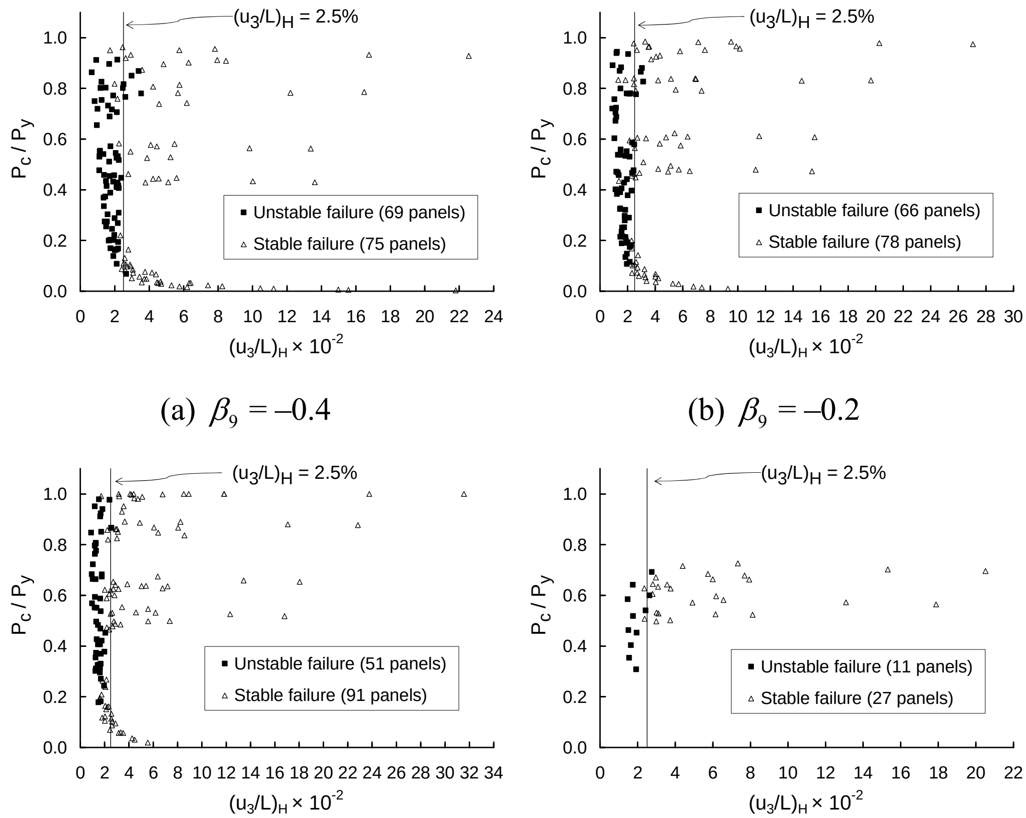

(a) $\beta_9 = -0.4$ (b) $\beta_9 = -0.2$

(c) $\beta_9 = 0$ (d) $\beta_9 = 0.2$

Figure 2-26 Distribution of unstable and stable plate induced failures ($(u_3/L)_H$ calculated using the minimum of P_c and P_{cH} and Equations [2-3], [2-4] and [2-5])

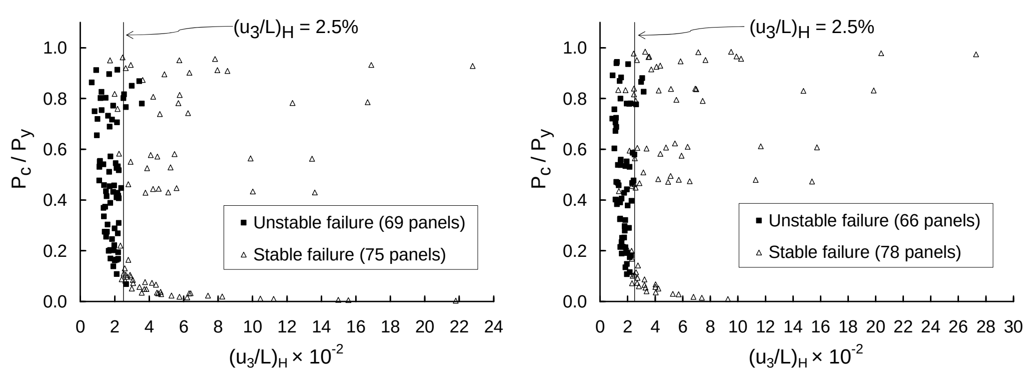

(a) $\beta_9 = -0.4$ (b) $\beta_9 = -0.2$

Figure 2-27 Distribution of unstable and stable plate induced failures ($(u_3/L)_H$ calculated using the minimum of P_c and P_{cH} and Equation [2-15])

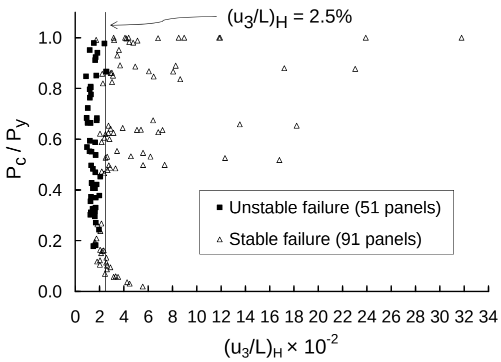

(c) $\beta_9 = 0$

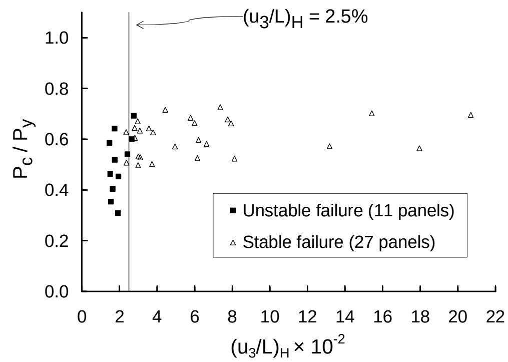

(d) $\beta_9 = 0.2$

Figure 2-27 Distribution of unstable and stable plate induced failures ($(u_3/L)_H$ calculated using the minimum of P_c and P_{cH} and Equation [2-15]) (continued)

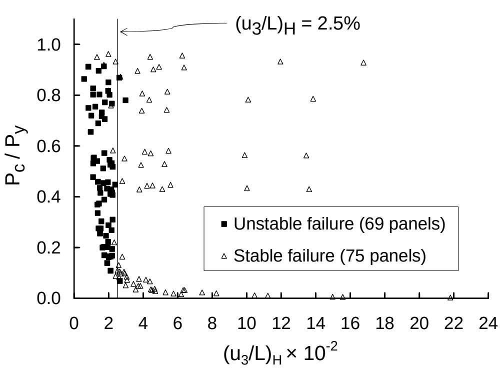

(a) $\beta_9 = -0.4$

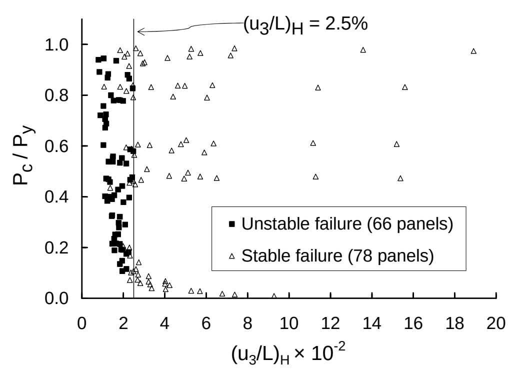

(b) $\beta_9 = -0.2$

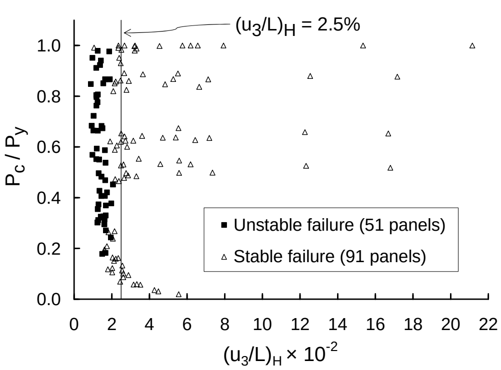

(c) $\beta_9 = 0$

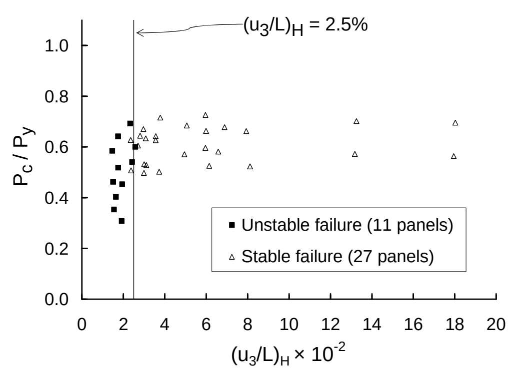

(d) $\beta_9 = 0.2$

Figure 2-28 Distribution of unstable and stable plate induced failures ($(u_3/L)_H$ calculated using P_c and Equation [2-15])

CHAPTER 3

A DESIGN APPROACH FOR STIFFENED STEEL PLATES UNDER COMPRESSION AND BENDING

3.1 INTRODUCTION

Traditional failure modes for stiffened steel plates include plate buckling, stiffener tripping, and overall buckling (Grondin *et al.*, 1998). While stiffener tripping has been considered as the only failure mode that leads to a sudden loss of load carrying capacity, the interaction of overall buckling with the formation of a plastic hinge was found in Chapter 2 to display similar post-peak behaviour. Although this instability results from the interaction of two failure modes, it will be treated as one failure mode in this research, namely, plastic hinge instability. It is desirable to predict this instability because its consequence of occurrence (the sudden loss of load carrying capacity) would require a lower probability of occurrence, hence a higher safety index.

These failure modes can be categorized as plate induced failure or stiffener induced failure, depending on the element that lies on the concave side (flexural compression side) of the panel when it buckles. Plate induced failure includes plate buckling, plate induced overall buckling and plate induced plastic hinge instability. Stiffener induced failure includes stiffener tripping, stiffener induced overall buckling and stiffener induced plastic hinge instability.

The plastic hinge instability failure mode is not recognized in any current design documents. The current design procedures do not specifically address the post-peak behaviour and treat plates that suffer from sudden loss of capacity after buckling the same way as plates with a stable post-buckling behaviour. The representative design documents dealing with the stiffened steel plates include DNV-RP-C201 [Det Norske Veritas (DNV), 2002], API bulletin 2V [American Petroleum Institute (API), 2000], the ABS guide [American Bureau of Shipping (ABS), 2007], AASHTO LRFD bridge design specifications [American

Association of State Highway Transportation Officials (AASHTO), 2007] and CAN/CSA-S6-06 [Canadian Standards Association (CSA), 2006a].

DNV-RP-C201 (DNV, 2002), API bulletin 2V (API, 2000), and the ABS guide (ABS, 2007) account for several failure modes such as plate buckling, stiffener tripping, and overall buckling. In these design documents, a stiffener with an effective plate width is treated as a beam-column. The effective width is used to reflect the loss of plate effectiveness when plate buckling occurs (Faulkner, 1975). This commonly used approach of dealing with the effect of plate buckling recognizes the post-buckling capacity of stiffened plates until flexural buckling of the overall panel is reached (Faulkner, 1975).

The overall buckling capacity of stiffened steel plates is most commonly calculated using beam column interaction equations for a stiffened plate panel with the effective plate width. Stiffener tripping is usually treated by analyzing the behaviour of the stiffener alone, twisting about the stiffener to plate junction. Different design concepts have been adopted for overall buckling and stiffener tripping. These concepts will be introduced in the following section.

AASHTO (2007) and CAN/CSA-S6-06 (CSA, 2006a), only consider plate buckling. Both design codes use classical elastic plate buckling equations (Timoshenko and Gere, 1961) to estimate the elastic plate buckling capacity, and use an arbitrarily selected sine curve between the elastic buckling curve and the yield load to calculate the inelastic buckling capacity (CSA, 2006b). The post-buckling behaviour and other failure modes are not concerned.

A number of researchers (Ghavami, 1994; Balaz and Murray, 1992; Sheikh *et al.,* 2002, 2003; Wang *et al.,* 2006; Sun and Wang, 2005) have assessed and compared various design methods including DNV-RP-C201 (DNV, 2002), API bulletin 2V (API, 2000), the ABS guide (ABS, 2004), Ontario Highway Bridge Design Code (Ministry of Transportation and Communications, 1983), and some other design codes that will not be introduced in this thesis. The 2004 version of the ABS guide (ABS, 2004) has the same design equations as the updated 2007 version (ABS, 2004) for the load cases investigated in this research. The Ontario Highway Bridge Design Code (Ministry of Transportation and Communications, 1983) also has the same design equations for stiffened plate as that of AASHTO (2007) and CAN/CSA-S6-06 (CSA, 2006a). The assessment work of these publications showed that the five current design procedures introduced previously need to improve their ability to predict stiffened plate capacity and understanding of failure behaviour.

This chapter will look at the effect of different post-buckling behaviours on the design process for stiffened steel plates loaded in compression parallel to the stiffeners, combined with out-of-plane bending. It is concerned with prediction of the ultimate load capacity and also failure mode of steel plates stiffened with longitudinal tee stiffeners. The load cases considered in this study are axial compression (applied parallel to the stiffeners) and a combination of compression and out-of-plane bending.

3.2 REVIEW OF DESIGN STANDARDS AND GUIDELINES

The design approaches for stiffened steel plates from three different sources were selected for evaluation since they provide the most comprehensive design guidelines for stiffened steel plates, namely, Bulletin 2V of the American Petroleum Institute (API, 2000), recommended practice DNV-RP-C201 of the Det Norske Veritas (DNV, 2002), and the design guide of the American Bureau of Shipping (ABS, 2007). A brief description of the procedures presented in these design documents is presented below.

3.2.1 API bulletin 2V (API, 2000)

API bulletin 2V (API, 2000) considers four failure modes for stiffened plates, namely, plate buckling, overall buckling, stiffener tripping and “plastic bending”. The last failure mode, “plastic bending”, is not the same as plastic hinge instability that was mentioned previously, while the difference will be introduced later. API bulletin 2V (API, 2000) uses the effective plate width, b_e, proposed by Faulkner (1975) as follows:

$$\begin{cases} \dfrac{b_e}{b} = 1 & if\ \beta_1 \le 1 \\ \dfrac{b_e}{b} = \dfrac{2}{\beta_1} - \dfrac{1}{\beta_1{}^2} & if\ \beta_1 > 1 \end{cases} \qquad [3\text{-}1]$$

where b is the plate width and β_1 is the plate slenderness ratio defined as:

$$\beta_1 = \frac{b}{t}\sqrt{\frac{F_{yp}}{E}} \qquad [3\text{-}2]$$

where t is the plate thickness; F_{yp} is the plate yield strength; and E is the modulus of elasticity. The stiffener and the effective plate width constitute an effective panel designed using the following beam-column interaction equation:

$$\frac{P}{P_{ue}} + \frac{\omega_1}{1 - P/P_{Ee}} \frac{|M_{ae}|}{M_{pe}} \le 1 \qquad [3\text{-}3]$$

where P is the applied axial load; P_{ue} is the overall buckling capacity of the effective panel; P_{Ee} is the Euler buckling load of the effective panel as given in Equation [3-4]; M_{ae} is the end moment about the centroid of the effective cross-section; M_{pe} is the plastic moment capacity of the effective panel; and ω_1 is an equivalent moment coefficient to account for the moment distribution along the plate length and is equal to 1.0 for a constant moment distribution. The axial load P cannot be greater than the torsional flexural buckling (stiffener tripping) capacity of the stiffened plate in API bulletin 2V (API, 2000).

$$P_{Ee} = \frac{\pi^2 E I_e}{(KL)^2} \qquad [3\text{-}4]$$

where I_e is the moment of inertia of the effective cross-section; L is the panel length; and KL is the effective length, which is a function of the boundary conditions. The load case of interest in this research is a constant out-of-plane moment, M_a, and an axial load P applied at the centroid of the full cross-section at both panel ends. When the effective panel is used in capacity calculation, the end moment should be taken about the centroid of the effective cross-section. Therefore, M_{ae} in Equation [3-3] would include the applied M_a and a moment equal to the applied axial force multiplied by the distance between the centroid of the full plate section and the centroid of the effective section. Both M_a and M_{ae} are first-order moments and an amplification factor, $\frac{\omega_1}{1-P/P_{Ee}}$, is used to account for the second order moment resulting from the action of the axial force on the deformed panel (P-δ effect). In calculation of the overall buckling capacity, inelastic behaviour of the stiffened plate is accounted for using the Ostenfeld-Bleich column curve expressed as follows:

$$\frac{P_{ue}}{P_{ye}} = \begin{cases} 1 - p_r(1-p_r)\lambda_e^2 & \text{if } \lambda_e \le 1/\sqrt{p_r} \\ 1/\lambda_e^2 & \text{if } \lambda_e > 1/\sqrt{p_r} \end{cases} \qquad [3\text{-}5]$$

where p_r is the ratio of the proportional limit to the yield strength of steel, taken as 0.5; P_{ye} is the yield capacity of the effective panel cross-section; and λ_e is the column slenderness ratio of the effective panel defined as:

$$\lambda_e = \sqrt{\frac{F_y}{F_{Ee}}} = \frac{KL}{r_e}\sqrt{\frac{F_y}{\pi^2 E}} \qquad [3\text{-}6]$$

where F_{Ee} is the Euler buckling (elastic buckling) stress of the effective specimen; F_y is the yield strength; and r_e is the radius of gyration of the effective cross-section about an axis through its centroid and parallel to the plate.

Stiffener tripping is considered as torsional flexural buckling of the effective panel. The elastic torsional flexural buckling capacity is calculated using the classical torsional flexural buckling equation derived by Timoshenko and Gere (1961). The inelastic torsional flexural buckling capacity is evaluated from the elastic buckling analysis results using the Ostenfeld-Bleich column curve in the same manner as the flexural buckling.

“Plastic bending” (this term is given by API) is also a mode considered by API. It was derived by Soreide (1981) for a symmetric I-section, but was adopted for monosymmetric sections by API. It calculates the plastic section capacity taking into account the interaction of the axial force and internal moment, but does not consider progression of plastic hinge and the effect of second-order moments. Therefore, it is not the same as the plastic hinge instability mode that was found in Chapter 2.

3.2.2 DNV-RP-C201 (DNV, 2002)

DNV-RP-C201 (DNV, 2002) considers three failure modes, namely, plate buckling, overall buckling and stiffener tripping. The plate effective width adopted by DNV (2002) is that proposed by Winter and is given as:

$$\begin{cases} \dfrac{b_e}{b} = 1 & \text{if } \beta_1 \le 1.28 \\ \dfrac{b_e}{b} = \dfrac{1.90}{\beta_1} - \dfrac{0.79}{\beta_1^2} & \text{if } \beta_1 > 1.28 \end{cases} \tag{3-7}$$

The design approach is based on the first yield criterion, and is expressed by the following interaction equations:

$$\frac{P}{F_k A_e} + \frac{1}{1 - P/P_{Ee}} \frac{|M_{ae}|}{M_{ye,c}} \le 1 \text{ (for the flexural compression side)} \tag{3-8a}$$

$$\frac{P}{F_k A_e} - 2\frac{P}{P_{ye}} + \frac{1}{1 - P/P_{Ee}} \frac{|M_{ae}|}{M_{ye,t}} \le 1 \text{ (for the flexural tension side)} \tag{3-8b}$$

where F_k is the characteristic buckling stress of the element being checked, which can be either the plate or the stiffener. Since the concept of effective width is implemented, F_k is taken as F_y for the plate side of the effective panel. For the stiffener side, F_k is taken as the torsional buckling stress of the stiffener for buckling about the stiffener to plate junction line to account for stiffener tripping. $M_{ye,c}$ and $M_{ye,t}$ in Equation [3-8] are the yield moments of the effective panel for yielding on the flexural compression side and on the flexural tension side, respectively; and A_e is the area of the effective cross-section. The general design philosophy is to ensure that the maximum stress on each side of a bending panel is below the yield strength. In the process of calculating the characteristic buckling stresses, the Ayrton-Perry formula (Ayrton and Perry, 1886) is adopted for the elasto-plastic behaviour. This formula entails calculation of a number of coefficients, and thus is not provided here. The form of Equation [3-8b] considers the possibility that the flexural tension side can be either in compression (when the axial compression force is dominant) or in tension, but the source of this equation is not clear.

3.2.3 The ABS guide (ABS, 2007)

The ABS guide (ABS, 2007) considers three failure modes, namely, plate buckling, overall buckling, and stiffener tripping. Its philosophy is also based on the first yield criterion expressed as follows:

$$\frac{P}{P_{ue}}+\frac{0.75}{1-\left(\left(P/A\right)/F_{Ee}\right)}\frac{\left|M_a\right|}{M_{ye2}}\leq 1 \qquad [3\text{-}9]$$

where M_{ye2} is the yield moment capacity for the effective cross-section. As for API Bulletin 2V (API, 2000), the axial load P cannot be greater than the torsional flexural buckling (stiffener tripping) capacity of the stiffened plate. Although Equation [3-9] is expressed in terms of stress in the ABS guide, it has been expressed in terms of axial force and moment here in order to be consistent with the presentation for other design guides and standards.

The effective plate width used to calculate P_{ue} and F_{Ee} is based on the Faulkner effective width formula (Equation [3-1]), which accounts for the loss of effectiveness due to plate buckling. However, the effective plate width used to calculate M_{ye2} accounts for the shear lag phenomenon associated with flexural bending (Faulkner, 1975). It is obtained from tabulated values in the ABS guide (ABS, 2007), which is believed to be derived from the work of Faulkner (Faulkner, 1975). In general, the first yield design philosophy of Equation [3-9] adopted by the ABS guide (ABS, 2007) is the same as Equation [3-8] of DNV-RP-C201 (DNV, 2002).

As for API Bulletin 2V (API, 2000), the ABS guide (ABS, 2007) uses the Ostenfeld-Bleich column curve (Equation [3-5]) for calculating the inelastic buckling capacity, P_{ue}, where the proportional limit ratio p_r is taken as 0.6 though.

The stiffener tripping calculation approach used in the ABS guide uses an iterative procedure to obtain the number of buckling waves corresponding to the minimum elastic torsional buckling capacity. The inelastic stiffener tripping capacity is accounted for using the Ostenfeld-Bleich column curve as well.

The ABS guide (ABS, 2007) also has a requirement for the minimum moment of inertia of the effective cross-section as follows:

$$I_e \geq \frac{bt^3}{12\left(1-\nu^2\right)}\left[\left(2.6+4.0\beta_5\right)\left(\frac{L}{b}\right)^2+12.4\frac{L}{b}-13.2\sqrt{\frac{L}{b}}\right] \qquad [3\text{-}10]$$

where I_e is the moment of inertia of the effective cross-section; ν is Poisson's ratio (taken as 0.3 for steel); and β_5 is the stiffener to plate area ratio. A stiffener satisfying this requirement is believed to have sufficient flexural stiffness to form a rigid nodal line between buckled plates. A similar requirement for the moment of inertia is found in CAN/CSA-S6-06 (CSA, 2006a) and the AASHTO LRFD bridge design specifications (AASHTO, 2007). Futhur discussion of this requirement will be introduced later when assessing the proposed method.

3.3 PROPOSED DESIGN APPROACH FOR STIFFENED PLATES UNDER COMPRESSION AND BENDING

3.3.1 Failure modes and underlying philosophy

The proposed approach considers the three traditional failure modes (plate buckling, overall buckling and stiffener tripping) that are included in current design documents (API, 2000; DNV, 2002; ABS, 2007), and adds the plastic hinge instability mode that was identified in Chapter 2.

Plate buckling is a common failure mode in stiffened plates. However, plate buckling does not represent the ultimate limit state for a stiffened steel plate. Since a plate can maintain its load carrying capacity in the post-buckling range (Faulkner, 1975), failure generally starts with plate buckling before overall buckling occurs. Therefore, the proposed approach uses the effective width concept to account for interaction between plate buckling and overall buckling. This approach is consistent with the other design approaches reviewed in the previous sections.

The work presented in Chapter 2 indicated that the capacity of stiffened steel plates is governed by the overall buckling mode. Due to the presence of local plate buckling, the overall buckling capacity would be obtained using the effective panel that consists of the effective plate and the stiffener.

Stiffener tripping has not been observed as the governing mode in all cases investigated in this research. It is believed that stiffened plates with tee stiffeners of sizes commonly available in rolled shapes would have stiffener tripping occurring only in the post-buckling range of overall buckling. This practical configuration is controlled by the slenderness ratios of the stiffener web and flange as given in Equations [3-11] and [3-12]

$$\beta_2 = \frac{h_w}{t_w}\sqrt{\frac{F_{ys}}{E}} \le 1.5 \qquad [3\text{-}11]$$

$$\beta_3 = \frac{b_f}{t_f}\sqrt{\frac{F_{ys}}{E}} \le 0.9 \qquad [3\text{-}12]$$

where h_w and t_w are the web height and thickness, respectively; F_{ys} is the stiffener yield strength; b_f and t_f are the flange width and thickness, respectively. These two requirements will be adopted in this proposed method. They are also consistent with the current design standards and guidelines as shown in Table 2-1.

The plastic hinge instability was found to affect significantly the post-buckling behaviour, resulting in a sudden loss of load carrying capacity. A criterion to determine whether a stiffened plate would be susceptible to such a sudden loss was proposed in Chapter 2. Although this plastic hinge instability does not reduce the ultimate stiffened plate capacity, the critical nature of the failure mode should be accounted for in the design process. Limit states design offers a rational approach to account for the severity of the failure mode since the probability of failure can be easily reduced for these undesirable failure modes through an increase of safety index (Kennedy and Gad Aly, 1980).

In general, the capacity of stiffened plates with tee stiffeners of most common sizes available is governed by the overall buckling capacity. Plate buckling affects the pre-buckling behaviour while stiffener tripping and plastic hinge formation affect the post-buckling behaviour. The post-buckling behaviour needs to be predicted. The formulations to evaluate the capacity and behaviour are presented in the following.

3.3.2 Fomulations of the proposed approach

Overall buckling capacity of stiffened steel plates is obtained by treating the effective panel as a beam-column. As for API Bulletin 2V (API, 2000) and the ABS guide (ABS, 2007), the beam-column formulation adopted here considers first yield as the ultimate limit state for plate induced overall buckling as given in

Equation [3-13a]. The beam-column formulation for stiffener induced overall buckling is given in Equation [3-13b].

$$\frac{P}{P_{ue}}+\frac{1}{1-P/P_{Ee}}\frac{Pe-\beta_9 M_p}{M_{ye,p}}\leq 1 \quad if\ Pe-\beta_9 M_p \geq 0 \qquad [3\text{-}13a]$$

$$\frac{P}{P_{ue}}+\frac{1}{1-P/P_{Ee}}\frac{\beta_9 M_p - Pe}{M_{pe}}\leq 1 \quad if\ Pe-\beta_9 M_p < 0 \qquad [3\text{-}13b]$$

The eccentricity e in the interaction equations is the distance between the centroids of the effective cross-section and the full cross-section, and $M_{ye,p}$ is the yield moment capacity of the effective section based on yielding of the extreme fibre on the plate side.

An effective plate width formula is needed to calculate the parameters P_{ue}, P_{Ee}, e, $M_{ye,p}$ and M_{pe} in Equation [3-13]. One option is the Faulkner formula (Equation [3-1]), which is used in the API bulletin 2V (API, 2000) and the ABS guide (ABS, 2007). Another choice is the Winter formula (Equation [3-7]), which is used in DNV-RP-C201 (DNV, 2002), CSA-S136-01 (CSA, 2002) and Eurocode EN 1993-1-5 [European Committee of Standardization (CEN), 2006]. The selection of a suitable effective width formula will be conducted in the later section of the model assessment.

The calculation of the parameter P_{ue} for the effective stiffened plate requires a column buckling model. One of the column buckling formulae currently used in CAN/CSA-S6-06 (CSA, 2006a) and CSA-S16-09 (CSA, 2009) corresponds to the SSRC column curve 2 and is given by Equation [3-14]. The one used in ANSI/AISC 360-05 (AISC, 2005) is given in Equation [3-15].

$$\frac{P_{ue}}{P_{ye}}=\left(1+\lambda_e^{2.68}\right)^{-1/1.34} \qquad [3\text{-}14]$$

$$\frac{P_{ue}}{P_{ye}}=\begin{cases}0.658^{\lambda_e^2} & if\ \lambda_e \leq 1.5\\ 0.877/\lambda_e^2 & if\ \lambda_e > 1.5\end{cases} \qquad [3\text{-}15]$$

The column curve used in the design guides for stiffened plates is the Ostenfeld-Bleich parabola (Equation [3-5]). It was adopted in API bulletin 2V (API, 2000) and the ABS guide (ABS, 2007), where the proportional limit ratio p_r is taken as 0.5 and 0.6, respectively. These four options, namely, Equation [3-14], Equation [3-15], Equation [3-5] with $p_r = 0.5$ and Equation [3-5] with $p_r = 0.6$ are plotted in Figure 3-1 and will also be tested in section 3.5 where they will be tried in the proposed design models 1 to 5 to find out the best option.

Equation [3-13a] applies to plate induced overall buckling. Under out-of-plane bending only the stiffener flange yields in tension before the plate yields in compression since the elastic neutral axis is much closer to the plate. As the axial load increases, the tensile stresses in the stiffener decrease, allowing the plate to yield in compression before yielding of the stiffener in tension. Therefore, the first yield criterion is applied on the plate side (the flexural compression side) for plate induced overall buckling by using $M_{ye,p}$ in Equation [3-13a]. Equation [3-13a] is applicable assuming small deformations prevail at the ultimate limit state. If external moments have already created a large deformation, the axial compression capacity may not be large enough to offset the tensile flexural stresses when the deflected shape is accentuated by the second order effect. In such cases, the panels would fail mainly due to the applied bending moment, with a small axial load. Some requirements to prevent this type of failure will be discussed in the next section for the range of load cases investigated.

Equation [3-13b] applies to stiffener induced overall buckling. When the stiffener extreme fibre is placed in flexural compression, the stiffener flange yields in compression before the plate outer surface yields in tension. As indicated in the previous section, the slenderness of the stiffener flange and web is controlled to prevent local buckling before full yielding of the stiffener. Therefore, the first yield criterion for the stiffener in flexural compression would be overly conservative. The full plastic moment capacity of the effective cross-section, M_{pe}, is therefore selected for the interaction Equation [3-13b]. Both the plate on the tension side and the stiffener on the compression side are allowed to fully yield. As for Equation [3-13a], Equation [3-13b] also assumes small deformations prevail at the ultimate limit state.

Equations [3-13a] and [3-13b] are therefore used to check the maximum stress on the flexural compression side of the buckled panel. The stresses on the flexural tension side do not govern since the simultaneous application of an axial compression force would reduce the tensile stresses.

When the left hand side of Equation [3-13a] reaches 1.0, the applied load, P, corresponds to plate induced overall buckling capacity, P_c. Similarly, P_c for stiffener induced overall buckling can be obtained by setting the left hand side of Equation [3-13b] equal to 1.0. The minimum value of the two values of P_c establishes the buckling direction and the ultimate capacity.

If plate induced overall buckling governs, the theoretical normalized out-of-plane deflection, $\left(u_3/L\right)_H$, can be evaluated from

$$\left(\frac{u_3}{L}\right)_H = \frac{\beta_9 M_p}{P_c L} + \left(\frac{P_y}{P_c} + 1\right)\left(\frac{z_p}{L} - \frac{P_y + P_c}{4F_y bL}\right) \quad [3\text{-}16]$$

where u_3 is the midspan out-of-plane deflection; z_p is the distance between the centroid of the full section to the plate outer surface. If the value of $\left(u_3/L\right)_H$ obtained from Equation [3-16] is less than 0.025, plate induced overall buckling will progress into plastic hinge instability. A higher safety index, β, should be used for this case.

If stiffener induced overall buckling governs, failure is usually accompanied by a sudden loss of strength immediately after the peak load due to plastic hinge instability. Therefore, a higher safety index should be used for all stiffener induced failure.

3.3.3 Area and slenderness requirements for the stiffener

Three slenderness requirements and one area requirement are set for stiffened plates in order to fully develop the capacity predicted by Equation [3-13]. The first two slenderness requirements are given in Equations [3-11] and [3-12] for the stiffener web slenderness ratio, β_2, and the flange slenderness ratio, β_3. They are consistent with the current design practice (CSA, 2009; API, 2000; DNV, 2002; ABS, 2007) and are set to prevent stiffener local buckling before yielding.

The third slenderness requirement and the area requirement are applied to the whole stiffener and are intended to provide sufficient support to the plate to prevent overall buckling before buckling of the plate panels bounded by the stiffeners. The slenderness requirement for stiffeners was first investigated by Timoshenko and Gere (1961). They investigated the behaviour of a compressed plate simply supported along the two unload edges. When the plate was stiffened by a longitudinal stiffener along its midline, it was found that the plate capacity could increase by a factor of four when the stiffener had sufficient stiffness to form a point of inflection across the width of the plate. In that case, the stiffener effectively divides the plate into two simply supported plates of width $b/2$. Timoshenko and Gere (1961) presented a relationship between the plate buckling strength and the stiffness of the stiffener.

$$\sigma_{cr} = k \frac{\pi^2 E}{12(1-\nu)^2} \left(\frac{t}{b} \right)^2 \qquad [3\text{-}17]$$

where k is the plate buckling coefficient, which reflects the boundary restraint from the stiffener to the plate. The minimum value of k applicable for a plate bounded by stiffeners is given by:

$$k = \frac{2\left[\sqrt{1 + I \Big/ \dfrac{bt^3}{12(1-\nu)^2}} + 1 \right]}{(m+1)^2 \left[1 + \beta_5 \right]} \qquad [3\text{-}18]$$

where I is the moment of inertia of the full section of one stiffener with its associated plate about the centroidal axis parallel to the plate; m is the number of stiffeners on a stiffened panel (between the adjacent girders or box-girder webs).

Based on the work of Timoshenko and Gere (1961), Mattock *et al*. (1967) proposed Equation [3-19] to be the minimum required moment of inertia of stiffeners. Equation [3-19] was believed to be an approximate expression of the exact but cumbersome Equations [3-17] and [3-18] (AASHTO, 2007) and was adopted by CAN/CSA-S6-06 (CSA, 2006a) and AASHTO LRFD bridge design specifications (AASHTO, 2007).

$$\begin{cases} I_s \geq 0.125k^3t^3b & for\ m=1 \\ I_s \geq 0.07k^3m^4t^3b & for\ m>1 \end{cases} \qquad [3\text{-}19]$$

where I_s is the moment of inertia of the stiffener about an axis parallel to the plate and taken at the base of the stiffener.

In North American bridge design practice a reasonable value of k (ranging normally from 2 to 4) is first assumed, from which the minimum required I_s value is obtained (AASHTO, 2007). However, in design practice the stiffness requirement expressed by equation [3-19] was found to be unreasonably conservative when m is large.

In the recent research, Yoo *et al*. (2001) and Choi (2002) made further investigation on the minimum stiffness requirement of tee stiffeners by using the finite element method. An iterative process was adopted to find out the minimum I_s that is required to cause buckling of the plate sub-panels bounded by the stiffeners before overall buckling of the stiffened panels. For each model, the iterative process used the same values of the aspect ratio L/b, the number of stiffeners m, the plate width b, and the plate thickness t, but with various I_s. Based on the regression analysis for the results of over one hundred models, Yoo *et al*. (2001) and Choi (2002) proposed Equation [3-20] for the minimum stiffness requirement where the effect of the aspect ratio was recognized.

$$I_s \geq 0.3\left(L/b\right)^2 \sqrt{m}\, t^3 b \qquad [3\text{-}20]$$

Although Equation [3-20] was demonstrated to be more rational than Equation [3-19], it is derived based on a limited range of m ($m \leq 4$). It has not been tested for the plate stiffened by more than four stiffeners. On the other hand, Equation [3-20] is derived for one load condition, axial compression, only.

The provisions for "under-stiffened" panels in API bulletin 2V (API, 2000) and CSA-S136-01 (CSA, 2002) are also applicable only for the axial compression load condition. The number of stiffeners, m, is included in the provisions but there is no limit for m though. Both design codes evaluate the plate buckling strength accounting for the reduced restraining effect of light stiffeners. Their provisions are also based on the work of Timoshenko and Gere (1961).

The ABS guide (ABS, 2007) is the only design guide reviewed in this study in which the stiffener stiffness requirement (Equation [3-10]) eliminates the variable m, i.e. applicable for the plate stiffened with any number of stiffeners. Therefore, Equation [3-10] can be directly applied to an isolated single stiffener–attached plate panel that represents the whole plate stiffened by multiple evenly spaced stiffeners. Equation [3-10] is applicable to both load cases of axial compression and combined compression and bending. Although the source of Equation [3-10] is not clear, it certainly has advantages over Equations [3-19] or [3-20] as the limitations for m and load conditions are removed. Therefore, Equation [3-10] is selected as the third slenderness requirement in the proposed approach to avoid "under-stiffened" configurations.

A requirement for the stiffener-to-plate area ratio, β_5, is also attempted here to supplement the slenderness requirement to prevent “under-stiffened” panels. Although desirable values have been adopted for β_5 in common design practice (such as a typical value of 0.2 in ship constructions (Smith *et al.*, 1992)), no literal requirement has been included in current design standards and guidelines studied in this research. Although the area ratio requirement does not have as explicit meaning as the three slenderness requirements, it is observed in later section that a requirement of $\beta_5 \geq 0.15$ is a reasonable supplement.

3.4 ASSESSMENT OF DESIGN MODELS

This section presents a comparison of predicted stiffened plate capacities with the FEA results obtained on 720 stiffened plate configurations presented in Appendix B and Appendix E. The effective plate width equations and column curves introduced in section 3.3.2 are combined into five different design models, all using the proposed interaction Equation [3-13]. The three current design guidelines, reviewed in section 3.2, are also introduced here as three more models. However, it should be noted that the three guides are not using the same interaction equations and failure mode classification as the proposed models. The total of eight models include:

(1) Model 1 (control model) – Faulkner effective plate width equation and CSA column curve (Equations [3-1] and [3-14]);

(2) Model 2 – Winter effective plate width equation and CSA column curve (Equations [3-7] and [3-14]);

(3) Model 3 – Faulkner effective plate width equation and AISC column curve (Equations [3-1] and [3-15]);

(4) Model 4 – Faulkner plate width equation and Ostenfeld-Bleich column curve with $p_r = 0.5$ (Equations [3-1] and [3-5]);

(5) Model 5 – Faulkner plate width equation and Ostenfeld-Bleich column curve with $p_r = 0.6$ (Equations [3-1] and [3-5]);

(6) Model 6 – API Bulletin 2V model (API, 2000);

(7) Model 7 – DNV-RP-C201 model (DNV, 2002);

(8) Model 8 – the ABS model (ABS, 2007).

When calculating the capacity using any of the design models presented above, the resistance factor is taken as 1.0. Mean FEA-to-predicted capacity ratio and the corresponding coefficient of variation (COV) are presented in Table 3-1. The ratio of the applied moment to the plastic moment, β_9, is positive if the applied moment causes compression in the stiffener flange. The mean and COV presented in Table 3-1 are based on a database of 720 samples (see Appendix B). The first column indicates the moment ratio (load case). There are 144 samples for each moment category and 720 in total. However, for the DNV-RP-C201 (2002) model some plate samples are not applicable because their predicted axial load carrying capacities are zero, which will be explained later. Due to the limited space, only the number of plate samples, N, used for DNV-RP-C201 (2002) model, which is different from other models, is tabulated in Table 3-1. A comparison between the predicted capacities and the FEA results is presented graphically in Figure 3-2. The points above the diagonal solid line represent the stiffened plates with the predicted capacity less than the FEA results (conservative prediction).

The 720 samples summarized in Table 3-1 and presented in Figure 3-2 all satisfy the requirements for stiffener web slenderness ratio (Equation [3-11]) and flange slenderness ratio (Equation [3-12]). Of these 720 samples, only 350 meet the moment of inertia requirement (Equation [3-10]). These are shown in Table 3-2 and Figure 3-3. If the area requirement is further applied with the moment of inertia requirement, the numbers of valid samples reduces to 280, and they are shown in Table 3-3 and Figure 3-4.

An examination of Tables 3-1 through 3-3 and Figures 3-2 through 3-4 indicates that the three design guidelines need to improve their ability to predict the stiffened steel plate capacities. Before the data screening, the maximum means of FEA-to-predicted capacity ratio for one load case are 1.347, 6.352 and 2.130, for the API model (API, 2000), the DNV model (DNV, 2002) and the ABS model (2007), respectively. These mean values are much larger than that of model 1, a maximum mean value of 1.074. The overall mean values for these three models are also larger than that of model 1.

The overall mean value for the DNV model (DNV, 2002) is based on a total number of 648 samples (Table 3-1). As shown in Figure 3-2 (g), 72 data points are located on the y-axis. These points represent 72 samples with $\beta_9 = -0.4$, 0.2 or 0.4 that are predicted to fail in bending before the application of the axial load. The predicted axial load carrying capacity of these samples is therefore zero. After these data points were excluded, the number of overall samples is 648 as presented in Table 3-1. There are also some data points located very close to the y-axis, i.e. with low predicted capacity and thus large FEA-to-predicted capacity ratios. These data points, although included in calculation of the mean and COV values, result in the substantially large mean values for the DNV model (DNV, 2002) as shown in Table 3-1.

A similar sample point that is close to the y-axis is observed in Figure 3-2 (h) for the ABS model (ABS, 2007) at (0.004, 0.546). The FEA-to-predicted ratio of this data point is 126.9, virtually in the same sense as those points on the y-axis in Figure 3-2 (g) that would have infinite FEA-to-predicted ratios. If this point (0.004, 0.546) is removed, the mean and COV for the rest of the overall set (719 samples) for the ABS model (ABS, 2007) will be 1.043 and 0.376, respectively.

The COV values of the overall set for the three design guides are larger than that of model 1 as well (Table 3-1). The COV values for the DNV model (DNV, 2002) and the ABS model (ABS, 2007) are even one order higher than that of model 1. Scatter of the data set for DNV model (DNV, 2002) is especially visually obvious as shown in Figure 3-2 (g).

Screening of the data does not help for the API model (API, 2000) and the DNV model (DNV, 2002) (Tables 3-1 through 3-3). Data screening by the moment of inertia requirement (Equation [3-10]) adopted in the ABS guide (ABS, 2007) itself doesn’t help the performance of the ABS model (ABS, 2007) (Tables 3-1 and 3-2). Data screening by both Equation [3-10] and $\beta_5 \geq 0.15$, however, reduces the mean values of the ABS model (ABS, 2007) from 1.218 to 1.050 and COV from 3.865 to 0.211 (Tables 3-1 and 3-3). The ABS model (ABS, 2007) is still not as good as the performance of model 1 though.

An examination of Tables 3-1 through 3-3 and Figures 3-2 through 3-4 indicates that models 1 and 2 yield very similar performance, i.e. they show a mean FEA-to-predicted ratio very close to 1.0 and almost identical COV values. Although screening of the data did not change significantly the mean FEA-to-predicted ratio, it resulted in a significant reduction in COV value, with COV = 0.21 for the unscreened data and COV = 0.10 for the screened data. The small differences between models 1 and 2 indicate that the Faulkner effective width formula or the Winter effective width formula yield similar predicted capacities.

Models 3 through 5 also have similar results to models 1 and 2 as shown in Figures 3-2 through 3-4, while the data points for models 4 and 5 are slightly skewed to the low side of the diagonal line. The data in Tables 3-1 through 3-3 indicate that models 3 through 5 have mean FEA-to-predicted values very slightly lower than the value for model 1 but they generally have lower COV values compared to model 1. The maximum difference between the means of model 1 and models 3 to 5 is 0.088, while the maximum difference between the COVs is 0.038. Model 1 certainly does a slightly better job in terms of the mean FEA-to-predicted ratio. Specifically for the 280 valid samples in Table 3-3, the mean value of the overall dataset is 1.000 and the mean values for various β_9 are in a narrow range of 0.983 to 1.014. Model 1 is slightly more scattered than models 3 through 5. The maximum COV of model 1 is 0.106 in Table 3-3, those of models 3 through 5 being 0.097, 0.094, and 0.094, respectively. However, the COV values for model 1 show more consistency with the maximum COV difference of 0.006 (Table 3-3), while those of models 3 through 5 are 0.011, 0.023, and 0.024, respectively.

In general, models 1 through 5 show a better performance than models 6 through 8, the design guidelines. Although the differences between models 1 through 5 are small. models 1 and 2 have an advantage that the CSA column buckling curve (Equation [3-14]) adopted in models 1 and 2 is one continuous equation instead of a combination of discrete segments (Loov, 1996). This will be a useful feature in terms of simplicity in the reliability analysis that will be conducted in Chapter 4. Therefore, model 1 is selected for the proposed approach, i.e. the beam-column equation (Equation [3-13]), the effective plate width formula proposed by Faulkner (Equation [3-1]) and CSA column curve (Equation [3-14]) are selected for the prediction of stiffened steel plate capacity.

3.4.1 Effect of moment of inertia and area requirements for the stiffener

Comparisons of the FEA results and the predicted capacities using model 1 are shown in Figure 3-2 (a) for all the data without screening. Screening of the data in terms of stiffener stiffness and area ratio lead to Figures 3-3 (a) and 3-4 (a). The same pool of data is correspondingly presented in Figure 3-5 with the FEA-to-predicted capacity ratio plotted against the FEA capacity.

Before screening of the data, a large portion of points on the left of $P_c / P_y (FEA) = 0.4$ show considerable scatter, with a large number of data points showing FEA-to-predicted ratios lower than 0.8 or higher than 1.2 (Figure 3-5(a)). The minimum and maximum FEA-to-predicted ratios are 0.300 and 1.715, respectively. The data points with low $P_c / P_y (FEA)$ values are the “under-stiffened” panels as presented previously in section 3.3.3, which undergo large deflection before reaching the desired overall buckling capacity of the effective panel.

Applying the moment of inertia requirement (Equation [3-10]) eliminates most of the points that show large scatter and reduces the COV from 0.211 to 0.120 (see Figure 3-5). After screening based on both the moment of inertia requirement

(Equation [3-10]) and the area ratio requirement ($\beta_5 \geq 0.15$), the remaining 280 valid samples are mostly controlled with the FEA-to-predicted ratio between 0.8 and 1.2, Figure 3-5 (c). Although the moment of inertia requirement has done an excellent job in reducing the scatter, the application of the extra area requirement makes the performance slightly better. The mean of the overall dataset is 1.000 and in the range of 0.983 to 1.014 when grouping the data according to the applied bending moment. The COV reduces to 0.102 for the overall dataset and varies from 0.100 to 0.106 for the five datasets with varying levels of bending moment.

The large scatter of the 720 data points could potentially be accounted for by a lower resistance factor in the limit states design if the moment of inertia and area requirements were not applied. However, the stiffened plates of practical configurations (the 280 panels) would be penalized in order to balance the effects of the large scatter of the undesired panels (the 440 panels). Therefore, it is recommended to apply the moment of inertial and area requirements in practice for a more economic design.

It is believed that in design practice and lab experiments the specimens have been designed to make sufficient use of the material strength. In the work of Soares and Gordo (1997), 115 test results from various sources were collected and about 95% of these specimens were found to have their test capacities greater than 40% of the yield capacity. According to these results, the moment of inertia requirement (Equation [3-10]) and the area requirement ($\beta_5 \geq 0.15$) may be automatically satisfied in design even though they were not explicitly checked. Since assessment of design methods are usually based on a database of test results, the specimens in the database most likely have already satisfied the moment of inertia and area requirements. It is possibly for this reason that setting explicit stiffener requirements hasn’t raised much attention.

3.5 CONCLUSIONS

The design methods currently used for stiffened plates still need improvements in both behaviour understanding and capacity prediction. Design philosophies among those methods are also not consistent. This chapter proposes a comprehensive design approach for stiffened plates with longitudinal tee stiffeners based on the work of behaviour understanding in Chapter 2.

The failure modes considered in the proposed approach are plate buckling, overall buckling, plastic hinge instability, and stiffener tripping. The ultimate capacity of the stiffened plate is governed by overall buckling. Plate buckling may take place in the pre overall buckling period, and its effect is taken into account by using the effective cross-section instead of the full cross-section in the design equations. Plastic hinge instability and stiffener tripping may cause sudden capacity loss in the post overall buckling period. This severe consequence can be predicted and given a lower resistance factor in limit states design.

The proposed approach (model 1) uses the beam-column equation (Equation [3-13]) to evaluate the stiffened plate capacity, while the various parameters in Equation [3-13] are obtained using Faulkner plate width formula (Equation [3-1]) and CSA column buckling curve (Equation [3-14]). When plate induced overall buckling governs, the capacity has to be used in Equation [3-16] to calculate $(u_3/L)_H$. If this $(u_3/L)_H$ is less than 0.025, the plate induced overall buckling will progress into plastic hinge instability and a lower resistance factor than that for normal overall buckling should apply. When stiffener induced overall buckling governs, a sudden capacity loss due to plastic hinge instability and stiffener tripping is believed to always occur, and a lower resistance factor should apply.

Four requirements were presented to ensure the stiffened plates reach the desired capacity. The requirements of the web slenderness ratio ($\beta_2 \leq 1.5$) and flange slenderness ratio ($\beta_3 \leq 0.9$) were set to prevent local bucking in the stiffener before yielding. The moment of inertial requirement (Equation [3-10]) and the area requirement ($\beta_5 \geq 0.15$) were to warrant sufficient stiffening from the stiffener to the plate, i.e. to prevent “under-stiffened” configurations.

Five models of equation combinations and three current design guidelines for stiffened plates were assessed based on a database of 720 finite element analysis models. The proposed approach (model 1) shows advantage in both mean and COV of the FEA-to-predicted capacity ratios.

References:

American Association of State Highway Transportation Officials (AASHTO). (2007). *AASHTO LRFD bridge design specifications*, 4ed, Washington, D.C.

American Bureau of Shipping (ABS) (2004). Guide for buckling and ultimate strength assessment for offshore structures. Houston, Texas.

American Bureau of Shipping (ABS) (2007). Guide for buckling and ultimate strength assessment for offshore structures. Houston, Texas.

American Institute of Steel Construction (AISC) (2005), *ANSI/AISC 360-05: Specification for Structural Steel Buildings*, USA.

American Petroleum Institute (API) (2000). *API Bulletin 2V: Design of flat plate structures*, Washington, D. C., USA.

Ayrton, W.E., and Perry, J.(1886)."On struts." *The Engineer*, 62, 464-513.

Balaz, I., and Murray, N. W.(1992)."A Comparison of Some Design Rules with Results from Tests on Longitudinally Stiffened Deck Plates of Box-Girders." *Journal of Constructional Steel Research*, 23 (1), 31–54.

Canadian Standards Association (CSA). (2002). CSA-S136-01: North American Specification for the Design of Cold-Formed Steel Structural Members, Ontario, Canada.

Canadian Standards Association (CSA). (2006a). *CAN/CSA-S6-06: Canadian Highway Bridge Design Code*, Toronto, Ontario, Canada.

Canadian Standards Association (CSA). (2006b). *CAN/CSA-S6.1-06: Commentary on CAN/CSA-S6-06, Canadian Highway Bridge Design Code*, Toronto, Ontario, Canada. 452-453

Canadian Standards Association (CSA). (2009). *CSA-S16-09: Design of Steel Structures*, Toronto, Ontario, Canada.

Choi, B.H.(2002). “Design requirements for longitudinal stiffeners for horizontally curved box girders.” PhD thesis, Auburn University, Auburn, Ala., USA.

Culver, C. G. (1972). Instability of Horizontally Curved Members: Design Recommendations for Curved Highway Bridges, Department of Civil and Engineering, Carnegie-Mellon University, Pennsylvania, USA.

Det Norske Veritas (DNV) (1995). Classification Notes No. 30.1: Buckling Strength Analysis, Norway.

Det Norske Veritas (DNV) (2002). Recommended Practice DNV-RP-C201: Buckling Strength of Plated Structures, Norway.

European Committee of Standardization (CEN) (2006). “Design of steel structures.” *EN 1993-1-5: Plated structural elements*, London.

Faulkner, D. (1975). "A review of effective plating for use in the analysis of stiffened plating in bending and compression" *Journal of Ship Research*, 19 (1), 1–17.

Ghavami, K.(1994)."Experimental Study of Stiffened Plates in Compression up to Collapse." *Journal of Construction Steel Research*, 28 (2), 197–221.

Grondin, G. Y., Chen, Q., Elwi, A. E., Cheng, J. J. R. (1998). "Stiffened plates under compression and bending." *Journal of Constructional Steel Research*, 45 (2), 125–148.

Kennedy, D.J.L and Gad Aly, M. (1980), “Limit states design of steel structures – performance factors.” *Canadian Journal of Civil Engineering*, 7 (1), 45-77.

Loov, R. (1996), “A simple equation for axially loaded steel column design curves.” *Canadian Journal of Civil Engineering*, 23 (1), 272-276.

Mattock,A.H., *et al.* (1967), “Commentary on Criteria for Design of Steel-Concrete Composite Box Girder Highway Bridges.” Report of Committee

Ministry of Transportation and Communications (1983), *Ontario Highway Bridge Design Code OHBDC*, Ontario

Sheikh, I. A., Grondin, G. Y., Elwi, A. E. (2002). "Stiffened steel plates under uniaxial compression" *Journal of Constructional Steel Research*, 58 (5), 1061-1080.

Sheikh, I. A., Elwi, A. E., Grondin, G. Y. (2003). "Stiffened steel plates under combined compression and bending." *Journal of Constructional Steel Research*, 59 (7), 911- 930.

Smith, C. S., Anderson, N., Chapman, J. C., Davidson, P. C., Dowling, P. J. (1992). "Strength of stiffened plating under combined compression and lateral pressure." *Transactions of the royal institute of naval architects*, 134, 131-147.

Soares, C.G., and Gordo, J.M.(1997)."Design methods for stiffened plates under predominantly uniaxial compression." *Marine Structures*, 10, 465–497.

Soreide, T. H.(1981). Ultimate load analysis of marine structures, 2.54-2.69, Tapir Press, Trondheim. Norway.

Sun, H. and Wang, X.(2005)."Buckling and Ultimate Strength Assessment of FPSO Structures." *2005 SNAME Marine Technology Conference & Expo*., Oct. 2005, Houston, Texas.

Timoshenko, S.P., and Gere, J.M.(1961), Theory of elastic stability, McGraw-Hill, 2ed, New York.

Yoo, C. H., Choi, B.H., and Ford, E.M. (2001), "Stiffness Requirements for Longitudinal Stiffened Box-Girder Flanges." ASCE Journal of Structural Engnieering, 127 (6), 705-711.

Wang, E. C. L., Grondin, G. Y. and Elwi, A. E. (2006), "Interaction Buckling Failure of Stiffened Steel Plates", *Structural Engineering Report No. 264*, Department of Civil and Environmental Engineering, University of Alberta, Canada.

Table 3-1 Mean and COV FEA-to-predicted capacity ratios for various models (Before screening with Eq. [3-10] and $\beta_5 \geq 0.15$)

	Model 1		Model 2		Model 3		Model 4		Model 5		API (2000)			DNV (2002)		ABS (2007)	
β_9	Mean	COV	Mean	COV	Mean	COV	Mean	COV	Mean	COV	Mean	COV	N	Mean	COV	Mean	COV
–0.4	0.876	0.318	0.868	0.316	0.863	0.315	0.824	0.326	0.822	0.326	1.347	0.286	128	1.669	0.564	0.791	0.410
–0.4	1.013	0.150	1.004	0.149	0.996	0.132	0.945	0.131	0.942	0.130	1.230	0.104	144	1.322	0.339	0.934	0.244
0	1.074	0.126	1.064	0.127	1.055	0.112	0.990	0.088	0.986	0.088	1.107	0.090	144	1.289	0.331	1.038	0.213
0.2	1.063	0.159	1.062	0.159	1.044	0.154	0.984	0.141	0.981	0.142	1.047	0.169	136	3.525	2.516	1.197	0.214
0.4	0.916	0.216	0.913	0.220	0.904	0.217	0.858	0.221	0.855	0.222	0.861	0.223	96	6.352	4.990	2.130	4.926
Ove-rall	0.988	0.211	0.982	0.211	0.972	0.205	0.920	0.201	0.917	0.202	1.118	0.246	648	2.591	4.994	1.218	3.865

Notes: The number of samples (N) is 144 for each load case and 720 overall, unless other wise noticed.

Table 3-2 Mean and COV of FEA-to-predicted capacity ratios for various models (After screening with Eq. [3-10])

	Model 1		Model 2		Model 3		Model 4		Model 5		API (2000)			DNV (2002)		ABS (2007)	
β_9	Mean	COV	Mean	COV	Mean	COV	Mean	COV	Mean	COV	Mean	COV	N	Mean	COV	Mean	COV
–0.4	0.999	0.135	0.988	0.136	0.993	0.137	0.966	0.141	0.964	0.142	1.560	0.100	66	1.092	0.391	0.991	0.231
–0.4	0.999	0.102	0.989	0.105	0.991	0.094	0.963	0.089	0.961	0.089	1.241	0.076	70	1.009	0.217	1.030	0.236
0	0.981	0.098	0.972	0.103	0.972	0.083	0.943	0.071	0.941	0.071	1.112	0.104	70	1.012	0.177	1.074	0.278
0.2	1.002	0.124	1.002	0.124	0.988	0.101	0.952	0.086	0.949	0.085	1.082	0.164	70	1.646	0.651	1.235	0.243
0.4	0.961	0.134	0.958	0.137	0.952	0.130	0.920	0.133	0.918	0.133	0.928	0.137	62	7.986	4.939	3.111	4.832
Ove-rall	0.988	0.120	0.982	0.122	0.979	0.111	0.949	0.108	0.947	0.108	1.185	0.213	338	2.438	6.972	1.488	4.527

Notes: The number of samples (N) is 70 for each load case and 350 overall, unless other wise noticed.

Table 3-3 Mean and COV of FEA-to-predicted capacity ratios for various models (After screening with Eq. [3-10] and $\beta_5 \geq 0.15$)

	Model 1		Model 2		Model 3		Model 4		Model 5		API (2000)			DNV (2002)		ABS (2007)	
β_9	Mean	COV	Mean	COV	Mean	COV	Mean	COV	Mean	COV	Mean	COV	N	Mean	COV	Mean	COV
–0.4	1.014	0.102	1.003	0.104	1.008	0.097	0.982	0.094	0.980	0.094	1.572	0.076	56	1.085	0.386	0.948	0.185
–0.4	1.002	0.102	0.992	0.107	0.995	0.089	0.969	0.078	0.967	0.077	1.242	0.082	56	1.015	0.227	0.959	0.173
0	0.983	0.103	0.973	0.109	0.975	0.086	0.948	0.071	0.946	0.070	1.110	0.114	56	1.019	0.190	0.984	0.187
0.2	1.000	0.106	1.002	0.105	0.989	0.088	0.957	0.079	0.955	0.078	1.087	0.164	56	1.595	0.681	1.158	0.155
0.4	0.999	0.100	0.997	0.102	0.991	0.092	0.959	0.091	0.957	0.091	0.968	0.095	53	8.438	5.046	1.199	0.215
Ove-rall	1.000	0.102	0.993	0.105	0.992	0.090	0.963	0.083	0.961	0.083	1.196	0.203	277	2.567	7.288	1.050	0.211

Notes: The number of samples (N) is 56 for each load case and 280 overall, unless other wise noticed.

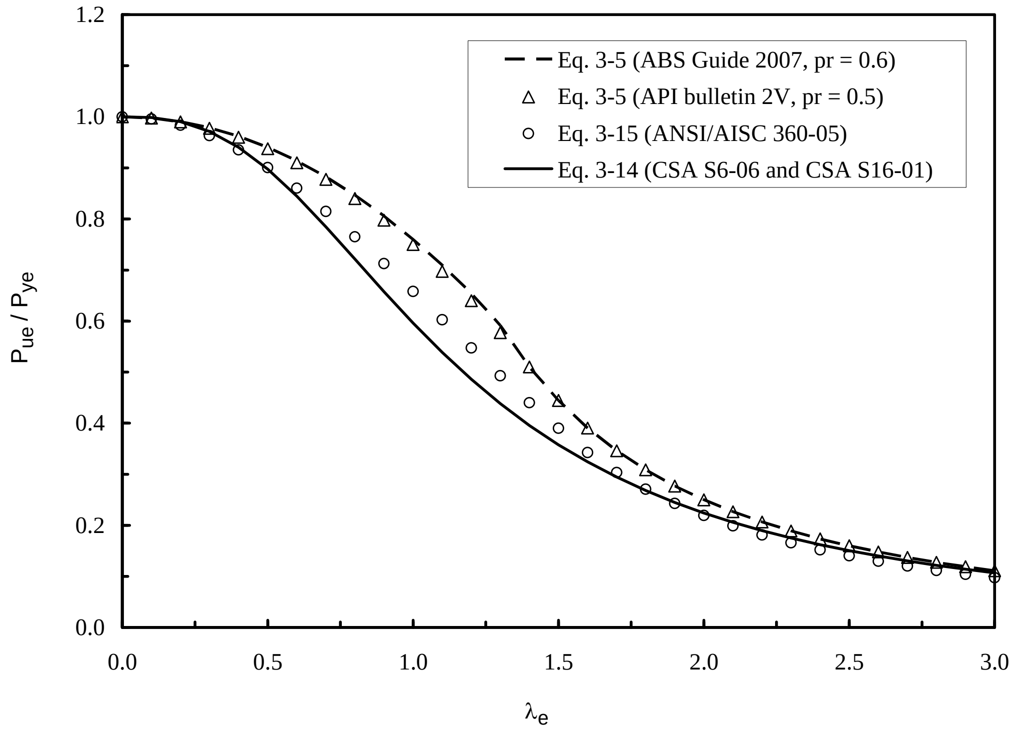

Figure 3-1 Comparison of the column curves

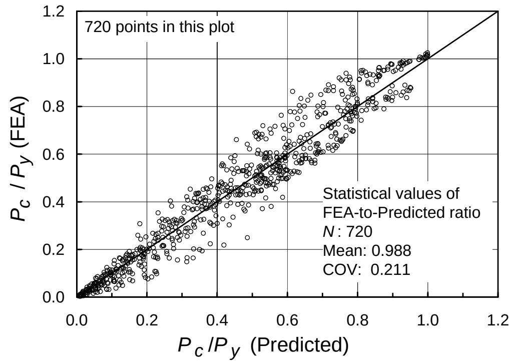

(a) Model 1

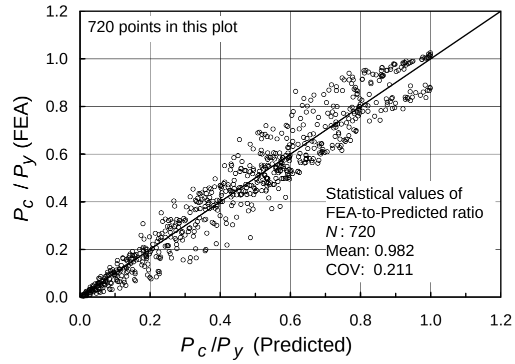

(b) Model 2

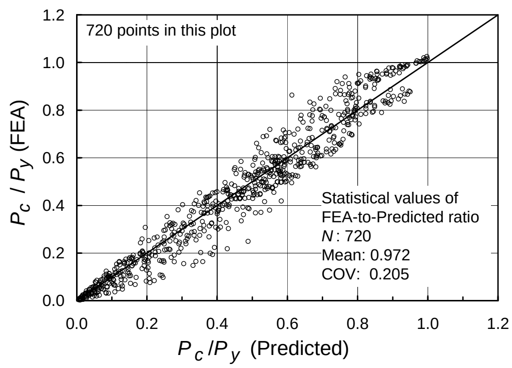

(c) Model 3

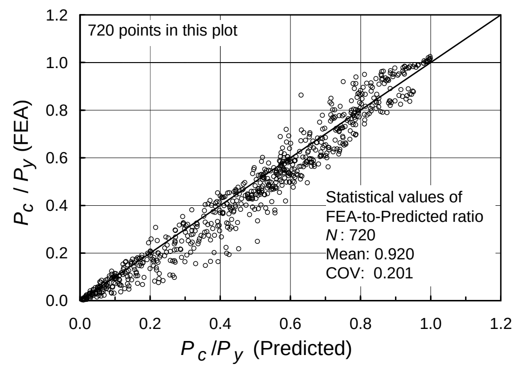

(d) Model 4

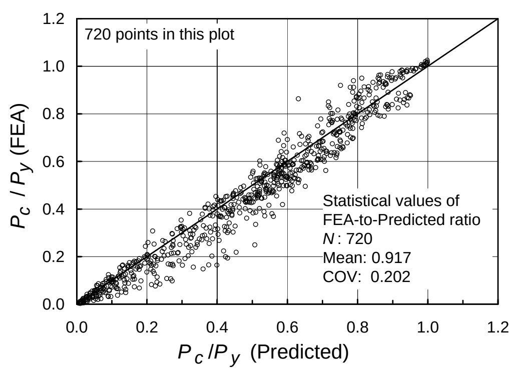

(e) Model 5

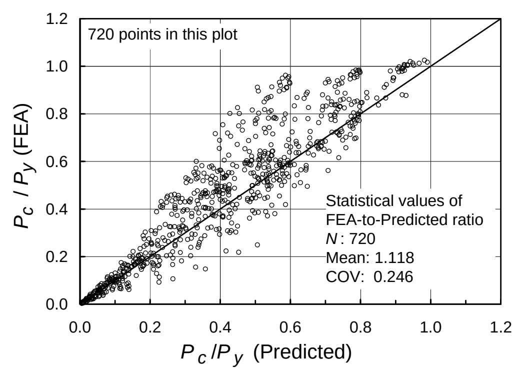

(f) API (2000)

Figure 3-2 Comparison between FEA results and capacities predicted using various design models (Before screening with Eq. [3-10] and $\beta_5 \geq 0.15$)

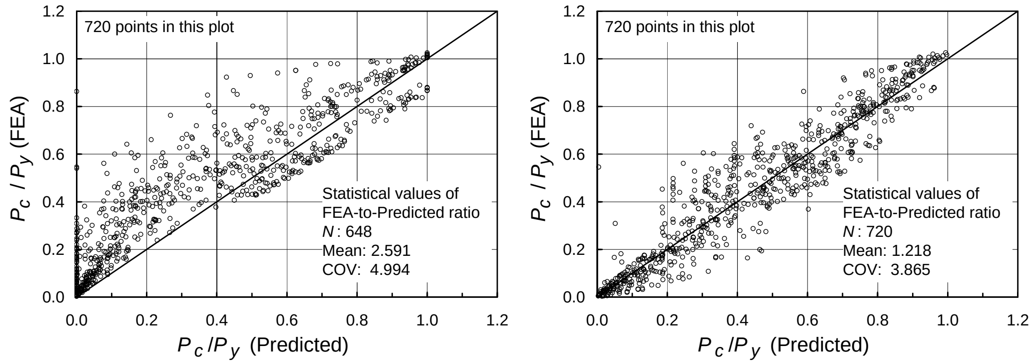

(g) DNV (2002) (h) ABS (2007)

Figure 3-2 Comparison between FEA results and capacities predicted using various design models (Before screening with Eq. [3-10] and $\beta_5 \geq 0.15$) (continued)

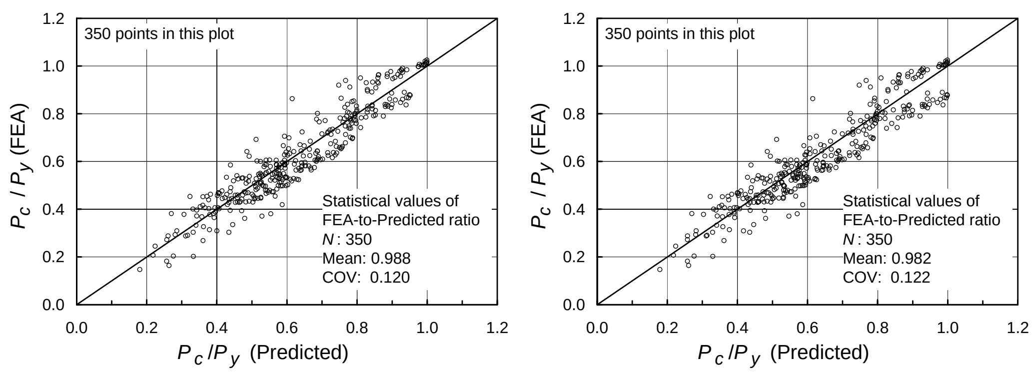

(a) Model 1 (b) Model 2

Figure 3-3 Comparison between FEA results and capacities predicted using various design models (After screening with Eq. [3-10])

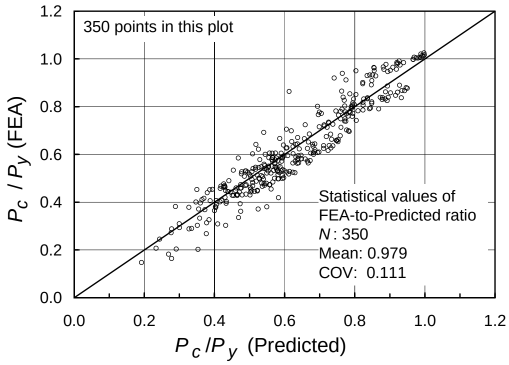

(c) Model 3

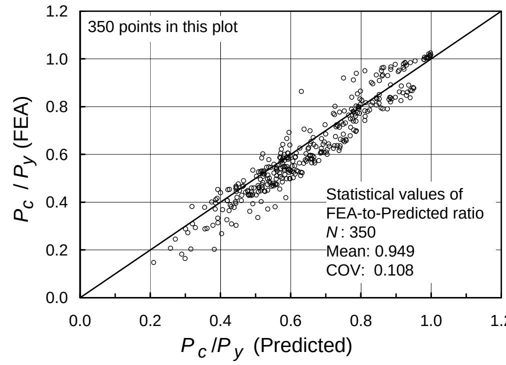

(b) Model 4

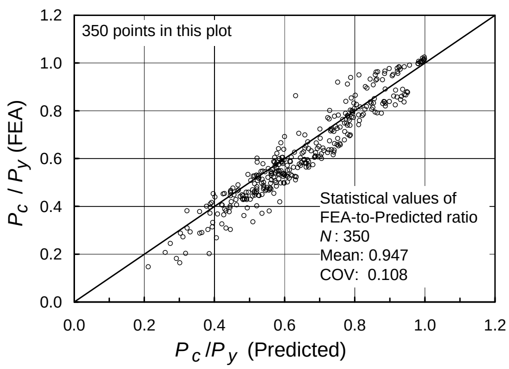

(e) Model 5

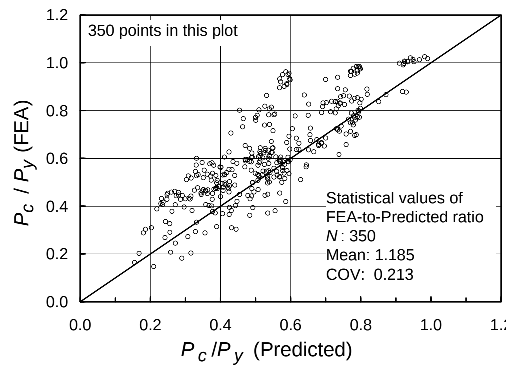

(f) API (2000)

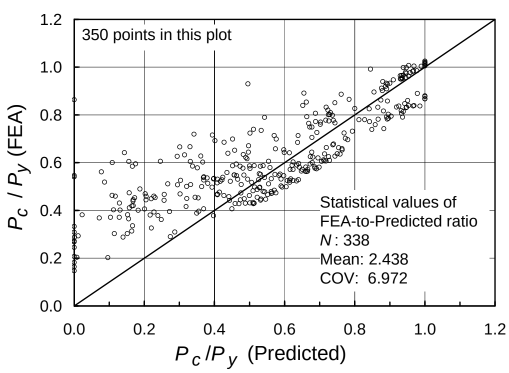

(g) DNV (2002)

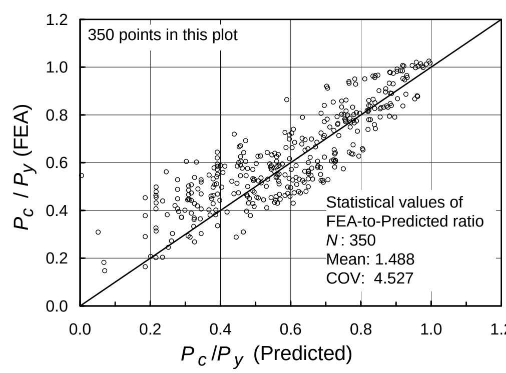

(h) ABS (2007)

Figure 3-3 Comparison between FEA results and capacities predicted using various design models (After screening with Eq. [3-10]) (continued)

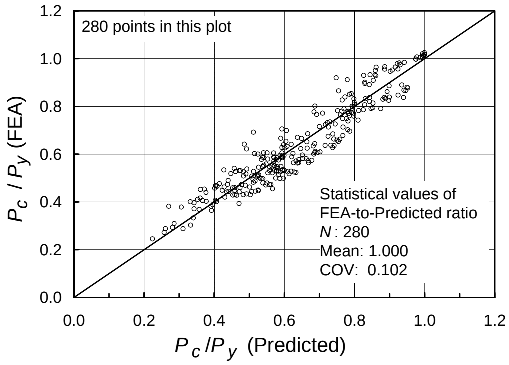

(a) Model 1

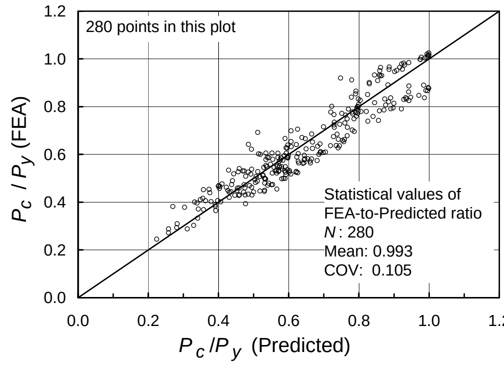

(b) Model 2

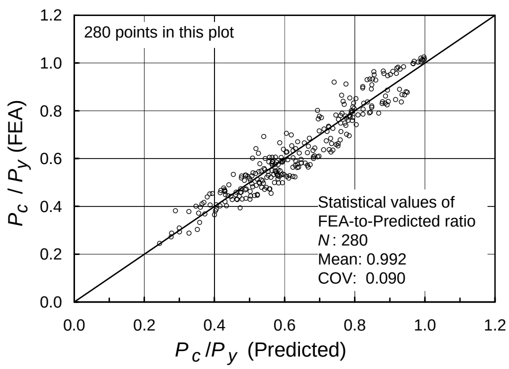

(c) Model 3

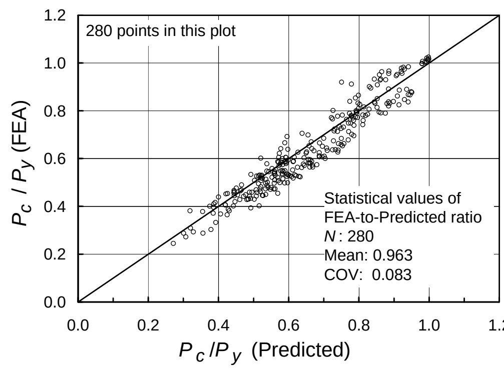

(d) Model 4

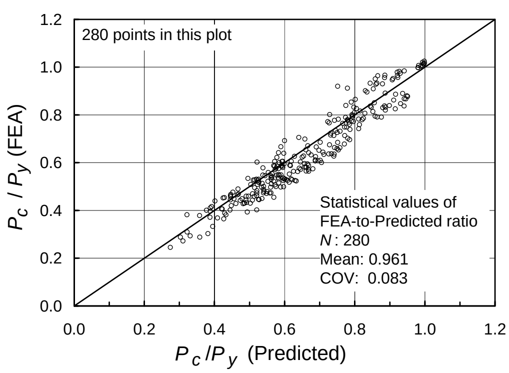

(e) Model 5

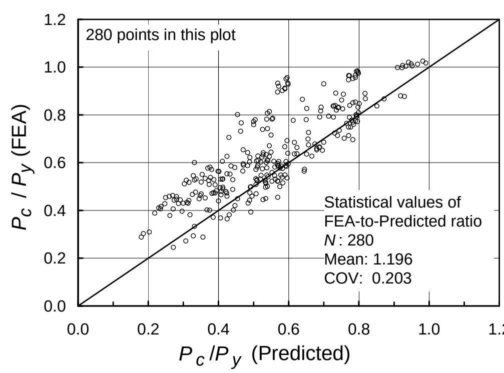

(f) API (2000)

Figure 3-4 Comparison between FEA results and capacities predicted using various design models (After screening with Eq. [3-10] and $\beta_5 \geq 0.15$)

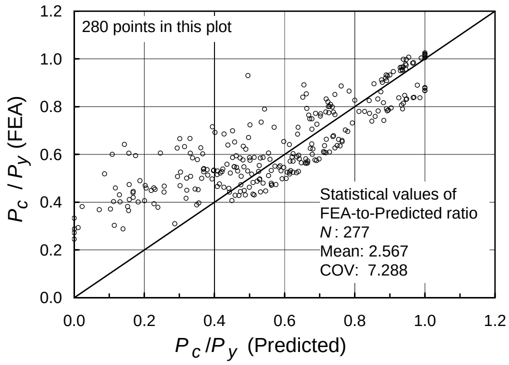

(g) DNV (2002)

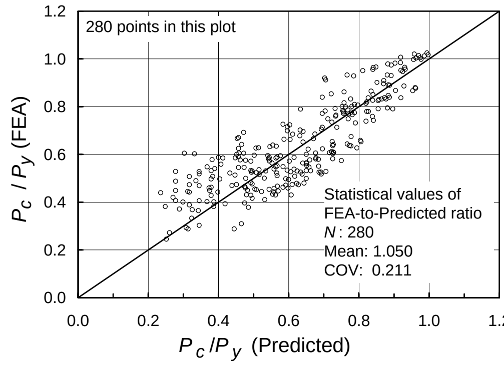

(h) ABS (2007)

Figure 3-4 Comparison between FEA results and capacities predicted using various design models (After screening with Eq. [3-10] and $\beta_5 \geq 0.15$)

(continued)

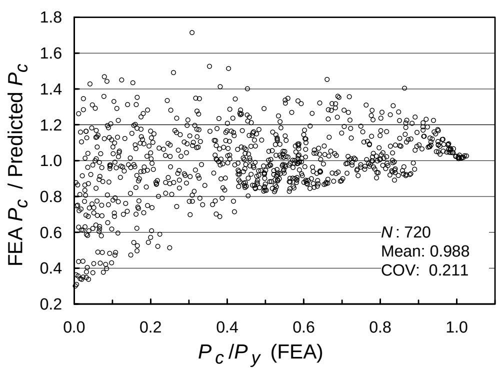

(a) Before screening

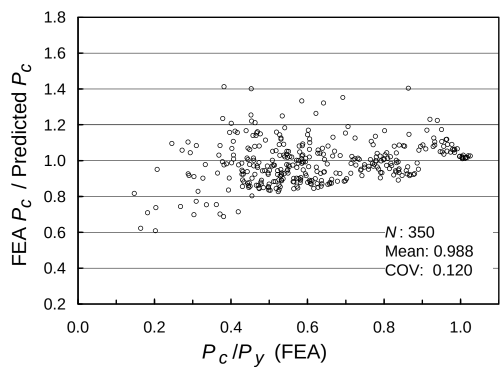

(b) After screening with Eq. [3-10]

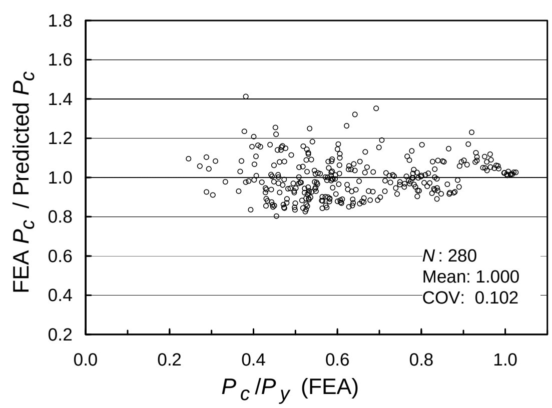

(c) After screening with Eq. [3-10] and $\beta_5 \geq 0.15$

Figure 3-5 Strength prediction using the proposed approach (Model 1)

CHAPTER 4

RESISTANCE FACTORS FOR STIFFENED STEEL PLATES UNDER COMPRESSION AND BENDING

4.1 INTRODUCTION

The actual capacity of a structural member cannot be described by a deterministic value. Uncertainties about structural components usually originate from three sources: member sizes, material properties, and the analytical model. Owing to the variability of these factors, the value of the actual capacity differs from the nominal one; the design capacity.

A method to predict the nominal capacity of steel plates stiffened by longitudinal tee stiffeners was presented in Chapter 3. This chapter presents the results of a reliability analysis conducted to assess the suitability of these design equations and determine an appropriate resistance factor for the design equations. The reliability analysis consists of the following steps:

(1) Select the design equations to be evaluated;

(2) Identify the basic variables that govern the design strength;

(3) Collect raw data to formulate probabilistic distributions for each basic variable;

(4) For each nominal panel previously analyzed using the non-linear finite element analysis procedure presented in Chapter 3, run Monte Carlo simulations to determine the variability of the predicted resistance due to the variability in material and geometric properties;

(5) For each nominal panel, determine the mean and C.O.V. for the professional factor (ratio of the actual capacity to the capacity predicted using the design equation to be evaluated);

(6) For each nominal panel, calculate the resistance factor for desired target safety index, β, using the procedure outlined in section 4.2.

(7) Select the appropriate resistance factor applicable to limit states design based on the values obtained from all panels.

4.2 METHODOLOGY FOR THE DETERMINATION OF RESISTANCE FACTORS

The resistance factor depends on the variability of both resistance and loads, as well as the selected target safety index, which is in turn dependent on the desired probability of failure. It can be obtained as (Kennedy and Baker, 1984; Schmidt and Bartlett, 2002b):

$$\phi = \rho_R \frac{\sum \alpha_i S_i}{\bar{S}} \exp\left(-\beta\sqrt{V_R^2 + V_S^2}\right) \qquad [4\text{-}1]$$

where ρ_R is the bias coefficient for the resistance (i.e. the ratio of the mean resistance to the nominal resistance), S_i is one nominal load, α_i is the associated load factor, $\bar{S}$ is the mean of the total load, β is the target safety index, and V_R and V_S are the coefficients of variation (COV) associated with ρ_R and $\bar{S}$, respectively. Equation [4-1] is applicable when the load statistics are known, otherwise a simplified equation should apply as (Galambos and Ravindra, 1973; Fisher *et al*., 1978; Grondin *et al.*, 2007):

$$\phi = C\rho_R \exp\left(-\beta\alpha_R V_R\right) \qquad [4\text{-}2]$$

where α_R is a separation variable used to separate the effect of loading and resistance on the probability of failure so that the resistance factor can be calculated using resistance statistics only. The value of α_R = 0.55 was proposed by Galambos and Ravindra (1973) as a value that provided a reasonable approximation over a wide range of load effects for steel buildings (the dead to live load ratio ranging from 0.1 to 4) and a safety index β = 3.0, which represents a probability of failure of 1.35×10^{-3} over the life of the structure. A correction factor C is applied to make Equation [4-2] applicable to different values of safety index (Fisher *et al*., 1978). For a range $1 \leq \beta \leq 5$ Grondin *et al.* (2007) derived the following expression for C based on the procedure outlined in Fisher *et al*. (1978):

$$C = 0.008\beta^2 - 0.1584\beta + 1.4056 \qquad [4\text{-}3]$$

Since the load variability on stiffened steel plates is not available at this point, Equation [4-1] cannot be used and the simplified equation, Equation [4-2], based on dead to live load ratio ranging from 1 to 4 for steel buildings (Galambos and Ravindra, 1973), will be adopted in this research in determining the resistance factors.

The basic form of the resistance parameters (ρ_R and V_R) is well established (Kennedy and Gad Aly, 1980; Ravindra and Galambos, 1978; MacGregor, 1976) as Equations [4-4] and [4-5], respectively:

$$\rho_R = \rho_M \rho_G \rho_P \qquad [4\text{-}4]$$

where ρ_M , ρ_G , ρ_P are bias coefficients for the material, geometry and professional factors, respectively. Since ρ_M , ρ_G , ρ_P are assumed to be independent quantities, the COV for the resistance is:

$$V_R = \sqrt{V_M^2 + V_G^2 + V_P^2} \qquad [4\text{-}5]$$

where V_M , V_G , and V_P are the COV associated with ρ_M , ρ_G , ρ_P , respectively.

The material and geometric factors recognize that the actual material properties and geometric properties are different from their nominal values. When the design equation is simply the product of a material property and a geometric property, such as the plastic moment capacity, the associated bias coefficient and COV are directly obtained from the known distribution of the calculated variables such as yield strength and plastic section modulus. As the complexity of the problem increases, such as when calculating the inelastic column buckling capacity, the procedure must be simplified. The simplification makes the statistical analysis only approximate when the distributions of various basic variables need to be combined. When the resistance expressions, such as the ones introduced later in this chapter, are too complex to have ρ_M and ρ_G clearly defined and calculated, the Monte Carlo simulation technique provides a good approach (Kennedy and Baker, 1984; Melchers, 1999).

The professional factors reflect the ability of the design equation to predict the actual capacity of the structural component. Although the results of a reliable analytical model could be assumed as an accurate simulation of the actual capacity, in this work test results will be considered as the actual capacity. Therefore, this chapter evaluates the ability of the proposed design equations to predict the finite element analysis results and the ability of the finite element analysis to predict the actual test results. The bias coefficient for the professional factor, ρ_P, and the associated COV, V_P, can be determined as follows:

$$\rho_P = \rho_{P1}\rho_{P2} = \left(mean\ of\ \frac{R_{FEA}}{R_n} \right)\left(mean\ of\ \frac{R_{Test}}{R_{FEA}} \right) \quad [4\text{-}6]$$

$$V_P = \sqrt{V_{P1}^2 + V_{P2}^2} \quad [4\text{-}7]$$

where ρ_{P1} and V_{P1} are the mean and COV for the ratio of the FEA results to the predicted capacities using the design equation; ρ_{P2} and V_{P2} are the mean and COV of the ratio of the test results to FEA results; R_{FEA} is the capacity predicted using the finite element analysis; R_n is the nominal resistance predicted using design equations; R_{Test} is the actual resistance from test results.

Another factor, the discretization factor, was also proposed as one of the parameters to include in the reliability analysis (Schmidt and Bartlett, 2002b; Kennedy and Baker, 1984). The discretization factor accounts for the fact that the capacity provided is usually larger than that required because the available member sizes are of discrete and limited sizes. The discretization factor is not considered in the present study for two reasons: (1) there are variables in stiffened plate design (plate width, and stiffener size for welded stiffeners) that permit asbuilt structures with a capacity very close to the required capacity; (2) since the design capacity is usually larger than required, ignoring the discretization factor will lead to a conservative estimate of the resistance factor.

4.3 DESIGN EQUATIONS

The design equations proposed in chapter 3 are used to calculate the nominal resistance, R_n, of stiffened plates. This approach uses the Faulkner formula (Equation [4-8]) for the effective plate width.

$$\begin{cases} \dfrac{b_e}{b} = 1 & if\ \beta_1 \le 1 \\ \dfrac{b_e}{b} = \dfrac{2}{\beta_1} - \dfrac{1}{\beta_1^{\,2}} & if\ \beta_1 > 1 \end{cases} \qquad [4\text{-}8]$$

where b_e is the effective plate width; b is the plate width (stiffener spacing); $\beta_1 = b/t\sqrt{F_{yp}/E}$ is the plate slenderness ratio; t is the plate thickness; F_{yp} is the plate yield strength; and E is the elastic modulus. The capacity of the stiffened panel is obtained by treating a single stiffener and the tributary plate width as a beam-column. The column slenderness ratio of the effective panel is defined as:

$$\lambda_e = \sqrt{\frac{F_y}{F_{Ee}}} = \frac{KL}{r_e}\sqrt{\frac{F_y}{\pi^2 E}} \qquad [4\text{-}9]$$

where F_{Ee} is the elastic buckling strength of the effective panel; F_y is the yield strength of the stiffened panel; L is the length; K *is* the effective length factor; and r_e is the radius of gyration of the effective cross-section about the centroidal axis parallel to the plate. Using the column equation presented in CSA-S16-09 (CSA, 2009), the overall buckling capacity of the effective panel, P_{ue}, is:

$$\frac{P_{ue}}{P_{ye}} = \left(1 + \lambda_e^{\,2.68}\right)^{-1/1.34} \qquad [4\text{-}10]$$

where P_{ye} is the yield strength of the effective cross-section. When the panel is subjected to combined axial compression and end moments, the following interaction equations are used:

$$\frac{P_c}{P_{ue}} + \frac{1}{1 - P_c / P_{Ee}} \frac{P_c e - M_a}{M_{ye,p}} = 1 \quad if\ P_c e - M_a \geq 0 \qquad [4\text{-}11a]$$

$$\frac{P_c}{P_{ue}} + \frac{1}{1 - P_c / P_{Ee}} \frac{M_a - P_c e}{M_{pe}} = 1 \quad if\ P_c e - M_a < 0 \qquad [4\text{-}11b]$$

where P_c is the stiffened plate axial load resistance; e is the distance between the centres of gravity of the effective cross-section and the full cross-section; M_a is the value of the applied moment (taken as positive when placing the stiffener flange in flexural compression); $M_{ye,p}$ is the yield moment of the effective cross-section calculated with respect to the plate outer surface; and M_{pe} is the plastic moment capacity of the effective cross-section. The axial load resistance, P_c, obtained from Equation [4-11] represents the nominal resistance R_n in the reliability analysis. The minimum resistance calculated from Equations [4-11a] and [4-11b] determines whether the failure is a plate induced mode (Equation [4-11a]) or stiffener induced mode (Equation [4-11b]).

The parameters required to calculate P_c using Equation [4-11] are P_{ue}, P_{Ee}, e, $M_{ye,p}$, M_{pe}, and M_a. M_a is a deterministic parameter when the load is given. Except for M_a, all the other parameters can be derived based on basic cross-section, length and material parameters: plate width (b), plate thickness (t), stiffener web height (h_w), stiffener web thickness (t_w), stiffener flange width (b_f), stiffener flange thickness (t_f), panel length (L), yield strength (F_y), and modulus of elasticity (E). These basic parameters will be the input variables in the Monte Carlo simulations performed in the present study.

An equation was proposed in Chapter 2 to determine whether the panel will experience a stable or unstable post-buckling behaviour. The unstable behaviour was found to be caused by the formation of a plastic hinge. Stiffened plates that fail by the formation of a plastic hinge display a rapid load drop after the formation of the plastic hinge. For all the stiffened plates with the wide range of tee stiffener sizes investigated in this study, which is believed to cover the full range of practical sizes, stiffener tripping was observed not to govern the axial load capacity but affects the post-buckling range, as discussed in Chapter 2. Although the post-buckling behaviour does not affect the axial load resistance of stiffened steel plates, it must be considered in the selection of the resistance factor. Plates that display a stable post-buckling behaviour such as observed in plate induced overall buckling can be designed with a lower safety index (higher probability of failure and higher resistance factor) than plates that display an unstable failure mode.

As presented in Chapter 3, the stiffeners were proportioned to prevent local buckling of the web and the flange before the capacity expressed by Equation [4-11] is reached.

4.4 DATA COLLECTION: VARIABILITY OF BASIC VARIABLES

The variability of resistance of stiffened steel plates comes from three sources: geometry, material, and analysis. A compilation of probabilistic data for calculated geometric properties (such as area and moment of inertia) and measurable (basic) geometric dimensions (such as plate thickness and web height) are available in the literature (Hess *et al.*, 1998; Schmidt and Bartlett, 2002a). The variability of the calculated geometric properties depends on the variability of the basic geometric variables. Therefore, the Monte Carlo simulation technique requires only the distributions of the basic geometric dimensions. For material properties, only the distributions of yield strength and modulus of elasticity are needed in the Monte Carlo simulations.

Hess *et al.* (1998) compiled a database of geometric and material data for stiffened plates used in ship structures. The part of this data that is relevant to this work is summarized in Table 4-1, where the statistics are presented in terms of the bias coefficient (i.e. ratio of the measured to the nominal value) for the variables. The plate width (stiffener spacing) and panel length are also included in Table 4-1, although they have usually been assumed deterministic in most research (Schmidt and Bartlett, 2002a; Hess *et al*., 1998). The plate and stiffeners are assumed to have identical material properties to simplify the analysis.

For the variables listed in Table 4-1 that follow a lognormal distribution, their mean and standard deviation have to be transformed to those of their natural logarithm for the subsequent operations in the Monte Carlo simulations. The following equations are used for the transformation (Melchers, 1999), and the results are presented in Table 4-2.

$$\sigma_{\ln x} = \sqrt{\ln(V_x{}^2 + 1)} \qquad [4\text{-}12]$$

$$\overline{\ln x} = \ln \bar{x} - \frac{\sigma_{\ln x}{}^2}{2} \qquad [4\text{-}13]$$

where x is a variable; $\sigma_{\ln x}$ is the standard deviation of $\ln x$; V_x is the COV of x; $\overline{\ln x}$ is the mean of $\ln x$; and $\bar{x}$ is the mean value of x.

The variability of initial imperfections and residual stresses is another source of uncertainty but difficult to quantify. Four half sine waves along the length of the stiffened plate, one half sine wave across the width and a magnitude representing the average plate imperfections of actual stiffened plates were used for initial imperfections in the finite element model as presented in Chapter 2. The selected distribution of the initial imperfections was demonstrated to be a conservative estimate for the actual imperfection of stiffened plates (Grondin, *et al*., 1999). As presented in Chapter 2, the selected distribution of the residual stresses used in the finite element model is representative of the actual residual stresses in stiffened plates and the selected magnitude in the model is a conservative estimate of the actual values. Since the initial imperfections and the residual stresses used in the finite element model in this research were both based on conservative estimates, the mean of the variability of the initial imperfections and the residual stresses will be assumed to be one and the corresponding COV to be zero.

4.5 MONTE CARLO SIMULATION

4.5.1 General

The Monte Carlo simulation provides an approach to derive the probability density function of a desired variable through a large number of simulated experiments (Melchers, 1999). By injecting into the design equation one random value of each input variable based on its distribution, one sample of the stiffened plate resistance is obtained. This process is repeated until the number of plate resistance values is sufficiently large to be representative of the population. Let's consider, for example, a generic problem where the variable Y is a function of basic variables (x_1, x_2, x_3, etc.), each with known statistical distributions. As demonstrated in Figure 4-1, one value of each x_i is generated randomly according to its distribution and is then used in the mathematical model describing the value of Y. If this procedure is repeated a large number of times, the statistical distribution of Y will eventually be revealed.

Few variables in structural engineering follow a uniform distribution[1] within a specified range. Therefore, an indirect method has to be used to generate random values for each variable x_i as demonstrated in Figure 4-2. The process is to generate a random number between 0 and 1, which is then used to obtain a value of x_i using its cumulative density function (CDF). A restriction is applied to exclude negative or zero sample values of the basic variables. Although negative or zero values are not realistic for member sizes and material properties, their

[1] A uniform distribution is a distribution where each value within a certain range has the same probability of occurrence.

probability of occurrence is not zero. For this reason, the imposed restriction is required.

In order to ensure the quality of the data set so that it is representative of the population, a sufficiently large number of data points must be sampled. Mirza and MacGregor (1982) used Monte Carlo simulations for reinforced concrete members under different load combinations and generated 500 to 5000 random data points for each nominal member. Grant *et al.* (1978) also used this method for concrete columns under eccentric loading and used 250 random columns for each nominal one. Melchers (1999) recommended a method to control the quality of the data by plotting the mean and coefficient of variation of the output variable against the number of samples. This provides a direct monitoring of the rate and accuracy of convergence of the statistical parameter.

4.5.2 Monte Carlo simulation Procedure

The Monte Carlo simulation method is adopted in the present work to derive the statistical parameters of the distribution of stiffened plate resistance, reflecting the uncertainties of the material and geometric properties. Since the strength Equation [4-11] is too complex to separate the material and geometric components, it is more efficient to treat their mutual influence as a whole. Correspondingly, the fundamental Equations [4-4] and [4-5] are converted to Equations [4-14] and [4-15] as follows:

$$\rho_R = \rho_{MG}\rho_P \qquad [4\text{-}14]$$

$$V_R = \sqrt{V_{MG}^2 + V_P^2} \qquad [4\text{-}15]$$

where ρ_{MG} is the combined material and geometry bias coefficient and V_{MG} is the corresponding coefficient of variation. Equations [4-14] and [4-15] are consistent with the philosophy of Equations [4-4] and [4-5] in determining ρ_R and V_R, which will be applied in Equation [4-2] for resistance factors.

In this chapter, 280 representative nominal panels have been selected based on the research presented in chapter 3. The 280 samples consist of 56 nominal stiffened plates under five different load conditions. The loading conditions represent different magnitudes of end moments, namely, –0.4, –0.2, 0, 0.2, and 0.4 times the nominal plastic moment capacity of the full cross-section, $\hat{M}_P$. The configurations of these nominal panels are presented in Table B-2 of Appendix B, and their capacities and associated failure modes, predicted using Equations [4-11] and the finite element analysis are presented in Tables B-4 to B-8 of Appendix B. The predicted nominal capacity is denoted as $\hat{R}_n$ or $\hat{R}_n(\hat{M},\hat{G})$, where $\hat{M}$ and $\hat{G}$ are nominal material and geometric parameters, respectively. For each of the 280 nominal specimens analyzed using the finite element model, the following procedure is adopted:

1. For each basic geometric and material variable presented in Table 4-1 (denoted as x_i), generate a random value ($x_{i,1}$) using the sampling method illustrated in Figure 4-2.

2. A set of random parameter values ($x_{1,1}$, $x_{2,1}$, $x_{3,1} \ldots$ $x_{i,1} \ldots$) obtained in step 1 constitutes a particular combination of material properties and geometric dimensions (M and G). These values are used as input to Equation [4-11] to calculate the nominal capacity R_n of this panel.

3. The nominal capacity R_n that is predicted using design equations and actual material and geometric properties (M and G) is divided by the nominal capacity $\hat{R}_n$ that is predicted using design equations and nominal material and geometric properties ($\hat{M}$ and $\hat{G}$). This gives one sample point of the sample set of $R_n / \hat{R}_n$.

4. Repeat steps 1 through 3 5000 times to establish the sample set for a particular nominal panel.

Steps 1 to 4 are repeated for each of the 280 nominal panels. It is recalled that the values of x_i generated in step 1 must be positive.

The sample size of $R_n/\hat{R}_n$ (or output variable Y) is 5000 for each nominal panel. This has been demonstrated to be a sufficiently large sample size (Mirza and MacGregor, 1982; Grant *et al.*, 1978; Melchers, 1999) to obtain an accurate representation of the population. The convergence of the mean and COV has also been monitored as a function of sample size. As an example, the estimated $\overline{Y}$ and V_Y of the observed results for panel 433_31 under $M_a/\hat{M}_P = -0.4$ are plotted in Figure 4-3 against the number of samples. The fluctuating amplitude is less than 0.005 for both parameters beyond the sample size of 2000, indicating convergence of the statistical parameters.

4.6 DETERMINATION OF ρ_{MG} AND V_{MG}

The resistance parameters ρ_{MG} and V_{MG} can now be determined for each of the 280 nominal panels based on the distribution of its 5000 samples of $R_n/\hat{R}_n$ (abbreviated as Y in the following discussion) obtained in the previous section. Lognormal curves are usually fitted to the observed distributions of the Monte Carlo simulation results. Since the lower range of the strength distribution is critical for the reliability analysis, the equivalent lognormal distribution curves will be obtained by fitting the lower 5% tail of the observed distributions. This normalization procedure was used by Kennedy and Baker (1984), and Mirza and MacGregor (1982). One example of panel 433_31 under $M_a/\hat{M}_P = -0.4$ is shown in Figure 4-4 to illustrate the fitting, where the range of interest (the lower 5% tail) shows excellent agreement while the insignificant range (the rest of the curve) may not have as good match.

In the present study, $Y_{0.001}$ and $Y_{0.05}$ are selected to determine the equivalent lognormal curve, where $Y_{0.001}$ and $Y_{0.05}$ are the 0.1% and 5% fractiles of the variable Y, respectively. Recognizing that, for a normal distribution the distance between the mean and the 0.1% and 5% fractiles are 3.090 and 1.645 standard deviations, respectively, it follows that:

$$\overline{\ln Y} - \ln Y_{0.001} = 3.090\,\sigma_{\ln Y} \qquad [4\text{-}16]$$

$$\overline{\ln Y} - \ln Y_{0.05} = 1.645\,\sigma_{\ln Y} \qquad [4\text{-}17]$$

A comparison can be made between a fractile obtained from the fitted lognormal curve and a fractile of the same percentage from the Monte Carlo simulation results to verify the goodness of fit. Since the fitted curve is determined from $Y_{0.001}$ and $Y_{0.05}$ fractiles, we assess the goodness of fit within the range of interest (the lower 5% tail) by comparing the fitted lognormal curve with the Monte Carlo simulation results at the 0.5% fractile, $Y_{0.005}$. A comparison of $Y_{0.005}$ between the fitted curve and the Monte Carlo simulation results for each of the 280 nominal panels is presented in Figure 4-5. The values of the fitted curves are in close agreement with the Monte Carlo simulation (MCS) results, where the mean of the MCS-to-fitted ratios is 1.002 and the COV is 0.015. A similar comparison at the 1% fractile, $Y_{0.01}$, is presented in Figure 4-6. The mean of the MCS-to-fitted ratios is 1.002 and the COV is 0.012. It is therefore concluded that the fitted curve is in excellent agreement with the distribution obtained from the Monte Carlo simulation within the range of interest, namely, the lower 5% tail.

The values of $\overline{\ln Y}$ and $\sigma_{\ln Y}$ obtained from Equations [4-16] and [4-17] are then substituted into Equations [4-18] and [4-19] (Melchers, 1999) to obtain $\bar{Y}$ and σ_Y, where $\bar{Y}$ is ρ_{MG} and σ_Y is the associated standard deviation.

$$\rho_{MG} = \bar{Y} = \exp\left(\overline{\ln Y} + 0.5\sigma_{\ln Y}^2\right) \qquad [4\text{-}18]$$

$$\rho_{MG} V_{MG} = \sigma_Y = \sqrt{\exp\left(2\overline{\ln Y} + \sigma_{\ln Y}^2\right) \times \left[\exp\left(\sigma_{\ln Y}^2\right) - 1\right]} \qquad [4\text{-}19]$$

Values of the observed and fitted $Y_{0.001}$, $Y_{0.05}$, $Y_{0.005}$ $Y_{0.01}$, ρ_{MG} and V_{MG} for the 280 nominal panels are presented in Appendix F.

4.7 DETERMINATION OF ρ_P AND V_P

The calculations presented in section 4.6 did not include the variability due to the difference between the capacity predicted from Equations [4-11] and that predicted using the finite element analysis, nor did they include the variation between the finite element analysis and the actual capacity (the test capacity). In this section we evaluate the ability of the proposed design equations to predict the finite element analysis results and the ability of the finite element analysis to predict the actual test results. The bias coefficient for the professional factor, ρ_P, and the associated COV, V_P, can be determined using Equations [4-6] and [4-7].

The factors ρ_{P1} and V_{P1} are obtained based on the same 280 nominal panels previously used. Their values for different failure modes in various slenderness ranges are presented in Table 4-3, where ρ_{P1} varies from 0.842 to 1.205, and V_{P1} varies from 0.018 to 0.152. It should be noted that the calculation of ρ_{P1} and V_{P1} has nothing to do with the Monte Carlo simulations. It simply represents the ability of the proposed design equations to predict the finite element analysis results.

The factors ρ_{P2} and V_{P2} are obtained based on the five test results presented by Grondin *et al.* (1998). For these tests the test set-up was carefully designed and the test procedures were carefully controlled to eliminate uncertainties in the numerical analysis as much as possible. This resulted in very accurate prediction of the test results, which may not reflect the majority of test data available in the literature. It is acknowledged that the size of this data set is limited and it is desirable to re-evaluate ρ_{P2} and V_{P2} when more data is available. The mean value of the ratio of the test capacity to finite element analysis capacity, predicted by the same numerical approach used in this investigation, ρ_{P2}, was found to be 0.972 and the corresponding COV 0.0439. Mirza and MacGregor (1982) pointed out that there are uncertainties in test measurements that need to be eliminated from the COV of this measured capacities. The measurement uncertainties result mainly from the variations of the actual specimen dimensions, differences between the material properties of the test panels and the material coupons, and inaccuracies in the load recordings. Mirza and MacGregor (1982) suggested reducing the COV of the test-to-predicted ratios by 0.04. Kennedy and Baker (1984) further recommended that the reduction should vary linearly when the COV of the test-to-predicted ratios is less than 0.06. This strategy is adopted in the present work in such a way that the COV of the test-to-FEA capacity ratio is reduced by the lesser of two thirds of itself and 0.04. Therefore the revised COV for the test-to-FEA ratio, V_{P2}, is 0.0327 $\left(\sqrt{0.0439^2 - \min(0.0439 \times 2/3, 0.04)^2}\right)$. The factors ρ_{P2} (0.972) and V_{P2} (0.0327) have negligible effect compared to ρ_{P1} (0.842 to 1.205) and V_{P1} (0.018 to 0.152) in Table 4-3 and the values of ρ_{MG} (1.168 to 1.935) and V_{MG} (0.077 to 0.337) in Appendix F. In fact, ρ_{P2} and V_{P2} have been ignored in some reliability analyses when the numerical model is able to predict the test results accurately as is the case for the present problem (Hess *et al.*, 1998).

The overall professional factors, ρ_P and V_P, are determined for each of the 280 nominal panels by using in Equations [4-6] and [4-7] the corresponding ρ_{P1} and V_{P1} from Table 4-3, the value of 0.972 for ρ_{P2}, and the value of 0.0327 for V_{P2}. The values of ρ_P and V_P are presented in Table 4-4.

4.8 DETERMINATION OF RESISTANCE FACTORS ϕ

Now that the parameters ρ_{MG}, V_{MG}, ρ_P and V_P are available, Equations [4-14] and [4-15] can be used to determine ρ_R and V_R, shown in Figures 4-7 and 4-8, respectively. The values of ρ_R and V_R are then used in Equation [4-2] to obtain the resistance factor ϕ for each of the 280 nominal panels. The safety index β in Equation [4-2] directly relates to the expected safety level of the structures and it reflects, among other things, the severity of limit state considered. A safety index of 3.0 is commonly used for ductile failure modes in steel building structures, and 4.5 for connection failures. For example, when considering failure of a bolted or riveted member, a safety index of 3.0 is used when considering the ultimate limit state of yielding of the gross section. However, when considering rupture at the net section, the safety index is increased to 4.5 to reflect the fact that there is no reserve of strength beyond rupture.

An appropriate selection of safety index for stiffened steel plates includes considerations of whether the failure has stable post-buckling behaviour and whether the stiffened plates are primary load carrying members (i.e. consequence of failure). An extensive analysis and a prediction method of stable and unstable post-buckling behaviour were presented in Chapter 2. There are three categories for combinations of post-buckling behaviour and the load carrying role of the stiffened plates. Stiffened plates that are primary load carrying members and have unstable post-buckling behaviour are in the worst category. Stiffened plates that are non-primary load carrying members and have stable post-buckling behaviour are in the best category. Stiffened plates that are primary load carrying members but have stable post-buckling behaviour and stiffened plates that are non-primary load carrying members but have unstable post-buckling behaviour are in the intermediate category. The worst category requires the largest safety index. In order to provide a comprehensive basis to facilitate further decision of code writers, five values for the safety index, namely, 2.5, 3.0, 3.5, 4.0 and 4.5, will be analyzed in this research.

The resistance factors are plotted in Figures 4-9 to 4-13 against the column slenderness ratio of the effective panel, λ_e, for the five values of the safety index. The points are divided by failure modes that were obtained from the finite element analysis results. Being the lowest value of the five, β = 2.5 should apply only to the best category, stiffened plates that are non-primary load carrying members and have stable post-buckling behaviour. From Figures 4-9 (c) and (d) that show the points of stable failure, ϕ = 0.90 is appropriate for β = 2.5.

Figures 4-10 to 4-12 show the values of ϕ for β = 3.0, 3.5 and 4.0, respectively. They may correspond to the intermediate category. Therefore, both unstable and stable failures need to be considered to determine the selection of ϕ. For β = 3.0 in Figure 4-10, a line representing ϕ = 0.87 (or 1/1.15) is drawn, where 1.15 is the material factor used in DNV-RP-C201 (DNV, 2002), which is analogous to the resistance factor. There are only five out of 280 points in Figure 4-10 that fall below ϕ = 0.87, and only one point lies below ϕ = 0.85. Therefore, ϕ = 0.85 is an appropriate resistance factor for β = 3.0. Resistance factors ϕ = 0.75 and 0.70 are applicable for β = 3.5 and 4.0, respectively, according to Figures 4-11 and 4-12.

For β = 4.5 in Figure 4-13, only the unstable failures need to be concerned since β = 4.5 can only correspond to the worst category. All the points in Figure 4-13 (a) is above ϕ = 0.65, and only two out of 65 points in Figure 4-13 (b) are below ϕ = 0.65. Therefore, ϕ = 0.65 may be selected for β = 4.5.

In general, ϕ = 0.90, 0.85, 0.75, 0.70, 0.65 are recommended for β = 2.5, 3.0, 3.5, 4.0, 4.5, respectively. Selection of appropriate β for various failure modes will depend on code writers' decision.

4.9 DISCUSSION

The separation factor, α_R, used in Equation [4-2] was found to give an acceptably small, but conservative, approximation of the more general Equation [4-1] (Galambos and Ravindra, 1973). The derivation of the value of 0.55 for α_R was mainly based on the reasonable variations of resistance and loads for steel buildings. A specific investigation of α_R for stiffened steel plate structures may be worthwhile if the data of load variability was available.

We should keep in mind that the accuracy of the calculated failure probability is highly dependent on the knowledge of the statistical distribution of the input variables and the type of distribution for the resistance and the load. MacGregor (1976) pointed out that the probability of failure could differ from the actual value by a factor of 10 in case of inadequate knowledge of the strength distribution. Ang and Cornell (1974) observed that the failure probability, implied by the safety index β, was not affected greatly by the choice of distribution type when the failure probability is high, but became sensitive for low failure probability. This is likely due to the fact that when a lower failure probability is set, the critical portion of the lower tail the distribution curve is smaller, and that it is easier to fit a shorter range of the observed distribution by a lognormal curve than for a longer portion of the curve as shown in Figure 4-4. Melchers (1999) clearly presented it as the tail sensitivity problem, which was merely a reflection of the uncertainties involved in quantifying the required statistical data. Allen (1975) indicated that β could be considered only as a relative measure of safety, even if the correct distribution were known. As β is considered as the nominal, or relative, safety index, it works effectively as a consistent indicator of the safety level of structures, especially when comparing and calibrating design rules. However, a more advanced analysis is recommended when the exact failure probability of a specific structure is required.

4.10 SUMMARY AND CONCLUSIONS

This chapter presented a reliability analysis to derive the adequate resistance factor for the design of stiffened steel plates under axial compression and out-of-plane bending moment, based on the statistical distributions of geometric and material properties presented by Hess *et al.* (1998), and data relating to the professional factor presented in the work of Grondin *et al.* (1998) and the finite element analysis of Chapter 2. The equations to predict stiffened plate capacity were presented in Chapter 3.

The Monte Carlo simulation technique was used to derive the distribution curves of the ratio of design capacities using random material and geometric properties to design capacities using nominal properties ($R_n / \hat{R}_n$), where the input variables are the basic material and geometric variables. A total of 280 representative nominal panels, of varying configurations and load conditions, were analyzed. For each nominal panel, a set of 5000 random panels were generated to form the probability density functions needed for the reliability analysis.

The 0.001 and 0.05 fractiles of the Monte Carlo results of $R_n / \hat{R}_n$ were used to determine the combined material and geometric factors (ρ_{MG} and V_{MG}) of the equivalent lognormal curve for each nominal panel.

Uncertainties due to accuracy of the design model are accounted for by the statistics for the professional factor, ρ_P and V_P. This includes the consideration of the ability of the design model to predict the FEA results, and the ability of the FEA to predict the actual capacity of stiffened steel plates.

The resistance factors ϕ = 0.90, 0.85, 0.75, 0.70, 0.65 are recommended for β = 2.5, 3.0, 3.5, 4.0, 4.5, respectively. Selection of appropriate safety index depends on the code writers' decision. These resistance factors are applicable for the design equations presented in section 4.3. The method to predict unstable failure was presented in Chapter 2.

References:

Allen, D.E.(1975). “Limit states design – a probabilistic study.” *Canadian Journal of Civil Engineering*, 2 (11), 36-49.

Ang, A.H.-S. and Cornell, C.A.(1974). “Reliability Bases of Structural Safety and Design.” *Journal of the Structural Engineering Division*, Proceedings of the ASCE, 100 (9), 1755-1769.

Canadian Standards Association (CSA). (2009). *CSA-S16-09: Design of Steel Structures*, Toronto, Ontario, Canada.

Det Norske Veritas (2002). Recommended Practice *DNV-RP-C201: Buckling Strength of Plated Structures*, Norway.

Fisher,J.W., Galambos,T.V., Kulak, G.L and Ravindra, M.K. (1978). “Load and Resistance Factor Design Criteria for Connectors.” *Journal of the Structural Division*, ASCE, 104(9), 1427-1441

Galambos,T.V. and Ravindra, M.K. (1973). Tentative load and resistance factor design criteria for steel buildings. Structural Division, Civil and Environmental Engineering Department, Washington University, St. Louis, MO. Research Report No. 18.

Grant, L.H., Mirza, S.A., and MacGregor, J.G. (1978). “Monte Carlo study of strength of concrete columns.” *American Concrete Institute Journal*, 75 (8), 348-358.

Grondin, G. Y., Chen, Q., Elwi, A. E., Cheng, J. J. R. (1998). "Stiffened plates under compression and bending." *Journal of Constructional Steel Research*, 45(2), 125–148.

Grondin, G. Y., Elwi, A.E., Cheng, J.J.R. (1999). "Buckling of Stiffened Steel Plates -A Parametric Study." *Journal of Constructional Steel Research*, 50(2), 151-175.

Grondin, G. Y., Jin, M., Josi, G.. (2007), "Slip Critical Bolted Connections - A Reliability Analysis for Design at the Ultimate Limit State", *Structural Engineering Report No. 270*, Department of Civil and Environmental Engineering, University of Alberta, Canada.

Hess, P.E., Bruchman, D., and Ayyub, B.M.(1998). “Uncertainties in material and geometric strength variables in marine structures.” *Uncertainty modeling and analysis in civil engineering*, edited by Ayyub, CRC Press LLC, 245-273.

Kennedy, D.J.L and Baker, K.A. (1984), “Resistance factors for steel highway bridges.” *Canadian Journal of Civil Engineering*, 11 (2), 324-334.

Kennedy, D.J.L and Gad Aly, M. (1980), “Limit states design of steel structures – performance factors.” *Canadian Journal of Civil Engineering*, 7 (1), 45-77.

MacGregor, J.G. (1976). “Safety and limit states design for reinforced concrete.” *Canadian Journal of Civil Engineering*, 3 (4), 484-513.

Melchers, R.E. (1999). *Structural reliability analysis and prediction*, 2nd edition, John Wiley & Sons, Toronto.

Mirza, S.A. and MacGregor, J.G. (1982). “Probabilistic study of strength of reinforced concrete members.” *Canadian Journal of Civil Engineering*, 9 (3), 431-448.

Ravindra, M.K. and Galambos, T.V. (1978). “Load and resistance factor design for steel.” *Journal of the Structural Engineering Division*, Proceedings of the ASCE, 104 (9), 1337-1353.

Schmidt, B.J., and Bartlett, F.M. (2002a). “Review of resistance factor for steel: data collection.” *Canadian Journal of Civil Engineering*, 29 (1), 98-108.

Schmidt, B.J., and Bartlett, F.M. (2002b). "Review of resistance factor for steel: resistance distributions and resistance factor calibration." *Canadian Journal of Civil Engineering*, 29 (1), 109-118.

Table 4-1 Statistical parameters for the bias coefficient of the basic variables (Hess *et al*., 1998)

x	b	t	h_w	t_w	b_f	t_f	L	F_y	E
Distri-bution*	N	LN	N	LN	LN	LN	LN	LN	N
$\bar{x}$	0.992	1.048	0.996	1.255	1.014	1.132	0.988	1.206	0.987
σ_x	0.028	0.045	0.019	0.113	0.016	0.104	0.047	0.183	0.075

* Note: N: normal distribution; LN: log normal distribution.

Table 4-2 Statistical parameters for the log of the bias coefficient for the basic variables in Table 4-1 that follow lognormal distribution

$\ln(x)$	$\ln(t)$	$\ln(t_w)$	$\ln(b_f)$	$\ln(t_f)$	$\ln(L)$	$\ln(F_y)$
$\overline{\ln(x)}$	0.046	0.223	0.014	0.120	-0.013	0.175
$\sigma_{\ln(x)}$	0.043	0.090	0.016	0.092	0.047	0.151

Table 4-3 Statistical parameters for professional factor ρ_{P1} and V_{P1}

$M_a/\hat{M}_p$	–0.4		–0.2		0		0.2		0.4	
λ_e	ρ_{P1}	V_{P1}	ρ_{P1}	V_{P1}	ρ_{P1}	V_{P1}	ρ_{P1}	V_{P1}	ρ_{P1}	V_{P1}
Plate induced failure										
(0.0,0.2]	0.981	0.107	0.956	0.091	0.934	0.078	0.842	0.018	—	—
(0.2,0.4]	0.990	0.100	0.962	0.079	0.938	0.064	0.886	0.039	—	—
(0.4,0.6]	1.022	0.086	1.002	0.081	0.978	0.079	0.959	0.075	—	—
(0.6,0.8]	1.085	0.076	1.086	0.060	1.066	0.059	1.078	0.088	—	—
(0.8,1.0]	1.079	0.118	1.187	0.056	1.205	0.053	1.159	0.15 †	—	—
Stiffener induced failure										
(0.0,0.2]	—	—	—	—	—	—	0.976	0.062	0.985	0.069
(0.2,0.4]	—	—	—	—	—	—	0.978	0.055	0.972	0.090
(0.4,0.6]	—	—	—	—	—	—	1.007	0.044	0.989	0.100
(0.6,0.8]	—	—	—	—	—	—	1.157	0.128	1.020	0.087
(0.8,1.0]	—	—	—	—	—	—	1.111	0.057	1.153	0.152

† The value of 0.15 is conservatively selected. It can not be calculated because only one sample lies in that range.

Table 4-4 Statistical parameters for overall professional factors ρ_P and V_P

$M_a/\hat{M}_p$	–0.4		–0.2		0		0.2		0.4	
λ_e	ρ_P	V_P	ρ_P	V_P	ρ_P	V_P	ρ_P	V_P	ρ_P	V_P
					Plate induced failure					
(0.0,0.2]	0.954	0.112	0.929	0.097	0.908	0.085	0.818	0.037	—	—
(0.2,0.4]	0.962	0.105	0.935	0.086	0.912	0.072	0.861	0.051	—	—
(0.4,0.6]	0.993	0.092	0.974	0.087	0.951	0.086	0.932	0.082	—	—
(0.6,0.8]	1.055	0.083	1.056	0.068	1.036	0.067	1.048	0.094	—	—
(0.8,1.0]	1.049	0.122	1.154	0.065	1.171	0.062	1.127	0.154	—	—
					Stiffener induced failure					
(0.0,0.2]	—	—	—	—	—	—	0.949	0.070	0.957	0.076
(0.2,0.4]	—	—	—	—	—	—	0.951	0.064	0.945	0.096
(0.4,0.6]	—	—	—	—	—	—	0.979	0.055	0.961	0.105
(0.6,0.8]	—	—	—	—	—	—	1.125	0.132	0.991	0.093
(0.8,1.0]	—	—	—	—	—	—	1.080	0.066	1.121	0.155

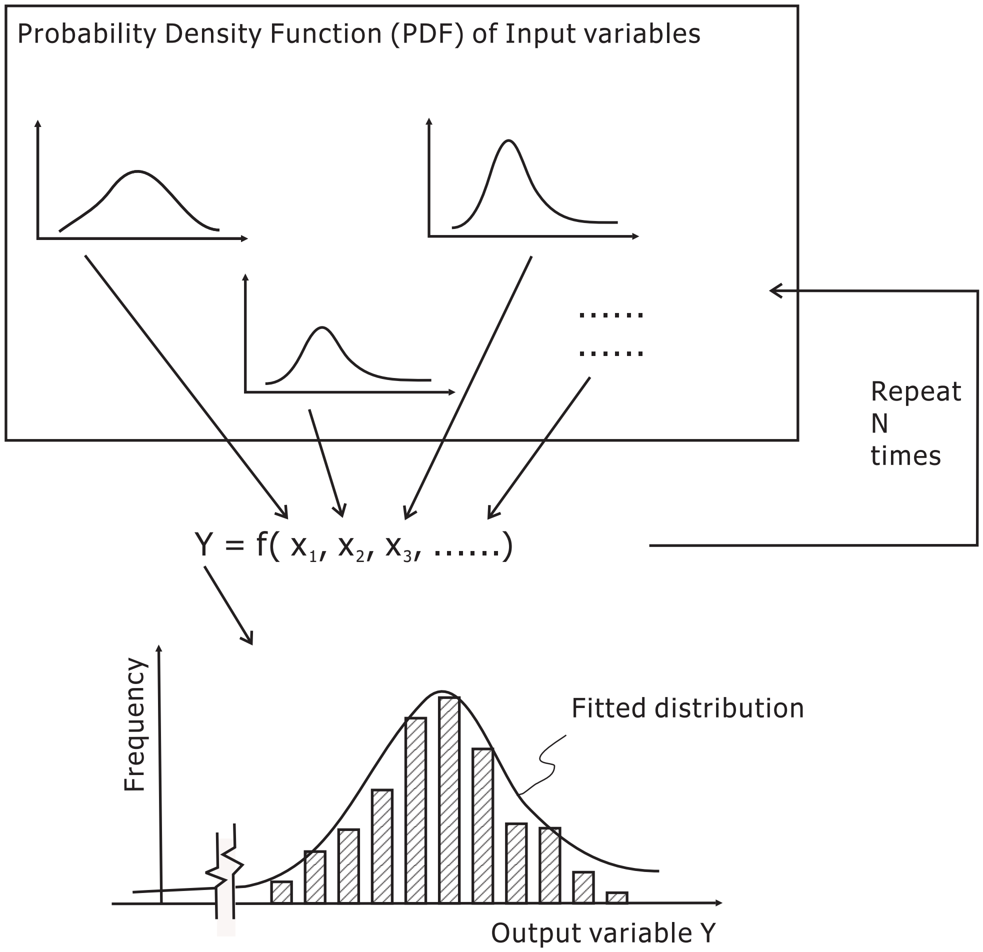

Figure 4-1 Schematic representation of Monte Carlo simulation

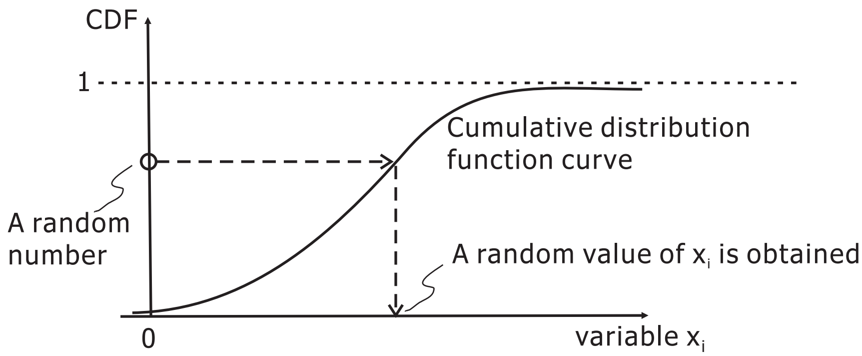

Figure 4-2 Generation of a random value of a variable of any arbitrary distribution

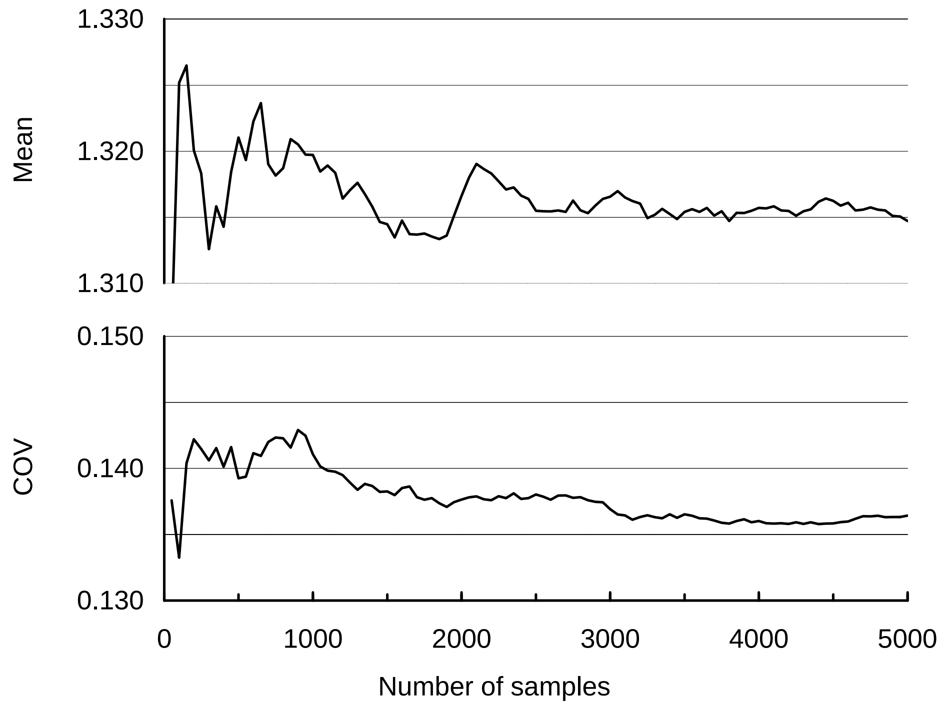

Figure 4-3 Convergence of observed statistics as a function of sample size

(panel 433_31, $M_a / \hat{M}_P = -0.4$)

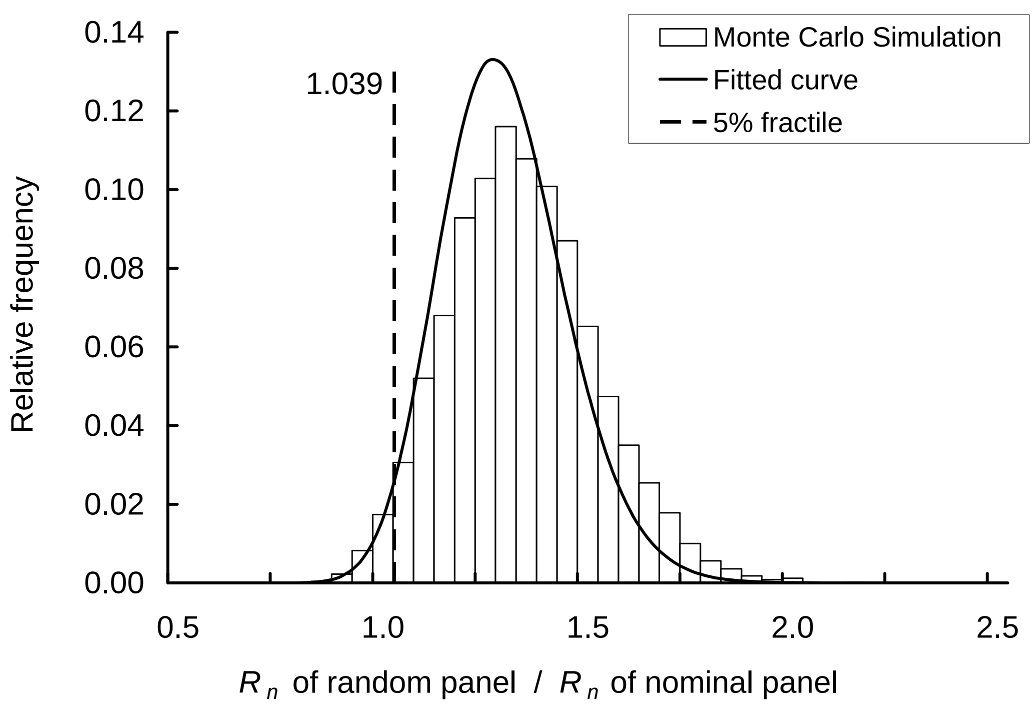

Figure 4-4 Distributions of $R_D / \hat{R}_D$ of panel 433_31 ($M_a / \hat{M}_P = -0.4$)

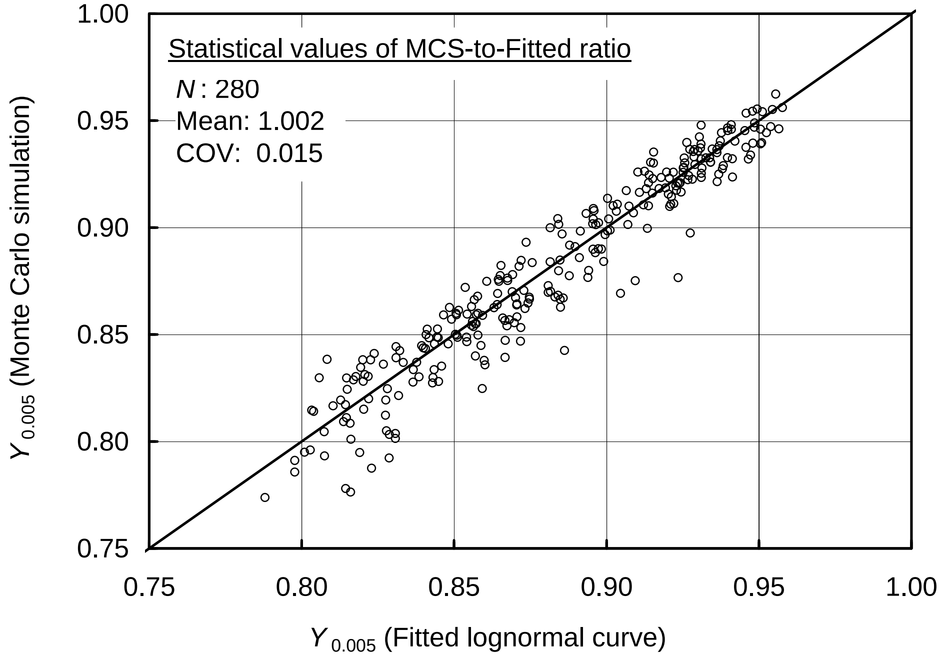

Figure 4-5 Comparison between the Monte Carlo simulation (MCS) results and the fitted lognormal curve at the lower 0.5% fractile

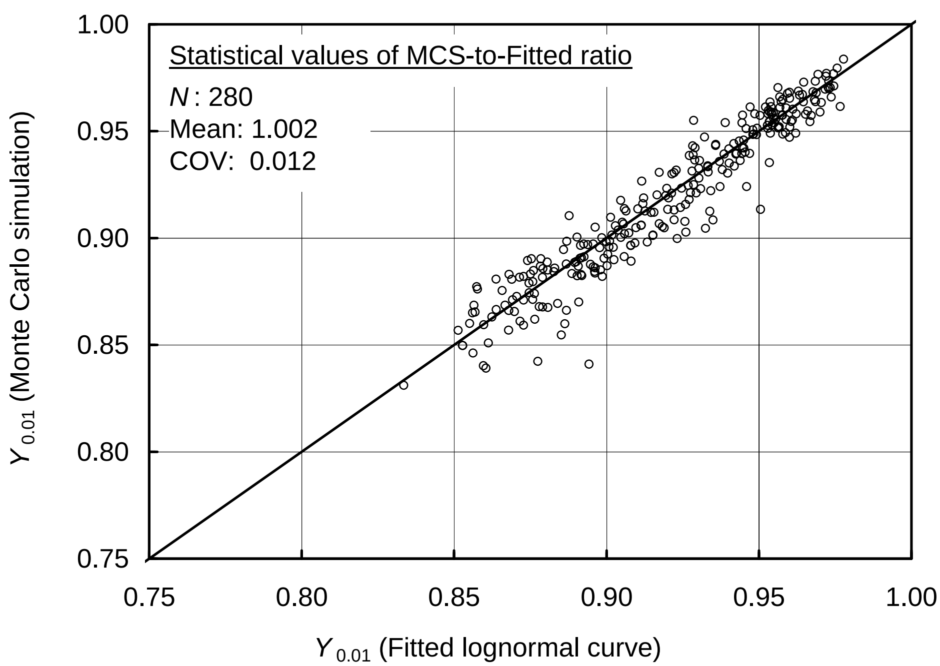

Figure 4-6 Comparison between the Monte Carlo simulation (MCS) results and the fitted lognormal curve at the lower 1% fractile

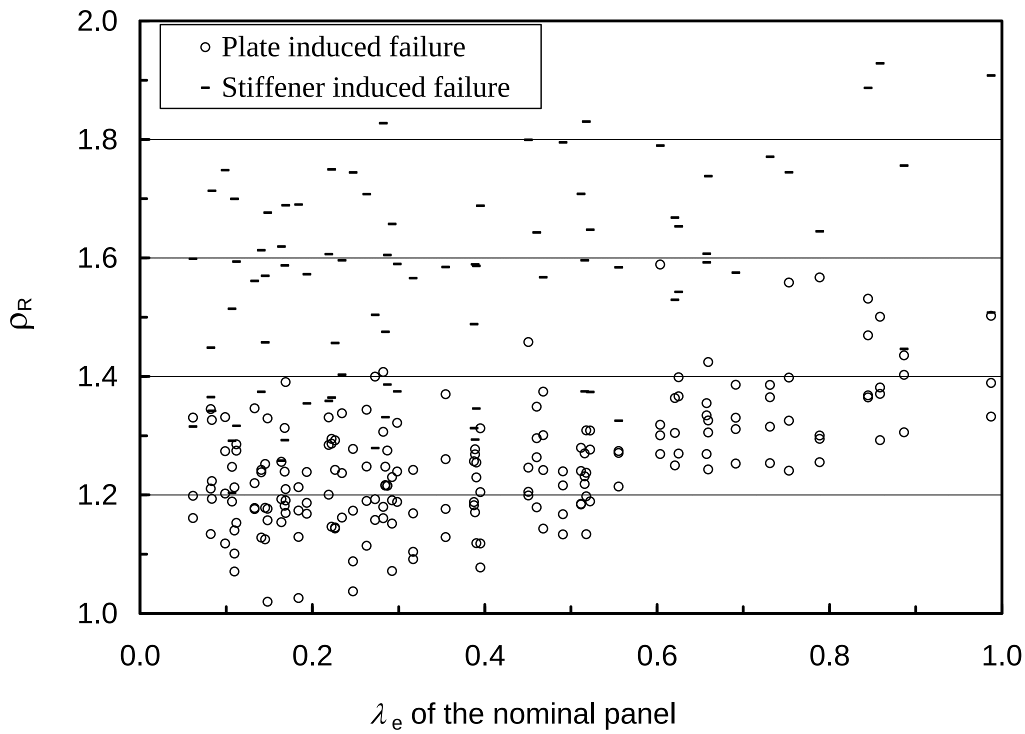

Figure 4-7 Professional factor, ρ_R, for the 280 nominal panels

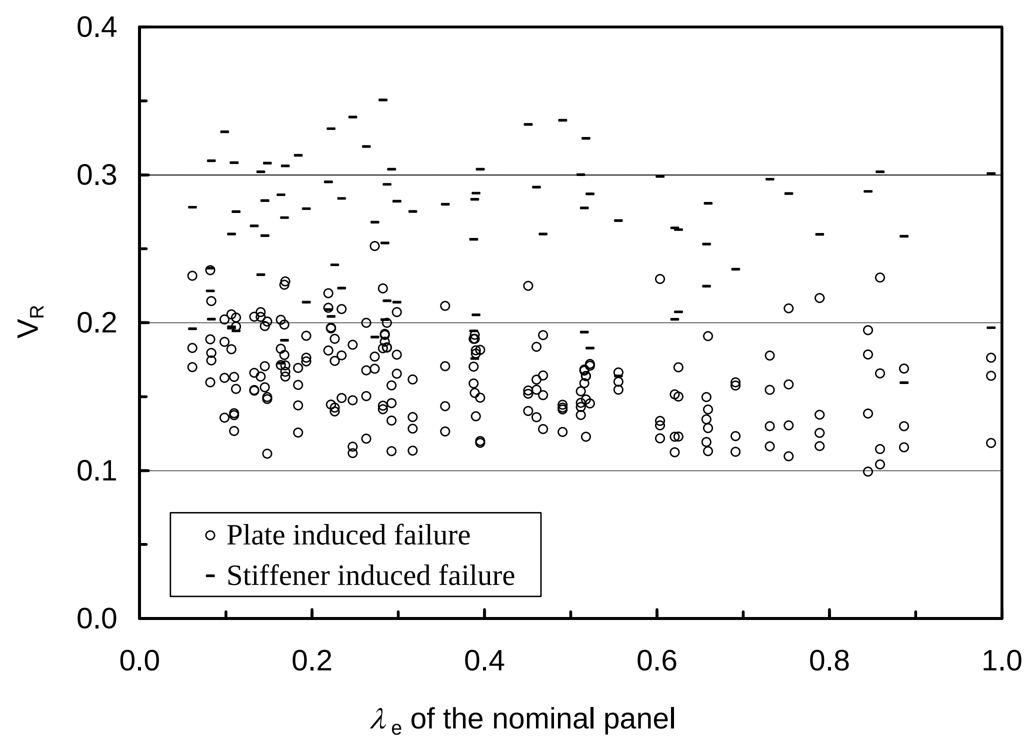

Figure 4-8 COV for the professional factor, V_R for the 280 nominal panels

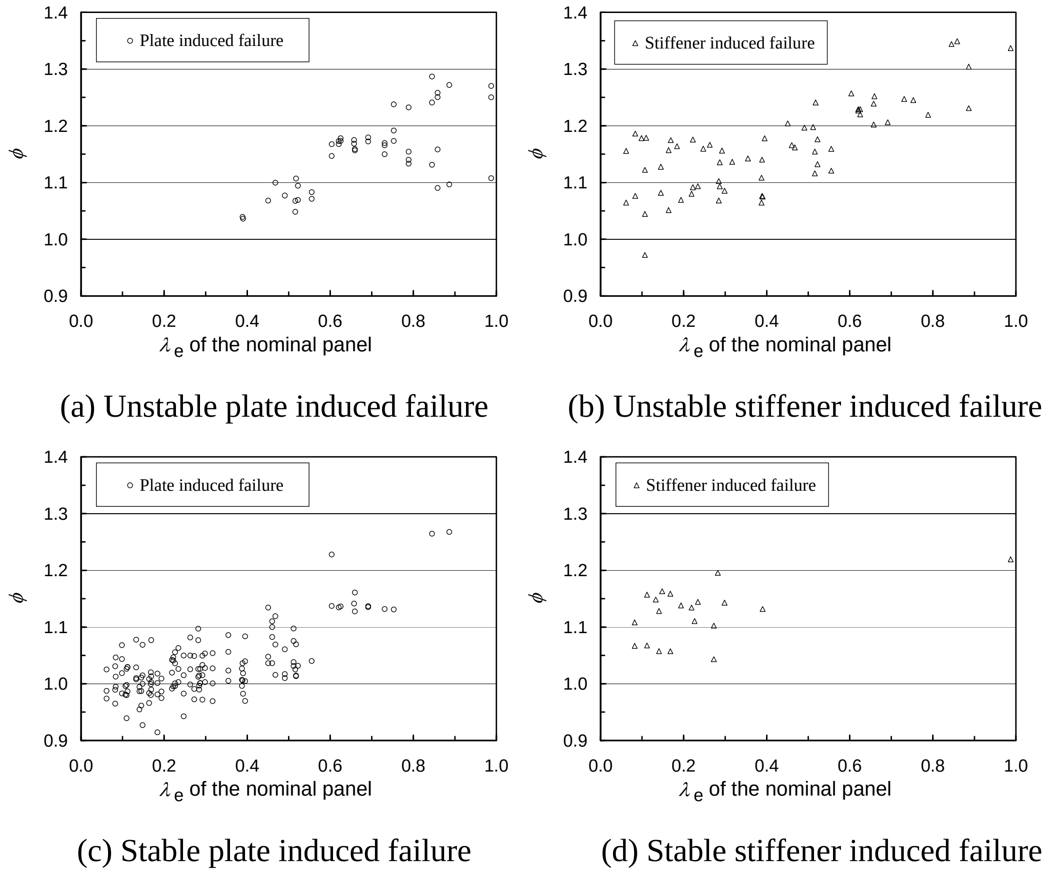

(a) Unstable plate induced failure (b) Unstable stiffener induced failure

(c) Stable plate induced failure (d) Stable stiffener induced failure

Figure 4-9 Values of resistance factor ϕ of the 280 nominal panels (β = 2.5)

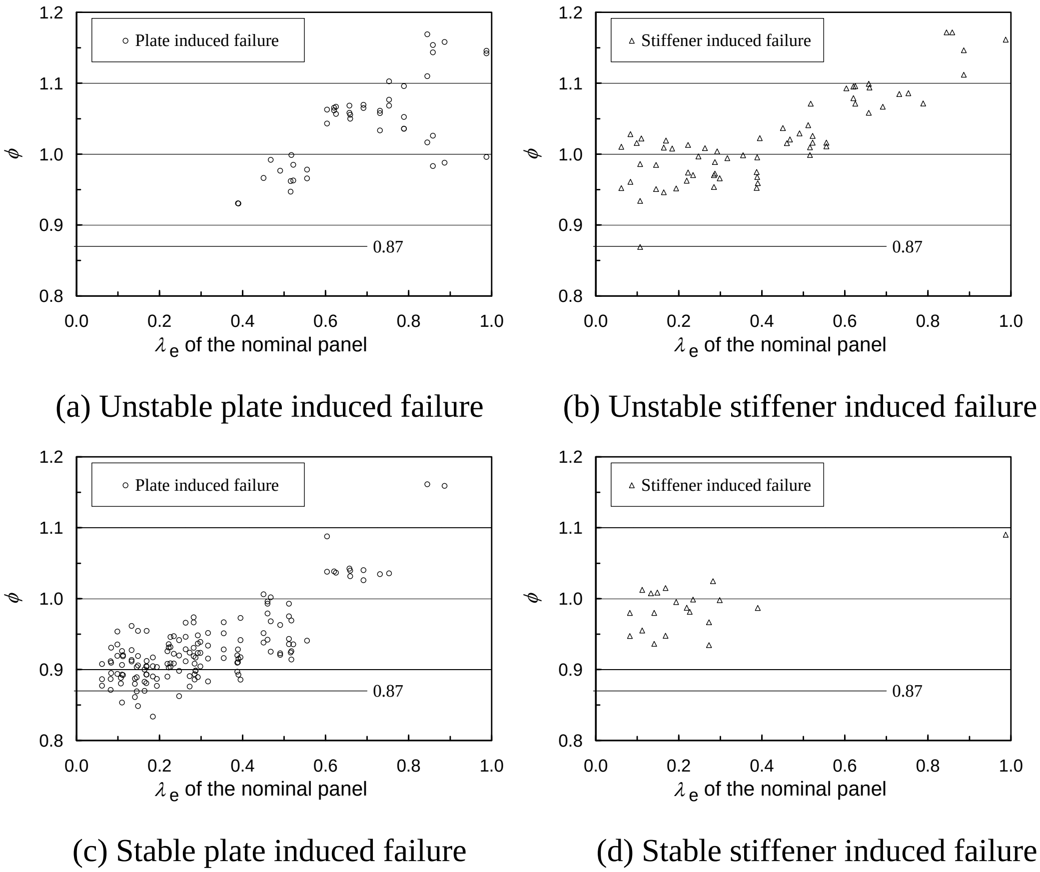

(a) Unstable plate induced failure (b) Unstable stiffener induced failure

(c) Stable plate induced failure (d) Stable stiffener induced failure

Figure 4-10 Values of resistance factor ϕ of the 280 nominal panels (β = 3.0)

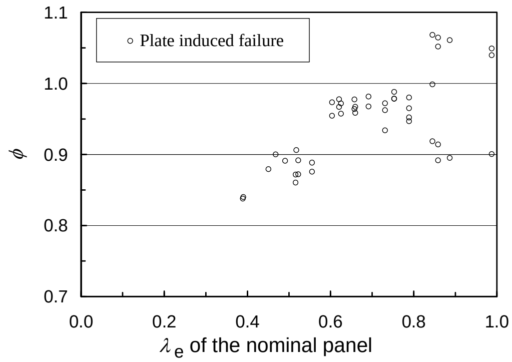

(a) Unstable plate induced failure

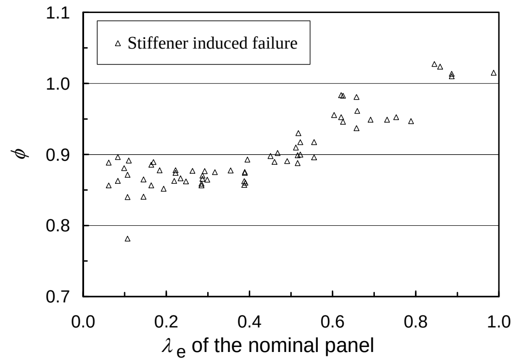

(b) Unstable stiffener induced failure

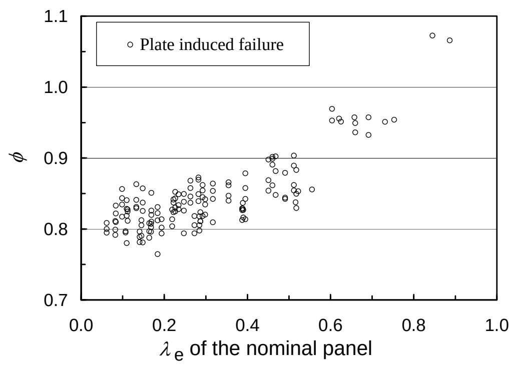

(c) Stable plate induced failure

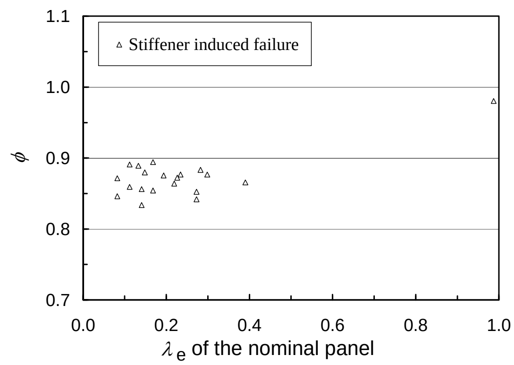

(d) Stable stiffener induced failure

Figure 4-11 Values of resistance factor ϕ of the 280 nominal panels (β = 3.5)

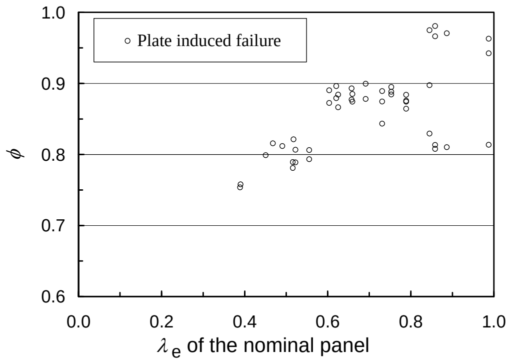

(a) Unstable plate induced failure

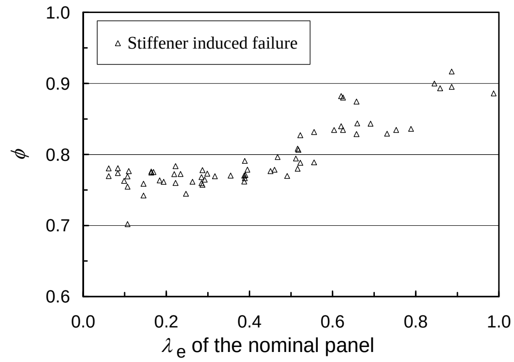

(b) Unstable stiffener induced failure

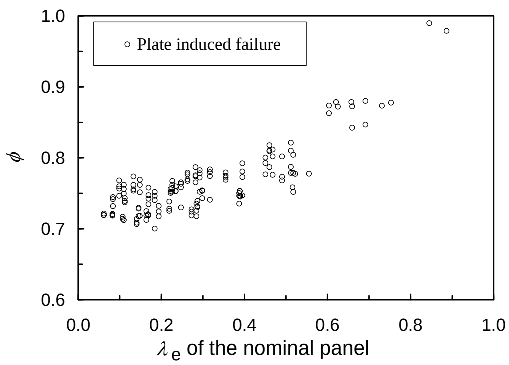

(c) Stable plate induced failure

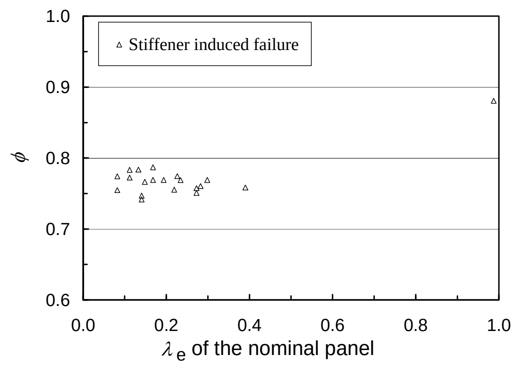

(d) Stable stiffener induced failure

Figure 4-12 Values of resistance factor ϕ of the 280 nominal panels (β = 4.0)

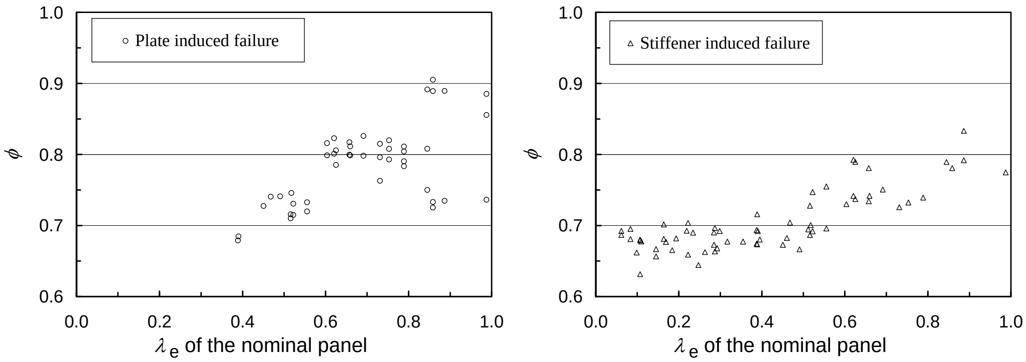

(a) Unstable plate induced failure (b) Unstable stiffener induced failure

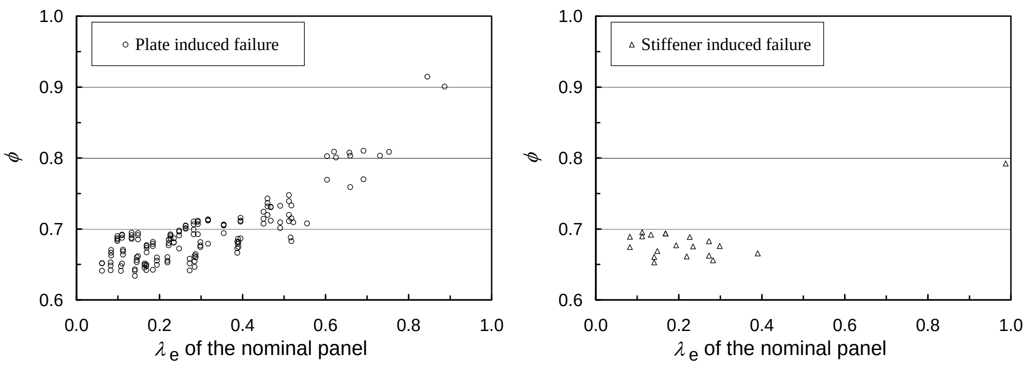

(c) Stable plate induced failure (d) Stable stiffener induced failure

Figure 4-13 Values of resistance factor ϕ of the 280 nominal panels (β = 4.5)

CHAPTER 5

SUMMARY AND CONCLUSIONS

5.1 SUMMARY AND CONCLUSIONS

An investigation of the behaviour of thin steel plates stiffened with longitudinal tee stiffeners was conducted. The loading conditions concerned in this study are compression parallel to the axis of the stiffeners, and combined compression and bending out of the plane of the plate.

The research was carried out mainly based on a database of finite element analysis results. The finite element model that was used to analyze various stiffened plates was presented in Chapter 2. The model incorporated initial imperfections, residual stresses and inelastic material behaviour, and it used large deformation theory. A total of 720 cases were run with the FEA model to form the database. These cases represented a fractional factorial design of a parameter matrix, where the parameter values were selected to cover the full range of practical stiffened panels.

The sudden loss of capacity observed in some plates of certain geometry and loading conditions was demonstrated to be associated with plastic behaviour where a sudden loss of load carrying capacity is observed once a plastic hinge is formed in the stiffened plate. A prediction model, developed using the principle of virtual work, was proposed to describe the development of a plastic hinge at midspan, and in turn predict the post-peak behaviour of stiffened plates. Showing excellent agreements with the finite element analysis results of the stiffened plate models where the sudden instability was observed, the virtual work model provided theoretical support to the conclusion that the sudden load drop is caused by the plastic hinge mechanism.

A method to predict the sudden loss of capacity experienced by some plates was proposed (Equation [2-15]) for plate induced failure. A sudden loss of capacity in plate failing by plate induced failure was found to occur if the calculated deformation ratio from Equation [2-15] is less than 0.025. On the other hand, all stiffened plates failing in a stiffener induced mode have been found to experience a sudden loss of capacity and should be treated as unstable in the post-peak range.

Based on the comprehensive behaviour investigation in Chapter 2, a design procedure was proposed in Chapter 3. The design philosophy is to treat the stiffened plate as an equivalent beam column, which consists of a stiffener and the associated effective plate width. Design equations are proposed for plate and stiffener induced failure. Plate induced failure prediction is based on the first-yield criterion since the panel is assumed to have failed once the plate outermost fibre yields in compression. For this case the stiffener side of the stiffened plate does not need to be checked. Stiffener induced failure is predicted based on the reduced plastic moment capacity obtained from interaction Equation [3-13b]. The second order effects due to the axial force acting on the deformed panel is accounted for using an amplification factor used to increase the applied bending moment. Once the buckling direction and capacity have been established, the method presented in Chapter 2 can be used to determine if the post peak behaviour will be stable or unstable. This is important in limit states design since the appropriate resistance factors need to be selected based on the consequence of reaching the peak capacity; plates that display an unstable post-peak behaviour are designed for a higher safety index.

Requirements for practical panel configurations were outlined in Chapter 3. The requirements were set to ensure that the panel can reach the expected resistance level. Three stiffener slenderness requirements and one stiffener area requirement were proposed.

Three design guidelines currently in use for the design of stiffened plates were reviewed. The proposed method and the three guidelines were assessed against the 720 stiffened plate samples contained in the database. It was found that the current design guidelines do not accurately predict the panel capacities mainly due to inappropriate design philosophy. The proposed method shows better correlation with the numerical results than the current design guidelines. A proposed screening process to avoid stiffened plates of impractical dimensions results in a mean value of the FEA-to-predicted ratios between 0.98 and 1.01, and a maximum coefficient of variation is 0.106.

The panels of practical dimensions from Chapter 3 were used in Chapter 4 to accomplish the final phase of the proposed design approach; the determination of appropriate resistance factors to provide a consistent level of safety. Due to the complexity of the proposed design equations in Chapter 3, a Monte Carlo simulation technique was used for the reliability analysis. Based on the probabilistic distributions of the basic variables, such as plate width and yield strength, random panel configurations were generated around the nominal one. For each representative nominal panel, 5000 random panels were generated to constitute the sample set of ratios of predicted resistance of actual panels to the nominal panel. The 5% lower tail of distribution curves of the Monte Carlo results was used to find the means and coefficient of variations of the equivalent log-normal curves, considering that the lower strength area is critical in design.

Uncertainties in strength prediction arise from the geometric and material factors and also from the accuracy of the design formulas. This is considered by using professional factors that come out of the statistical distributions of the FEA-to-predicted and the test-to-FEA capacity ratios.

Resistance factors varying from 0.90 to 0.65 are recommended for safety indices from 2.5 to 4.5, respectively.

5.2 FUTURE WORK

As noted in Chapter 2, the parameter values of the fractional factorial design is determined to fully and evenly cover the practical configurations of stiffened steel plates. Based on the parameters in the current study, future work should aim at developing a more refined database of practical configurations. This may need sufficient collections of panel configurations from realistic design. Chapter 3 discusses the requirements to screen out the impractical configurations. However, they seem to be conservative and need further refinement.

Additional research is required to establish a criterion for unstable failure modes. In the current work unstable failure was defined as a sudden loss of capacity within a nominal longitudinal strain of 1%, which is about five times the yield strain. This strain limit may be too conservative for most design applications.

In the parametric study the initial geometric imperfections and residual stresses are set at the average and severe levels, respectively. These two variables and their magnitude and distribution should have been considered as statistical parameters in the Monte Carlo simulation. The parametric study should be expanded to include a wider variety of initial imperfections and residual stress magnitudes and distributions.

The current work presents only two common load cases; axial compression loading, and compression plus bending. Additional research is necessary to investigate the interaction of other loads, such as transverse in-plane compression and edge shear. The moment distribution is another aspect that would affect the strength of a stiffened steel plate panel. The constant moment distribution assumed in this research is conservative.

The mean and COV for the ratio of the test results to FEA results used in the reliability analysis were calculated based on a limited set of test results by Grondin *et al.* (1998). This data set of test results should be expanded. When new data are added to the data set, it is important that the test conditions, initial imperfections of the specimens tested and material properties be representative of the specific test specimens since all these parameters will affect the magnitude of the test to FEA result ratio. The test data reported by Grondin *et al*. (1998) were the only ones where all these factors had been specifically measured. More data of this kind is needed to better quantify the test to FEA ratio.

Only tee shaped stiffeners were considered in this study. Given that the torsional rigidity of the other open-sectioned stiffeners, such as bar shape or L shape, is considerably smaller than the tee stiffeners, the findings and formulas proposed in this study may not apply directly to stiffeners of other shapes. The scope of this study should be expanded to include other stiffener shapes.

References:

American Bureau of Shipping (ABS) (2007). *Guide for buckling and ultimate strength assessment for offshore structures*. Houston, Texas

American Petroleum Institute (API) (2000). *API Bulletin 2V: Design of flat plate structures*, Washington, D. C., U.S.

Det Norske Veritas (2002). Recommended Practice *DNV-RP-C201: Buckling Strength of Plated Structures*, Norway.

Grondin, G. Y., Chen, Q., Elwi, A. E., Cheng, J. J. R. (1998). "Stiffened plates under compression and bending." *Journal of Constructional Steel Research*, 45(2), 125–148.

APPENDIX A

SAMPLE ABAQUS INPUT FILE

This appendix presents a sample input file for the load condition of β_9 = 0.4 and the boundary condtion that the unloaded plate edges are free in transverse in-plane direction. Change of load condition and boundary condition will result in minor modification to the input file, and the modification will be pointed out in the text boxes next to the corresponding input lines. The explaination of the finite element model is presented in Chapter 2. The general coordination definition is shown in Figure 2-1.

The sample input file as below is for panel 122_14. Its geometry shape and meshing are shown in Figure 2-21. In the sample input file, the command lines in normal fonts are general lines that are common to all specimens. The command lines in *Italic fonts* are specific for the target panel.

*heading

This is the parametric study. Case A: Unloaded edges free to expand transversely.

Hardening=iso

UNITS: mm,kg,s,N,MPa

*parameter

#

#geometric/load parameters,
L,tp,tw,tf,bp,bf,h0(hw+tp/2+tf/2),centroid(height),MP(Plastic M)

#independent

L=3123.44897078438

tp=32.7326835353989

tw=6.29732085890498

tf=6.39335592627242

bp=500

bf=83.7086785055319

h0=129.498065488384

centroid=6.74605508466603

MP=105782915.509366

#dependent

```
PercentL=0.01*L
HalfL=L/2
Halfbp=bp/2
Quaterbf=bf/4
Halfbf=bf/2
Quaterh0=h0/4
Halfh0=h0/2
ThreeQuaterh0=0.75*h0
Mapply=0.4*MP
#
#material parameters, E, fyp,fyw,fyf
E=200000
fyp=420
fyw=420
fyf=420
fypp=fyp+100
fywp=fyw+100
fyfp=fyf+100
****************************
** Build the stiffened plate
****************************
**
** Node definiton
**
*node
1,-1561.72448539219,-250,-3.93003487252386E-16
2,-1464.11670505518,-250,-0.613786528606488
3,-1366.50892471816,-250,-1.13412962222138
4,-1268.90114438115,-250,-1.48181176176368
5,-1171.29336404414,-250,-1.60390149323454
6,-1073.68558370713,-250,-1.48181176176369
7,-976.077803370118,-250,-1.13412962222138
8,-878.470023033106,-250,-0.613786528606488
9,-780.862242696094,-250,1.96501743626193E-16
10,-683.254462359082,-250,0.613786528606489
```

Indicates 40% of plastic moment applied (β_9 = 0.4)

11,-585.646682022071,-250,1.13412962222137

12,-488.038901685059,-250,1.48181176176368

13,-390.431121348047,-250,1.60390149323454

14,-292.823341011035,-250,1.48181176176369

15,-195.215560674024,-250,1.13412962222138

16,-97.6077803370117,-250,0.613786528606488

17,0,-250,0

18,97.6077803370117,-250,-0.613786528606488

19,195.215560674024,-250,-1.13412962222138

20,292.823341011035,-250,-1.48181176176369

21,390.431121348047,-250,-1.60390149323454

22,488.038901685059,-250,-1.48181176176369

23,585.646682022071,-250,-1.13412962222138

24,683.254462359083,-250,-0.613786528606487

25,780.862242696094,-250,5.15773603181671E-16

26,878.470023033106,-250,0.613786528606488

27,976.077803370118,-250,1.13412962222138

28,1073.68558370713,-250,1.48181176176368

29,1171.29336404414,-250,1.60390149323454

30,1268.90114438115,-250,1.48181176176368

31,1366.50892471817,-250,1.13412962222137

32,1464.11670505518,-250,0.613786528606488

33,1561.72448539219,-250,3.93003487252386E-16

101,-1561.72448539219,-218.75,-3.85452035444279E-16

102,-1464.11670505518,-218.75,-0.601992792567039

⋮

⋮

⋮

For brevity, the lines for nodes 103 to 133, 201 to 233, 301 to 333, 401 to 433,..., 2301 to 2333, 2401 to 2431, are omitted.

2432,1464.11670505518,-37.191726187369,132.512019222867

2433,1561.72448539219,-37.1691657965894,132.52660245615

*nset,nset=EndA,generate

1,2401,100

*nset,nset=EndB,generate

33,2433,100

*nset,nset=Mid,generate

```
17,2417,100
*nset,nset=MidPlate,generate
17,1617,100
*nset,nset=MidWeb,unsorted
817,1717,1817,1917,2017
*nset,nset=MidFlange,unsorted
2417,2317,2017,2117,2217
*nset,nset=Clamp,generate
2,32,1
1602,1632,1
******nset,nset=Clamp
*****5,11,17,23,29,
*****1605,1611,1617,1623,1629
*NSET,NSET=P1,GENERATE
1,33,1
*NSET,NSET=P2,GENERATE
101,133,1
*NSET,NSET=P3,GENERATE
201,233,1
*NSET,NSET=P4,GENERATE
301,333,1
*NSET,NSET=P5,GENERATE
401,433,1
*NSET,NSET=P6,GENERATE
501,533,1
*NSET,NSET=P7,GENERATE
601,633,1
*NSET,NSET=P8,GENERATE
701,733,1
*NSET,NSET=P9,GENERATE
801,833,1
*NSET,NSET=P10,GENERATE
901,933,1
*NSET,NSET=P11,GENERATE
1001,1033,1
```

```
*NSET,NSET=P12,GENERATE
1101,1133,1
*NSET,NSET=P13,GENERATE
1201,1233,1
*NSET,NSET=P14,GENERATE
1301,1333,1
*NSET,NSET=P15,GENERATE
1401,1433,1
*NSET,NSET=P16,GENERATE
1501,1533,1
*NSET,NSET=P17,GENERATE
1601,1633,1
*NSET,NSET=W1,GENERATE
1701,1733,1
*NSET,NSET=W2,GENERATE
1801,1833,1
*NSET,NSET=W3,GENERATE
1901,1933,1
*NSET,NSET=W4,GENERATE
2001,2033,1
*NSET,NSET=F1,GENERATE
2101,2133,1
*NSET,NSET=F2,GENERATE
2201,2233,1
*NSET,NSET=F3,GENERATE
2301,2333,1
*NSET,NSET=F4,GENERATE
2401,2433,1
**
**element connectivity
**
*element,type=s4r
1,   1,2,102,101
513, 801,802,1702,1701
514, 1701,1702,1802,1801
```

```
641, 2401,2402,2302,2301
642, 2301,2302,2002,2001
643, 2001,2002,2102,2101
644, 2101,2102,2202,2201
*elgen,elset=Plate
1,  16,100,1,    32,1,16
*elgen,elset=Web
513,  32,1,4
514,  3,100,1,   32,1,4
*elgen,elset=Flange
641,  32,1,4
642,  32,1,4
643,  32,1,4
644,  32,1,4
**
** Section & Material
**
*shell section, elset=plate, material=plate
<tp>
*material,name=plate
*elastic
<E>, 0.3
*plastic, HARDENING=isotropic
<fyp>,0
<fypp>,1
*EXPANSION, TYPE=ORTHO
.0000117,0,0
*shell section, elset=web, material=web
<tw>
*material,name=web
*ELASTIC
<E>, 0.3
*PLASTIC, HARDENING=isotropic
<fyw>,0
<fywp>,1
```

```
*EXPANSION, TYPE=ORTHO
.0000117,0,0
*shell section, elset=flange, material=flange
<tf>
*MATERIAL, NAME=FLANGE
*ELASTIC
<E>, 0.3
*PLASTIC, HARDENING=isotropic
<fyf>,0
<fyfp>,1
*EXPANSION, TYPE=ORTHO
.0000117,0,0
****************************
** Build the rigid frames
****************************
**
** Node definiton
**
*node,nset=RBEndA
10001,-<HalfL>,-<Halfbp>
11601,-<HalfL>, <Halfbp>
11701,-<HalfL>,        0,   <Quaterh0>
11801,-<HalfL>,        0,   <Halfh0>
11901,-<HalfL>,        0,   <ThreeQuaterh0>
12001,-<HalfL>,        0,   <h0>
12101,-<HalfL>, <Quaterbf>, <h0>
12201,-<HalfL>, <Halfbf>,   <h0>
12301,-<HalfL>,-<Quaterbf>, <h0>
12401,-<HalfL>,-<Halfbf>,   <h0>
*ngen,nset=RBEndA
10001,11601,100
**11701,12001,100
*ncopy,old set=RBEndA,new set=RBEndB,
reflect=mirror,change number=32
0,0,0,    0,1,0
```

```
0,0,1
*node
20001,-<HalfL>, 0, <centroid>
20033, <HalfL> ,0, <centroid>
**
** element conectivity
**
*element, type=rb3d2,elset=RBEndA
1001,10001,10101
1017,10801,20001
1018,20001,11701
1019,11701,11801
1022,12401,12301
1023,12301,12001
1024,12001,12101
1025,12101,12201
*elgen, elset=RBenda
1001,16,100,1
1019, 3,100,1
*elcopy,old set=RBenda,element shift=1000,
shift nodes=32,new set=RBendb
*rigid body,elset=RBenda,ref node=20001
*rigid body,elset=RBendb,ref node=20033
**
** MPC
**
*mpc
beam,enda,RBenda
beam,endb,RBendb
*nset,nset=Ppoint
20033
*nset,nset=RFpoint
20001
*boundary
Ppoint,2,4
```

Ppoint,6
RFpoint,1,4
RFpoint,6
**clamp,2
clamp,4
clamp,6
*initial conditions,type=temperature
P1,0
P2,0
P3,0
P4,0
P5,0
P6,0
P7,0
P8,0
P9,0
P10,0
P11,0
P12,0
P13,0
P14,0
P15,0
P16,0
P17,0
W1,0
W2,0
W3,0
W4,0
F1,0
F2,0
F3,0
F4,0
****
** History
****

Note:
For the boundary condition that has transverse in-plane restraints along unloaded plate edges, this line is "clamp,2"

```
**
** step 1
**
*step,nlgeom
apply residual stress
*static
0.01,0.1
*temperature
P1,53.8461538461538
P2,53.8461538461538
P3,53.8461538461538
P4,53.8461538461538
P5,53.8461538461538
P6,16.1928651059085
P7,-52.6755852842809
P8,-116.08138238573
P9,-179.48717948718
P10,-116.08138238573
P11,-52.6755852842809
P12,16.1928651059085
P13,53.8461538461538
P14,53.8461538461538
P15,53.8461538461538
P16,53.8461538461538
P17,53.8461538461538
W1,94.2307692307692
W2,32.9059828461538
W3,-10.4700855
W4,-53.8461538461538
F1,0
F2,53.8461538461538
F3,0
F4,53.8461538461538
*end step
**
```

```
** step 2
**
*step,nlgeom
40% plastic moment
*static
0.01,0.1
*cload
Ppoint,  5,-<Mapply>
RFpoint, 5, <Mapply>
*monitor, dof=1, node=Ppoint
*output,field,frequency=1
*node output
u
*node output,nset=Ppoint
cf
*node output,nset=RFpoint
rf
*element output
s,e
*output,history,frequency=1
*energy output
allwk
*energy output,elset=Plate
allse,allpd,allie
*energy output,elset=Web
allse,allpd,allie
*energy output,elset=Flange
allse,allpd,allie
*end step
**
** step 3
**
*step,nlgeom,inc=1000
axial load
*static, riks
```

Note:
If β_9 = 0, step 2 should be removed.

```
0.05,1,,,,Ppoint,1,-<PercentL>
*cload
Ppoint,1,-10000
*monitor, dof=1, node=Ppoint
*output,field,frequency=1
*node output
u
*node output,nset=Ppoint
cf
*node output,nset=RFpoint
rf
*element output
s,e
*output,history,frequency=1
*energy output
allwk
*energy output,elset=Plate
allse,allpd,allie
*energy output,elset=Web
allse,allpd,allie
*energy output,elset=Flange
allse,allpd,allie
*end step
```

APPENDIX B

FINITE ELEMENT ANALYSIS RESULTS

A total of 720 stiffened steel plates were analysed as described in the fractional factorial design matrix shown in Table B-1, where β_2 and β_3 are taken as only three different pairs, namely, (0.17, 0.17), (0.8, 0.6), and (1.5, 0.9). The 720 cases consist of 144 panel configurations and five load cases (five values of β_9). The dimensions of the panels and the values of the dimensionless parameters for the 144 specimens are presented in Table B-2 and Table B-3, respectively. The material properties are selected as F_{yp} = 420 MPa, F_{ys} = 420 MPa, E = 200000 MPa for all the panels. The numbering convention for the panel designation is explained in Figure B-1.

The failure modes for stiffened steel plates include plate and stiffener induced modes. Refined classifications may be also needed to provide more information. The refined modes are as follows:

PB (Plate Buckling): Buckling of the plate between the stiffeners;

PI (Plate Induced overall buckling): Stable plate induced overall buckling mode;

PP (Plate induced Plastic hinge instability): Formation of a plastic hinge following plate induced overall buckling;

SI (Stiffener Induced overall buckling): Stable stiffener induced overall buckling mode;

ST (Stiffener Tripping): Tripping of the stiffener about the stiffener to plate junction;

SP (Stiffener induced Plastic hinge instability): Formation of a plastic hinge following stiffener induced overall buckling.

One stiffened plate must undergo an overall buckling mode in failure and may normally have other failure modes before, after, or simultaneously with overall buckling. The detailed analysis of these behaviours was presented in Chapter 2.

When a stiffend plate undergoes evident plate buckling deformation, the plate induced overall buckling displacement is less evident, and the post-buckling behaviour is stable, the failure is designated as PB. When a stiffend plate undergoes more evident plate induced overall buckling than plate buckling and the post-buckling behaviour is stable, the failure is designated as PI. When a stiffened plate fails in plate induced overall buckling and the post-buckling behaviour is unstable, the failure is designated as PP.

For stiffener induced failure, stiffener tripping and stiffener local buckling is normally seen shortly after or at the peak axial load. However, as analyzed in Chapter 2, stiffener induced overall buckling is the mode governing the axial load capacity and the plastic hinge mechanism is the main reason for the post-buckling instability. Therefore, the stiffener induced failure mode in this appendix will be simply designated as SI if the post-buckling range is stable and as SP if the post-buckling range is unstable. Stiffener tripping and stiffener local buckling will not show in the mode designation for simplicity, although they may take place with plastic hinging in the post-buckling range.

The observed capacities and failure modes from the finite element analysis, and the calculated capacities and failure modes using the proposed design method, are presented in Tables B-4 to B-8 for β_9 = –0.4, –0.2, 0, 0.2, and 0.4, respectively. The normalized out-of-plane deflection that is to determine the plastic hinge instability, $(u_3/L)_H$, is also presented in Tables B-4 to B-8. It is calculated using both the observed and calculated capacities and Equation [B-1] or [B-2].

$$\left(\frac{u_3}{L}\right)_H = \frac{\beta_9 M_p}{P_c L} + \left(\frac{P_y}{P_c} + 1\right)\left(\frac{z_p}{L} - \frac{P_y + P_c}{4F_y bL}\right) \text{ for plate induced failure} \qquad \text{[B-1]}$$

$$\left(\frac{u_3}{L}\right)_H = \frac{\beta_9 M_p}{P_c L} - \left(\frac{P_y}{P_c} - 1\right)\left(\frac{z_p}{L} - \frac{P_y - P_c}{4F_y bL}\right) \text{ for stiffener induced failure} \qquad \text{[B-2]}$$

Figures B-2 to B-4, each including three force versus deformation plots, the extend of yielding and the deformed shape, show three examples that fail in the mode of plate induced plastic hinge instability (PP) with the predicted deflection magnitude in ranges of 0 < $\left(u_3/L\right)_H$ < 1%, 1% < $\left(u_3/L\right)_H$ < 2.5%, and $\left(u_3/L\right)_H$ > 2.5% respectively. Figures B-5 and B-6 show two examples failing in other plate induced modes with the predicted deflection magnitude in ranges of 1% < $\left(u_3/L\right)_H$ < 2.5% and $\left(u_3/L\right)_H$ > 2.5% respectively, while the range of 0 < $\left(u_3/L\right)_H$ < 1% is missing here since no sample falls in it.

Figures B-7 to B-9, each including three force versus deformation plots, the extend of yielding and the deformed shape, show three examples that fail in the mode of stiffener induced plastic hinge instability (SP) with the predicted deflection in ranges of of –1% < $\left(u_3/L\right)_H$ < 0, –2% < $\left(u_3/L\right)_H$ < –1%, and $\left(u_3/L\right)_H$ < –2% respectively. Figures B-10 and B-12 show examples failing in the mode of stiffener induced overall buckling (SI) with the predicted deflection in ranges of –1% < $\left(u_3/L\right)_H$ < 0, –2% < $\left(u_3/L\right)_H$ < –1%, and $\left(u_3/L\right)_H$ < –2%, respectively.

Table B-1 Parameter values

β_1	β_2	β_3	β^*	β_5	β_6	β_7	β_8	β_9
0.7	0.17	0.17	0.15	0.075	$0.1\,\beta_1^2$	0.0015	0.3	–0.4
1.28	0.8	0.6	0.4	0.15				–0.2
2.0	1.5	0.9	0.7	0.3				0
2.7			1.0					0.2
								0.4

Table B-2 Dimensions of analyzed specimens (mm)

Specimen	b	t	h_w	t_w	b_f	t_f	L
111_11	500	32.73	50.7	13.66	44.6	12.01	514
111_12	500	32.73	50.7	13.66	44.6	12.01	1370
111_13	500	32.73	50.7	13.66	44.6	12.01	2397
111_14	500	32.73	50.7	13.66	44.6	12.01	3424
211_11	500	17.90	37.5	10.10	33.0	8.88	514
211_12	500	17.90	37.5	10.10	33.0	8.88	1370
211_13	500	17.90	37.5	10.10	33.0	8.88	2397
211_14	500	17.90	37.5	10.10	33.0	8.88	3424
311_11	500	11.46	30.0	8.08	26.4	7.11	514
311_12	500	11.46	30.0	8.08	26.4	7.11	1370
311_13	500	11.46	30.0	8.08	26.4	7.11	2397
311_14	500	11.46	30.0	8.08	26.4	7.11	3424
411_11	500	8.49	25.8	6.96	22.7	6.12	514
411_12	500	8.49	25.8	6.96	22.7	6.12	1370
411_13	500	8.49	25.8	6.96	22.7	6.12	2397
411_14	500	8.49	25.8	6.96	22.7	6.12	3424
111_21	500	32.73	71.7	19.32	63.0	16.99	514
111_22	500	32.73	71.7	19.32	63.0	16.99	1370
111_23	500	32.73	71.7	19.32	63.0	16.99	2397
111_24	500	32.73	71.7	19.32	63.0	16.99	3424
211_21	500	17.90	53.0	14.29	46.6	12.56	514
211_22	500	17.90	53.0	14.29	46.6	12.56	1370
211_23	500	17.90	53.0	14.29	46.6	12.56	2397
211_24	500	17.90	53.0	14.29	46.6	12.56	3424
311_21	500	11.46	42.4	11.43	37.3	10.05	514
311_22	500	11.46	42.4	11.43	37.3	10.05	1370

Table B-2 Dimensions of analyzed specimens (mm)

Specimen	b	t	h_w	t_w	b_f	t_f	L
311_23	500	11.46	42.4	11.43	37.3	10.05	2397
311_24	500	11.46	42.4	11.43	37.3	10.05	3424
411_21	500	8.49	36.5	9.84	32.1	8.65	514
411_22	500	8.49	36.5	9.84	32.1	8.65	1370
411_23	500	8.49	36.5	9.84	32.1	8.65	2397
411_24	500	8.49	36.5	9.84	32.1	8.65	3424
111_31	500	32.73	101.4	27.32	89.1	24.02	514
111_32	500	32.73	101.4	27.32	89.1	24.02	1370
111_33	500	32.73	101.4	27.32	89.1	24.02	2397
111_34	500	32.73	101.4	27.32	89.1	24.02	3424
211_31	500	17.90	75.0	20.20	65.9	17.76	514
211_32	500	17.90	75.0	20.20	65.9	17.76	1370
211_33	500	17.90	75.0	20.20	65.9	17.76	2397
211_34	500	17.90	75.0	20.20	65.9	17.76	3424
311_31	500	11.46	60.0	16.16	52.7	14.21	514
311_32	500	11.46	60.0	16.16	52.7	14.21	1370
311_33	500	11.46	60.0	16.16	52.7	14.21	2397
311_34	500	11.46	60.0	16.16	52.7	14.21	3424
411_31	500	8.49	51.6	13.91	45.4	12.23	514
411_32	500	8.49	51.6	13.91	45.4	12.23	1370
411_33	500	8.49	51.6	13.91	45.4	12.23	2397
411_34	500	8.49	51.6	13.91	45.4	12.23	3424
122_11	500	32.73	109.9	6.30	83.7	6.39	469
122_12	500	32.73	109.9	6.30	83.7	6.39	1249
122_13	500	32.73	109.9	6.30	83.7	6.39	2186
122_14	500	32.73	109.9	6.30	83.7	6.39	3123

Table B-2 Dimensions of analyzed specimens (mm)

Specimen	b	t	h_w	t_w	b_f	t_f	L
222_11	500	17.90	81.3	4.66	61.9	4.73	469
222_12	500	17.90	81.3	4.66	61.9	4.73	1249
222_13	500	17.90	81.3	4.66	61.9	4.73	2186
222_14	500	17.90	81.3	4.66	61.9	4.73	3123
322_11	500	11.46	65.0	3.73	49.5	3.78	469
322_12	500	11.46	65.0	3.73	49.5	3.78	1249
322_13	500	11.46	65.0	3.73	49.5	3.78	2186
322_14	500	11.46	65.0	3.73	49.5	3.78	3123
422_11	500	8.49	56.0	3.21	42.6	3.26	469
422_12	500	8.49	56.0	3.21	42.6	3.26	1249
422_13	500	8.49	56.0	3.21	42.6	3.26	2186
422_14	500	8.49	56.0	3.21	42.6	3.26	3123
122_21	500	32.73	155.5	8.91	118.4	9.04	469
122_22	500	32.73	155.5	8.91	118.4	9.04	1249
122_23	500	32.73	155.5	8.91	118.4	9.04	2186
122_24	500	32.73	155.5	8.91	118.4	9.04	3123
222_21	500	17.90	115.0	6.59	87.5	6.69	469
222_22	500	17.90	115.0	6.59	87.5	6.69	1249
222_23	500	17.90	115.0	6.59	87.5	6.69	2186
222_24	500	17.90	115.0	6.59	87.5	6.69	3123
322_21	500	11.46	92.0	5.27	70.0	5.35	469
322_22	500	11.46	92.0	5.27	70.0	5.35	1249
322_23	500	11.46	92.0	5.27	70.0	5.35	2186
322_24	500	11.46	92.0	5.27	70.0	5.35	3123
422_21	500	8.49	79.2	4.53	60.3	4.60	469
422_22	500	8.49	79.2	4.53	60.3	4.60	1249

Table B-2 Dimensions of analyzed specimens (mm)

Specimen	b	t	h_w	t_w	b_f	t_f	L
422_23	500	8.49	79.2	4.53	60.3	4.60	2186
422_24	500	8.49	79.2	4.53	60.3	4.60	3123
122_31	500	32.73	219.9	12.59	167.4	12.79	469
122_32	500	32.73	219.9	12.59	167.4	12.79	1249
122_33	500	32.73	219.9	12.59	167.4	12.79	2186
122_34	500	32.73	219.9	12.59	167.4	12.79	3123
222_31	500	17.90	162.6	9.31	123.8	9.46	469
222_32	500	17.90	162.6	9.31	123.8	9.46	1249
222_33	500	17.90	162.6	9.31	123.8	9.46	2186
222_34	500	17.90	162.6	9.31	123.8	9.46	3123
322_31	500	11.46	130.1	7.45	99.0	7.56	469
322_32	500	11.46	130.1	7.45	99.0	7.56	1249
322_33	500	11.46	130.1	7.45	99.0	7.56	2186
322_34	500	11.46	130.1	7.45	99.0	7.56	3123
422_31	500	8.49	112.0	6.41	85.2	6.51	469
422_32	500	8.49	112.0	6.41	85.2	6.51	1249
422_33	500	8.49	112.0	6.41	85.2	6.51	2186
422_34	500	8.49	112.0	6.41	85.2	6.51	3123
133_11	500	32.73	150.5	4.60	102.5	5.22	466
133_12	500	32.73	150.5	4.60	102.5	5.22	1243
133_13	500	32.73	150.5	4.60	102.5	5.22	2174
133_14	500	32.73	150.5	4.60	102.5	5.22	3106
233_11	500	17.90	111.3	3.40	75.8	3.86	466
233_12	500	17.90	111.3	3.40	75.8	3.86	1243
233_13	500	17.90	111.3	3.40	75.8	3.86	2174
233_14	500	17.90	111.3	3.40	75.8	3.86	3106

Table B-2 Dimensions of analyzed specimens (mm)

Specimen	b	t	h_w	t_w	b_f	t_f	L
333_11	500	11.46	89.1	2.72	60.7	3.09	466
333_12	500	11.46	89.1	2.72	60.7	3.09	1243
333_13	500	11.46	89.1	2.72	60.7	3.09	2174
333_14	500	11.46	89.1	2.72	60.7	3.09	3106
433_11	500	8.49	76.6	2.34	52.2	2.66	466
433_12	500	8.49	76.6	2.34	52.2	2.66	1243
433_13	500	8.49	76.6	2.34	52.2	2.66	2174
433_14	500	8.49	76.6	2.34	52.2	2.66	3106
133_21	500	32.73	212.9	6.50	145.0	7.38	466
133_22	500	32.73	212.9	6.50	145.0	7.38	1243
133_23	500	32.73	212.9	6.50	145.0	7.38	2174
133_24	500	32.73	212.9	6.50	145.0	7.38	3106
233_21	500	17.90	157.4	4.81	107.2	5.46	466
233_22	500	17.90	157.4	4.81	107.2	5.46	1243
233_23	500	17.90	157.4	4.81	107.2	5.46	2174
233_24	500	17.90	157.4	4.81	107.2	5.46	3106
333_21	500	11.46	125.9	3.85	85.8	4.37	466
333_22	500	11.46	125.9	3.85	85.8	4.37	1243
333_23	500	11.46	125.9	3.85	85.8	4.37	2174
333_24	500	11.46	125.9	3.85	85.8	4.37	3106
433_21	500	8.49	108.4	3.31	73.8	3.76	466
433_22	500	8.49	108.4	3.31	73.8	3.76	1243
433_23	500	8.49	108.4	3.31	73.8	3.76	2174
433_24	500	8.49	108.4	3.31	73.8	3.76	3106
133_31	500	32.73	301.1	9.20	205.0	10.44	466
133_32	500	32.73	301.1	9.20	205.0	10.44	1243

Table B-2 Dimensions of analyzed specimens (mm)

Specimen	b	t	h_w	t_w	b_f	t_f	L
133_33	500	32.73	301.1	9.20	205.0	10.44	2174
133_34	500	32.73	301.1	9.20	205.0	10.44	3106
233_31	500	17.90	222.6	6.80	151.6	7.72	466
233_32	500	17.90	222.6	6.80	151.6	7.72	1243
233_33	500	17.90	222.6	6.80	151.6	7.72	2174
233_34	500	17.90	222.6	6.80	151.6	7.72	3106
333_31	500	11.46	178.1	5.44	121.3	6.18	466
333_32	500	11.46	178.1	5.44	121.3	6.18	1243
333_33	500	11.46	178.1	5.44	121.3	6.18	2174
333_34	500	11.46	178.1	5.44	121.3	6.18	3106
433_31	500	8.49	153.3	4.68	104.4	5.32	466
433_32	500	8.49	153.3	4.68	104.4	5.32	1243
433_33	500	8.49	153.3	4.68	104.4	5.32	2174
433_34	500	8.49	153.3	4.68	104.4	5.32	3106

Table B-3 Dimensionless parameters for the analyzed specimens

Specimen	β_1	β_2	β_3	β_4	β_5	β^*	L/b
111_11	0.70	0.17	0.17	1.59	0.075	0.15	1.03
111_12	0.70	0.17	0.17	4.23	0.075	0.40	2.74
111_13	0.70	0.17	0.17	7.41	0.075	0.70	4.79
111_14	0.70	0.17	0.17	10.59	0.075	1.00	6.85
211_11	1.28	0.17	0.17	1.17	0.075	0.15	1.03
211_12	1.28	0.17	0.17	3.13	0.075	0.40	2.74
211_13	1.28	0.17	0.17	5.48	0.075	0.70	4.79
211_14	1.28	0.17	0.17	7.83	0.075	1.00	6.85
311_11	2.00	0.17	0.17	0.94	0.075	0.15	1.03
311_12	2.00	0.17	0.17	2.50	0.075	0.40	2.74
311_13	2.00	0.17	0.17	4.38	0.075	0.70	4.79
311_14	2.00	0.17	0.17	6.26	0.075	1.00	6.85
411_11	2.70	0.17	0.17	0.81	0.075	0.15	1.03
411_12	2.70	0.17	0.17	2.16	0.075	0.40	2.74
411_13	2.70	0.17	0.17	3.77	0.075	0.70	4.79
411_14	2.70	0.17	0.17	5.39	0.075	1.00	6.85
111_21	0.70	0.17	0.17	1.12	0.150	0.15	1.03
111_22	0.70	0.17	0.17	2.99	0.150	0.40	2.74
111_23	0.70	0.17	0.17	5.24	0.150	0.70	4.79
111_24	0.70	0.17	0.17	7.48	0.150	1.00	6.85
211_21	1.28	0.17	0.17	0.83	0.150	0.15	1.03
211_22	1.28	0.17	0.17	2.21	0.150	0.40	2.74
211_23	1.28	0.17	0.17	3.87	0.150	0.70	4.79
211_24	1.28	0.17	0.17	5.54	0.150	1.00	6.85
311_21	2.00	0.17	0.17	0.66	0.150	0.15	1.03
311_22	2.00	0.17	0.17	1.77	0.150	0.40	2.74

Table B-3 Dimensionless parameters for the analyzed specimens

Specimen	β_1	β_2	β_3	β_4	β_5	β^*	L/b
311_23	2.00	0.17	0.17	3.10	0.150	0.70	4.79
311_24	2.00	0.17	0.17	4.43	0.150	1.00	6.85
411_21	2.70	0.17	0.17	0.57	0.150	0.15	1.03
411_22	2.70	0.17	0.17	1.52	0.150	0.40	2.74
411_23	2.70	0.17	0.17	2.67	0.150	0.70	4.79
411_24	2.70	0.17	0.17	3.81	0.150	1.00	6.85
111_31	0.70	0.17	0.17	0.79	0.300	0.15	1.03
111_32	0.70	0.17	0.17	2.12	0.300	0.40	2.74
111_33	0.70	0.17	0.17	3.70	0.300	0.70	4.79
111_34	0.70	0.17	0.17	5.29	0.300	1.00	6.85
211_31	1.28	0.17	0.17	0.59	0.300	0.15	1.03
211_32	1.28	0.17	0.17	1.57	0.300	0.40	2.74
211_33	1.28	0.17	0.17	2.74	0.300	0.70	4.79
211_34	1.28	0.17	0.17	3.91	0.300	1.00	6.85
311_31	2.00	0.17	0.17	0.47	0.300	0.15	1.03
311_32	2.00	0.17	0.17	1.25	0.300	0.40	2.74
311_33	2.00	0.17	0.17	2.19	0.300	0.70	4.79
311_34	2.00	0.17	0.17	3.13	0.300	1.00	6.85
411_31	2.70	0.17	0.17	0.40	0.300	0.15	1.03
411_32	2.70	0.17	0.17	1.08	0.300	0.40	2.74
411_33	2.70	0.17	0.17	1.89	0.300	0.70	4.79
411_34	2.70	0.17	0.17	2.69	0.300	1.00	6.85
122_11	0.70	0.80	0.60	0.75	0.075	0.15	0.94
122_12	0.70	0.80	0.60	2.01	0.075	0.40	2.50
122_13	0.70	0.80	0.60	3.52	0.075	0.70	4.37
122_14	0.70	0.80	0.60	5.02	0.075	1.00	6.25

Table B-3 Dimensionless parameters for the analyzed specimens

Specimen	β_1	β_2	β_3	β_4	β_5	β^*	L/b
222_11	1.28	0.80	0.60	0.56	0.075	0.15	0.94
222_12	1.28	0.80	0.60	1.49	0.075	0.40	2.50
222_13	1.28	0.80	0.60	2.60	0.075	0.70	4.37
222_14	1.28	0.80	0.60	3.71	0.075	1.00	6.25
322_11	2.00	0.80	0.60	0.45	0.075	0.15	0.94
322_12	2.00	0.80	0.60	1.19	0.075	0.40	2.50
322_13	2.00	0.80	0.60	2.08	0.075	0.70	4.37
322_14	2.00	0.80	0.60	2.97	0.075	1.00	6.25
422_11	2.70	0.80	0.60	0.38	0.075	0.15	0.94
422_12	2.70	0.80	0.60	1.02	0.075	0.40	2.50
422_13	2.70	0.80	0.60	1.79	0.075	0.70	4.37
422_14	2.70	0.80	0.60	2.56	0.075	1.00	6.25
122_21	0.70	0.80	0.60	0.53	0.150	0.15	0.94
122_22	0.70	0.80	0.60	1.42	0.150	0.40	2.50
122_23	0.70	0.80	0.60	2.49	0.150	0.70	4.37
122_24	0.70	0.80	0.60	3.55	0.150	1.00	6.25
222_21	1.28	0.80	0.60	0.39	0.150	0.15	0.94
222_22	1.28	0.80	0.60	1.05	0.150	0.40	2.50
222_23	1.28	0.80	0.60	1.84	0.150	0.70	4.37
222_24	1.28	0.80	0.60	2.63	0.150	1.00	6.25
322_21	2.00	0.80	0.60	0.32	0.150	0.15	0.94
322_22	2.00	0.80	0.60	0.84	0.150	0.40	2.50
322_23	2.00	0.80	0.60	1.47	0.150	0.70	4.37
322_24	2.00	0.80	0.60	2.10	0.150	1.00	6.25
422_21	2.70	0.80	0.60	0.27	0.150	0.15	0.94
422_22	2.70	0.80	0.60	0.72	0.150	0.40	2.50

Table B-3 Dimensionless parameters for the analyzed specimens

Specimen	β_1	β_2	β_3	β_4	β_5	β^*	L/b
422_23	2.70	0.80	0.60	1.27	0.150	0.70	4.37
422_24	2.70	0.80	0.60	1.81	0.150	1.00	6.25
122_31	0.70	0.80	0.60	0.38	0.300	0.15	0.94
122_32	0.70	0.80	0.60	1.00	0.300	0.40	2.50
122_33	0.70	0.80	0.60	1.76	0.300	0.70	4.37
122_34	0.70	0.80	0.60	2.51	0.300	1.00	6.25
222_31	1.28	0.80	0.60	0.28	0.300	0.15	0.94
222_32	1.28	0.80	0.60	0.74	0.300	0.40	2.50
222_33	1.28	0.80	0.60	1.30	0.300	0.70	4.37
222_34	1.28	0.80	0.60	1.86	0.300	1.00	6.25
322_31	2.00	0.80	0.60	0.22	0.300	0.15	0.94
322_32	2.00	0.80	0.60	0.59	0.300	0.40	2.50
322_33	2.00	0.80	0.60	1.04	0.300	0.70	4.37
322_34	2.00	0.80	0.60	1.49	0.300	1.00	6.25
422_31	2.70	0.80	0.60	0.19	0.300	0.15	0.94
422_32	2.70	0.80	0.60	0.51	0.300	0.40	2.50
422_33	2.70	0.80	0.60	0.89	0.300	0.70	4.37
422_34	2.70	0.80	0.60	1.28	0.300	1.00	6.25
133_11	0.70	1.50	0.90	0.56	0.075	0.15	0.93
133_12	0.70	1.50	0.90	1.50	0.075	0.40	2.49
133_13	0.70	1.50	0.90	2.63	0.075	0.70	4.35
133_14	0.70	1.50	0.90	3.75	0.075	1.00	6.21
233_11	1.28	1.50	0.90	0.42	0.075	0.15	0.93
233_12	1.28	1.50	0.90	1.11	0.075	0.40	2.49
233_13	1.28	1.50	0.90	1.94	0.075	0.70	4.35
233_14	1.28	1.50	0.90	2.77	0.075	1.00	6.21

Table B-3 Dimensionless parameters for the analyzed specimens

Specimen	β_1	β_2	β_3	β_4	β_5	β^*	L/b
333_11	2.00	1.50	0.90	0.33	0.075	0.15	0.93
333_12	2.00	1.50	0.90	0.89	0.075	0.40	2.49
333_13	2.00	1.50	0.90	1.55	0.075	0.70	4.35
333_14	2.00	1.50	0.90	2.22	0.075	1.00	6.21
433_11	2.70	1.50	0.90	0.29	0.075	0.15	0.93
433_12	2.70	1.50	0.90	0.76	0.075	0.40	2.49
433_13	2.70	1.50	0.90	1.34	0.075	0.70	4.35
433_14	2.70	1.50	0.90	1.91	0.075	1.00	6.21
133_21	0.70	1.50	0.90	0.40	0.150	0.15	0.93
133_22	0.70	1.50	0.90	1.06	0.150	0.40	2.49
133_23	0.70	1.50	0.90	1.86	0.150	0.70	4.35
133_24	0.70	1.50	0.90	2.65	0.150	1.00	6.21
233_21	1.28	1.50	0.90	0.29	0.150	0.15	0.93
233_22	1.28	1.50	0.90	0.78	0.150	0.40	2.49
233_23	1.28	1.50	0.90	1.37	0.150	0.70	4.35
233_24	1.28	1.50	0.90	1.96	0.150	1.00	6.21
333_21	2.00	1.50	0.90	0.24	0.150	0.15	0.93
333_22	2.00	1.50	0.90	0.63	0.150	0.40	2.49
333_23	2.00	1.50	0.90	1.10	0.150	0.70	4.35
333_24	2.00	1.50	0.90	1.57	0.150	1.00	6.21
433_21	2.70	1.50	0.90	0.20	0.150	0.15	0.93
433_22	2.70	1.50	0.90	0.54	0.150	0.40	2.49
433_23	2.70	1.50	0.90	0.95	0.150	0.70	4.35
433_24	2.70	1.50	0.90	1.35	0.150	1.00	6.21
133_31	0.70	1.50	0.90	0.28	0.300	0.15	0.93
133_32	0.70	1.50	0.90	0.75	0.300	0.40	2.49

Table B-3 Dimensionless parameters for the analyzed specimens

Specimen	β_1	β_2	β_3	β_4	β_5	β^*	L/b
133_33	0.70	1.50	0.90	1.31	0.300	0.70	4.35
133_34	0.70	1.50	0.90	1.88	0.300	1.00	6.21
233_31	1.28	1.50	0.90	0.21	0.300	0.15	0.93
233_32	1.28	1.50	0.90	0.55	0.300	0.40	2.49
233_33	1.28	1.50	0.90	0.97	0.300	0.70	4.35
233_34	1.28	1.50	0.90	1.39	0.300	1.00	6.21
333_31	2.00	1.50	0.90	0.17	0.300	0.15	0.93
333_32	2.00	1.50	0.90	0.44	0.300	0.40	2.49
333_33	2.00	1.50	0.90	0.78	0.300	0.70	4.35
333_34	2.00	1.50	0.90	1.11	0.300	1.00	6.21
433_31	2.70	1.50	0.90	0.14	0.300	0.15	0.93
433_32	2.70	1.50	0.90	0.38	0.300	0.40	2.49
433_33	2.70	1.50	0.90	0.67	0.300	0.70	4.35
433_34	2.70	1.50	0.90	0.95	0.300	1.00	6.21

Table B-4 Analysis results (β_9 = –0.4)

	FEA			Proposed Method		
Specimen	P_c/P_y	Mode	$(u_3/L)_H$ (%)	P_c/P_y	Mode	$(u_3/L)_H$ (%)
111_11	0.863	PP	0.58	0.615	PP	1.63
111_12	0.220	PI	2.32	0.275	PP	1.83
111_13	0.066	PI	4.39	0.107	PI	2.74
111_14	0.032	PI	6.32	0.054	PI	3.74
211_11	0.541	PP	1.34	0.530	PP	1.38
211_12	0.073	PI	4.16	0.151	PP	2.06
211_13	0.023	PI	7.42	0.053	PI	3.29
211_14	0.011	PI	10.46	0.026	PI	4.59
311_11	0.268	PP	2.18	0.361	PP	1.60
311_12	0.032	PI	6.40	0.086	PP	2.48
311_13	0.010	PI	11.23	0.029	PI	4.04
311_14	0.005	PI	15.56	0.015	PI	5.67
411_11	0.164	PI	2.79	0.263	PP	1.76
411_12	0.020	PI	8.24	0.058	PI	2.83
411_13	0.006	PI	14.98	0.020	PI	4.67
411_14	0.003	PI	21.80	0.010	PI	6.57
111_21	0.920	PB	1.72	0.748	PI	2.51
111_22	0.719	PP	1.00	0.530	PP	1.48
111_23	0.246	PP	1.85	0.272	PP	1.68
111_24	0.105	PI	2.89	0.148	PP	2.08
211_21	0.772	PP	1.79	0.709	PP	1.99
211_22	0.373	PP	1.44	0.371	PP	1.45
211_23	0.105	PI	2.64	0.153	PP	1.87
211_24	0.049	PI	3.84	0.079	PP	2.43

Table B-4 Analysis results (β_9 = –0.4)

	FEA			Proposed Method		
Specimen	P_c/P_y	Mode	$(u_3/L)_H$ (%)	P_c/P_y	Mode	$(u_3/L)_H$ (%)
311_21	0.545	PP	2.05	0.527	PP	2.12
311_22	0.168	PP	2.20	0.229	PP	1.67
311_23	0.057	PI	3.44	0.089	PP	2.25
311_24	0.028	PI	4.70	0.045	PI	3.00
411_21	0.407	PP	2.23	0.403	PP	2.25
411_22	0.098	PI	2.93	0.159	PP	1.89
411_23	0.035	PI	4.45	0.060	PI	2.65
411_24	0.019	PI	5.76	0.030	PI	3.57
111_31	0.912	PB	4.92	0.779	PI	5.79
111_32	0.850	PP	1.99	0.695	PP	2.42
111_33	0.689	PP	1.40	0.507	PP	1.84
111_34	0.415	PP	1.53	0.336	PP	1.83
211_31	0.782	PB	4.35	0.752	PI	4.50
211_32	0.706	PP	1.78	0.593	PP	2.04
211_33	0.434	PP	1.49	0.346	PP	1.79
211_34	0.201	PP	1.95	0.199	PP	1.96
311_31	0.571	PB	4.44	0.570	PI	4.45
311_32	0.457	PP	1.96	0.401	PP	2.17
311_33	0.222	PP	1.97	0.207	PP	2.08
311_34	0.110	PI	2.51	0.115	PP	2.42
411_31	0.444	PB	4.55	0.442	PI	4.57
411_32	0.310	PP	2.23	0.286	PP	2.37
411_33	0.131	PI	2.58	0.139	PP	2.45
411_34	0.072	PI	3.07	0.075	PI	2.96

Table B-4 Analysis results (β_9 = –0.4)

Specimen	FEA			Proposed Method		
	P_c/P_y	Mode	$(u_3/L)_H$ (%)	P_c/P_y	Mode	$(u_3/L)_H$ (%)
122_11	0.950	PB	1.32	0.810	PP	1.92
122_12	0.749	PP	0.83	0.629	PP	1.09
122_13	0.194	PP	2.20	0.357	PP	1.21
122_14	0.076	PI	3.76	0.203	PP	1.48
222_11	0.803	PP	1.47	0.778	PP	1.54
222_12	0.369	PP	1.35	0.476	PP	1.04
222_13	0.085	PI	3.05	0.213	PP	1.29
222_14	0.038	PI	4.67	0.112	PP	1.65
322_11	0.572	PP	1.75	0.595	PP	1.68
322_12	0.165	PP	2.07	0.314	PP	1.16
322_13	0.049	PI	3.72	0.131	PP	1.47
322_14	0.024	PI	5.30	0.067	PP	1.92
422_11	0.432	PP	1.91	0.467	PP	1.78
422_12	0.098	PI	2.72	0.228	PP	1.26
422_13	0.032	PI	4.52	0.092	PP	1.65
422_14	0.016	PI	6.20	0.047	PP	2.17
122_21	0.951	PB	4.40	0.859	PI	4.93
122_22	0.913	PP	1.73	0.805	PP	1.98
122_23	0.826	PP	1.10	0.658	PP	1.38
122_24	0.551	PP	1.13	0.485	PP	1.27
222_21	0.807	PB	3.94	0.829	PI	3.85
222_22	0.732	PP	1.61	0.722	PP	1.62
222_23	0.554	PP	1.15	0.498	PP	1.25
222_24	0.255	PP	1.50	0.314	PP	1.27

Table B-4 Analysis results (β_9 = –0.4)

Specimen	FEA P_c/P_y	FEA Mode	FEA $(u_3/L)_H$ (%)	Proposed Method P_c/P_y	Proposed Method Mode	Proposed Method $(u_3/L)_H$ (%)
322_21	0.577	PB	4.09	0.641	PI	3.78
322_22	0.511	PP	1.68	0.524	PP	1.65
322_23	0.275	PP	1.55	0.325	PP	1.36
322_24	0.139	PP	1.92	0.193	PP	1.44
422_21	0.443	PB	4.22	0.507	PI	3.83
422_22	0.388	PP	1.75	0.396	PP	1.72
422_23	0.162	PP	2.00	0.231	PP	1.49
422_24	0.088	PI	2.40	0.134	PP	1.65
122_31	0.932	PB	11.95	0.844	PI	12.82
122_32	0.902	PB	4.59	0.829	PI	4.87
122_33	0.873	PB	2.68	0.782	PI	2.90
122_34	0.817	PP	1.97	0.703	PP	2.18
222_31	0.783	PB	10.09	0.812	PI	9.86
222_32	0.739	PB	3.92	0.781	PI	3.79
222_33	0.766	PP	2.19	0.692	PP	2.33
222_34	0.717	PP	1.60	0.565	PP	1.86
322_31	0.564	PB	9.89	0.626	PI	9.27
322_32	0.525	PB	3.88	0.588	PI	3.61
322_33	0.518	PP	2.24	0.490	PP	2.32
322_34	0.454	PP	1.70	0.372	PP	1.95
422_31	0.433	PB	10.02	0.492	PI	9.23
422_32	0.429	PB	3.78	0.453	PI	3.65
422_33	0.416	PP	2.20	0.360	PP	2.43
422_34	0.288	PP	1.99	0.261	PP	2.14

Table B-4 Analysis results (β_9 = –0.4)

	FEA			Proposed Method		
Specimen	P_c/P_y	Mode	$(u_3/L)_H$ (%)	P_c/P_y	Mode	$(u_3/L)_H$ (%)
133_11	0.962	PB	1.99	0.861	PP	2.44
133_12	0.912	PP	0.83	0.753	PP	1.12
133_13	0.477	PP	1.10	0.523	PP	1.00
133_14	0.164	PP	2.11	0.331	PP	1.10
233_11	0.818	PB	1.99	0.830	PP	1.95
233_12	0.655	PP	0.96	0.634	PP	1.00
233_13	0.200	PP	1.65	0.350	PP	1.00
233_14	0.082	PI	2.61	0.196	PP	1.18
333_11	0.582	PB	2.25	0.643	PP	2.05
333_12	0.336	PP	1.36	0.445	PP	1.07
333_13	0.108	PP	2.11	0.222	PP	1.11
333_14	0.051	PI	2.99	0.121	PP	1.34
433_11	0.447	PP	2.38	0.510	PP	2.13
433_12	0.202	PP	1.74	0.333	PP	1.14
433_13	0.068	PP	2.66	0.159	PP	1.23
433_14	0.034	PI	3.57	0.085	PP	1.51
133_21	0.956	PB	6.26	0.886	PI	6.72
133_22	0.932	PB	2.40	0.858	PI	2.59
133_23	0.896	PP	1.42	0.774	PP	1.62
133_24	0.802	PP	1.10	0.648	PP	1.31
233_21	0.814	PB	5.40	0.852	PI	5.22
233_22	0.759	PI	2.13	0.798	PP	2.06
233_23	0.754	PP	1.23	0.650	PP	1.37
233_24	0.531	PP	1.11	0.477	PP	1.20

Table B-4 Analysis results (β_9 = –0.4)

	FEA			Proposed Method		
Specimen	P_c/P_y	Mode	$(u_3/L)_H$ (%)	P_c/P_y	Mode	$(u_3/L)_H$ (%)
333_21	0.581	PB	5.47	0.662	PI	5.00
333_22	0.532	PP	2.18	0.600	PP	2.01
333_23	0.459	PP	1.38	0.452	PP	1.40
333_24	0.275	PP	1.41	0.309	PP	1.29
433_21	0.447	PB	5.59	0.525	PI	5.00
433_22	0.428	PP	2.16	0.464	PP	2.04
433_23	0.303	PP	1.58	0.333	PP	1.48
433_24	0.170	PP	1.75	0.219	PP	1.42
133_31	0.928	PB	16.77	0.861	PI	17.57
133_32	0.909	PB	6.37	0.853	PI	6.63
133_33	0.895	PB	3.67	0.830	PI	3.85
133_34	0.869	PP	2.62	0.787	PI	2.79
233_31	0.786	PB	13.85	0.825	PI	13.47
233_32	0.742	PB	5.37	0.810	PI	5.10
233_33	0.780	PP	2.98	0.764	PI	3.02
233_34	0.801	PP	2.05	0.687	PP	2.25
333_31	0.563	PB	13.45	0.638	PI	12.50
333_32	0.529	PB	5.24	0.619	PI	4.77
333_33	0.551	PI	2.92	0.565	PI	2.88
333_34	0.526	PP	2.10	0.483	PP	2.22
433_31	0.430	PB	13.62	0.503	PI	12.36
433_32	0.430	PB	5.10	0.483	PI	4.75
433_33	0.462	PI	2.79	0.428	PI	2.93
433_34	0.411	PP	2.10	0.353	PP	2.33

Table B-5 Analysis results (β_9 = –0.2)

	FEA			Proposed Method		
Specimen	P_c/P_y	Mode	$(u_3/L)_H$ (%)	P_c/P_y	Mode	$(u_3/L)_H$ (%)
111_11	0.939	PP	0.80	0.767	PP	1.52
111_12	0.458	PP	1.36	0.368	PP	1.77
111_13	0.142	PI	2.75	0.145	PI	2.68
111_14	0.067	PI	4.03	0.074	PI	3.68
211_11	0.724	PP	1.16	0.643	PP	1.42
211_12	0.182	PP	2.26	0.193	PP	2.12
211_13	0.057	PI	4.02	0.068	PI	3.41
211_14	0.028	PI	5.70	0.034	PI	4.76
311_11	0.428	PP	1.74	0.434	PP	1.72
311_12	0.087	PI	3.22	0.108	PI	2.62
311_13	0.030	PI	5.28	0.037	PI	4.26
311_14	0.015	PI	7.38	0.018	PI	5.99
411_11	0.290	PP	2.09	0.317	PP	1.92
411_12	0.051	PI	4.23	0.073	PI	3.02
411_13	0.018	PI	6.78	0.025	PI	4.96
411_14	0.009	PI	9.28	0.012	PI	6.98
111_21	0.964	PB	2.20	0.862	PI	2.70
111_22	0.834	PI	1.07	0.638	PP	1.55
111_23	0.435	PI	1.37	0.339	PP	1.76
111_24	0.206	PI	1.99	0.187	PP	2.19
211_21	0.816	PI	2.15	0.799	PP	2.21
211_22	0.538	PP	1.29	0.442	PP	1.57
211_23	0.190	PP	1.98	0.186	PP	2.02
211_24	0.093	PI	2.71	0.096	PI	2.65

Table B-5 Analysis results (β_9 = –0.2)

	FEA			Proposed Method		
Specimen	P_c/P_y	Mode	$(u_3/L)_H$ (%)	P_c/P_y	Mode	$(u_3/L)_H$ (%)
311_21	0.589	PI	2.39	0.594	PP	2.38
311_22	0.279	PP	1.79	0.273	PP	1.83
311_23	0.106	PI	2.49	0.107	PP	2.47
311_24	0.055	PI	3.29	0.055	PI	3.29
411_21	0.449	PI	2.57	0.458	PI	2.52
411_22	0.168	PI	2.32	0.190	PP	2.08
411_23	0.065	PI	3.22	0.073	PI	2.89
411_24	0.036	PI	4.04	0.037	PI	3.89
111_31	0.966	PB	5.72	0.886	PI	6.28
111_32	0.915	PI	2.28	0.805	PI	2.60
111_33	0.779	PP	1.54	0.608	PP	1.94
111_34	0.552	PP	1.49	0.412	PP	1.92
211_31	0.837	PB	4.97	0.843	PI	4.94
211_32	0.777	PP	1.99	0.684	PP	2.22
211_33	0.559	PP	1.50	0.415	PP	1.92
211_34	0.297	PP	1.78	0.242	PP	2.11
311_31	0.623	PB	5.04	0.647	PI	4.89
311_32	0.530	PP	2.14	0.471	PP	2.35
311_33	0.321	PP	1.83	0.252	PP	2.24
311_34	0.175	PP	2.15	0.141	PI	2.61
411_31	0.495	PB	5.12	0.510	PI	5.00
411_32	0.397	PP	2.28	0.343	PI	2.56
411_33	0.200	PI	2.29	0.171	PI	2.61
411_34	0.115	PI	2.61	0.094	PI	3.14

Table B-5 Analysis results (β_9 = –0.2)

	FEA			Proposed Method		
Specimen	P_c/P_y	Mode	$(u_3/L)_H$ (%)	P_c/P_y	Mode	$(u_3/L)_H$ (%)
122_11	0.977	PB	1.84	0.896	PP	2.22
122_12	0.891	PP	0.84	0.717	PP	1.21
122_13	0.471	PP	1.17	0.423	PP	1.32
122_14	0.214	PP	1.83	0.243	PP	1.62
222_11	0.833	PB	1.85	0.843	PP	1.81
222_12	0.603	PP	1.04	0.538	PP	1.18
222_13	0.215	PP	1.65	0.247	PP	1.45
222_14	0.101	PI	2.37	0.130	PP	1.87
322_11	0.594	PB	2.14	0.642	PP	1.97
322_12	0.324	PP	1.44	0.353	PP	1.33
322_13	0.115	PP	2.15	0.150	PP	1.68
322_14	0.060	PI	2.82	0.077	PP	2.20
422_11	0.455	PI	2.30	0.505	PP	2.09
422_12	0.192	PP	1.90	0.256	PP	1.46
422_13	0.073	PI	2.69	0.105	PP	1.89
422_14	0.040	PI	3.37	0.054	PP	2.50
122_21	0.982	PB	5.28	0.928	PI	5.63
122_22	0.952	PB	2.05	0.876	PP	2.25
122_23	0.883	PP	1.27	0.731	PP	1.54
122_24	0.706	PP	1.12	0.551	PP	1.41
222_21	0.838	PB	4.63	0.885	PI	4.40
222_22	0.780	PP	1.85	0.782	PP	1.85
222_23	0.688	PP	1.18	0.554	PP	1.42
222_24	0.396	PP	1.31	0.357	PP	1.43

Table B-5 Analysis results (β_9 = –0.2)

	FEA			Proposed Method		
Specimen	P_c/P_y	Mode	$(u_3/L)_H$ (%)	P_c/P_y	Mode	$(u_3/L)_H$ (%)
322_21	0.607	PB	4.78	0.687	PI	4.34
322_22	0.552	PP	1.93	0.571	PP	1.88
322_23	0.391	PP	1.46	0.364	PP	1.54
322_24	0.234	PP	1.56	0.220	PP	1.64
422_21	0.471	PB	4.93	0.547	PI	4.40
422_22	0.442	PP	1.95	0.436	PP	1.97
422_23	0.252	PP	1.75	0.261	PP	1.70
422_24	0.148	PP	1.94	0.154	PP	1.88
122_31	0.979	PB	13.58	0.922	PI	14.21
122_32	0.952	PB	5.20	0.908	PI	5.39
122_33	0.930	PB	3.02	0.863	PI	3.20
122_34	0.880	PP	2.21	0.785	PP	2.40
222_31	0.830	PB	11.40	0.881	PI	10.95
222_32	0.795	PB	4.40	0.852	PI	4.20
222_33	0.827	PP	2.45	0.765	PI	2.58
222_34	0.781	PP	1.78	0.636	PP	2.05
322_31	0.612	PB	11.16	0.688	PI	10.32
322_32	0.582	PB	4.33	0.652	PI	4.01
322_33	0.579	PP	2.48	0.553	PI	2.56
322_34	0.534	PP	1.84	0.427	PP	2.15
422_31	0.479	PB	11.29	0.550	PI	10.26
422_32	0.482	PB	4.21	0.512	PI	4.04
422_33	0.477	PP	2.43	0.415	PI	2.68
422_34	0.378	PP	2.01	0.306	PP	2.35

Table B-5 Analysis results (β_9 = –0.2)

	FEA			Proposed Method		
Specimen	P_c/P_y	Mode	$(u_3/L)_H$ (%)	P_c/P_y	Mode	$(u_3/L)_H$ (%)
133_11	0.985	PB	2.61	0.926	PI	2.90
133_12	0.945	PP	1.05	0.822	PP	1.30
133_13	0.721	PP	0.89	0.588	PP	1.13
133_14	0.384	PP	1.23	0.381	PP	1.24
233_11	0.839	PB	2.46	0.880	PP	2.32
233_12	0.757	PP	1.04	0.686	PP	1.16
233_13	0.402	PP	1.12	0.391	PP	1.15
233_14	0.189	PP	1.57	0.221	PP	1.36
333_11	0.605	PB	2.70	0.680	PP	2.42
333_12	0.468	PP	1.28	0.483	PP	1.25
333_13	0.215	PP	1.47	0.248	PP	1.29
333_14	0.107	PP	1.95	0.135	PP	1.57
433_11	0.466	PB	2.86	0.540	PI	2.51
433_12	0.326	PP	1.46	0.362	PP	1.34
433_13	0.135	PP	1.84	0.177	PP	1.43
433_14	0.072	PI	2.32	0.096	PP	1.77
133_21	0.984	PB	7.37	0.942	PI	7.68
133_22	0.965	PB	2.82	0.916	PI	2.96
133_23	0.936	PP	1.66	0.835	PP	1.84
133_24	0.869	PP	1.24	0.710	PP	1.48
233_21	0.839	PB	6.30	0.899	PI	5.96
233_22	0.791	PB	2.47	0.847	PP	2.34
233_23	0.800	PP	1.40	0.702	PP	1.55
233_24	0.672	PP	1.12	0.525	PP	1.36

Table B-5 Analysis results (β_9 = –0.2)

	FEA			Proposed Method		
Specimen	P_c/P_y	Mode	$(u_3/L)_H$ (%)	P_c/P_y	Mode	$(u_3/L)_H$ (%)
333_21	0.610	PB	6.36	0.702	PI	5.73
333_22	0.565	PB	2.52	0.641	PP	2.30
333_23	0.538	PP	1.49	0.493	PP	1.60
333_24	0.400	PP	1.31	0.343	PP	1.48
433_21	0.474	PB	6.51	0.561	PI	5.75
433_22	0.462	PI	2.48	0.501	PP	2.34
433_23	0.406	PP	1.57	0.366	PP	1.69
433_24	0.251	PP	1.60	0.245	PP	1.63
133_31	0.974	PB	18.91	0.930	PI	19.51
133_32	0.957	PB	7.18	0.924	PI	7.35
133_33	0.947	PB	4.13	0.902	PI	4.27
133_34	0.925	PB	2.94	0.861	PI	3.08
233_31	0.832	PB	15.60	0.888	PI	14.97
233_32	0.790	PB	6.04	0.875	PI	5.67
233_33	0.832	PI	3.34	0.831	PI	3.35
233_34	0.865	PP	2.28	0.755	PP	2.49
333_31	0.608	PB	15.20	0.696	PI	13.94
333_32	0.574	PB	5.91	0.678	PI	5.31
333_33	0.603	PB	3.27	0.625	PI	3.20
333_34	0.586	PP	2.33	0.541	PP	2.46
433_31	0.473	PB	15.38	0.558	PI	13.77
433_32	0.480	PB	5.71	0.539	PI	5.29
433_33	0.509	PI	3.14	0.483	PI	3.25
433_34	0.467	PP	2.33	0.404	PI	2.57

Table B-6 Analysis results (β_9 = 0)

Specimen	FEA P_c/P_y	FEA Mode	FEA $(u_3/L)_H$ (%)	Proposed Method P_c/P_y	Proposed Method Mode	Proposed Method $(u_3/L)_H$ (%)
111_11	0.991	PB	1.06	0.930	PP	1.31
111_12	0.665	PP	1.02	0.518	PP	1.47
111_13	0.264	PI	1.82	0.226	PP	2.14
111_14	0.133	PI	2.56	0.118	PI	2.88
211_11	0.807	PP	1.26	0.773	PP	1.36
211_12	0.321	PP	1.57	0.273	PP	1.86
211_13	0.113	PI	2.55	0.100	PI	2.88
211_14	0.057	PI	3.52	0.050	PI	3.97
311_11	0.538	PP	1.67	0.522	PP	1.73
311_12	0.160	PI	2.21	0.147	PP	2.40
311_13	0.059	PI	3.33	0.052	PI	3.76
311_14	0.031	PI	4.47	0.026	PI	5.20
411_11	0.378	PP	1.98	0.380	PP	1.96
411_12	0.095	PI	2.88	0.097	PI	2.81
411_13	0.036	PI	4.27	0.035	PI	4.44
411_14	0.019	PI	5.55	0.017	PI	6.13
111_21	1.007	PB	2.64	0.978	PI	2.79
111_22	0.912	PP	1.18	0.767	PP	1.52
111_23	0.593	PP	1.20	0.450	PP	1.62
111_24	0.315	PP	1.62	0.264	PP	1.93
211_21	0.862	PB	2.46	0.893	PP	2.35
211_22	0.664	PP	1.26	0.539	PP	1.57
211_23	0.295	PP	1.61	0.247	PP	1.90
211_24	0.151	PI	2.12	0.131	PP	2.42

Table B-6 Analysis results (β_9 = 0)

Specimen	FEA			Proposed Method		
	P_c/P_y	Mode	$(u_3/L)_H$ (%)	P_c/P_y	Mode	$(u_3/L)_H$ (%)
311_21	0.625	PB	2.72	0.665	PI	2.56
311_22	0.369	PP	1.68	0.332	PP	1.86
311_23	0.164	PI	2.04	0.139	PP	2.39
311_24	0.087	PI	2.61	0.073	PI	3.10
411_21	0.488	PB	2.87	0.516	PI	2.72
411_22	0.239	PI	2.06	0.232	PP	2.12
411_23	0.101	PI	2.62	0.094	PI	2.80
411_24	0.058	PI	3.16	0.049	PI	3.67
111_31	1.020	PB	6.42	0.994	PI	6.62
111_32	0.983	PB	2.51	0.921	PI	2.70
111_33	0.867	PP	1.64	0.731	PP	1.95
111_34	0.683	PP	1.46	0.528	PP	1.85
211_31	0.890	PB	5.51	0.935	PI	5.27
211_32	0.851	PI	2.15	0.786	PP	2.31
211_33	0.674	PP	1.51	0.511	PP	1.92
211_34	0.407	PP	1.63	0.316	PP	2.03
311_31	0.674	PB	5.54	0.725	PI	5.23
311_32	0.606	PI	2.27	0.551	PP	2.45
311_33	0.421	PP	1.75	0.313	PP	2.24
311_34	0.243	PP	1.95	0.182	PI	2.52
411_31	0.546	PB	5.58	0.580	PI	5.32
411_32	0.465	PI	2.38	0.408	PI	2.65
411_33	0.268	PI	2.15	0.217	PI	2.58
411_34	0.162	PI	2.34	0.124	PI	3.00

Table B-6 Analysis results (β_9 = 0)

	FEA			Proposed Method		
Specimen	P_c/P_y	Mode	$(u_3/L)_H$ (%)	P_c/P_y	Mode	$(u_3/L)_H$ (%)
122_11	1.004	PB	2.34	0.983	PP	2.44
122_12	0.952	PP	0.98	0.815	PP	1.27
122_13	0.683	PP	0.94	0.519	PP	1.31
122_14	0.374	PP	1.30	0.317	PP	1.53
222_11	0.858	PB	2.21	0.909	PP	2.03
222_12	0.723	PP	1.04	0.613	PP	1.26
222_13	0.355	PP	1.26	0.305	PP	1.45
222_14	0.182	PP	1.67	0.167	PP	1.82
322_11	0.620	PB	2.48	0.690	PP	2.22
322_12	0.427	PP	1.35	0.402	PP	1.43
322_13	0.196	PI	1.61	0.181	PP	1.73
322_14	0.106	PI	2.02	0.096	PP	2.21
422_11	0.478	PB	2.66	0.543	PP	2.35
422_12	0.271	PP	1.69	0.292	PP	1.58
422_13	0.122	PI	2.03	0.126	PP	1.97
422_14	0.069	PI	2.45	0.067	PI	2.54
122_21	1.014	PB	6.09	0.996	PI	6.22
122_22	0.991	PB	2.35	0.949	PP	2.46
122_23	0.941	PP	1.42	0.811	PP	1.66
122_24	0.804	PP	1.17	0.634	PP	1.48
222_21	0.868	PB	5.27	0.941	PI	4.88
222_22	0.820	PB	2.08	0.844	PP	2.03
222_23	0.777	PP	1.25	0.621	PP	1.52
222_24	0.552	PP	1.18	0.418	PP	1.50

Table B-6 Analysis results (β_9 = 0)

	FEA			Proposed Method		
Specimen	P_c/P_y	Mode	$(u_3/L)_H$ (%)	P_c/P_y	Mode	$(u_3/L)_H$ (%)
322_21	0.638	PB	5.40	0.733	PI	4.81
322_22	0.589	PB	2.16	0.621	PP	2.07
322_23	0.483	PP	1.45	0.412	PP	1.66
322_24	0.325	PP	1.42	0.258	PP	1.73
422_21	0.498	PB	5.58	0.587	PI	4.88
422_22	0.473	PB	2.18	0.478	PP	2.16
422_23	0.330	PP	1.68	0.298	PP	1.83
422_24	0.209	PI	1.74	0.182	PP	1.97
122_31	1.025	PB	15.04	0.999	PI	15.35
122_32	1.004	PB	5.74	0.987	PI	5.81
122_33	0.988	PB	3.32	0.946	PI	3.43
122_34	0.952	PI	2.39	0.873	PI	2.56
222_31	0.880	PB	12.54	0.950	PI	11.87
222_32	0.847	PB	4.83	0.924	PI	4.54
222_33	0.891	PB	2.66	0.842	PI	2.77
222_34	0.867	PP	1.90	0.717	PP	2.18
322_31	0.659	PB	12.26	0.750	PI	11.19
322_32	0.637	PB	4.71	0.716	PI	4.33
322_33	0.642	PB	2.68	0.619	PI	2.74
322_34	0.622	PI	1.92	0.492	PP	2.27
422_31	0.526	PB	12.32	0.609	PI	11.09
422_32	0.533	PB	4.58	0.572	PI	4.35
422_33	0.531	PB	2.62	0.474	PI	2.85
422_34	0.452	PP	2.07	0.360	PP	2.46

Table B-6 Analysis results (β_9 = 0)

Specimen	FEA			Proposed Method		
	P_c/P_y	Mode	$(u_3/L)_H$ (%)	P_c/P_y	Mode	$(u_3/L)_H$ (%)
133_11	1.007	PB	3.20	0.991	PI	3.28
133_12	0.979	PP	1.26	0.895	PP	1.44
133_13	0.848	PP	0.89	0.667	PP	1.20
133_14	0.661	SP	-0.37	0.455	PP	1.27
233_11	0.861	PB	2.90	0.930	PI	2.64
233_12	0.797	PP	1.19	0.744	PP	1.29
233_13	0.569	PP	0.97	0.448	PP	1.22
233_14	0.302	PP	1.24	0.266	PP	1.40
333_11	0.625	PB	3.14	0.717	PI	2.75
333_12	0.550	PP	1.33	0.524	PP	1.39
333_13	0.312	PP	1.28	0.283	PP	1.39
333_14	0.179	PP	1.49	0.160	PP	1.65
433_11	0.485	PB	3.31	0.571	PI	2.86
433_12	0.407	PP	1.45	0.394	PP	1.49
433_13	0.191	PI	1.63	0.202	PP	1.55
433_14	0.118	PI	1.80	0.113	PP	1.87
133_21	1.013	SP	0.10	0.998	PI	8.53
133_22	0.997	PB	3.20	0.975	PI	3.27
133_23	0.977	PP	1.87	0.898	PP	2.02
133_24	0.923	PP	1.38	0.777	PP	1.61
233_21	0.867	PB	7.12	0.946	PI	6.62
233_22	0.825	PB	2.78	0.898	PI	2.59
233_23	0.851	PP	1.55	0.757	PP	1.71
233_24	0.763	PP	1.19	0.583	PP	1.48

Table B-6 Analysis results (β_9 = 0)

	FEA			Proposed Method		
Specimen	P_c/P_y	Mode	$(u_3/L)_H$ (%)	P_c/P_y	Mode	$(u_3/L)_H$ (%)
333_21	0.636	PB	7.18	0.742	PI	6.38
333_22	0.600	PB	2.82	0.684	PI	2.55
333_23	0.587	PP	1.64	0.537	PP	1.75
333_24	0.496	PP	1.31	0.385	PP	1.60
433_21	0.499	PB	7.35	0.597	PI	6.40
433_22	0.497	PB	2.76	0.539	PI	2.60
433_23	0.469	PP	1.65	0.404	PP	1.86
433_24	0.326	PP	1.55	0.278	PP	1.77
133_31	1.017	PB	20.89	1.000	PI	21.16
133_32	1.005	PB	7.90	0.994	PI	7.97
133_33	0.998	PB	4.54	0.974	PI	4.62
133_34	0.980	PB	3.22	0.937	PI	3.32
233_31	0.877	PB	17.17	0.952	PI	16.26
233_32	0.837	PB	6.64	0.940	PI	6.15
233_33	0.887	PB	3.65	0.899	PI	3.62
233_34	0.930	PB	2.48	0.826	PI	2.68
333_31	0.653	PB	16.68	0.754	PI	15.15
333_32	0.627	PB	6.43	0.738	PI	5.76
333_33	0.644	PB	3.61	0.687	PI	3.46
333_34	0.654	PB	2.50	0.605	PI	2.64
433_31	0.518	PB	16.79	0.613	PI	14.92
433_32	0.532	PB	6.18	0.595	PI	5.71
433_33	0.554	PB	3.43	0.541	PI	3.49
433_34	0.527	PB	2.49	0.461	PI	2.74

Table B-7 Analysis results (β_9 = 0.2)

	FEA			Proposed Method		
Specimen	P_c/P_y	Mode	$(u_3/L)_H$ (%)	P_c/P_y	Mode	$(u_3/L)_H$ (%)
111_11	0.719	SI	-0.73	0.716	SP	-0.75
111_12	0.317	SP	-1.71	0.335	SP	-1.59
111_13	0.127	SI	-2.86	0.131	SP	-2.75
111_14	0.066	SI	-3.95	0.067	SP	-3.91
211_11	0.511	SP	-1.20	0.579	SP	-0.90
211_12	0.159	SP	-2.30	0.164	SP	-2.21
211_13	0.058	SI	-3.83	0.057	SP	-3.87
211_14	0.029	SI	-5.46	0.028	SP	-5.54
311_11	0.444	SP	-1.06	0.415	SP	-1.19
311_12	0.098	SP	-2.65	0.088	SP	-2.97
311_13	0.033	SI	-4.66	0.029	SP	-5.26
311_14	0.017	SI	-6.51	0.014	SP	-7.54
411_11	0.453	PP	1.94	0.323	SP	-1.35
411_12	0.078	SP	-2.63	0.057	SP	-3.61
411_13	0.024	SI	-5.00	0.019	SP	-6.44
411_14	0.012	SI	-7.32	0.009	SP	-9.25
111_21	0.790	SI	-0.43	0.770	SP	-0.54
111_22	0.587	SP	-0.72	0.551	SP	-0.85
111_23	0.321	SP	-1.28	0.284	SP	-1.52
111_24	0.176	SI	-1.92	0.155	SP	-2.21
211_21	0.724	SP	-0.49	0.717	SP	-0.52
211_22	0.418	SP	-0.90	0.367	SP	-1.12
211_23	0.175	SP	-1.71	0.149	SP	-2.07
211_24	0.090	SI	-2.52	0.076	SP	-3.01

Table B-7 Analysis results (β_9 = 0.2)

	FEA			Proposed Method		
Specimen	P_c/P_y	Mode	$(u_3/L)_H$ (%)	P_c/P_y	Mode	$(u_3/L)_H$ (%)
311_21	0.671	PB	2.97	0.637	SP	-0.60
311_22	0.327	SP	-0.95	0.243	SP	-1.42
311_23	0.112	SP	-2.04	0.086	SP	-2.69
311_24	0.055	SI	-3.02	0.043	SP	-3.93
411_21	0.528	PB	3.11	0.578	PI	2.86
411_22	0.308	PP	1.92	0.180	SP	-1.66
411_23	0.086	SI	-2.18	0.059	SP	-3.22
411_24	0.041	SI	-3.29	0.029	SP	-4.74
111_31	0.854	SI	0.03	0.790	SP	-0.50
111_32	0.772	SP	-0.25	0.707	SP	-0.49
111_33	0.617	SP	-0.51	0.517	SP	-0.84
111_34	0.433	SP	-0.86	0.343	SP	-1.28
211_31	0.840	SP	-0.01	0.773	SP	-0.38
211_32	0.699	SP	-0.32	0.606	SP	-0.60
211_33	0.437	SP	-0.78	0.347	SP	-1.17
211_34	0.253	SP	-1.30	0.197	SP	-1.79
311_31	0.726	PB	5.97	0.745	SP	-0.38
311_32	0.692	PP	2.33	0.512	SP	-0.71
311_33	0.318	SP	-0.99	0.236	SP	-1.52
311_34	0.165	SI	-1.66	0.122	SP	-2.37
411_31	0.596	PB	5.96	0.652	PI	5.55
411_32	0.540	PP	2.42	0.457	SP	-0.75
411_33	0.260	SP	-1.10	0.174	SP	-1.84
411_34	0.124	SI	-1.92	0.086	SP	-2.91

Table B-7 Analysis results (β_9 = 0.2)

	FEA			Proposed Method		
Specimen	P_c/P_y	Mode	$(u_3/L)_H$ (%)	P_c/P_y	Mode	$(u_3/L)_H$ (%)
122_11	0.740	SI	-0.74	0.777	SP	-0.51
122_12	0.495	SP	-1.06	0.597	SP	-0.67
122_13	0.294	SP	-1.41	0.336	SP	-1.17
122_14	0.171	SP	-1.93	0.190	SP	-1.70
222_11	0.616	SP	-0.96	0.730	SP	-0.46
222_12	0.384	SP	-1.01	0.428	SP	-0.84
222_13	0.175	SP	-1.64	0.186	SP	-1.52
222_14	0.093	SI	-2.29	0.097	SP	-2.22
322_11	0.644	PB	2.81	0.640	SP	-0.58
322_12	0.320	SP	-0.93	0.299	SP	-1.03
322_13	0.118	SP	-1.80	0.112	SP	-1.91
322_14	0.060	SI	-2.59	0.056	SP	-2.80
422_11	0.498	PB	2.99	0.583	PI	2.57
422_12	0.354	PP	1.55	0.232	SP	-1.14
422_13	0.096	SP	-1.81	0.079	SP	-2.22
422_14	0.046	SI	-2.76	0.039	SP	-3.28
122_21	0.792	SI	-0.47	0.794	SP	-0.45
122_22	0.690	SP	-0.54	0.737	SP	-0.36
122_23	0.583	SP	-0.59	0.593	SP	-0.56
122_24	0.447	SP	-0.77	0.430	SP	-0.83
222_21	0.749	SP	-0.51	0.777	SP	-0.35
222_22	0.652	SP	-0.43	0.664	SP	-0.40
222_23	0.456	SP	-0.68	0.440	SP	-0.73
222_24	0.295	SP	-0.99	0.270	SP	-1.12

Table B-7 Analysis results (β_9 = 0.2)

	FEA			Proposed Method		
Specimen	P_c/P_y	Mode	$(u_3/L)_H$ (%)	P_c/P_y	Mode	$(u_3/L)_H$ (%)
322_21	0.663	PB	5.99	0.741	SP	-0.39
322_22	0.628	PI	2.36	0.593	SP	-0.44
322_23	0.366	SP	-0.74	0.329	SP	-0.88
322_24	0.202	SP	-1.22	0.179	SP	-1.41
422_21	0.525	PB	6.14	0.628	PI	5.30
422_22	0.508	PI	2.37	0.524	PP	2.31
422_23	0.404	PP	1.64	0.267	SP	-0.99
422_24	0.160	SP	-1.34	0.133	SP	-1.66
122_31	0.832	SI	0.00	0.798	SP	-0.48
122_32	0.770	SP	-0.34	0.782	SP	-0.27
122_33	0.726	SP	-0.35	0.734	SP	-0.32
122_34	0.681	SP	-0.37	0.656	SP	-0.44
222_31	0.800	SI	-0.24	0.793	SP	-0.32
222_32	0.764	SP	-0.23	0.760	SP	-0.25
222_33	0.685	SP	-0.33	0.666	SP	-0.39
222_34	0.584	SP	-0.46	0.535	SP	-0.60
322_31	0.702	PB	13.25	0.781	SP	-0.31
322_32	0.685	PB	5.06	0.738	SP	-0.25
322_33	0.633	SP	-0.37	0.608	SP	-0.43
322_34	0.474	SP	-0.62	0.438	SP	-0.74
422_31	0.572	PB	13.18	0.668	PI	11.76
422_32	0.571	PB	4.95	0.634	PI	4.58
422_33	0.606	PI	2.71	0.540	PI	2.95
422_34	0.402	SI	-0.73	0.377	SP	-0.82

Table B-7 Analysis results (β_9 = 0.2)

	FEA			Proposed Method		
Specimen	P_c/P_y	Mode	$(u_3/L)_H$ (%)	P_c/P_y	Mode	$(u_3/L)_H$ (%)
133_11	0.699	SP	-1.08	0.787	SP	-0.46
133_12	0.562	SP	-0.87	0.678	SP	-0.46
133_13	0.389	SP	-1.04	0.459	SP	-0.78
133_14	0.250	SP	-1.37	0.287	SP	-1.14
233_11	0.658	SP	-0.84	0.756	SP	-0.38
233_12	0.498	SP	-0.70	0.553	SP	-0.55
233_13	0.274	SP	-1.08	0.290	SP	-1.00
233_14	0.156	SP	-1.51	0.159	SP	-1.47
333_11	0.643	PB	3.57	0.687	SP	-0.47
333_12	0.585	PP	1.46	0.439	SP	-0.64
333_13	0.200	SP	-1.16	0.192	SP	-1.22
333_14	0.102	SP	-1.76	0.098	SP	-1.83
433_11	0.502	PB	3.73	0.602	PI	3.16
433_12	0.463	PP	1.51	0.382	SP	-0.65
433_13	0.181	SP	-1.05	0.143	SP	-1.39
433_14	0.079	SP	-1.87	0.070	SP	-2.12
133_21	0.772	SP	-0.69	0.797	SP	-0.44
133_22	0.713	SP	-0.50	0.767	SP	-0.28
133_23	0.643	SP	-0.48	0.682	SP	-0.37
133_24	0.544	SP	-0.58	0.560	SP	-0.54
233_21	0.760	SP	-0.49	0.785	SP	-0.32
233_22	0.714	SP	-0.31	0.726	SP	-0.28
233_23	0.565	SP	-0.48	0.573	SP	-0.46
233_24	0.437	SP	-0.63	0.406	SP	-0.72

Table B-7 Analysis results (β_9 = 0.2)

	FEA			Proposed Method		
Specimen	P_c/P_y	Mode	$(u_3/L)_H$ (%)	P_c/P_y	Mode	$(u_3/L)_H$ (%)
333_21	0.663	PB	7.94	0.758	SP	-0.35
333_22	0.634	PB	3.08	0.683	SP	-0.29
333_23	0.642	PP	1.74	0.486	SP	-0.53
333_24	0.324	SP	-0.79	0.301	SP	-0.88
433_21	0.523	PB	8.12	0.633	PI	6.98
433_22	0.532	PB	3.00	0.578	PI	2.81
433_23	0.519	PP	1.75	0.447	PP	1.97
433_24	0.277	SP	-0.82	0.242	SP	-0.99
133_31	0.810	SP	-0.28	0.799	SP	-0.47
133_32	0.774	SP	-0.35	0.791	SP	-0.23
133_33	0.749	SP	-0.31	0.766	SP	-0.23
133_34	0.710	SP	-0.34	0.723	SP	-0.30
233_31	0.799	SP	-0.26	0.795	SP	-0.31
233_32	0.778	SP	-0.20	0.779	SP	-0.19
233_33	0.735	SP	-0.24	0.730	SP	-0.26
233_34	0.666	SP	-0.34	0.649	SP	-0.38
333_31	0.696	PB	18.03	0.787	SP	-0.29
333_32	0.678	PB	6.89	0.767	SP	-0.19
333_33	0.716	PI	3.79	0.700	SP	-0.27
333_34	0.595	SP	-0.42	0.588	SP	-0.43
433_31	0.564	PB	17.95	0.669	PI	15.88
433_32	0.582	PB	6.58	0.653	PI	6.06
433_33	0.627	PI	3.56	0.602	PI	3.67
433_34	0.600	PP	2.57	0.525	PI	2.84

Table B-8 Analysis results (β_9 = 0.4)

	FEA			Proposed Method		
Specimen	P_c/P_y	Mode	$(u_3/L)_H$ (%)	P_c/P_y	Mode	$(u_3/L)_H$ (%)
111_11	0.546	SI	-1.00	0.519	SP	-1.17
111_12	0.167	SI	-2.71	0.225	SP	-1.89
111_13	0.061	SI	-4.59	0.087	SP	-3.13
111_14	0.031	SI	-6.41	0.044	SP	-4.43
211_11	0.309	SI	-1.89	0.400	SP	-1.22
211_12	0.065	SI	-4.39	0.108	SP	-2.57
211_13	0.023	SI	-7.33	0.037	SP	-4.44
211_14	0.012	SI	-10.14	0.019	SP	-6.35
311_11	0.182	SI	-2.57	0.257	SP	-1.66
311_12	0.037	SI	-5.45	0.053	SP	-3.71
311_13	0.013	SI	-9.01	0.018	SP	-6.47
311_14	0.007	SI	-12.41	0.009	SP	-9.26
411_11	0.147	SI	-2.56	0.180	SP	-2.02
411_12	0.028	SI	-5.57	0.033	SP	-4.79
411_13	0.009	SI	-9.75	0.011	SP	-8.42
411_14	0.005	SI	-13.76	0.005	SP	-12.06
111_21	0.605	SI	-0.70	0.569	SP	-0.96
111_22	0.308	SI	-1.60	0.382	SP	-1.10
111_23	0.161	SI	-2.18	0.190	SP	-1.78
111_24	0.091	SI	-2.91	0.103	SP	-2.53
211_21	0.445	SI	-1.25	0.517	SP	-0.80
211_22	0.217	SI	-1.62	0.245	SP	-1.37
211_23	0.093	SI	-2.52	0.098	SP	-2.40
211_24	0.049	SI	-3.55	0.050	SP	-3.45

Table B-8 Analysis results (β_9 = 0.4)

	FEA			Proposed Method		
Specimen	P_c/P_y	Mode	$(u_3/L)_H$ (%)	P_c/P_y	Mode	$(u_3/L)_H$ (%)
311_21	0.420	SP	-0.99	0.430	SP	-0.94
311_22	0.161	SI	-1.68	0.151	SP	-1.81
311_23	0.062	SI	-2.81	0.054	SP	-3.24
311_24	0.031	SI	-4.01	0.027	SP	-4.69
411_21	0.440	SP	-0.69	0.377	SP	-0.99
411_22	0.140	SI	-1.60	0.106	SP	-2.20
411_23	0.048	SI	-3.01	0.036	SP	-4.00
411_24	0.024	SI	-4.28	0.018	SP	-5.80
111_31	0.666	SI	-0.16	0.590	SP	-0.95
111_32	0.514	SP	-0.71	0.511	SP	-0.73
111_33	0.380	SP	-0.94	0.357	SP	-1.07
111_34	0.251	SP	-1.35	0.231	SP	-1.52
211_31	0.585	SI	-0.56	0.571	SP	-0.67
211_32	0.449	SP	-0.69	0.423	SP	-0.81
211_33	0.268	SP	-1.14	0.232	SP	-1.42
211_34	0.156	SI	-1.68	0.130	SP	-2.09
311_31	0.578	SI	-0.41	0.535	SP	-0.67
311_32	0.401	SP	-0.67	0.332	SP	-1.01
311_33	0.192	SP	-1.37	0.150	SP	-1.89
311_34	0.104	SI	-2.05	0.078	SP	-2.83
411_31	0.602	SP	-0.21	0.515	SP	-0.64
411_32	0.382	SP	-0.61	0.270	SP	-1.18
411_33	0.154	SI	-1.51	0.107	SP	-2.34
411_34	0.079	SI	-2.31	0.054	SP	-3.52

Table B-8 Analysis results (β_9 = 0.4)

Specimen	FEA P_c/P_y	FEA Mode	FEA $(u_3/L)_H$ (%)	Proposed Method P_c/P_y	Proposed Method Mode	Proposed Method $(u_3/L)_H$ (%)
122_11	0.562	SI	-1.03	0.576	SP	-0.92
122_12	0.219	SI	-2.55	0.419	SP	-0.90
122_13	0.107	SI	-3.39	0.226	SP	-1.40
122_14	0.062	SI	-4.24	0.127	SP	-1.96
222_11	0.371	SI	-1.82	0.529	SP	-0.74
222_12	0.156	SI	-2.36	0.287	SP	-1.05
222_13	0.071	SI	-3.24	0.122	SP	-1.78
222_14	0.039	SI	-4.29	0.063	SP	-2.55
322_11	0.303	SI	-1.79	0.434	SP	-0.89
322_12	0.129	SI	-2.08	0.184	SP	-1.35
322_13	0.051	SI	-3.24	0.070	SP	-2.35
322_14	0.027	SI	-4.41	0.035	SP	-3.38
422_11	0.314	SP	-1.33	0.379	SP	-0.94
422_12	0.121	SI	-1.79	0.133	SP	-1.59
422_13	0.044	SI	-3.08	0.047	SP	-2.83
422_14	0.021	SI	-4.50	0.023	SP	-4.11
122_21	0.605	SI	-0.75	0.593	SP	-0.88
122_22	0.416	SI	-1.28	0.538	SP	-0.57
122_23	0.328	SP	-1.19	0.416	SP	-0.74
122_24	0.239	SP	-1.39	0.292	SP	-1.02
222_21	0.500	SI	-1.23	0.575	SP	-0.61
222_22	0.393	SP	-0.92	0.471	SP	-0.57
222_23	0.260	SP	-1.13	0.297	SP	-0.91
222_24	0.164	SP	-1.49	0.179	SP	-1.34

Table B-8 Analysis results (β_9 = 0.4)

	FEA			Proposed Method		
Specimen	P_c/P_y	Mode	$(u_3/L)_H$ (%)	P_c/P_y	Mode	$(u_3/L)_H$ (%)
322_21	0.497	SI	-0.88	0.534	SP	-0.65
322_22	0.365	SP	-0.78	0.392	SP	-0.67
322_23	0.204	SP	-1.18	0.207	SP	-1.16
322_24	0.116	SI	-1.69	0.113	SP	-1.74
422_21	0.528	SP	-0.54	0.512	SP	-0.61
422_22	0.371	SP	-0.61	0.343	SP	-0.72
422_23	0.173	SP	-1.21	0.157	SP	-1.37
422_24	0.092	SI	-1.82	0.082	SP	-2.08
122_31	0.639	SI	-0.21	0.598	SP	-0.95
122_32	0.539	SI	-0.82	0.581	SP	-0.48
122_33	0.497	SP	-0.68	0.536	SP	-0.48
122_34	0.446	SP	-0.70	0.467	SP	-0.61
222_31	0.587	SI	-0.67	0.591	SP	-0.61
222_32	0.530	SI	-0.56	0.558	SP	-0.40
222_33	0.459	SP	-0.60	0.473	SP	-0.54
222_34	0.371	SP	-0.76	0.368	SP	-0.78
322_31	0.577	SI	-0.55	0.576	SP	-0.56
322_32	0.513	SP	-0.49	0.527	SP	-0.42
322_33	0.402	SP	-0.67	0.407	SP	-0.65
322_34	0.293	SP	-0.93	0.281	SP	-1.00
422_31	0.587	SI	-0.34	0.570	SP	-0.50
422_32	0.508	SP	-0.42	0.507	SP	-0.42
422_33	0.368	SP	-0.69	0.357	SP	-0.74
422_34	0.245	SP	-1.05	0.224	SP	-1.22

Table B-8 Analysis results (β_9 = 0.4)

Specimen	FEA			Proposed Method		
	P_c/P_y	Mode	$(u_3/L)_H$ (%)	P_c/P_y	Mode	$(u_3/L)_H$ (%)
133_11	0.419	SP	-2.61	0.586	SP	-0.86
133_12	0.250	SP	-2.38	0.486	SP	-0.67
133_13	0.148	SI	-2.63	0.313	SP	-0.96
133_14	0.093	SI	-3.13	0.192	SP	-1.34
233_11	0.381	SP	-1.92	0.554	SP	-0.65
233_12	0.224	SP	-1.71	0.380	SP	-0.72
233_13	0.114	SI	-2.23	0.192	SP	-1.19
233_14	0.066	SI	-2.83	0.105	SP	-1.72
333_11	0.362	SP	-1.49	0.480	SP	-0.75
333_12	0.204	SP	-1.38	0.276	SP	-0.89
333_13	0.090	SI	-2.11	0.119	SP	-1.53
333_14	0.047	SI	-2.98	0.062	SP	-2.22
433_11	0.395	SP	-0.98	0.438	SP	-0.76
433_12	0.207	SP	-1.08	0.218	SP	-1.01
433_13	0.075	SI	-2.07	0.085	SP	-1.81
433_14	0.037	SI	-3.06	0.043	SP	-2.65
133_21	0.536	SP	-1.69	0.596	SP	-0.86
133_22	0.455	SP	-1.16	0.566	SP	-0.47
133_23	0.387	SP	-1.01	0.489	SP	-0.53
133_24	0.301	SP	-1.15	0.390	SP	-0.69
233_21	0.516	SP	-1.23	0.584	SP	-0.58
233_22	0.450	SP	-0.76	0.525	SP	-0.42
233_23	0.342	SP	-0.85	0.397	SP	-0.61
233_24	0.239	SP	-1.09	0.272	SP	-0.89

Table B-8 Analysis results (β_9 = 0.4)

	FEA			Proposed Method		
Specimen	P_c/P_y	Mode	$(u_3/L)_H$ (%)	P_c/P_y	Mode	$(u_3/L)_H$ (%)
333_21	0.522	SP	-0.82	0.553	SP	-0.59
333_22	0.442	SP	-0.58	0.471	SP	-0.47
333_23	0.288	SP	-0.86	0.311	SP	-0.75
333_24	0.183	SP	-1.19	0.190	SP	-1.14
433_21	0.548	SP	-0.50	0.538	SP	-0.55
433_22	0.490	SP	-0.33	0.440	SP	-0.48
433_23	0.272	SP	-0.78	0.257	SP	-0.86
433_24	0.147	SP	-1.32	0.145	SP	-1.35
133_31	0.594	SP	-1.05	0.599	SP	-0.94
133_32	0.549	SP	-0.83	0.590	SP	-0.43
133_33	0.522	SP	-0.65	0.566	SP	-0.38
133_34	0.483	SP	-0.65	0.526	SP	-0.44
233_31	0.585	SP	-0.75	0.594	SP	-0.59
233_32	0.548	SP	-0.53	0.577	SP	-0.33
233_33	0.501	SP	-0.52	0.530	SP	-0.38
233_34	0.431	SP	-0.64	0.459	SP	-0.52
333_31	0.575	SP	-0.65	0.583	SP	-0.53
333_32	0.546	SP	-0.40	0.558	SP	-0.33
333_33	0.470	SP	-0.51	0.488	SP	-0.44
333_34	0.382	SP	-0.68	0.391	SP	-0.64
433_31	0.585	SP	-0.40	0.579	SP	-0.47
433_32	0.559	SP	-0.27	0.548	SP	-0.31
433_33	0.459	SP	-0.46	0.459	SP	-0.47
433_34	0.333	SP	-0.79	0.340	SP	-0.75

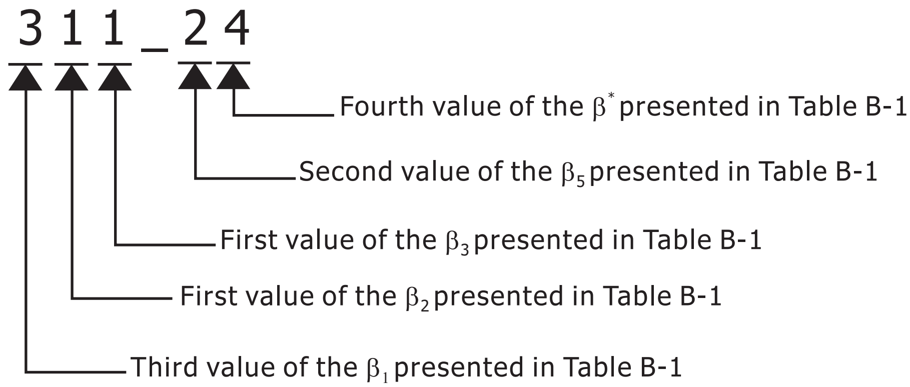

Examples:

Name	β_1	β_2	β_3	β_5	β^*
311_24	2.0	0.17	0.17	0.15	1.0
233_12	1.28	1.5	0.9	0.075	0.4

Figure B-1 Panel naming convention

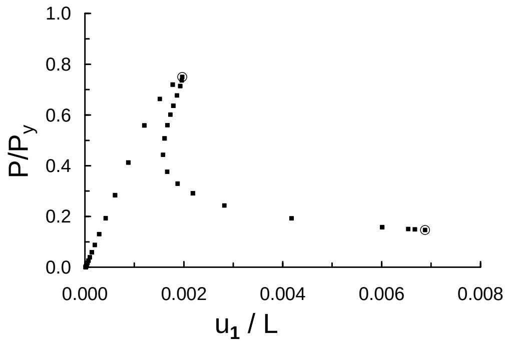

(a) Axial load vs. axial deformation

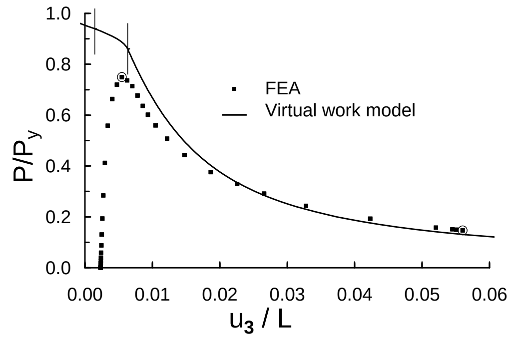

(b) Axial load vs. lateral deflection at centre of the stiffened panel

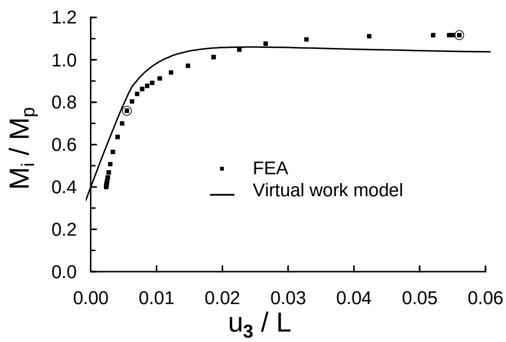

(c) Internal moment vs. lateral deflection

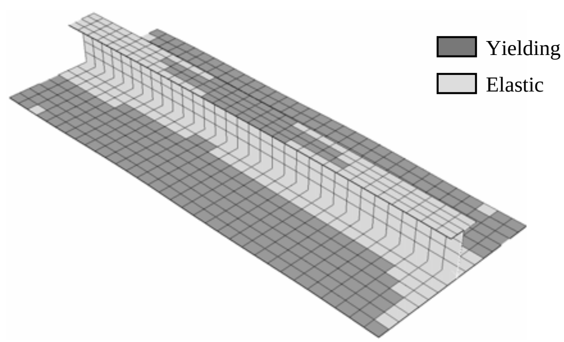

(d) Extend of yielding at the stage of the peak axial load

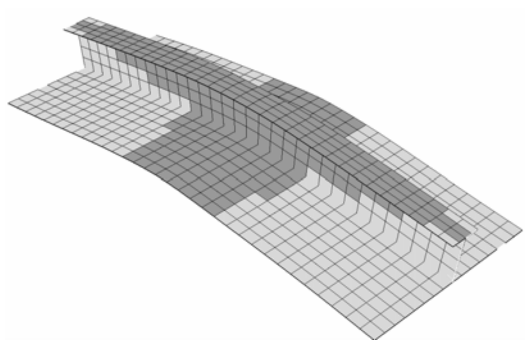

(e) Extend of yielding in the end of the analysis

Figure B-2 Sample plate induced plastic hinging mode ($0 < \left(u_3/L\right)_H < 1\%$)

(Panel 122_12, $\beta_9 = -0.4$, $\left(u_3/L\right)_H = 0.008$)

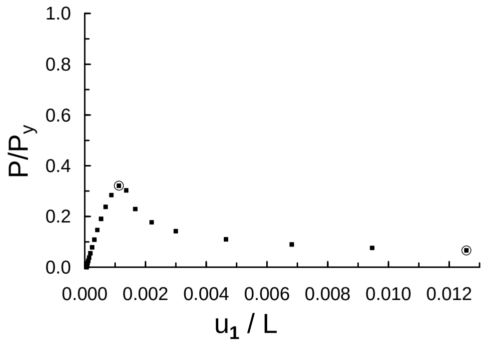

(a) Axial load vs. axial deformation

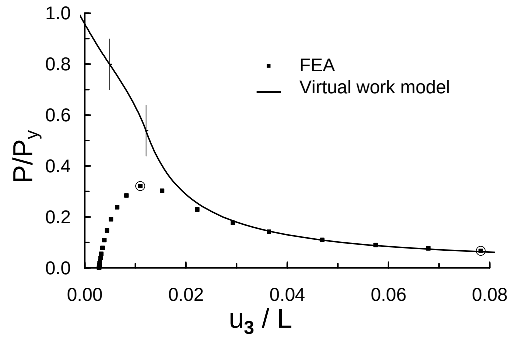

(b) Axial load vs. lateral deflection at centre of the stiffened panel

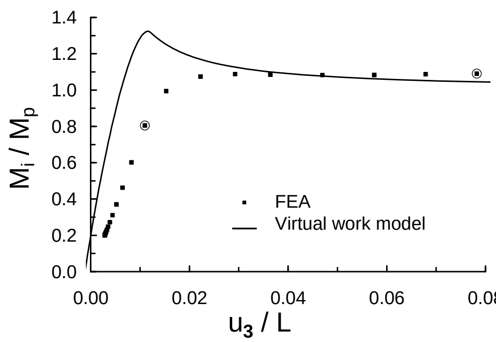

(c) Internal moment vs. lateral deflection

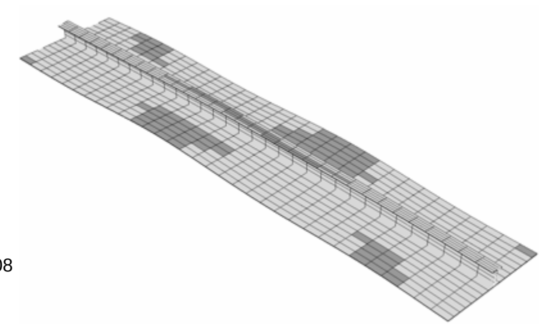

(d) Extend of yielding at the stage of the peak axial load

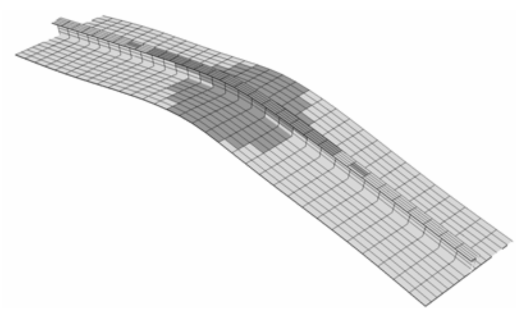

(e) Extend of yielding in the end of the analysis

Figure B-3 Sample plate induced plastic hinging mode (1% < $(u_3/L)_H$ < 2.5%)

(Panel 311_33, $\beta_9 = -0.2$, $(u_3/L)_H = 0.018$)

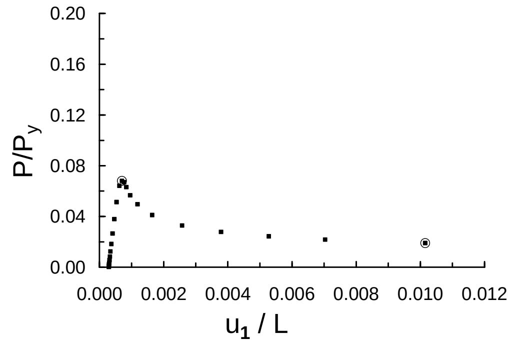

(a) Axial load vs. axial deformation

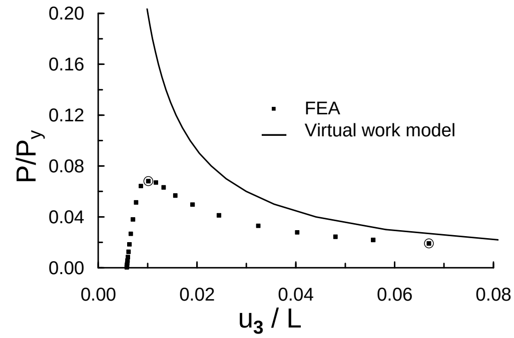

(b) Axial load vs. lateral deflection at centre of the stiffened panel

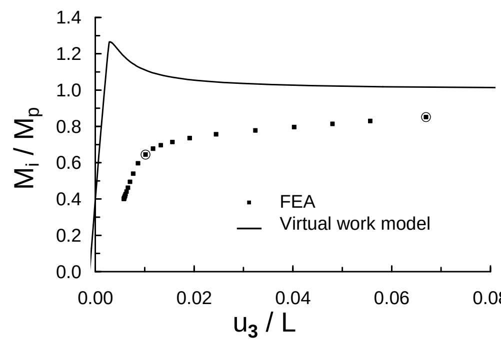

(c) Internal moment vs. lateral deflection

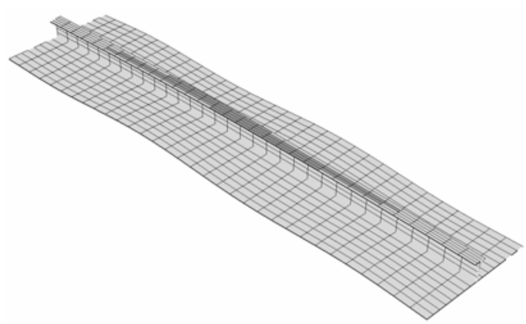

(d) Extend of yielding at the stage of the peak axial load

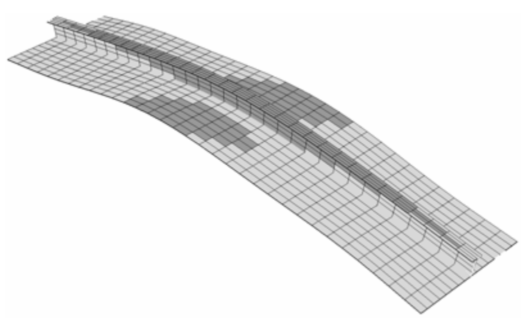

(e) Extend of yielding in the end of the analysis

Figure B-4 Sample plate induced plastic hinging mode ($\left(u_3/L\right)_H$ > 2.5%)

(Panel 433_13, β_9 = –0.4, $\left(u_3/L\right)_H$ = 0.027)

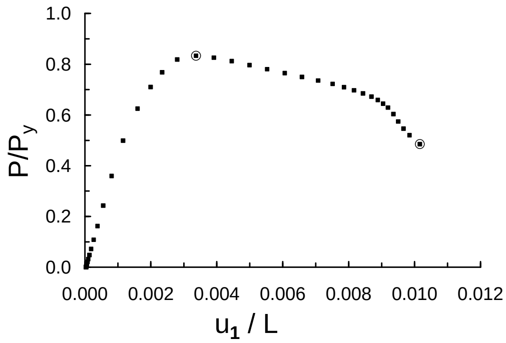

(a) Axial load vs. axial deformation

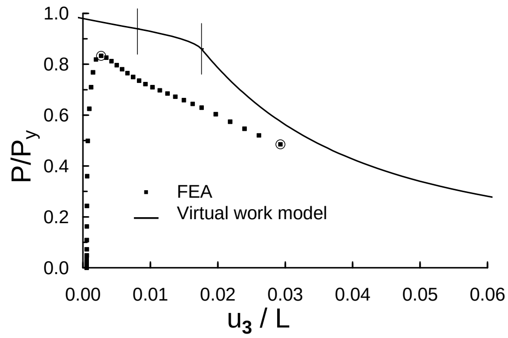

(b) Axial load vs. lateral deflection at centre of the stiffened panel

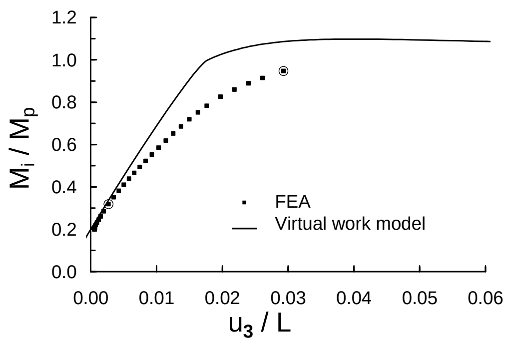

(c) Internal moment vs. lateral deflection

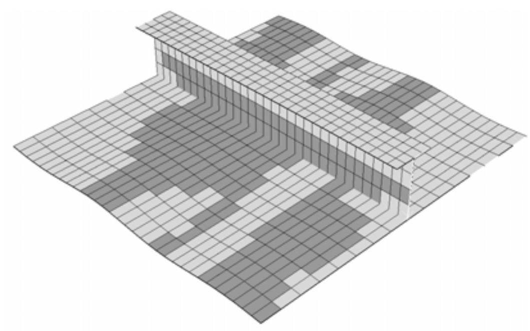

(d) Extend of yielding at the stage of the peak axial load

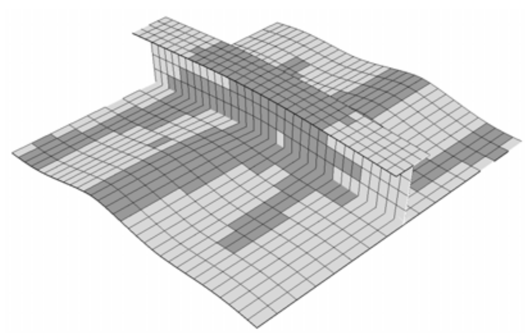

(e) Extend of yielding in the end of the analysis

Figure B-5 Sample plate buckling mode (1% < $\left(u_3/L\right)_H$ < 2.5%)

(Panel 222_11, $\beta_9 = -0.2$, $\left(u_3/L\right)_H = 0.018$)

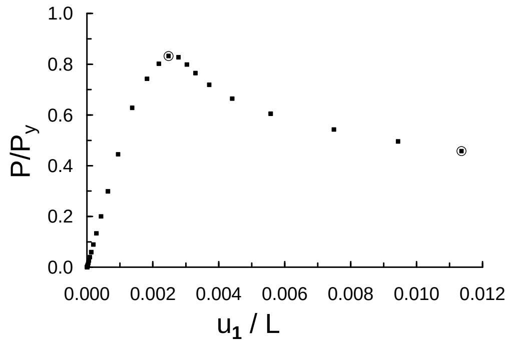

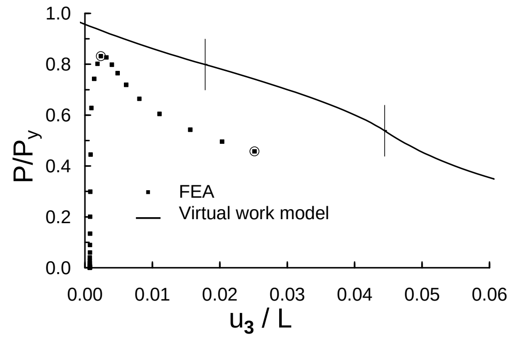

(a) Axial load vs. axial deformation

(b) Axial load vs. lateral deflection at centre of the stiffened panel

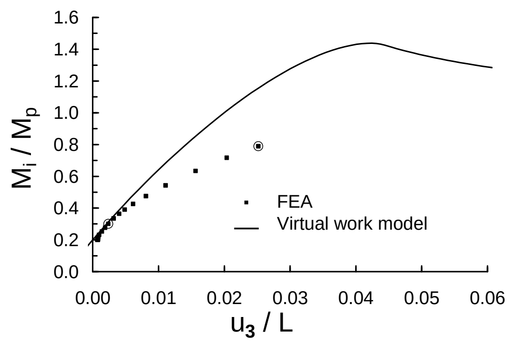

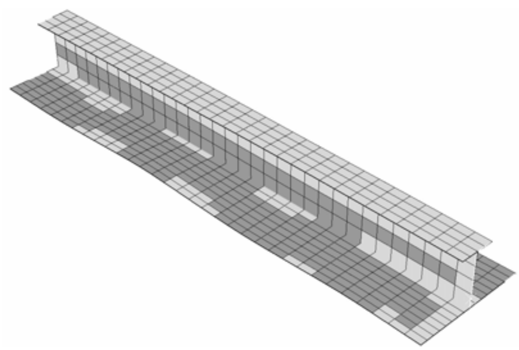

(c) Internal moment vs. lateral deflection

(d) Extend of yielding at the stage of the peak axial load

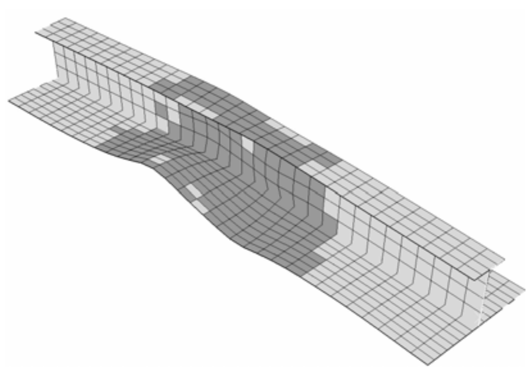

(e) Extend of yielding in the end of the analysis

Figure B-6 Sample plate induced overall buckling mode ($(u_3/L)_H$ > 2.5%)

(Panel 233_33, $\beta_9 = -0.2$, $(u_3/L)_H = 0.033$)

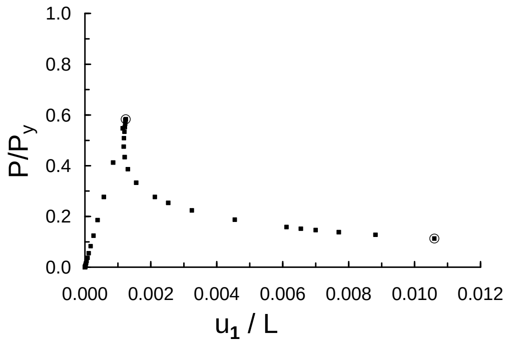

(a) Axial load vs. axial deformation

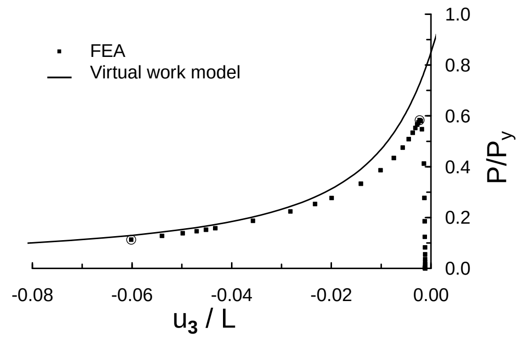

(b) Axial load vs. lateral deflection at centre of the stiffened panel

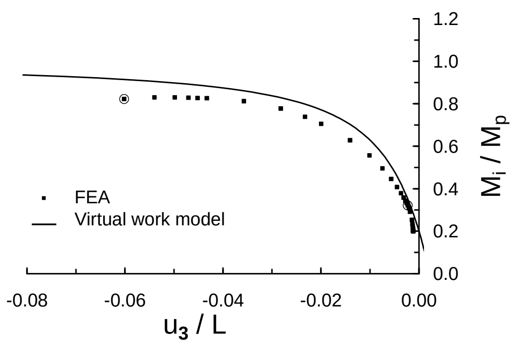

(c) Internal moment vs. lateral deflection

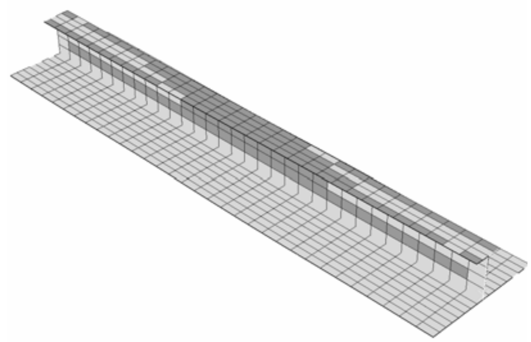

(d) Extend of yielding at the stage of the peak axial load

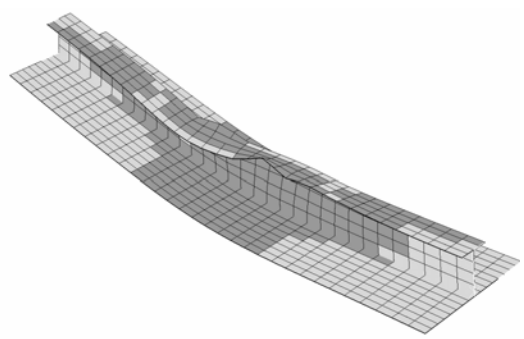

(e) Extend of yielding in the end of the analysis

Figure B-7 Sample stiffener induced plastic hinge mode (–1% < $(u_3/L)_H$ < 0)

(Panel 122_23, $\beta_9 = 0.2$, $(u_3/L)_H = -0.006$)

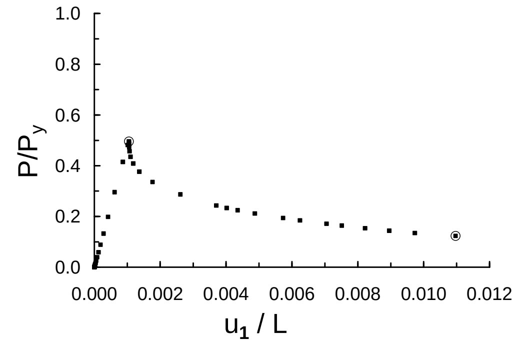

(a) Axial load vs. axial deformation

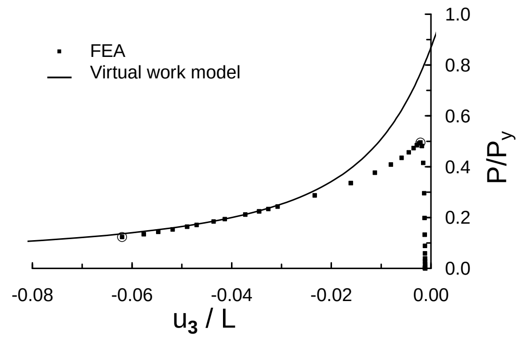

(b) Axial load vs. lateral deflection at centre of the stiffened panel

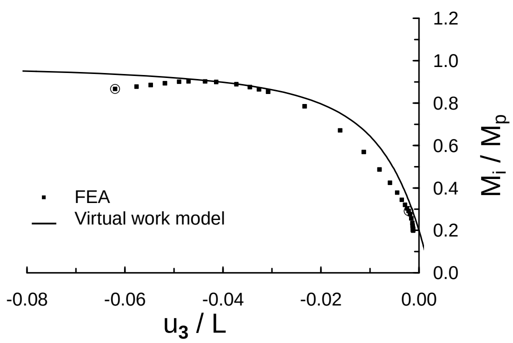

(c) Internal moment vs. lateral deflection

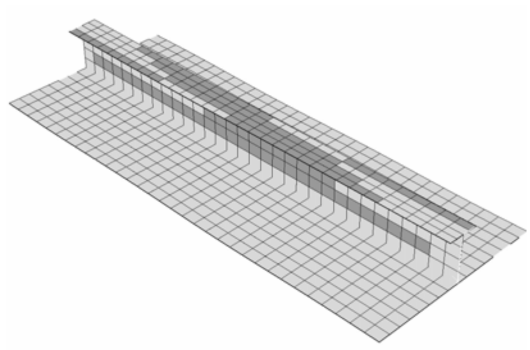

(d) Extend of yielding at the stage of the peak axial load

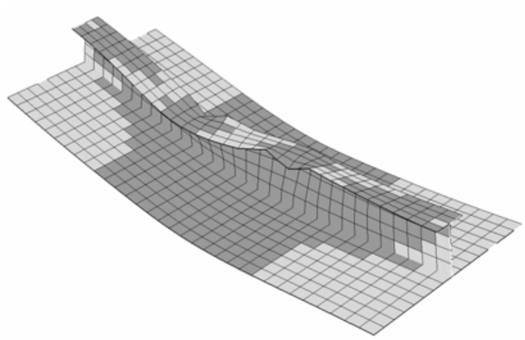

(e) Extend of yielding in the end of the analysis

Figure B-8 Sample stiffener induced plastic hinge mode (–2% < $(u_3/L)_H$ < –1%)

(Panel 122_12, β_9 = 0.2, $(u_3/L)_H$ = –0.011)

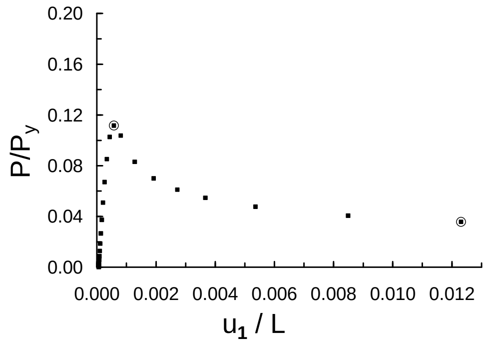

(a) Axial load vs. axial deformation

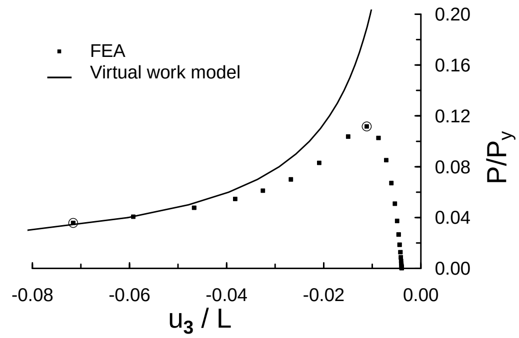

(b) Axial load vs. lateral deflection at centre of the stiffened panel

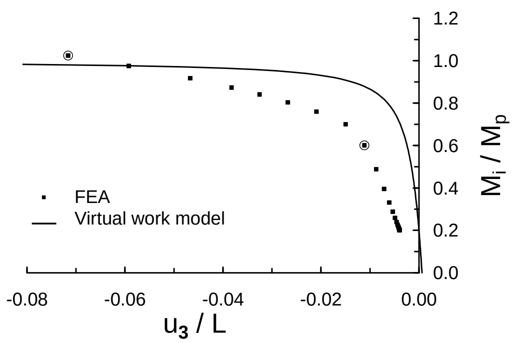

(c) Internal moment vs. lateral deflection

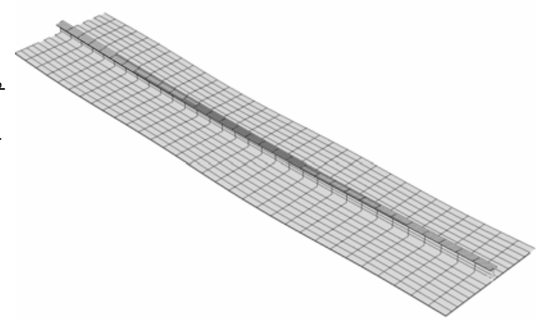

(d) Extend of yielding at the stage of the peak axial load

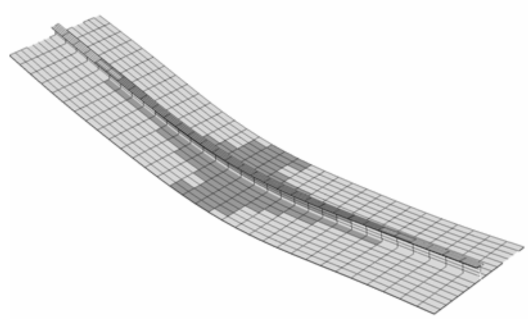

(e) Extend of yielding in the end of the analysis

Figure B-9 Sample stiffener induced plastic hinge mode ($(u_3/L)_H < -2\%$)

(Panel 311_23, $\beta_9 = 0.2$, $(u_3/L)_H = -0.035$)

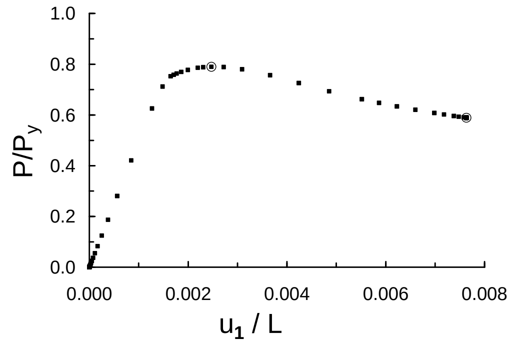

(a) Axial load vs. axial deformation

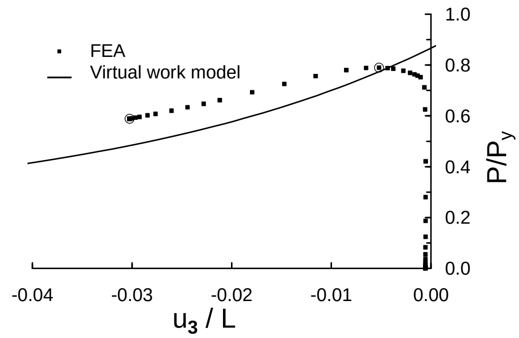

(b) Axial load vs. lateral deflection at centre of the stiffened panel

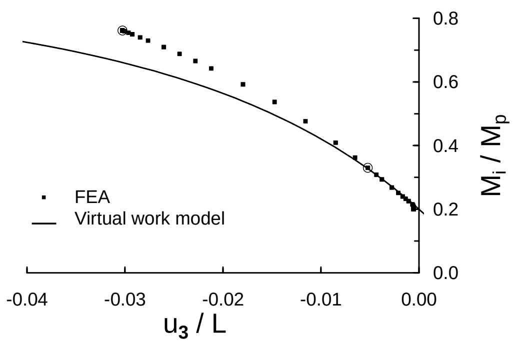

(c) Internal moment vs. lateral deflection

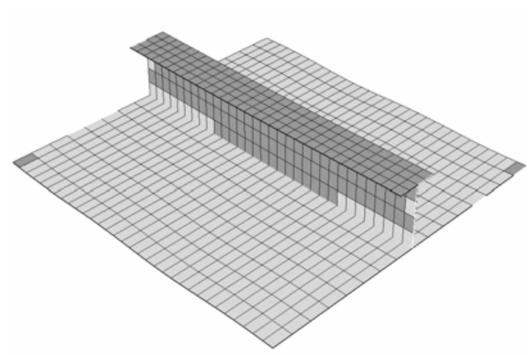

(d) Extend of yielding at the stage of the peak axial load

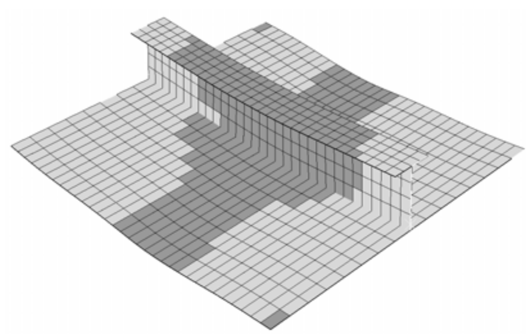

(e) Extend of yielding in the end of the analysis

Figure B-10 Sample stiffener induced overall buckling mode (–1%< $(u_3/L)_H$ < 0)

(Panel 111_21, $\beta_9 = 0.2$, $(u_3/L)_H = -0.004$)

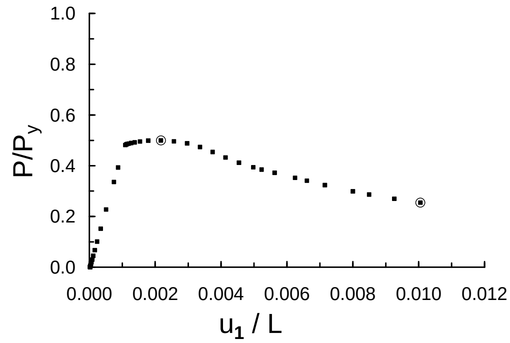

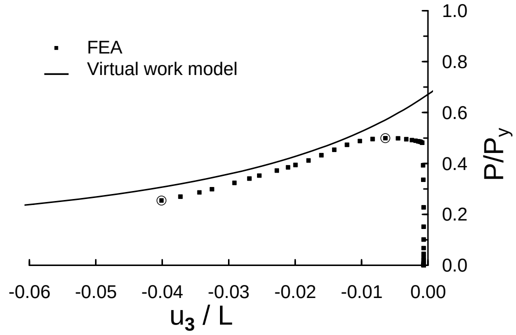

(a) Axial load vs. axial deformation

(b) Axial load vs. lateral deflection at centre of the stiffened panel

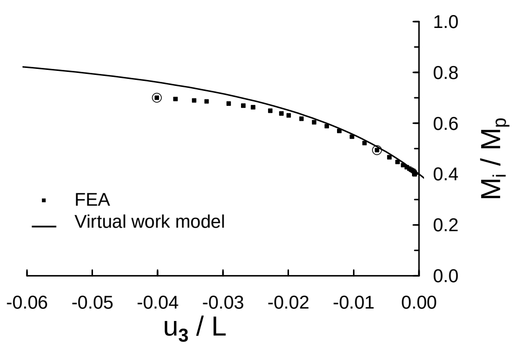

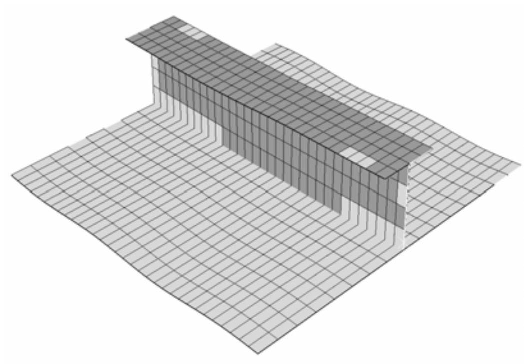

(c) Internal moment vs. lateral deflection

(d) Extend of yielding at the stage of the peak axial load

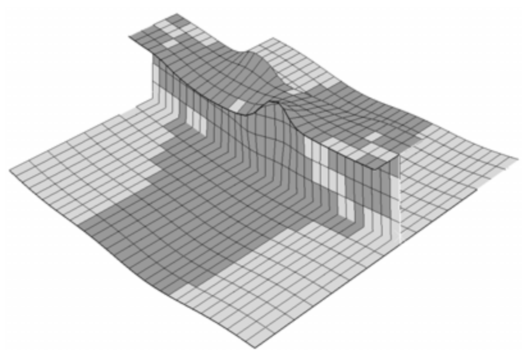

(e) Extend of yielding in the end of the analysis

Figure B-11 Sample stiffener induced overall buckling mode

(–2% < $(u_3/L)_H$ < –1%) (Panel 222_21, β_9 = 0.4, $(u_3/L)_H$ = –0.012)

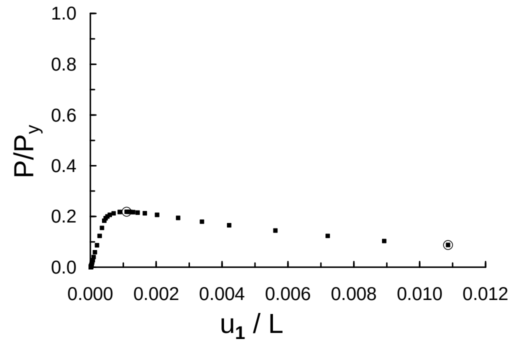

(a) Axial load vs. axial deformation

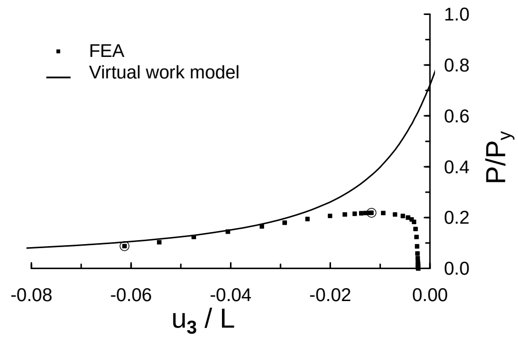

(b) Axial load vs. lateral deflection at centre of the stiffened panel

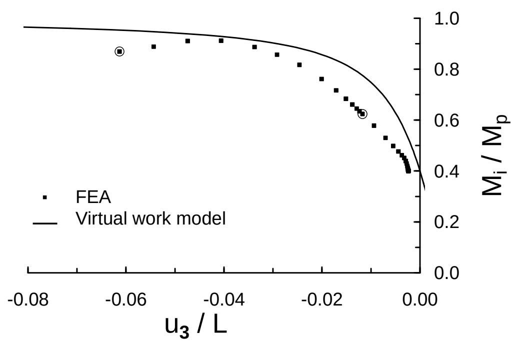

(c) Internal moment vs. lateral deflection

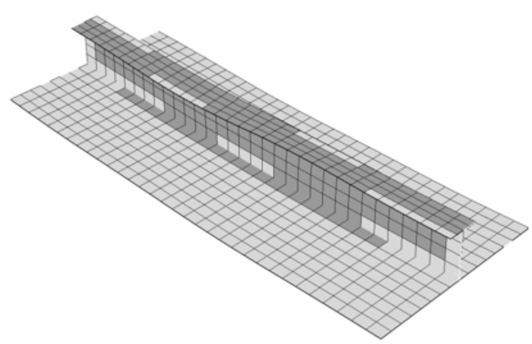

(d) Extend of yielding at the stage of the peak axial load

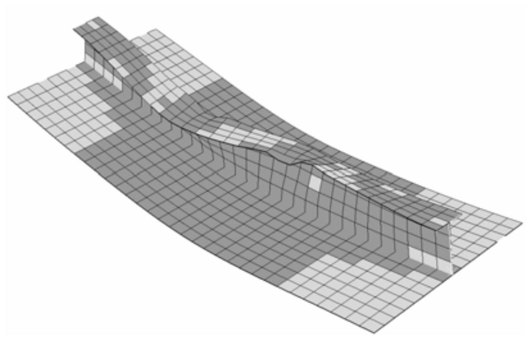

(e) Extend of yielding in the end of the analysis

Figure B-12 Sample stiffener induced overall buckling mode ($(u_3/L)_H < -2\%$)

(Panel 122_12, $\beta_9 = 0.4$, $(u_3/L)_H = -0.026$)

APPENDIX C

COMPARISON OF FINITE ELEMENT ANALYSIS RESULTS UNDER DIFFERENT BOUNDARY CONDITIONS

The finite element analysis was conducted with two different boundary conditions: one was fully restrained laterally along both unloaded edges of the panel plate and the other was free to expand laterally. The 720 models described in Table B-1 were run with each of these two boundary conditions. The results for boundary condition that has the unloaded edges free to translate in the transverse direction were presented in Appendix B. The results for boundary condition that has the unloaded edges fully restrained in the transverse direction are presented in Table C-1. Comparisons between the results for the two boundary conditions are shown in Figures C-1 to C-5 by load case. The comparisons for all the five load cases are shown in Figure C-6. Results of the two panels, panels 122_11 and 122_12, under boundary condition that has the unloaded edges fully restrained in the transverse direction and $\beta_9 = 0.4$ are missing because the two panels had convergence problem in the finite element analysis.

Table C-1 Finite element analysis results, P_c/P_y , for plates with unloaded edges fully restrained laterally in the plane of the plate

Specimen	β_9 = –0.4	β_9 = –0.2	β_9 = 0	β_9 = 0.2	β_9 = 0.4
111_11	0.921	1.022	1.080	0.730	0.549
111_12	0.222	0.487	1.103	0.314	0.167
111_13	0.067	0.144	0.271	0.126	0.061
111_14	0.032	0.068	0.134	0.066	0.031
211_11	0.548	0.736	0.819	0.510	0.309
211_12	0.075	0.187	0.333	0.158	0.066
211_13	0.024	0.059	0.116	0.058	0.024
211_14	0.012	0.029	0.058	0.029	0.012
311_11	0.277	0.440	0.552	0.439	0.183
311_12	0.038	0.095	0.167	0.101	0.040
311_13	0.013	0.033	0.063	0.035	0.015
311_14	0.006	0.017	0.033	0.018	0.008
411_11	0.172	0.301	0.388	0.458	0.149
411_12	0.028	0.063	0.106	0.084	0.033
411_13	0.010	0.024	0.043	0.027	0.012
411_14	0.005	0.012	0.023	0.013	0.006
111_21	1.010	1.055	1.100	0.794	0.609
111_22	0.794	0.937	1.027	0.578	0.307
111_23	0.256	0.451	0.628	0.314	0.162
111_24	0.107	0.211	0.321	0.174	0.091
211_21	0.778	0.826	0.870	0.716	0.445
211_22	0.385	0.549	0.685	0.408	0.218
211_23	0.108	0.199	0.307	0.175	0.094
211_24	0.050	0.097	0.156	0.090	0.049
311_21	0.549	0.588	0.627	0.671	0.418

Table C-1 Finite element analysis results, P_c/P_y, for plates with unloaded edges fully restrained laterally in the plane of the plate

Specimen	β_9 = –0.4	β_9 = –0.2	β_9 = 0	β_9 = 0.2	β_9 = 0.4
311_22	0.182	0.295	0.394	0.332	0.165
311_23	0.062	0.113	0.171	0.114	0.064
311_24	0.031	0.057	0.090	0.056	0.032
411_21	0.413	0.453	0.489	0.531	0.441
411_22	0.116	0.189	0.261	0.329	0.145
411_23	0.044	0.078	0.116	0.088	0.050
411_24	0.022	0.040	0.063	0.043	0.026
111_31	1.002	1.055	1.103	0.855	0.668
111_32	0.966	1.035	1.109	0.764	0.511
111_33	0.784	0.883	0.991	0.604	0.377
111_34	0.463	0.615	0.738	0.423	0.252
211_31	0.791	0.845	0.897	0.819	0.584
211_32	0.722	0.786	0.866	0.691	0.446
211_33	0.448	0.588	0.726	0.430	0.267
211_34	0.208	0.304	0.429	0.249	0.157
311_31	0.572	0.627	0.679	0.729	0.577
311_32	0.485	0.547	0.622	0.705	0.402
311_33	0.231	0.332	0.442	0.319	0.194
311_34	0.115	0.180	0.250	0.166	0.106
411_31	0.444	0.496	0.544	0.598	0.588
411_32	0.344	0.419	0.485	0.557	0.389
411_33	0.152	0.222	0.302	0.256	0.155
411_34	0.081	0.125	0.174	0.126	0.080
122_11	1.038	1.066	1.035	0.747	#N/A
122_12	0.822	0.985	1.064	0.491	#N/A

Table C-1 Finite element analysis results, P_c/P_y , for plates with unloaded edges fully restrained laterally in the plane of the plate

Specimen	β_9 = –0.4	β_9 = –0.2	β_9 = 0	β_9 = 0.2	β_9 = 0.4
122_13	0.198	0.505	0.618	0.289	0.107
122_14	0.077	0.222	0.352	0.169	0.062
222_11	0.812	0.838	0.863	0.612	0.371
222_12	0.388	0.616	0.737	0.379	0.156
222_13	0.087	0.218	0.359	0.174	0.072
222_14	0.039	0.103	0.182	0.094	0.039
322_11	0.572	0.594	0.619	0.642	0.303
322_12	0.178	0.341	0.447	0.327	0.133
322_13	0.054	0.124	0.203	0.122	0.054
322_14	0.026	0.063	0.109	0.062	0.028
422_11	0.434	0.456	0.478	0.498	0.314
422_12	0.113	0.215	0.304	0.374	0.127
422_13	0.041	0.087	0.139	0.099	0.047
422_14	0.020	0.044	0.076	0.048	0.023
122_21	1.033	1.065	1.027	0.795	0.606
122_22	1.021	1.059	1.029	0.685	0.415
122_23	0.945	1.008	1.079	0.557	0.326
122_24	0.610	0.780	0.734	0.435	0.237
222_21	0.811	0.842	0.873	0.746	0.500
222_22	0.736	0.775	0.819	0.635	0.390
222_23	0.589	0.713	0.789	0.454	0.258
222_24	0.260	0.426	0.517	0.290	0.163
322_21	0.577	0.607	0.636	0.665	0.494
322_22	0.524	0.565	0.601	0.642	0.369
322_23	0.299	0.424	0.529	0.370	0.207

Table C-1 Finite element analysis results, P_c/P_y , for plates with unloaded edges fully restrained laterally in the plane of the plate

Specimen	β_9 = –0.4	β_9 = –0.2	β_9 = 0	β_9 = 0.2	β_9 = 0.4
322_24	0.145	0.240	0.336	0.203	0.120
422_21	0.444	0.472	0.498	0.526	0.524
422_22	0.410	0.455	0.485	0.529	0.384
422_23	0.194	0.289	0.381	0.335	0.177
422_24	0.102	0.164	0.234	0.161	0.095
122_31	1.003	1.051	1.030	0.833	0.640
122_32	1.003	1.053	1.023	0.768	0.537
122_33	0.998	1.056	1.020	0.715	0.496
122_34	0.944	1.016	1.012	0.670	0.442
222_31	0.789	0.837	0.883	0.799	0.587
222_32	0.732	0.785	0.837	0.758	0.530
222_33	0.756	0.815	0.878	0.676	0.454
222_34	0.727	0.802	0.890	0.571	0.368
322_31	0.563	0.610	0.658	0.703	0.576
322_32	0.541	0.589	0.644	0.695	0.517
322_33	0.573	0.631	0.698	0.638	0.407
322_34	0.510	0.597	0.683	0.475	0.299
422_31	0.434	0.479	0.527	0.568	0.588
422_32	0.440	0.493	0.540	0.580	0.520
422_33	0.484	0.541	0.598	0.742	0.378
422_34	0.370	0.444	0.532	0.412	0.255
133_11	1.049	1.072	1.019	0.700	0.426
133_12	1.019	1.055	1.018	0.557	0.250
133_13	0.518	0.786	0.663	0.382	0.147
133_14	0.169	0.390	0.509	0.246	0.093

Table C-1 Finite element analysis results, P_c/P_y , for plates with unloaded edges fully restrained laterally in the plane of the plate

Specimen	β_9 = –0.4	β_9 = –0.2	β_9 = 0	β_9 = 0.2	β_9 = 0.4
233_11	0.823	0.844	0.865	0.653	0.381
233_12	0.687	0.758	0.797	0.491	0.225
233_13	0.203	0.411	0.565	0.273	0.115
233_14	0.084	0.193	0.296	0.155	0.067
333_11	0.581	0.604	0.624	0.642	0.364
333_12	0.366	0.487	0.568	0.604	0.208
333_13	0.116	0.222	0.326	0.204	0.093
333_14	0.054	0.113	0.183	0.104	0.049
433_11	0.447	0.467	0.485	0.502	0.404
433_12	0.224	0.353	0.423	0.480	0.216
433_13	0.081	0.150	0.224	0.174	0.080
433_14	0.041	0.082	0.129	0.082	0.041
133_21	1.038	1.067	1.019	0.775	0.526
133_22	1.036	1.070	1.009	0.711	0.453
133_23	1.022	1.064	0.971	0.635	0.384
133_24	0.898	0.987	0.834	0.534	0.298
233_21	0.816	0.844	0.872	0.740	0.514
233_22	0.754	0.788	0.818	0.698	0.445
233_23	0.752	0.796	0.842	0.571	0.340
233_24	0.539	0.693	0.744	0.422	0.241
333_21	0.581	0.608	0.635	0.662	0.520
333_22	0.546	0.572	0.608	0.643	0.445
333_23	0.512	0.599	0.647	0.548	0.298
333_24	0.292	0.436	0.546	0.325	0.186
433_21	0.447	0.474	0.499	0.524	0.547

Table C-1 Finite element analysis results, P_c/P_y , for plates with unloaded edges fully restrained laterally in the plane of the plate

Specimen	β_9 = –0.4	β_9 = –0.2	β_9 = 0	β_9 = 0.2	β_9 = 0.4
433_22	0.443	0.476	0.510	0.544	0.483
433_23	0.373	0.466	0.539	0.597	0.268
433_24	0.199	0.304	0.392	0.270	0.150
133_31	1.004	1.051	1.024	0.810	0.595
133_32	1.008	1.056	1.011	0.772	0.548
133_33	1.019	1.071	1.004	0.746	0.519
133_34	0.999	1.057	0.981	0.706	0.477
233_31	0.789	0.835	0.880	0.798	0.585
233_32	0.734	0.781	0.826	0.775	0.547
233_33	0.766	0.824	0.878	0.729	0.499
233_34	0.795	0.851	0.917	0.661	0.435
333_31	0.560	0.606	0.652	0.696	0.578
333_32	0.538	0.579	0.632	0.684	0.547
333_33	0.610	0.660	0.716	0.775	0.476
333_34	0.618	0.682	0.749	0.598	0.386
433_31	0.430	0.473	0.519	0.564	0.585
433_32	0.442	0.492	0.543	0.590	0.562
433_33	0.521	0.589	0.641	0.702	0.461
433_34	0.452	0.519	0.594	0.561	0.344

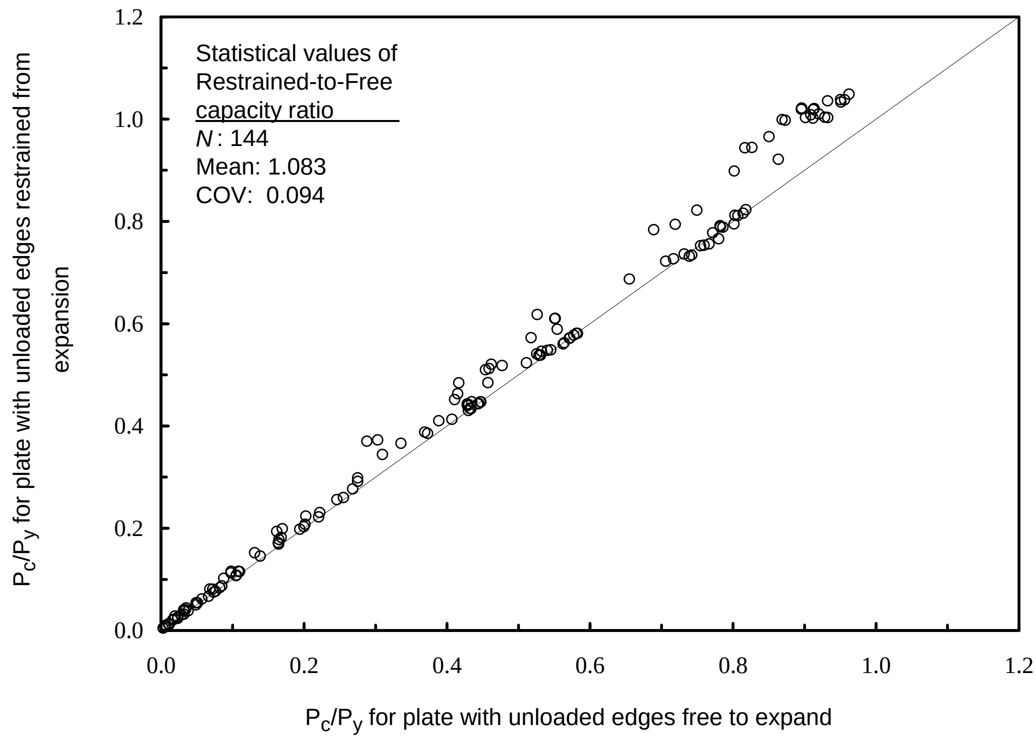

Figure C-1 Comparison between two boundary conditions (β_9 = –0.4)

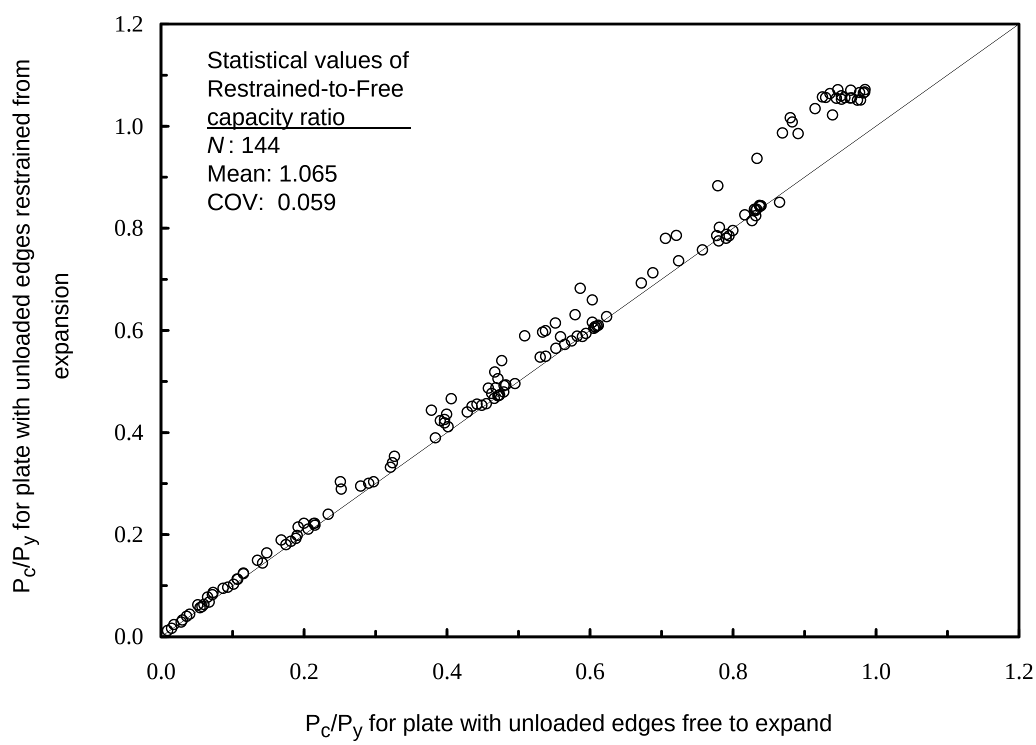

Figure C-2 Comparison between two boundary conditions (β_9 = –0.2)

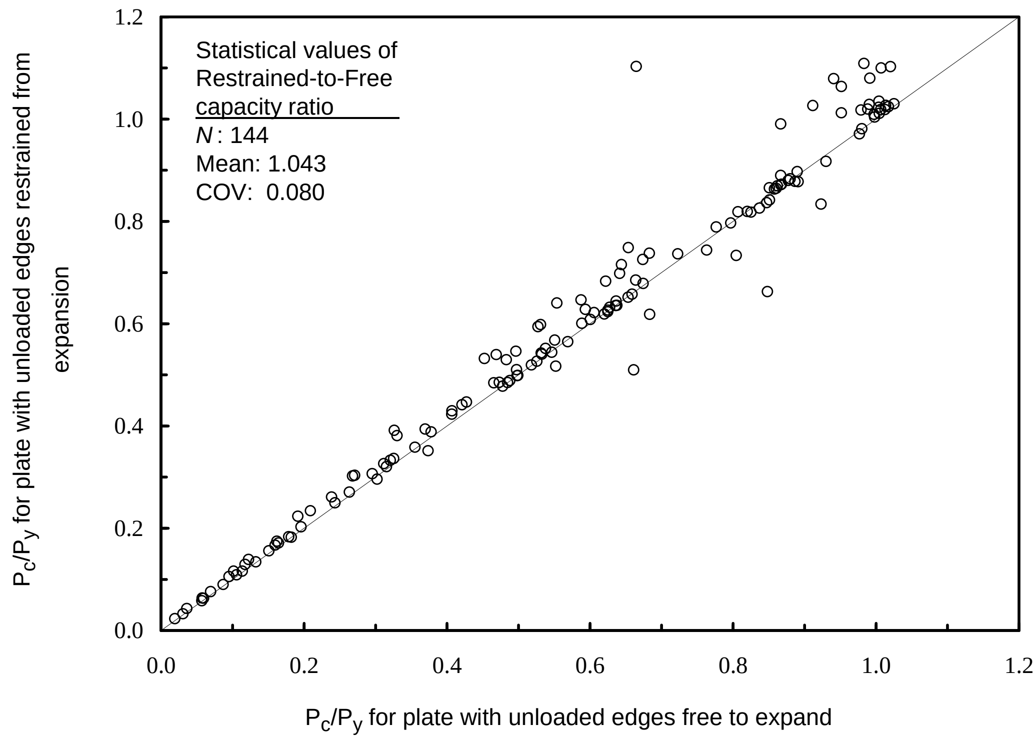

Figure C-3 Comparison between two boundary conditions (β_9 = 0)

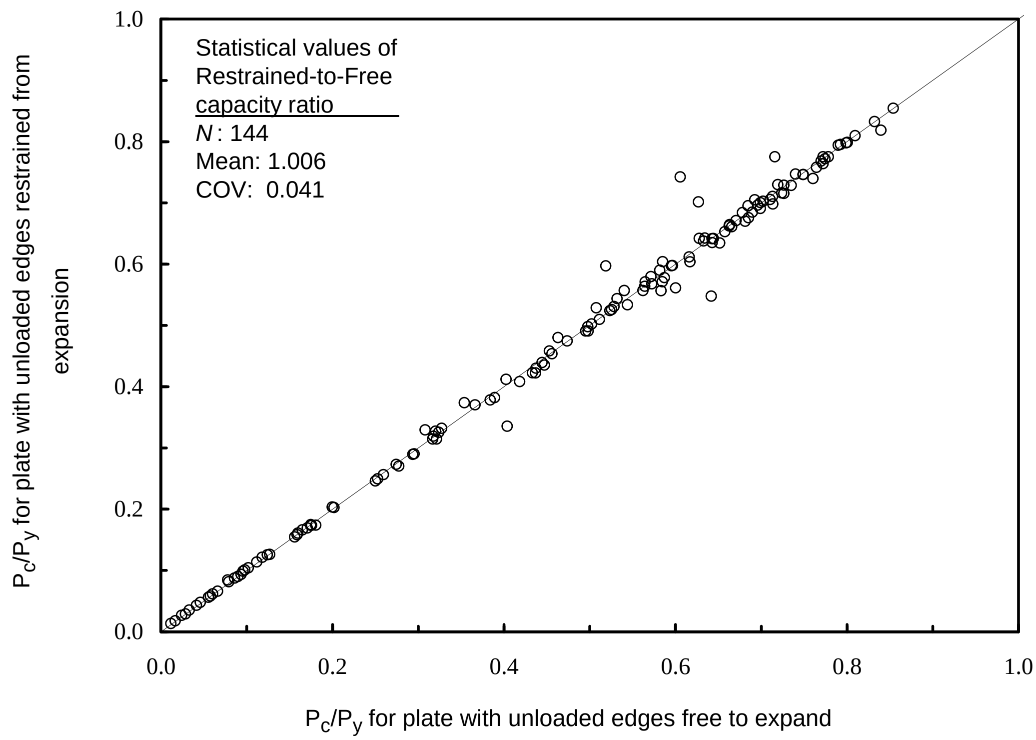

Figure C-4 Comparison between two boundary conditions (β_9 = 0.2)

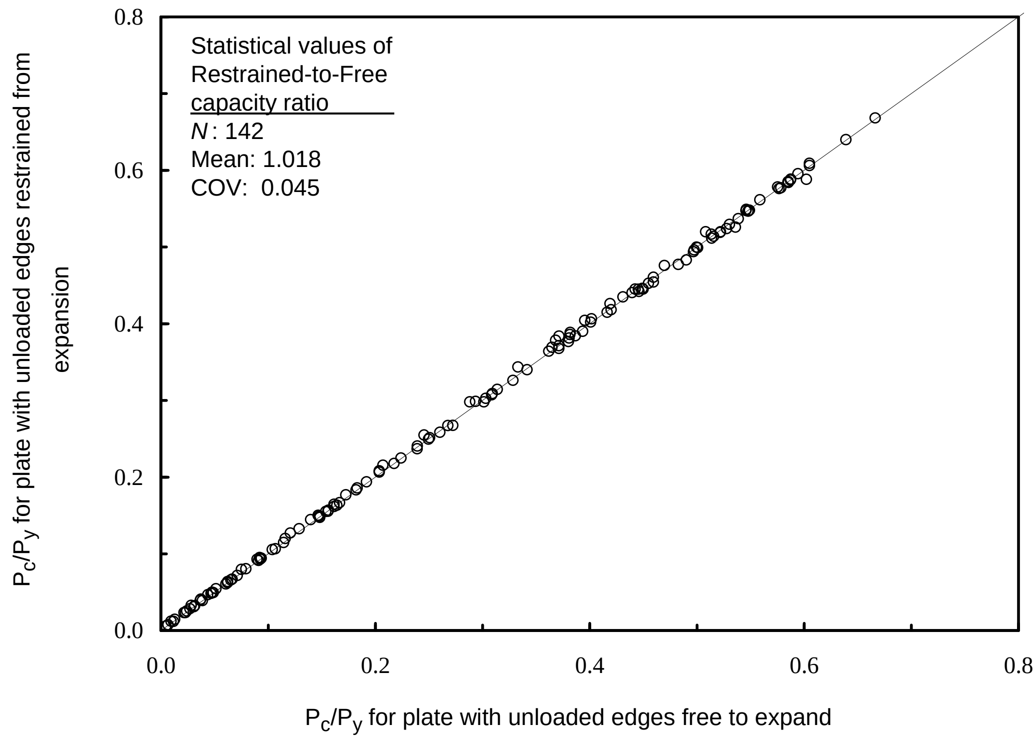

Figure C-5 Comparison between two boundary conditions (β_9 = 0.4)

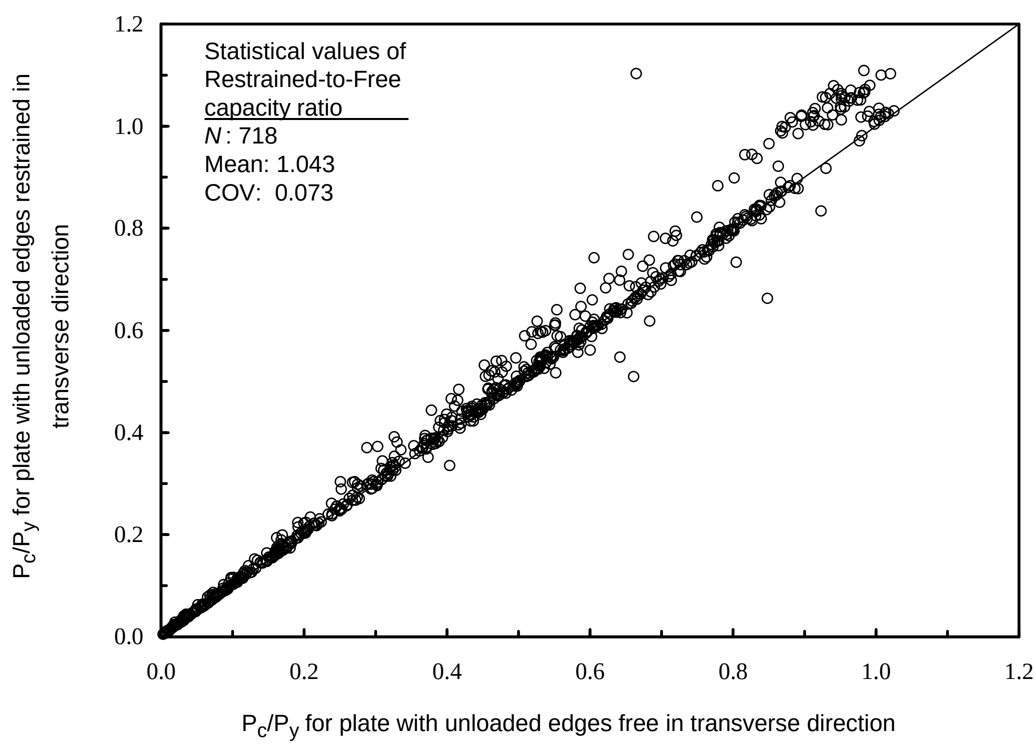

Figure C-6 Comparison between two boundary conditions (β_9 = all)

APPENDIX D

VIRTUAL WORK MODEL FOR PLASTIC HINGE MECHANISMS

For most stiffened plate proportions currently used in engineering practice, the plate area is usually larger than the stiffener area. The investigation presented in this report used a stiffener to plate area ratio (β_5) ranging from 0.075 to 0.3. Therefore, the plastic neutral axis for the pure bending loading condition is located in the plate. For a plastic hinge with the plate outer surface in flexural compression (plate induced plastic hinge), the portion of the cross-section in compression will extend from the plate outer surface to the pure bending P.N.A. If an axial compression force is superimposed to the bending moment, the portion of the cross-section in compression will be larger than the tension portion, and the P.N.A can be anywhere above the pure bending P.N.A., including above the flange of the stiffener (entire cross-section in compression). Therefore, three cases, namely, the P.N.A. in the plate (between the pure bending P.N.A. and the plate to web junction), the web, and the flange, will be analyzed respectively.

Similarly, when a stiffener induced plastic hinge is formed under flexure only, the portion of the cross-section in compression is between the flange outer surface and the pure bending P.N.A. If an axial compression force is superimposed to the bending moment, the compression portion can spread to anywhere below the pure bending P.N.A. Therefore, only one case needs to be analyzed, namely, the P.N.A. in the plate only (between the pure bending P.N.A. and the plate outer surface).

A virtual work model will be established to predict the plastic hinge mechanism. The case of plate induced plastic hinge with the P.N.A. in the plate will be first considered. Figure D-1(b) illustrates the deformed shape at any instant after the formation of a plastic hinge at midspan. The stiffened plate is subjected to the axial load (P) and the applied moment (M_a) at both ends. The applied moments are defined positive when placing the stiffener flange in flexural compression. This sign convention is consistent with the previous research (Sheikh *et al.*, 2002, 2003). The direction of the end moments shown in Figure D-1 are consistent with the deflected shape shown and are negative according to the sign convention. The panel is simply supported and the left end support is free to translate in the span direction. Because of the symmetry, the plastic hinge is expected to form at midspan. If the left end of the specimen is given a virtual displacement of δu_1 as shown in Figure D-1 (c), the two halves rotate by the same amount, the virtual rotation, $\delta\theta$. The virtual work done by the external force and moments is

$$External\,Work = P \times \delta u_1 - 2\left(M_a \times \delta\theta\right) \quad \text{[D-1]}$$

Assuming the member is not compressible axially, the end translation in the longitudinal direction is:

$$\delta u_1 = 2\left[a\cos\theta - a\cos(\theta + \delta\theta)\right] = 4a\sin\left(\theta + \frac{\delta\theta}{2}\right)\sin\frac{\delta\theta}{2} \quad \text{[D-2]}$$

where a is the chord distance between the end support and the midspan cross-section; θ is the angle between the chord and the horizontal line. Since the virtual rotation $\delta\theta$ is an infinitesimal deformation, the virtual displacement δu_1 can be approximated as:

$$\delta u_1 = 4a\sin\left(\theta + \frac{\delta\theta}{2}\right)\left(\frac{\delta\theta}{2}\right) = 2u_3 \times \delta\theta \quad \text{[D-3]}$$

where u_3 is the midspan deflection, taken as positive if towards the stiffener. Substituting Equation [D-3] into Equation [D-1] yields

$$External\,Work = 2Pu_3 \times \delta\theta - 2M_a \times \delta\theta = \left(Pu_3 - M_a\right) \times 2\delta\theta \quad \text{[D-4]}$$

The internal virtual work of a plastic hinge mechanism comes from the hinge rotation as:

$$Internal\ Work = M_i \times 2\delta\theta \quad \text{[D-5]}$$

where M_i is the internal moment about the centroid axis.

As shown in Figure D-1, the stress distribution of the midspan cross-section is separated into two components to facilitate the derivation. The values of P and M_i can be found from the sum of the forces and moments about the centroid. This gives

$$P = -P_y + 2F_y b t_1 \qquad \text{[D-6]}$$

$$M_i = 2F_y b t_1 \left(z_p - \frac{t_1}{2} \right) \qquad \text{[D-7]}$$

where t_1 is the thickness of the compression block in the plate. Solving for t_1 from Equation [D-6] and then substituting the solution into Equation [D-7] there comes out

$$M_i = \left(P_y + P\right)\left(z_p - \frac{P_y + P}{4F_y b} \right) \qquad \text{[D-8]}$$

Equating the external work and the internal work gives

$$\left(Pu_3 - M_a\right) \times 2\delta\theta = M_i \times 2\delta\theta \qquad \text{[D-9]}$$

or simply

$$Pu_3 - M_a = M_i \qquad \text{[D-10]}$$

Substituting $\beta_9 M_p$ for M_a and Equation [D-8] for M_i , Equation [D-10] becomes

$$u_3 = \frac{\beta_9 M_p}{P} + \left(\frac{P_y}{P} + 1 \right)\left(z_p - \frac{P_y + P}{4F_y b} \right), \quad \frac{P}{P_y} \le 1 - \frac{2A_s}{A} \quad N.A.\ in\ plate \qquad \text{[D-11]}$$

or in nomalizd form

$$\frac{u_3}{L} = \frac{\beta_9 M_p}{PL} + \left(\frac{P_y}{P} + 1 \right)\left(\frac{z_p}{L} - \frac{P_y + P}{4F_y bL} \right), \quad \frac{P}{P_y} \le 1 - \frac{2A_s}{A} \quad N.A.\ in\ plate \qquad \text{[D-12]}$$

The above equations were derived considering the P.N.A. to be located in the plate. The case where plate induced plastic hinge takes place with the P.N.A. in the web will now be examined. Its original shape, deflected shape, and the virtual displacements, can still be referred to Figure D-1 (a), (b), and (c), respectively. Its stress distribution is shown in Figure D-2. The stress distribution is separated into three components to facilitate the derivation. The values of P and M_i can be found from the sum of the forces and moments about the centroid. This gives

$$P = P_y - 2F_y A_f - 2F_y t_2 t_w \tag{D-13}$$

$$M_i = 2F_y A_f \left(z_s - \frac{t_f}{2} \right) + 2F_y t_2 t_w \left(z_s - t_f - \frac{t_2}{2} \right) \tag{D-14}$$

where t_2 is the height of the tension block in the web. Solving for t_2 from Equation [D-13] and then substituting the solution into Equation [D-14] there comes out

$$M_i = 2F_y A_f \left(z_s - \frac{t_f}{2} \right) + \left(P_y - P - 2F_y A_f \right) \left(z_s - t_f - \frac{P_y - P - 2F_y A_f}{4F_y t_w} \right) \tag{D-15}$$

Substituting $\beta_9 M_p$ for M_a and Equation [D-15] for M_i , Equation [D-10] becomes

$$u_3 = \frac{\beta_9 M_p}{P} + \frac{2F_y A_f}{P} \left(z_s - \frac{t_f}{2} \right) + \left(\frac{P_y - 2F_y A_f}{P} - 1 \right) \left(z_s - t_f - \frac{P_y - P}{4F_y t_w} + \frac{A_f}{2t_w} \right)$$
$$, 1 - \frac{2A_s}{A} \le \frac{P}{P_y} \le 1 - \frac{2A_f}{A} \quad N.A.\ in\ web$$

[D-16]

or in nomalizd form,

$$\frac{u_3}{L} = \frac{\beta_9 M_p}{PL} + \frac{2F_y A_f}{P} \left(\frac{z_s}{L} - \frac{t_f}{2L} \right) + \left(\frac{P_y - 2F_y A_f}{P} - 1 \right) \left(\frac{z_s}{L} - \frac{t_f}{L} - \frac{P_y - P}{4F_y t_w L} + \frac{A_f}{2t_w L} \right)$$
$$, 1 - \frac{2A_s}{A} \le \frac{P}{P_y} \le 1 - \frac{2A_f}{A} \quad N.A.\ in\ web$$

[D-17]

Similar approach is used for the case with the P.N.A. in the flange, as displayed in Figure D-3. The flange thickness is exaggerated in this figure to show the neutral axis clearly. The values of P and M_i can be found from the sum of the forces and moments about the centroid. This gives

$$P = P_y - 2F_y t_3 b_f \tag{D-18}$$

$$M_i = 2F_y t_3 b_f \left(z_s - \frac{t_3}{2} \right) \tag{D-19}$$

where t_3 is the thickness of the tension block in the flange. Solving for t_3 from Equation [D-18] and then substituting the solution into Equation [D-19] there comes out

$$M_i = \left(P_y - P\right)\left(z_s - \frac{P_y - P}{4F_y b_f}\right) \qquad \text{[D-20]}$$

Substituting $\beta_9 M_p$ for M_a and Equation [D-20] for M_i, Equation [D-10] becomes

$$u_3 = \frac{\beta_9 M_p}{P} + \left(\frac{P_y}{P} - 1\right)\left(z_s - \frac{P_y - P}{4F_y b_f}\right), \quad \frac{P}{P_y} \geq 1 - \frac{2A_f}{A} \quad N.A.\ in\ flange \qquad \text{[D-21]}$$

or in nomalizd form,

$$\frac{u_3}{L} = \frac{\beta_9 M_p}{PL} + \left(\frac{P_y}{P} - 1\right)\left(\frac{z_s}{L} - \frac{P_y - P}{4F_y b_f L}\right), \quad \frac{P}{P_y} \geq 1 - \frac{2A_f}{A} \quad N.A.\ in\ flange \qquad \text{[D-22]}$$

For stiffener induced plastic hinge mechanism, the P.N.A. can be located in the plate only. Derivation process of its formula is almost the same as the processes above for plate induced hinge, except that the internal moment and the deflection are now in the opposite direction. The deformed shape and stress distribution for stiffener induced plastic hinge are shown in Figure D-4. If the left end support of the specimen is given a virtual displacement of δu_1 (Figure D-4 (c)), the two halves then have a virtual rotation by the same amount of $\delta\theta$. The virtual work done by the external force and moments is

$$External\,Work = P \times \delta u_1 + 2\left(M_a \times \delta\theta\right) \qquad \text{[D-23]}$$

where

$$\delta u_1 = 2\left[a\cos\theta - a\cos\left(\theta + \delta\theta\right)\right] = 4a\sin\left(\theta + \frac{\delta\theta}{2}\right)\sin\frac{\delta\theta}{2} \qquad \text{[D-24]}$$

Since the virtual rotation $\delta\theta$ is an infinitesimal deformation, the virtual displacement δu_1 can be approximated as:

$$\delta u_1 = 2a\sin\left(\theta + \frac{\delta\theta}{2}\right)\delta\theta = 2(-u_3)\delta\theta \qquad \text{[D-25]}$$

where u_3 is the midspan deflection and it is negative in Figure D-4 according to the sign convention described before. Substitute Equation [D-25] into Equation [D-23] gives:

$$External\,Work = 2P(-u_3)\times\delta\theta + 2M_a\times\delta\theta = (-Pu_3 + M_a)\times 2\delta\theta \qquad \text{[D-26]}$$

The internal virtual work of a plastic hinge mechanism comes from the hinge rotation as:

$$Internal\ Work = M_i \times 2\delta\theta \qquad \text{[D-27]}$$

The values of P and M_i can be found from the sum of the forces and moments about the centroid. This gives

$$P = P_y - 2F_y bt_4 \qquad \text{[D-28]}$$

$$M_i = 2F_y bt_4\left(z_p - \frac{t_4}{2}\right) \qquad \text{[D-29]}$$

where t_4 is the thickness of the tension block in the plate. Solving for t_4 from Equation [D-28] and then substituting the solution into Equation [D-29] there comes out

$$M_i = (P_y - P)\left(z_p - \frac{P_y - P}{4F_y b}\right) \qquad \text{[D-30]}$$

Equating the external work and the internal work gives

$$-Pu_3 + M_a = M_i \qquad \text{[D-31]}$$

Substituting $\beta_9 M_p$ for M_a and Equation [D-30] for M_i, Equation [D-31] becomes

$$u_3 = \frac{\beta_9 M_p}{P} - \left(\frac{P_y}{P} - 1\right)\left(z_p - \frac{P_y - P}{4F_y b}\right), \quad stiffener\ induced\ plastic\ hinge \qquad \text{[D-32]}$$

or in normalized form,

$$\frac{u_3}{L} = \frac{\beta_9 M_p}{PL} - \left(\frac{P_y}{P} - 1\right)\left(\frac{z_p}{L} - \frac{P_y - P}{4F_y bL}\right), \quad \textit{stiffener induced plastic hinge} \quad \text{[D-33]}$$

Equations [D-12], [D-17], [D-22], and [D-33] together present the complete description of the plastic hinge mechanisms. They form the upper bound curve shown in Chapter 2.

When the stress block used for the axial load is located in the plate, it is also possible to derive more concise equations for the plastic hinge mechanisms, by splitting the stress distribution in a different manner. The case of plate induced plastic hinge with the P.N.A. in the plate will be first considered, as shown in Figure D-5. The stress distribution is seperated into a flexural component and a compression component. The compression component is indicated as the shaded area in the plate. Since this area is a regular rectangle, the location of its resultant force conincides with the pure bending P.N.A. The distance between this axis and the centroid of the cross-section is denoted as d_c. The resultant forces or moments about the pure bending P.N.A. are

$$P = F_y b t_c \quad \text{[D-34]}$$

$$M_p^{'} = M_p - \frac{F_y b t_c^2}{4} \quad \text{[D-35]}$$

where $M_p^{'}$ is the reduced plastic moment about the pure bending P.N.A. due to the axial load, and t_c is the thickness of the stress block used by the axial compression force. Solving for t_c from Equation [D-34] and then substituting the solution into Equation [D-35] there comes out

$$M_p^{'} = M_p - \frac{P^2}{4F_y b} \quad \text{[D-36]}$$

And the internal moment about the centroid is

$$M_i = M_p^{'} + Pd_c = M_p - \frac{P^2}{4F_y b} + Pd_c \qquad \text{[D-37]}$$

Substituting $\beta_9 M_p$ for M_a and Equation [D-37] for M_i, Equation [D-10] becomes

$$u_3 = d_c + \frac{(1+\beta_9)M_p}{P} - \frac{P}{4F_y b}, \quad \frac{P}{P_y} \le 1 - \frac{2A_s}{A} \quad N.A.\ in\ plate \qquad \text{[D-38]}$$

or in normalized form,

$$\frac{u_3}{L} = \frac{d_c}{L} + \frac{(1+\beta_9)M_p}{PL} - \frac{P}{4F_y bL}, \quad \frac{P}{P_y} \le 1 - \frac{2A_s}{A} \quad N.A.\ in\ plate \qquad \text{[D-39]}$$

The expression of the axial force may also be obtained as below,

$$P = -2F_y b(u_3 - d_c) + 2\sqrt{F_y^2 b^2 (u_3 - d_c)^2 + F_y b(1+\beta_9)M_p}, \quad \frac{P}{P_y} \le 1 - \frac{2A_s}{A} \quad N.A.\ in\ plate \qquad \text{[D-40]}$$

or in normalized form,

$$\frac{P}{P_y} = -\frac{2F_y b(u_3 - d_c)}{P_y} + 2\sqrt{\frac{F_y^2 b^2 (u_3 - d_c)^2}{P_y^2} + \frac{F_y b(1+\beta_9)M_p}{P_y^2}}, \quad \frac{P}{P_y} \le 1 - \frac{2A_s}{A} \quad N.A.\ in\ plate \qquad \text{[D-41]}$$

Stiffener induced plastic hinge case is shown in Figure D-6. The resultant forces and momoents of the two stress distribution components are the same as the above Equations [D-34] and [D-35]. The internal moment is

$$M_i = M_p^{'} - Pd_c = M_p - \frac{P^2}{4F_y b} - Pd_c \qquad \text{[D-42]}$$

Substituting $\beta_9 M_p$ for M_a and Equation [D-42] for M_i, Equation [D-31] becomes

$$u_3 = d_c - \frac{(1-\beta_9)M_p}{P} + \frac{P}{4F_y b}, \quad \textit{stiffener induced plastic hinge} \qquad \text{[D-43]}$$

or in normalized form,

$$\frac{u_3}{L} = \frac{d_c}{L} - \frac{(1-\beta_9)M_p}{PL} + \frac{P}{4F_y bL}, \quad \textit{stiffener induced plastic hinge} \qquad \text{[D-43]}$$

The expression of the axial force may also be obtained as below,

$$P = 2F_y b(u_3 - d_c) + 2\sqrt{F_y^2 b^2 (u_3 - d_c)^2 + F_y b(1-\beta_9)M_p}, \qquad \text{[D-44]}$$
$$\textit{stiffener induced plastic hinge}$$

or in normalized form,

$$\frac{P}{P_y} = \frac{2F_y b(u_3 - d_c)}{P_y} + 2\sqrt{\frac{F_y^2 b^2 (u_3 - d_c)^2}{P_y^2} + \frac{F_y b(1-\beta_9)M_p}{P_y^2}}, \qquad \text{[D-45]}$$
$$\textit{stiffener induced plastic hinge}$$

The theoretical internal moment, M_i, can be either obtained from equilibrium or from the virtual work model (Equations [D-10] and [D-31]). Regardless of the flexural direction, the maganitude of the internal moment can be expressed as

$$M_i = \left| Pu_3 - \beta_9 M_p \right| \qquad \text{[D-46]}$$

It is useful to know when M_i reaches its maximum. If the rotation of the plastic hinge is considered as the action of a rotational spring, the stiffness of the spring would be zero when M_i reaches its maximum. A panel in plate induced failure (plate outmost fibre in flexural compression) is shown in Figure D-7 to illustrate the qualitative analysis of the variation of M_i with moving P.N.A. The cross-section is fully plasticized and the magnitude of M_i simply depends on the location of the P.N.A. The stress distribution results in the internal moment M_i and the axial force P, while only the former is of interest here. The internal moment of case 0 is equal to M_0 where the P.N.A. is at the centroid. For cases 1 and 2 where the P.N.A. is above or below the centroid, M_i will be less than M_0 because the additional M_1 and M_2 as shown in Figure D-7 are in the opposite direction to M_0. Thus M_i is at maximum when the P.N.A. passes through the centroid. These conclusions apply to both plate induced failure (plate outer surface in flexural compression) and stiffener induced failure (stiffener flange in flexural compression).

All of the above analysis in this appendix is for stiffened plates assuming the full plate width effective. When local buckling takes place in the plate of the stiffened panel, the virtual work model is correspondingly modified. The effective plate width can be used with the stiffener to form the effective cross-section. It is is assumed that the yield strength can be fully reached across the effective cross-section. The plate induced plastic hinge mechanism with the P.N.A. in the plate is taken for illustration. Its effective cross-section and stress distribution are shown in Figure D-8. Using the same approach as for the full cross-section (Figure D-1), the values of P and M_{ie} can be found from the sum of the forces and moments about the centroid of the effective cross-section, where M_{ie} is the internal moment about the centroid of the effective cross-section. This gives

$$P = -P_{ye} + 2F_y b_e t_1 \qquad \text{[D-47]}$$

$$M_{ie} = 2F_y b_e t_1 \left(z_{pe} - \frac{t_1}{2} \right) \qquad \text{[D-48]}$$

where P_{ye} is the yield force of the effective cross-section; b_e is the effective plate width; z_{pe} is the distance between the plate outer surface and the centroid of the effective cross-section. Solving for t_1 from Equation [D-47] and then substituting the solution into Equation [D-48] there comes out

$$M_{ie} = \left(P_{ye} + P\right)\left(z_{pe} - \frac{P_{ye} + P}{4F_y b_e} \right) \qquad \text{[D-49]}$$

Since the external axial loads are applied at the centroid of the full section at both ends of the stiffened plate (Figure D-1), the virtual work model uses the internal moment about the centroid of the full section, M_i. The value of M_i is obtained simply by adding up the eccentricity effect of P to M_{ie} as below:

$$M_i = \left(P_{ye} + P\right)\left(z_{pe} - \frac{P_{ye} + P}{4F_y b_e}\right) - P\left(z_{pe} - z_p\right) \qquad \text{[D-50]}$$

Substituting $\beta_9 M_p$ for M_a and Equation [D-50] for M_i in Equation [D-10], there comes:

$$\frac{u_3}{L} = \frac{\beta_9 M_p}{PL} + \left(\frac{P_{ye}}{P} + 1\right)\left(\frac{z_{pe}}{L} - \frac{P_{ye} + P}{4F_y b_e L}\right) - \frac{z_{pe}}{L} + \frac{z_p}{L}, \quad \frac{P}{P_{ye}} \le 1 - \frac{2A_s}{A_e} \qquad \text{[D-51]}$$
$$N.A.\ in\ plate$$

where A_e is the area of the effective cross-section.

The other two equations for effective cross-sections using the similar approach for plate induced plastic hinge are as follows:

$$\frac{u_3}{L} = \frac{\beta_9 M_p}{PL} + \frac{2F_y A_f}{P}\left(\frac{z_{se}}{L} - \frac{t_f}{2L}\right) + \left(\frac{P_{ye} - 2F_y A_f}{P} - 1\right)\left(\frac{z_{se}}{L} - \frac{t_f}{L} - \frac{P_{ye} - P}{4F_y t_w L} + \frac{A_f}{2t_w L}\right)$$
$$- \frac{z_{pe}}{L} + \frac{z_p}{L}, \qquad 1 - \frac{2A_s}{A_e} \le \frac{P}{P_{ye}} \le 1 - \frac{2A_f}{A_e} \quad N.A.\ in\ web \qquad \text{[D-52]}$$

$$\frac{u_3}{L} = \frac{\beta_9 M_p}{PL} + \left(\frac{P_{ye}}{P} - 1\right)\left(\frac{z_{se}}{L} - \frac{P_{ye} - P}{4F_y b_f L}\right) - \frac{z_{pe}}{L} + \frac{z_p}{L}, \quad \frac{P}{P_{ye}} \ge 1 - \frac{2A_f}{A_e} \qquad \text{[D-53]}$$
$$N.A.\ in\ flange$$

where z_{se} is the distance between the flange outer surface and the centroid of the effective cross-section.

The one equation for stiffener induced plastic hinge with effective cross-sections is

$$\frac{u_3}{L} = \frac{\beta_9 M_p}{PL} - \left(\frac{P_{ye}}{P} - 1\right)\left(\frac{z_{pe}}{L} - \frac{P_{ye} - P}{4F_y b_e L}\right) + \frac{z_{pe}}{L} - \frac{z_p}{L}, \qquad \text{[D-54]}$$

stiffener induced plastic hinge

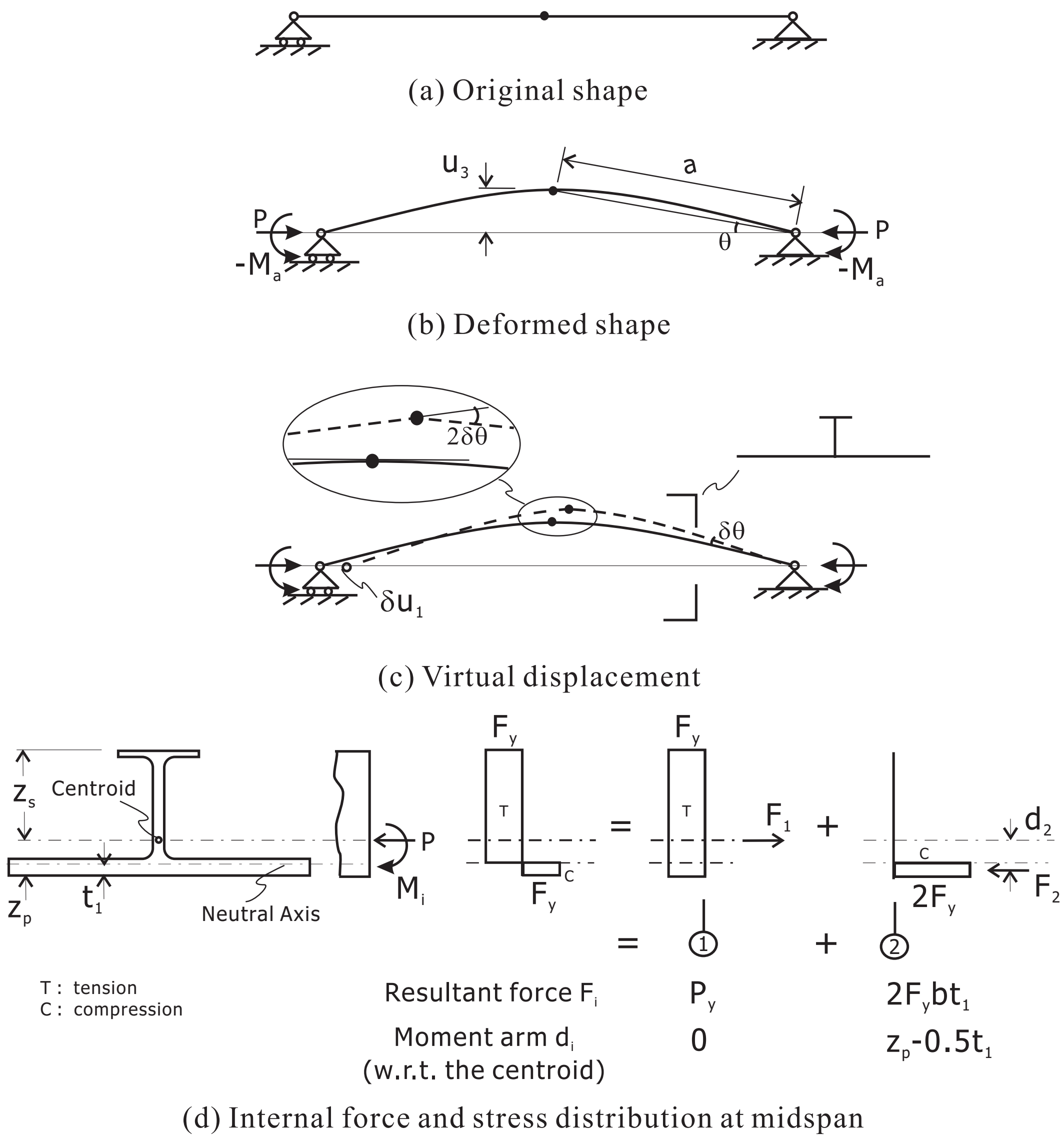

Figure D-1 Virtual work model for plate induced plastic hinge mechanism with the neutral axis in the plate

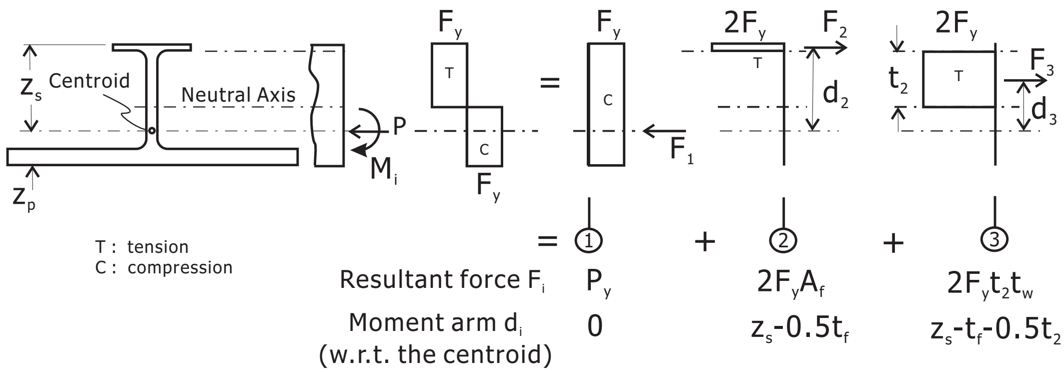

Figure D-2 Virtual work model for plate induced plastic hinge mechanism with the neutral axis in the web

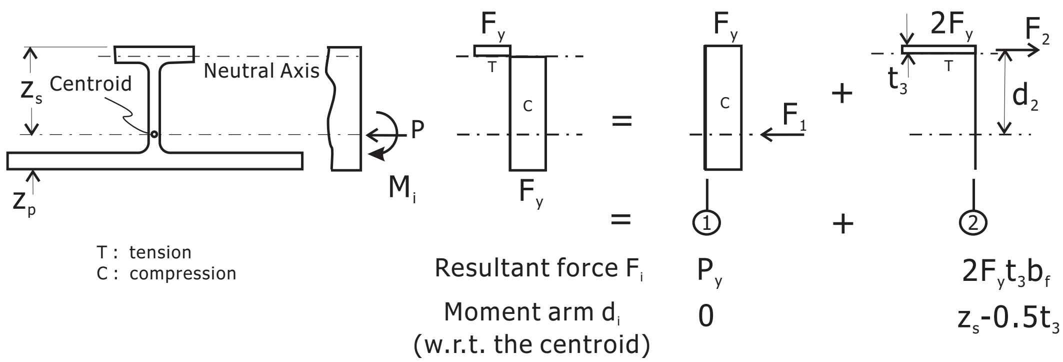

Figure D-3 Virtual work model for plate induced plastic hinge mechanism with the neutral axis in the flange

(a) Original shape

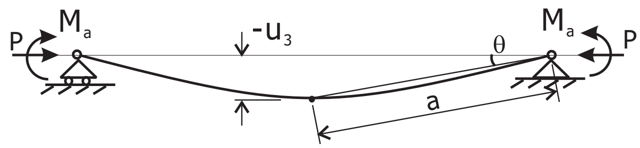

(b) Deformed shape

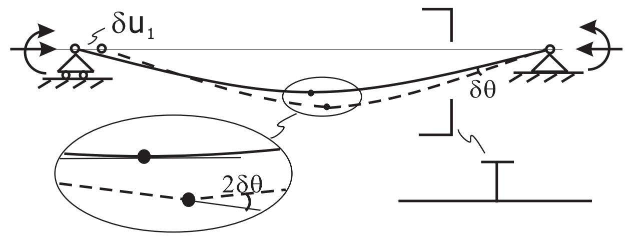

(c) Virtual displacement

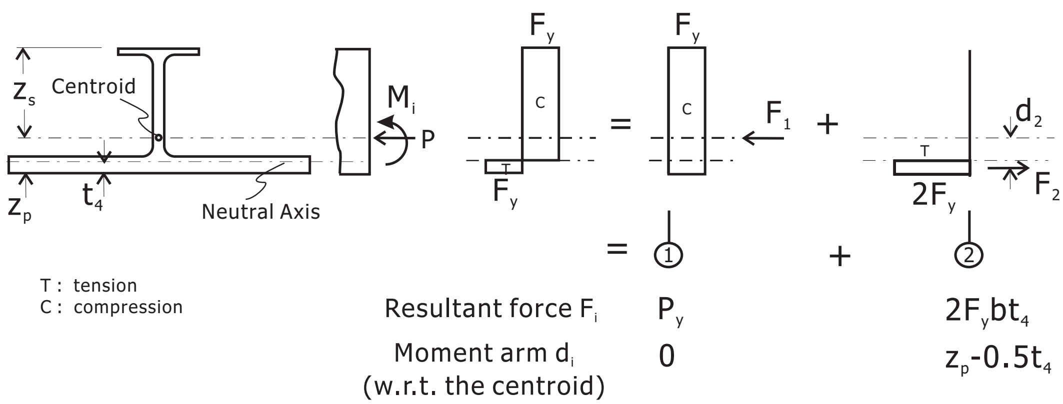

(d) Internal force and stress distribution at midspan

Figure D-4 Virtual work model for stiffener induced plastic hinge mechanism

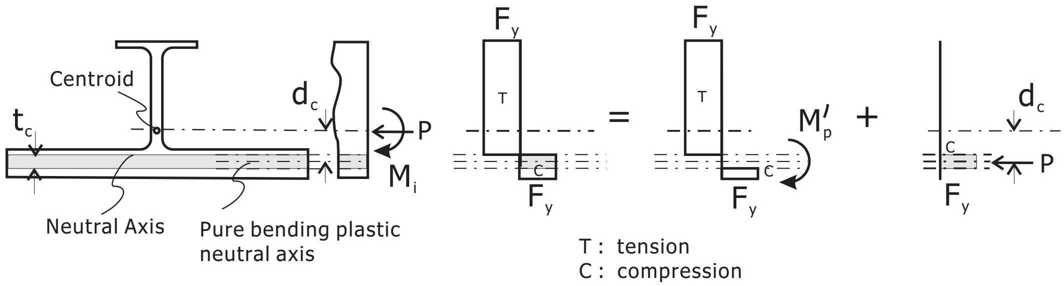

Figure D-5 Virtual work model for plate induced plastic hinge mechanism with the neutral axis in the plate

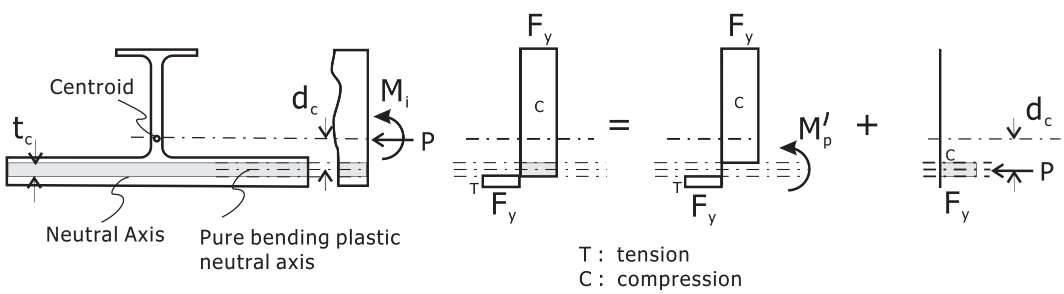

Figure D-6 Virtual work model for stiffener induced plastic hinge mechanism

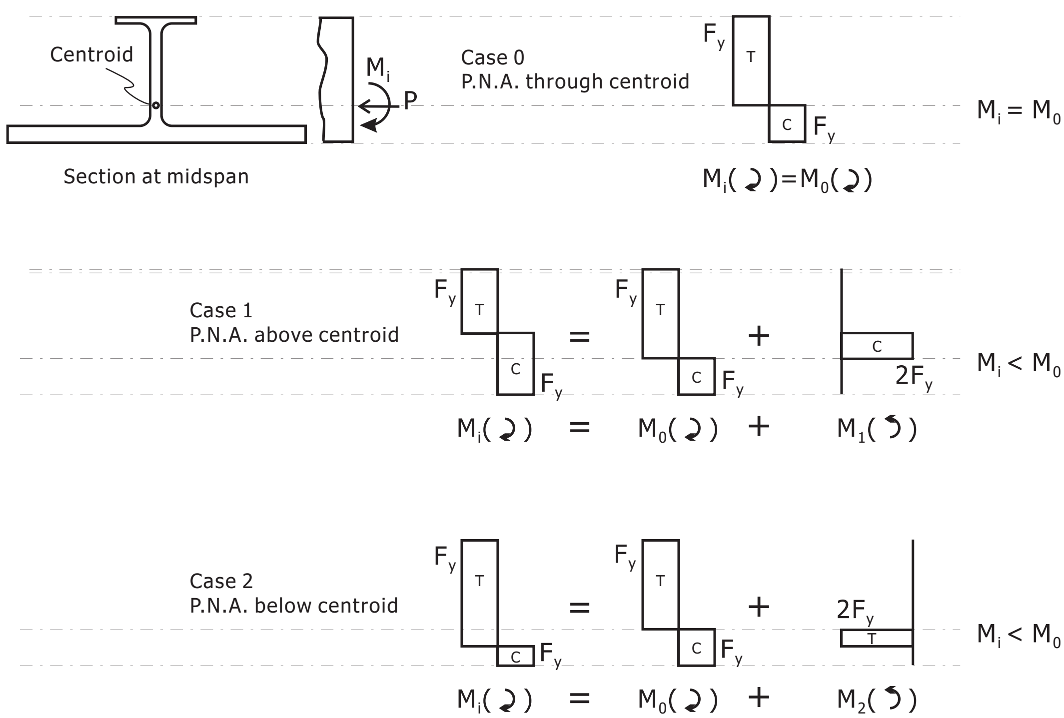

Figure D-7 Maximum internal moment about the centroid

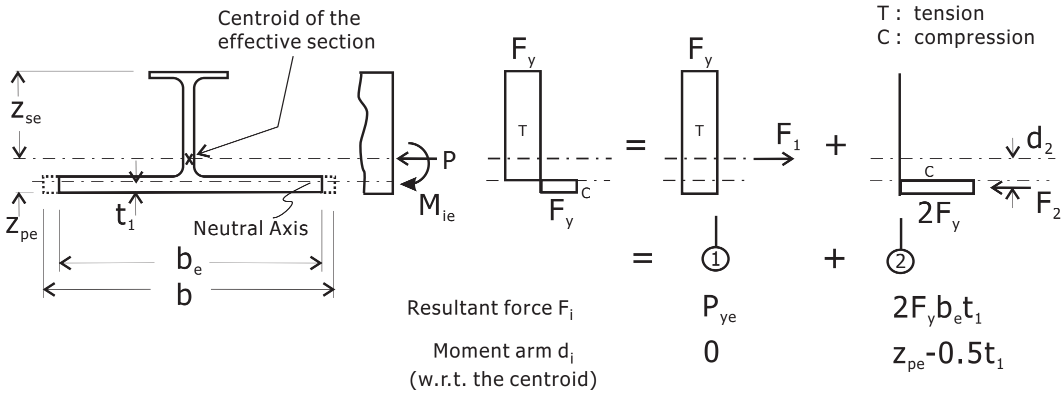

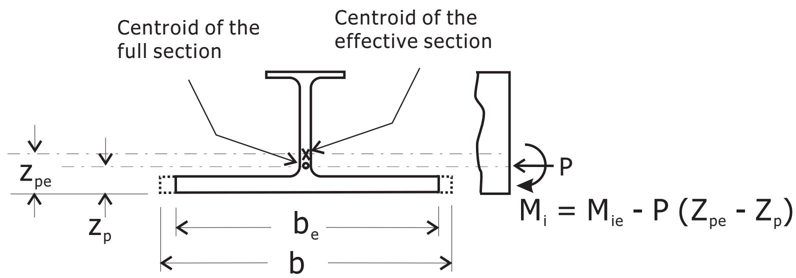

Figure D-8 Calculation of internal moment about the centroid of the full cross-section

APPENDIX E

LOAD VERSUS DEFORMATION CURVES OF THE 720 CASES FROM FINITE ELEMENT ANALYSIS

In this section, the axial load versus axial shortening curves and the axial load versus midspan lateral deflection curves of all the 720 panels are shown in the following figures. The boundary condition for all the 720 panels is the condition that the unloaded plate edges are free to move in the transverse in-plane direction (denoted by Case A in the figures). Each figure shows the curves of eight panels with identical β_2, β_3, and β_5, with their values displayed in the figure caption. In all the figures, $\beta\beta$ denotes the parameter β^* described in Chapter 2 and Appendix B; U_1 denotes the axial shortening displacement; and U_3 denotes the midspan lateral deflection.

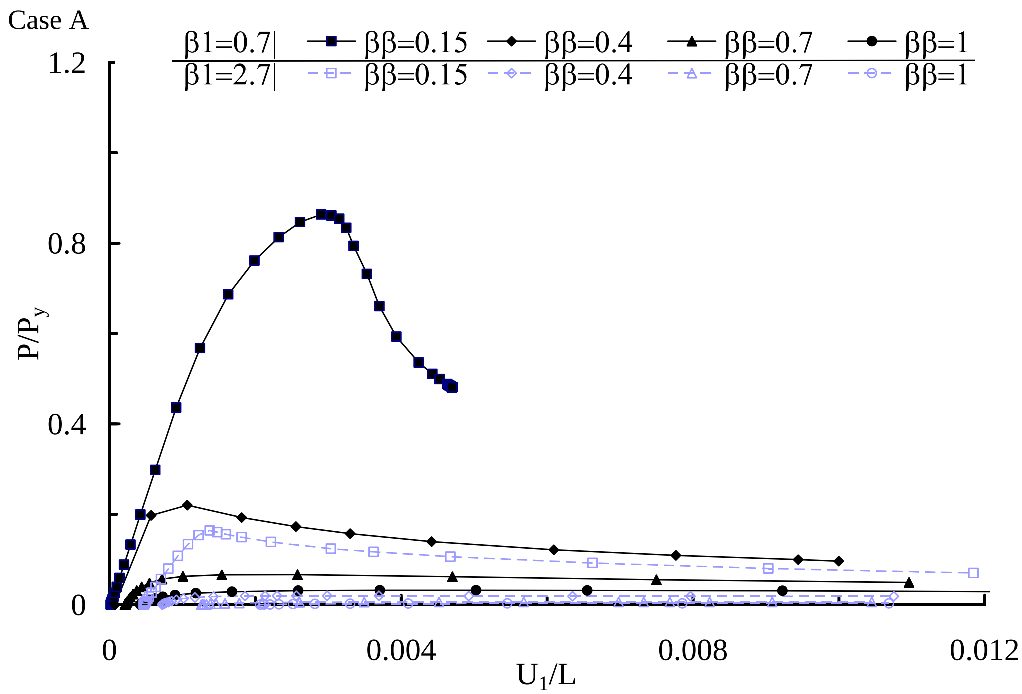

Figure E-1 Axial load versus axial shortening ($\beta_9 = -0.4$, $\beta_1 = 0.7$ & 2.7, $\beta_2 = 0.17$, $\beta_3 = 0.17$, $\beta_5 = 0.075$)

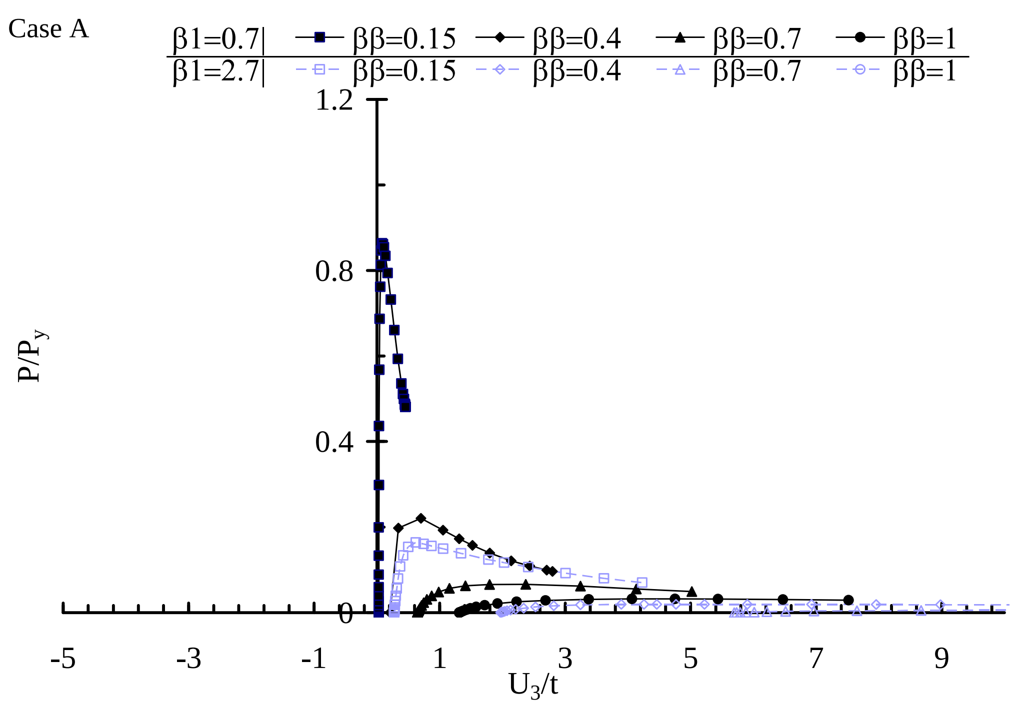

Figure E-2 Axial load versus lateral deflection ($\beta_9 = -0.4$, $\beta_1 = 0.7$ & 2.7, $\beta_2 = 0.17$, $\beta_3 = 0.17$, $\beta_5 = 0.075$)

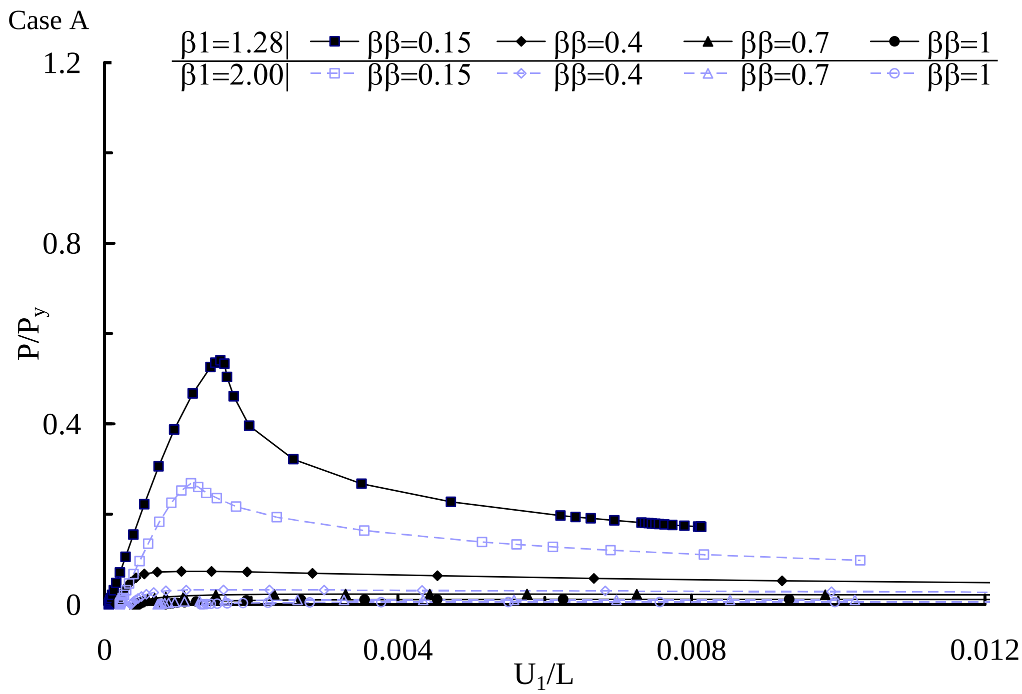

Figure E-3 Axial load versus axial shortening ($\beta_9 = -0.4$, $\beta_1 = 1.28$ & 2.0, $\beta_2 = 0.17$, $\beta_3 = 0.17$, $\beta_5 = 0.075$)

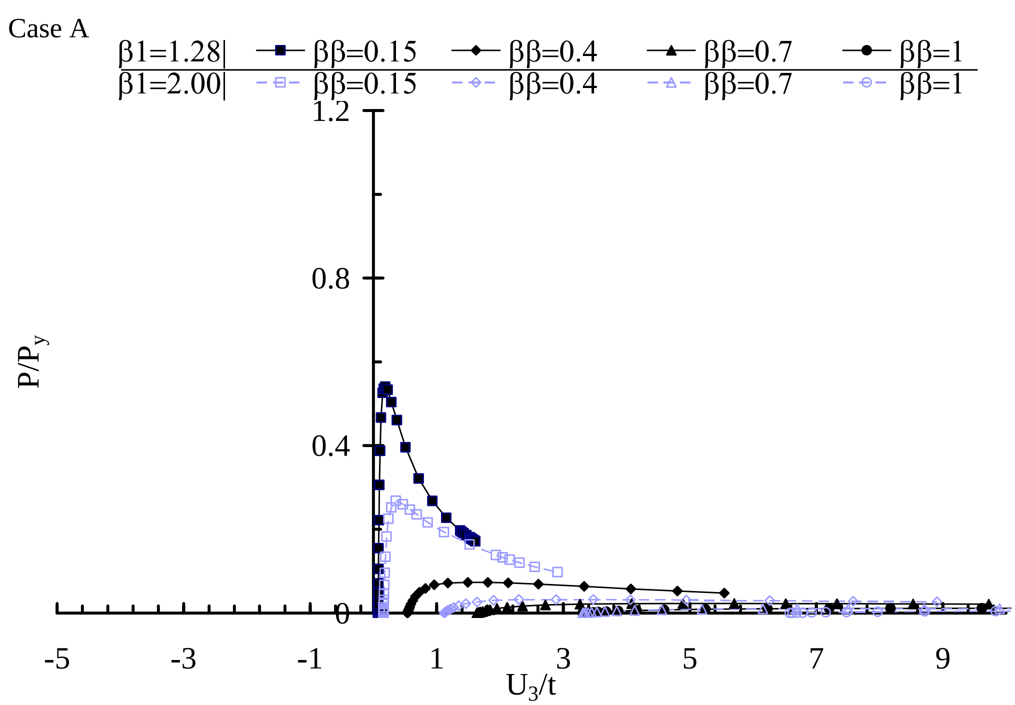

Figure E-4 Axial load versus lateral deflection ($\beta_9 = -0.4$, $\beta_1 = 1.28$ & 2.0, $\beta_2 = 0.17$, $\beta_3 = 0.17$, $\beta_5 = 0.075$)

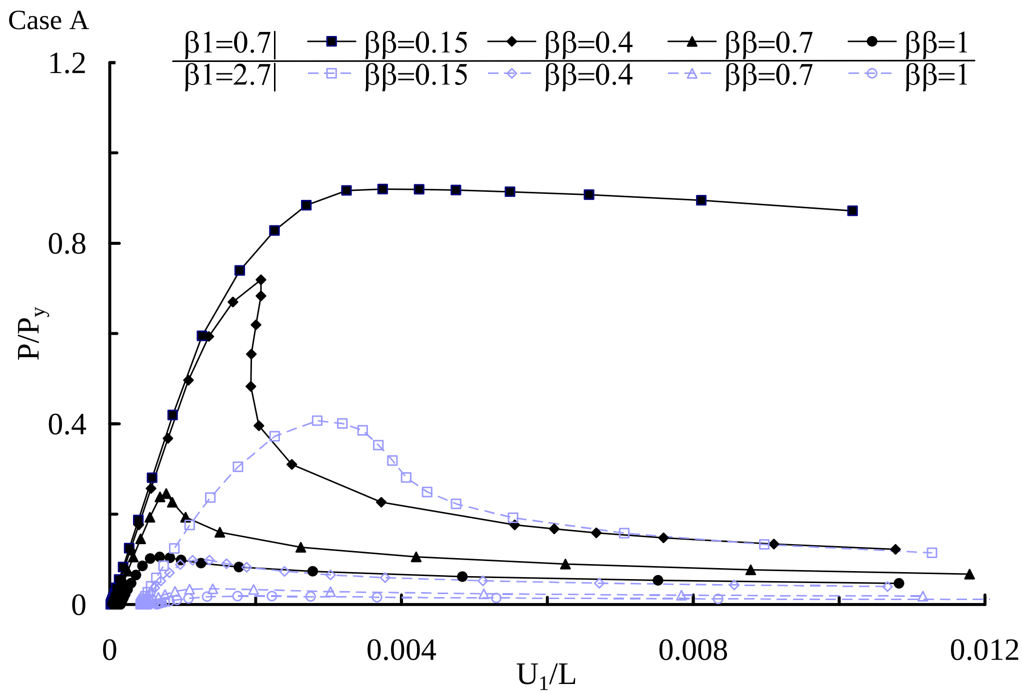

Figure E-5 Axial load versus axial shortening ($\beta_9 = -0.4$, $\beta_1 = 0.7$ & 2.7, $\beta_2 = 0.17$, $\beta_3 = 0.17$, $\beta_5 = 0.15$)

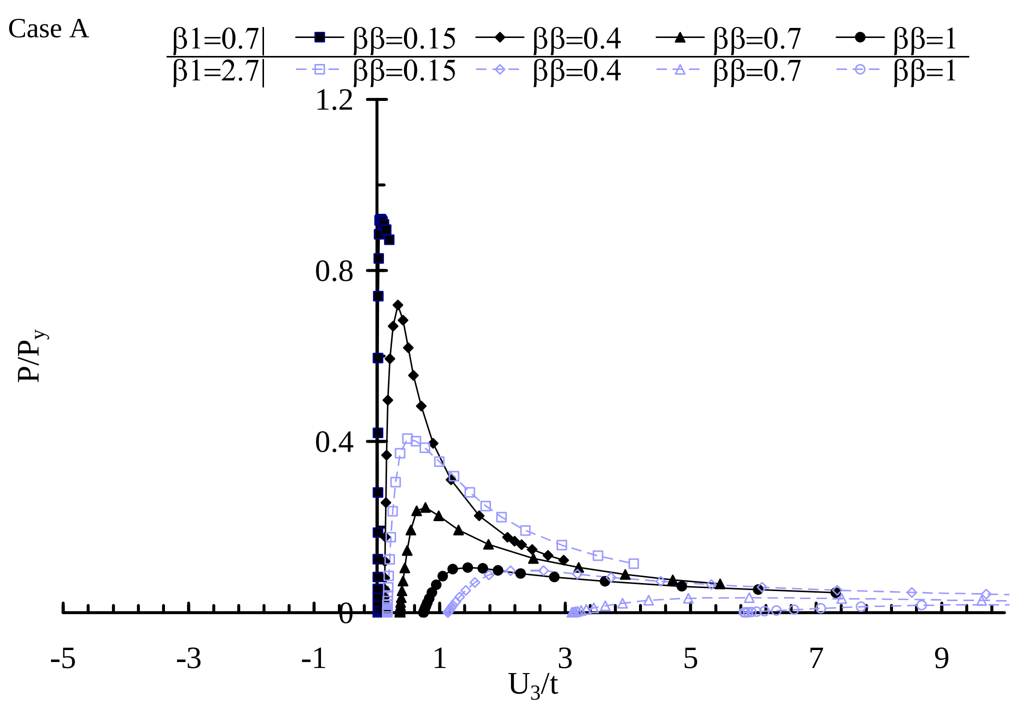

Figure E-6 Axial load versus lateral deflection ($\beta_9 = -0.4$, $\beta_1 = 0.7$ & 2.7, $\beta_2 = 0.17$, $\beta_3 = 0.17$, $\beta_5 = 0.15$)

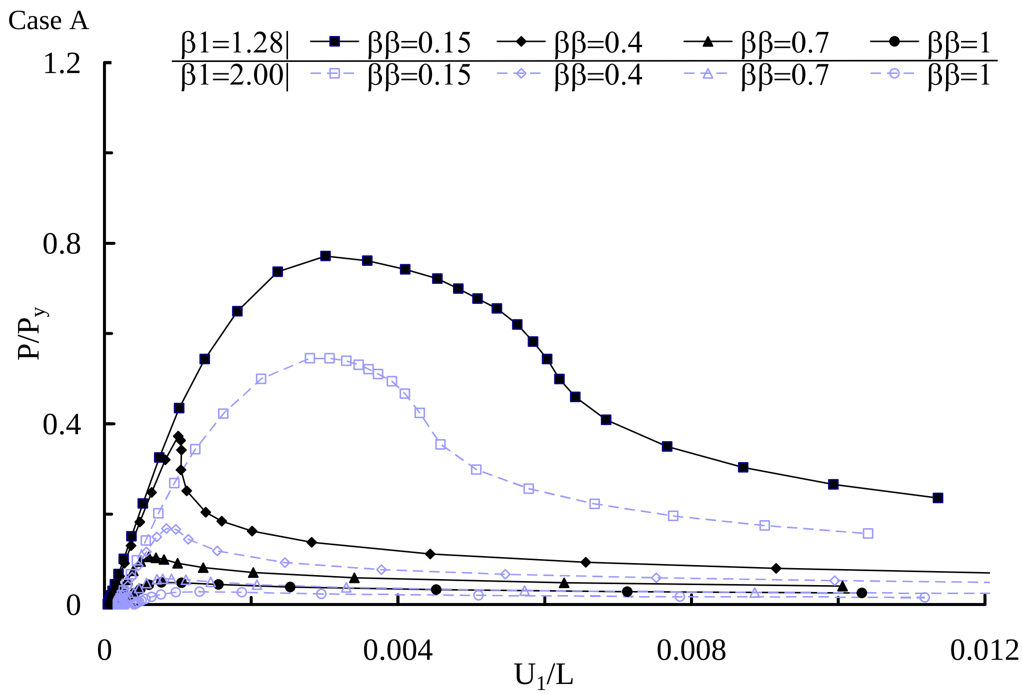

Figure E-7 Axial load versus axial shortening ($\beta_9 = -0.4$, $\beta_1 = 1.28$ & 2.0, $\beta_2 = 0.17$, $\beta_3 = 0.17$, $\beta_5 = 0.15$)

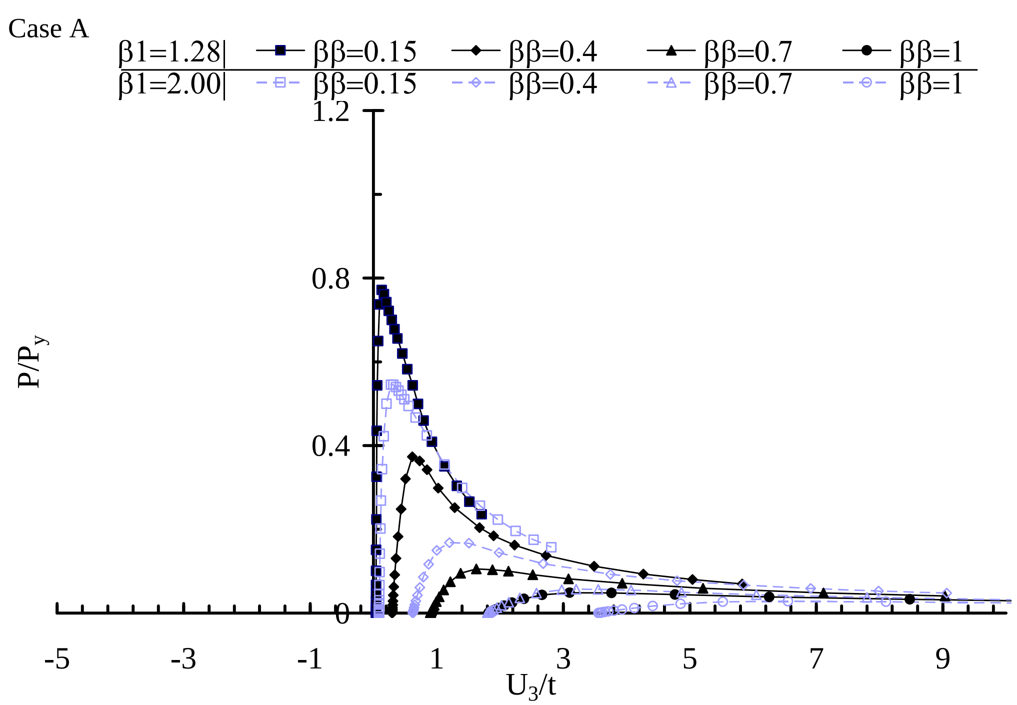

Figure E-8 Axial load versus lateral deflection ($\beta_9 = -0.4$, $\beta_1 = 1.28$ & 2.0, $\beta_2 = 0.17$, $\beta_3 = 0.17$, $\beta_5 = 0.15$)

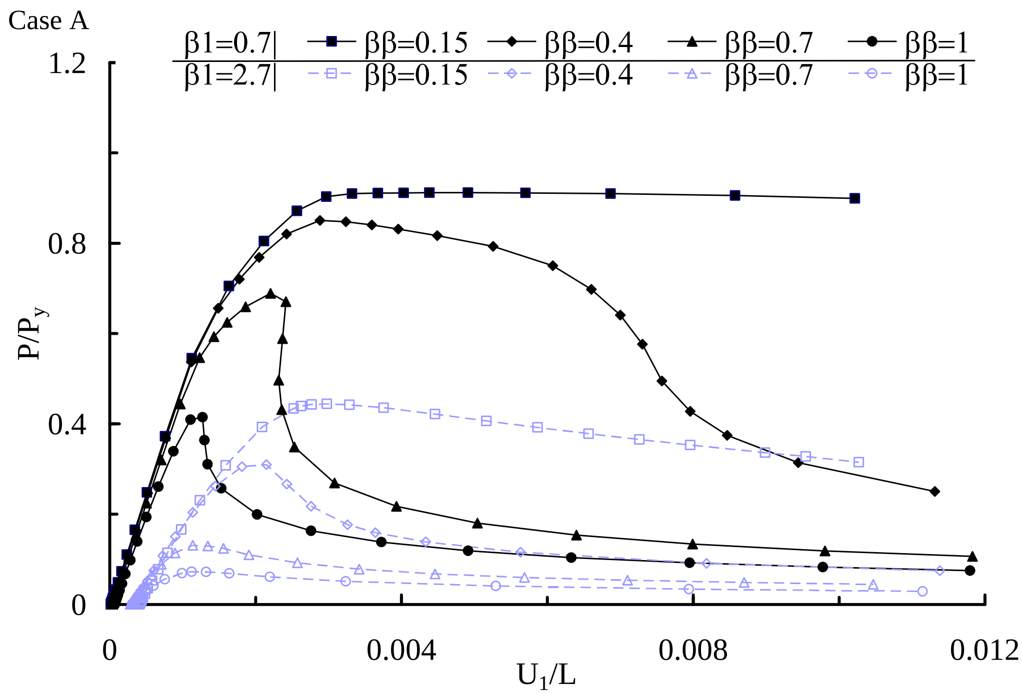

Figure E-9 Axial load versus axial shortening ($\beta_9 = -0.4$, $\beta_1 = 0.7$ & 2.7, $\beta_2 = 0.17$, $\beta_3 = 0.17$, $\beta_5 = 0.3$)

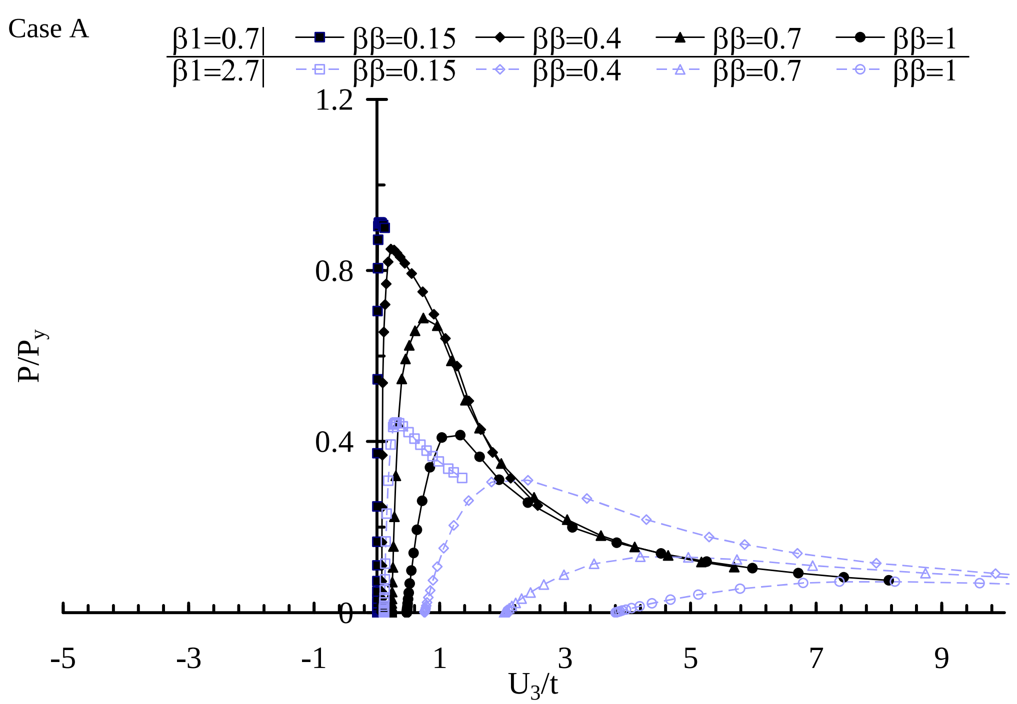

Figure E-10 Axial load versus lateral deflection ($\beta_9 = -0.4$, $\beta_1 = 0.7$ & 2.7, $\beta_2 = 0.17$, $\beta_3 = 0.17$, $\beta_5 = 0.3$)

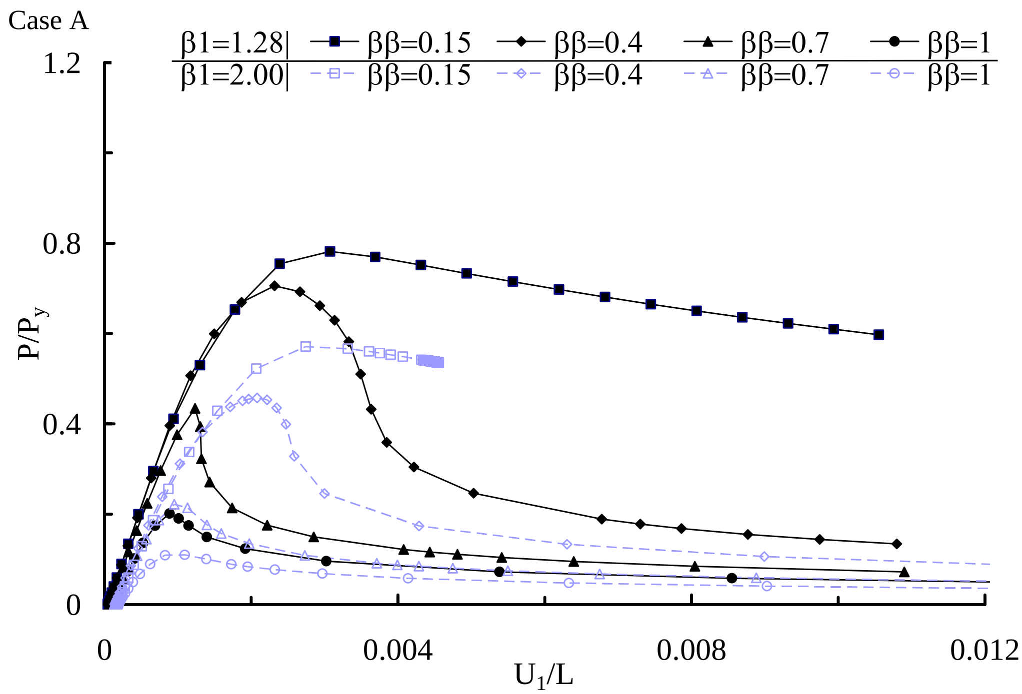

Figure E-11 Axial load versus axial shortening ($\beta_9 = -0.4$, $\beta_1 = 1.28$ & 2.0, $\beta_2 = 0.17$, $\beta_3 = 0.17$, $\beta_5 = 0.3$)

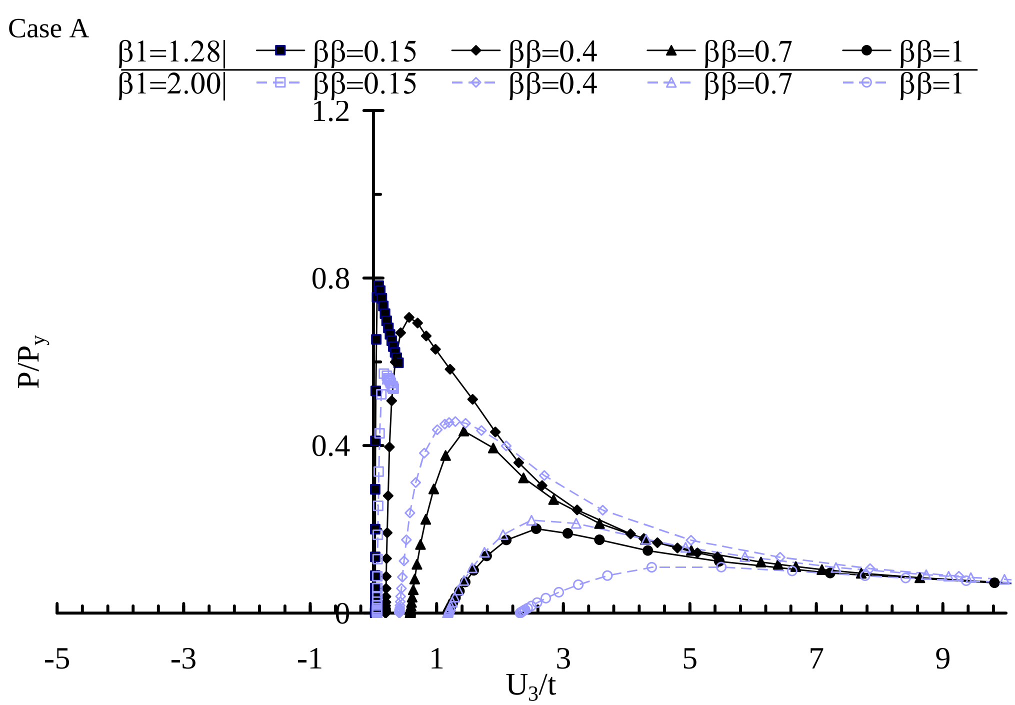

Figure E-12 Axial load versus lateral deflection ($\beta_9 = -0.4$, $\beta_1 = 1.28$ & 2.0, $\beta_2 = 0.17$, $\beta_3 = 0.17$, $\beta_5 = 0.3$)

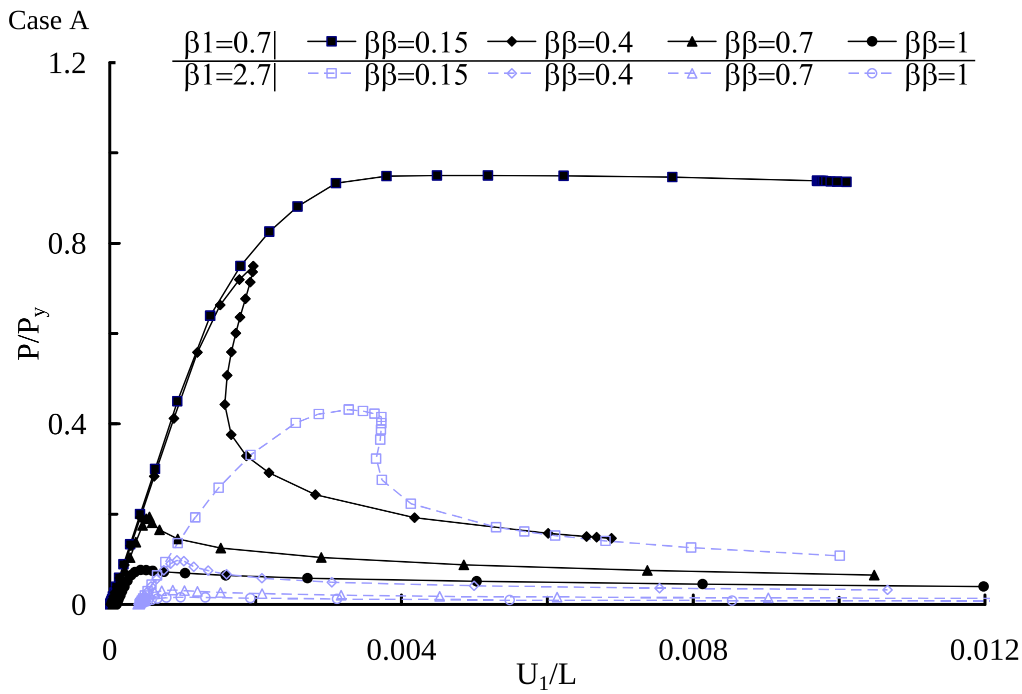

Figure E-13 Axial load versus axial shortening ($\beta_9 = -0.4$, $\beta_1 = 0.7$ & 2.7, $\beta_2 = 0.8$, $\beta_3 = 0.6$, $\beta_5 = 0.075$)

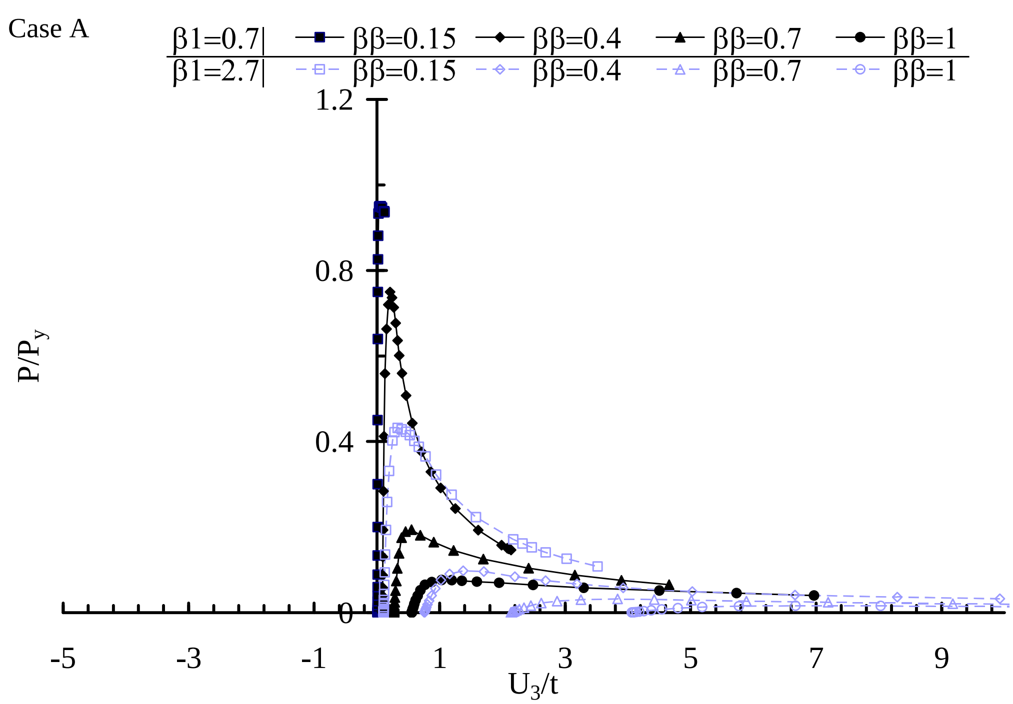

Figure E-14 Axial load versus lateral deflection ($\beta_9 = -0.4$, $\beta_1 = 0.7$ & 2.7, $\beta_2 = 0.8$, $\beta_3 = 0.6$, $\beta_5 = 0.075$)

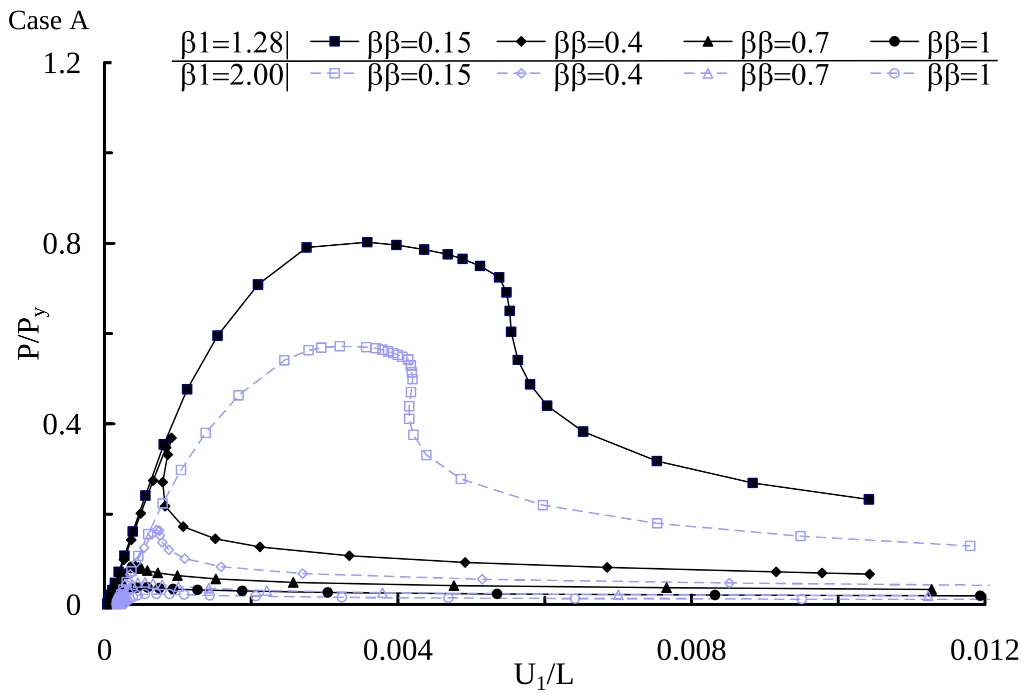

Figure E-15 Axial load versus axial shortening ($\beta_9 = -0.4$, $\beta_1 = 1.28$ & 2.0, $\beta_2 = 0.8$, $\beta_3 = 0.6$, $\beta_5 = 0.075$)

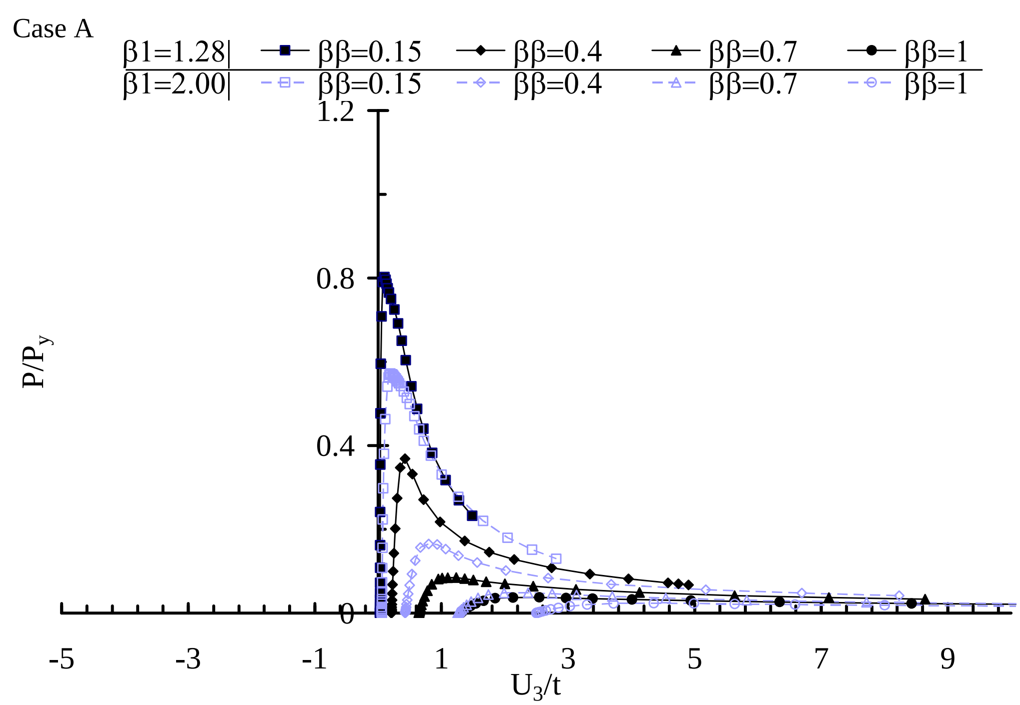

Figure E-16 Axial load versus lateral deflection ($\beta_9 = -0.4$, $\beta_1 = 1.28$ & 2.0, $\beta_2 = 0.8$, $\beta_3 = 0.6$, $\beta_5 = 0.075$)

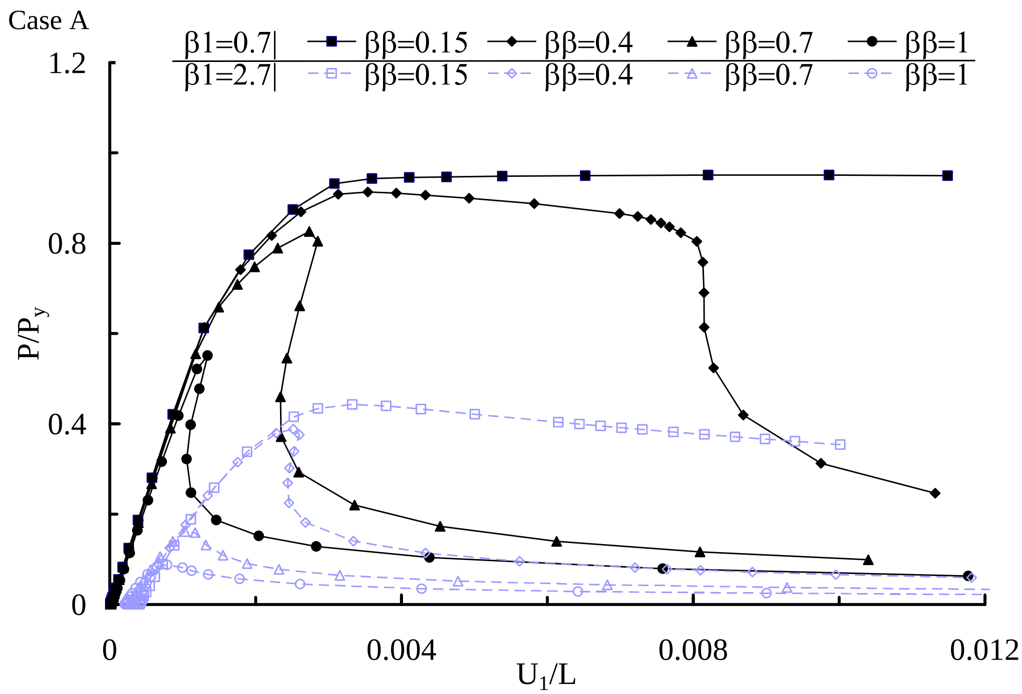

Figure E-17 Axial load versus axial shortening ($\beta_9 = -0.4$, $\beta_1 = 0.7$ & 2.7, $\beta_2 = 0.8$, $\beta_3 = 0.6$, $\beta_5 = 0.15$)

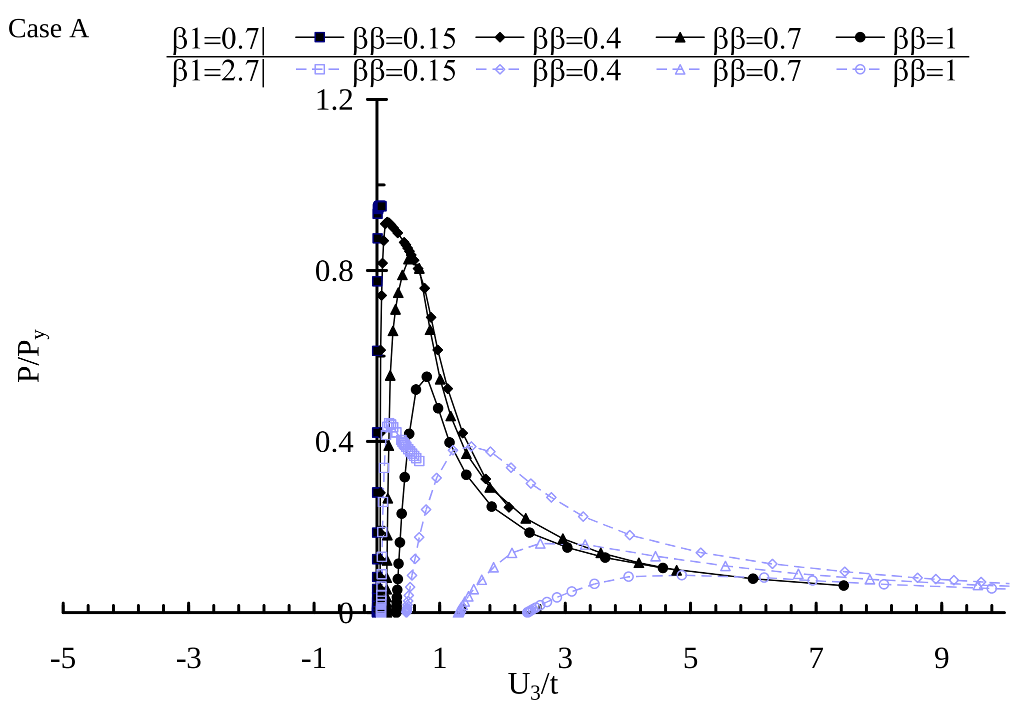

Figure E-18 Axial load versus lateral deflection ($\beta_9 = -0.4$, $\beta_1 = 0.7$ & 2.7, $\beta_2 = 0.8$, $\beta_3 = 0.6$, $\beta_5 = 0.15$)

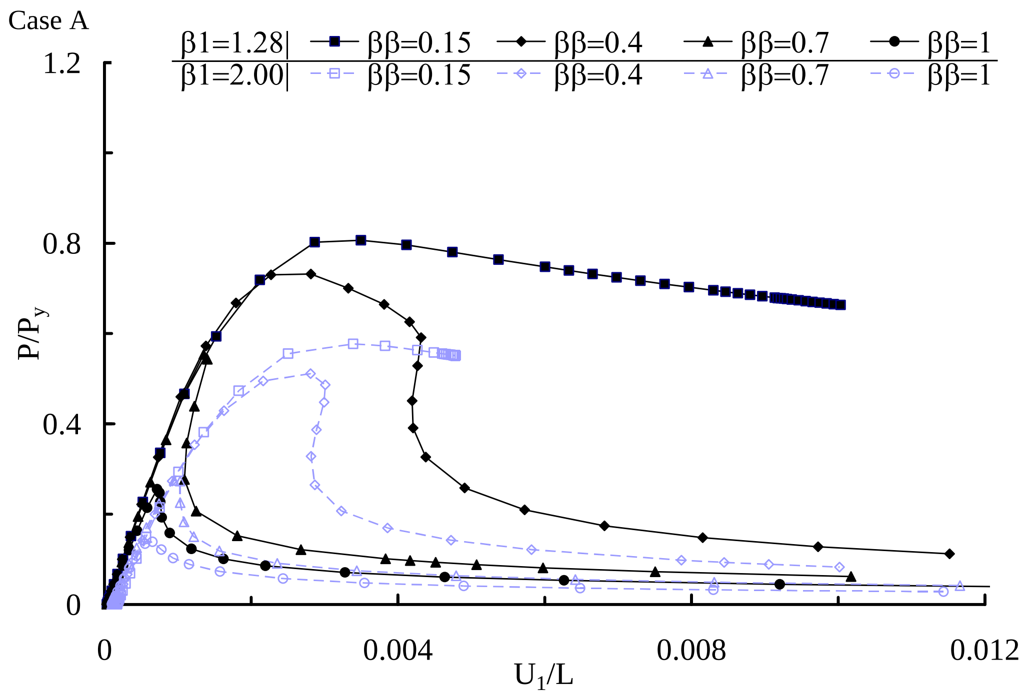

Figure E-19 Axial load versus axial shortening ($\beta_9 = -0.4$, $\beta_1 = 1.28$ & 2.0, $\beta_2 = 0.8$, $\beta_3 = 0.6$, $\beta_5 = 0.15$)

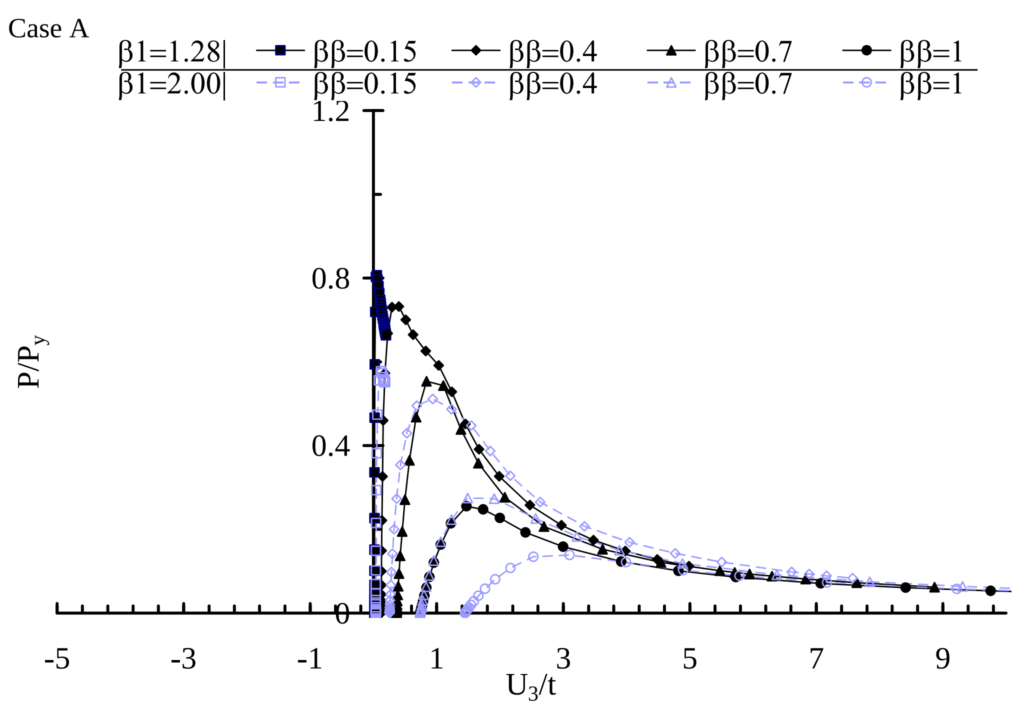

Figure E-20 Axial load versus lateral deflection ($\beta_9 = -0.4$, $\beta_1 = 1.28$ & 2.0, $\beta_2 = 0.8$, $\beta_3 = 0.6$, $\beta_5 = 0.15$)

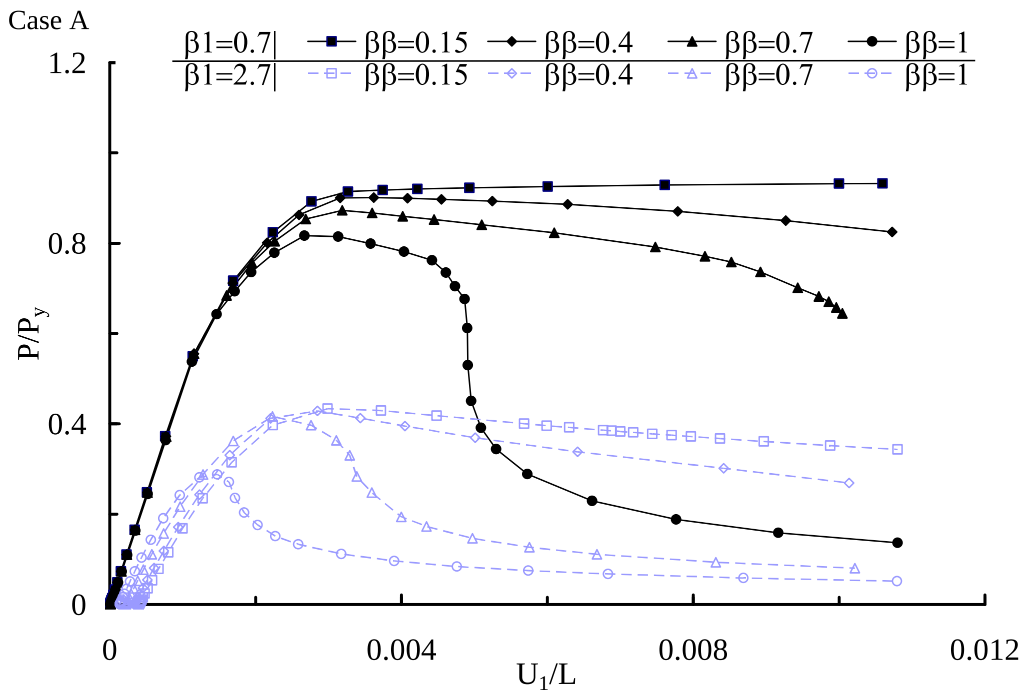

Figure E-21 Axial load versus axial shortening ($\beta_9 = -0.4$, $\beta_1 = 0.7$ & 2.7, $\beta_2 = 0.8$, $\beta_3 = 0.6$, $\beta_5 = 0.3$)

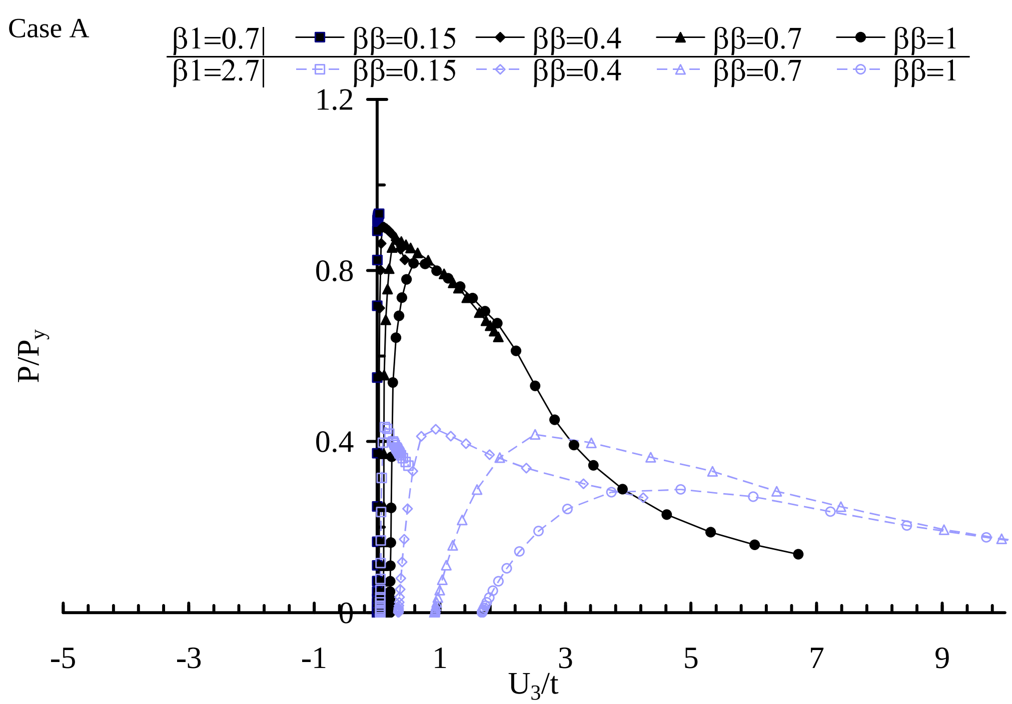

Figure E-22 Axial load versus lateral deflection ($\beta_9 = -0.4$, $\beta_1 = 0.7$ & 2.7, $\beta_2 = 0.8$, $\beta_3 = 0.6$, $\beta_5 = 0.3$)

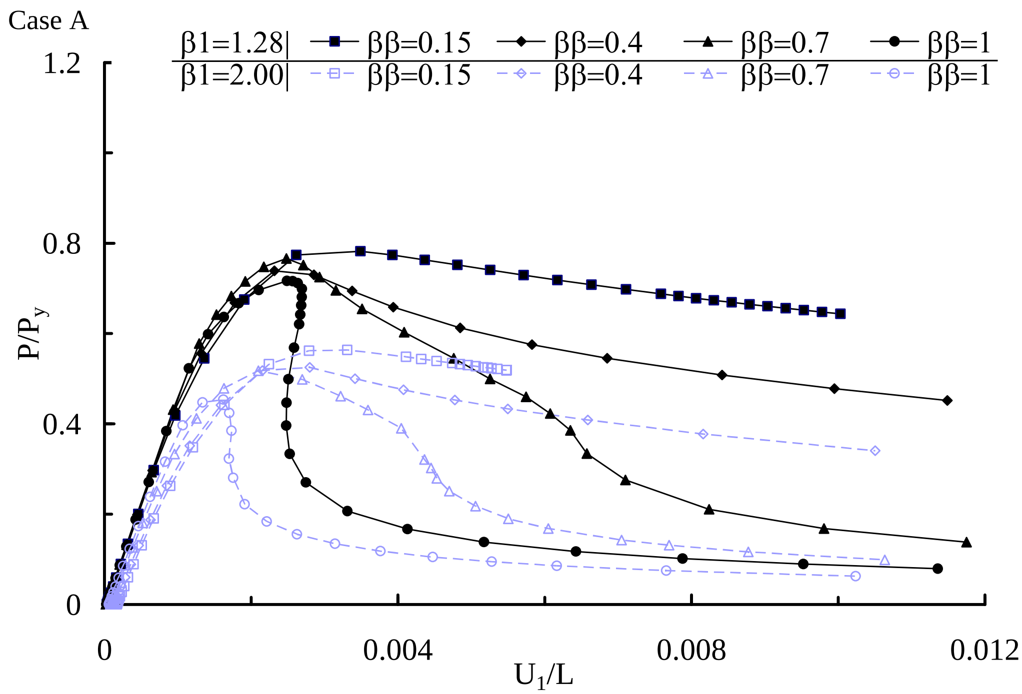

Figure E-23 Axial load versus axial shortening ($\beta_9 = -0.4$, $\beta_1 = 1.28$ & 2.0, $\beta_2 = 0.8$, $\beta_3 = 0.6$, $\beta_5 = 0.3$)

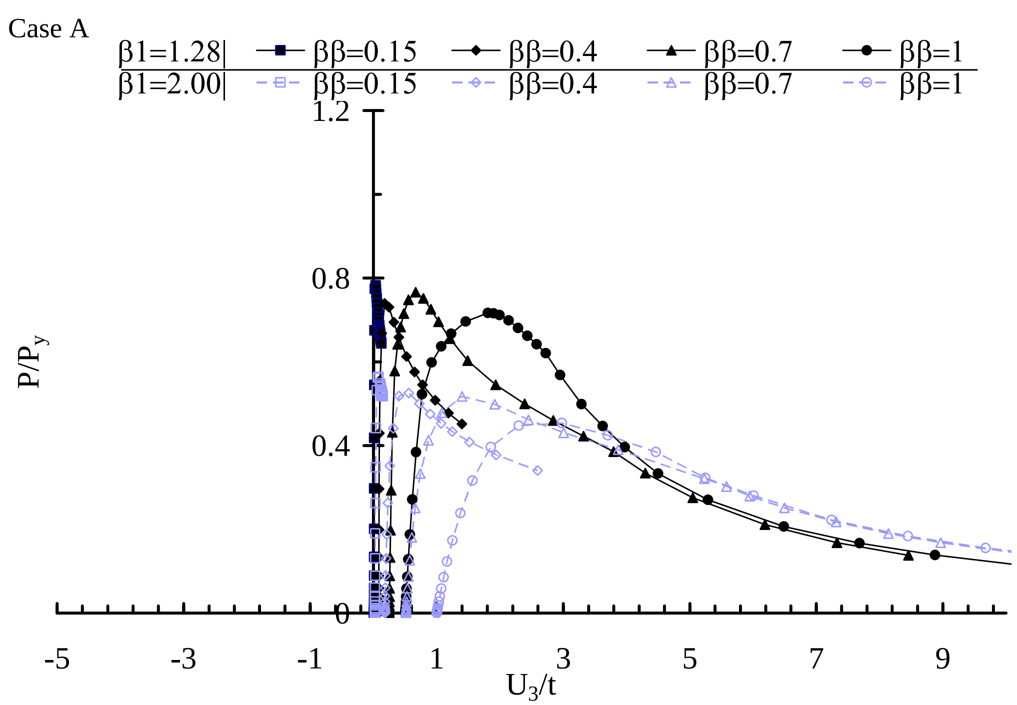

Figure E-24 Axial load versus lateral deflection ($\beta_9 = -0.4$, $\beta_1 = 1.28$ & 2.0, $\beta_2 = 0.8$, $\beta_3 = 0.6$, $\beta_5 = 0.3$)

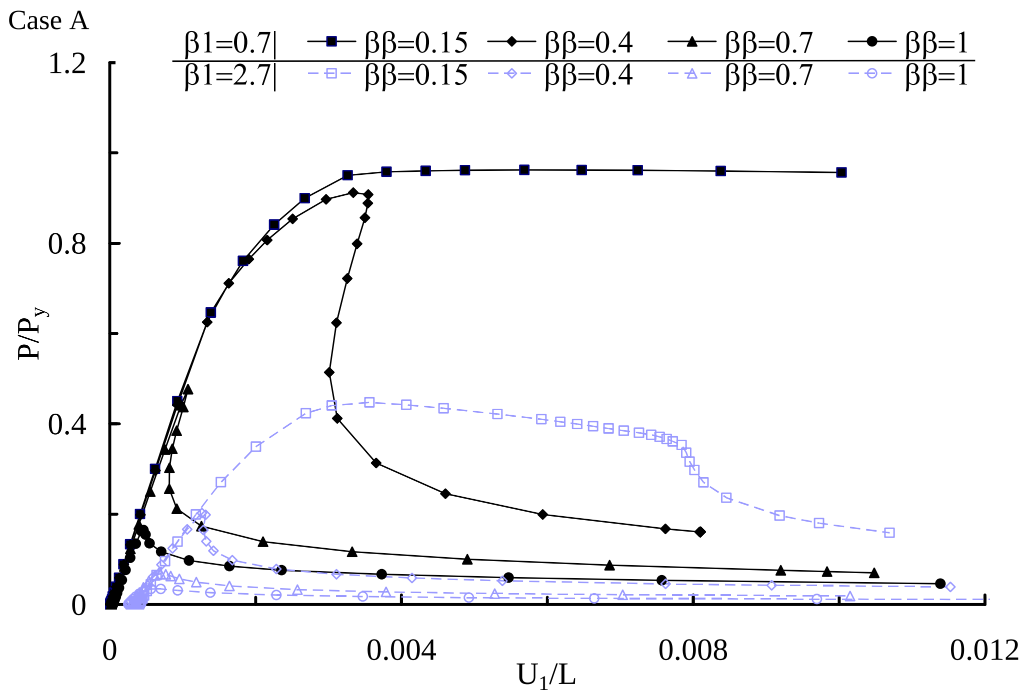

Figure E-25 Axial load versus axial shortening ($\beta_9 = -0.4$, $\beta_1 = 0.7$ & 2.7, $\beta_2 = 1.5$, $\beta_3 = 0.9$, $\beta_5 = 0.075$)

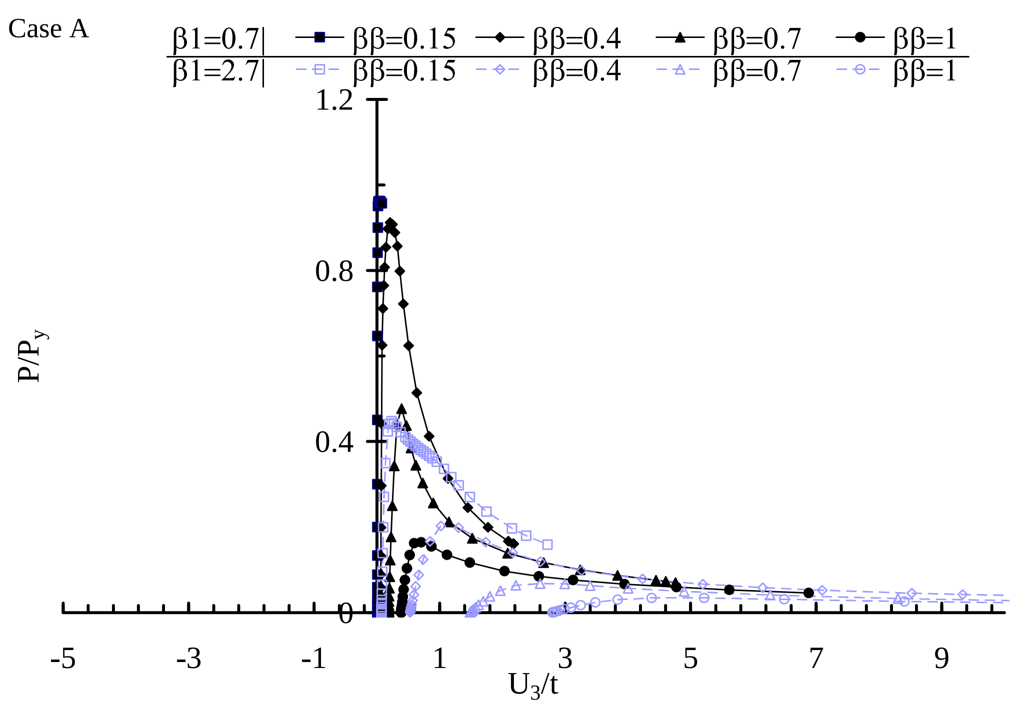

Figure E-26 Axial load versus lateral deflection ($\beta_9 = -0.4$, $\beta_1 = 0.7$ & 2.7, $\beta_2 = 1.5$, $\beta_3 = 0.9$, $\beta_5 = 0.075$)

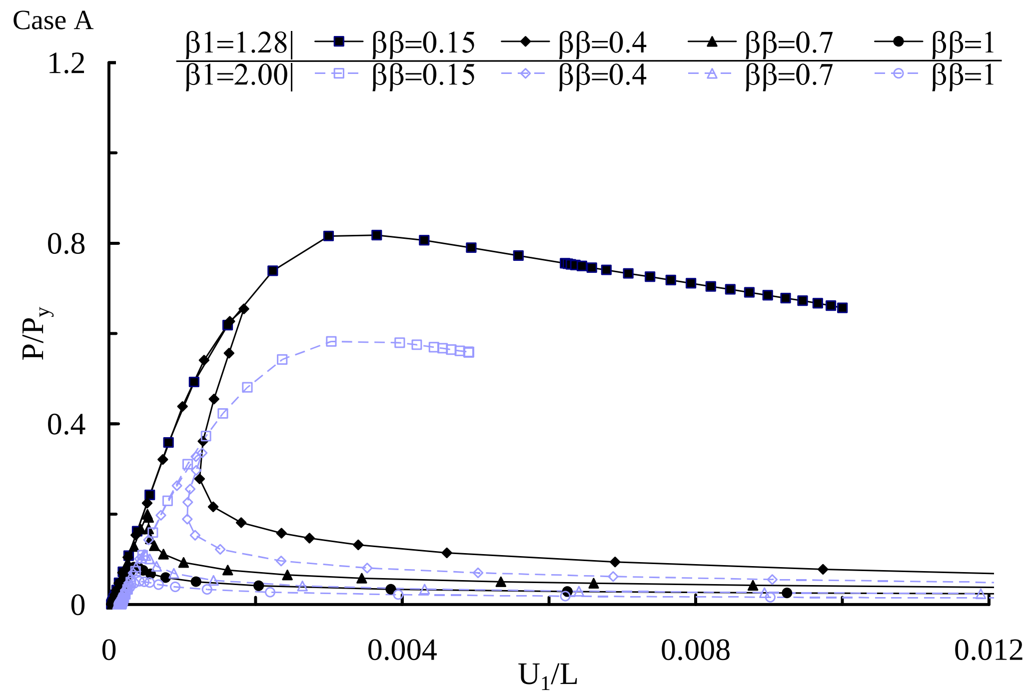

Figure E-27 Axial load versus axial shortening ($\beta_9 = -0.4$, $\beta_1 = 1.28$ & 2.0, $\beta_2 = 1.5$, $\beta_3 = 0.9$, $\beta_5 = 0.075$)

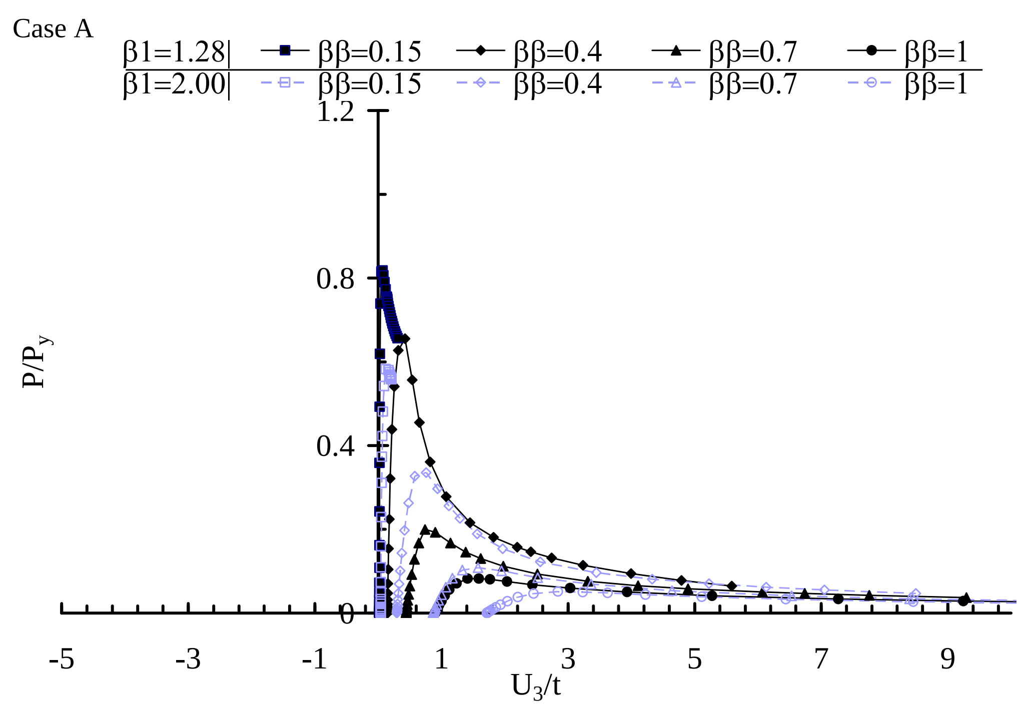

Figure E-28 Axial load versus lateral deflection ($\beta_9 = -0.4$, $\beta_1 = 1.28$ & 2.0, $\beta_2 = 1.5$, $\beta_3 = 0.9$, $\beta_5 = 0.075$)

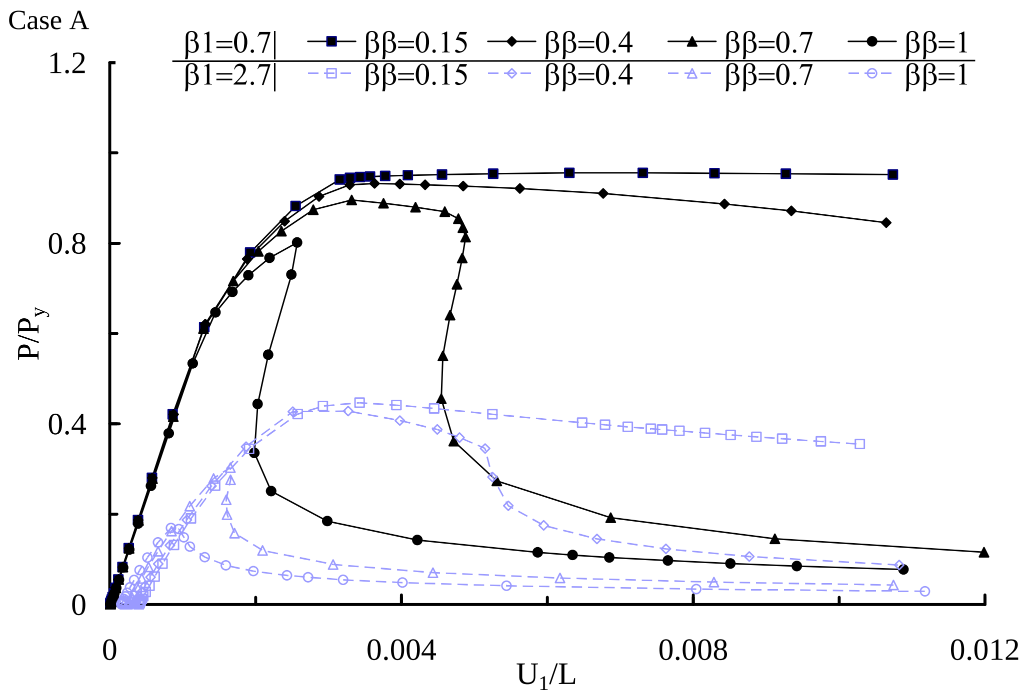

Figure E-29 Axial load versus axial shortening ($\beta_9 = -0.4$, $\beta_1 = 0.7$ & 2.7, $\beta_2 = 1.5$, $\beta_3 = 0.9$, $\beta_5 = 0.15$)

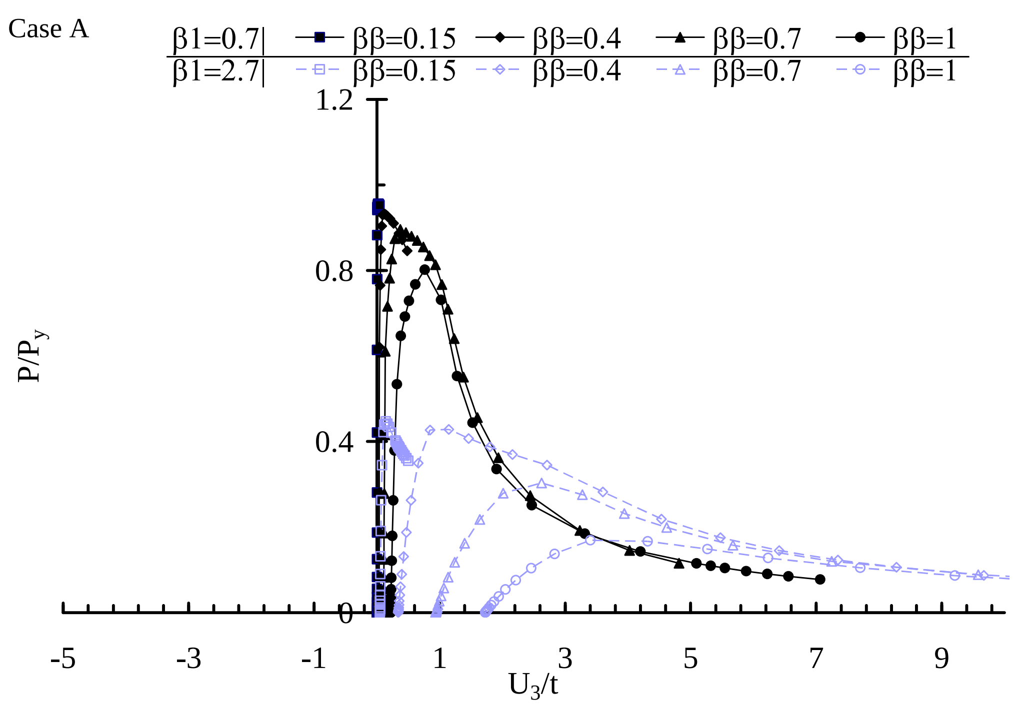

Figure E-30 Axial load versus lateral deflection ($\beta_9 = -0.4$, $\beta_1 = 0.7$ & 2.7, $\beta_2 = 1.5$, $\beta_3 = 0.9$, $\beta_5 = 0.15$)

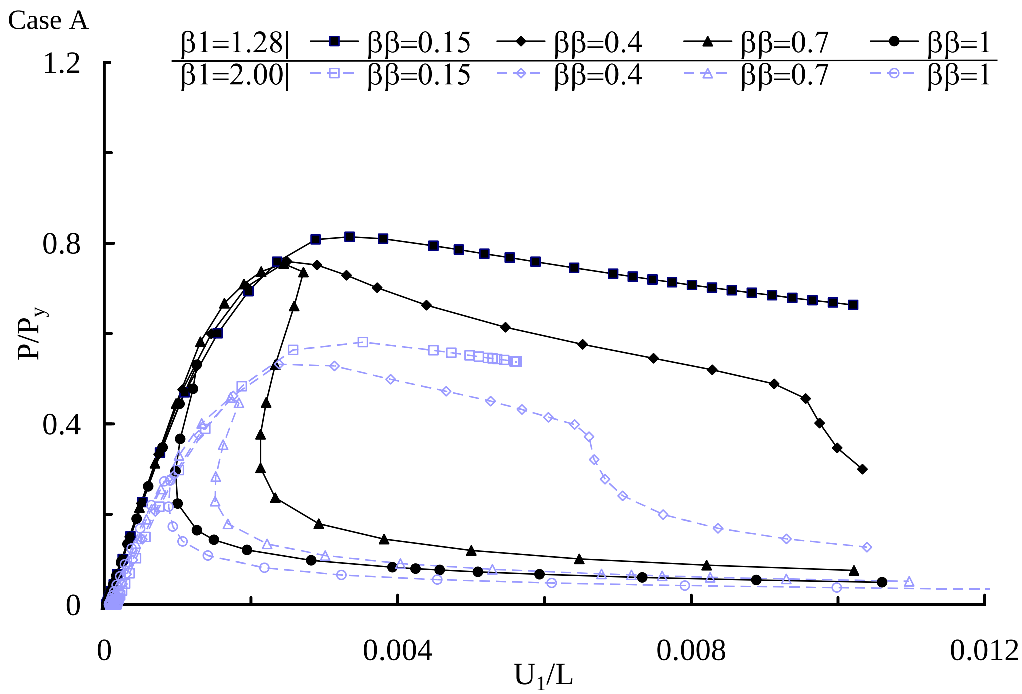

Figure E-31 Axial load versus axial shortening ($\beta_9 = -0.4$, $\beta_1 = 1.28$ & 2.0, $\beta_2 = 1.5$, $\beta_3 = 0.9$, $\beta_5 = 0.15$)

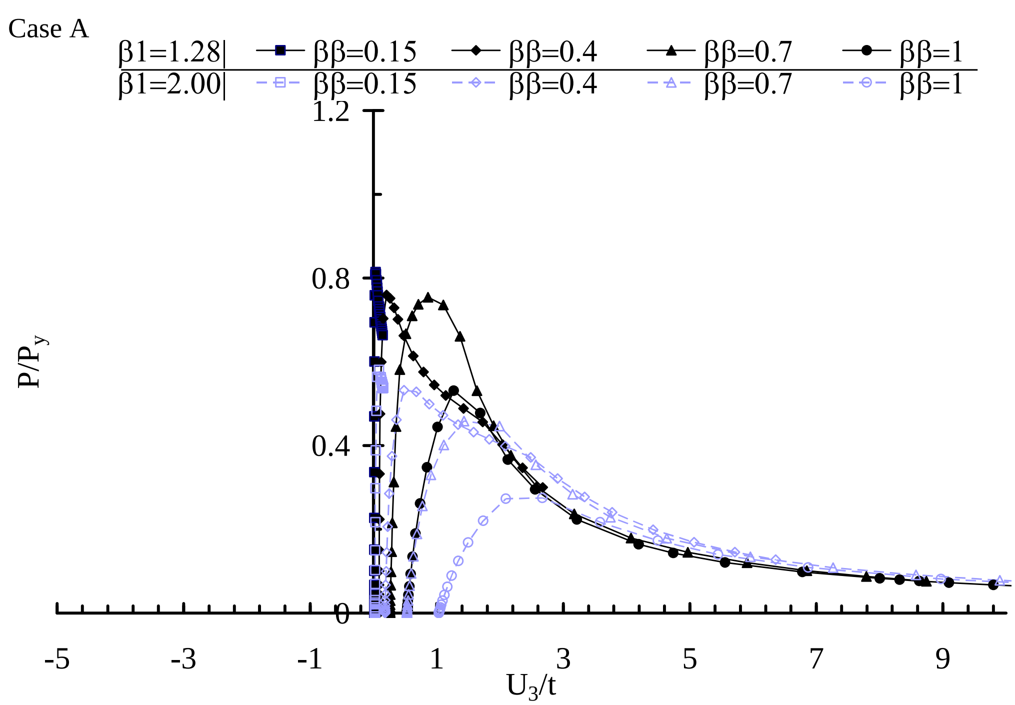

Figure E-32 Axial load versus lateral deflection ($\beta_9 = -0.4$, $\beta_1 = 1.28$ & 2.0, $\beta_2 = 1.5$, $\beta_3 = 0.9$, $\beta_5 = 0.15$)

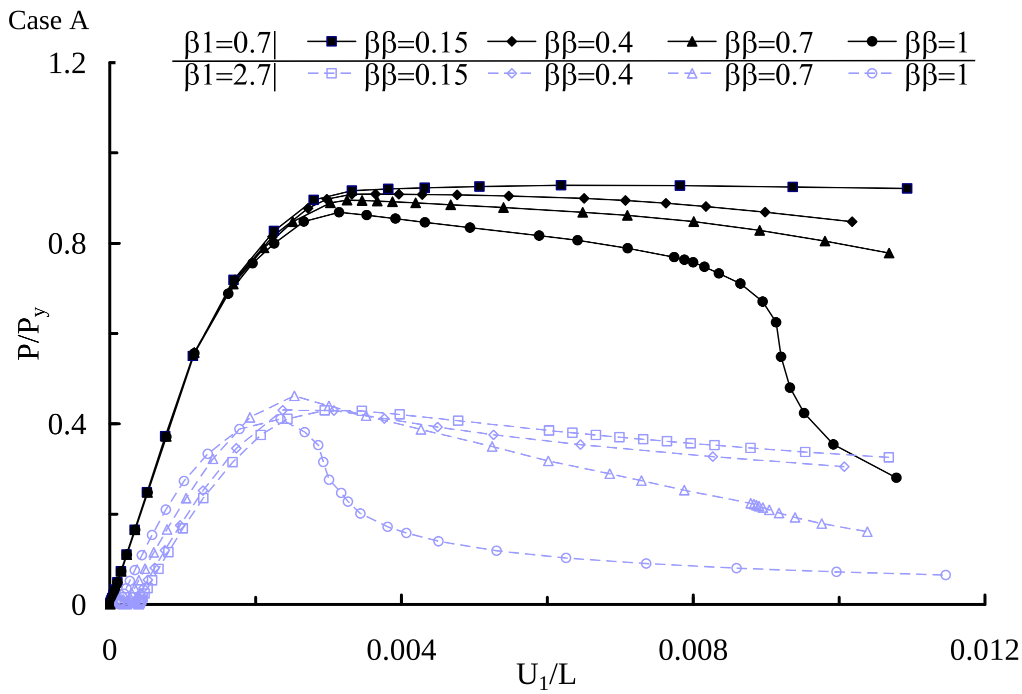

Figure E-33 Axial load versus axial shortening ($\beta_9 = -0.4$, $\beta_1 = 0.7$ & 2.7, $\beta_2 = 1.5$, $\beta_3 = 0.9$, $\beta_5 = 0.3$)

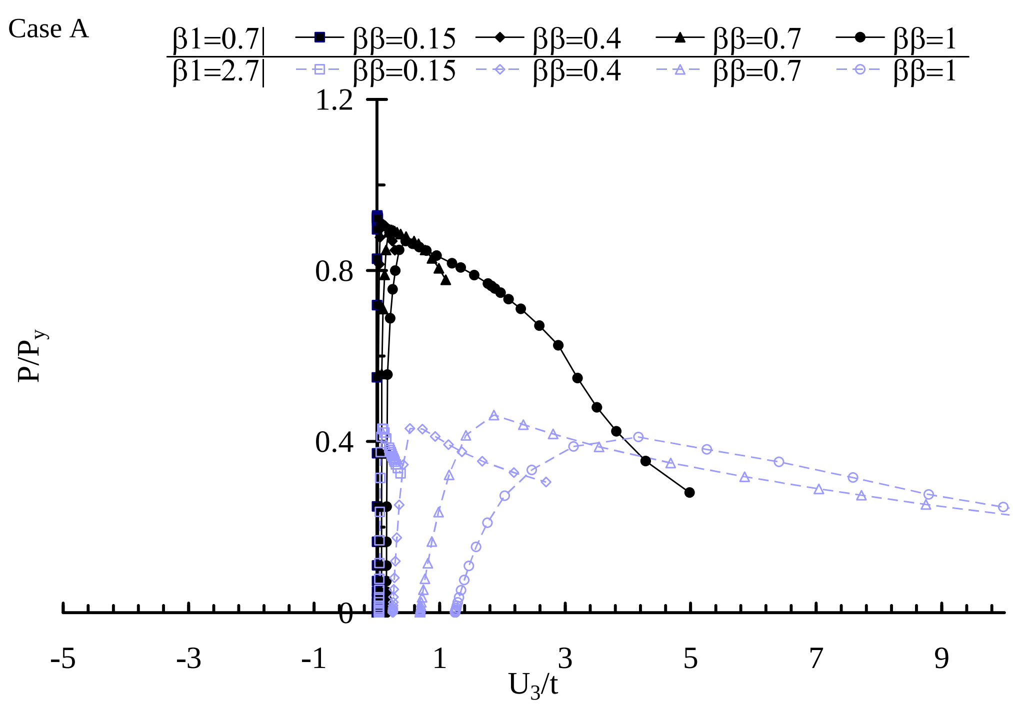

Figure E-34 Axial load versus lateral deflection ($\beta_9 = -0.4$, $\beta_1 = 0.7$ & 2.7, $\beta_2 = 1.5$, $\beta_3 = 0.9$, $\beta_5 = 0.3$)

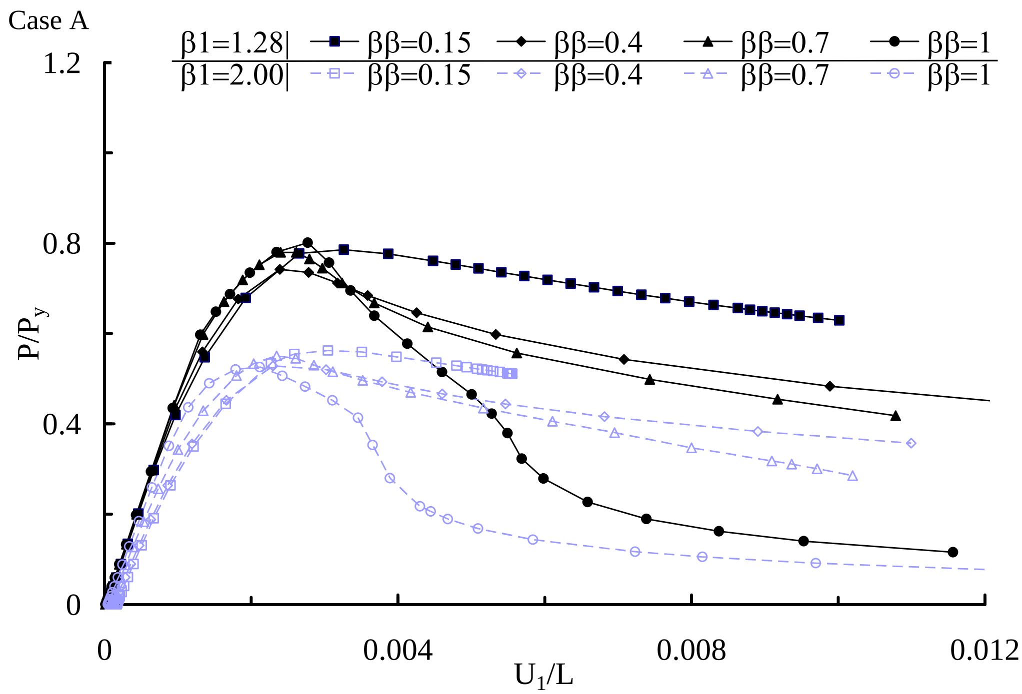

Figure E-35 Axial load versus axial shortening ($\beta_9 = -0.4$, $\beta_1 = 1.28$ & 2.0, $\beta_2 = 1.5$, $\beta_3 = 0.9$, $\beta_5 = 0.3$)

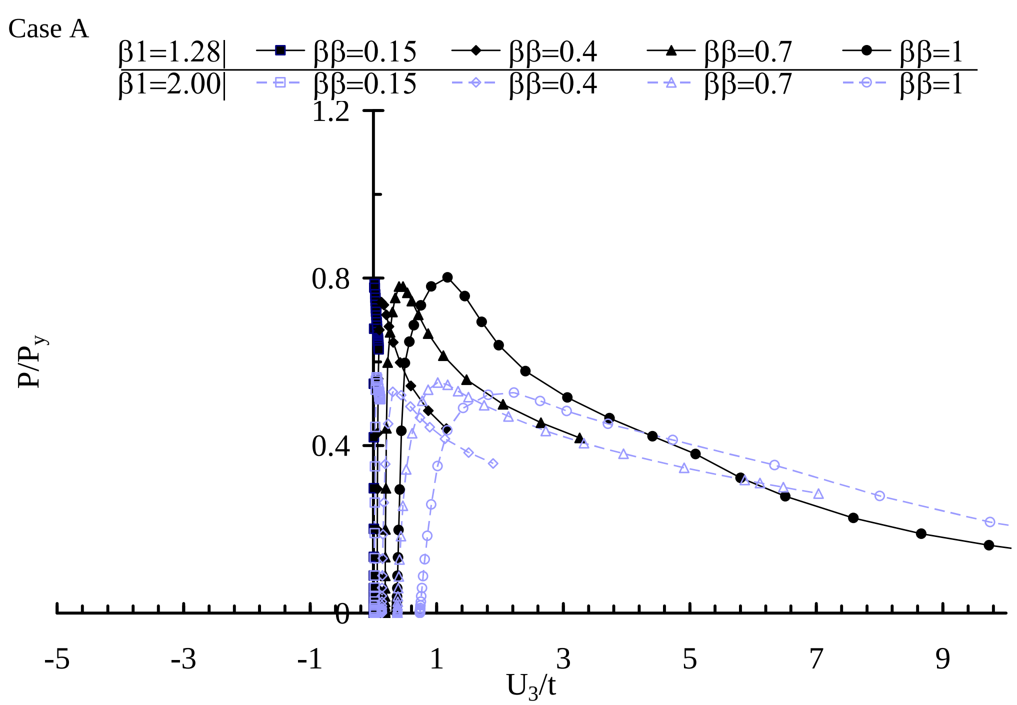

Figure E-36 Axial load versus lateral deflection ($\beta_9 = -0.4$, $\beta_1 = 1.28$ & 2.0, $\beta_2 = 1.5$, $\beta_3 = 0.9$, $\beta_5 = 0.3$)

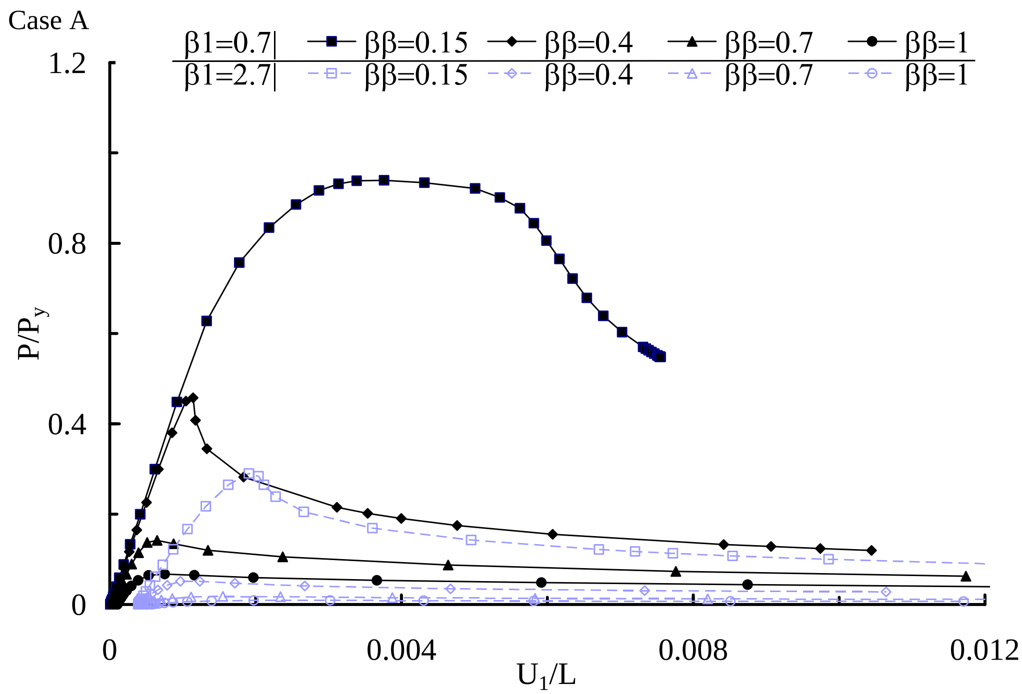

Figure E-37 Axial load versus axial shortening ($\beta_9 = -0.2$, $\beta_1 = 0.7$ & 2.7, $\beta_2 = 0.17$, $\beta_3 = 0.17$, $\beta_5 = 0.075$)

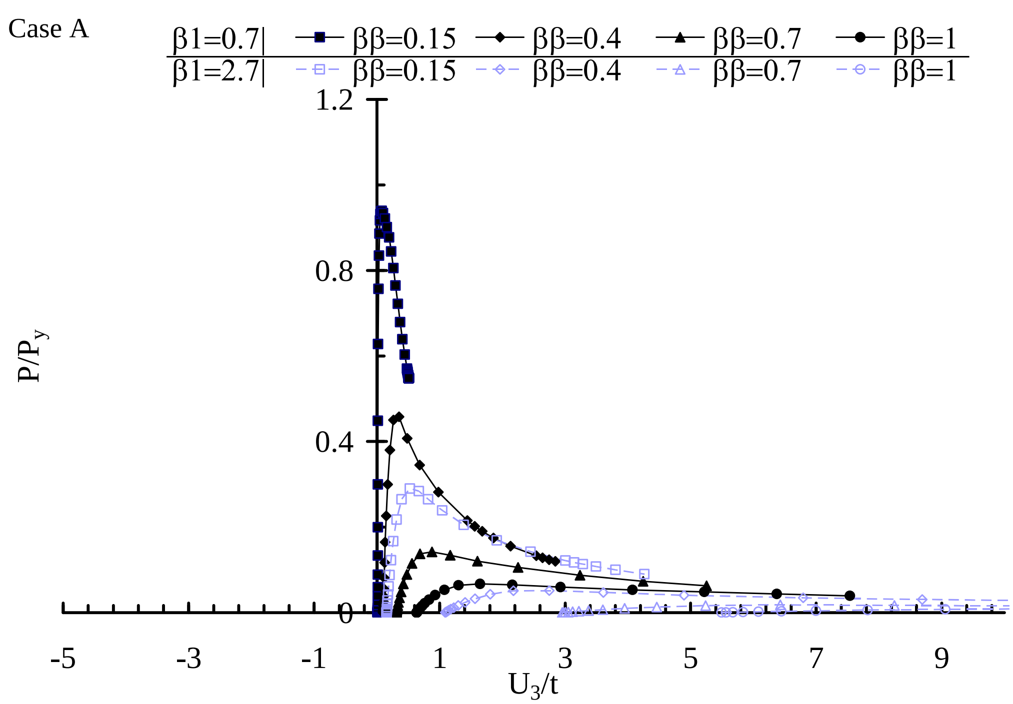

Figure E-38 Axial load versus lateral deflection ($\beta_9 = -0.2$, $\beta_1 = 0.7$ & 2.7, $\beta_2 = 0.17$, $\beta_3 = 0.17$, $\beta_5 = 0.075$)

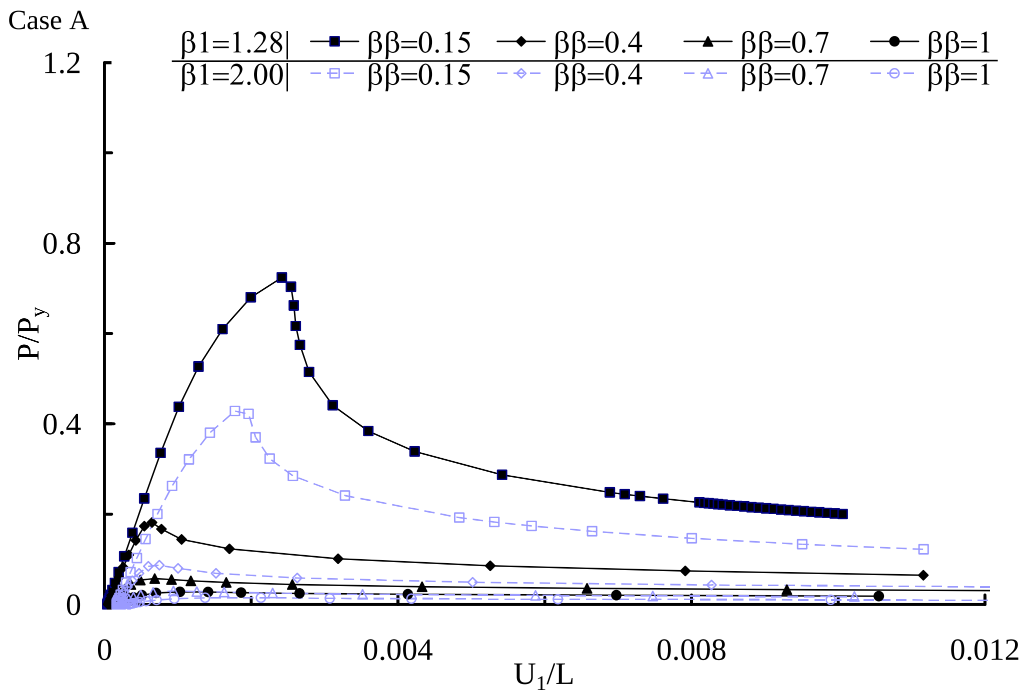

Figure E-39 Axial load versus axial shortening ($\beta_9 = -0.2$, $\beta_1 = 1.28$ & 2.0, $\beta_2 = 0.17$, $\beta_3 = 0.17$, $\beta_5 = 0.075$)

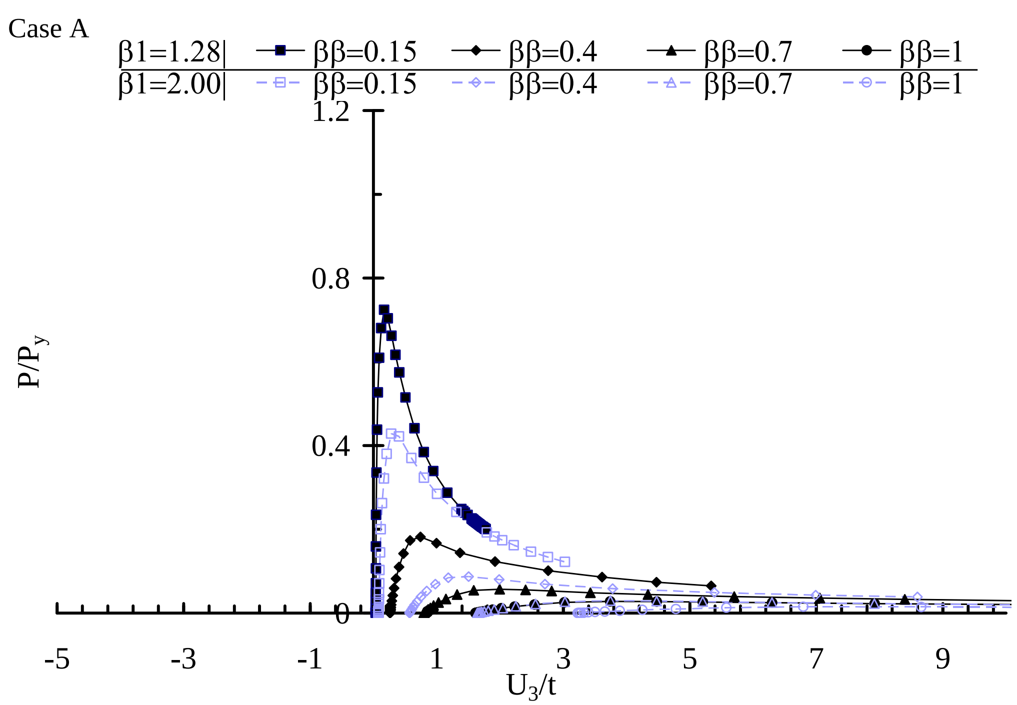

Figure E-40 Axial load versus lateral deflection ($\beta_9 = -0.2$, $\beta_1 = 1.28$ & 2.0, $\beta_2 = 0.17$, $\beta_3 = 0.17$, $\beta_5 = 0.075$)

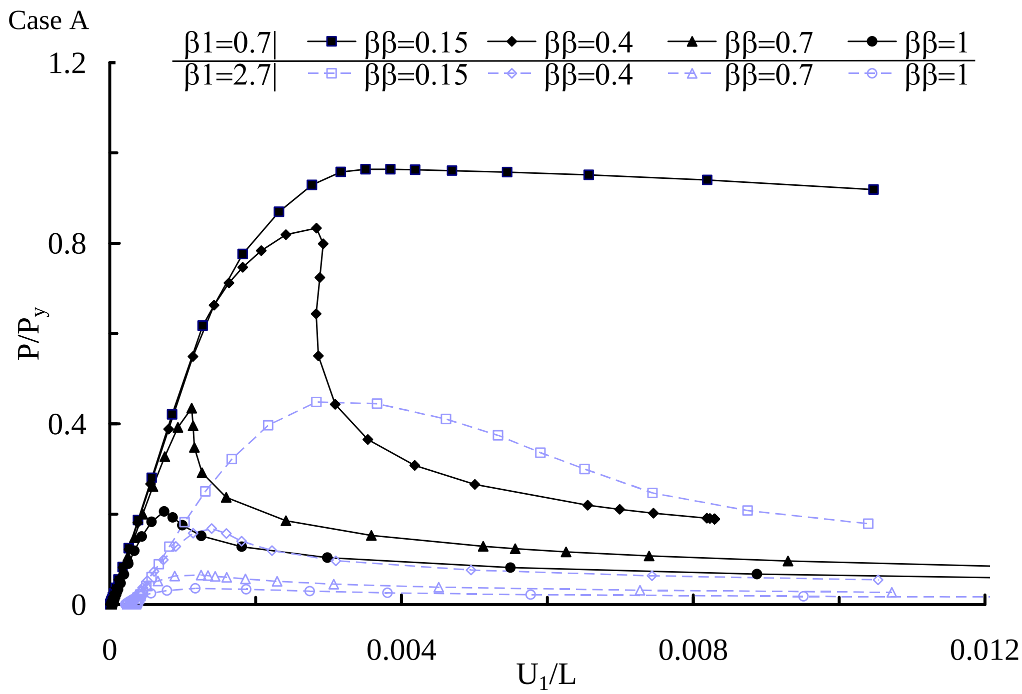

Figure E-41 Axial load versus axial shortening ($\beta_9 = -0.2$, $\beta_1 = 0.7$ & 2.7, $\beta_2 = 0.17$, $\beta_3 = 0.17$, $\beta_5 = 0.15$)

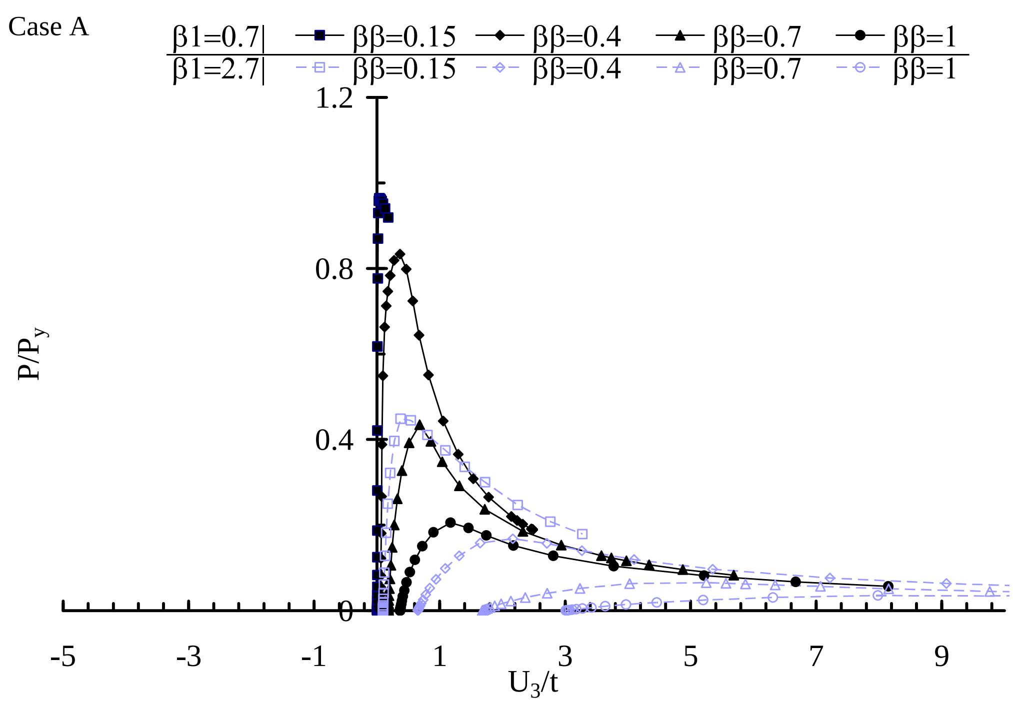

Figure E-42 Axial load versus lateral deflection ($\beta_9 = -0.2$, $\beta_1 = 0.7$ & 2.7, $\beta_2 = 0.17$, $\beta_3 = 0.17$, $\beta_5 = 0.15$)

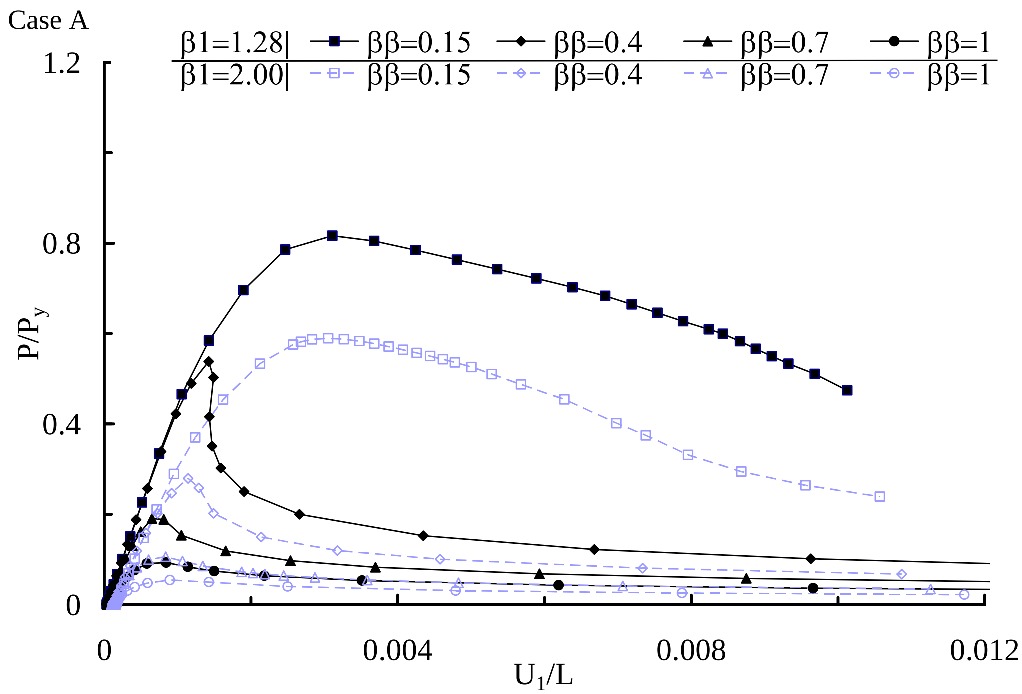

Figure E-43 Axial load versus axial shortening ($\beta_9 = -0.2$, $\beta_1 = 1.28$ & 2.0, $\beta_2 = 0.17$, $\beta_3 = 0.17$, $\beta_5 = 0.15$)

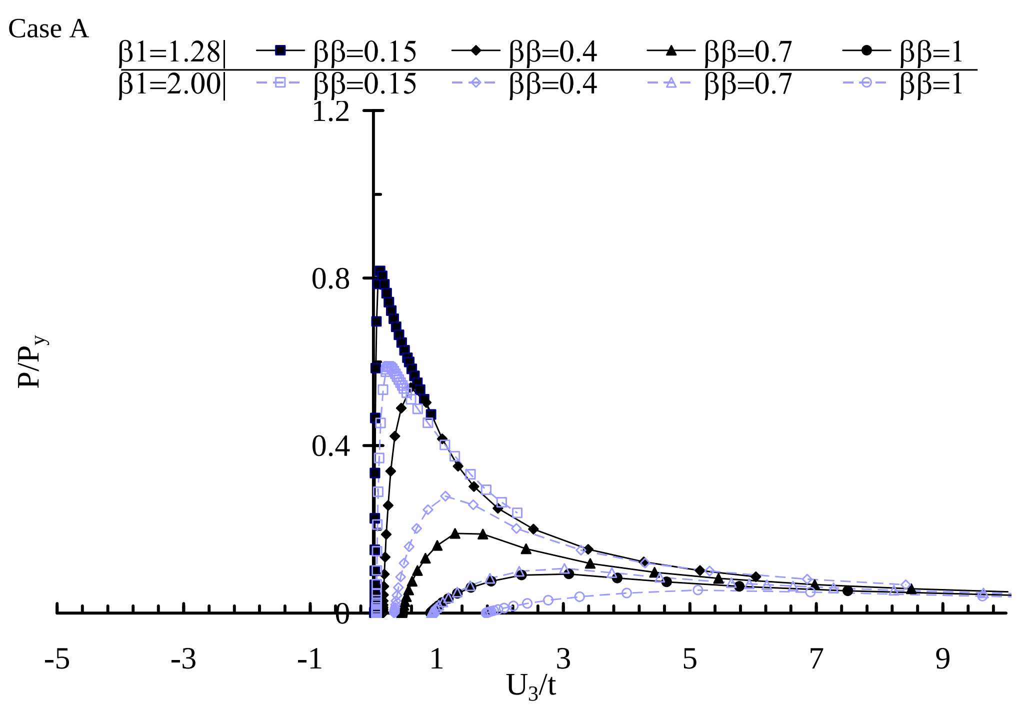

Figure E-44 Axial load versus lateral deflection ($\beta_9 = -0.2$, $\beta_1 = 1.28$ & 2.0, $\beta_2 = 0.17$, $\beta_3 = 0.17$, $\beta_5 = 0.15$)

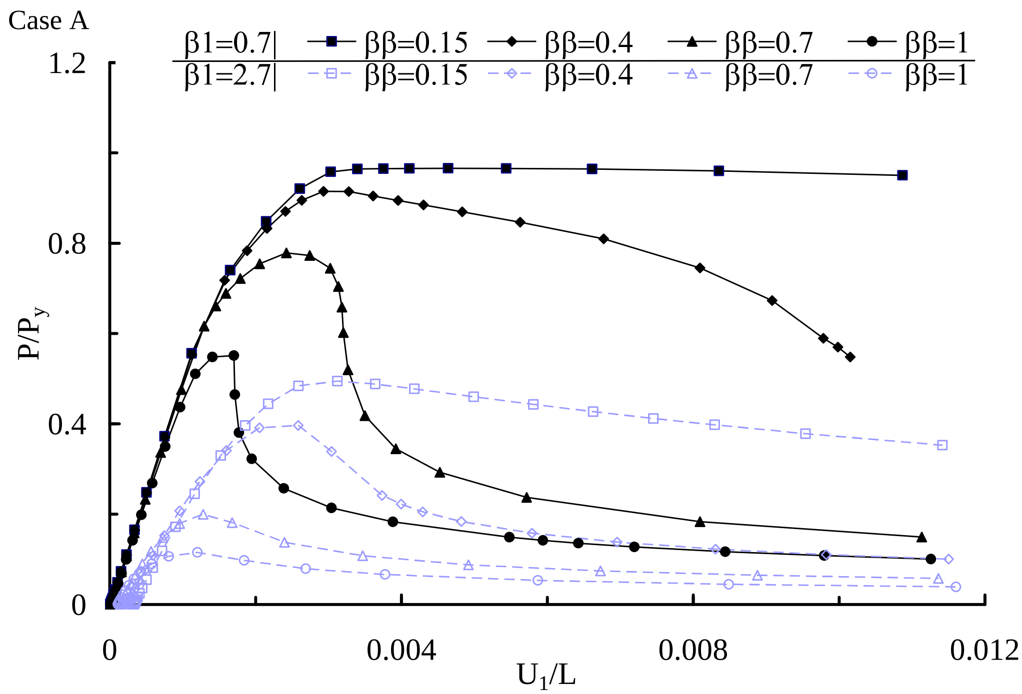

Figure E-45 Axial load versus axial shortening ($\beta_9 = -0.2$, $\beta_1 = 0.7$ & 2.7, $\beta_2 = 0.17$, $\beta_3 = 0.17$, $\beta_5 = 0.3$)

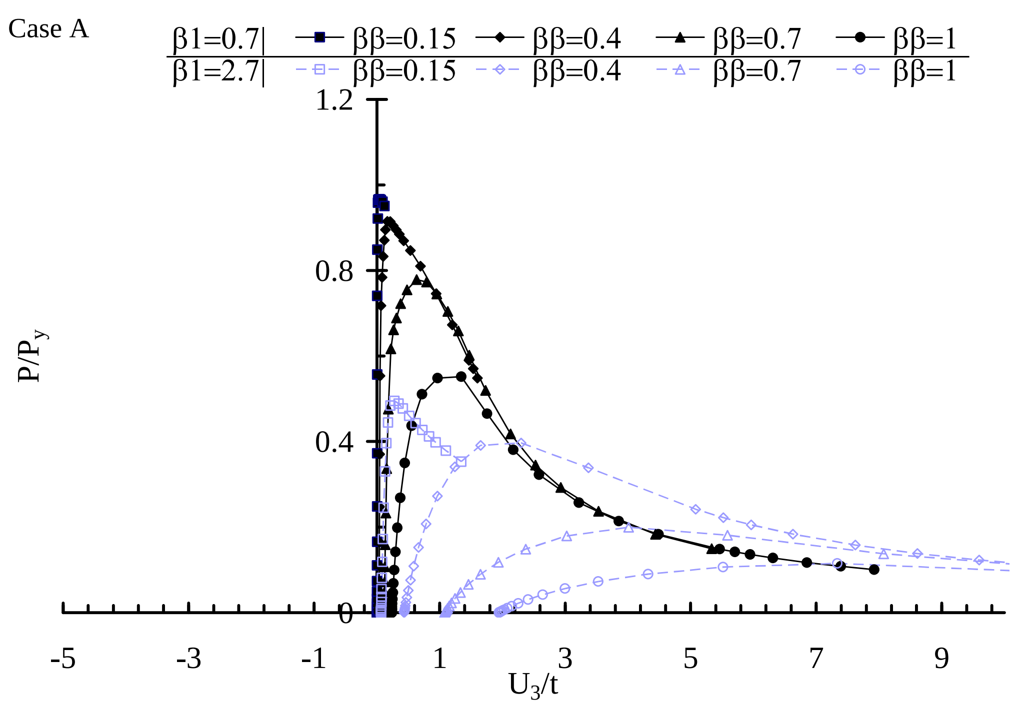

Figure E-46 Axial load versus lateral deflection ($\beta_9 = -0.2$, $\beta_1 = 0.7$ & 2.7, $\beta_2 = 0.17$, $\beta_3 = 0.17$, $\beta_5 = 0.3$)

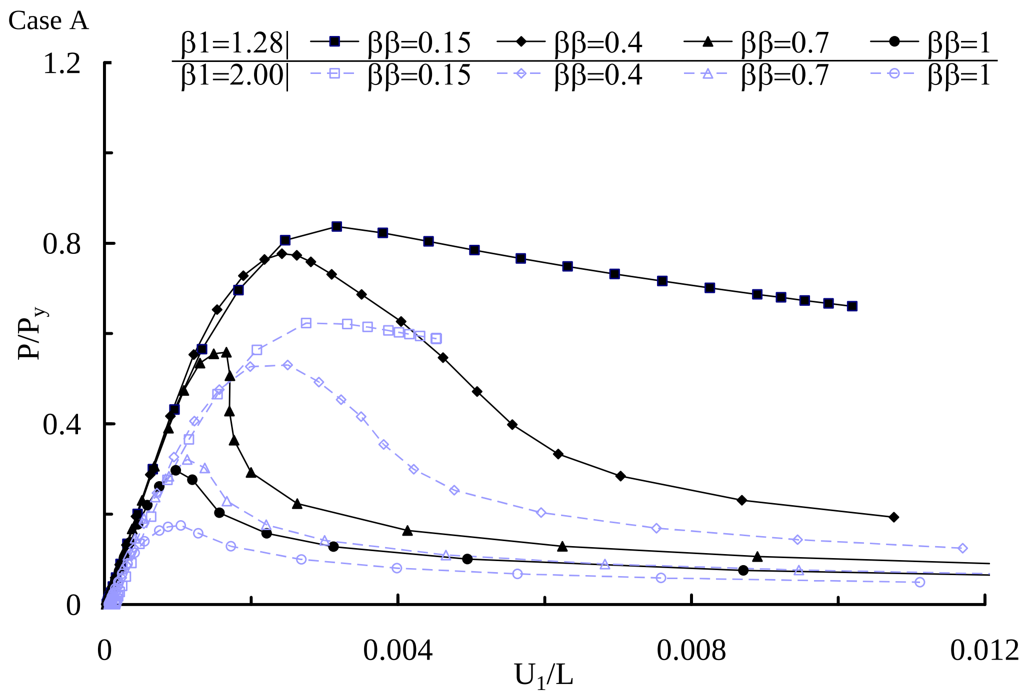

Figure E-47 Axial load versus axial shortening ($\beta_9 = -0.2$, $\beta_1 = 1.28$ & 2.0, $\beta_2 = 0.17$, $\beta_3 = 0.17$, $\beta_5 = 0.3$)

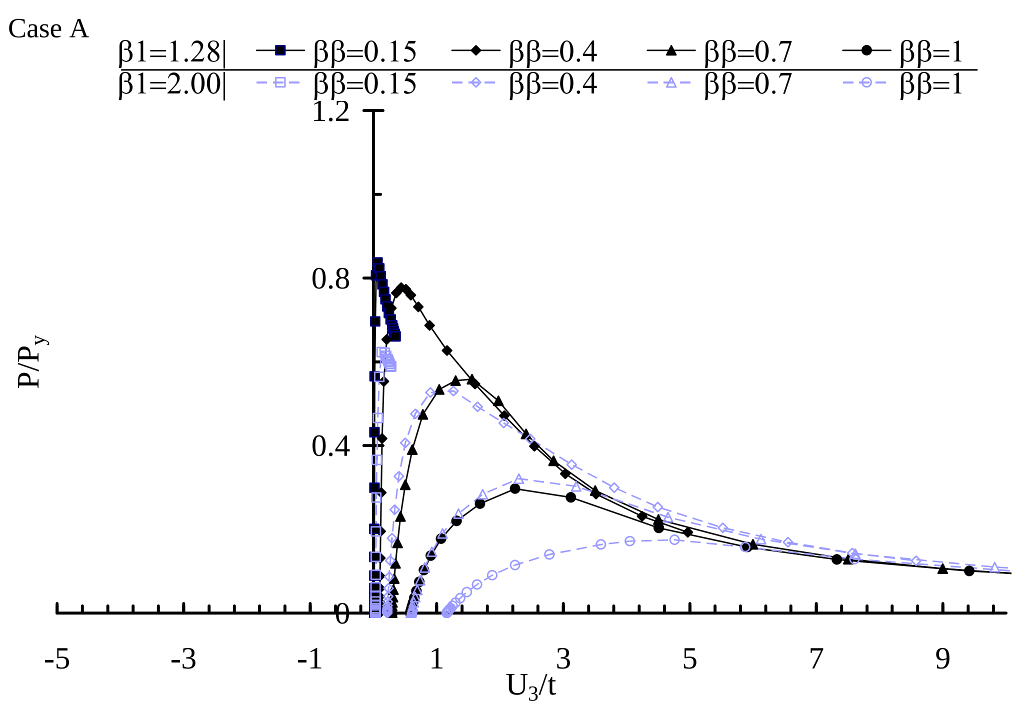

Figure E-48 Axial load versus lateral deflection ($\beta_9 = -0.2$, $\beta_1 = 1.28$ & 2.0, $\beta_2 = 0.17$, $\beta_3 = 0.17$, $\beta_5 = 0.3$)

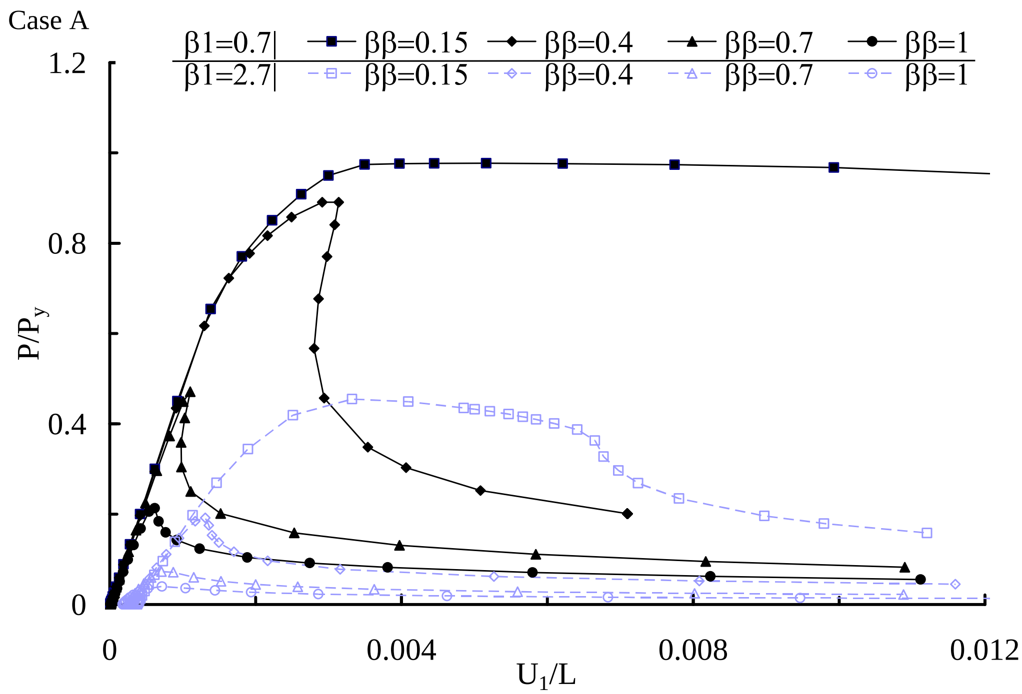

Figure E-49 Axial load versus axial shortening ($\beta_9 = -0.2$, $\beta_1 = 0.7$ & 2.7, $\beta_2 = 0.8$, $\beta_3 = 0.6$, $\beta_5 = 0.075$)

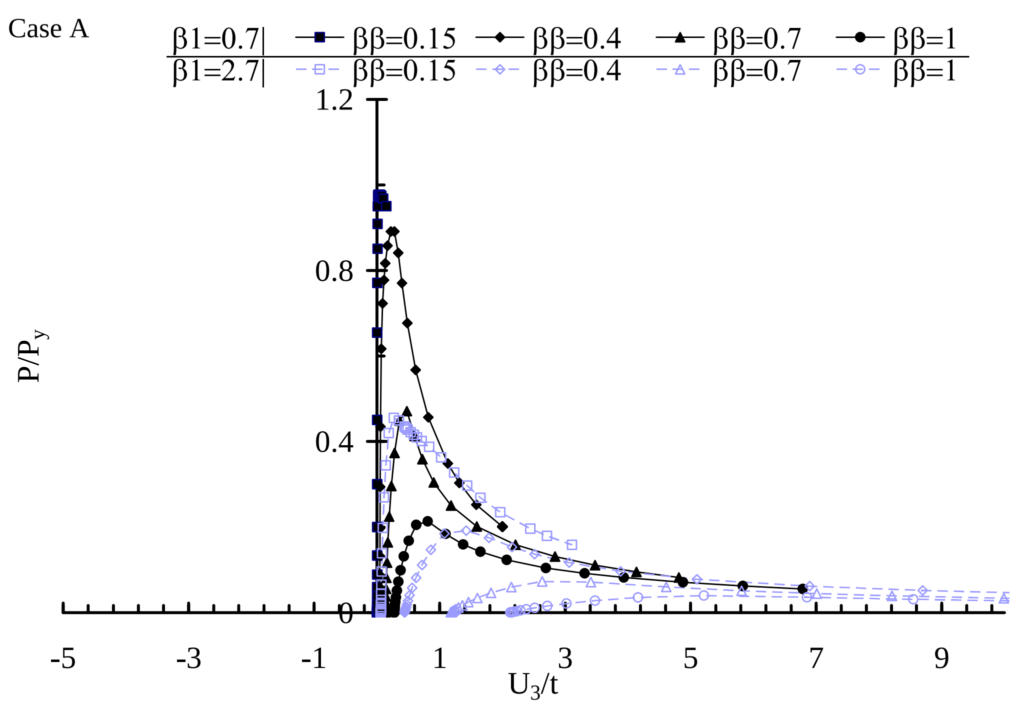

Figure E-50 Axial load versus lateral deflection ($\beta_9 = -0.2$, $\beta_1 = 0.7$ & 2.7, $\beta_2 = 0.8$, $\beta_3 = 0.6$, $\beta_5 = 0.075$)

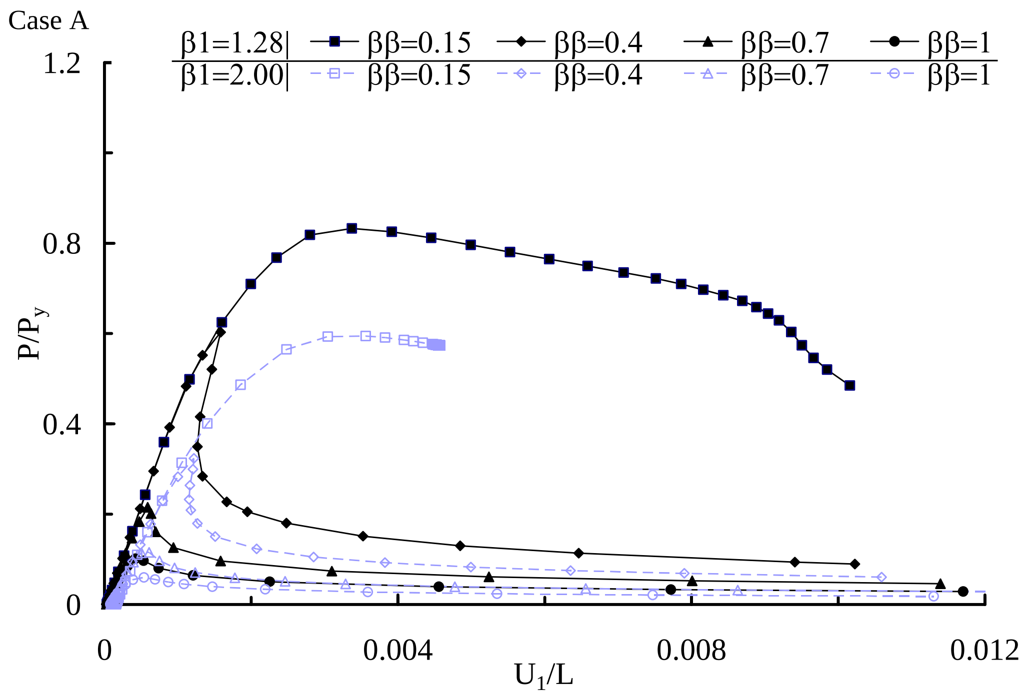

Figure E-51 Axial load versus axial shortening ($\beta_9 = -0.2$, $\beta_1 = 1.28$ & 2.0, $\beta_2 = 0.8$, $\beta_3 = 0.6$, $\beta_5 = 0.075$)

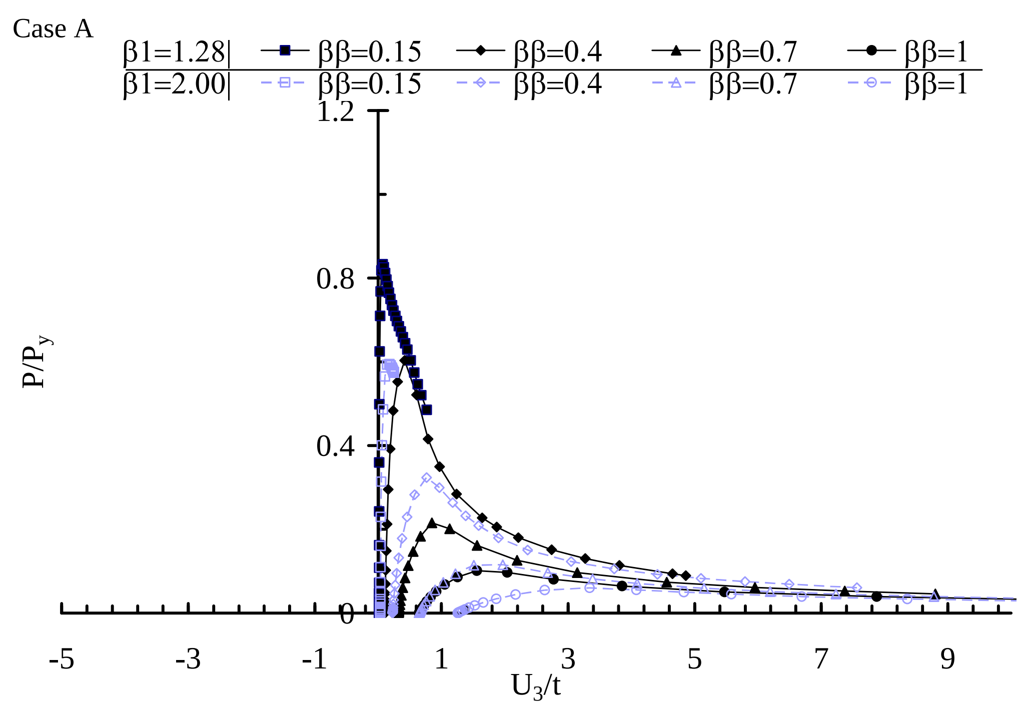

Figure E-52 Axial load versus lateral deflection ($\beta_9 = -0.2$, $\beta_1 = 1.28$ & 2.0, $\beta_2 = 0.8$, $\beta_3 = 0.6$, $\beta_5 = 0.075$)

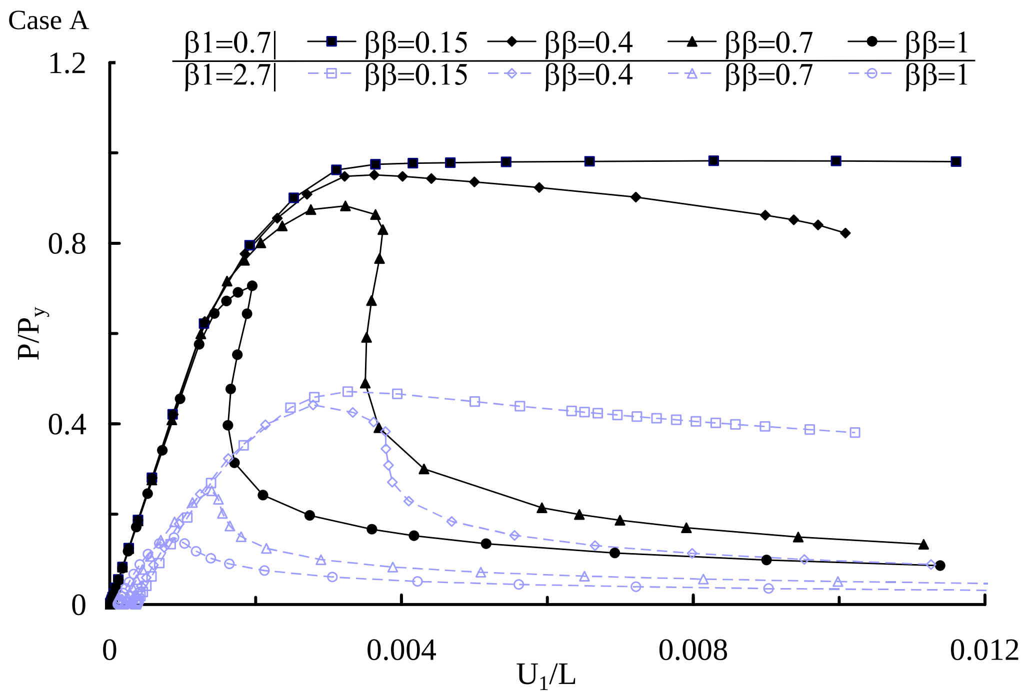

Figure E-53 Axial load versus axial shortening ($\beta_9 = -0.2$, $\beta_1 = 0.7$ & 2.7, $\beta_2 = 0.8$, $\beta_3 = 0.6$, $\beta_5 = 0.15$)

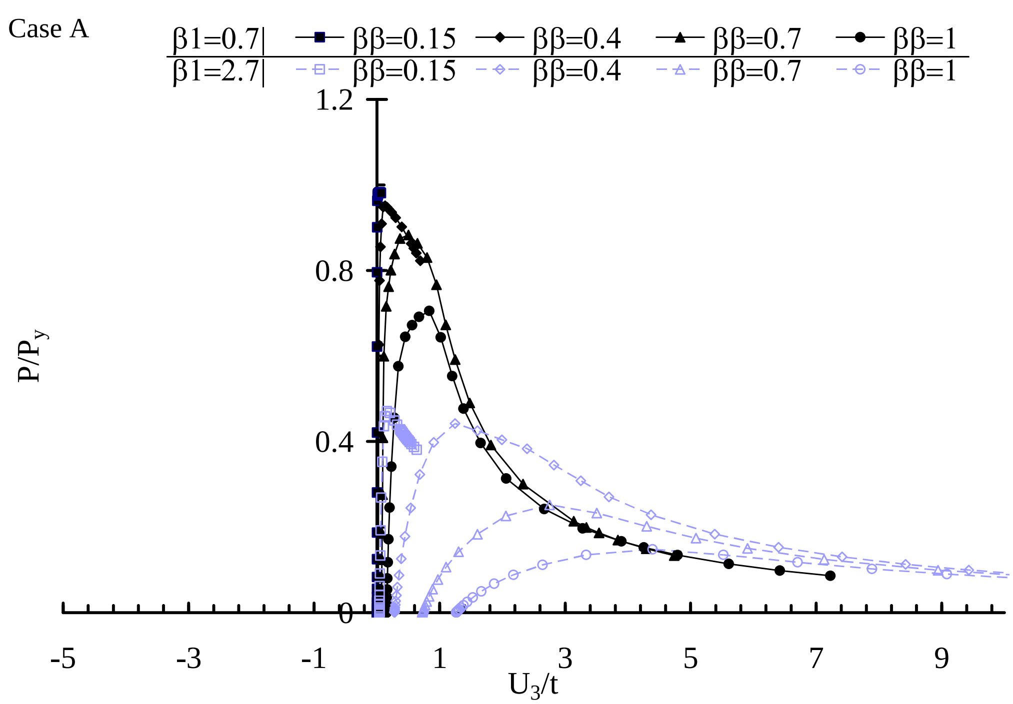

Figure E-54 Axial load versus lateral deflection ($\beta_9 = -0.2$, $\beta_1 = 0.7$ & 2.7, $\beta_2 = 0.8$, $\beta_3 = 0.6$, $\beta_5 = 0.15$)

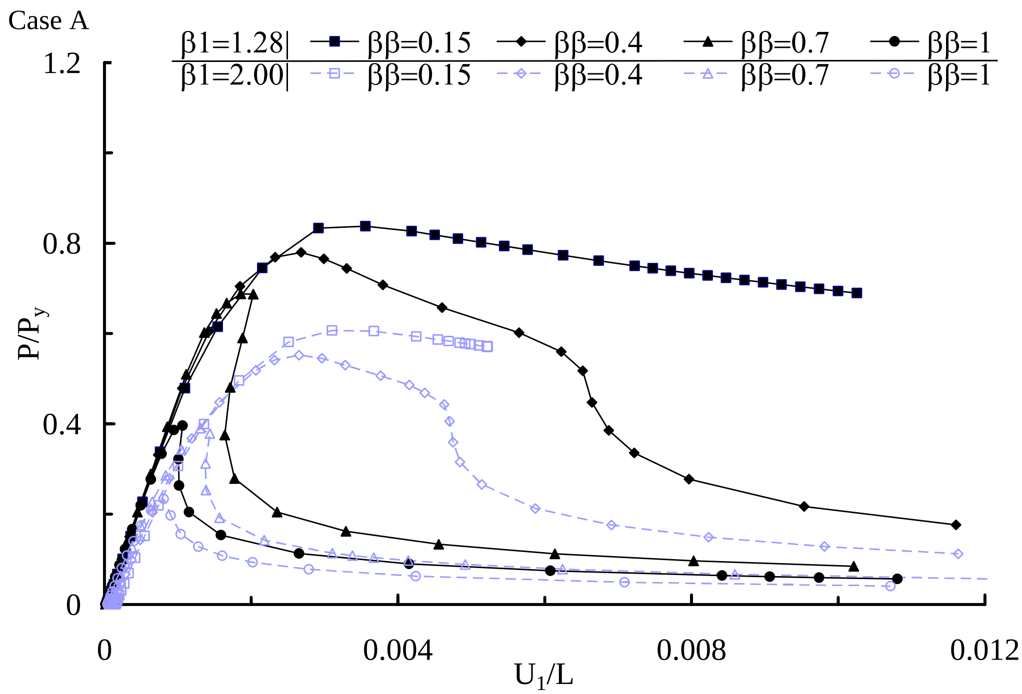

Figure E-55 Axial load versus axial shortening ($\beta_9 = -0.2$, $\beta_1 = 1.28$ & 2.0, $\beta_2 = 0.8$, $\beta_3 = 0.6$, $\beta_5 = 0.15$)

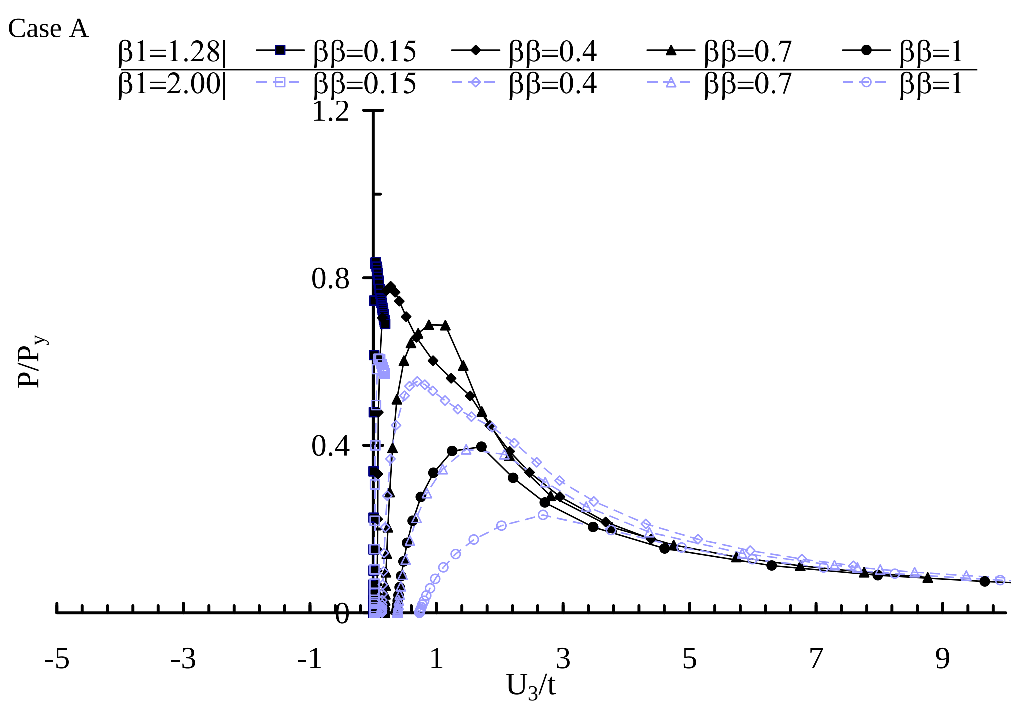

Figure E-56 Axial load versus lateral deflection ($\beta_9 = -0.2$, $\beta_1 = 1.28$ & 2.0, $\beta_2 = 0.8$, $\beta_3 = 0.6$, $\beta_5 = 0.15$)

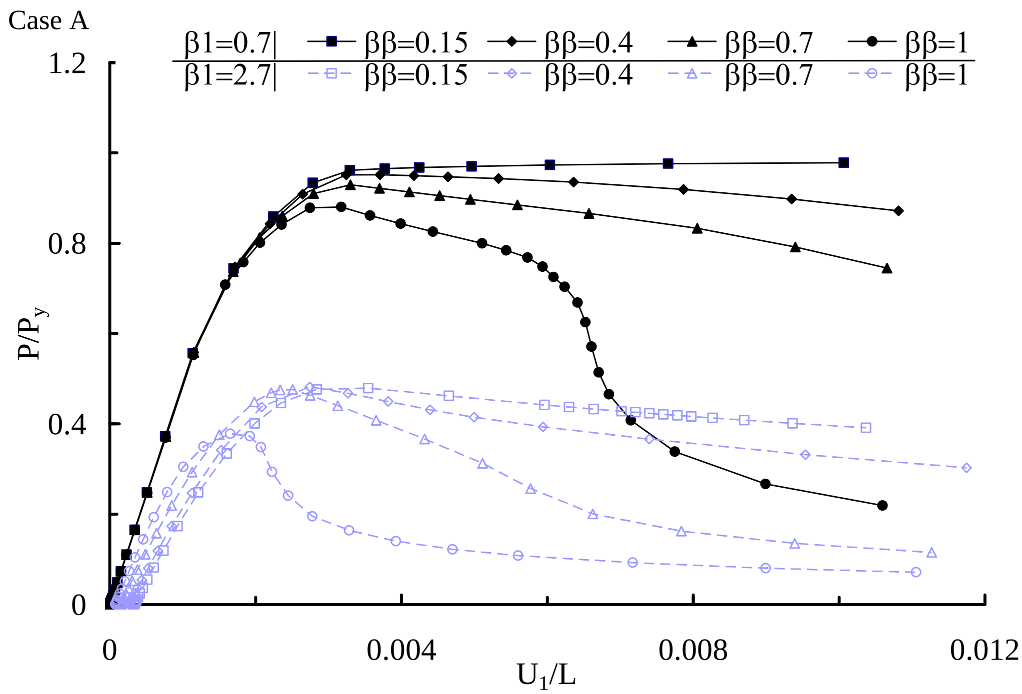

Figure E-57 Axial load versus axial shortening ($\beta_9 = -0.2$, $\beta_1 = 0.7$ & 2.7, $\beta_2 = 0.8$, $\beta_3 = 0.6$, $\beta_5 = 0.3$)

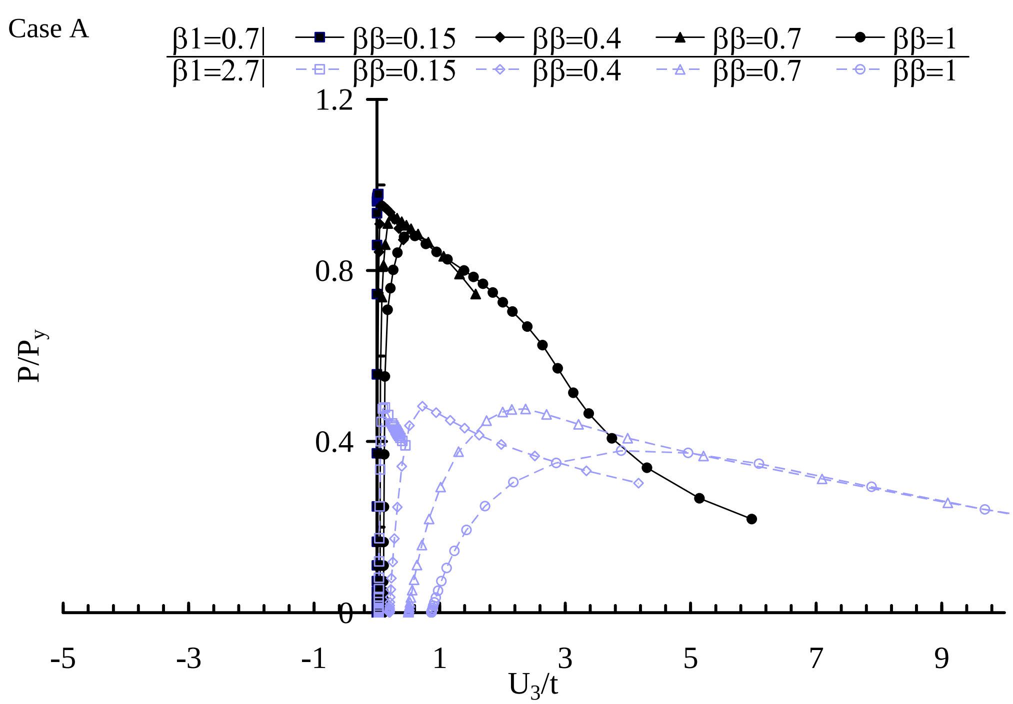

Figure E-58 Axial load versus lateral deflection ($\beta_9 = -0.2$, $\beta_1 = 0.7$ & 2.7, $\beta_2 = 0.8$, $\beta_3 = 0.6$, $\beta_5 = 0.3$)

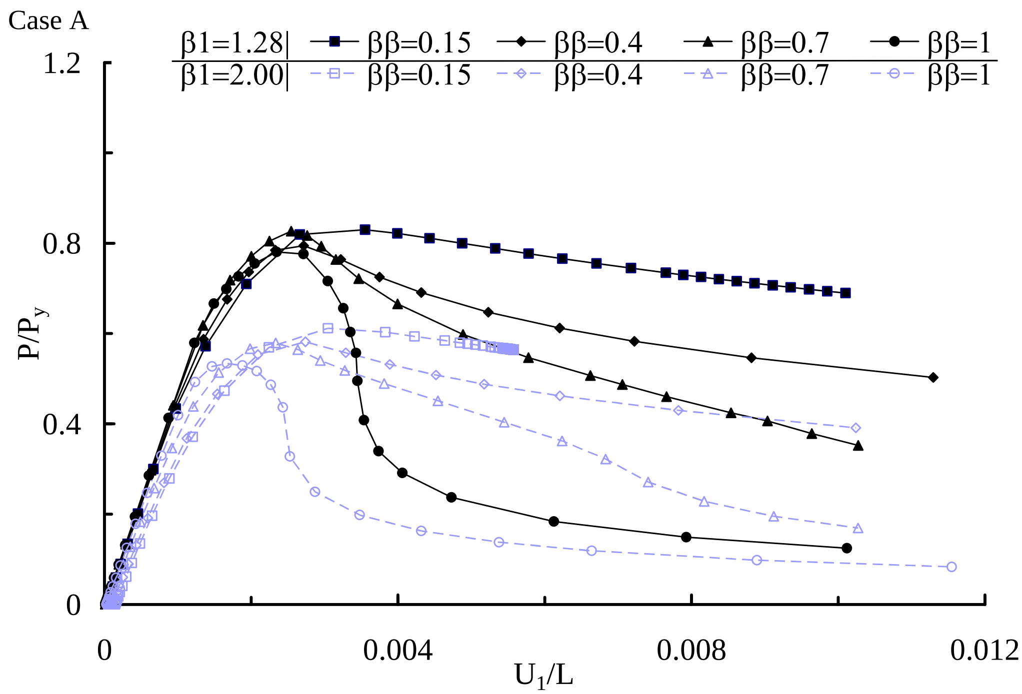

Figure E-59 Axial load versus axial shortening ($\beta_9 = -0.2$, $\beta_1 = 1.28$ & 2.0, $\beta_2 = 0.8$, $\beta_3 = 0.6$, $\beta_5 = 0.3$)

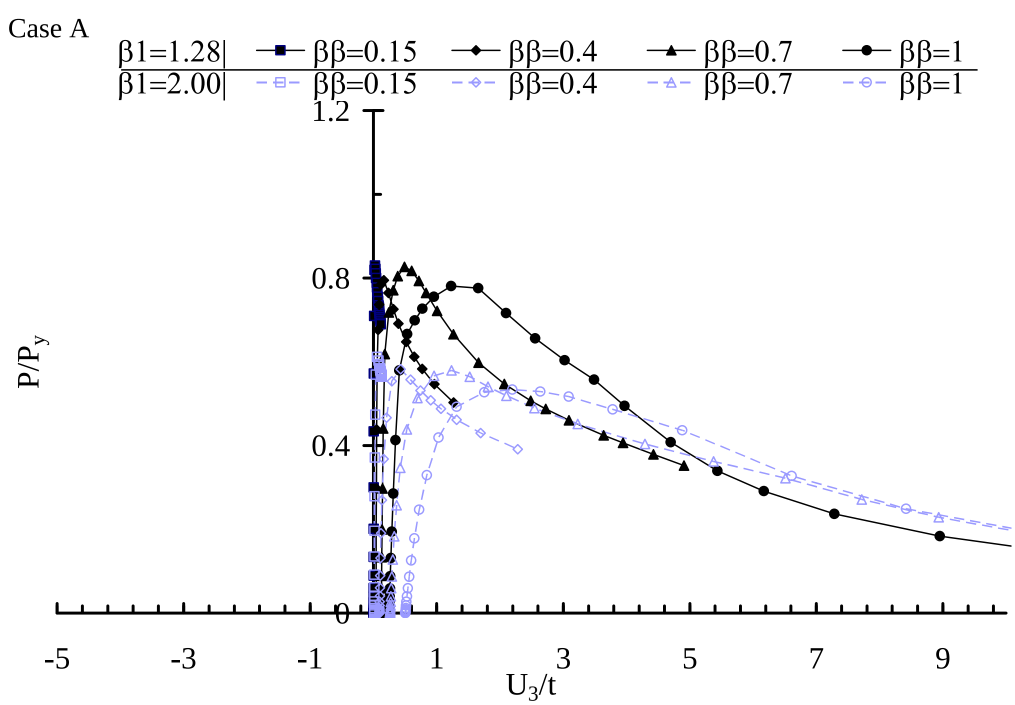

Figure E-60 Axial load versus lateral deflection ($\beta_9 = -0.2$, $\beta_1 = 1.28$ & 2.0, $\beta_2 = 0.8$, $\beta_3 = 0.6$, $\beta_5 = 0.3$)

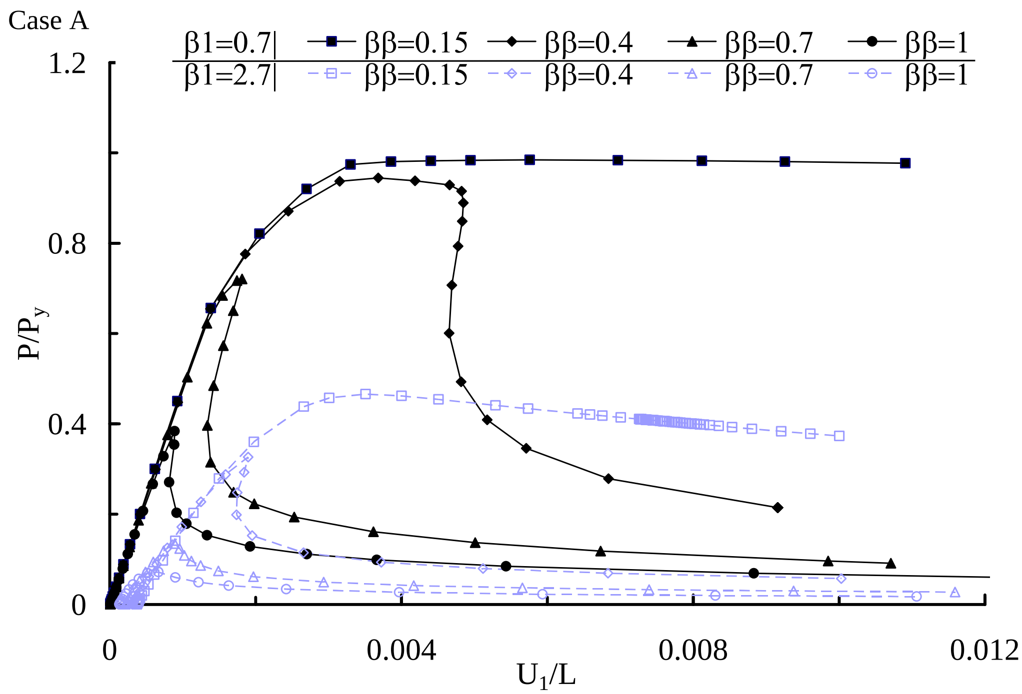

Figure E-61 Axial load versus axial shortening ($\beta_9 = -0.2$, $\beta_1 = 0.7$ & 2.7, $\beta_2 = 1.5$, $\beta_3 = 0.9$, $\beta_5 = 0.075$)

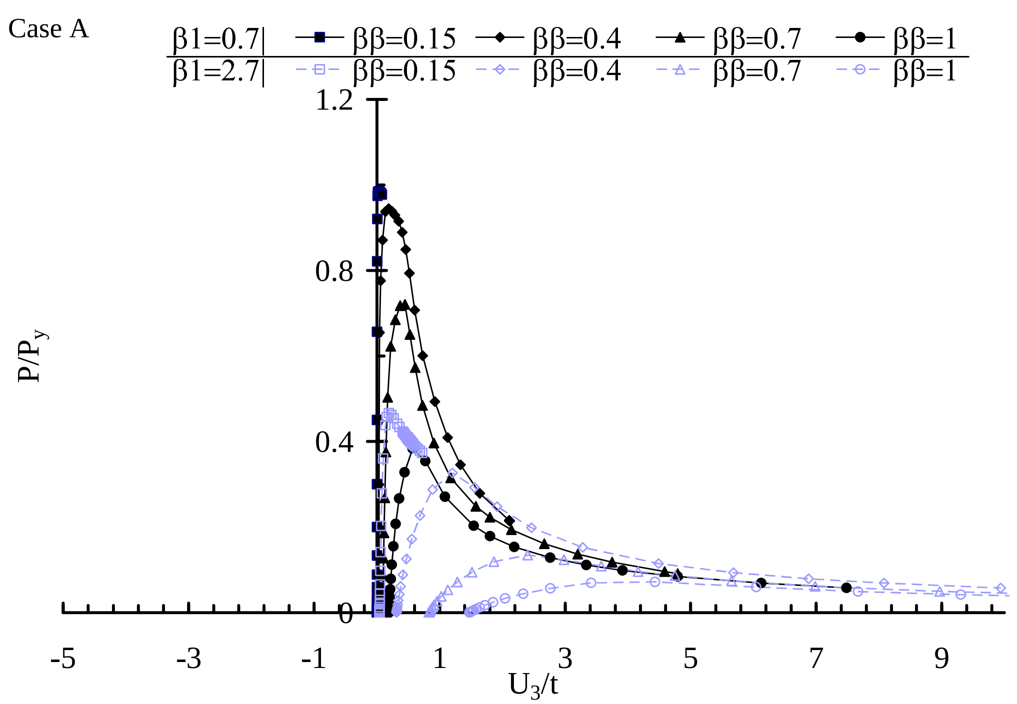

Figure E-62 Axial load versus lateral deflection ($\beta_9 = -0.2$, $\beta_1 = 0.7$ & 2.7, $\beta_2 = 1.5$, $\beta_3 = 0.9$, $\beta_5 = 0.075$)

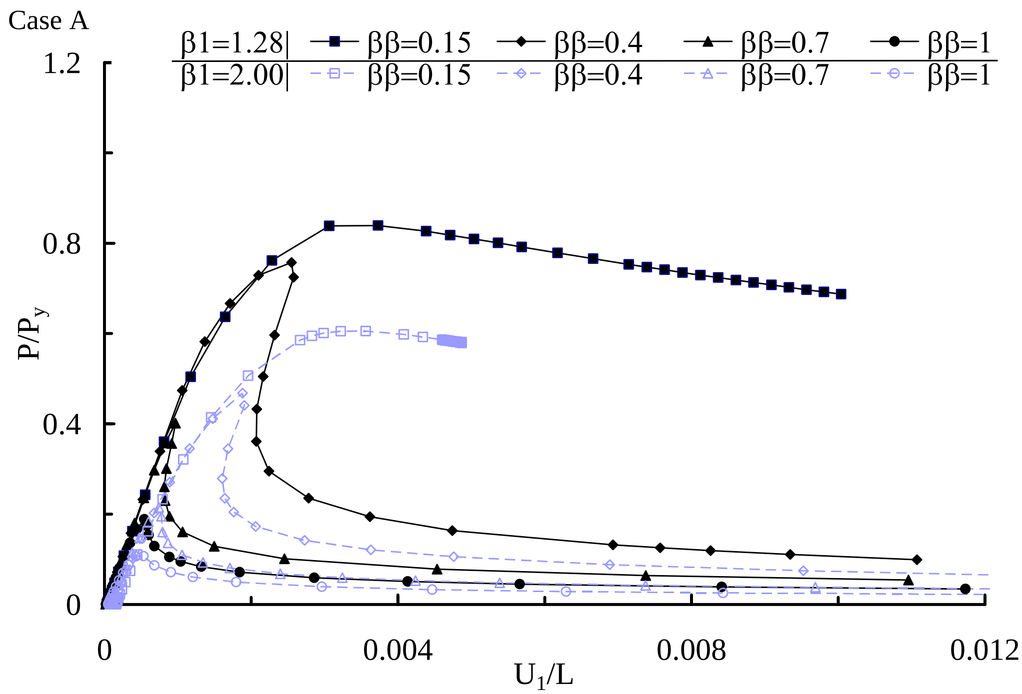

Figure E-63 Axial load versus axial shortening ($\beta_9 = -0.2$, $\beta_1 = 1.28$ & 2.0, $\beta_2 = 1.5$, $\beta_3 = 0.9$, $\beta_5 = 0.075$)

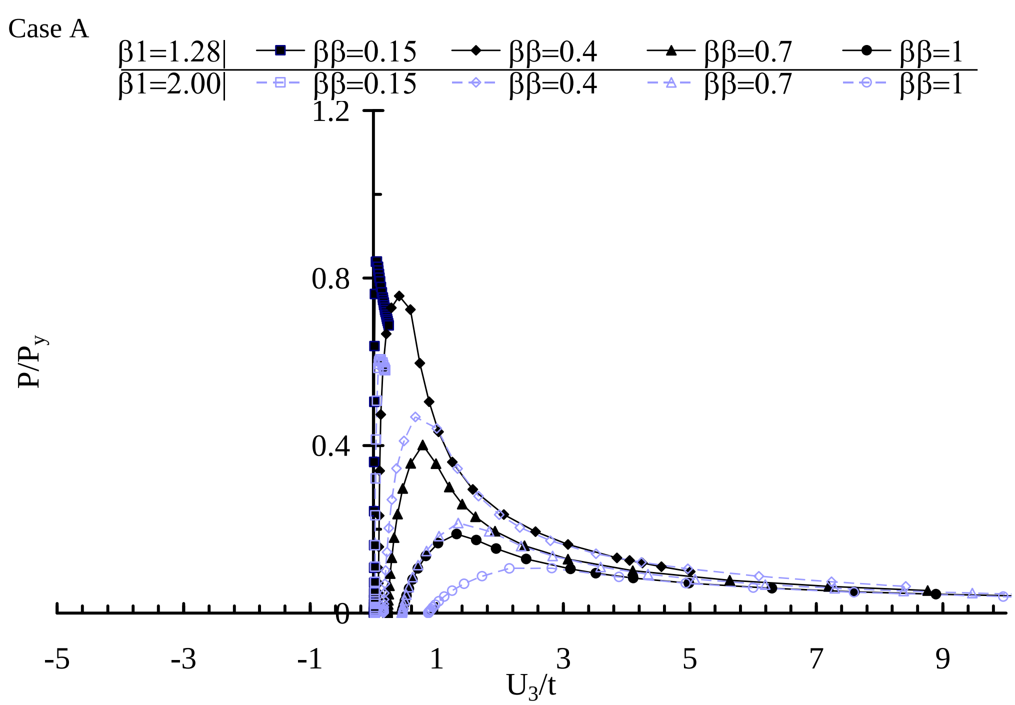

Figure E-64 Axial load versus lateral deflection ($\beta_9 = -0.2$, $\beta_1 = 1.28$ & 2.0, $\beta_2 = 1.5$, $\beta_3 = 0.9$, $\beta_5 = 0.075$)

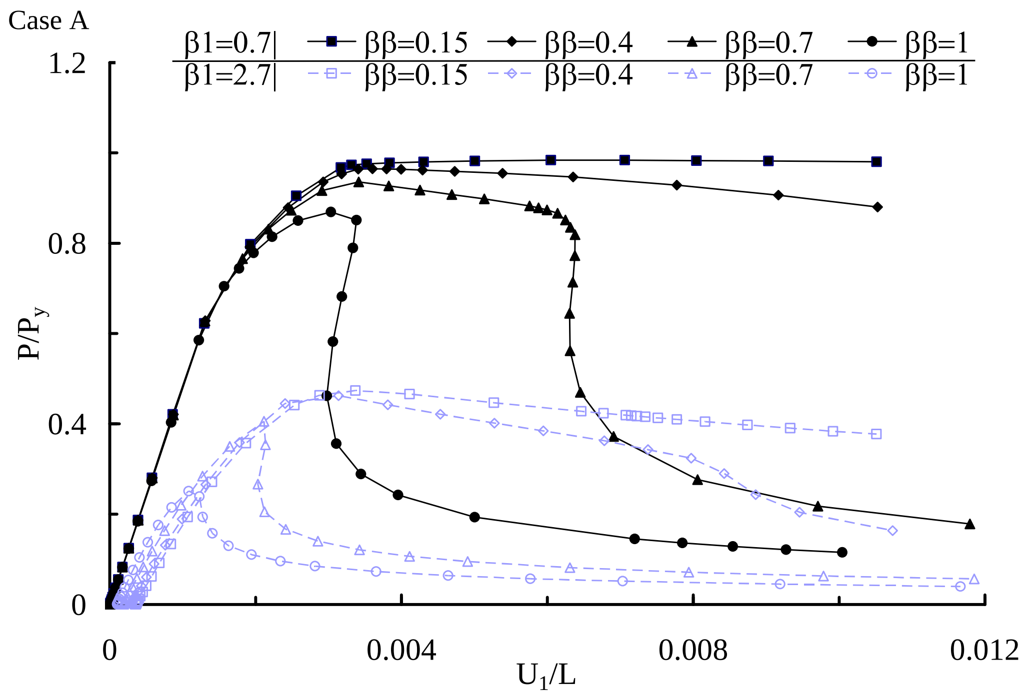

Figure E-65 Axial load versus axial shortening (β_9 = −0.2, β_1 = 0.7 & 2.7, β_2 = 1.5, β_3 = 0.9, β_5 = 0.15)

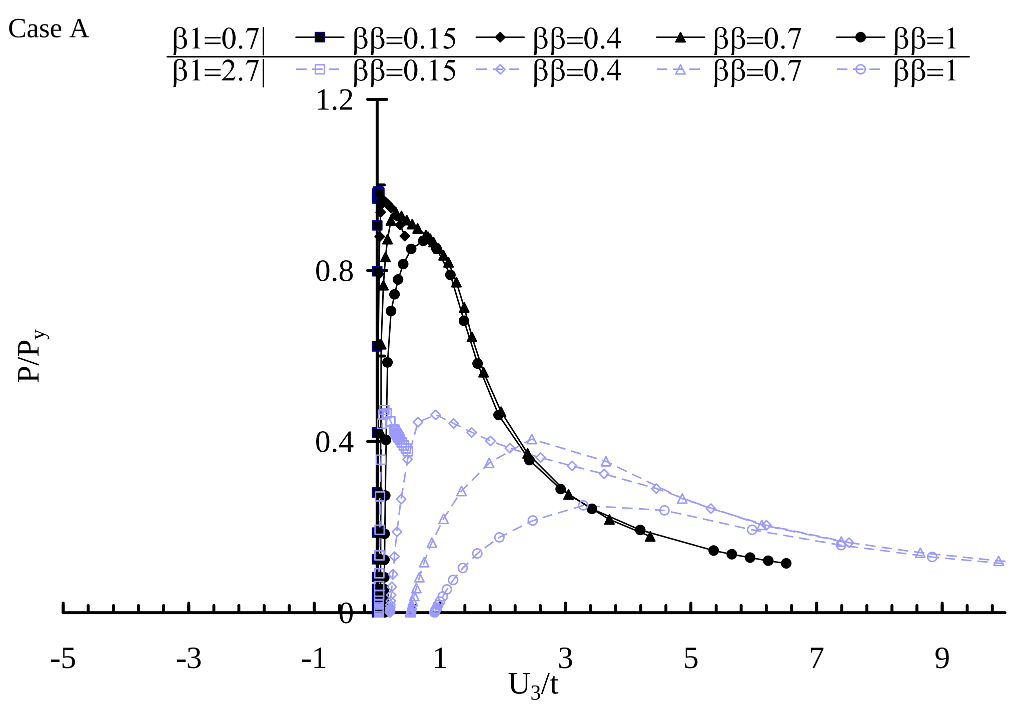

Figure E-66 Axial load versus lateral deflection (β_9 = −0.2, β_1 = 0.7 & 2.7, β_2 = 1.5, β_3 = 0.9, β_5 = 0.15)

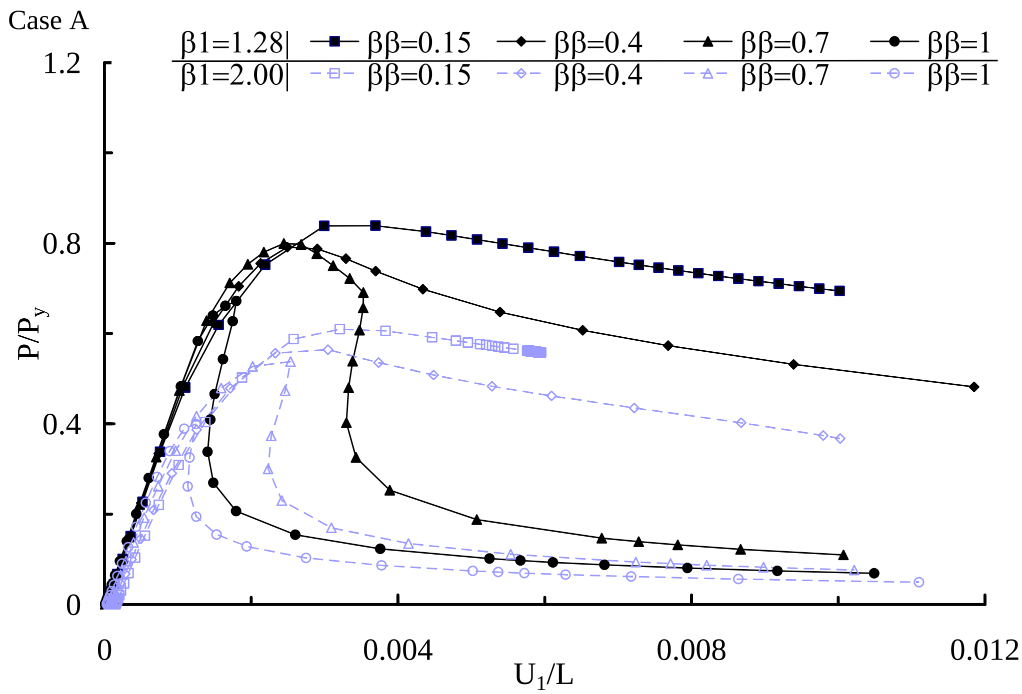

Figure E-67 Axial load versus axial shortening ($\beta_9 = -0.2$, $\beta_1 = 1.28$ & 2.0, $\beta_2 = 1.5$, $\beta_3 = 0.9$, $\beta_5 = 0.15$)

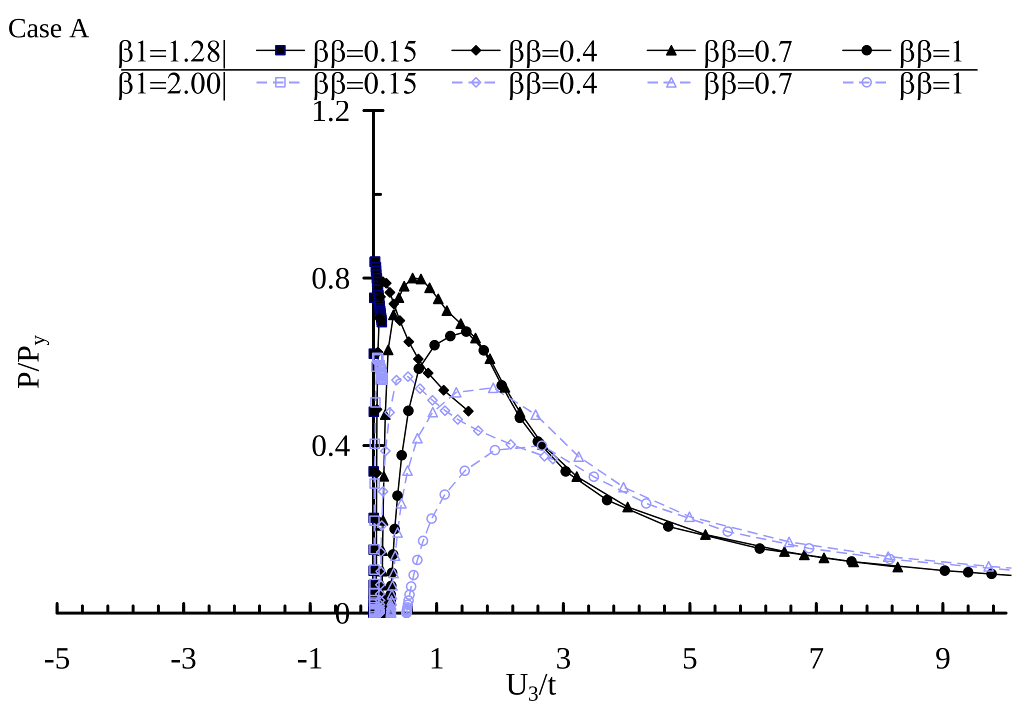

Figure E-68 Axial load versus lateral deflection ($\beta_9 = -0.2$, $\beta_1 = 1.28$ & 2.0, $\beta_2 = 1.5$, $\beta_3 = 0.9$, $\beta_5 = 0.15$)

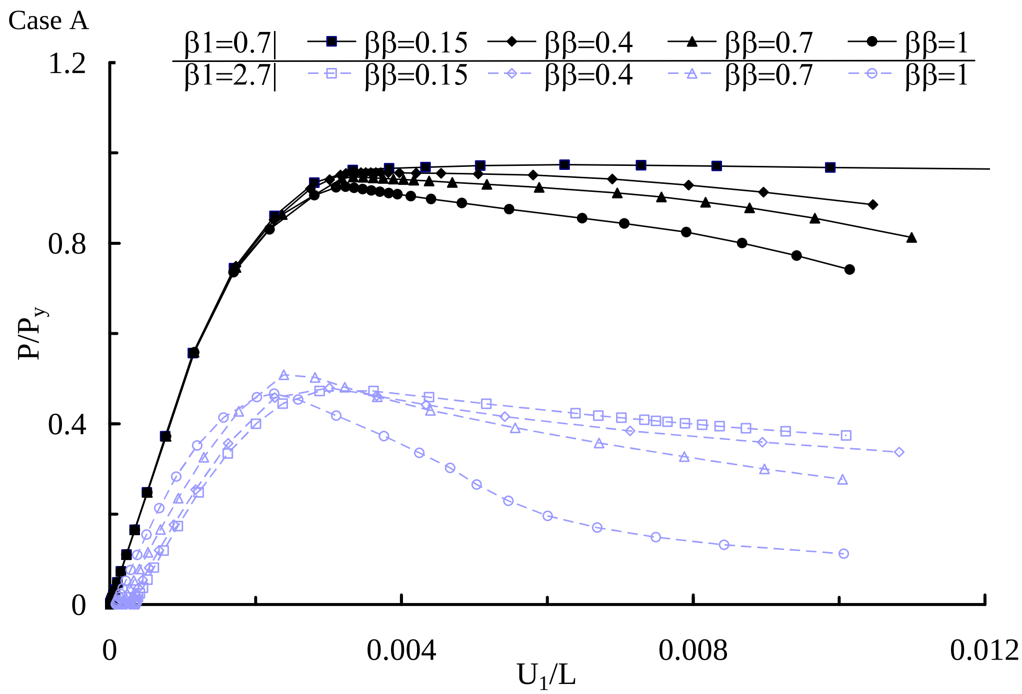

Figure E-69 Axial load versus axial shortening ($\beta_9 = -0.2$, $\beta_1 = 0.7$ & 2.7, $\beta_2 = 1.5$, $\beta_3 = 0.9$, $\beta_5 = 0.3$)

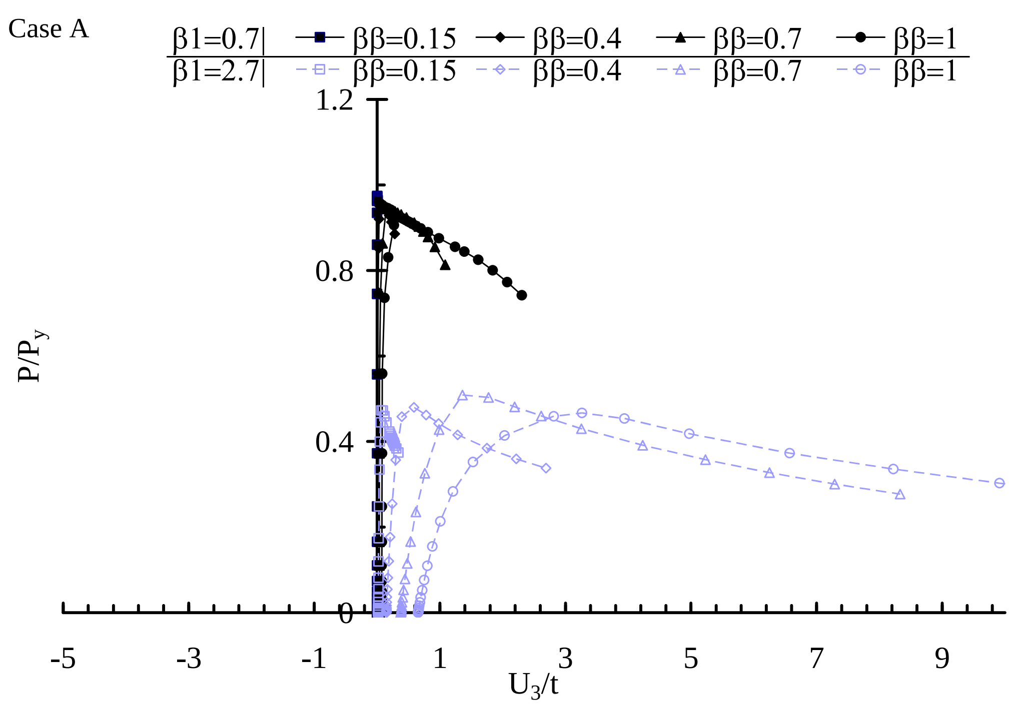

Figure E-70 Axial load versus lateral deflection ($\beta_9 = -0.2$, $\beta_1 = 0.7$ & 2.7, $\beta_2 = 1.5$, $\beta_3 = 0.9$, $\beta_5 = 0.3$)

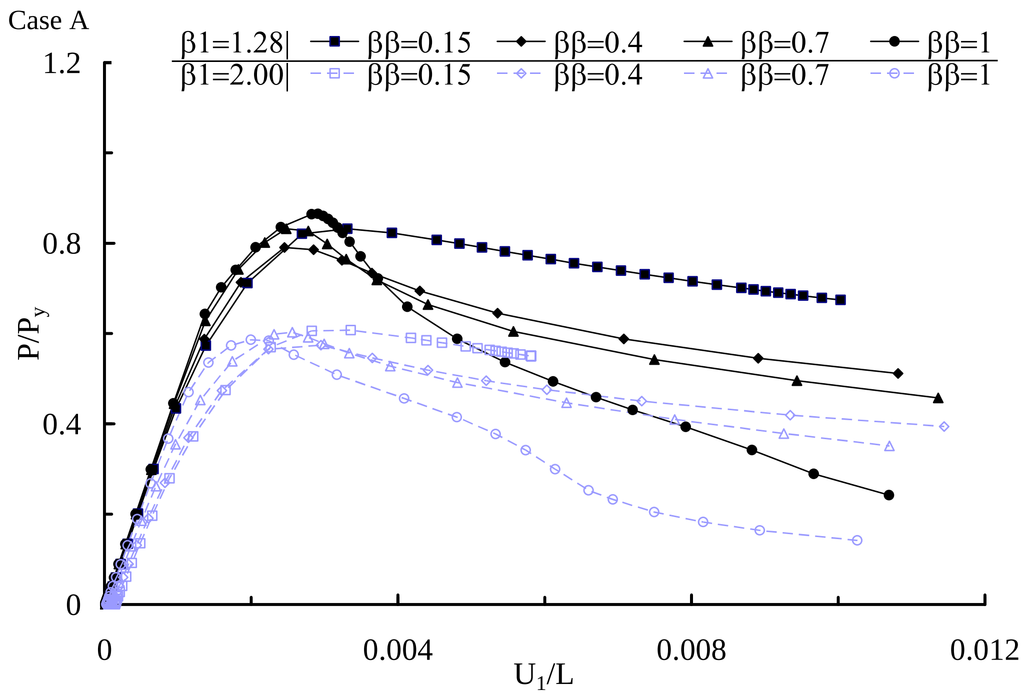

Figure E-71 Axial load versus axial shortening ($\beta_9 = -0.2$, $\beta_1 = 1.28$ & 2.0, $\beta_2 = 1.5$, $\beta_3 = 0.9$, $\beta_5 = 0.3$)

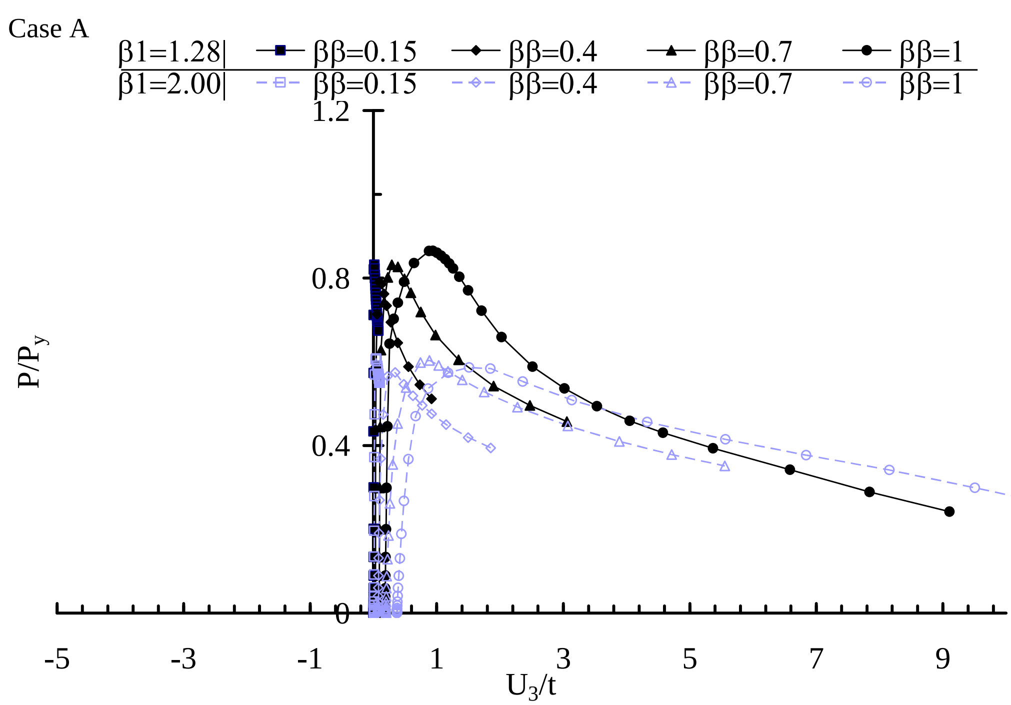

Figure E-72 Axial load versus lateral deflection ($\beta_9 = -0.2$, $\beta_1 = 1.28$ & 2.0, $\beta_2 = 1.5$, $\beta_3 = 0.9$, $\beta_5 = 0.3$)

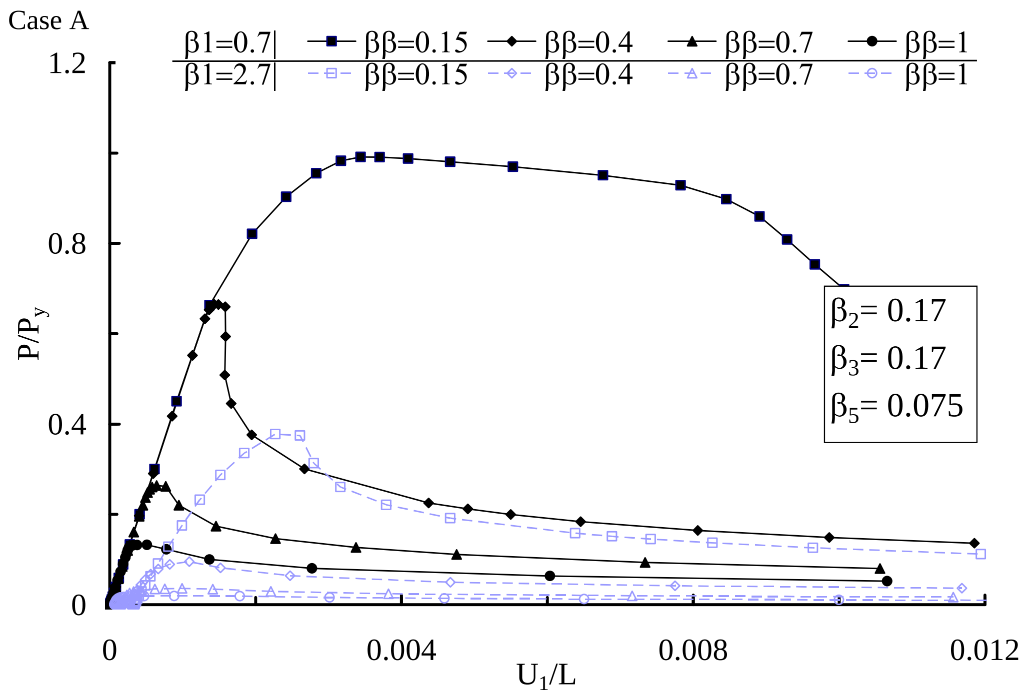

Figure E-73 Axial load versus axial shortening ($\beta_9 = 0$, $\beta_1 = 0.7$ & 2.7, $\beta_2 = 0.17$, $\beta_3 = 0.17$, $\beta_5 = 0.075$)

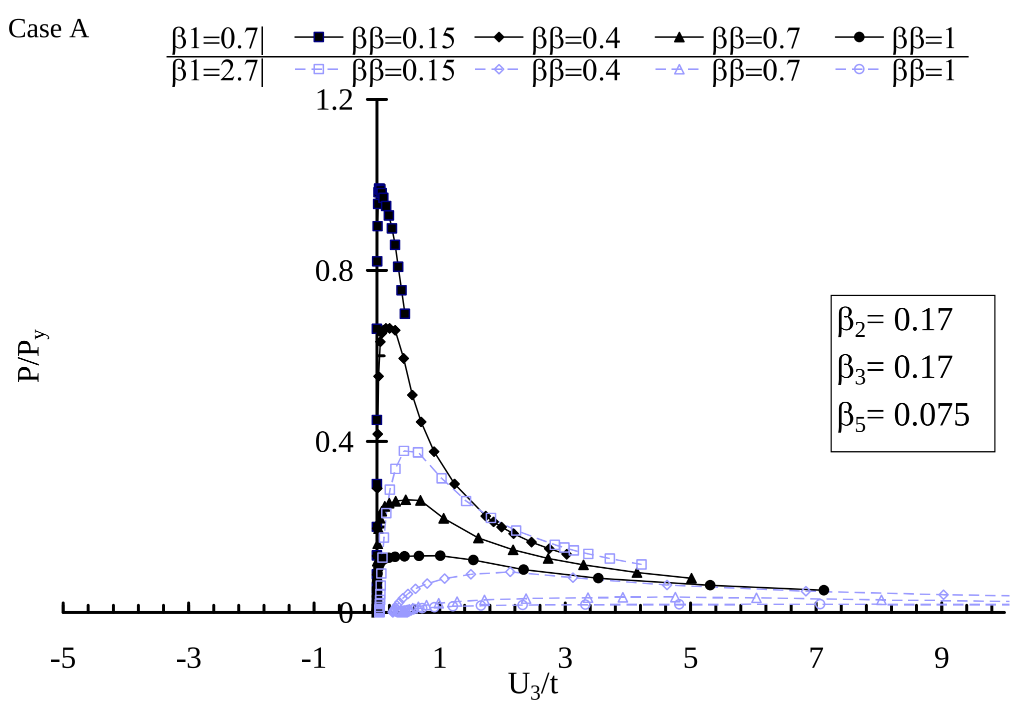

Figure E-74 Axial load versus lateral deflection ($\beta_9 = 0$, $\beta_1 = 0.7$ & 2.7, $\beta_2 = 0.17$, $\beta_3 = 0.17$, $\beta_5 = 0.075$)

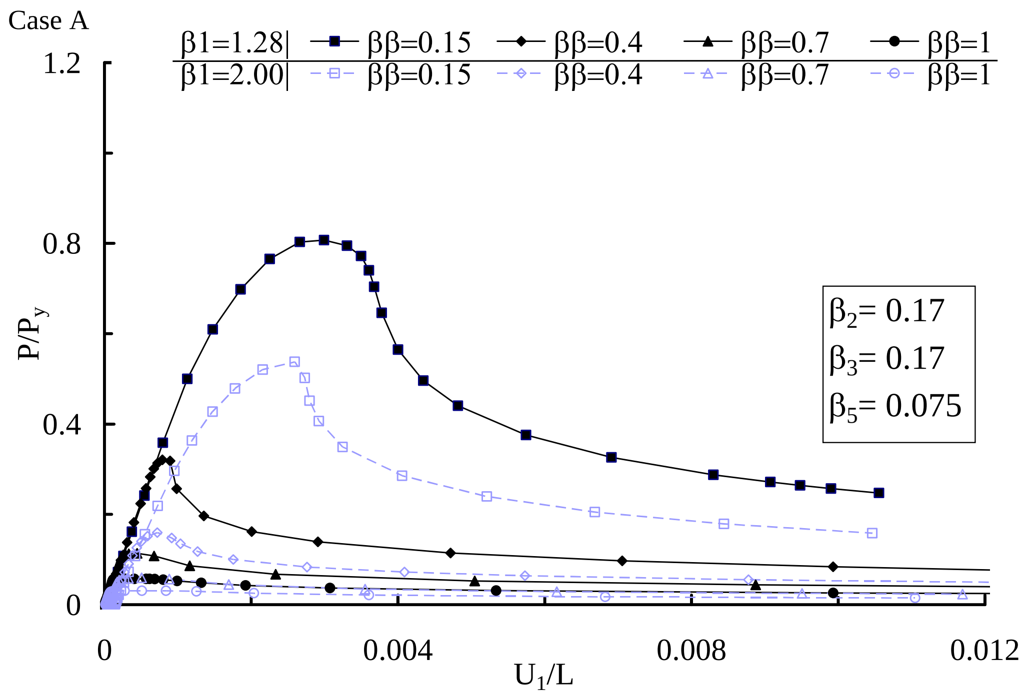

Figure E-75 Axial load versus axial shortening ($\beta_9 = 0$, $\beta_1 = 1.28$ & 2.0, $\beta_2 = 0.17$, $\beta_3 = 0.17$, $\beta_5 = 0.075$)

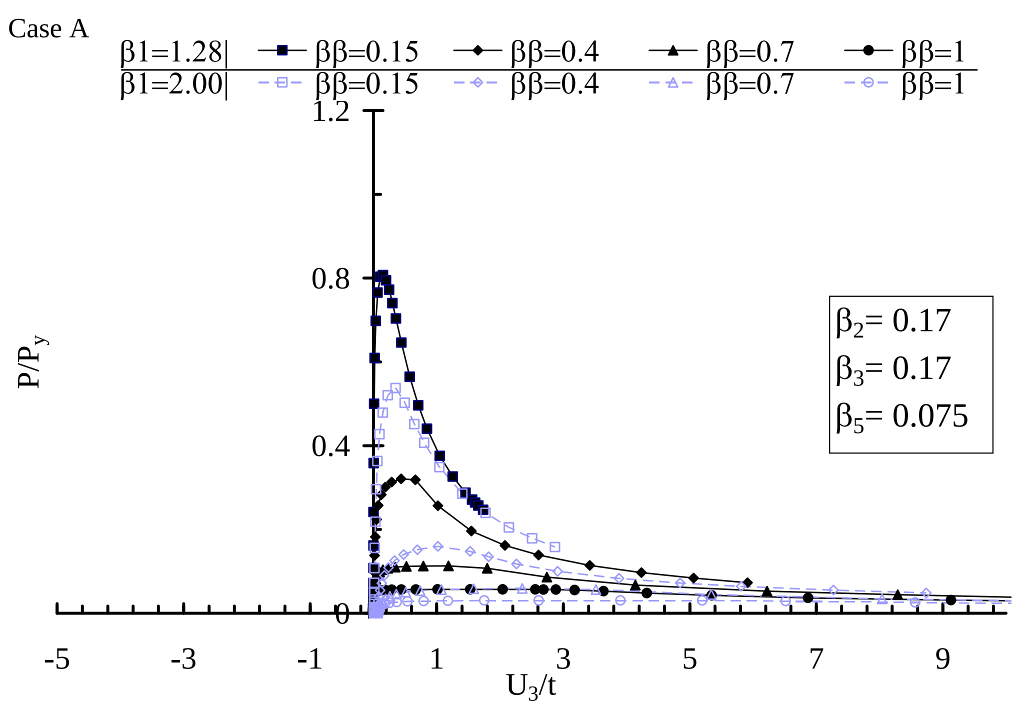

Figure E-76 Axial load versus lateral deflection ($\beta_9 = 0$, $\beta_1 = 1.28$ & 2.0, $\beta_2 = 0.17$, $\beta_3 = 0.17$, $\beta_5 = 0.075$)

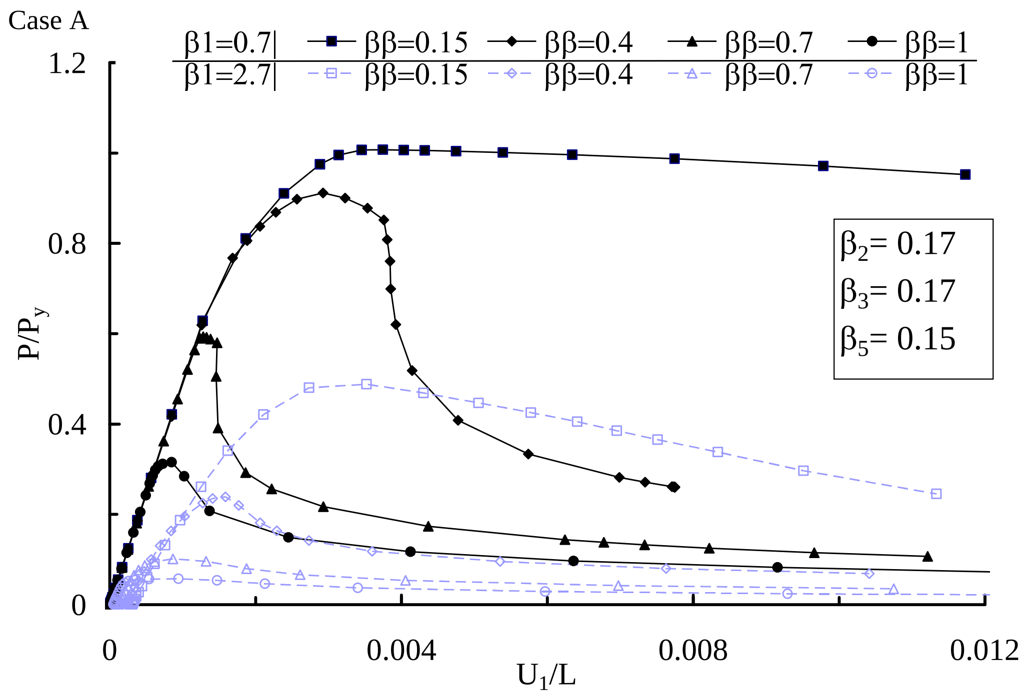

Figure E-77 Axial load versus axial shortening ($\beta_9 = 0$, $\beta_1 = 0.7$ & 2.7, $\beta_2 = 0.17$, $\beta_3 = 0.17$, $\beta_5 = 0.15$)

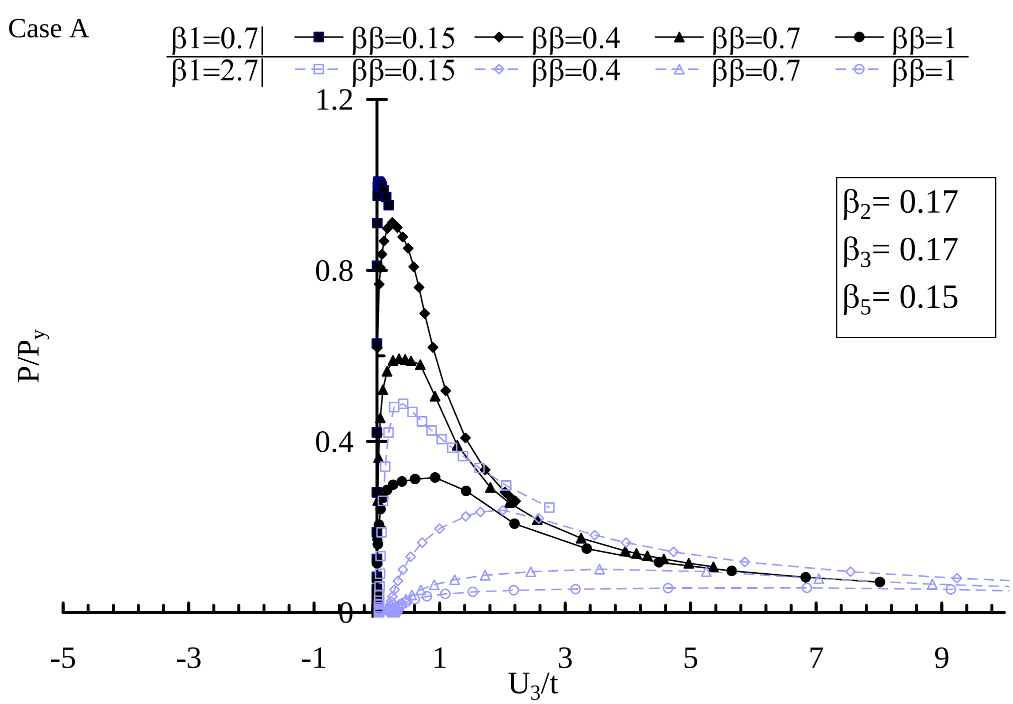

Figure E-78 Axial load versus lateral deflection ($\beta_9 = 0$, $\beta_1 = 0.7$ & 2.7, $\beta_2 = 0.17$, $\beta_3 = 0.17$, $\beta_5 = 0.15$)

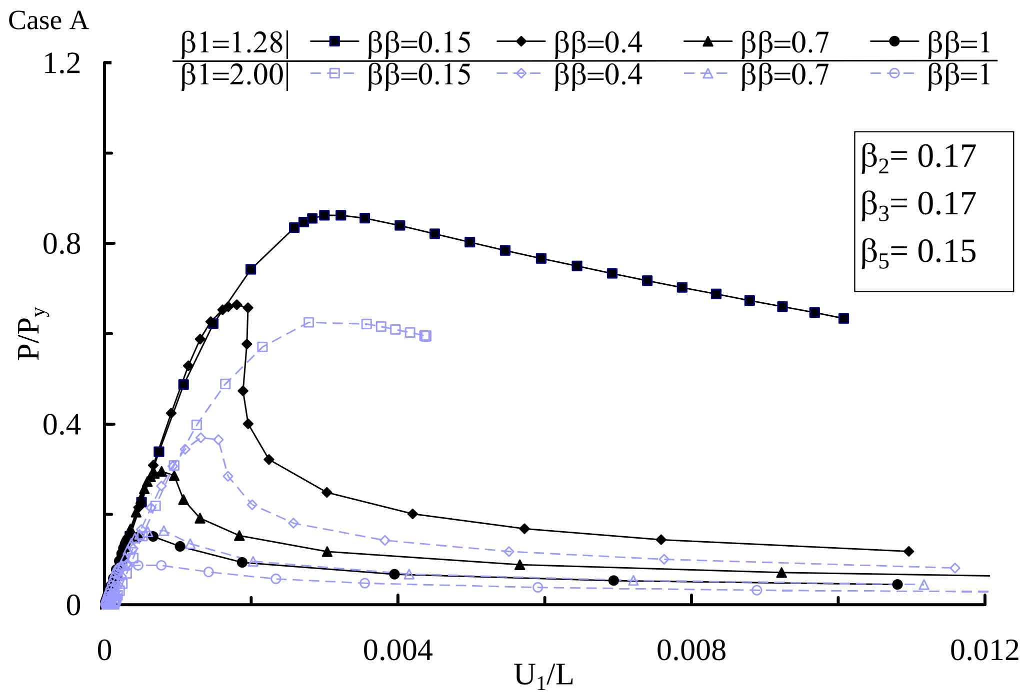

Figure E-79 Axial load versus axial shortening ($\beta_9 = 0$, $\beta_1 = 1.28$ & 2.0, $\beta_2 = 0.17$, $\beta_3 = 0.17$, $\beta_5 = 0.15$)

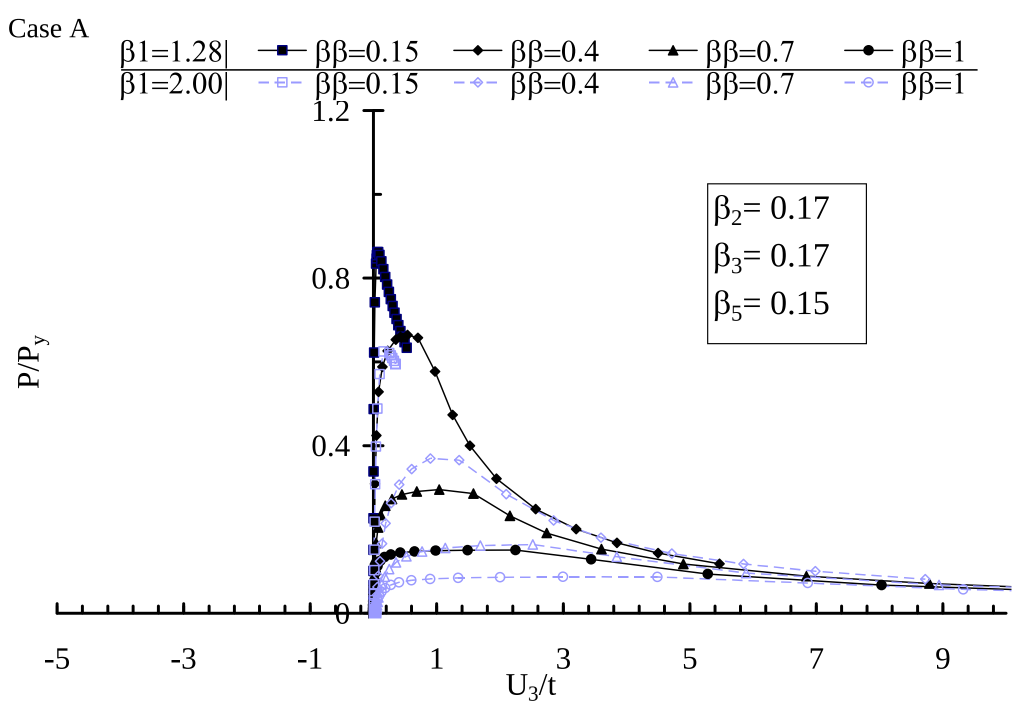

Figure E-80 Axial load versus lateral deflection ($\beta_9 = 0$, $\beta_1 = 1.28$ & 2.0, $\beta_2 = 0.17$, $\beta_3 = 0.17$, $\beta_5 = 0.15$)

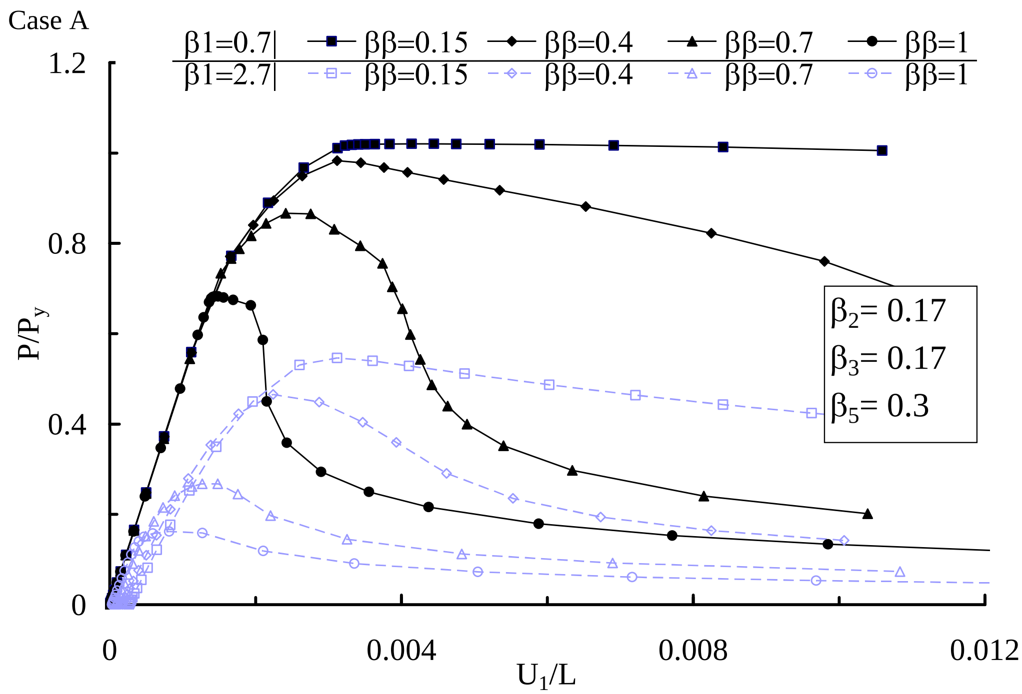

Figure E-81 Axial load versus axial shortening ($\beta_9 = 0$, $\beta_1 = 0.7$ & 2.7, $\beta_2 = 0.17$, $\beta_3 = 0.17$, $\beta_5 = 0.3$)

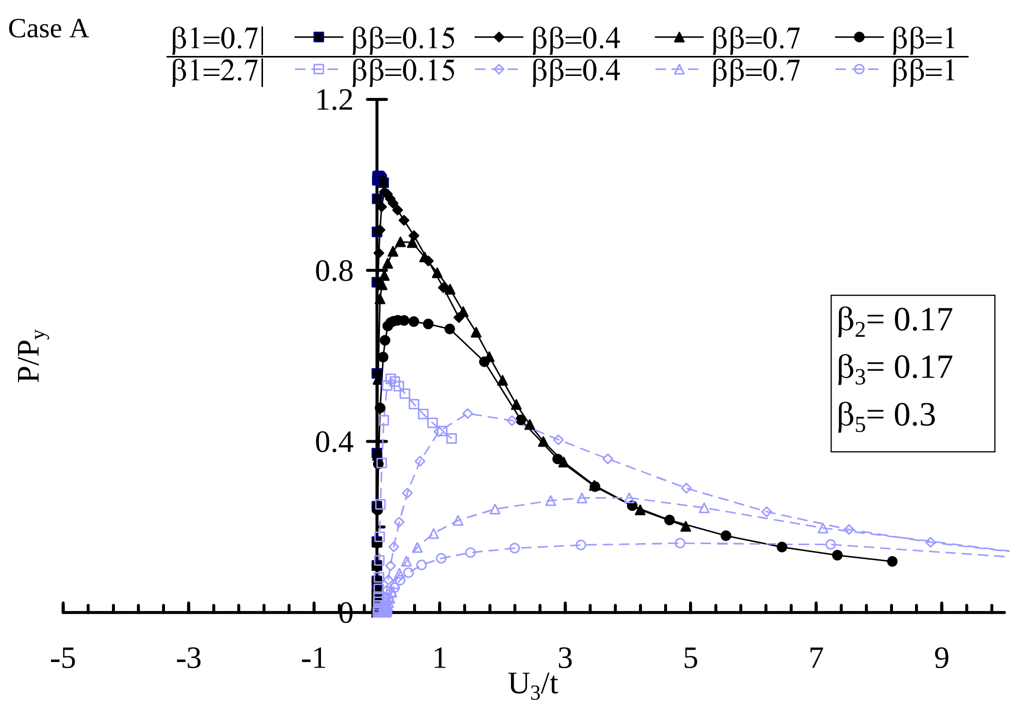

Figure E-82 Axial load versus lateral deflection ($\beta_9 = 0$, $\beta_1 = 0.7$ & 2.7, $\beta_2 = 0.17$, $\beta_3 = 0.17$, $\beta_5 = 0.3$)

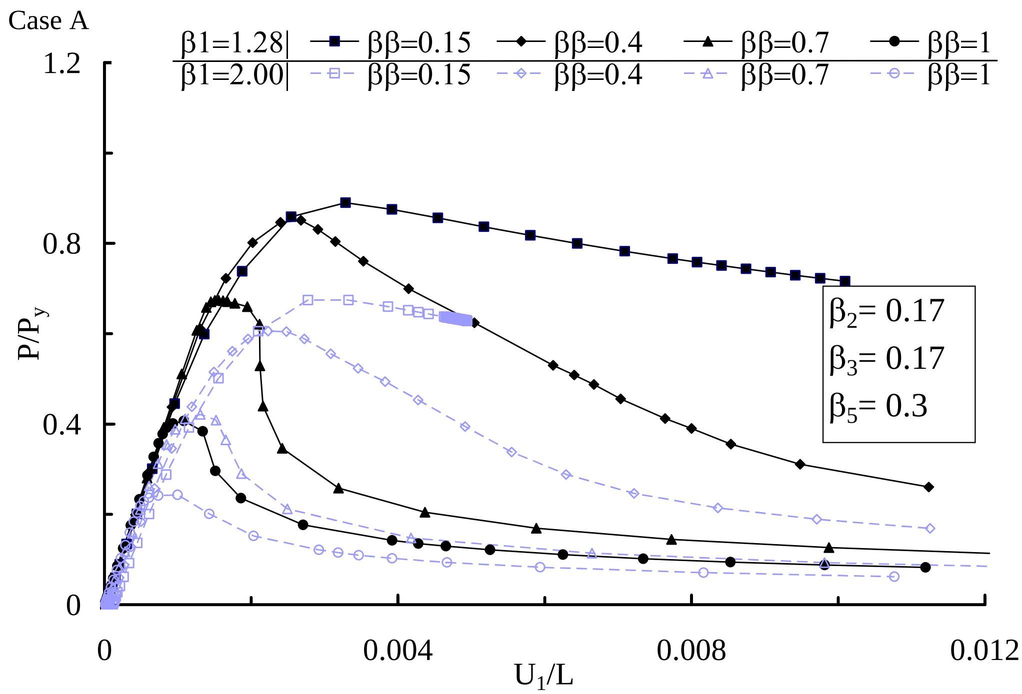

Figure E-83 Axial load versus axial shortening ($\beta_9 = 0$, $\beta_1 = 1.28$ & 2.0, $\beta_2 = 0.17$, $\beta_3 = 0.17$, $\beta_5 = 0.3$)

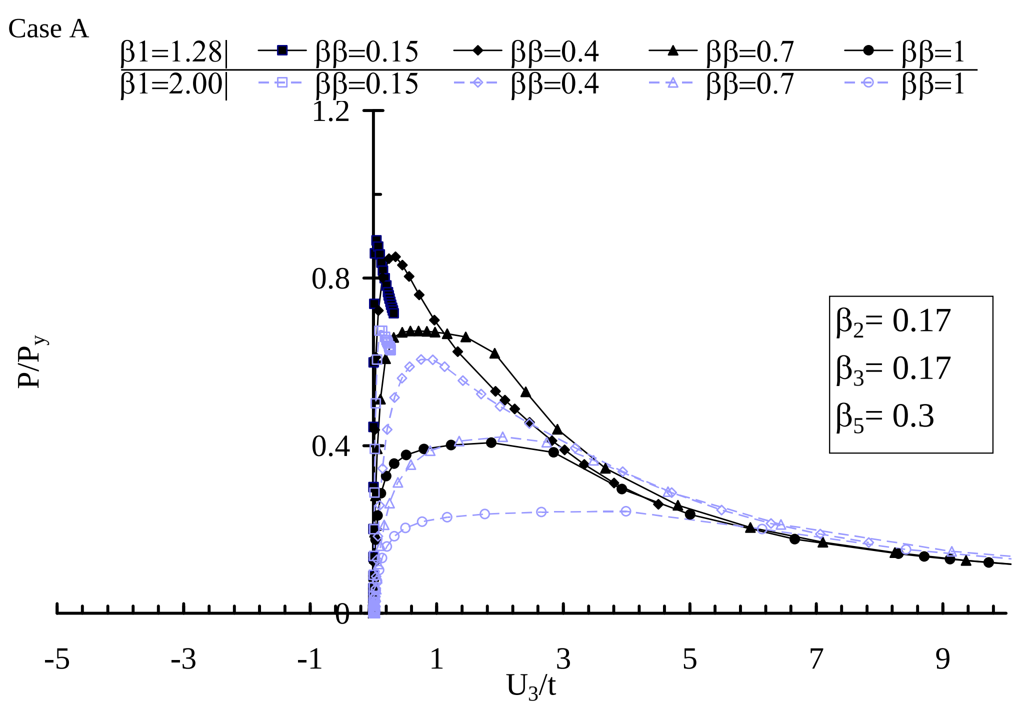

Figure E-84 Axial load versus lateral deflection ($\beta_9 = 0$, $\beta_1 = 1.28$ & 2.0, $\beta_2 = 0.17$, $\beta_3 = 0.17$, $\beta_5 = 0.3$)

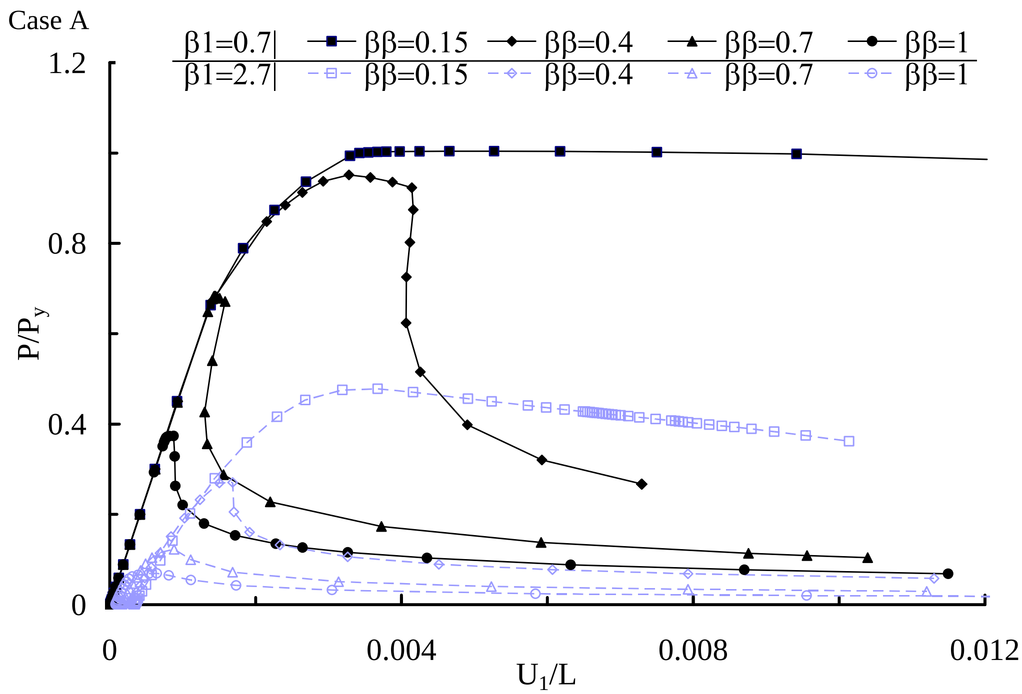

Figure E-85 Axial load versus axial shortening ($\beta_9 = 0$, $\beta_1 = 0.7$ & 2.7, $\beta_2 = 0.8$, $\beta_3 = 0.6$, $\beta_5 = 0.075$)

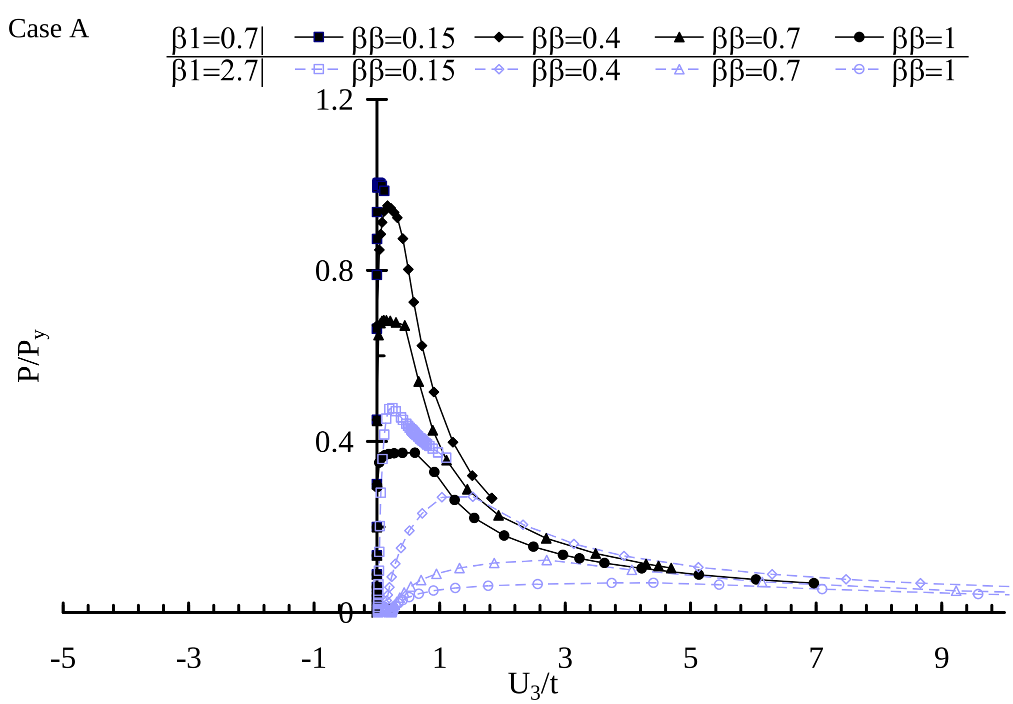

Figure E-86 Axial load versus lateral deflection ($\beta_9 = 0$, $\beta_1 = 0.7$ & 2.7, $\beta_2 = 0.8$, $\beta_3 = 0.6$, $\beta_5 = 0.075$)

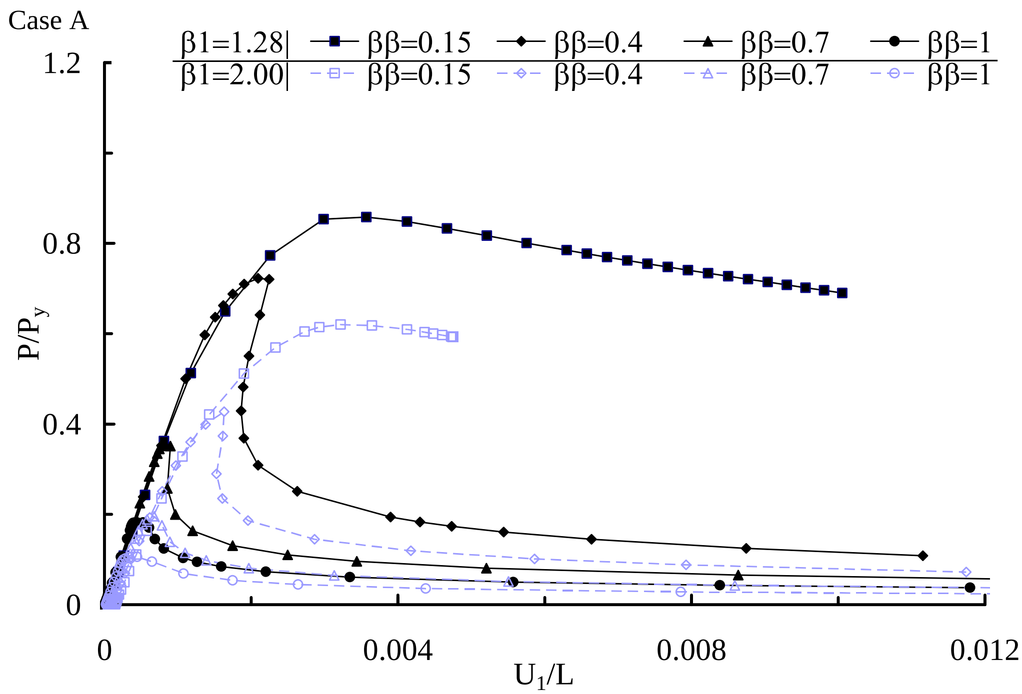

Figure E-87 Axial load versus axial shortening ($\beta_9 = 0$, $\beta_1 = 1.28$ & 2.0, $\beta_2 = 0.8$, $\beta_3 = 0.6$, $\beta_5 = 0.075$)

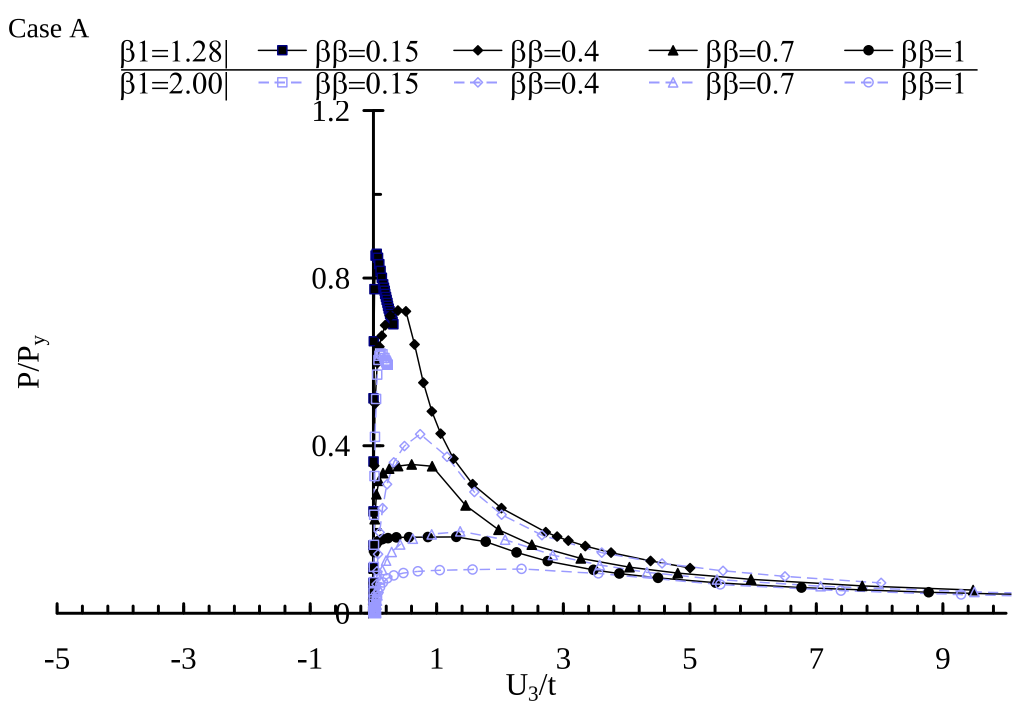

Figure E-88 Axial load versus lateral deflection ($\beta_9 = 0$, $\beta_1 = 1.28$ & 2.0, $\beta_2 = 0.8$, $\beta_3 = 0.6$, $\beta_5 = 0.075$)

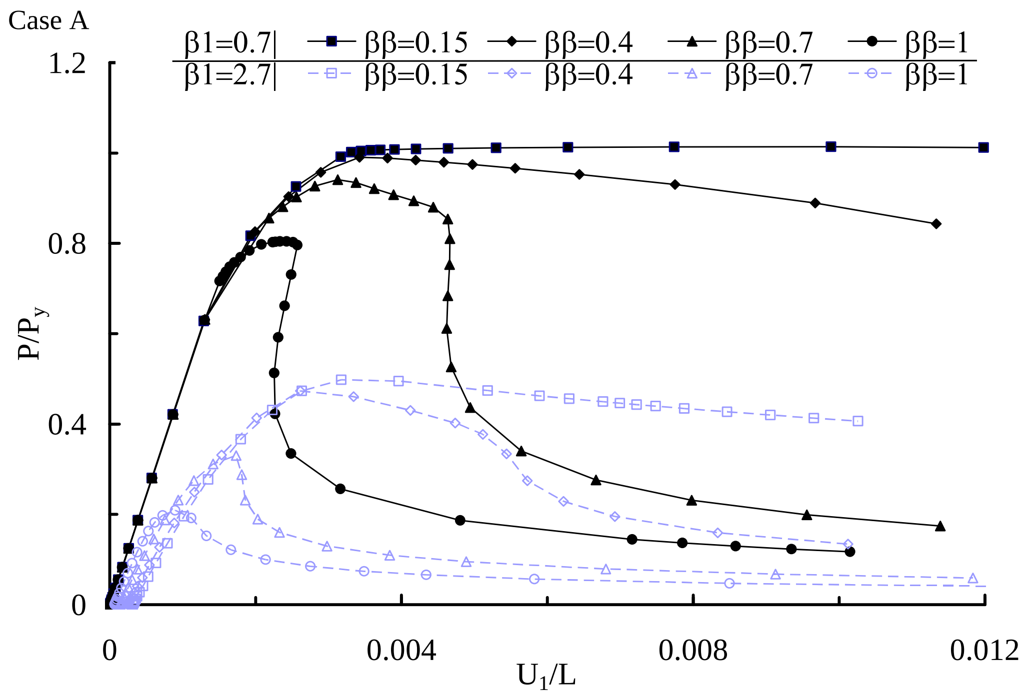

Figure E-89 Axial load versus axial shortening ($\beta_9 = 0$, $\beta_1 = 0.7$ & 2.7, $\beta_2 = 0.8$, $\beta_3 = 0.6$, $\beta_5 = 0.15$)

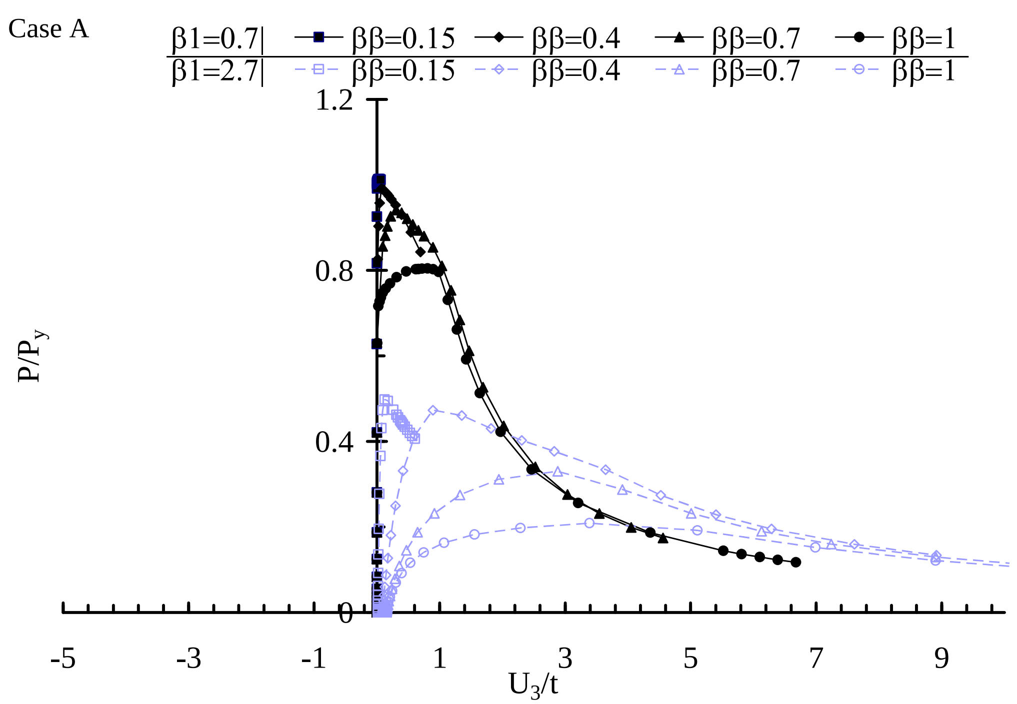

Figure E-90 Axial load versus lateral deflection ($\beta_9 = 0$, $\beta_1 = 0.7$ & 2.7, $\beta_2 = 0.8$, $\beta_3 = 0.6$, $\beta_5 = 0.15$)

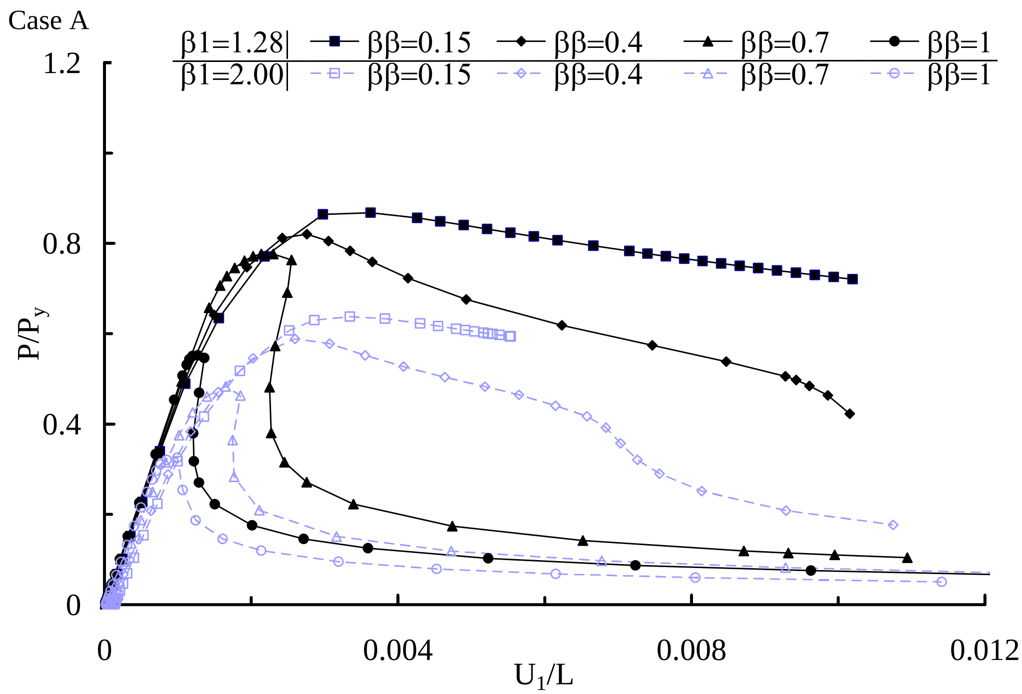

Figure E-91 Axial load versus axial shortening ($\beta_9 = 0$, $\beta_1 = 1.28$ & 2.0, $\beta_2 = 0.8$, $\beta_3 = 0.6$, $\beta_5 = 0.15$)

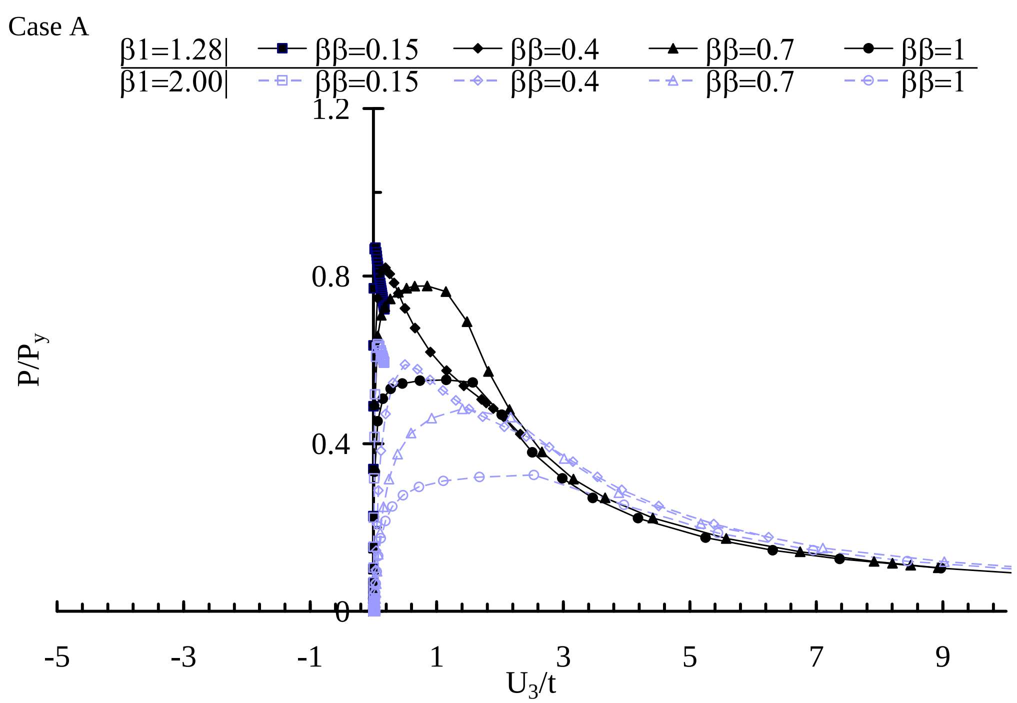

Figure E-92 Axial load versus lateral deflection ($\beta_9 = 0$, $\beta_1 = 1.28$ & 2.0, $\beta_2 = 0.8$, $\beta_3 = 0.6$, $\beta_5 = 0.15$)

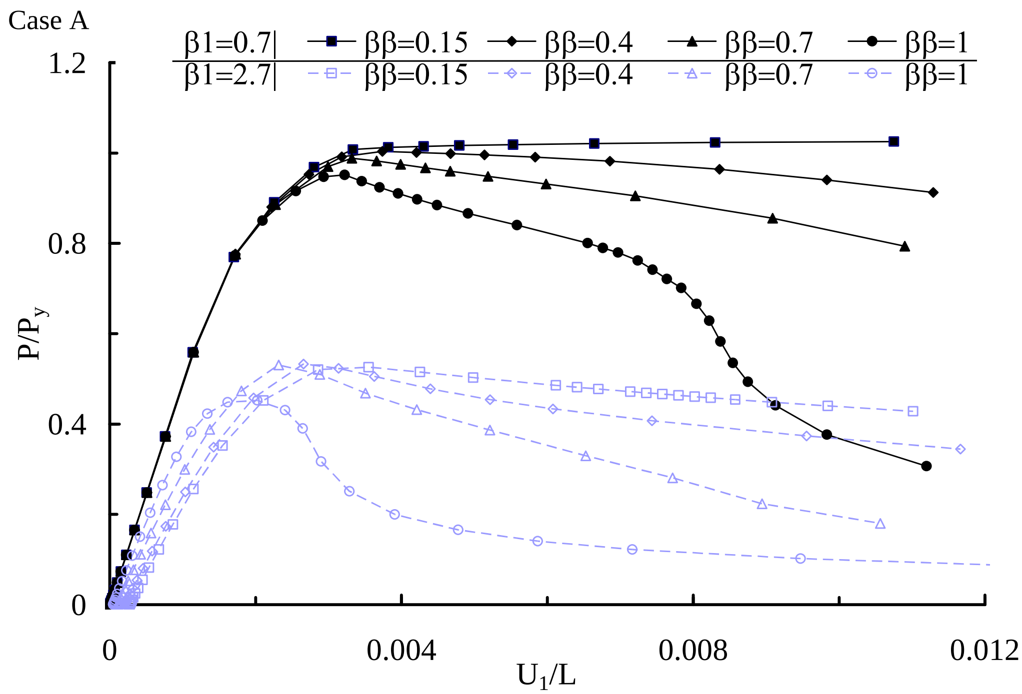

Figure E-93 Axial load versus axial shortening ($\beta_9 = 0$, $\beta_1 = 0.7$ & 2.7, $\beta_2 = 0.8$, $\beta_3 = 0.6$, $\beta_5 = 0.3$)

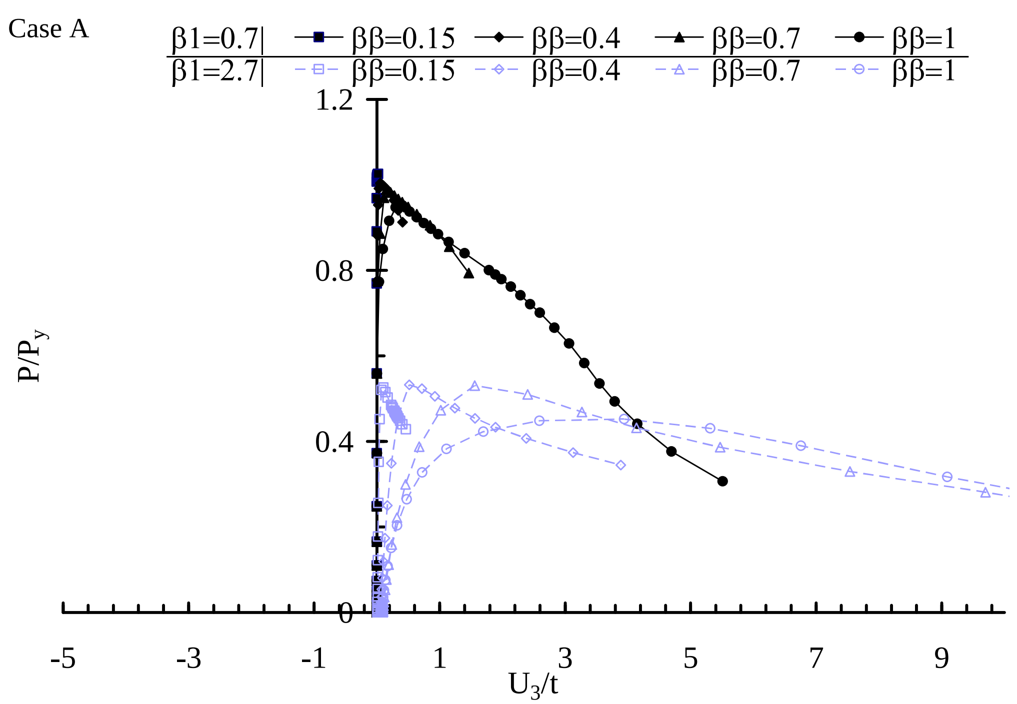

Figure E-94 Axial load versus lateral deflection ($\beta_9 = 0$, $\beta_1 = 0.7$ & 2.7, $\beta_2 = 0.8$, $\beta_3 = 0.6$, $\beta_5 = 0.3$)

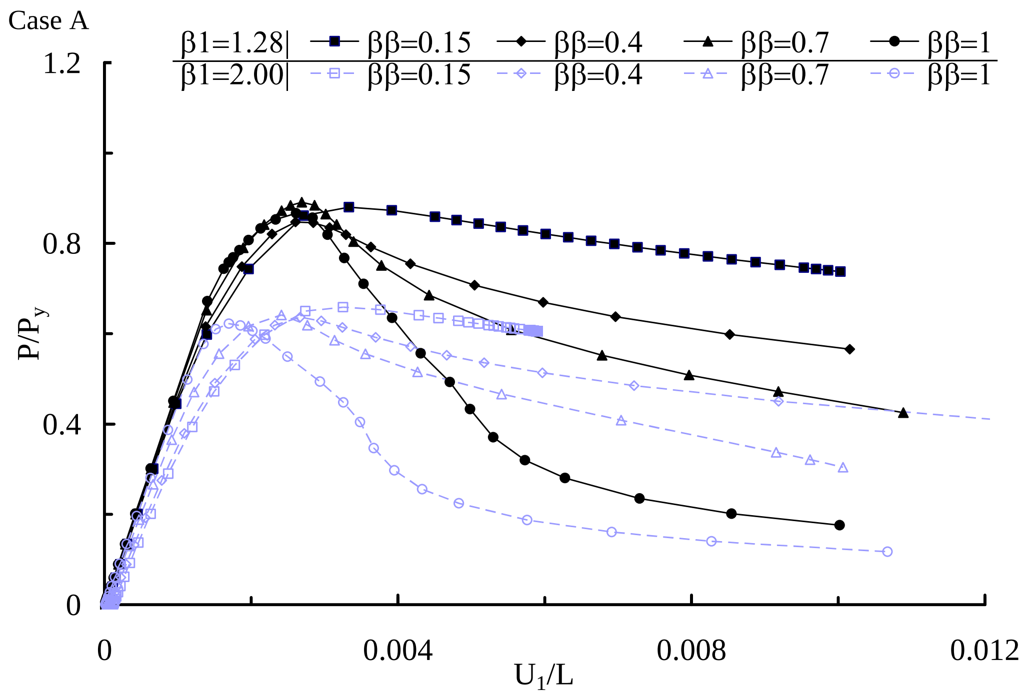

Figure E-95 Axial load versus axial shortening ($\beta_9 = 0$, $\beta_1 = 1.28$ & 2.0, $\beta_2 = 0.8$, $\beta_3 = 0.6$, $\beta_5 = 0.3$)

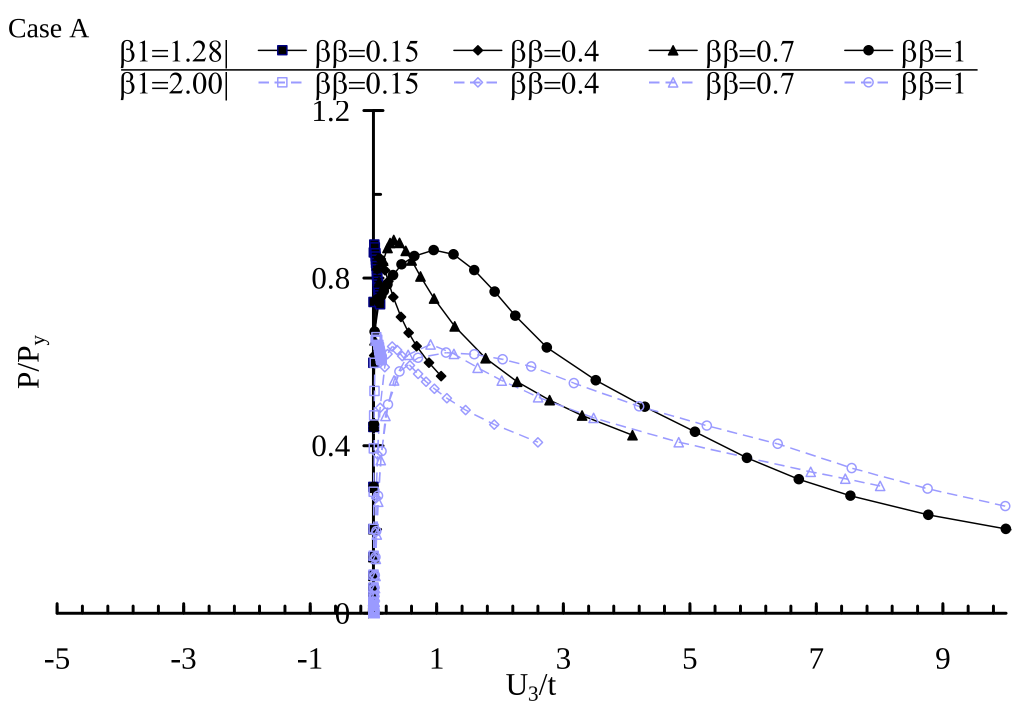

Figure E-96 Axial load versus lateral deflection ($\beta_9 = 0$, $\beta_1 = 1.28$ & 2.0, $\beta_2 = 0.8$, $\beta_3 = 0.6$, $\beta_5 = 0.3$)

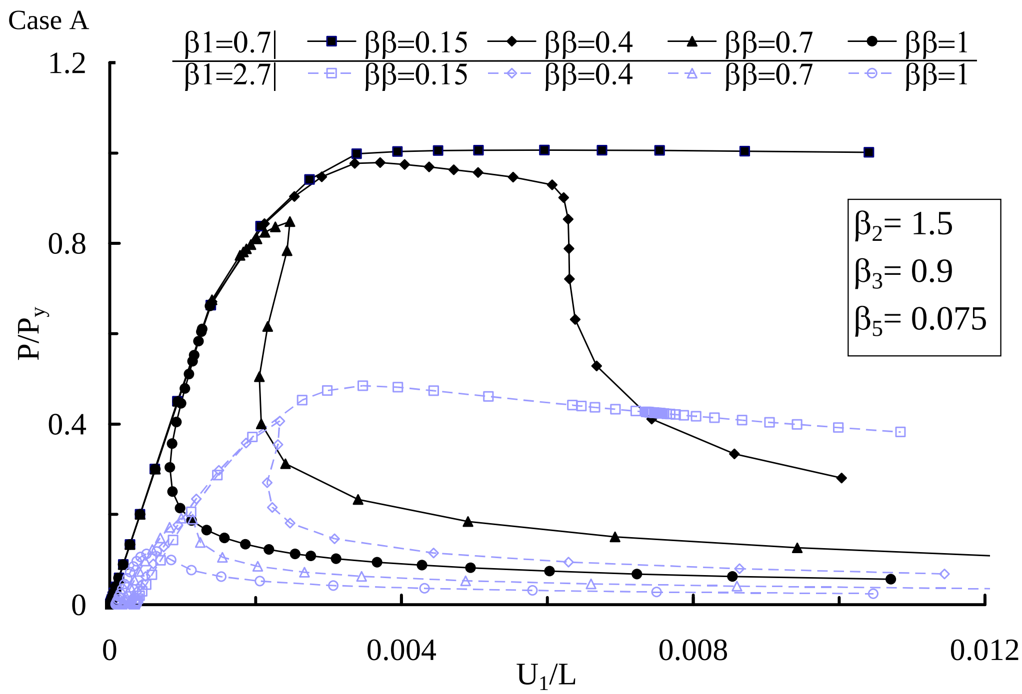

Figure E-97 Axial load versus axial shortening ($\beta_9 = 0$, $\beta_1 = 0.7$ & 2.7, $\beta_2 = 1.5$, $\beta_3 = 0.9$, $\beta_5 = 0.075$)

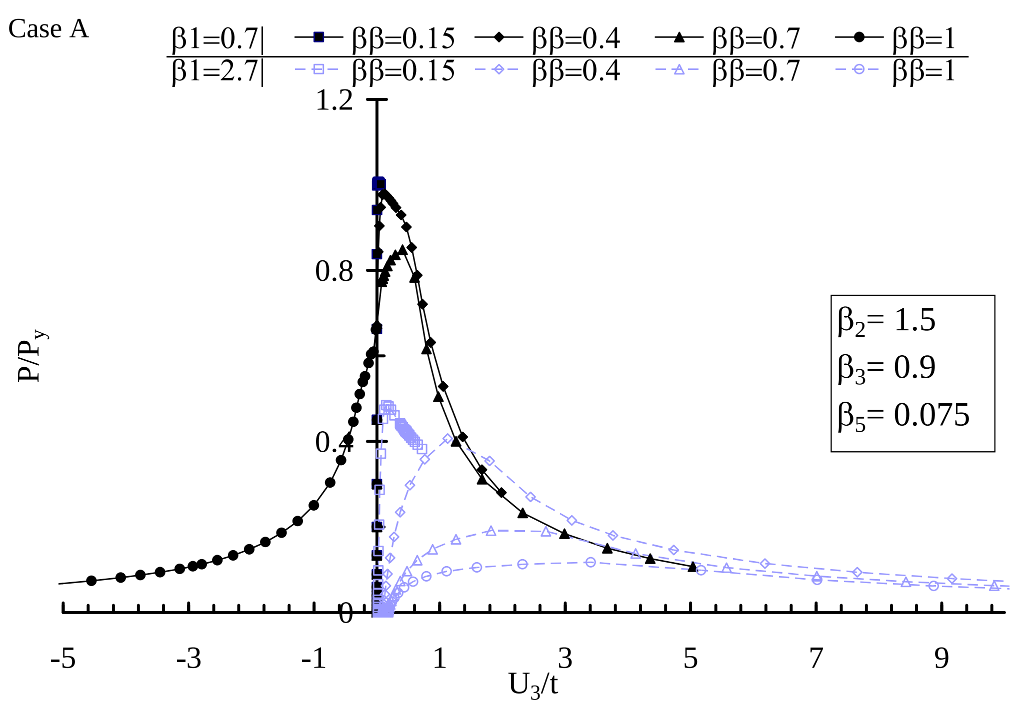

Figure E-98 Axial load versus lateral deflection ($\beta_9 = 0$, $\beta_1 = 0.7$ & 2.7, $\beta_2 = 1.5$, $\beta_3 = 0.9$, $\beta_5 = 0.075$)

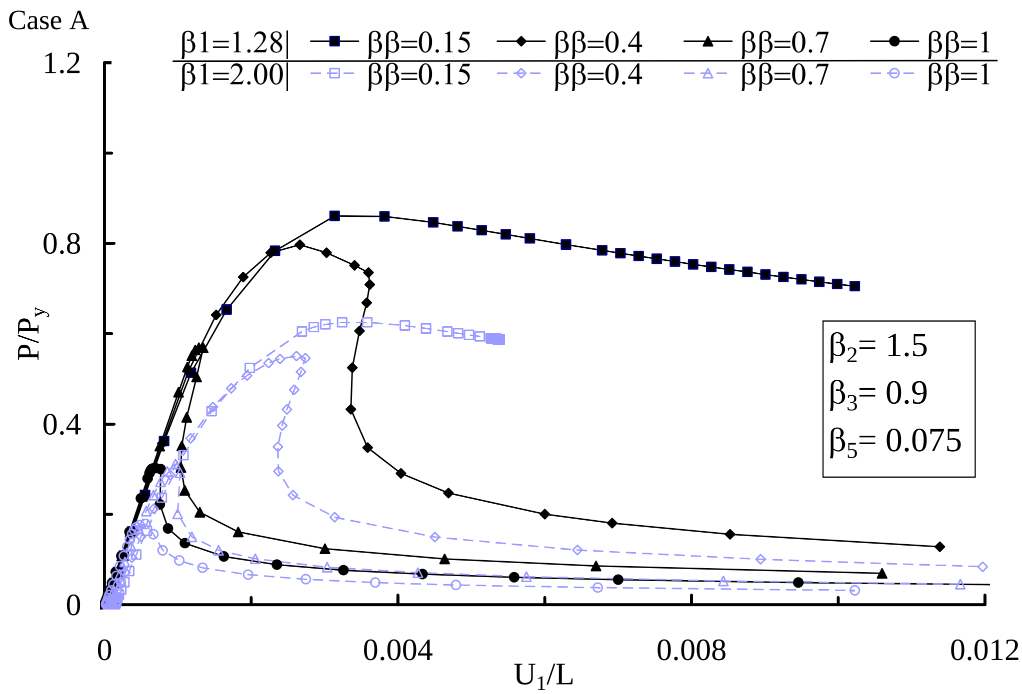

Figure E-99 Axial load versus axial shortening ($\beta_9 = 0$, $\beta_1 = 1.28$ & 2.0, $\beta_2 = 1.5$, $\beta_3 = 0.9$, $\beta_5 = 0.075$)

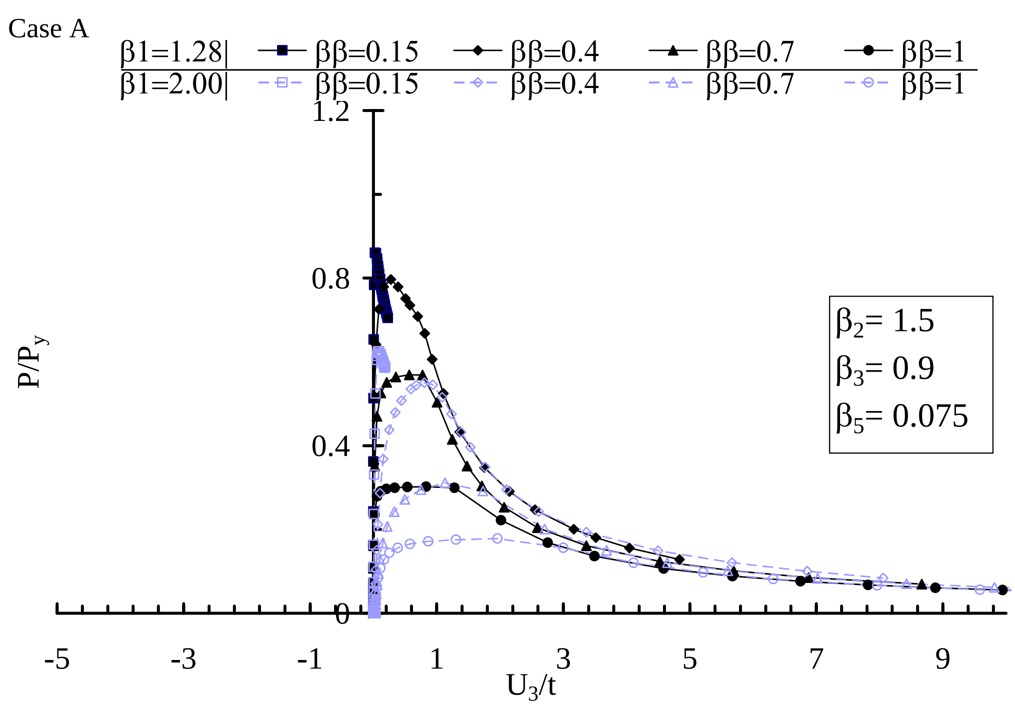

Figure E-100 Axial load versus lateral deflection ($\beta_9 = 0$, $\beta_1 = 1.28$ & 2.0, $\beta_2 = 1.5$, $\beta_3 = 0.9$, $\beta_5 = 0.075$)

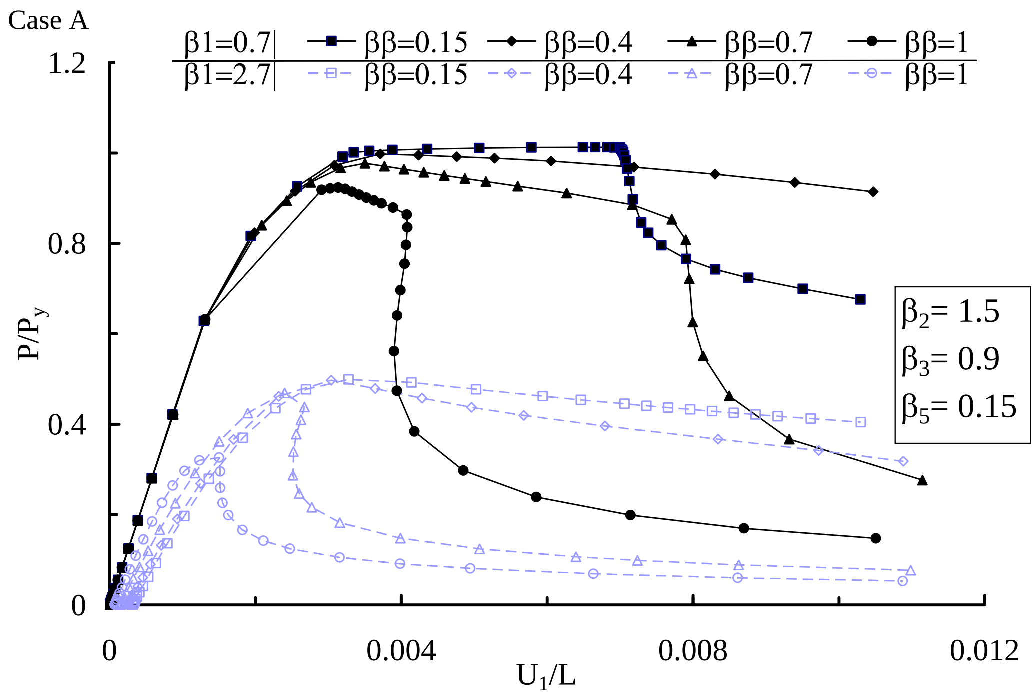

Figure E-101 Axial load versus axial shortening ($\beta_9 = 0$, $\beta_1 = 0.7$ & 2.7, $\beta_2 = 1.5$, $\beta_3 = 0.9$, $\beta_5 = 0.15$)

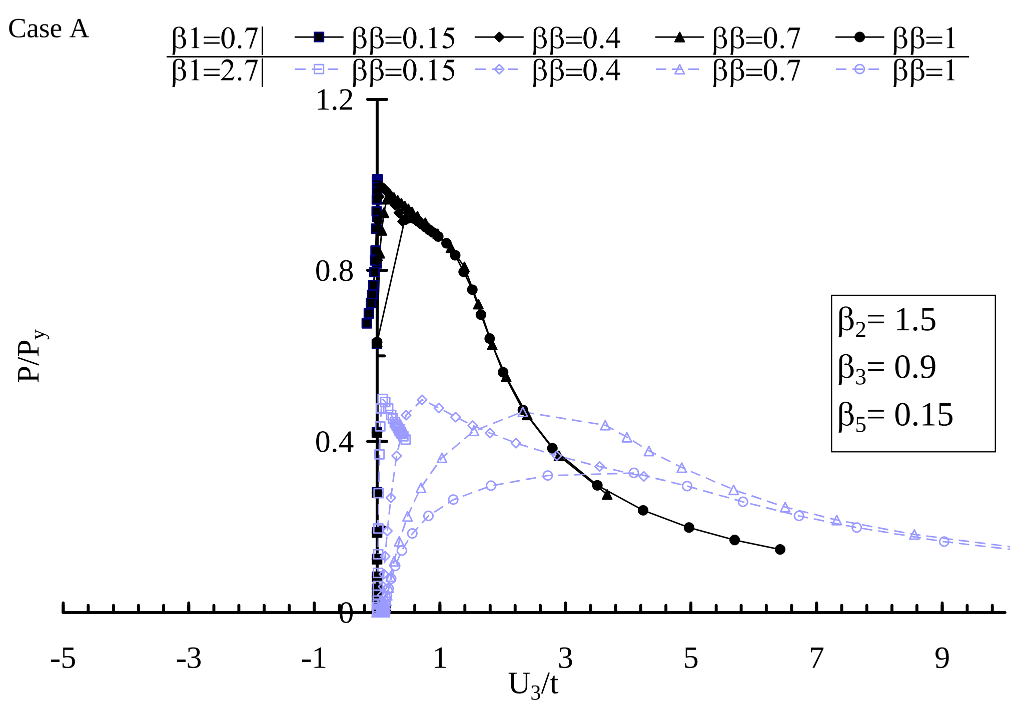

Figure E-102 Axial load versus lateral deflection ($\beta_9 = 0$, $\beta_1 = 0.7$ & 2.7, $\beta_2 = 1.5$, $\beta_3 = 0.9$, $\beta_5 = 0.15$)

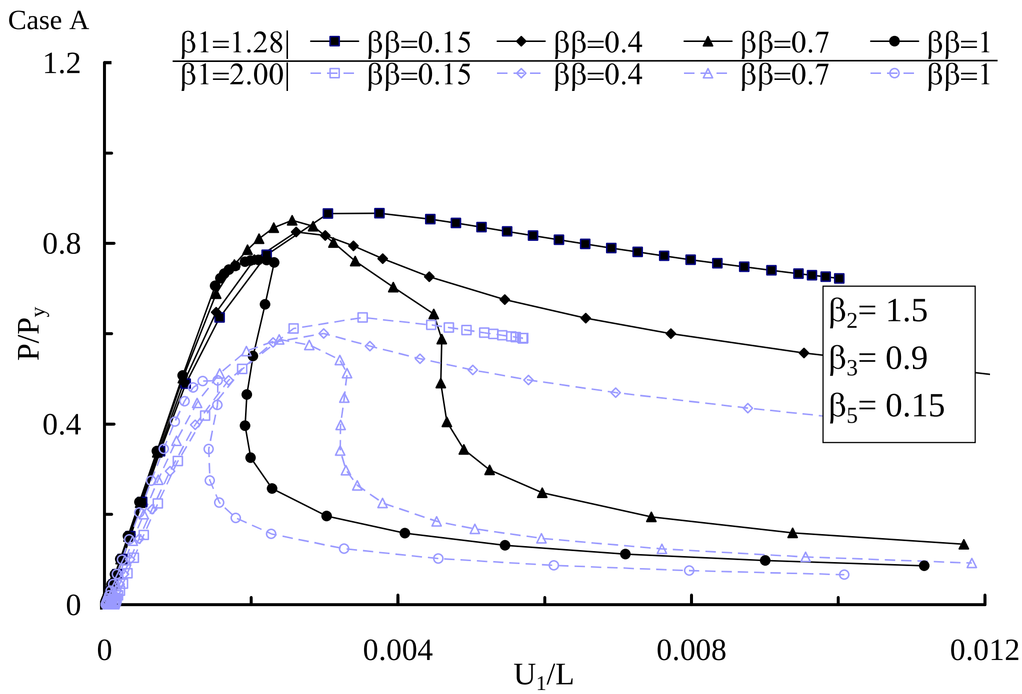

Figure E-103 Axial load versus axial shortening ($\beta_9 = 0$, $\beta_1 = 1.28$ & 2.0, $\beta_2 = 1.5$, $\beta_3 = 0.9$, $\beta_5 = 0.15$)

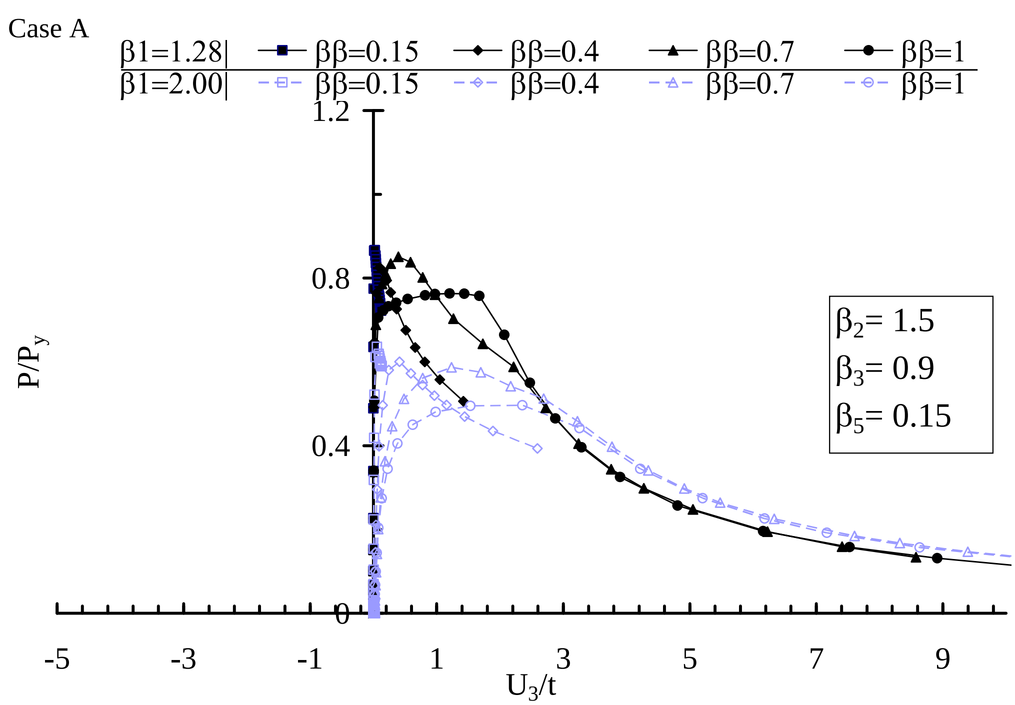

Figure E-104 Axial load versus lateral deflection ($\beta_9 = 0$, $\beta_1 = 1.28$ & 2.0, $\beta_2 = 1.5$, $\beta_3 = 0.9$, $\beta_5 = 0.15$)

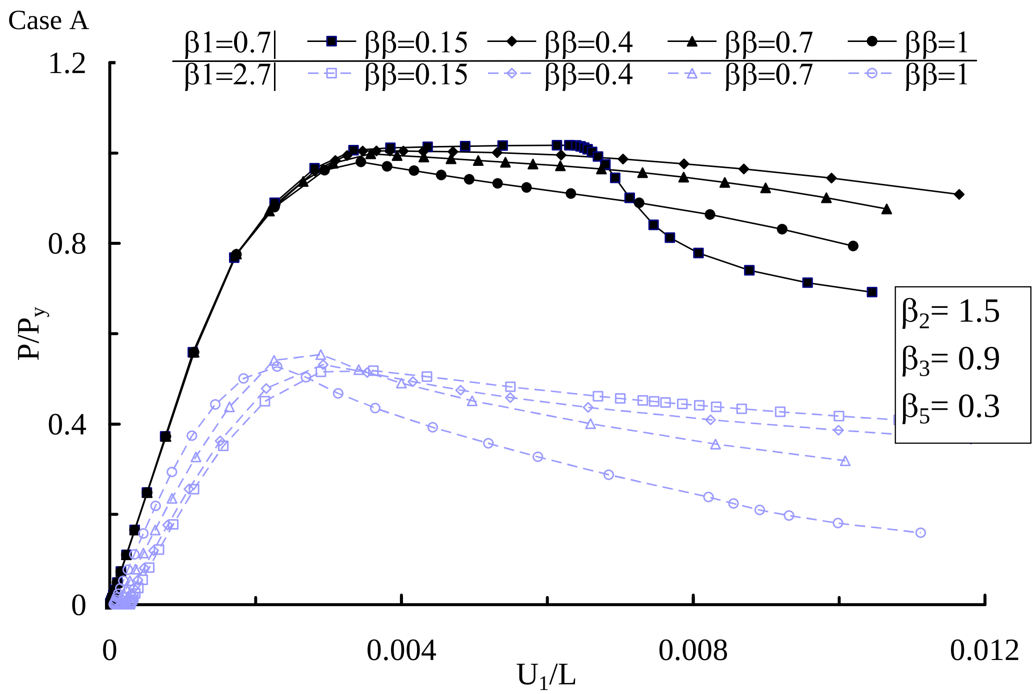

Figure E-105 Axial load versus axial shortening ($\beta_9 = 0$, $\beta_1 = 0.7$ & 2.7, $\beta_2 = 1.5$, $\beta_3 = 0.9$, $\beta_5 = 0.3$)

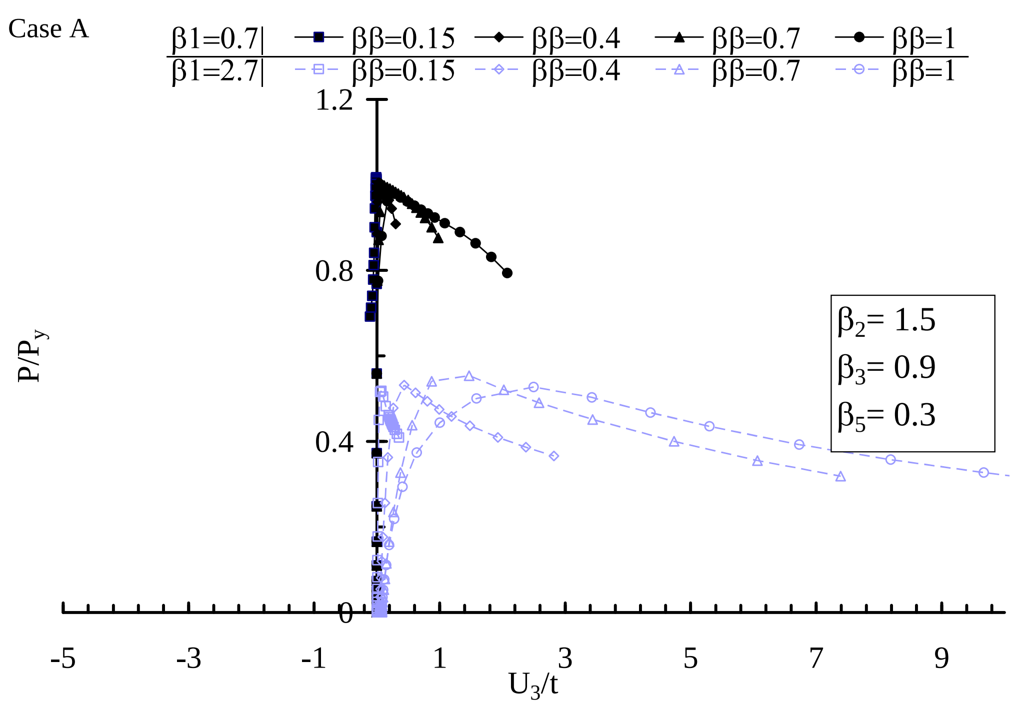

Figure E-106 Axial load versus lateral deflection ($\beta_9 = 0$, $\beta_1 = 0.7$ & 2.7, $\beta_2 = 1.5$, $\beta_3 = 0.9$, $\beta_5 = 0.3$)

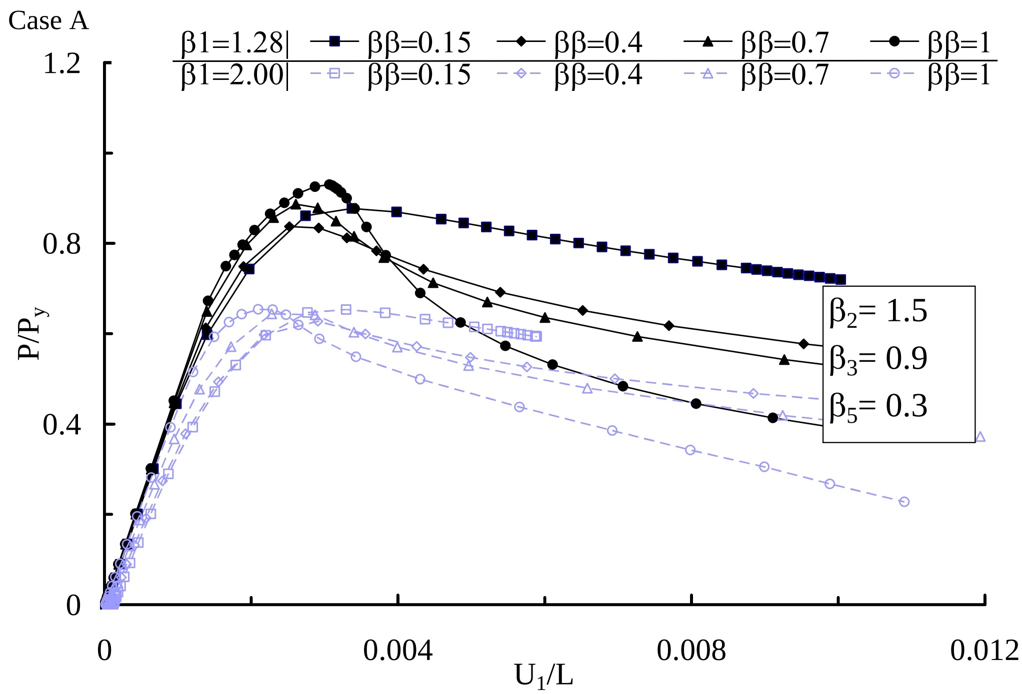

Figure E-107 Axial load versus axial shortening ($\beta_9 = 0$, $\beta_1 = 1.28$ & 2.0, $\beta_2 = 1.5$, $\beta_3 = 0.9$, $\beta_5 = 0.3$)

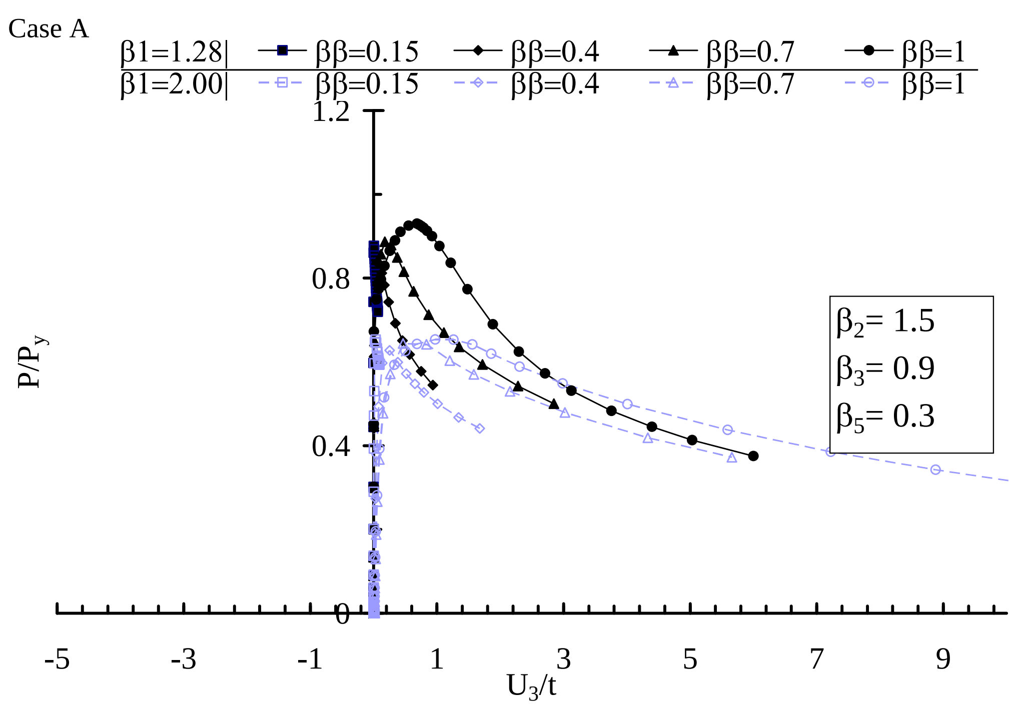

Figure E-108 Axial load versus lateral deflection ($\beta_9 = 0$, $\beta_1 = 1.28$ & 2.0, $\beta_2 = 1.5$, $\beta_3 = 0.9$, $\beta_5 = 0.3$)

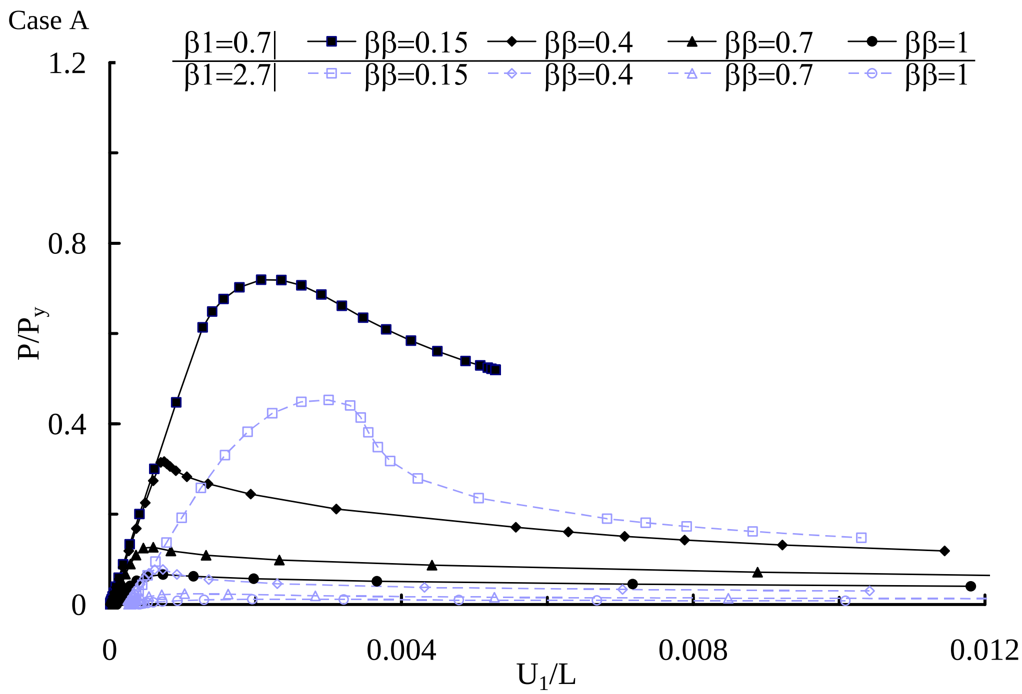

Figure E-109 Axial load versus axial shortening ($\beta_9 = 0.2$, $\beta_1 = 0.7$ & 2.7, $\beta_2 = 0.17$, $\beta_3 = 0.17$, $\beta_5 = 0.075$)

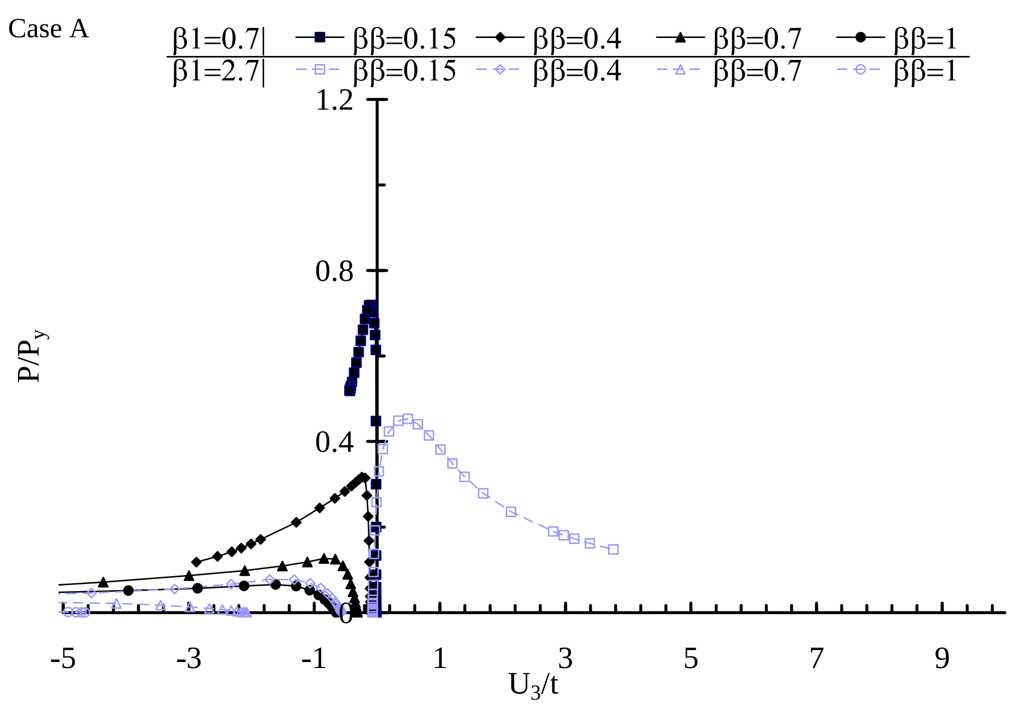

Figure E-110 Axial load versus lateral deflection ($\beta_9 = 0.2$, $\beta_1 = 0.7$ & 2.7, $\beta_2 = 0.17$, $\beta_3 = 0.17$, $\beta_5 = 0.075$)

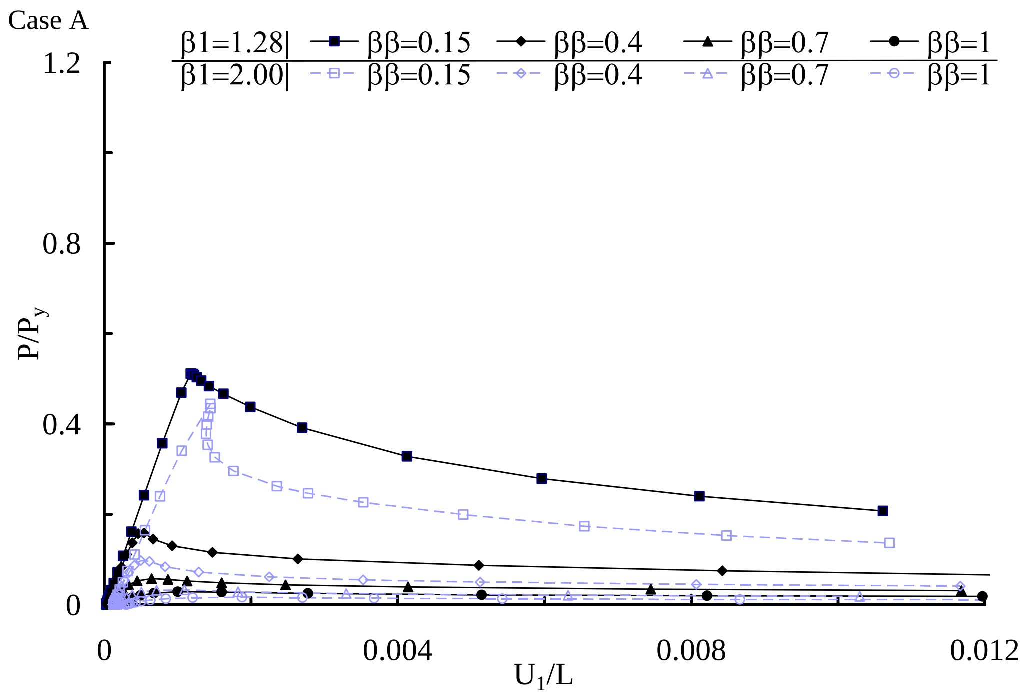

Figure E-111 Axial load versus axial shortening ($\beta_9 = 0.2$, $\beta_1 = 1.28$ & 2.0, $\beta_2 = 0.17$, $\beta_3 = 0.17$, $\beta_5 = 0.075$)

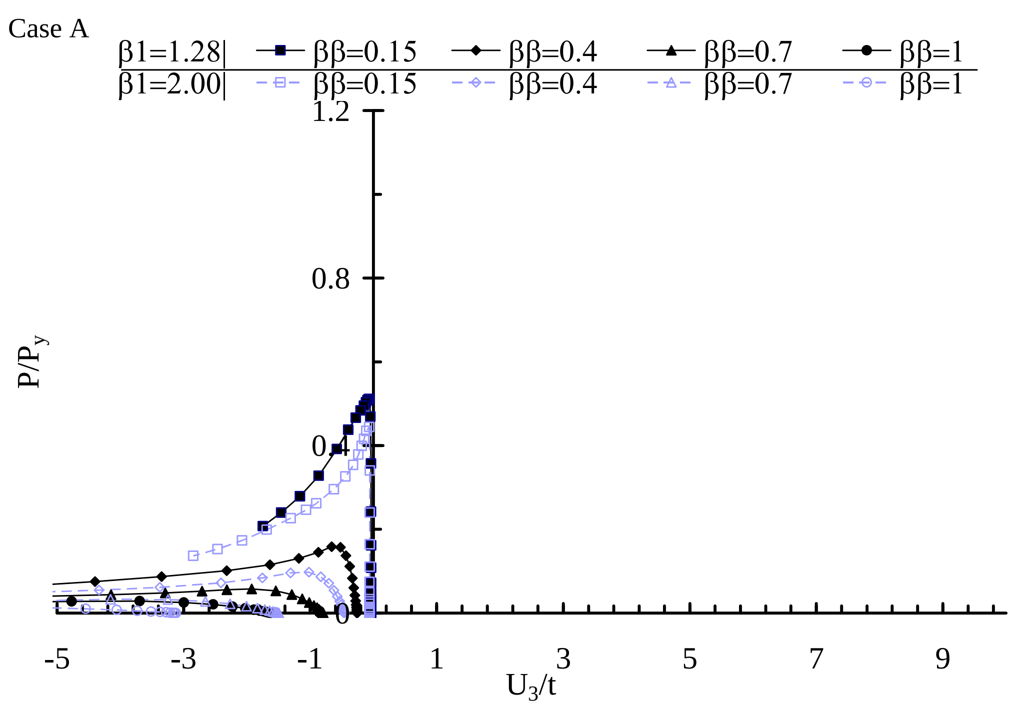

Figure E-112 Axial load versus lateral deflection ($\beta_9 = 0.2$, $\beta_1 = 1.28$ & 2.0, $\beta_2 = 0.17$, $\beta_3 = 0.17$, $\beta_5 = 0.075$)

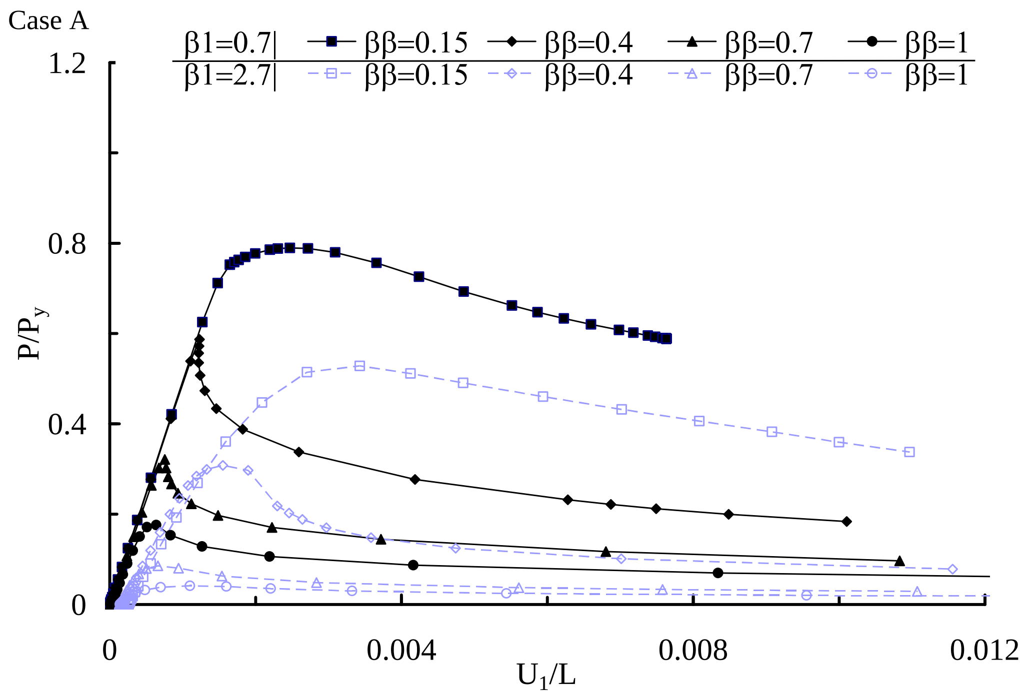

Figure E-113 Axial load versus axial shortening ($\beta_9 = 0.2$, $\beta_1 = 0.7$ & 2.7, $\beta_2 = 0.17$, $\beta_3 = 0.17$, $\beta_5 = 0.15$)

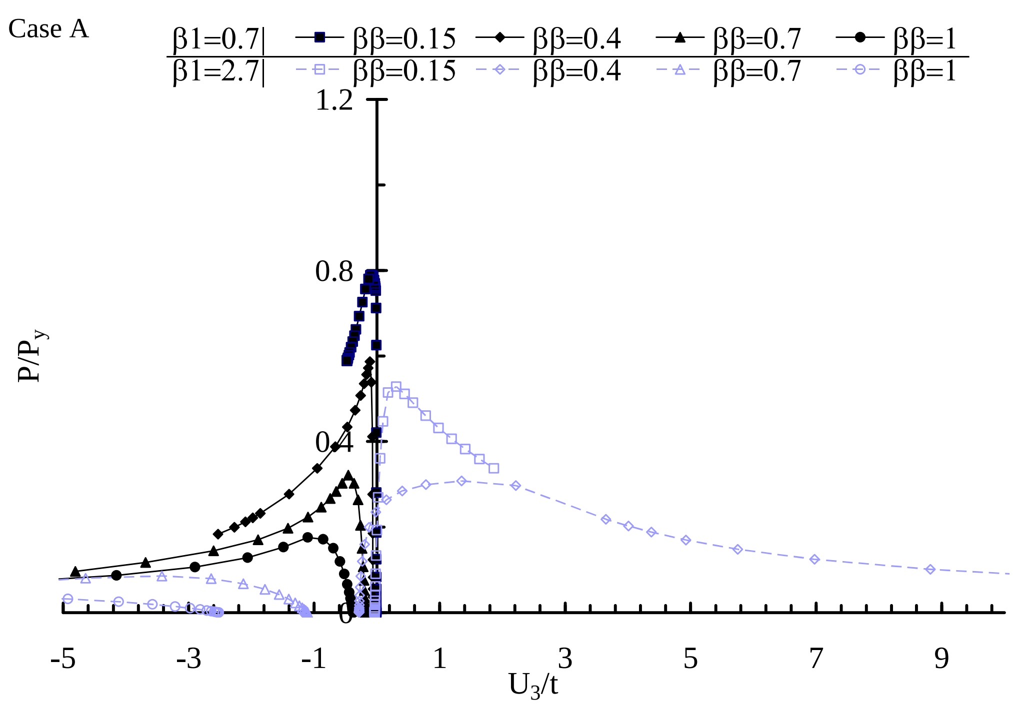

Figure E-114 Axial load versus lateral deflection ($\beta_9 = 0.2$, $\beta_1 = 0.7$ & 2.7, $\beta_2 = 0.17$, $\beta_3 = 0.17$, $\beta_5 = 0.15$)

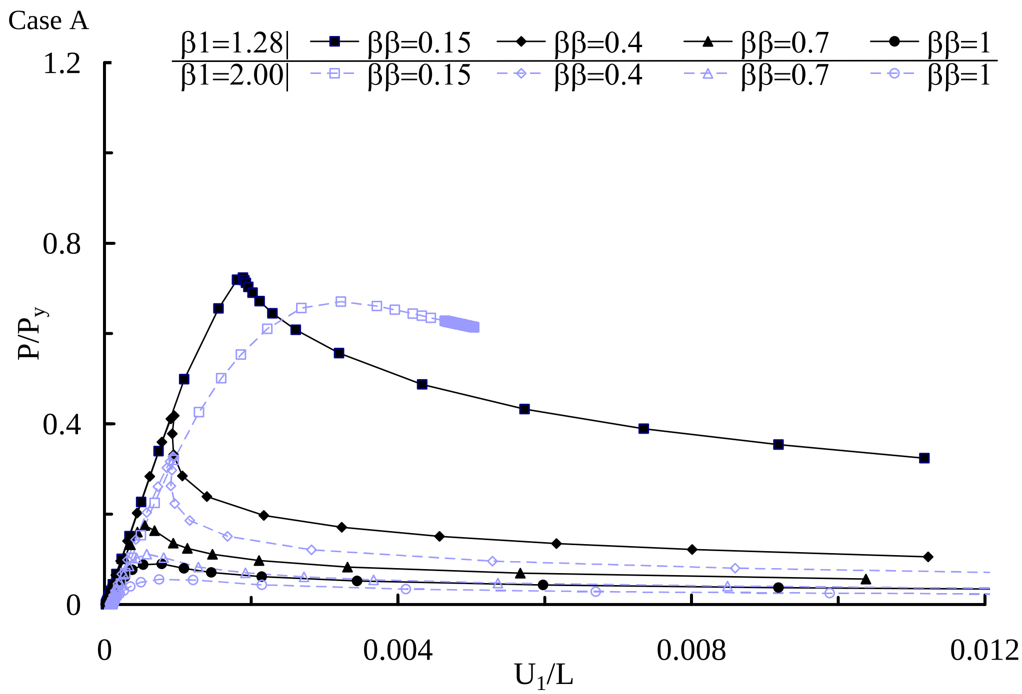

Figure E-115 Axial load versus axial shortening ($\beta_9 = 0.2$, $\beta_1 = 1.28$ & 2.0, $\beta_2 = 0.17$, $\beta_3 = 0.17$, $\beta_5 = 0.15$)

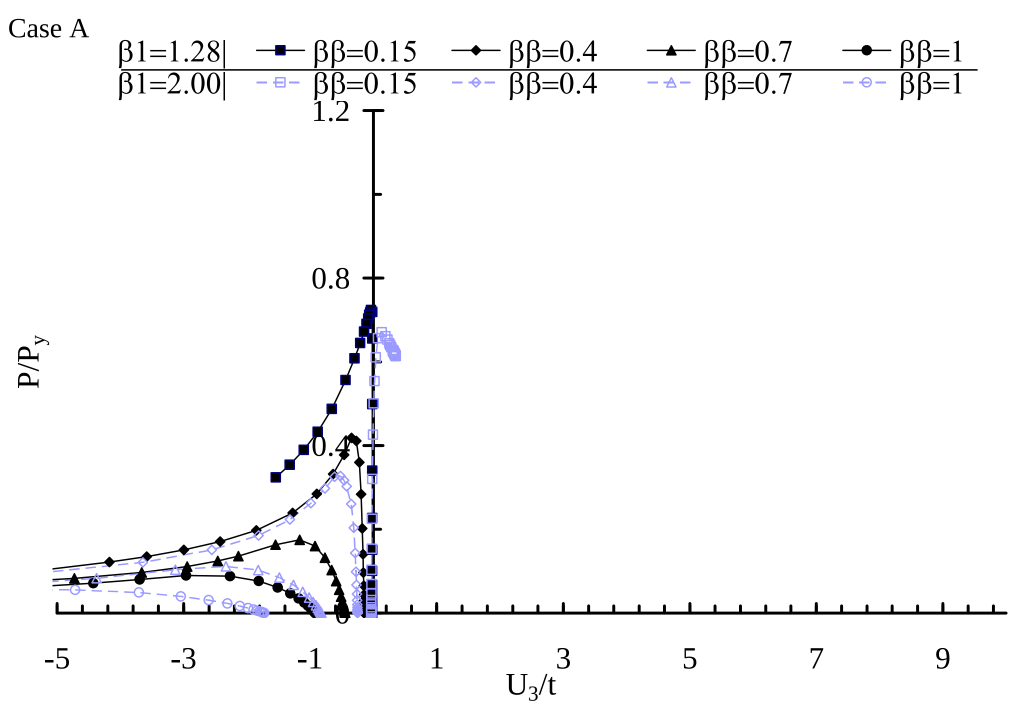

Figure E-116 Axial load versus lateral deflection ($\beta_9 = 0.2$, $\beta_1 = 1.28$ & 2.0, $\beta_2 = 0.17$, $\beta_3 = 0.17$, $\beta_5 = 0.15$)

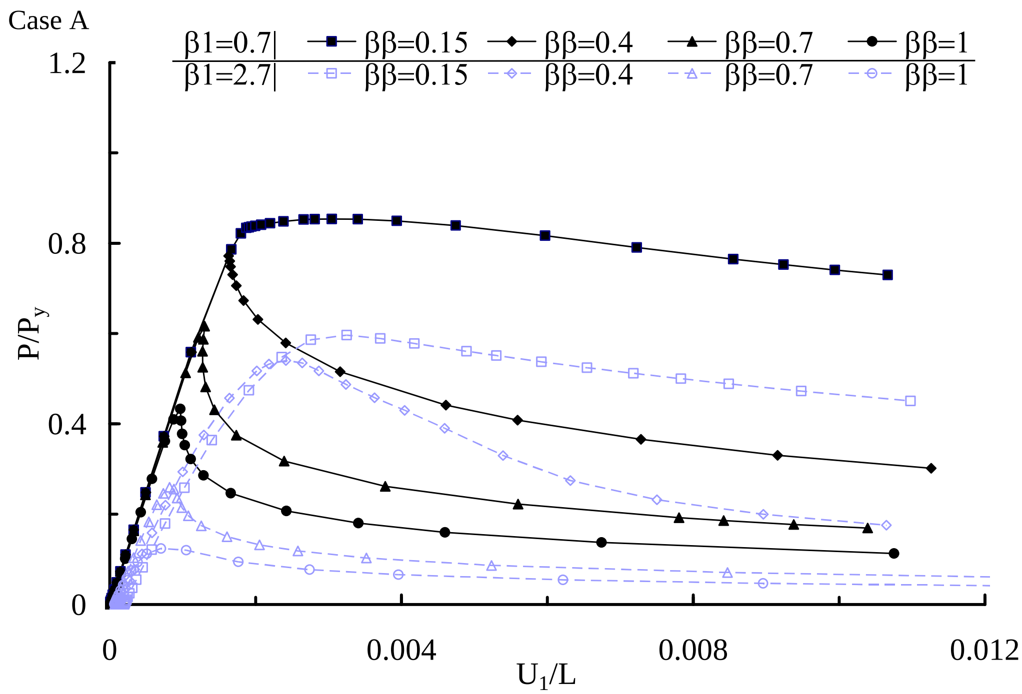

Figure E-117 Axial load versus axial shortening ($\beta_9 = 0.2$, $\beta_1 = 0.7$ & 2.7, $\beta_2 = 0.17$, $\beta_3 = 0.17$, $\beta_5 = 0.3$)

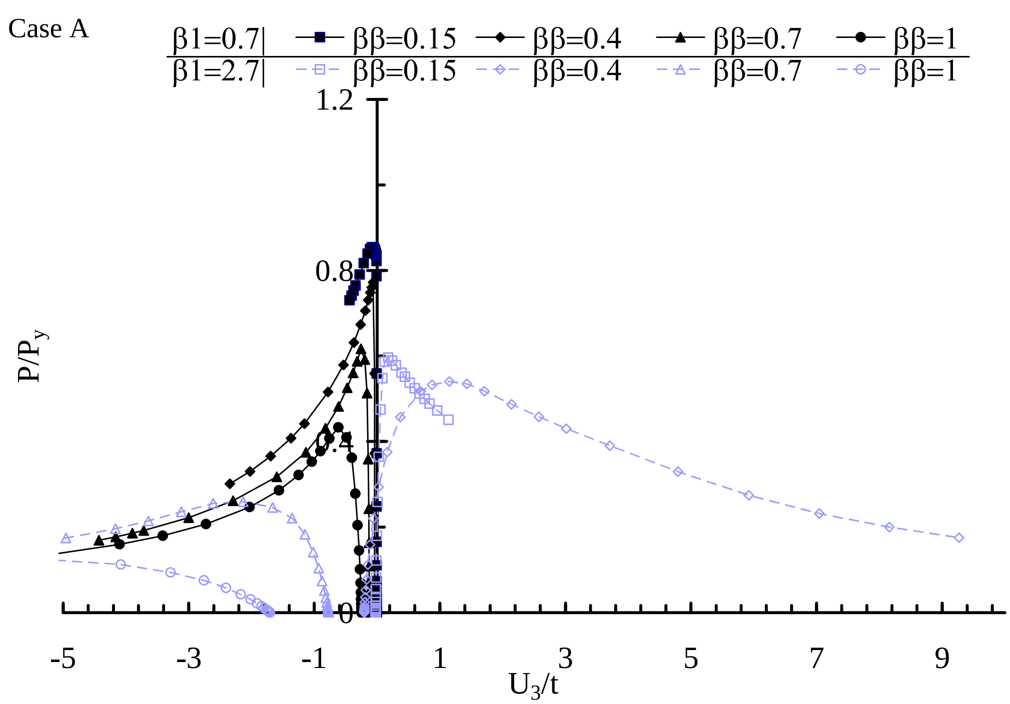

Figure E-118 Axial load versus lateral deflection ($\beta_9 = 0.2$, $\beta_1 = 0.7$ & 2.7, $\beta_2 = 0.17$, $\beta_3 = 0.17$, $\beta_5 = 0.3$)

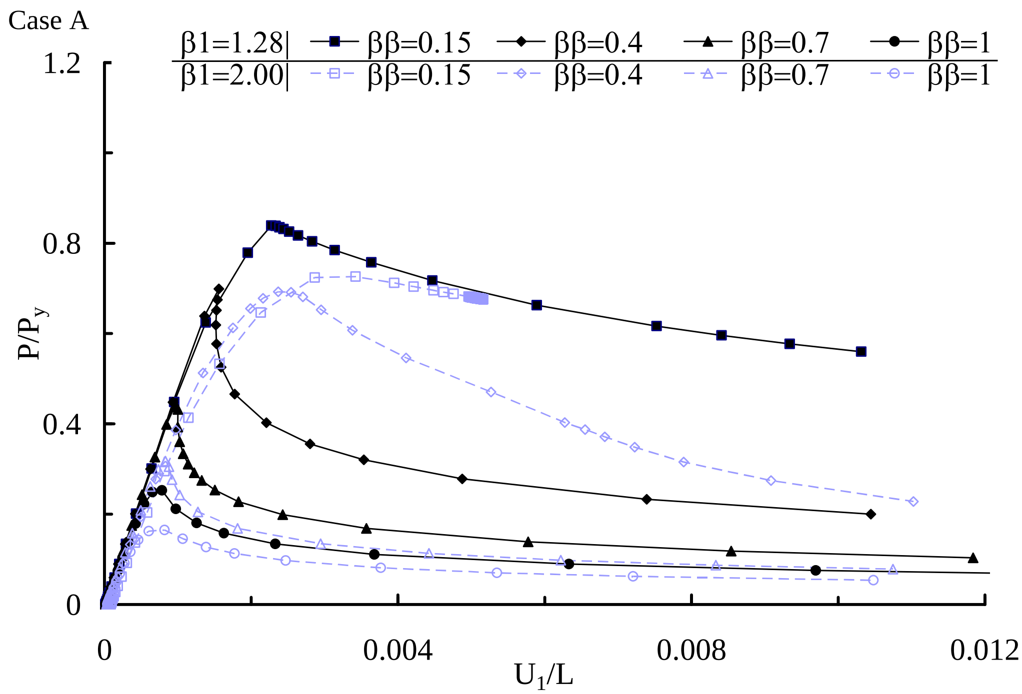

Figure E-119 Axial load versus axial shortening ($\beta_9 = 0.2$, $\beta_1 = 1.28$ & 2.0, $\beta_2 = 0.17$, $\beta_3 = 0.17$, $\beta_5 = 0.3$)

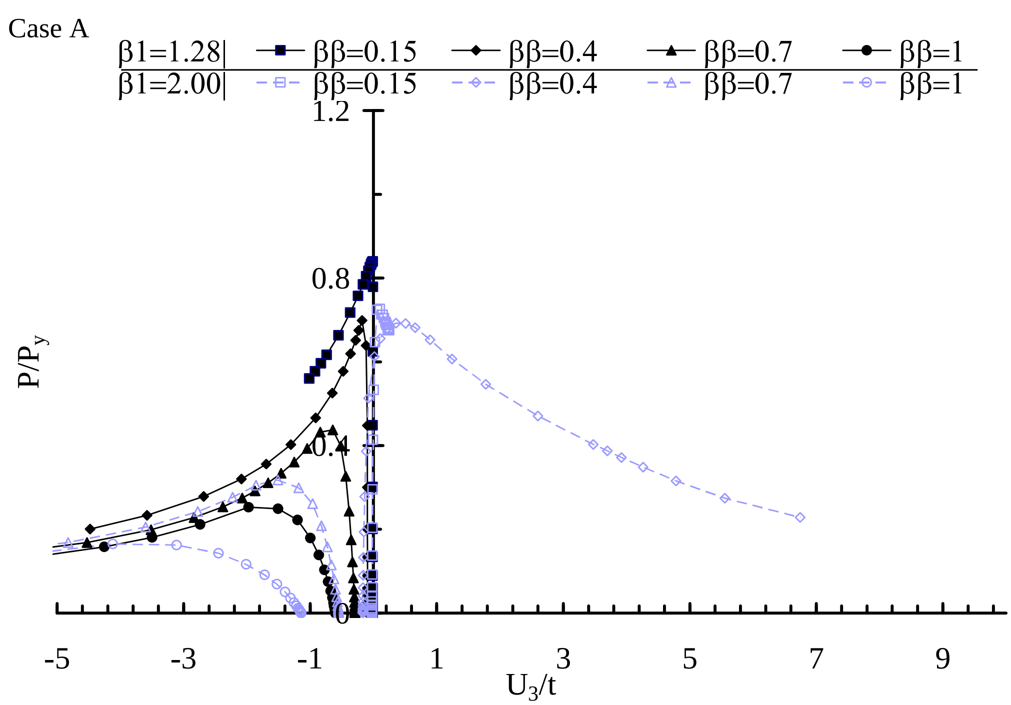

Figure E-120 Axial load versus lateral deflection ($\beta_9 = 0.2$, $\beta_1 = 1.28$ & 2.0, $\beta_2 = 0.17$, $\beta_3 = 0.17$, $\beta_5 = 0.3$)

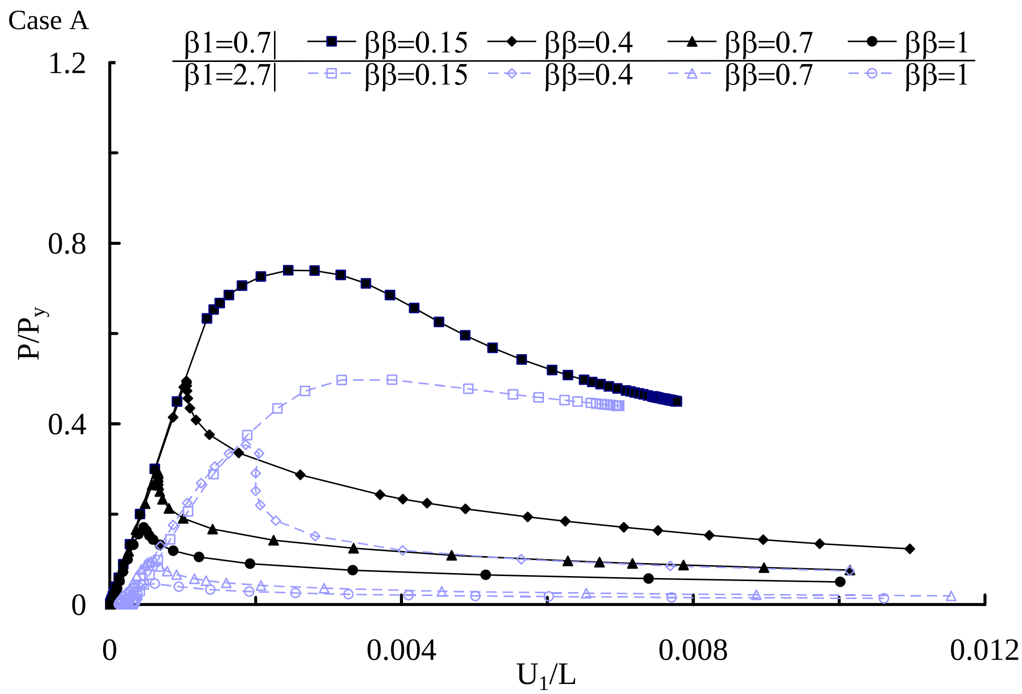

Figure E-121 Axial load versus axial shortening ($\beta_9 = 0.2$, $\beta_1 = 0.7$ & 2.7, $\beta_2 = 0.8$, $\beta_3 = 0.6$, $\beta_5 = 0.075$)

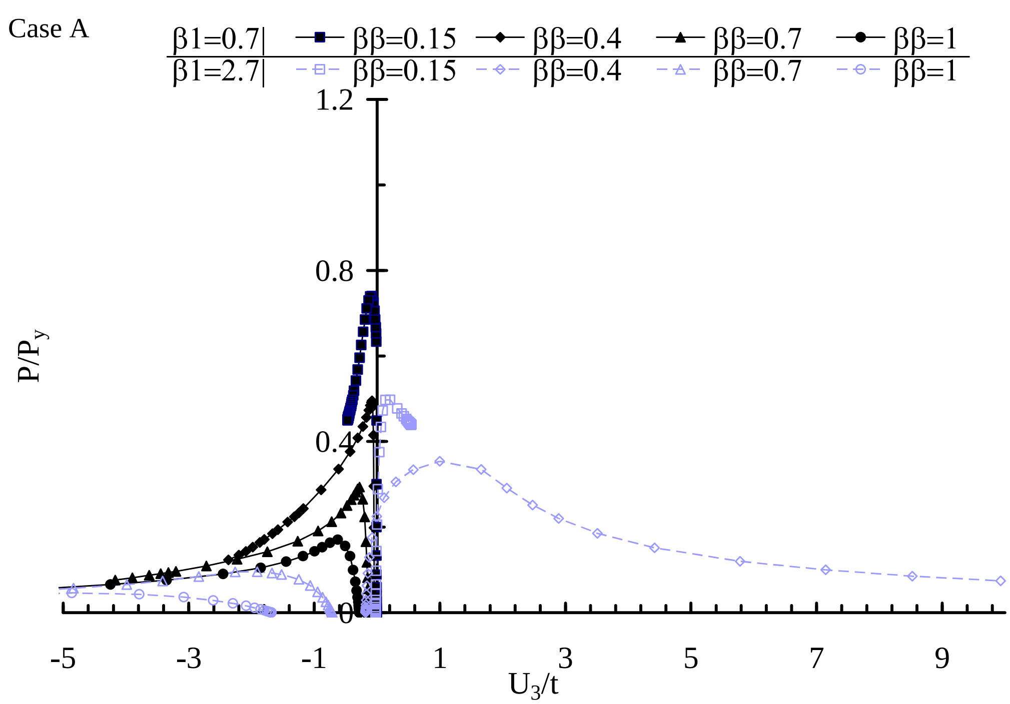

Figure E-122 Axial load versus lateral deflection ($\beta_9 = 0.2$, $\beta_1 = 0.7$ & 2.7, $\beta_2 = 0.8$, $\beta_3 = 0.6$, $\beta_5 = 0.075$)

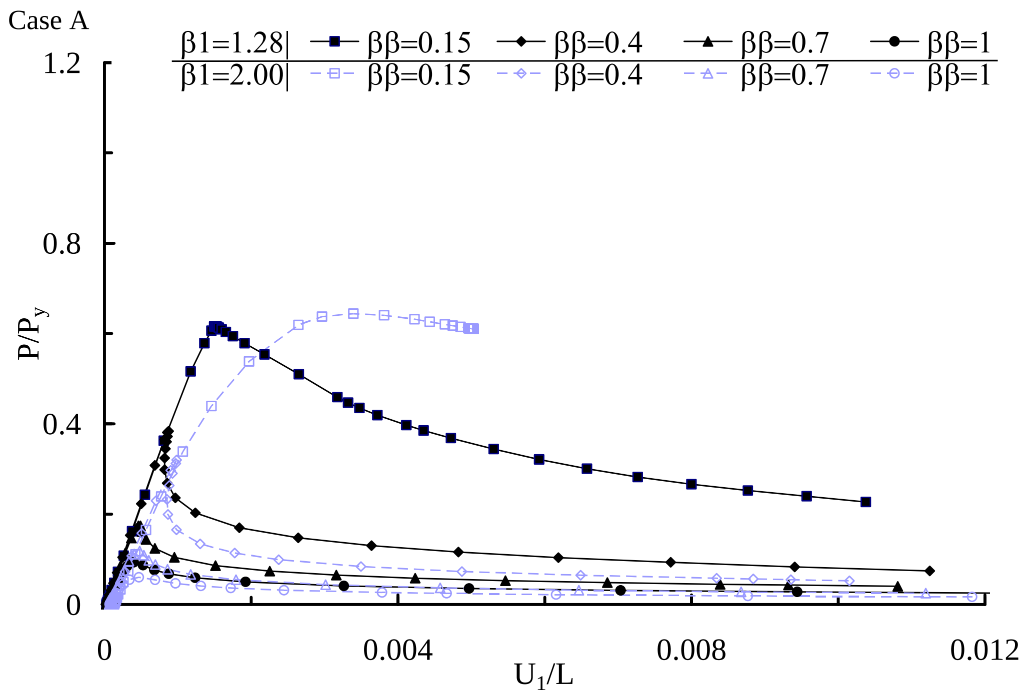

Figure E-123 Axial load versus axial shortening ($\beta_9 = 0.2$, $\beta_1 = 1.28$ & 2.0, $\beta_2 = 0.8$, $\beta_3 = 0.6$, $\beta_5 = 0.075$)

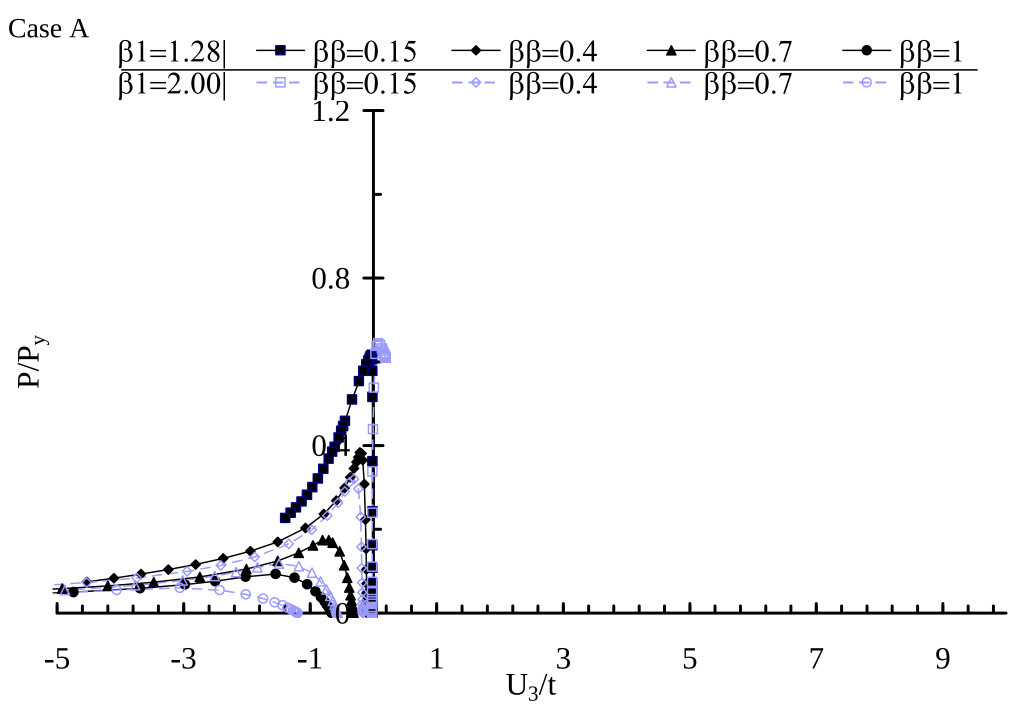

Figure E-124 Axial load versus lateral deflection ($\beta_9 = 0.2$, $\beta_1 = 1.28$ & 2.0, $\beta_2 = 0.8$, $\beta_3 = 0.6$, $\beta_5 = 0.075$)

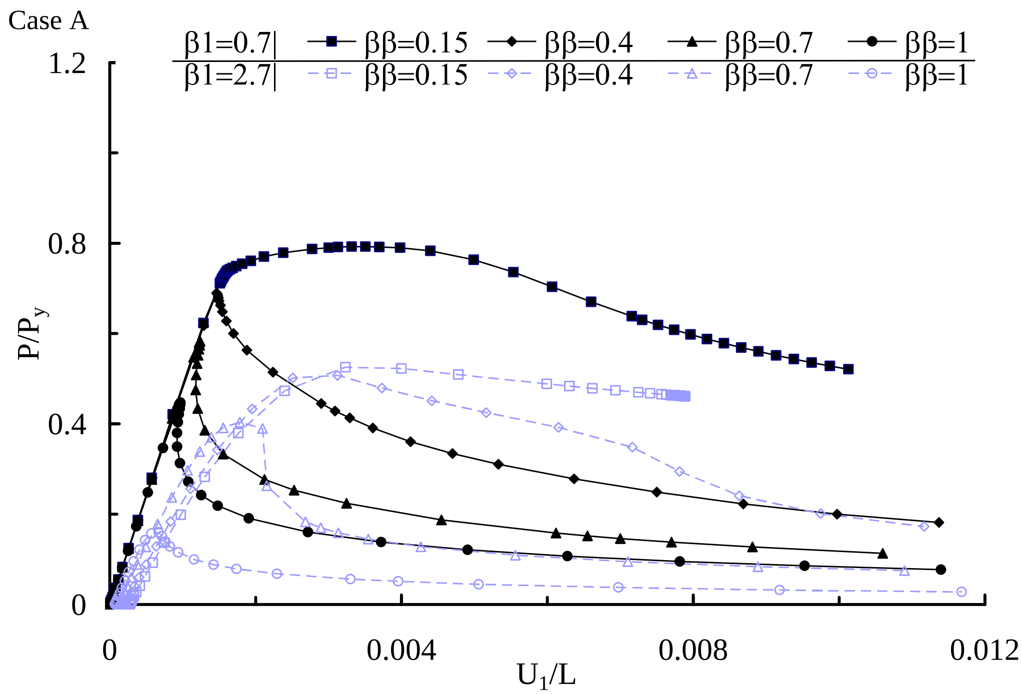

Figure E-125 Axial load versus axial shortening ($\beta_9 = 0.2$, $\beta_1 = 0.7$ & 2.7, $\beta_2 = 0.8$, $\beta_3 = 0.6$, $\beta_5 = 0.15$)

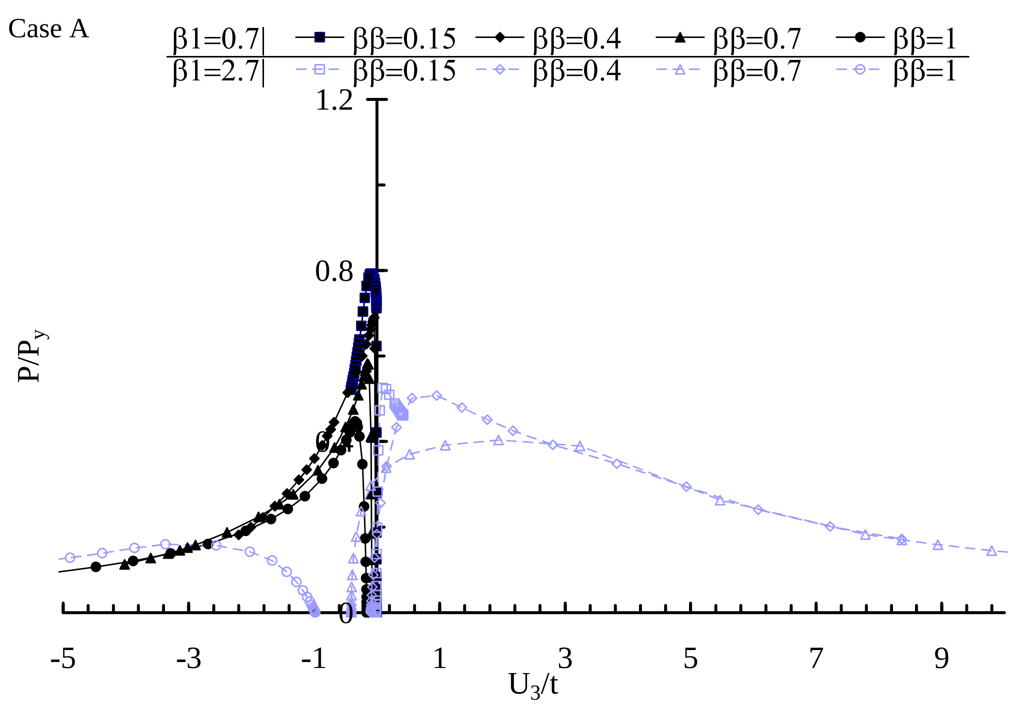

Figure E-126 Axial load versus lateral deflection ($\beta_9 = 0.2$, $\beta_1 = 0.7$ & 2.7, $\beta_2 = 0.8$, $\beta_3 = 0.6$, $\beta_5 = 0.15$)

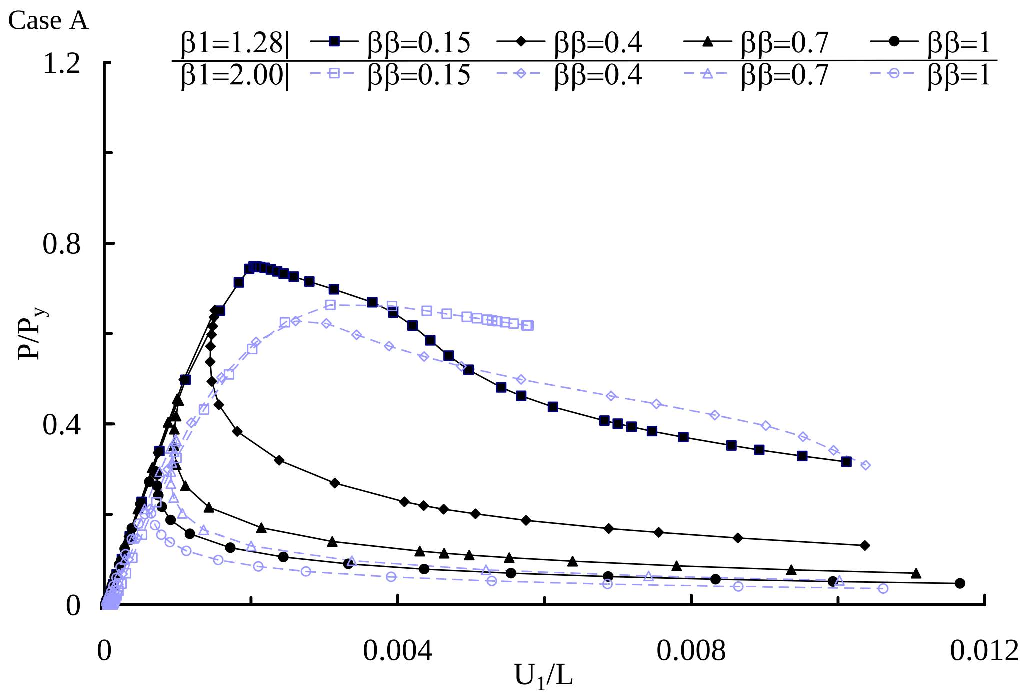

Figure E-127 Axial load versus axial shortening ($\beta_9 = 0.2$, $\beta_1 = 1.28$ & 2.0, $\beta_2 = 0.8$, $\beta_3 = 0.6$, $\beta_5 = 0.15$)

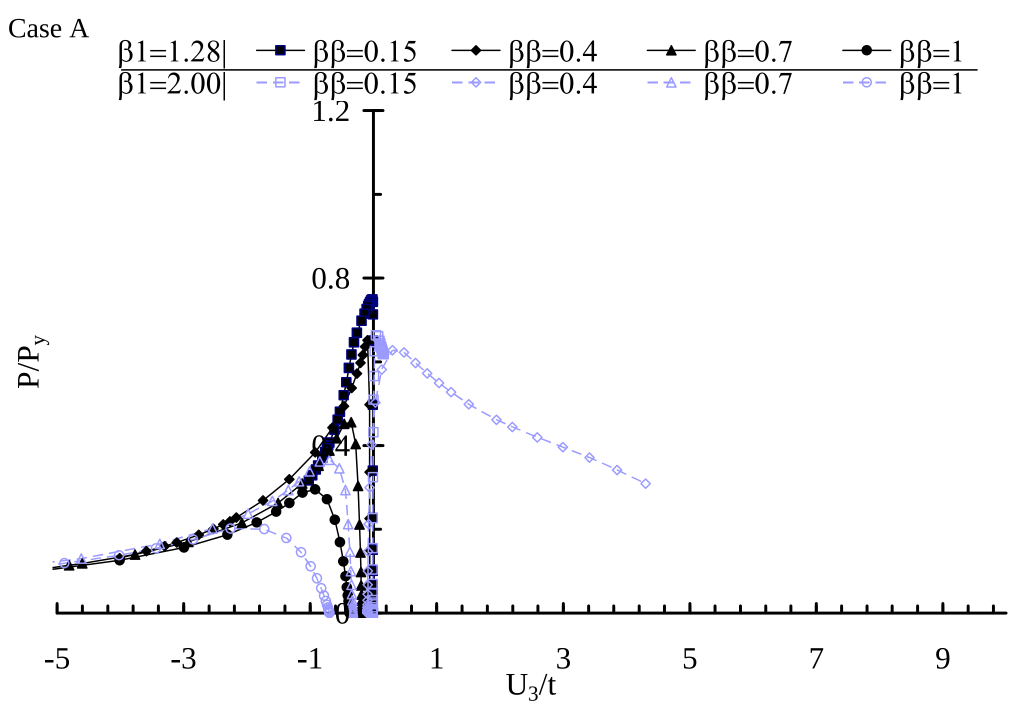

Figure E-128 Axial load versus lateral deflection ($\beta_9 = 0.2$, $\beta_1 = 1.28$ & 2.0, $\beta_2 = 0.8$, $\beta_3 = 0.6$, $\beta_5 = 0.15$)

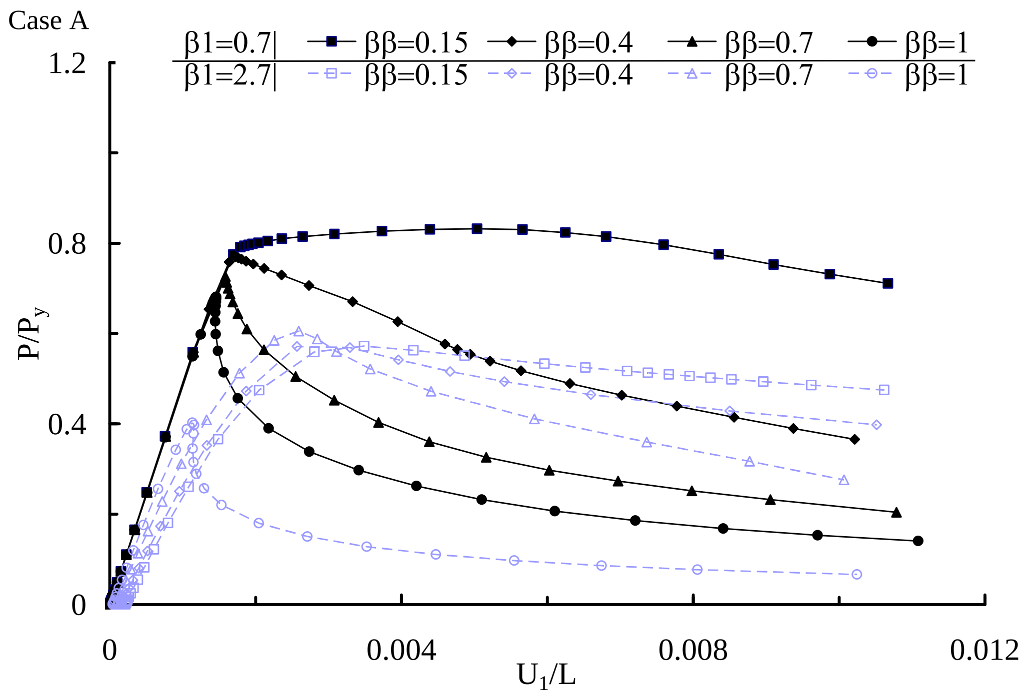

Figure E-129 Axial load versus axial shortening ($\beta_9 = 0.2$, $\beta_1 = 0.7$ & 2.7, $\beta_2 = 0.8$, $\beta_3 = 0.6$, $\beta_5 = 0.3$)

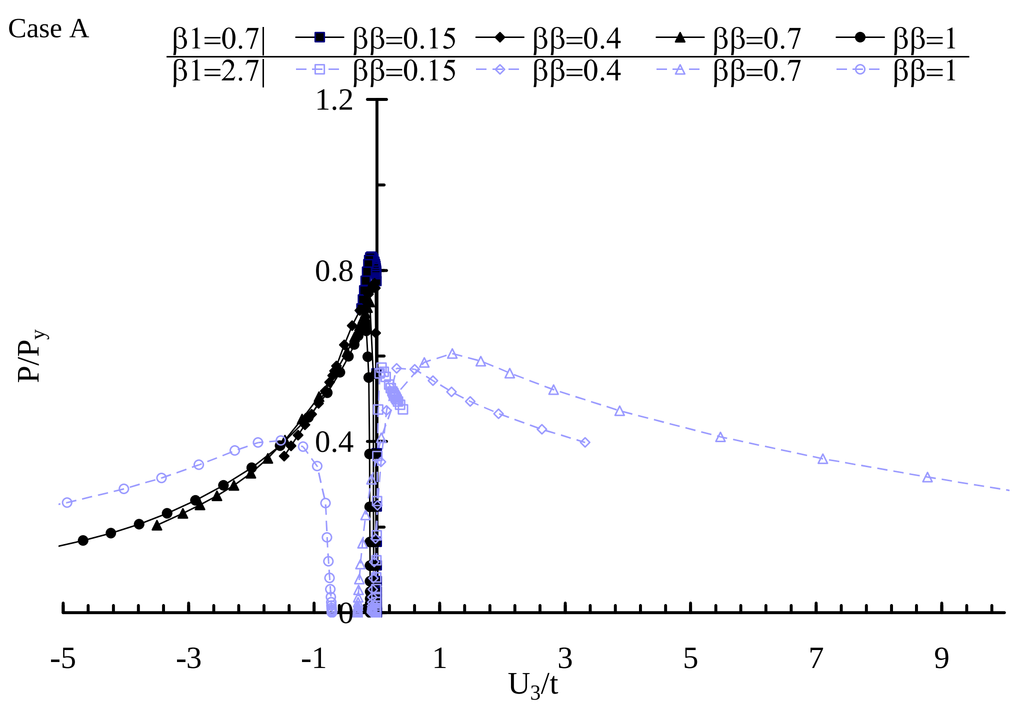

Figure E-130 Axial load versus lateral deflection ($\beta_9 = 0.2$, $\beta_1 = 0.7$ & 2.7, $\beta_2 = 0.8$, $\beta_3 = 0.6$, $\beta_5 = 0.3$)

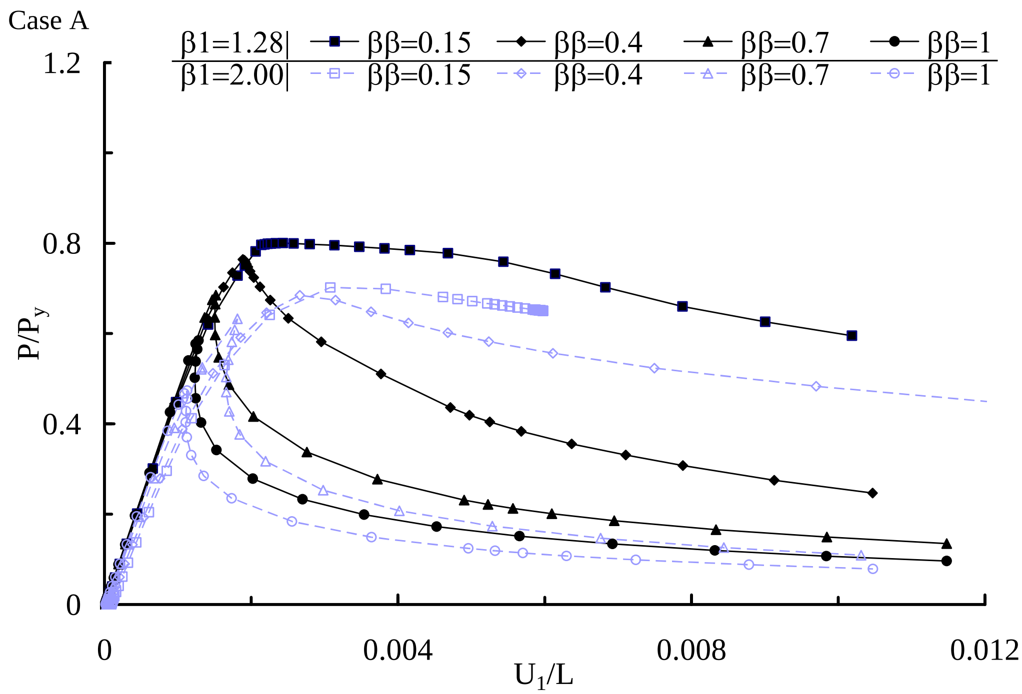

Figure E-131 Axial load versus axial shortening ($\beta_9 = 0.2$, $\beta_1 = 1.28$ & 2.0, $\beta_2 = 0.8$, $\beta_3 = 0.6$, $\beta_5 = 0.3$)

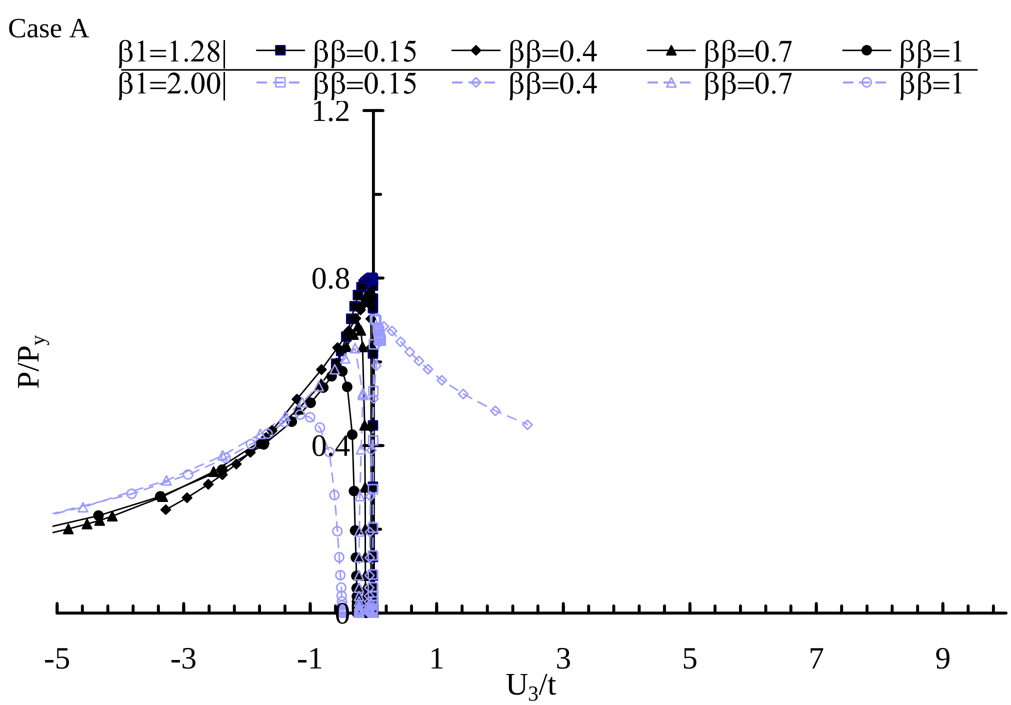

Figure E-132 Axial load versus lateral deflection ($\beta_9 = 0.2$, $\beta_1 = 1.28$ & 2.0, $\beta_2 = 0.8$, $\beta_3 = 0.6$, $\beta_5 = 0.3$))

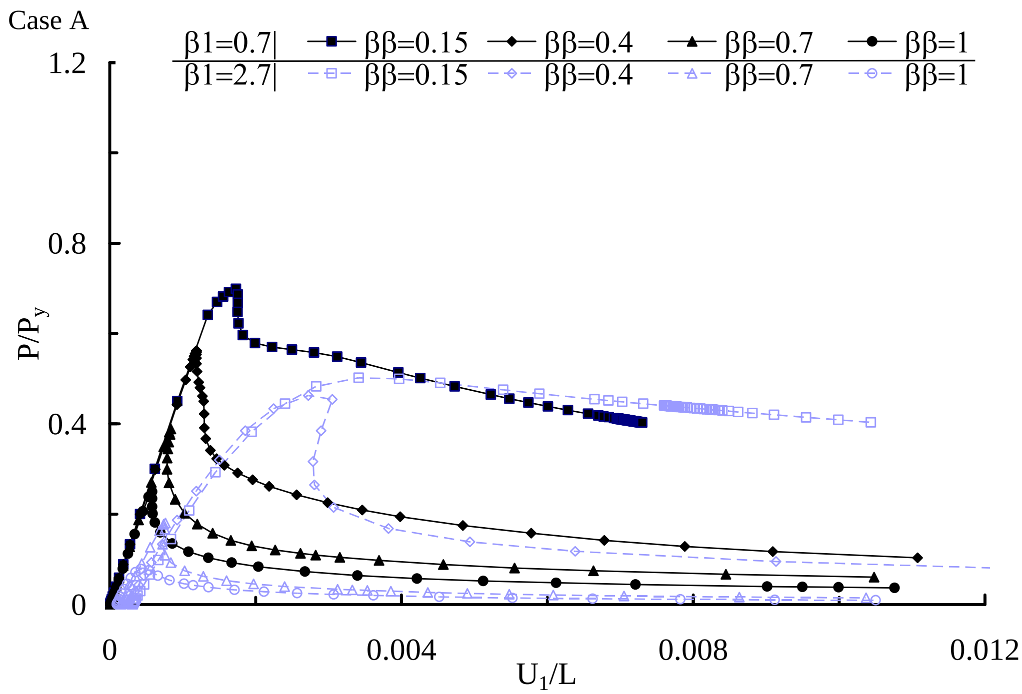

Figure E-133 Axial load versus axial shortening ($\beta_9 = 0.2$, $\beta_1 = 0.7$ & 2.7, $\beta_2 = 1.5$, $\beta_3 = 0.9$, $\beta_5 = 0.075$)

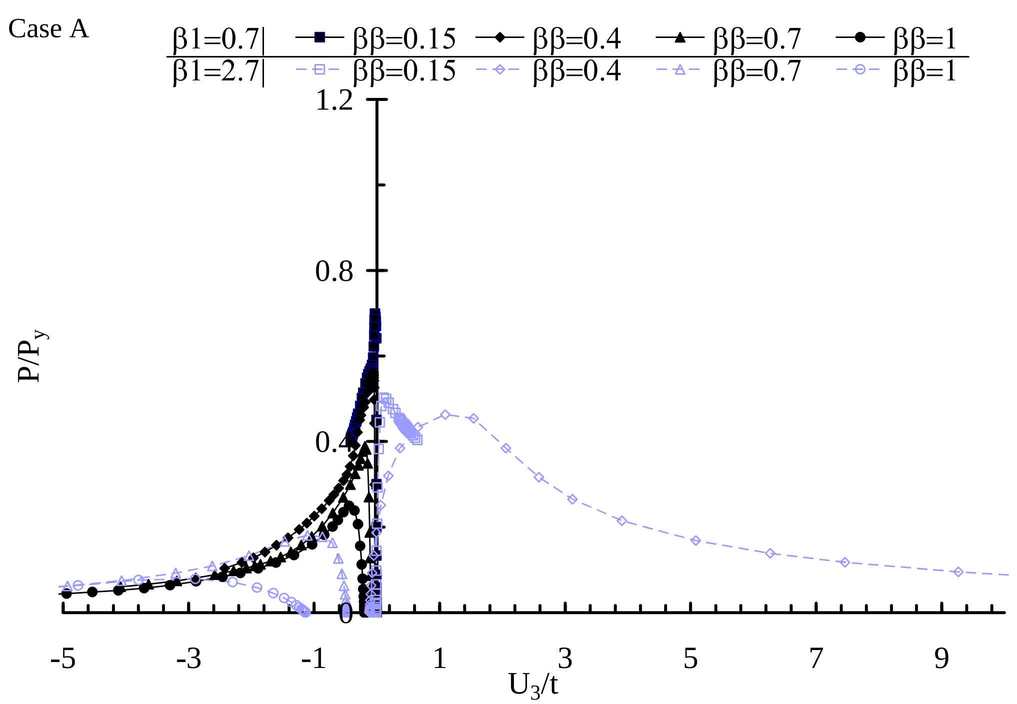

Figure E-134 Axial load versus lateral deflection ($\beta_9 = 0.2$, $\beta_1 = 0.7$ & 2.7, $\beta_2 = 1.5$, $\beta_3 = 0.9$, $\beta_5 = 0.075$)

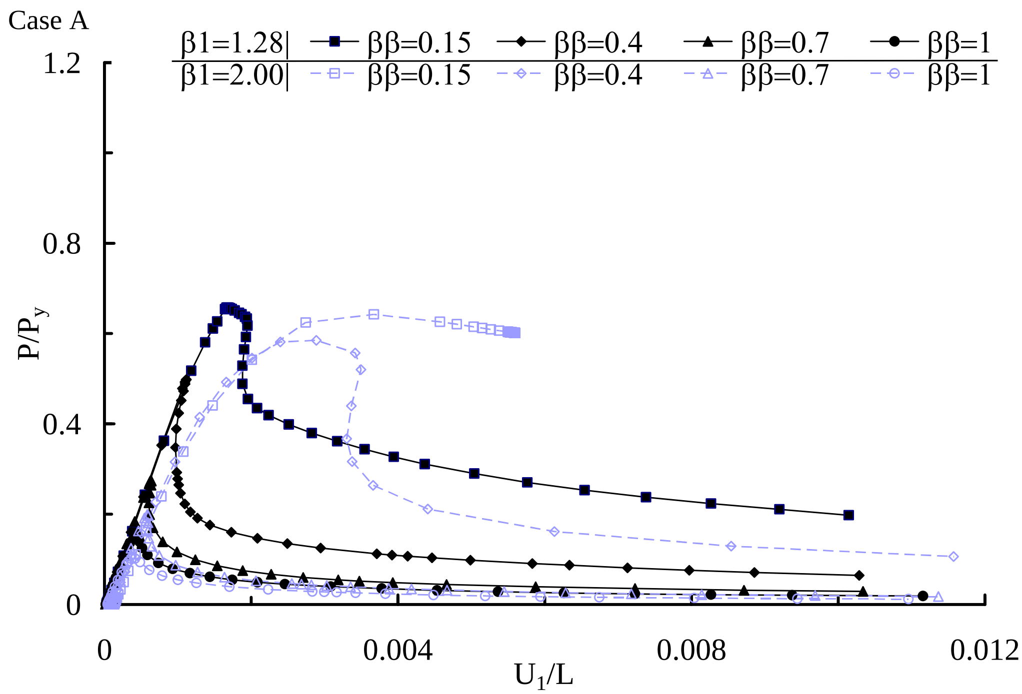

Figure E-135 Axial load versus axial shortening ($\beta_9 = 0.2$, $\beta_1 = 1.28$ & 2.0, $\beta_2 = 1.5$, $\beta_3 = 0.9$, $\beta_5 = 0.075$)

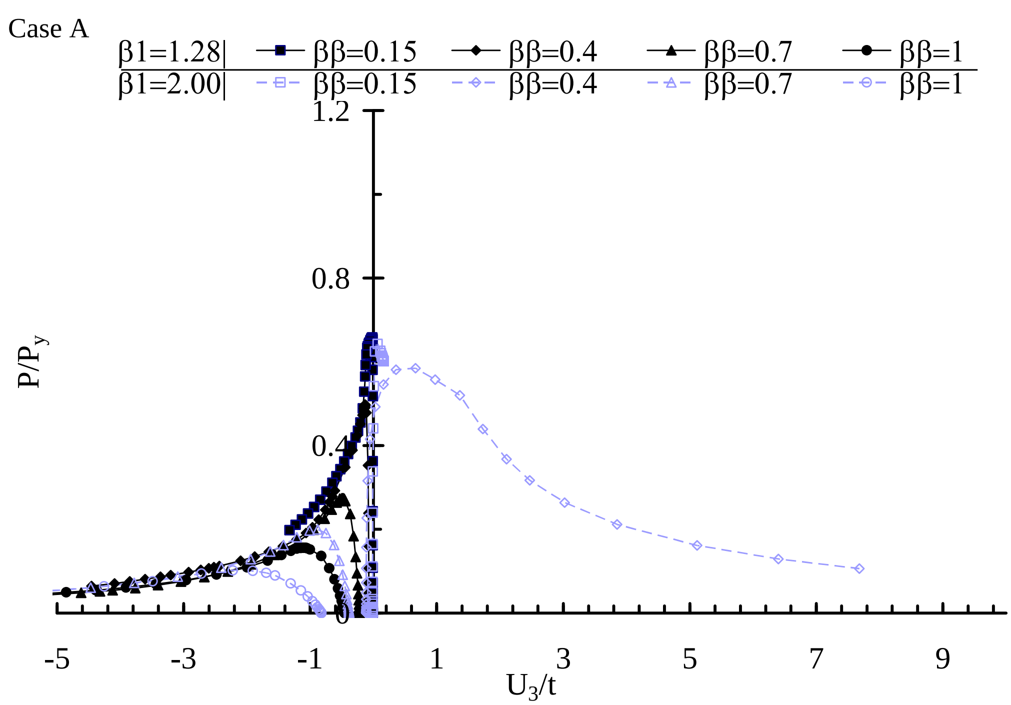

Figure E-136 Axial load versus lateral deflection ($\beta_9 = 0.2$, $\beta_1 = 1.28$ & 2.0, $\beta_2 = 1.5$, $\beta_3 = 0.9$, $\beta_5 = 0.075$)

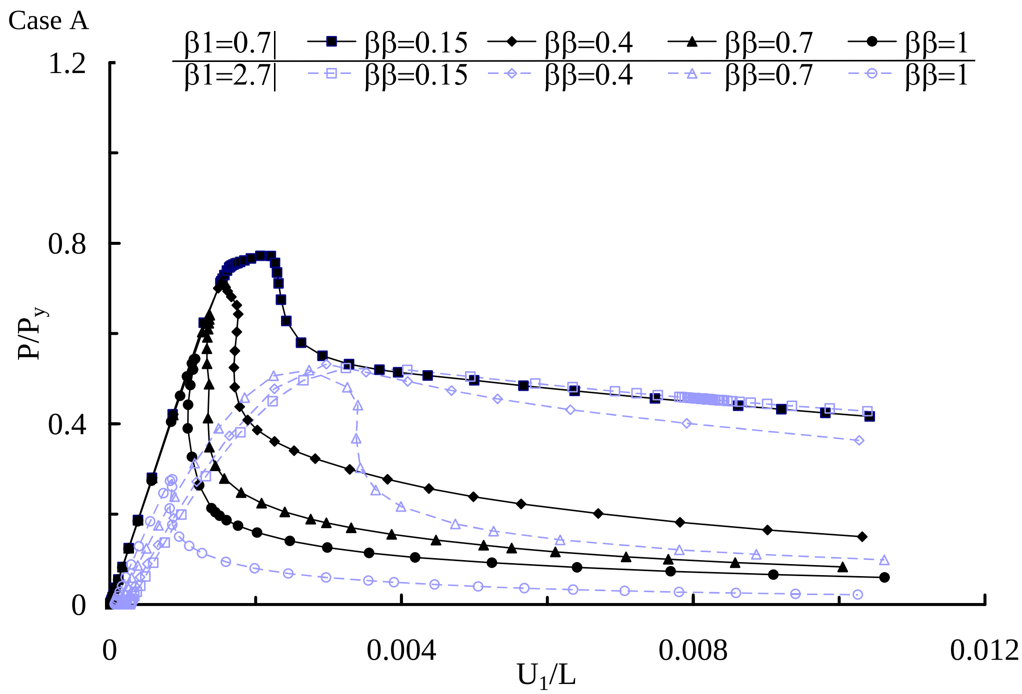

Figure E-137 Axial load versus axial shortening ($\beta_9 = 0.2$, $\beta_1 = 0.7$ & 2.7, $\beta_2 = 1.5$, $\beta_3 = 0.9$, $\beta_5 = 0.15$)

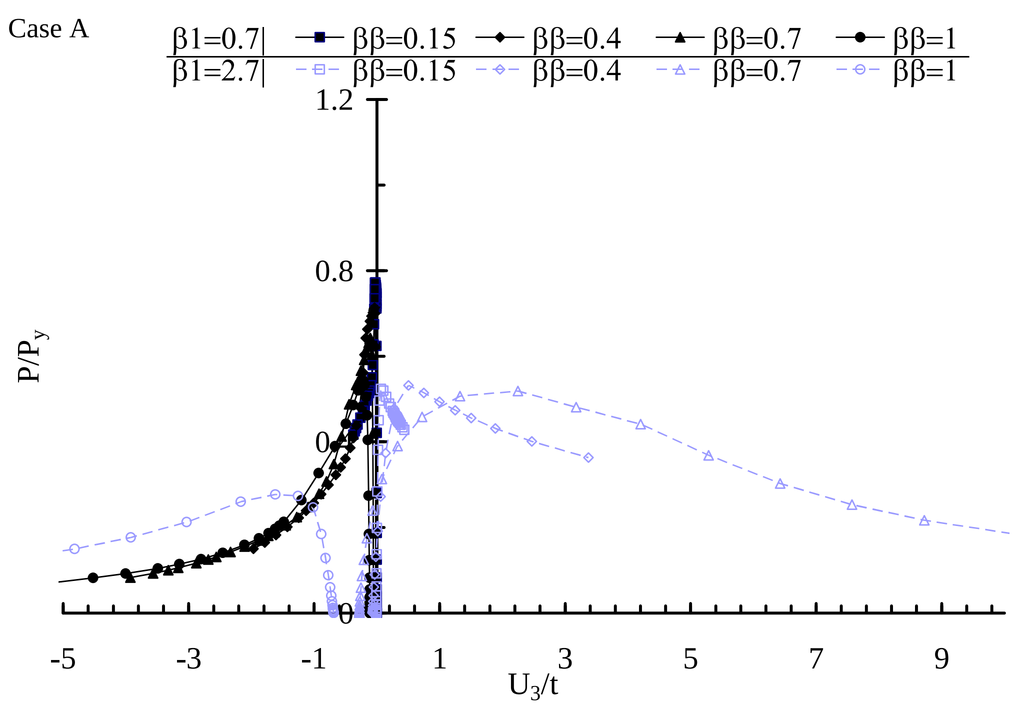

Figure E-138 Axial load versus lateral deflection ($\beta_9 = 0.2$, $\beta_1 = 0.7$ & 2.7, $\beta_2 = 1.5$, $\beta_3 = 0.9$, $\beta_5 = 0.15$)

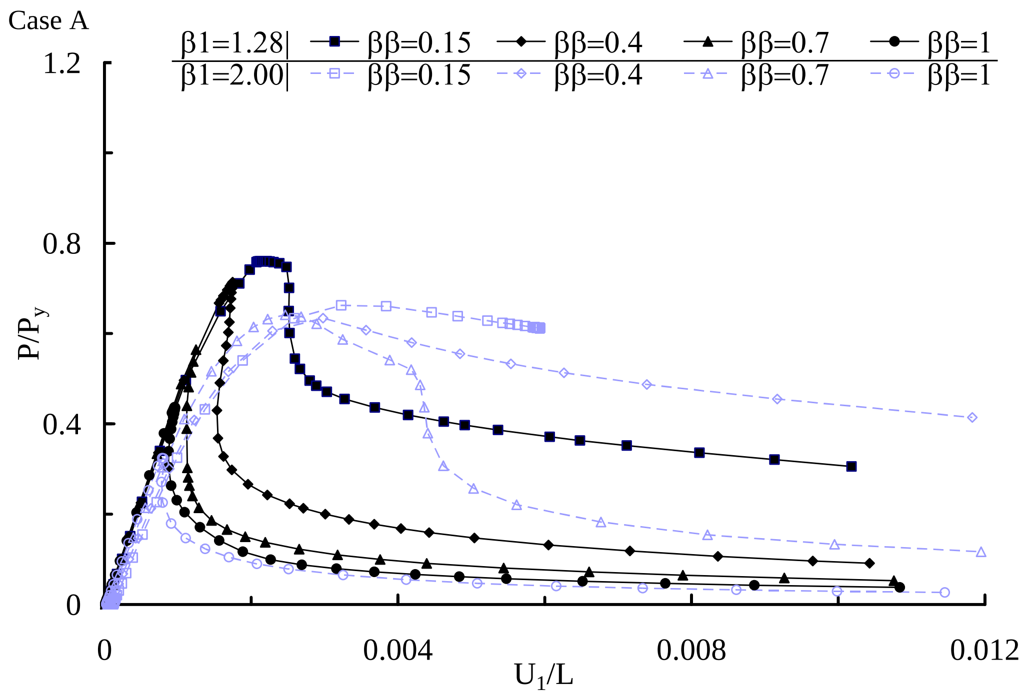

Figure E-139 Axial load versus axial shortening ($\beta_9 = 0.2$, $\beta_1 = 1.28$ & 2.0, $\beta_2 = 1.5$, $\beta_3 = 0.9$, $\beta_5 = 0.15$)

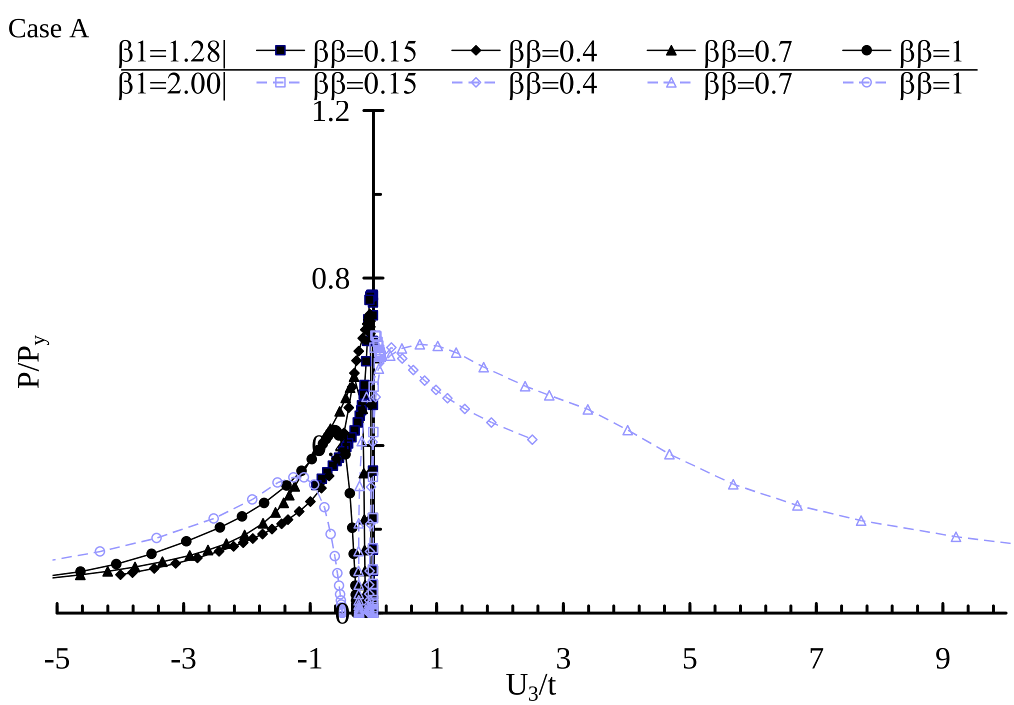

Figure E-140 Axial load versus lateral deflection ($\beta_9 = 0.2$, $\beta_1 = 1.28$ & 2.0, $\beta_2 = 1.5$, $\beta_3 = 0.9$, $\beta_5 = 0.15$)

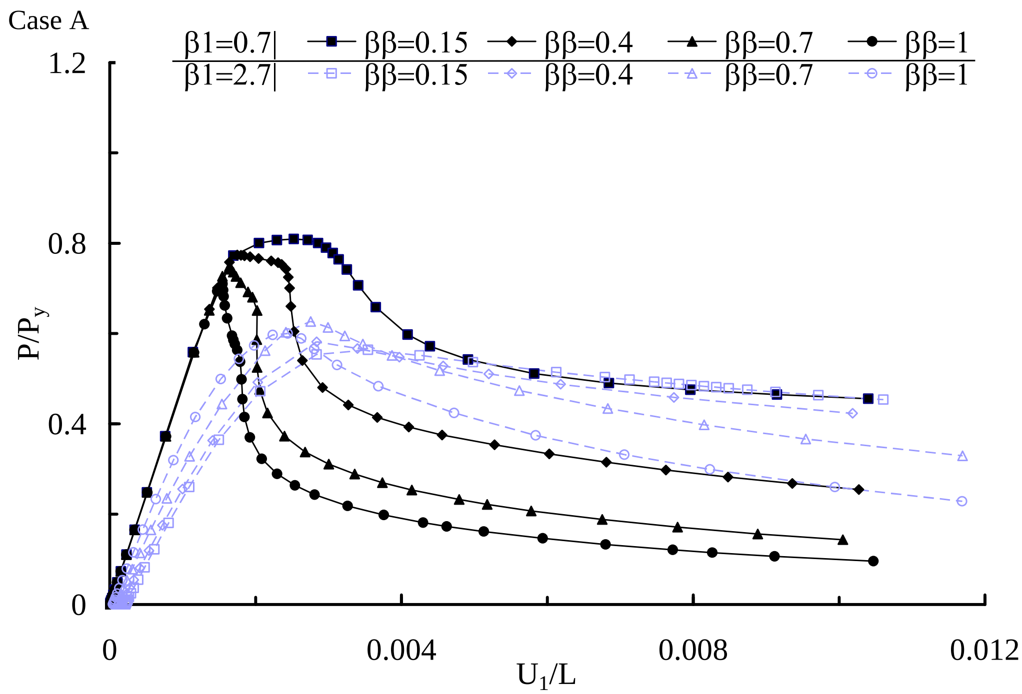

Figure E-141 Axial load versus axial shortening ($\beta_9 = 0.2$, $\beta_1 = 0.7$ & 2.7, $\beta_2 = 1.5$, $\beta_3 = 0.9$, $\beta_5 = 0.3$)

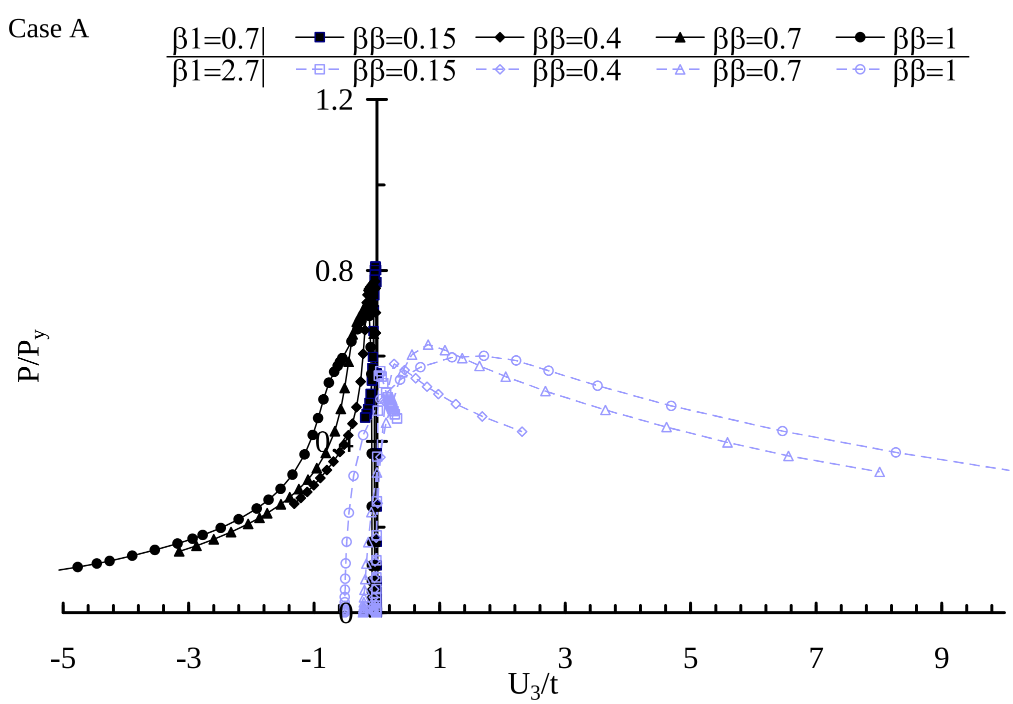

Figure E-142 Axial load versus lateral deflection ($\beta_9 = 0.2$, $\beta_1 = 0.7$ & 2.7, $\beta_2 = 1.5$, $\beta_3 = 0.9$, $\beta_5 = 0.3$)

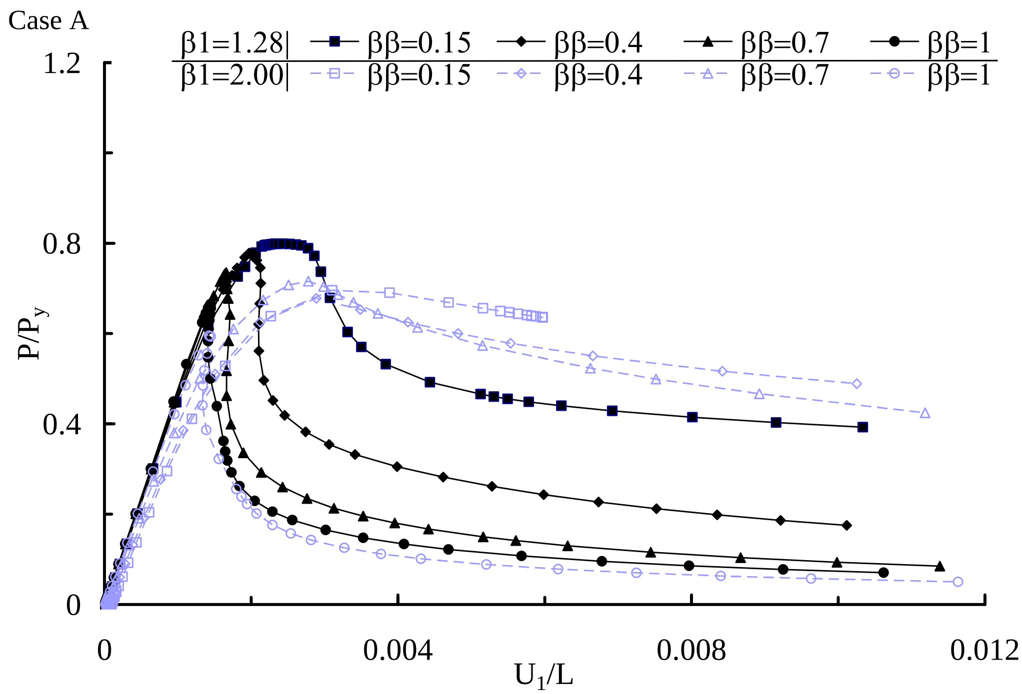

Figure E-143 Axial load versus axial shortening ($\beta_9 = 0.2$, $\beta_1 = 1.28$ & 2.0, $\beta_2 = 1.5$, $\beta_3 = 0.9$, $\beta_5 = 0.3$)

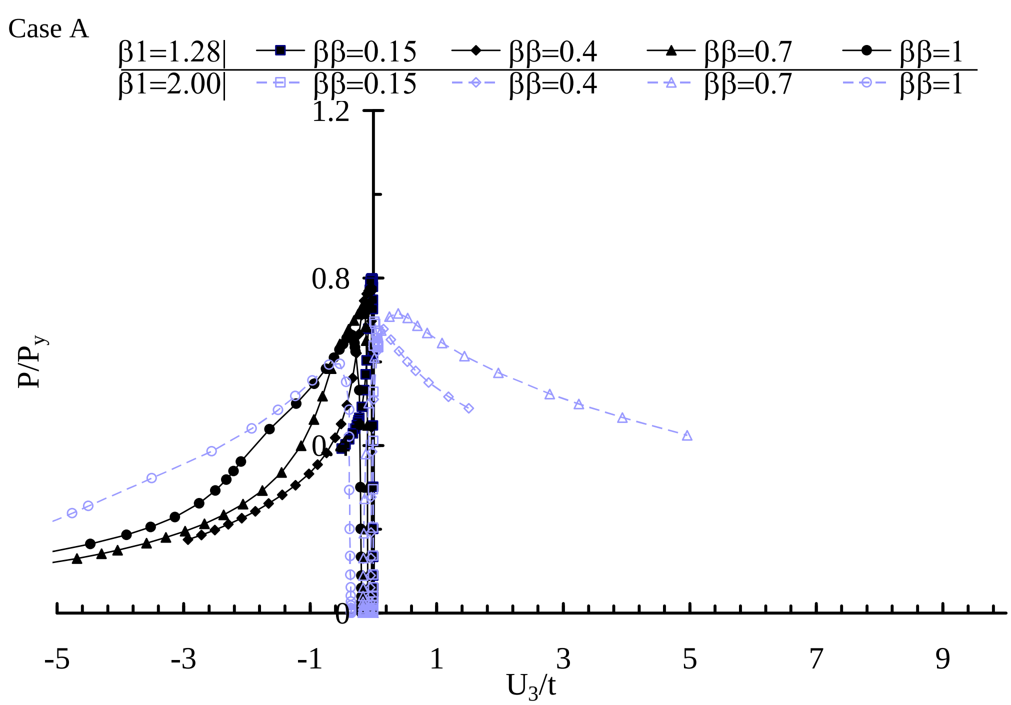

Figure E-144 Axial load versus lateral deflection ($\beta_9 = 0.2$, $\beta_1 = 1.28$ & 2.0, $\beta_2 = 1.5$, $\beta_3 = 0.9$, $\beta_5 = 0.3$)

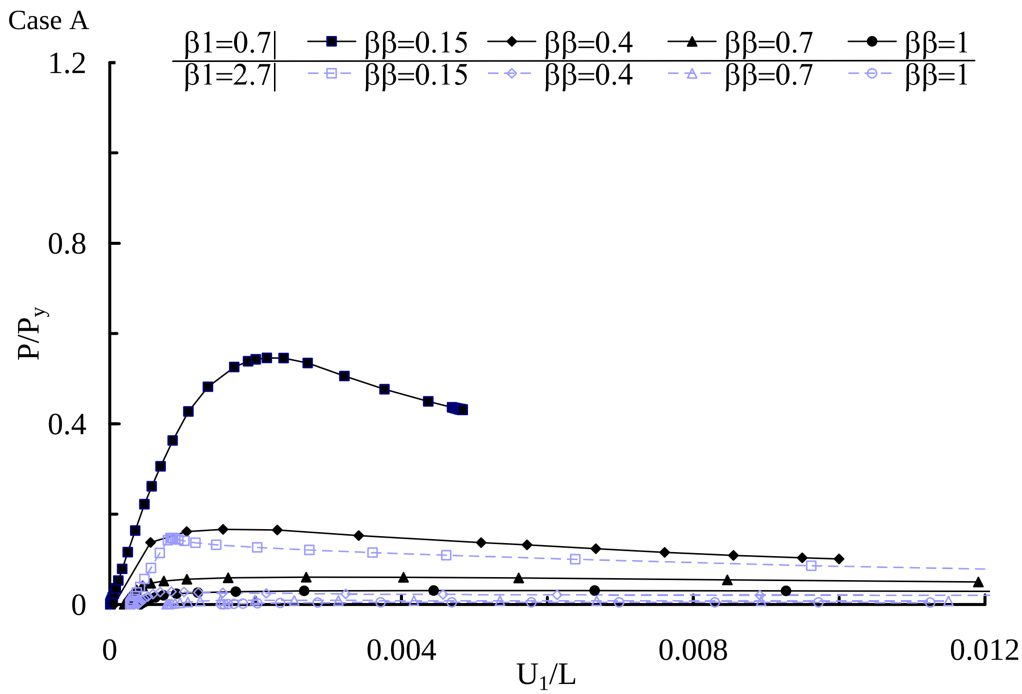

Figure E-145 Axial load versus axial shortening ($\beta_9 = 0.4$, $\beta_1 = 0.7$ & 2.7, $\beta_2 = 0.17$, $\beta_3 = 0.17$, $\beta_5 = 0.075$)

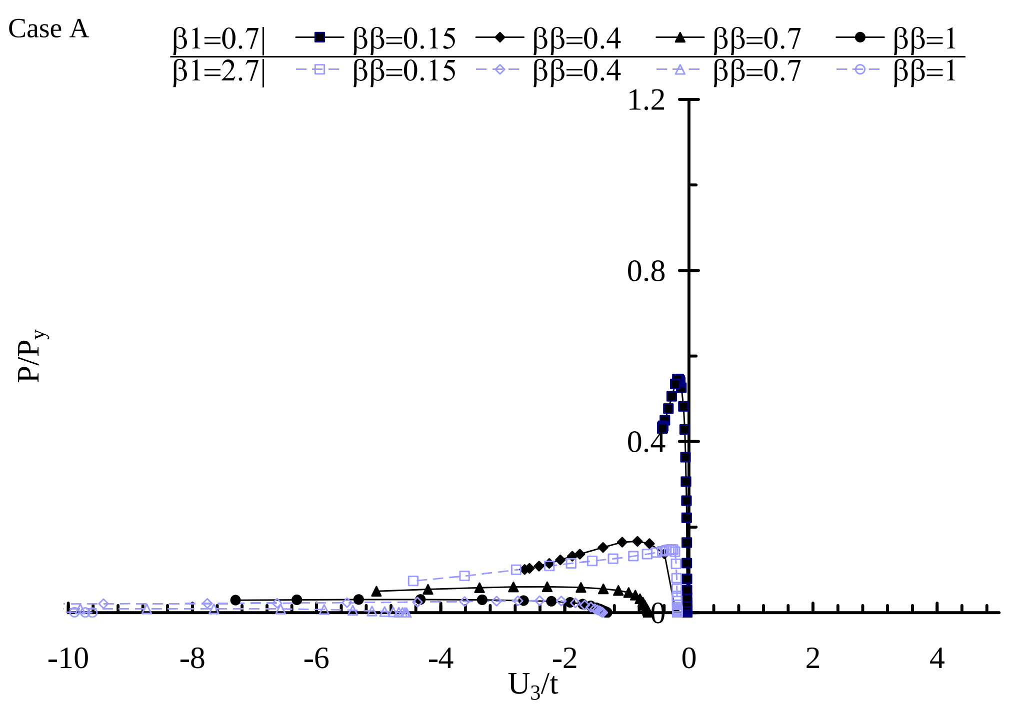

Figure E-146 Axial load versus lateral deflection ($\beta_9 = 0.4$, $\beta_1 = 0.7$ & 2.7, $\beta_2 = 0.17$, $\beta_3 = 0.17$, $\beta_5 = 0.075$)

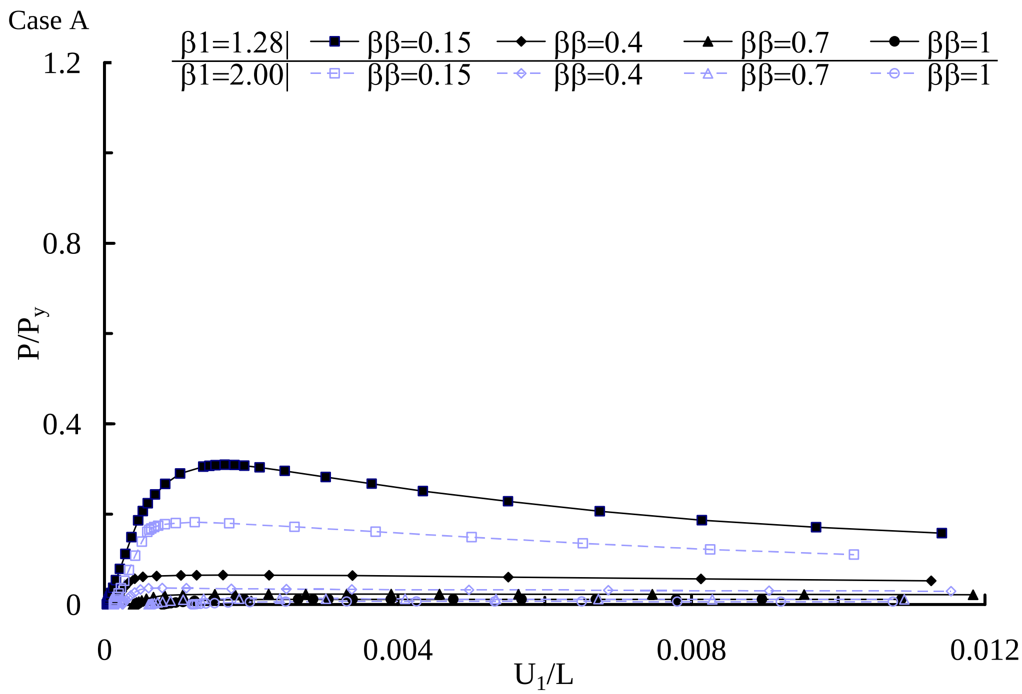

Figure E-147 Axial load versus axial shortening ($\beta_9 = 0.4$, $\beta_1 = 1.28$ & 2.0, $\beta_2 = 0.17$, $\beta_3 = 0.17$, $\beta_5 = 0.075$)

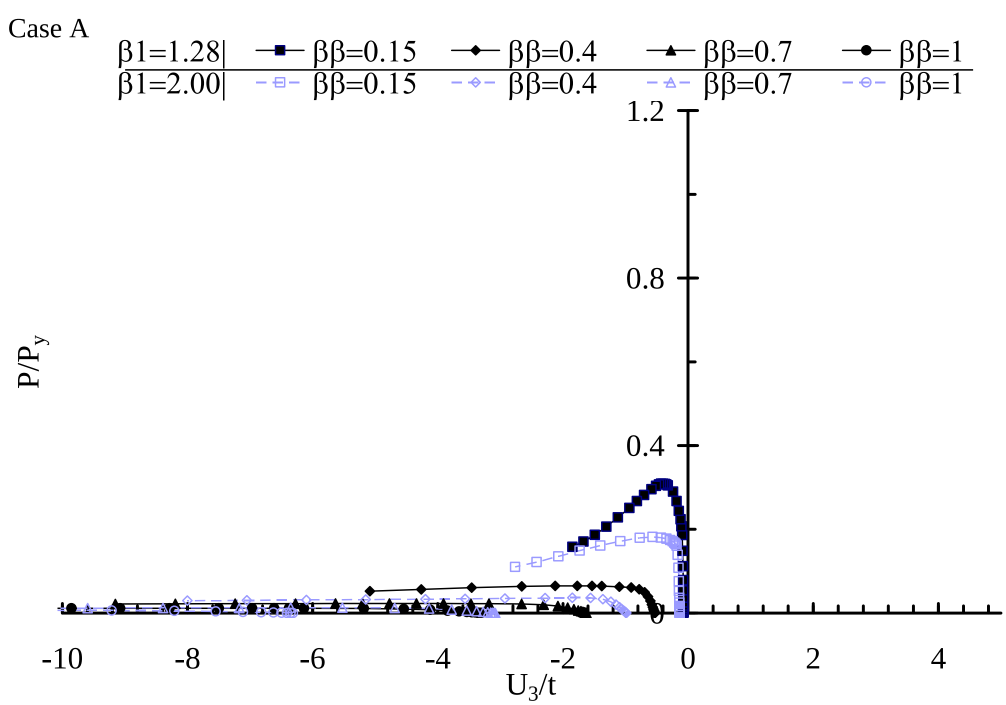

Figure E-148 Axial load versus lateral deflection ($\beta_9 = 0.4$, $\beta_1 = 1.28$ & 2.0, $\beta_2 = 0.17$, $\beta_3 = 0.17$, $\beta_5 = 0.075$)

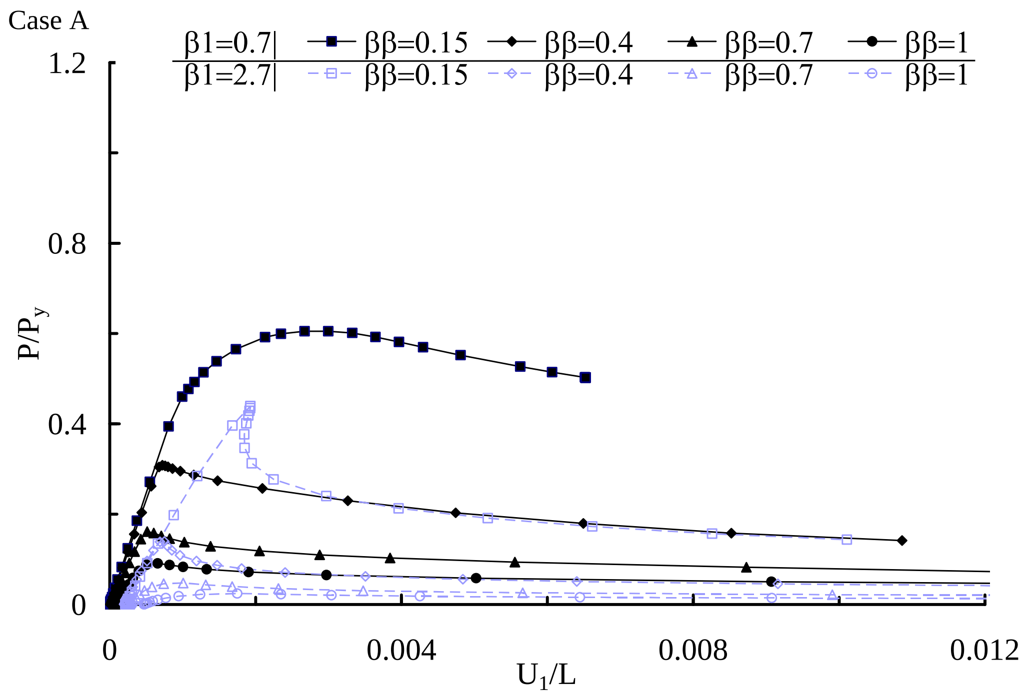

Figure E-149 Axial load versus axial shortening ($\beta_9 = 0.4$, $\beta_1 = 0.7$ & 2.7, $\beta_2 = 0.17$, $\beta_3 = 0.17$, $\beta_5 = 0.15$)

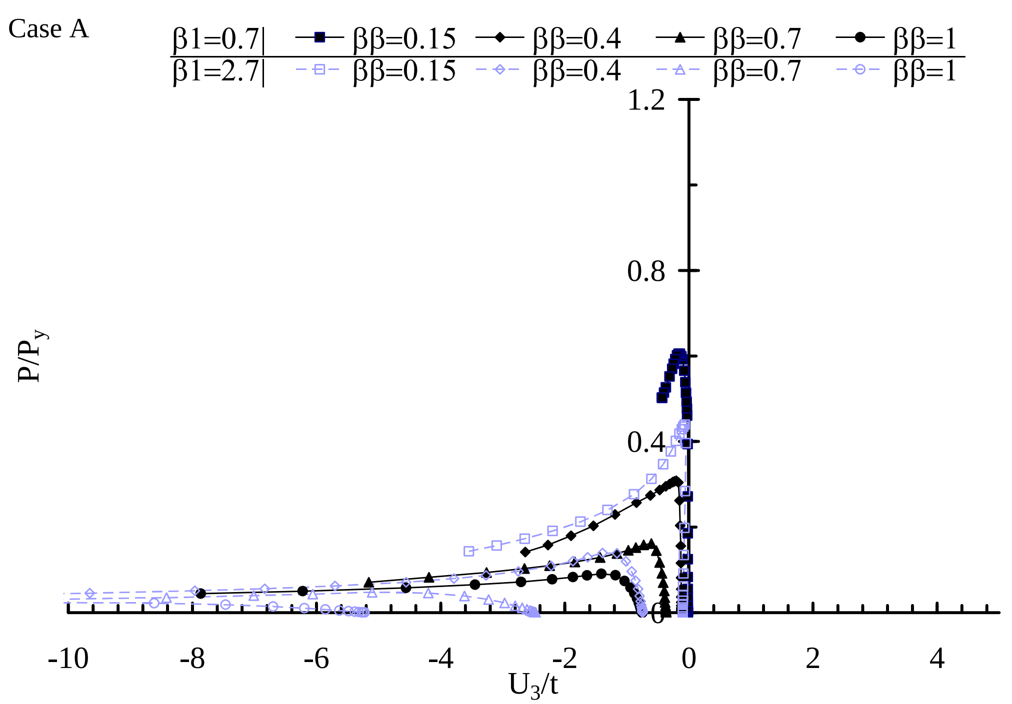

Figure E-150 Axial load versus lateral deflection ($\beta_9 = 0.4$, $\beta_1 = 0.7$ & 2.7, $\beta_2 = 0.17$, $\beta_3 = 0.17$, $\beta_5 = 0.15$)

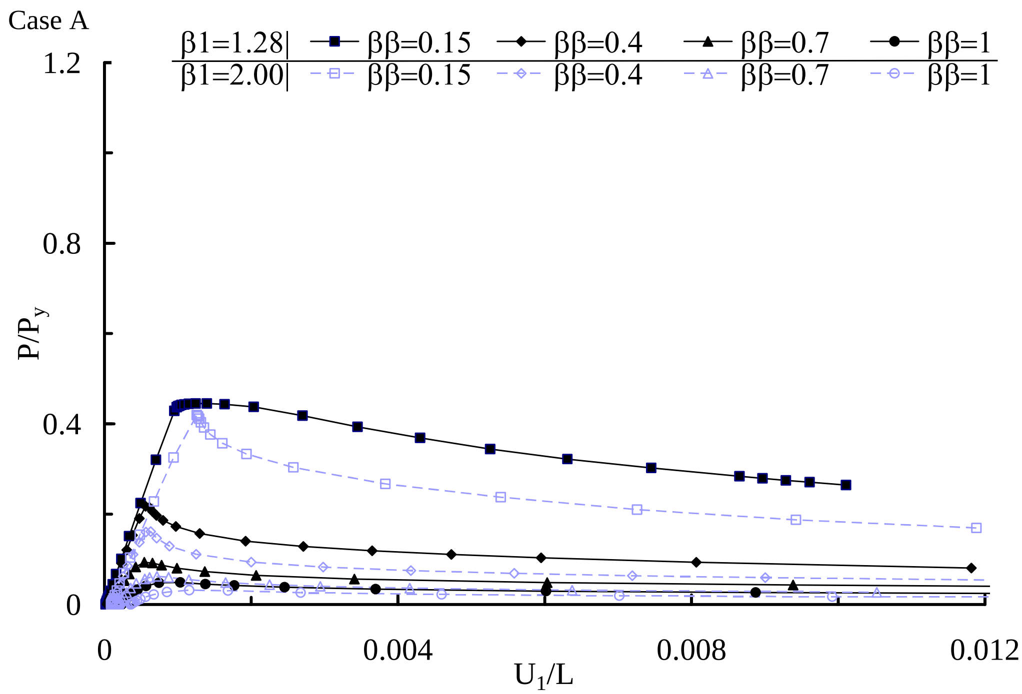

Figure E-151 Axial load versus axial shortening ($\beta_9 = 0.4$, $\beta_1 = 1.28$ & 2.0, $\beta_2 = 0.17$, $\beta_3 = 0.17$, $\beta_5 = 0.15$)

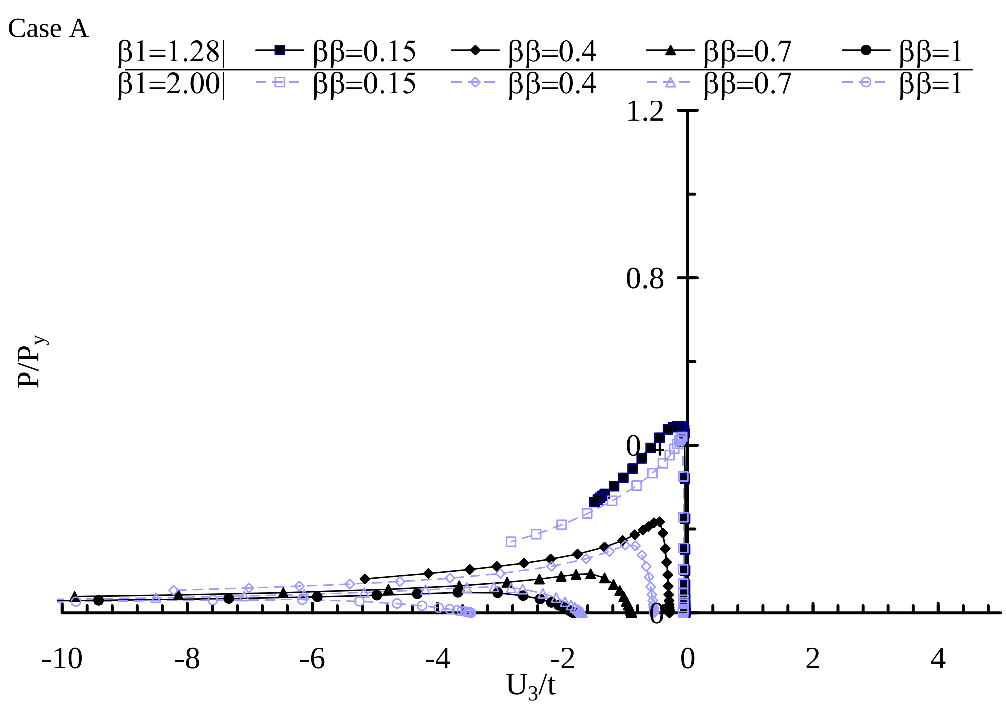

Figure E-152 Axial load versus lateral deflection ($\beta_9 = 0.4$, $\beta_1 = 1.28$ & 2.0, $\beta_2 = 0.17$, $\beta_3 = 0.17$, $\beta_5 = 0.15$)

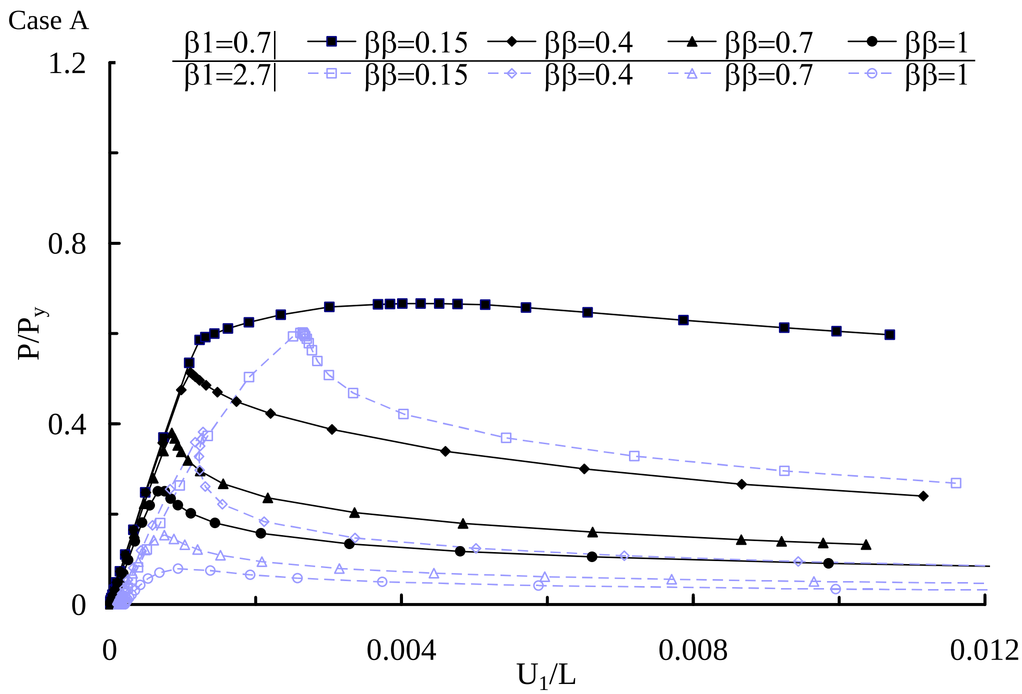

Figure E-153 Axial load versus axial shortening ($\beta_9 = 0.4$, $\beta_1 = 0.7$ & 2.7, $\beta_2 = 0.17$, $\beta_3 = 0.17$, $\beta_5 = 0.3$)

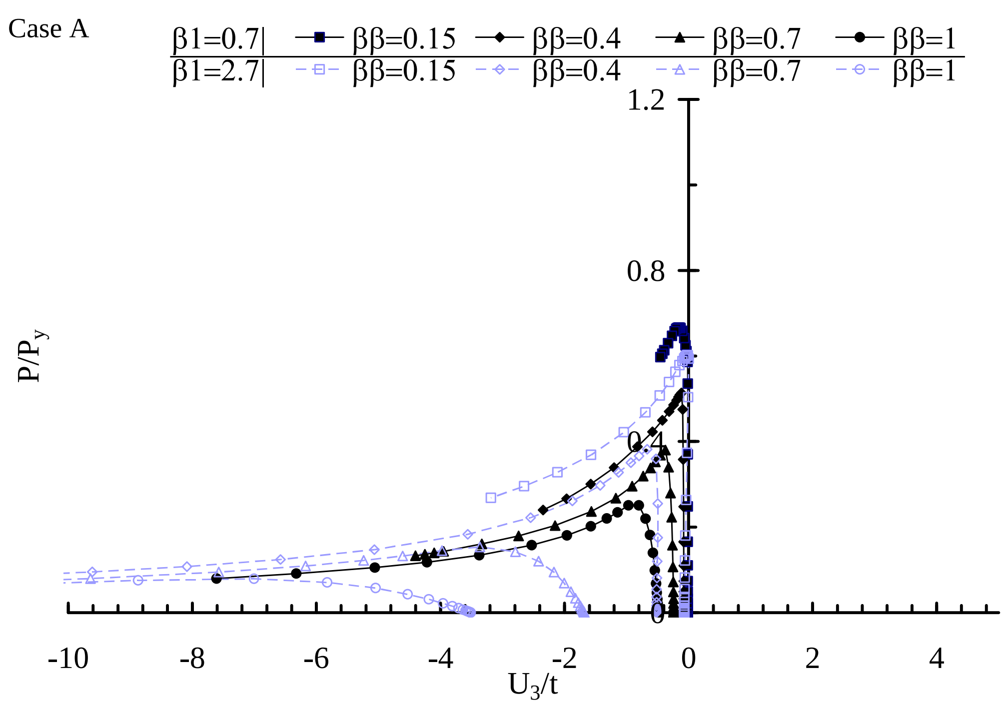

Figure E-154 Axial load versus lateral deflection ($\beta_9 = 0.4$, $\beta_1 = 0.7$ & 2.7, $\beta_2 = 0.17$, $\beta_3 = 0.17$, $\beta_5 = 0.3$)

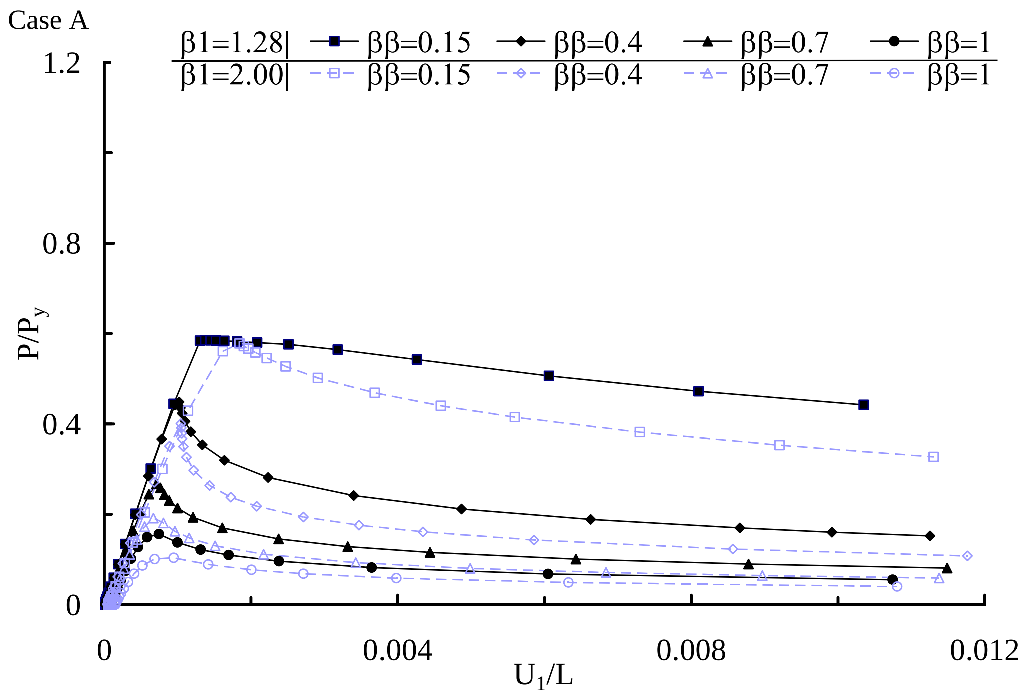

Figure E-155 Axial load versus axial shortening ($\beta_9 = 0.4$, $\beta_1 = 1.28$ & 2.0, $\beta_2 = 0.17$, $\beta_3 = 0.17$, $\beta_5 = 0.3$)

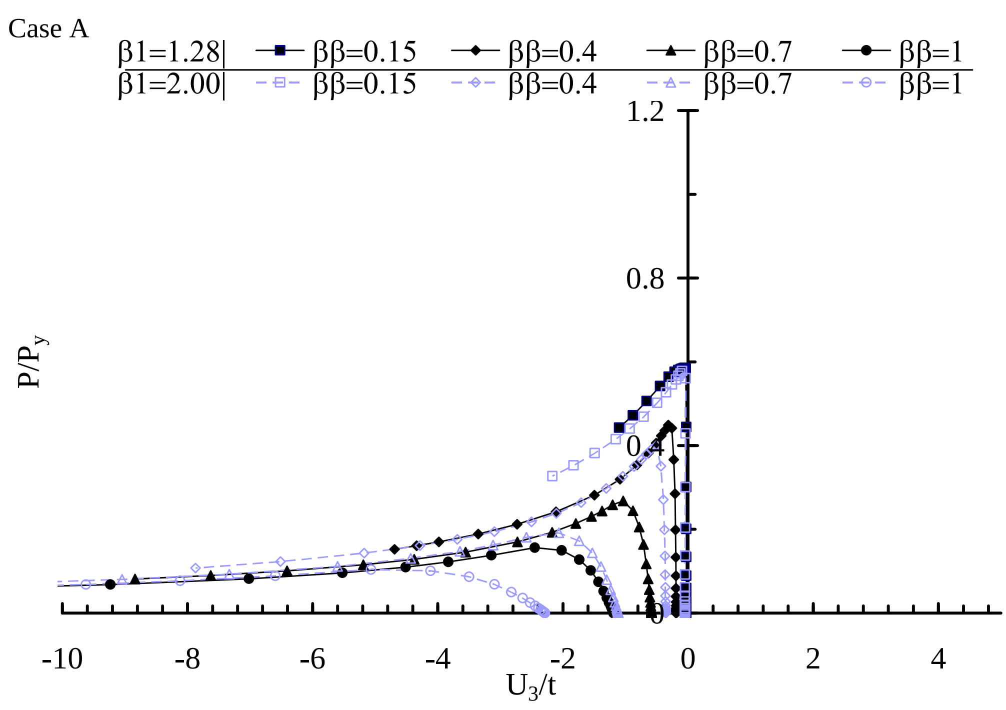

Figure E-156 Axial load versus lateral deflection ($\beta_9 = 0.4$, $\beta_1 = 1.28$ & 2.0, $\beta_2 = 0.17$, $\beta_3 = 0.17$, $\beta_5 = 0.3$)

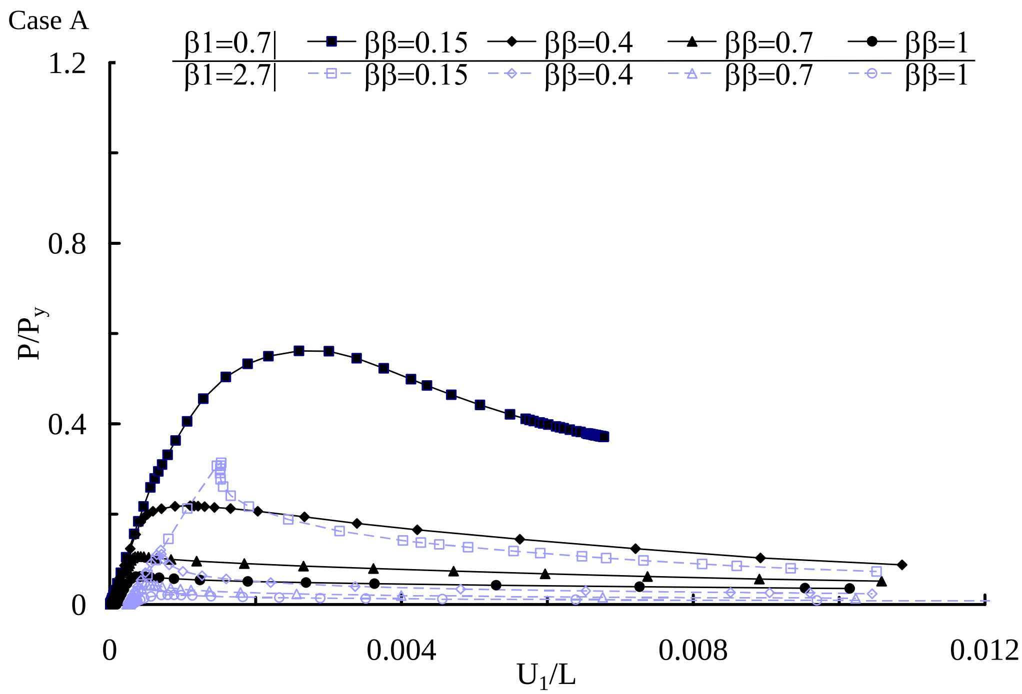

Figure E-157 Axial load versus axial shortening ($\beta_9 = 0.4$, $\beta_1 = 0.7$ & 2.7, $\beta_2 = 0.8$, $\beta_3 = 0.6$, $\beta_5 = 0.075$)

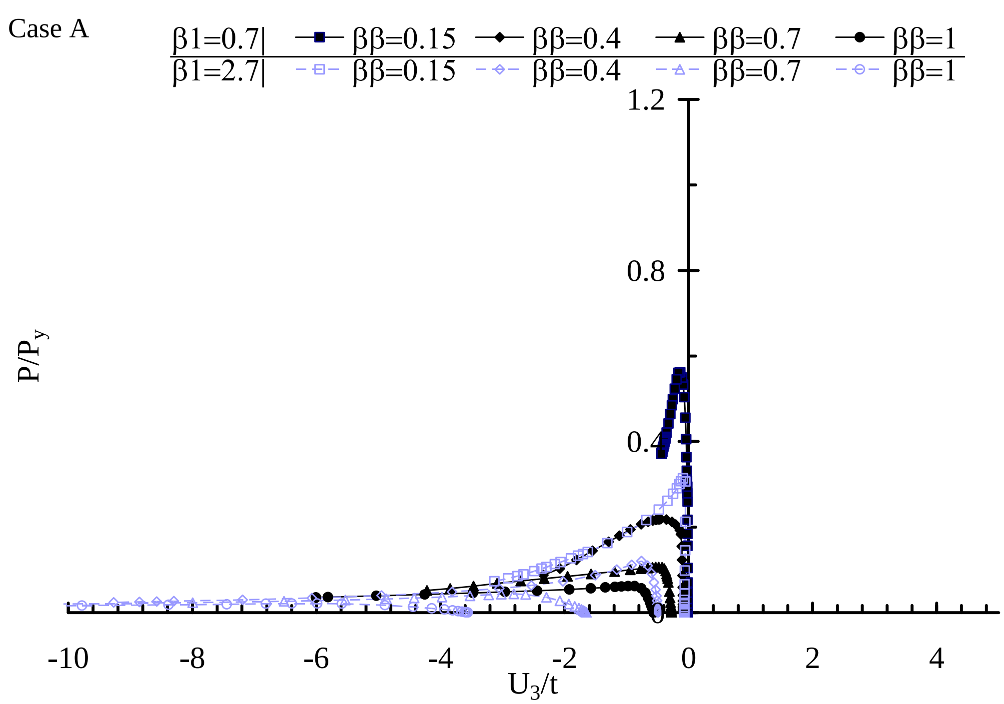

Figure E-158 Axial load versus lateral deflection ($\beta_9 = 0.4$, $\beta_1 = 0.7$ & 2.7, $\beta_2 = 0.8$, $\beta_3 = 0.6$, $\beta_5 = 0.075$)

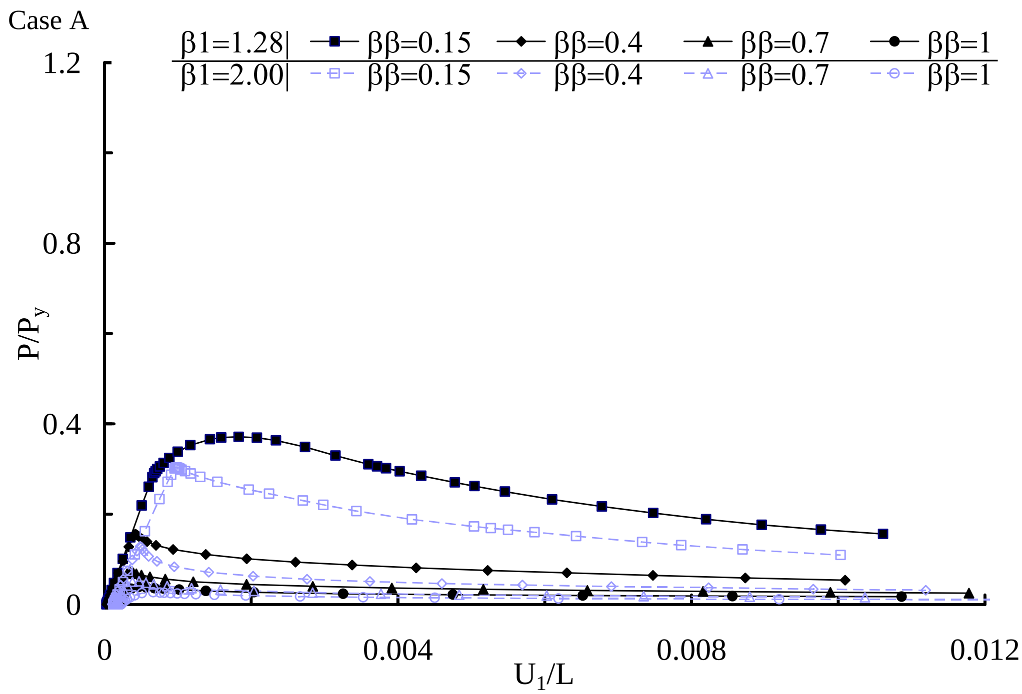

Figure E-159 Axial load versus axial shortening ($\beta_9 = 0.4$, $\beta_1 = 1.28$ & 2.0, $\beta_2 = 0.8$, $\beta_3 = 0.6$, $\beta_5 = 0.075$)

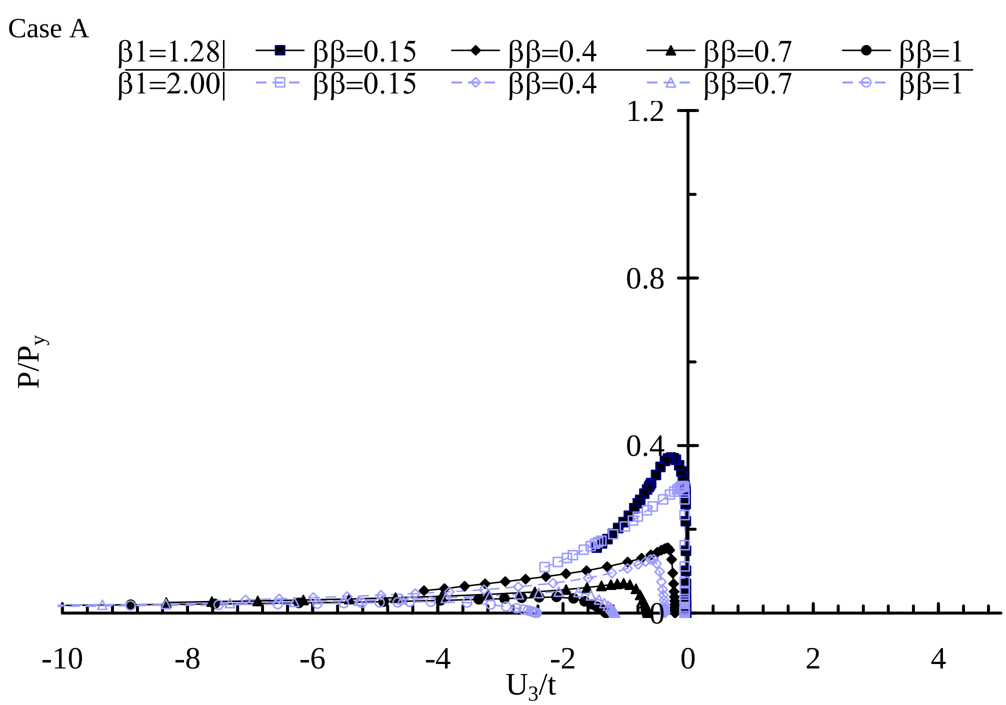

Figure E-160 Axial load versus lateral deflection ($\beta_9 = 0.4$, $\beta_1 = 1.28$ & 2.0, $\beta_2 = 0.8$, $\beta_3 = 0.6$, $\beta_5 = 0.075$)

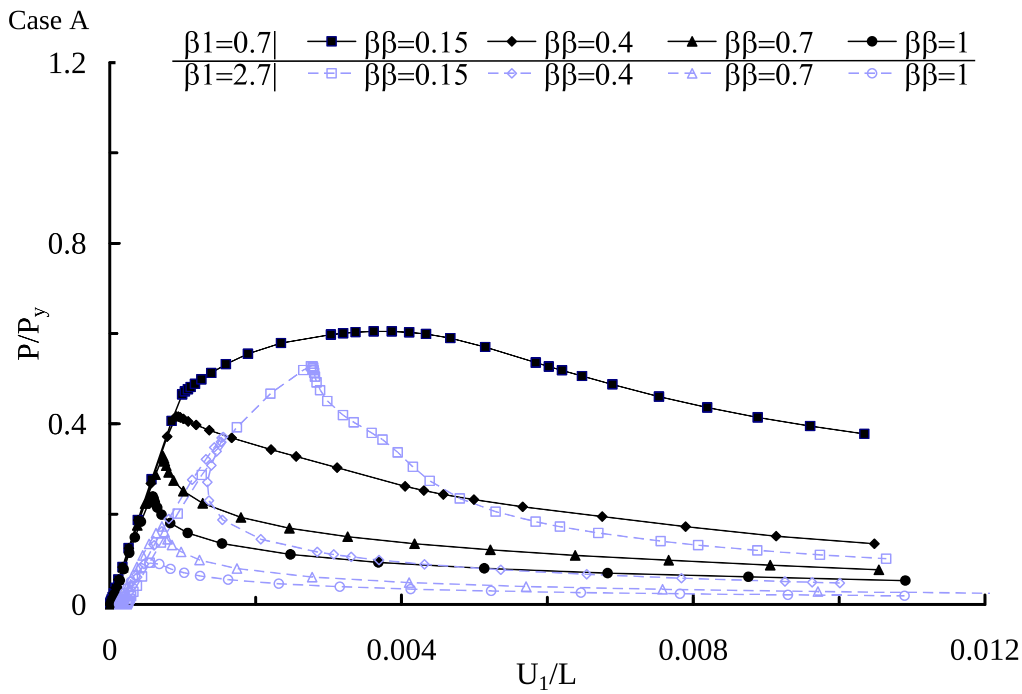

Figure E-161 Axial load versus axial shortening ($\beta_9 = 0.4$, $\beta_1 = 0.7$ & 2.7, $\beta_2 = 0.8$, $\beta_3 = 0.6$, $\beta_5 = 0.15$)

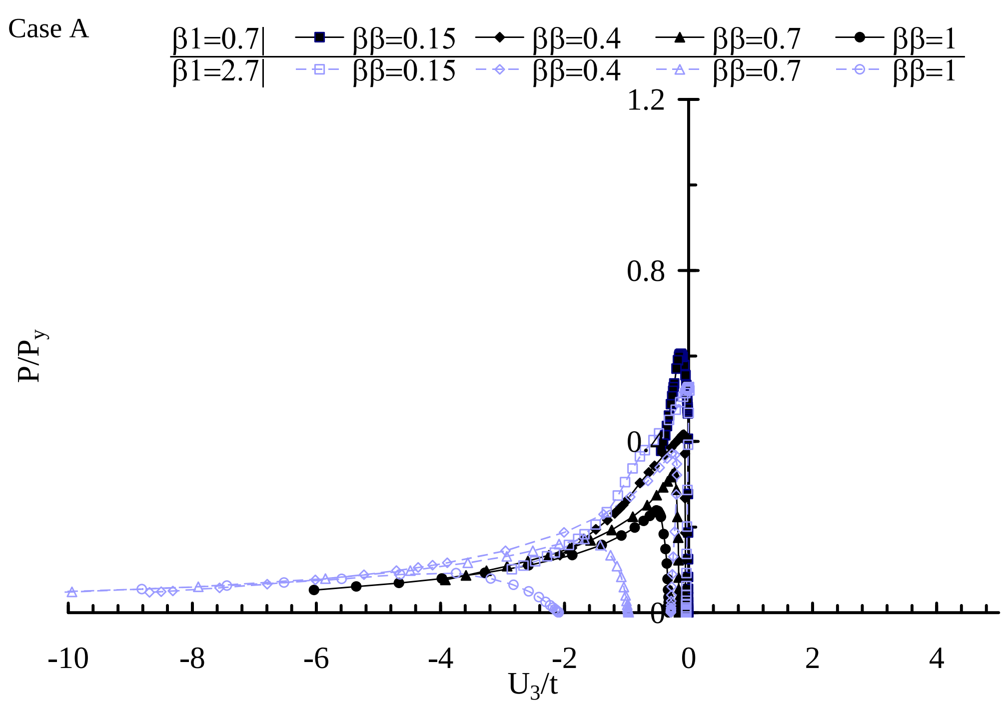

Figure E-162 Axial load versus lateral deflection ($\beta_9 = 0.4$, $\beta_1 = 0.7$ & 2.7, $\beta_2 = 0.8$, $\beta_3 = 0.6$, $\beta_5 = 0.15$)

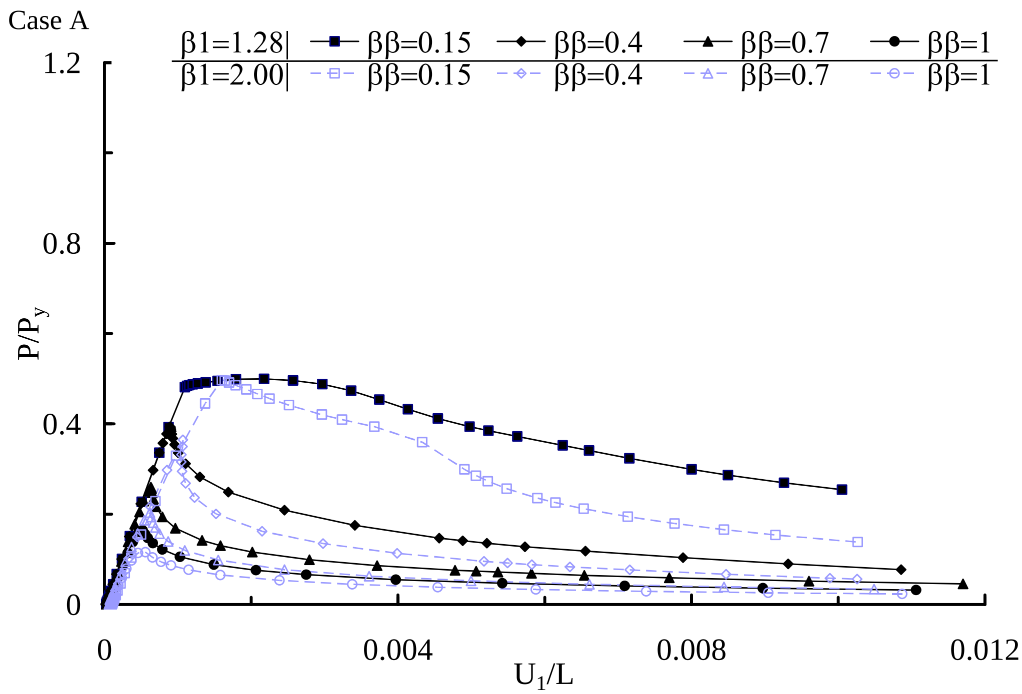

Figure E-163 Axial load versus axial shortening ($\beta_9 = 0.4$, $\beta_1 = 1.28$ & 2.0, $\beta_2 = 0.8$, $\beta_3 = 0.6$, $\beta_5 = 0.15$)

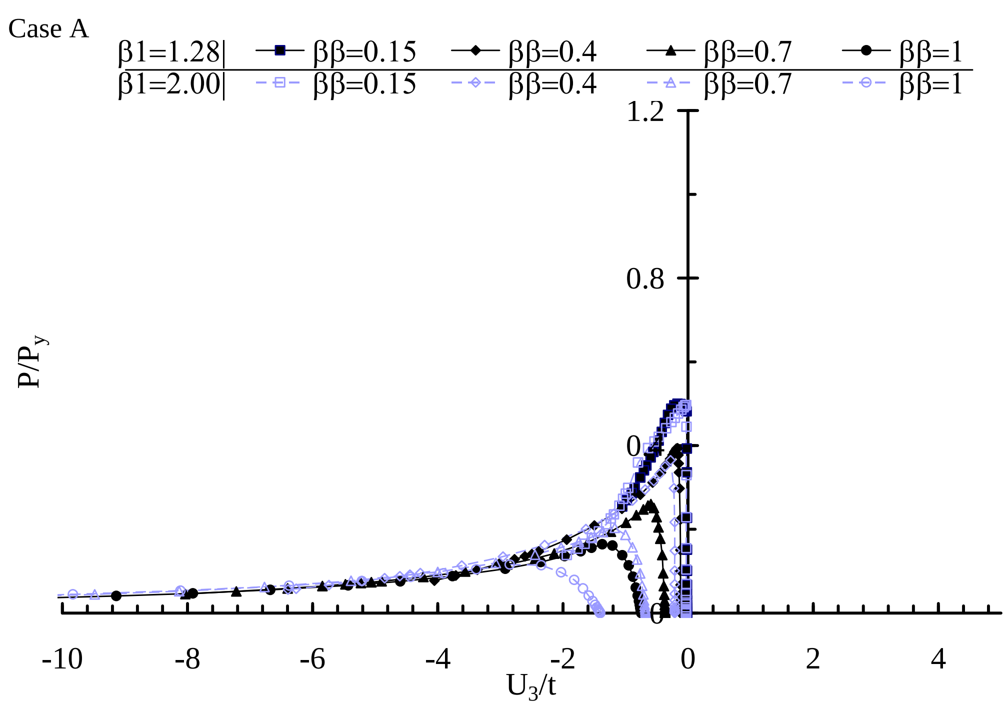

Figure E-164 Axial load versus lateral deflection ($\beta_9 = 0.4$, $\beta_1 = 1.28$ & 2.0, $\beta_2 = 0.8$, $\beta_3 = 0.6$, $\beta_5 = 0.15$)

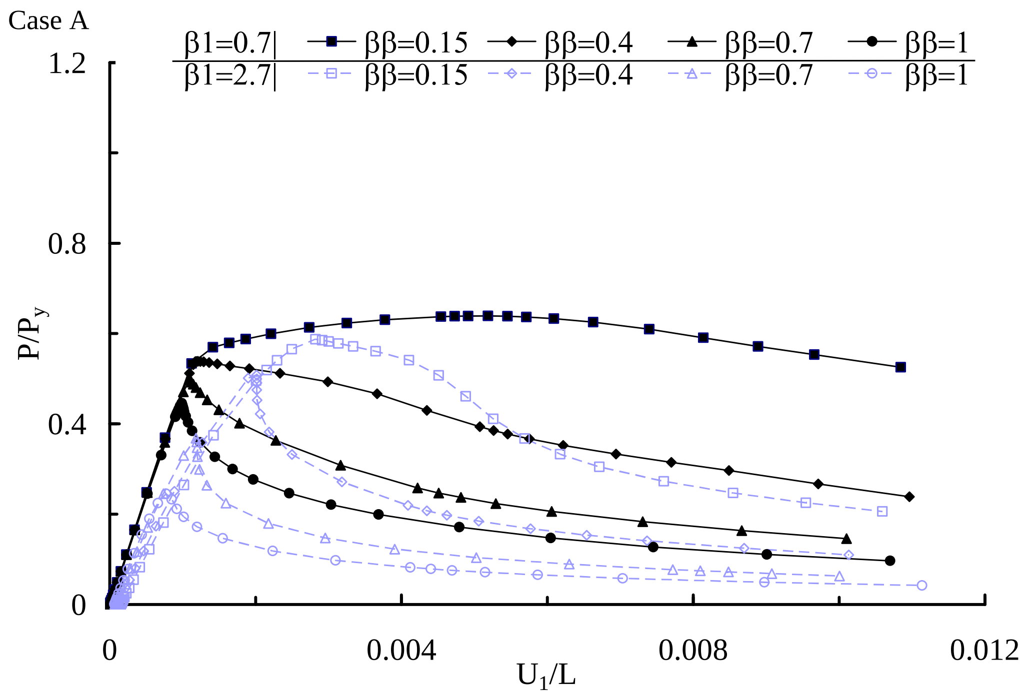

Figure E-165 Axial load versus axial shortening ($\beta_9 = 0.4$, $\beta_1 = 0.7$ & 2.7, $\beta_2 = 0.8$, $\beta_3 = 0.6$, $\beta_5 = 0.3$)

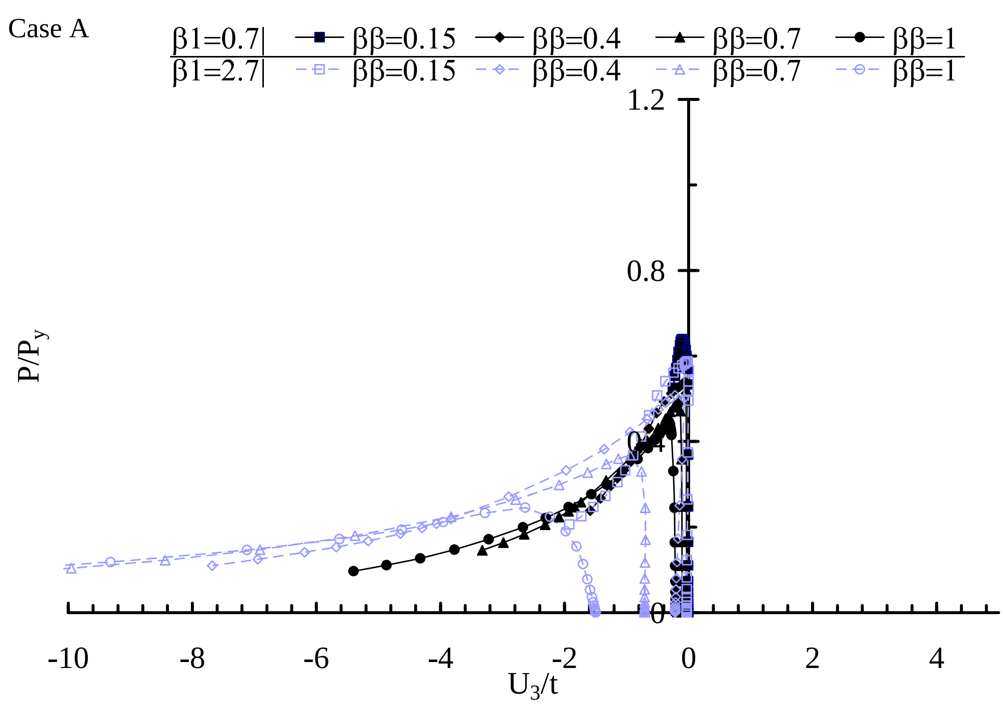

Figure E-166 Axial load versus lateral deflection ($\beta_9 = 0.4$, $\beta_1 = 0.7$ & 2.7, $\beta_2 = 0.8$, $\beta_3 = 0.6$, $\beta_5 = 0.3$)

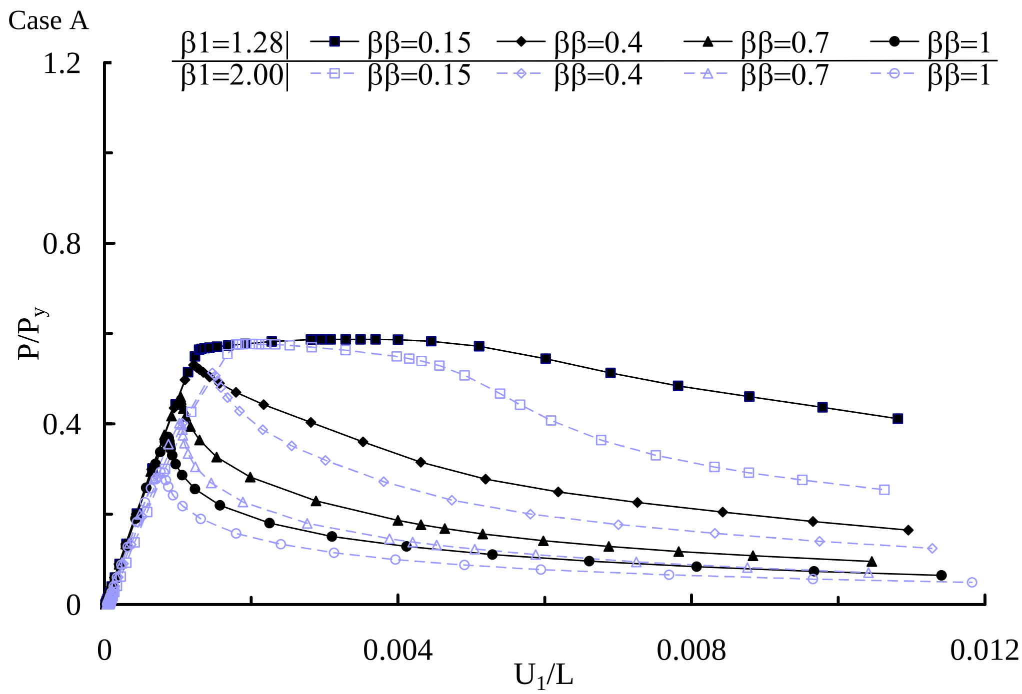

Figure E-167 Axial load versus axial shortening ($\beta_9 = 0.4$, $\beta_1 = 1.28$ & 2.0, $\beta_2 = 0.8$, $\beta_3 = 0.6$, $\beta_5 = 0.3$)

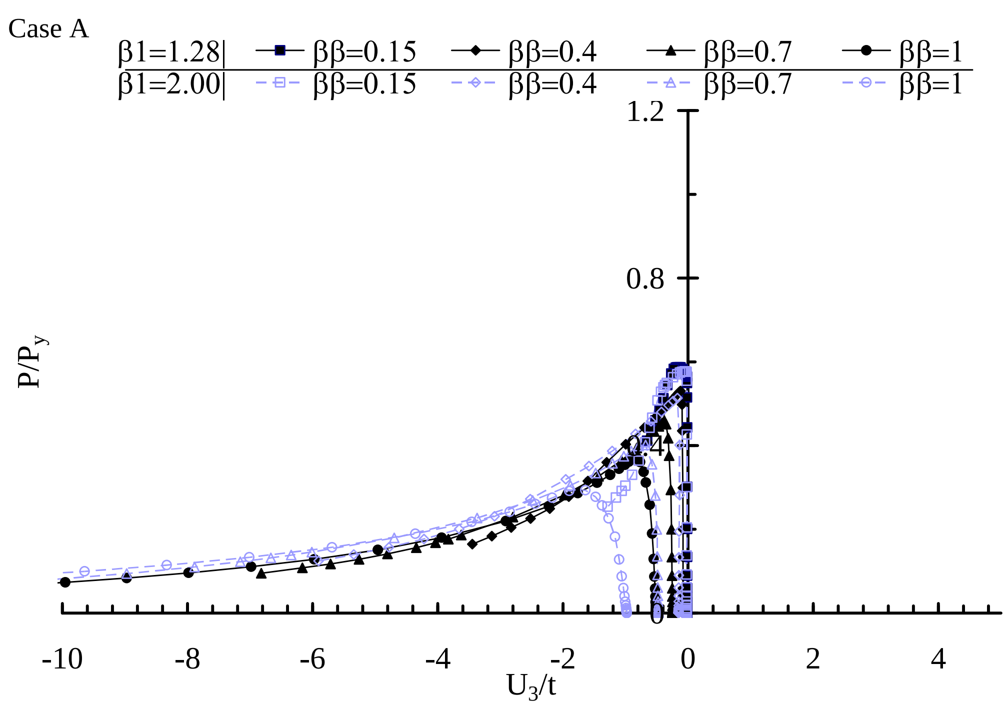

Figure E-168 Axial load versus lateral deflection ($\beta_9 = 0.4$, $\beta_1 = 1.28$ & 2.0, $\beta_2 = 0.8$, $\beta_3 = 0.6$, $\beta_5 = 0.3$)

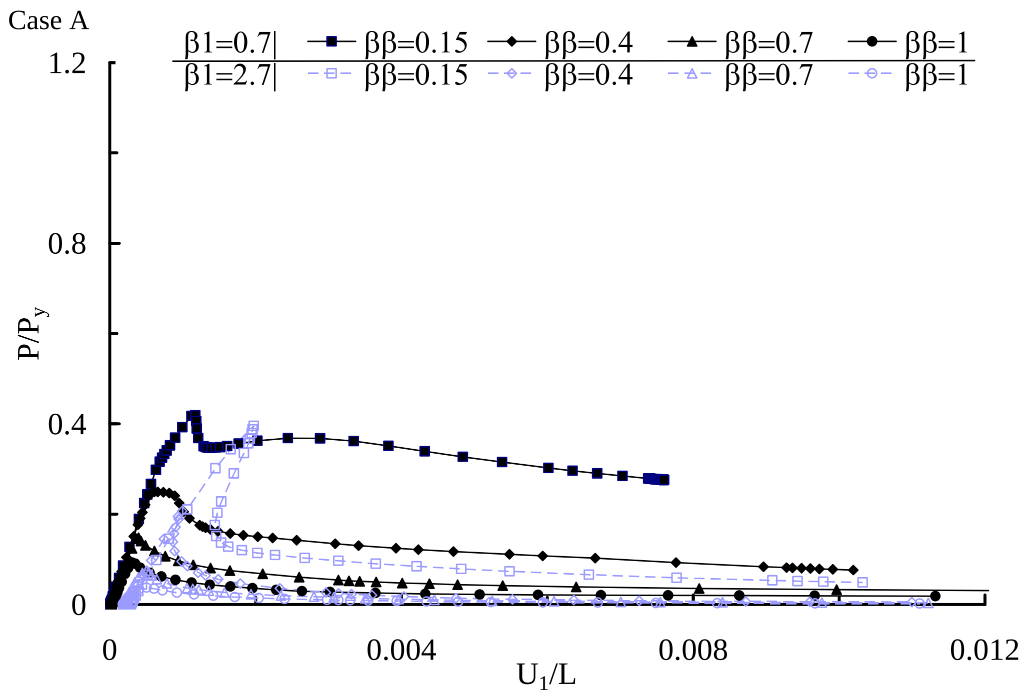

Figure E-169 Axial load versus axial shortening ($\beta_9 = 0.4$, $\beta_1 = 0.7$ & 2.7, $\beta_2 = 1.5$, $\beta_3 = 0.9$, $\beta_5 = 0.075$)

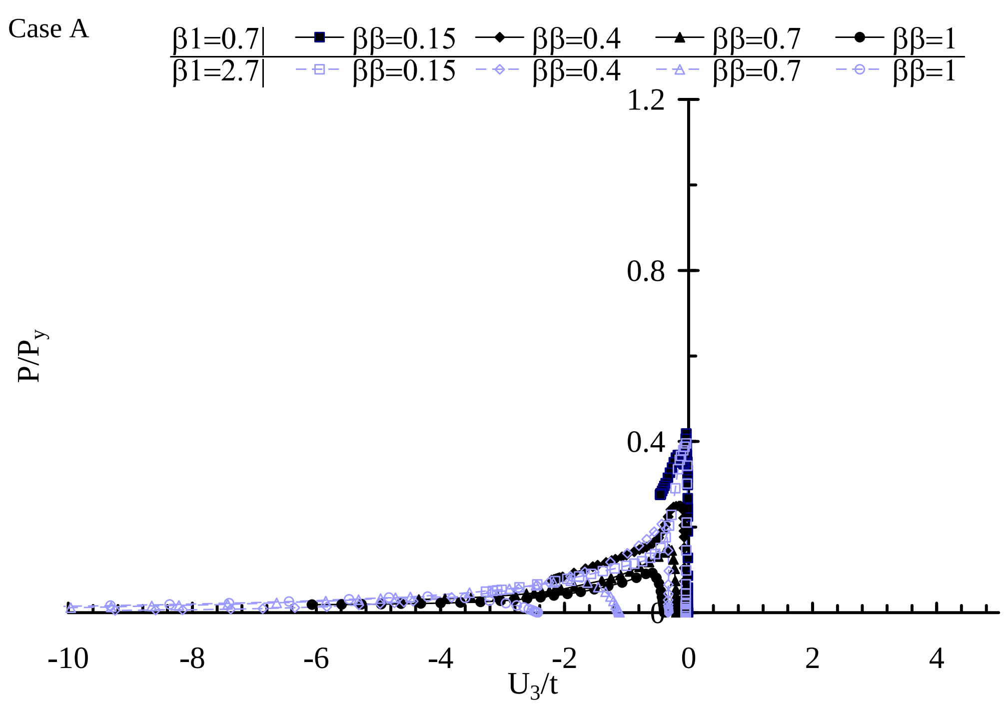

Figure E-170 Axial load versus lateral deflection ($\beta_9 = 0.4$, $\beta_1 = 0.7$ & 2.7, $\beta_2 = 1.5$, $\beta_3 = 0.9$, $\beta_5 = 0.075$)

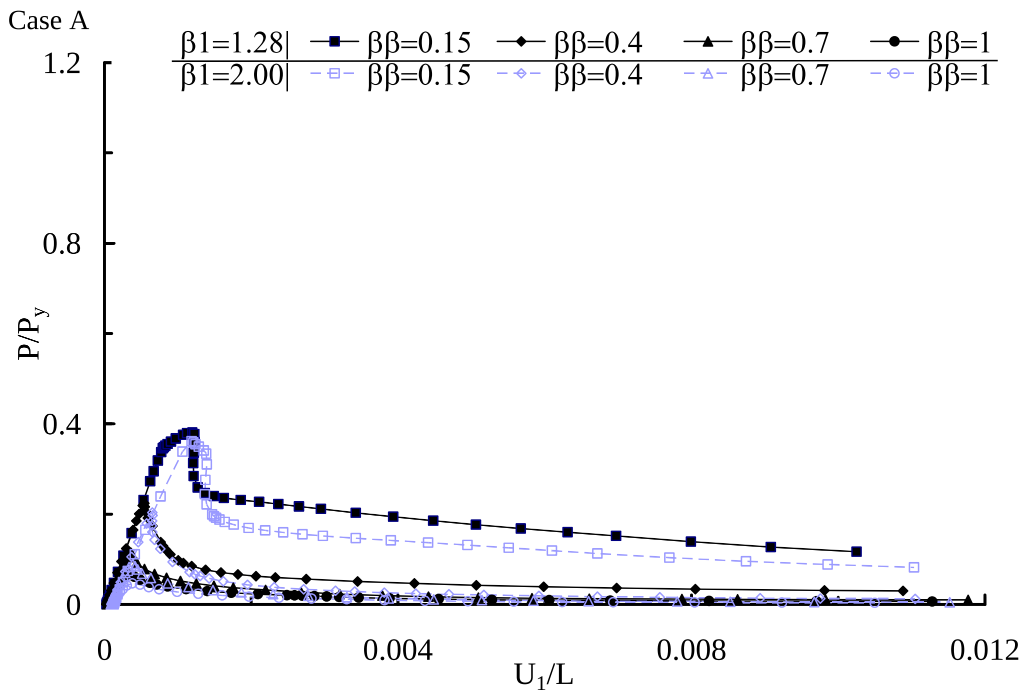

Figure E-171 Axial load versus axial shortening ($\beta_9 = 0.4$, $\beta_1 = 1.28$ & 2.0, $\beta_2 = 1.5$, $\beta_3 = 0.9$, $\beta_5 = 0.075$)

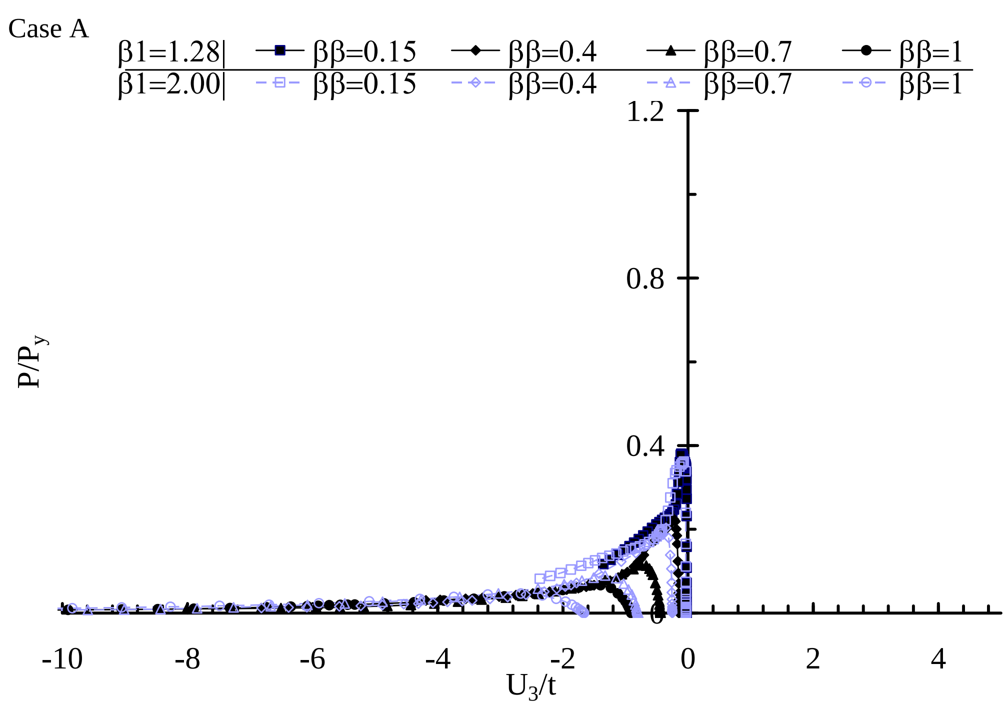

Figure E-172 Axial load versus lateral deflection ($\beta_9 = 0.4$, $\beta_1 = 1.28$ & 2.0, $\beta_2 = 1.5$, $\beta_3 = 0.9$, $\beta_5 = 0.075$)

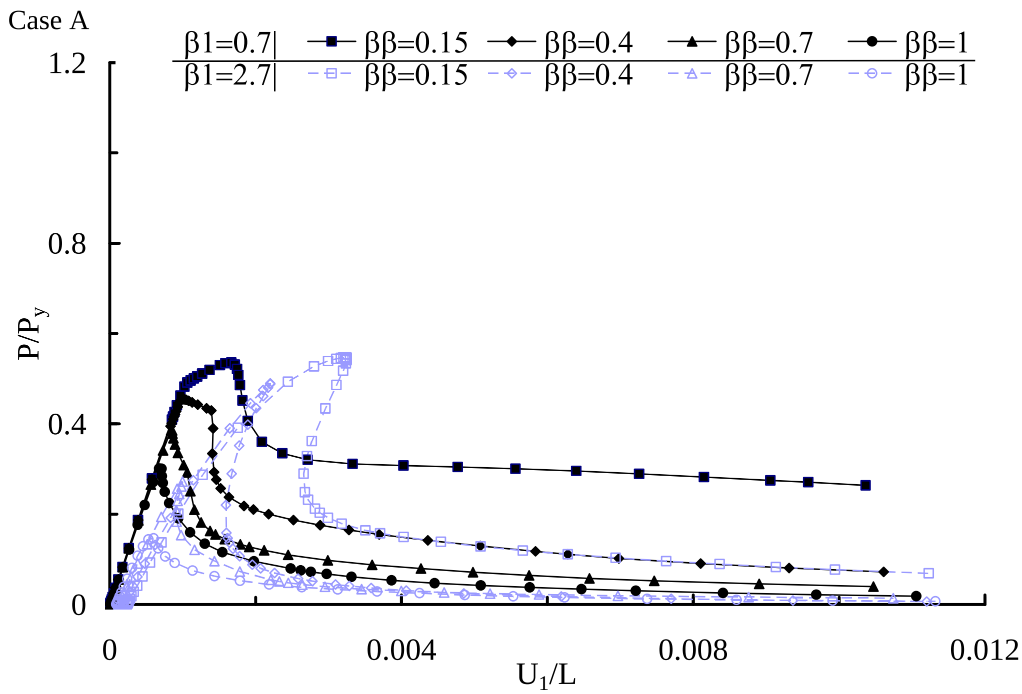

Figure E-173 Axial load versus axial shortening ($\beta_9 = 0.4$, $\beta_1 = 0.7$ & 2.7, $\beta_2 = 1.5$, $\beta_3 = 0.9$, $\beta_5 = 0.15$)

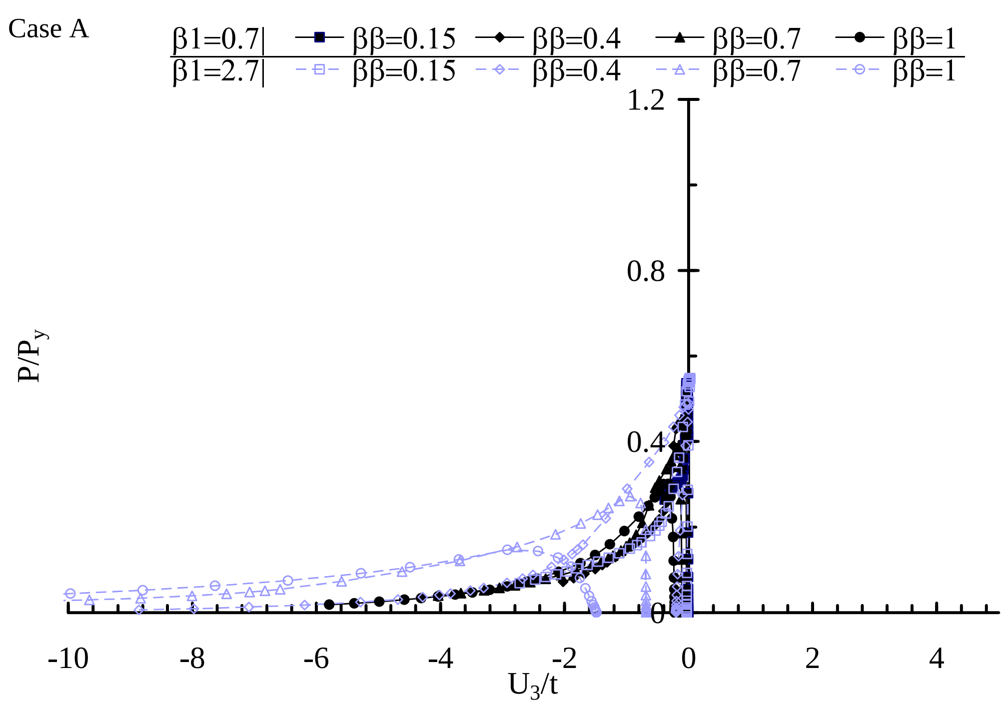

Figure E-174 Axial load versus lateral deflection ($\beta_9 = 0.4$, $\beta_1 = 0.7$ & 2.7, $\beta_2 = 1.5$, $\beta_3 = 0.9$, $\beta_5 = 0.15$)

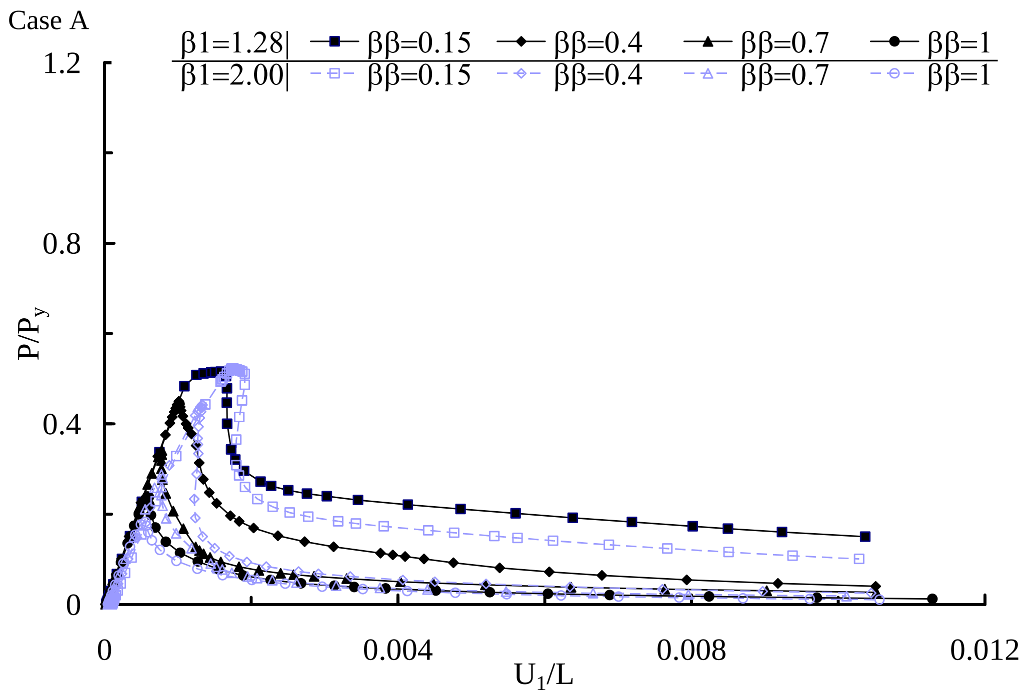

Figure E-175 Axial load versus axial shortening ($\beta_9 = 0.4$, $\beta_1 = 1.28$ & 2.0, $\beta_2 = 1.5$, $\beta_3 = 0.9$, $\beta_5 = 0.15$)

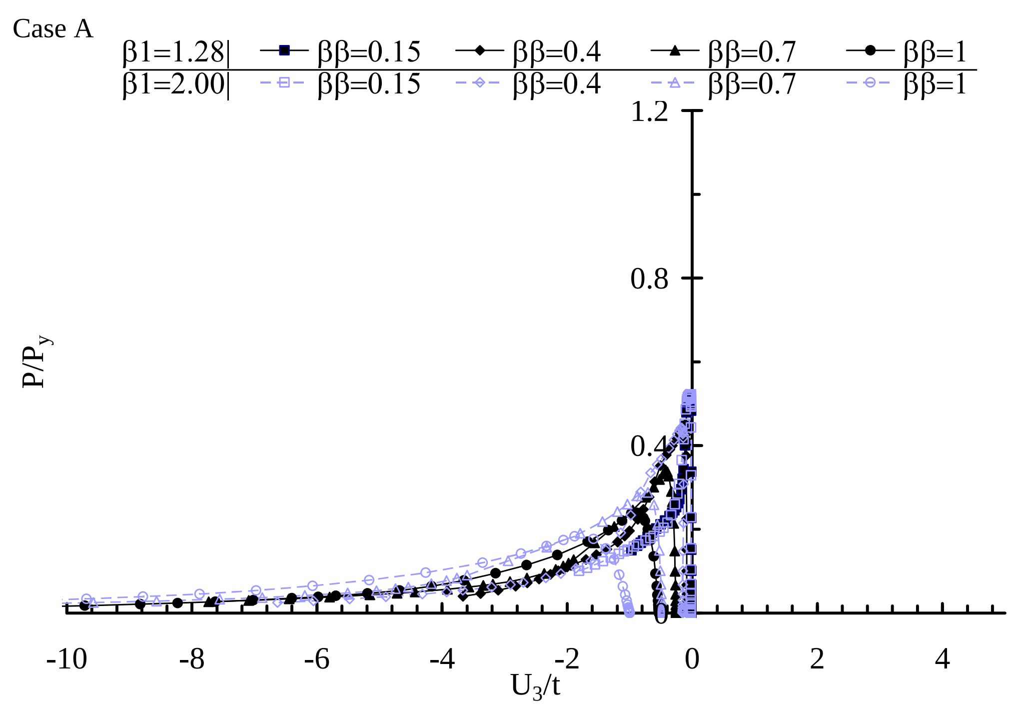

Figure E-176 Axial load versus lateral deflection ($\beta_9 = 0.4$, $\beta_1 = 1.28$ & 2.0, $\beta_2 = 1.5$, $\beta_3 = 0.9$, $\beta_5 = 0.15$)

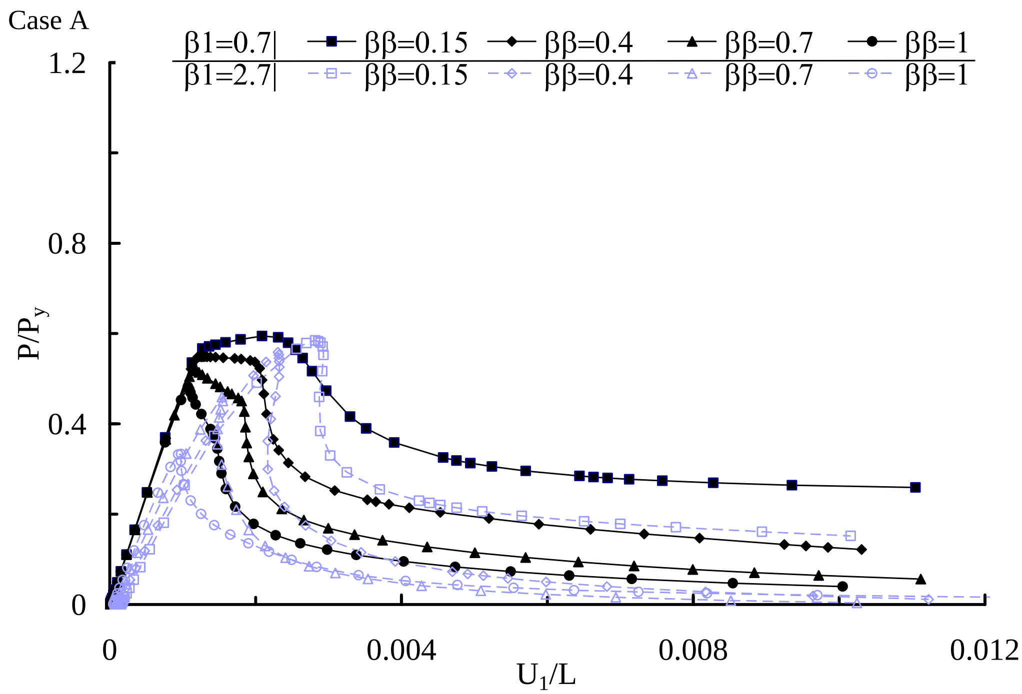

Figure E-177 Axial load versus axial shortening ($\beta_9 = 0.4$, $\beta_1 = 0.7$ & 2.7, $\beta_2 = 1.5$, $\beta_3 = 0.9$, $\beta_5 = 0.3$)

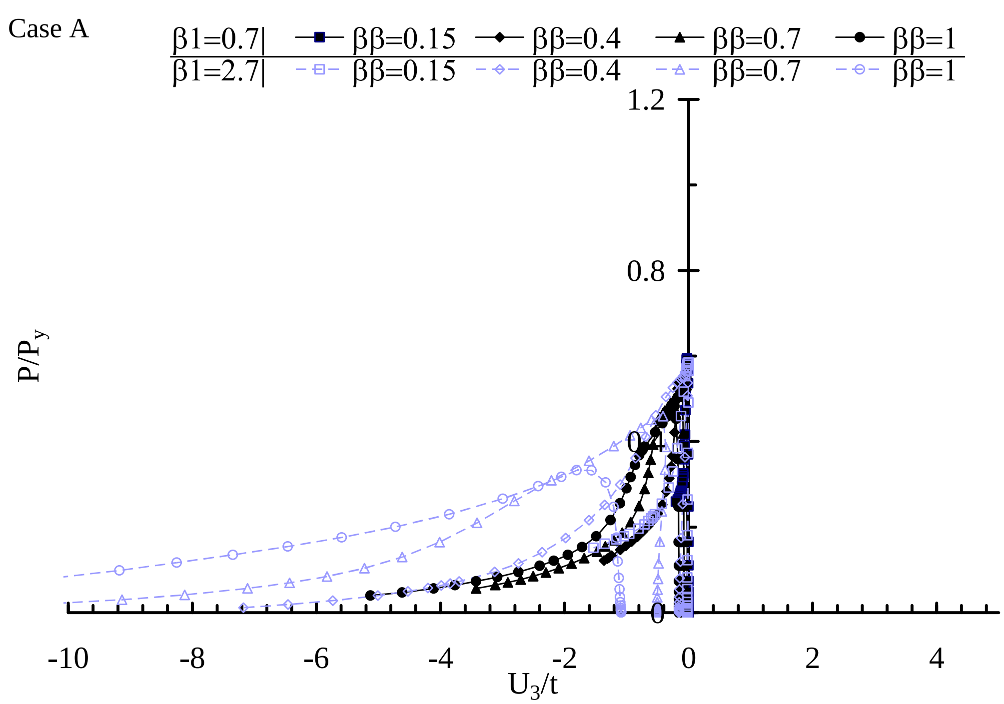

Figure E-178 Axial load versus lateral deflection ($\beta_9 = 0.4$, $\beta_1 = 0.7$ & 2.7, $\beta_2 = 1.5$, $\beta_3 = 0.9$, $\beta_5 = 0.3$)

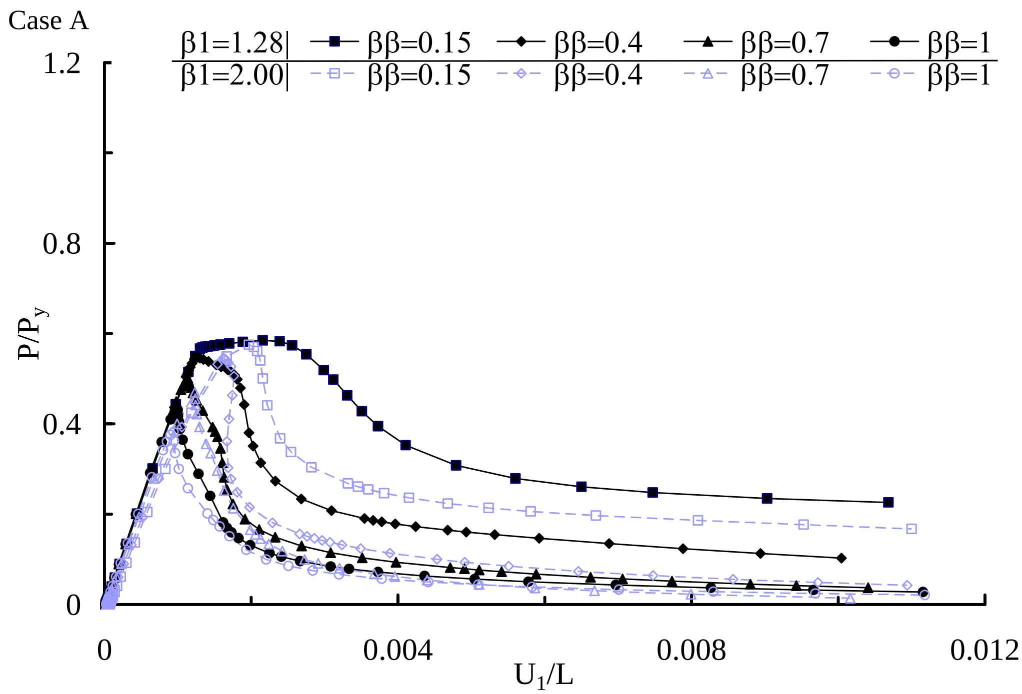

Figure E-179 Axial load versus axial shortening ($\beta_9 = 0.4$, $\beta_1 = 1.28$ & 2.0, $\beta_2 = 1.5$, $\beta_3 = 0.9$, $\beta_5 = 0.3$)

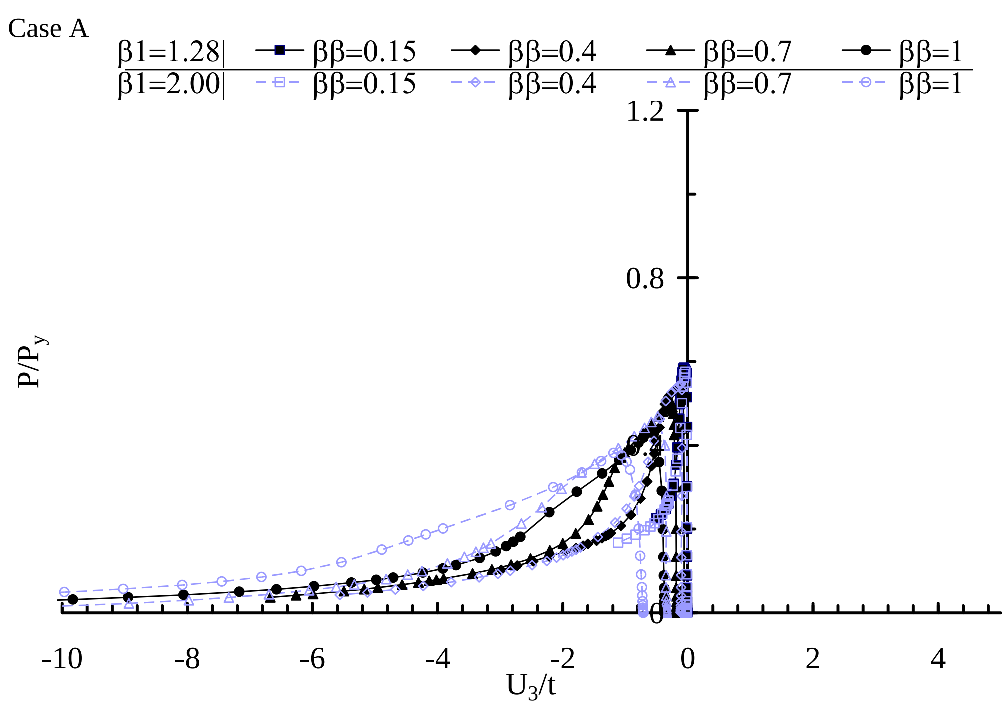

Figure E-180 Axial load versus lateral deflection ($\beta_9 = 0.4$, $\beta_1 = 1.28$ & 2.0, $\beta_2 = 1.5$, $\beta_3 = 0.9$, $\beta_5 = 0.3$)

APPENDIX F

MONTE CARLO SIMULATION RESULTS AND FITTED LOGNORMAL CURVE RESUTLS

This appendix presents the results of the Monte Carlo simulations and the results of the corresponding fitted lognormal curves for each of the 280 nominal panels that were used in the reliability analysis in Chapter 4. The results include $Y_{0.001}$, $Y_{0.05}$, $Y_{0.005}$ $Y_{0.01}$, ρ_{MG} and V_{MG} as given in Tables F-1 to F-5 for five load conditions (β_9 = –0.4, –0.2, 0, 0.2, 0.4). Each of the statistical parameters in Tables F-1 to F-5 is based on a data set of 5000 samples for the corresponding nominal panel. Since the fitted lognormal curve is determined from $Y_{0.001}$ and $Y_{0.05}$ fractiles of the Monte Carlo simulation results, $Y_{0.001}/Y_{0.05}$ from the Monte Carlo results are identical to $Y_{0.001}/Y_{0.05}$ of the fitted curves. The other parameters, namely, $Y_{0.005}$ $Y_{0.01}$, ρ_{MG} and V_{MG}, from the Monte Carlo results and from the fitted curves are given separately.

Table F-1 Results of the Monte Carlo simulations and fitted lognormal curve (β_9 = –0.4)

			Monte Carlo simulations				Fitted lognormal curve			
Specimen	$Y_{0.001}$	$Y_{0.05}$	$Y_{0.005}$	$Y_{0.01}$	ρ_{MG}	V_{MG}	$Y_{0.005}$	$Y_{0.01}$	ρ_{MG}	V_{MG}
111_21	0.706	0.979	0.808	0.860	1.366	0.187	0.793	0.839	1.455	0.229
211_21	0.820	1.014	0.872	0.905	1.314	0.145	0.885	0.918	1.304	0.147
311_21	0.854	1.039	0.920	0.960	1.292	0.126	0.916	0.947	1.310	0.136
411_21	0.860	1.046	0.927	0.955	1.285	0.119	0.922	0.954	1.318	0.136
111_31	0.741	0.982	0.813	0.855	1.380	0.189	0.819	0.860	1.377	0.196
211_31	0.787	1.019	0.863	0.906	1.332	0.155	0.863	0.902	1.391	0.181
211_32	0.831	1.029	0.885	0.922	1.306	0.135	0.897	0.931	1.326	0.148
311_31	0.786	1.042	0.905	0.934	1.328	0.139	0.869	0.913	1.463	0.197
311_32	0.867	1.053	0.929	0.957	1.296	0.123	0.929	0.961	1.325	0.135
411_31	0.880	1.049	0.929	0.960	1.332	0.134	0.937	0.965	1.291	0.122
411_32	0.866	1.043	0.937	0.961	1.291	0.124	0.925	0.955	1.300	0.130
122_21	0.761	0.972	0.839	0.868	1.323	0.173	0.830	0.866	1.303	0.171
222_21	0.797	0.996	0.856	0.894	1.282	0.144	0.863	0.897	1.299	0.155
222_22	0.821	1.005	0.865	0.906	1.268	0.130	0.882	0.914	1.279	0.141
322_21	0.835	1.019	0.900	0.930	1.270	0.129	0.897	0.928	1.291	0.139
322_22	0.888	1.032	0.927	0.952	1.254	0.114	0.937	0.961	1.233	0.105
422_21	0.823	1.024	0.898	0.946	1.275	0.126	0.890	0.924	1.328	0.152
422_22	0.877	1.035	0.914	0.950	1.247	0.109	0.930	0.957	1.257	0.114
122_31	0.733	0.985	0.804	0.851	1.349	0.181	0.814	0.857	1.410	0.207
122_32	0.753	0.992	0.822	0.873	1.345	0.177	0.830	0.871	1.383	0.193
222_31	0.801	1.011	0.869	0.903	1.317	0.149	0.870	0.906	1.337	0.163
222_32	0.783	1.011	0.866	0.908	1.309	0.146	0.858	0.896	1.374	0.178
222_33	0.834	1.028	0.891	0.928	1.295	0.129	0.898	0.931	1.317	0.145
322_31	0.870	1.038	0.912	0.929	1.312	0.138	0.926	0.955	1.279	0.123
322_32	0.860	1.043	0.924	0.957	1.302	0.128	0.921	0.952	1.310	0.134
322_33	0.868	1.041	0.922	0.959	1.277	0.118	0.926	0.956	1.292	0.127

Table F-1 Results of the Monte Carlo simulations and fitted lognormal curve (β_9 = –0.4)

			Monte Carlo simulations				Fitted lognormal curve			
Specimen	$Y_{0.001}$	$Y_{0.05}$	$Y_{0.005}$	$Y_{0.01}$	ρ_{MG}	V_{MG}	$Y_{0.005}$	$Y_{0.01}$	ρ_{MG}	V_{MG}
322_34	0.864	1.022	0.907	0.942	1.252	0.116	0.917	0.944	1.244	0.116
422_31	0.824	1.047	0.927	0.953	1.318	0.134	0.897	0.935	1.394	0.167
422_32	0.857	1.060	0.914	0.954	1.310	0.125	0.925	0.959	1.364	0.148
422_33	0.855	1.041	0.923	0.962	1.274	0.117	0.917	0.949	1.314	0.137
422_34	0.853	1.024	0.902	0.942	1.251	0.117	0.910	0.939	1.270	0.127
133_21	0.759	0.972	0.817	0.856	1.312	0.172	0.829	0.865	1.308	0.173
133_22	0.782	0.985	0.845	0.868	1.306	0.165	0.849	0.883	1.297	0.161
233_21	0.785	0.993	0.856	0.890	1.280	0.144	0.854	0.889	1.313	0.163
233_22	0.797	0.999	0.864	0.900	1.271	0.135	0.864	0.898	1.306	0.157
333_21	0.846	1.012	0.895	0.921	1.274	0.131	0.902	0.930	1.249	0.124
333_22	0.851	1.017	0.909	0.940	1.259	0.119	0.907	0.935	1.255	0.124
333_23	0.873	1.023	0.918	0.954	1.236	0.107	0.923	0.949	1.233	0.110
433_21	0.853	1.024	0.907	0.939	1.272	0.125	0.910	0.939	1.272	0.127
433_22	0.880	1.033	0.931	0.953	1.254	0.114	0.932	0.958	1.248	0.111
433_23	0.868	1.020	0.923	0.944	1.226	0.109	0.920	0.945	1.232	0.111
133_31	0.735	0.983	0.820	0.868	1.341	0.176	0.815	0.857	1.395	0.203
133_32	0.775	0.987	0.839	0.869	1.342	0.175	0.845	0.881	1.317	0.168
133_33	0.776	0.990	0.854	0.892	1.336	0.169	0.847	0.883	1.325	0.170
233_31	0.780	1.015	0.868	0.908	1.311	0.148	0.857	0.897	1.391	0.183
233_32	0.798	1.012	0.884	0.919	1.310	0.146	0.868	0.905	1.346	0.166
233_33	0.802	1.009	0.882	0.918	1.298	0.141	0.870	0.905	1.327	0.160
233_34	0.850	1.026	0.896	0.928	1.283	0.129	0.909	0.939	1.282	0.131
333_31	0.833	1.034	0.913	0.942	1.309	0.135	0.900	0.934	1.336	0.150
333_32	0.862	1.039	0.914	0.946	1.305	0.132	0.921	0.951	1.297	0.130
333_33	0.860	1.041	0.923	0.956	1.288	0.122	0.921	0.952	1.305	0.132
333_34	0.868	1.039	0.931	0.953	1.266	0.115	0.925	0.955	1.284	0.125

Table F-1 Results of the Monte Carlo simulations and fitted lognormal curve (β_9 = –0.4)

			Monte Carlo simulations				Fitted lognormal curve			
Specimen	$Y_{0.001}$	$Y_{0.05}$	$Y_{0.005}$	$Y_{0.01}$	ρ_{MG}	V_{MG}	$Y_{0.005}$	$Y_{0.01}$	ρ_{MG}	V_{MG}
433_31	0.875	1.039	0.915	0.949	1.315	0.136	0.930	0.958	1.272	0.119
433_32	0.886	1.048	0.942	0.960	1.308	0.130	0.940	0.968	1.279	0.117
433_33	0.876	1.045	0.934	0.954	1.287	0.119	0.933	0.962	1.288	0.123
433_34	0.859	1.036	0.917	0.948	1.264	0.114	0.918	0.948	1.294	0.130

Table F-2 Results of the Monte Carlo simulations and fitted lognormal curve ($\beta_9 = -0.2$)

			Monte Carlo simulations				Fitted lognormal curve			
Specimen	$Y_{0.001}$	$Y_{0.05}$	$Y_{0.005}$	$Y_{0.01}$	ρ_{MG}	V_{MG}	$Y_{0.005}$	$Y_{0.01}$	ρ_{MG}	V_{MG}
111_21	0.784	0.979	0.842	0.871	1.314	0.167	0.848	0.882	1.276	0.155
211_21	0.802	1.005	0.864	0.904	1.271	0.133	0.869	0.904	1.316	0.157
311_21	0.866	1.034	0.928	0.953	1.259	0.116	0.923	0.951	1.275	0.123
411_21	0.873	1.037	0.925	0.955	1.248	0.109	0.928	0.956	1.271	0.120
111_31	0.772	0.990	0.840	0.864	1.333	0.168	0.844	0.881	1.334	0.173
211_31	0.810	1.014	0.888	0.915	1.299	0.139	0.877	0.912	1.323	0.156
211_32	0.851	1.031	0.904	0.940	1.271	0.120	0.911	0.942	1.295	0.134
311_31	0.879	1.038	0.926	0.953	1.290	0.125	0.933	0.960	1.262	0.115
311_32	0.885	1.040	0.946	0.969	1.252	0.107	0.937	0.964	1.256	0.111
411_31	0.898	1.046	0.941	0.968	1.289	0.119	0.948	0.973	1.251	0.106
411_32	0.867	1.034	0.931	0.960	1.245	0.108	0.923	0.952	1.273	0.122
122_21	0.748	0.973	0.832	0.860	1.301	0.167	0.821	0.859	1.333	0.183
222_21	0.803	0.993	0.857	0.887	1.264	0.138	0.866	0.898	1.277	0.147
222_22	0.832	1.008	0.890	0.921	1.252	0.123	0.891	0.921	1.264	0.133
322_21	0.866	1.016	0.924	0.945	1.252	0.122	0.917	0.942	1.225	0.111
322_22	0.881	1.034	0.940	0.970	1.236	0.104	0.933	0.959	1.250	0.111
422_21	0.861	1.024	0.915	0.936	1.254	0.119	0.916	0.944	1.255	0.120
422_22	0.878	1.028	0.938	0.961	1.224	0.101	0.929	0.955	1.237	0.109
122_31	0.783	0.987	0.850	0.876	1.324	0.167	0.850	0.885	1.303	0.162
122_32	0.750	0.987	0.843	0.881	1.317	0.166	0.827	0.867	1.374	0.192
222_31	0.787	1.017	0.873	0.915	1.292	0.140	0.862	0.901	1.384	0.179
222_32	0.811	1.015	0.869	0.913	1.284	0.135	0.878	0.913	1.326	0.156
222_33	0.826	1.020	0.897	0.931	1.268	0.122	0.890	0.923	1.311	0.147
322_31	0.871	1.035	0.910	0.944	1.286	0.126	0.926	0.954	1.268	0.120
322_32	0.877	1.035	0.934	0.958	1.278	0.119	0.931	0.958	1.259	0.115
322_33	0.898	1.040	0.951	0.973	1.248	0.105	0.946	0.970	1.236	0.102

Table F-2 Results of the Monte Carlo simulations and fitted lognormal curve (β_9 = –0.2)

			Monte Carlo simulations				Fitted lognormal curve			
Specimen	$Y_{0.001}$	$Y_{0.05}$	$Y_{0.005}$	$Y_{0.01}$	ρ_{MG}	V_{MG}	$Y_{0.005}$	$Y_{0.01}$	ρ_{MG}	V_{MG}
322_34	0.874	1.028	0.925	0.956	1.224	0.104	0.926	0.952	1.244	0.112
422_31	0.886	1.044	0.931	0.957	1.294	0.124	0.939	0.966	1.267	0.114
422_32	0.878	1.047	0.936	0.957	1.274	0.116	0.935	0.964	1.289	0.122
422_33	0.900	1.044	0.949	0.973	1.239	0.101	0.949	0.974	1.242	0.103
422_34	0.810	1.006	0.909	0.935	1.212	0.106	0.875	0.908	1.301	0.151
133_21	0.788	0.983	0.841	0.879	1.295	0.165	0.853	0.886	1.280	0.154
133_22	0.771	0.979	0.831	0.875	1.294	0.161	0.839	0.874	1.302	0.166
233_21	0.816	0.998	0.867	0.905	1.266	0.135	0.876	0.907	1.268	0.140
233_22	0.831	1.007	0.896	0.919	1.257	0.127	0.890	0.920	1.265	0.134
333_21	0.836	1.024	0.900	0.940	1.260	0.124	0.898	0.930	1.302	0.141
333_22	0.873	1.022	0.921	0.948	1.243	0.112	0.923	0.949	1.231	0.110
333_23	0.882	1.026	0.934	0.955	1.215	0.100	0.931	0.955	1.227	0.105
433_21	0.855	1.022	0.921	0.947	1.253	0.120	0.911	0.940	1.264	0.125
433_22	0.881	1.034	0.933	0.955	1.235	0.106	0.933	0.959	1.248	0.111
433_23	0.891	1.021	0.915	0.945	1.207	0.099	0.935	0.958	1.197	0.094
133_31	0.792	0.989	0.849	0.892	1.319	0.167	0.857	0.891	1.290	0.155
133_32	0.789	0.986	0.856	0.895	1.320	0.168	0.854	0.888	1.284	0.155
133_33	0.781	0.986	0.854	0.889	1.312	0.160	0.849	0.883	1.300	0.162
233_31	0.818	1.017	0.899	0.927	1.294	0.140	0.884	0.918	1.317	0.151
233_32	0.789	1.017	0.871	0.907	1.290	0.139	0.864	0.902	1.377	0.176
233_33	0.798	1.016	0.881	0.917	1.277	0.130	0.870	0.907	1.357	0.169
233_34	0.836	1.025	0.901	0.933	1.262	0.118	0.899	0.931	1.305	0.142
333_31	0.859	1.036	0.913	0.949	1.284	0.126	0.918	0.948	1.294	0.131
333_32	0.864	1.032	0.924	0.959	1.281	0.122	0.921	0.949	1.273	0.123
333_33	0.869	1.044	0.938	0.967	1.261	0.112	0.927	0.957	1.297	0.128
333_34	0.878	1.038	0.941	0.966	1.240	0.104	0.932	0.960	1.264	0.116

Table F-2 Results of the Monte Carlo simulations and fitted lognormal curve (β_9 = –0.2)

			Monte Carlo simulations				Fitted lognormal curve			
Specimen	$Y_{0.001}$	$Y_{0.05}$	$Y_{0.005}$	$Y_{0.01}$	ρ_{MG}	V_{MG}	$Y_{0.005}$	$Y_{0.01}$	ρ_{MG}	V_{MG}
433_31	0.899	1.037	0.941	0.972	1.289	0.125	0.946	0.970	1.227	0.099
433_32	0.881	1.044	0.930	0.954	1.280	0.120	0.936	0.964	1.274	0.118
433_33	0.883	1.044	0.931	0.958	1.258	0.109	0.937	0.965	1.274	0.117
433_34	0.881	1.033	0.947	0.962	1.233	0.102	0.932	0.958	1.246	0.111

Table F-3 Results of the Monte Carlo simulations and fitted lognormal curve ($\beta_9 = 0$)

			Monte Carlo simulations				Fitted lognormal curve			
Specimen	$Y_{0.001}$	$Y_{0.05}$	$Y_{0.005}$	$Y_{0.01}$	ρ_{MG}	V_{MG}	$Y_{0.005}$	$Y_{0.01}$	ρ_{MG}	V_{MG}
111_21	0.785	0.978	0.844	0.879	1.275	0.154	0.849	0.882	1.270	0.153
211_21	0.852	1.007	0.884	0.917	1.241	0.123	0.904	0.931	1.227	0.116
311_21	0.892	1.023	0.936	0.954	1.224	0.105	0.936	0.959	1.202	0.095
411_21	0.905	1.028	0.940	0.959	1.218	0.100	0.947	0.968	1.193	0.088
111_31	0.795	0.996	0.852	0.898	1.298	0.158	0.861	0.895	1.302	0.156
211_31	0.846	1.020	0.901	0.933	1.268	0.127	0.904	0.934	1.275	0.131
211_32	0.889	1.030	0.935	0.959	1.241	0.105	0.937	0.961	1.226	0.103
311_31	0.868	1.035	0.927	0.953	1.257	0.114	0.924	0.953	1.273	0.122
311_32	0.915	1.036	0.958	0.974	1.211	0.092	0.956	0.977	1.198	0.086
411_31	0.920	1.044	0.956	0.978	1.256	0.109	0.962	0.984	1.211	0.088
411_32	0.917	1.026	0.948	0.965	1.203	0.094	0.954	0.973	1.168	0.077
122_21	0.801	0.979	0.851	0.879	1.279	0.158	0.860	0.890	1.243	0.140
222_21	0.798	0.993	0.885	0.901	1.251	0.134	0.863	0.896	1.287	0.152
222_22	0.814	1.002	0.894	0.922	1.227	0.115	0.877	0.909	1.281	0.144
322_21	0.852	1.017	0.903	0.937	1.239	0.116	0.908	0.936	1.254	0.123
322_22	0.892	1.032	0.948	0.970	1.213	0.095	0.939	0.963	1.225	0.101
422_21	0.897	1.023	0.926	0.947	1.235	0.111	0.940	0.961	1.194	0.091
422_22	0.904	1.030	0.948	0.968	1.206	0.093	0.947	0.968	1.200	0.091
122_31	0.817	0.992	0.868	0.896	1.295	0.154	0.875	0.905	1.249	0.135
122_32	0.780	0.990	0.851	0.896	1.296	0.154	0.849	0.884	1.317	0.166
222_31	0.844	1.018	0.897	0.923	1.276	0.132	0.902	0.932	1.270	0.130
222_32	0.815	1.010	0.894	0.922	1.262	0.127	0.880	0.913	1.304	0.149
222_33	0.865	1.024	0.919	0.945	1.245	0.111	0.919	0.946	1.251	0.118
322_31	0.864	1.040	0.915	0.954	1.264	0.119	0.923	0.953	1.295	0.129
322_32	0.893	1.038	0.930	0.964	1.252	0.109	0.942	0.967	1.238	0.104
322_33	0.911	1.037	0.951	0.972	1.221	0.095	0.954	0.976	1.206	0.090

Table F-3 Results of the Monte Carlo simulations and fitted lognormal curve ($\beta_9 = 0$)

			Monte Carlo simulations				Fitted lognormal curve			
Specimen	$Y_{0.001}$	$Y_{0.05}$	$Y_{0.005}$	$Y_{0.01}$	ρ_{MG}	V_{MG}	$Y_{0.005}$	$Y_{0.01}$	ρ_{MG}	V_{MG}
322_34	0.883	1.016	0.931	0.948	1.194	0.095	0.928	0.951	1.198	0.098
422_31	0.870	1.037	0.920	0.953	1.262	0.115	0.926	0.954	1.274	0.122
422_32	0.908	1.043	0.946	0.969	1.247	0.105	0.953	0.977	1.227	0.096
422_33	0.912	1.039	0.949	0.972	1.213	0.092	0.955	0.977	1.209	0.090
422_34	0.864	1.000	0.914	0.933	1.183	0.097	0.910	0.933	1.186	0.101
133_21	0.756	0.976	0.820	0.857	1.278	0.159	0.828	0.865	1.325	0.178
133_22	0.761	0.982	0.837	0.869	1.268	0.151	0.834	0.871	1.334	0.178
233_21	0.820	0.991	0.865	0.906	1.252	0.133	0.878	0.907	1.239	0.131
233_22	0.802	1.001	0.883	0.915	1.241	0.123	0.868	0.901	1.304	0.154
333_21	0.830	1.015	0.888	0.920	1.239	0.119	0.892	0.923	1.288	0.140
333_22	0.854	1.024	0.922	0.945	1.227	0.107	0.911	0.940	1.268	0.126
333_23	0.900	1.032	0.945	0.969	1.202	0.091	0.945	0.968	1.211	0.095
433_21	0.863	1.021	0.911	0.936	1.241	0.116	0.916	0.943	1.244	0.116
433_22	0.892	1.020	0.928	0.958	1.221	0.102	0.936	0.957	1.192	0.093
433_23	0.901	1.017	0.937	0.961	1.187	0.090	0.940	0.960	1.170	0.084
133_31	0.805	0.994	0.858	0.898	1.301	0.158	0.868	0.900	1.279	0.147
133_32	0.796	0.986	0.859	0.893	1.297	0.157	0.859	0.891	1.271	0.149
133_33	0.784	0.998	0.867	0.899	1.287	0.151	0.854	0.891	1.334	0.169
233_31	0.814	1.013	0.884	0.910	1.274	0.132	0.880	0.914	1.314	0.152
233_32	0.848	1.016	0.896	0.930	1.274	0.129	0.904	0.933	1.257	0.126
233_33	0.841	1.021	0.907	0.938	1.262	0.123	0.901	0.932	1.284	0.135
233_34	0.852	1.025	0.921	0.944	1.241	0.110	0.910	0.940	1.277	0.129
333_31	0.884	1.029	0.929	0.954	1.261	0.118	0.933	0.958	1.231	0.106
333_32	0.899	1.035	0.940	0.963	1.258	0.113	0.945	0.969	1.222	0.098
333_33	0.890	1.037	0.951	0.968	1.239	0.105	0.940	0.965	1.240	0.106
333_34	0.901	1.038	0.954	0.973	1.219	0.096	0.947	0.971	1.225	0.098

Table F-3 Results of the Monte Carlo simulations and fitted lognormal curve (β_9 = 0)

			Monte Carlo simulations				Fitted lognormal curve			
Specimen	$Y_{0.001}$	$Y_{0.05}$	$Y_{0.005}$	$Y_{0.01}$	ρ_{MG}	V_{MG}	$Y_{0.005}$	$Y_{0.01}$	ρ_{MG}	V_{MG}
433_31	0.903	1.034	0.931	0.956	1.267	0.118	0.948	0.970	1.213	0.094
433_32	0.886	1.043	0.951	0.974	1.259	0.110	0.939	0.966	1.263	0.113
433_33	0.888	1.037	0.937	0.965	1.235	0.101	0.938	0.964	1.245	0.108
433_34	0.900	1.031	0.938	0.963	1.205	0.092	0.944	0.967	1.210	0.095

Table F-4 Results of the Monte Carlo simulations and fitted lognormal curve (β_9 = 0.2)

			Monte Carlo simulations				Fitted lognormal curve			
Specimen	$Y_{0.001}$	$Y_{0.05}$	$Y_{0.005}$	$Y_{0.01}$	ρ_{MG}	V_{MG}	$Y_{0.005}$	$Y_{0.01}$	ρ_{MG}	V_{MG}
111_21	0.765	0.989	0.820	0.858	1.365	0.183	0.838	0.876	1.346	0.179
211_21	0.765	1.011	0.859	0.896	1.369	0.167	0.845	0.887	1.416	0.195
311_21	0.788	1.024	0.874	0.910	1.342	0.135	0.865	0.905	1.405	0.183
411_21	0.822	1.008	0.882	0.926	1.191	0.094	0.884	0.916	1.285	0.142
111_31	0.786	1.010	0.857	0.893	1.395	0.182	0.859	0.897	1.363	0.174
211_31	0.751	1.019	0.838	0.892	1.395	0.179	0.837	0.882	1.476	0.214
211_32	0.829	1.043	0.882	0.931	1.381	0.160	0.900	0.936	1.372	0.160
311_31	0.802	1.025	0.865	0.906	1.309	0.124	0.875	0.913	1.375	0.171
311_32	0.829	1.048	0.884	0.927	1.377	0.140	0.901	0.939	1.386	0.163
411_31	0.876	1.038	0.926	0.965	1.230	0.099	0.930	0.958	1.267	0.118
411_32	0.795	1.034	0.881	0.920	1.229	0.093	0.873	0.913	1.418	0.184
122_21	0.719	0.986	0.807	0.853	1.368	0.186	0.805	0.850	1.448	0.222
222_21	0.754	1.007	0.827	0.875	1.366	0.176	0.836	0.879	1.428	0.202
222_22	0.782	1.021	0.858	0.905	1.367	0.165	0.860	0.900	1.405	0.186
322_21	0.776	1.001	0.851	0.887	1.271	0.126	0.850	0.888	1.360	0.178
322_22	0.781	1.022	0.854	0.890	1.320	0.126	0.860	0.900	1.413	0.188
422_21	0.882	1.018	0.925	0.949	1.220	0.106	0.928	0.951	1.204	0.099
422_22	0.805	1.022	0.923	0.951	1.185	0.087	0.877	0.913	1.359	0.166
122_31	0.741	1.001	0.828	0.867	1.396	0.187	0.825	0.869	1.439	0.210
122_32	0.763	1.014	0.831	0.891	1.393	0.178	0.844	0.887	1.430	0.199
222_31	0.783	1.016	0.847	0.901	1.395	0.180	0.859	0.899	1.388	0.181
222_32	0.759	1.017	0.832	0.883	1.388	0.177	0.842	0.886	1.446	0.204
222_33	0.811	1.041	0.891	0.929	1.378	0.164	0.886	0.925	1.404	0.174
322_31	0.776	1.020	0.857	0.891	1.287	0.124	0.855	0.897	1.419	0.191
322_32	0.763	1.018	0.848	0.881	1.289	0.120	0.846	0.889	1.441	0.201
322_33	0.839	1.046	0.896	0.928	1.325	0.119	0.908	0.943	1.360	0.153

Table F-4 Results of the Monte Carlo simulations and fitted lognormal curve (β_9 = 0.2)

			Monte Carlo simulations				Fitted lognormal curve			
Specimen	$Y_{0.001}$	$Y_{0.05}$	$Y_{0.005}$	$Y_{0.01}$	ρ_{MG}	V_{MG}	$Y_{0.005}$	$Y_{0.01}$	ρ_{MG}	V_{MG}
322_34	0.848	1.045	0.900	0.932	1.378	0.147	0.914	0.947	1.340	0.145
422_31	0.897	1.043	0.957	0.975	1.243	0.106	0.946	0.971	1.245	0.105
422_32	0.894	1.043	0.952	0.973	1.227	0.096	0.944	0.970	1.251	0.107
422_33	0.854	1.024	0.912	0.943	1.181	0.083	0.911	0.940	1.270	0.126
422_34	0.778	1.015	0.870	0.902	1.276	0.110	0.856	0.896	1.397	0.185
133_21	0.764	0.993	0.808	0.857	1.374	0.184	0.838	0.877	1.361	0.183
133_22	0.765	1.006	0.841	0.883	1.363	0.178	0.843	0.884	1.401	0.192
233_21	0.698	0.996	0.829	0.877	1.370	0.179	0.792	0.842	1.537	0.249
233_22	0.774	1.007	0.841	0.874	1.367	0.172	0.850	0.889	1.381	0.184
333_21	0.739	1.007	0.859	0.891	1.257	0.123	0.825	0.870	1.466	0.217
333_22	0.748	1.022	0.860	0.899	1.275	0.118	0.836	0.882	1.490	0.218
333_23	0.810	1.037	0.885	0.925	1.352	0.133	0.885	0.923	1.394	0.172
433_21	0.860	1.022	0.921	0.945	1.227	0.106	0.914	0.942	1.253	0.120
433_22	0.868	1.027	0.936	0.958	1.205	0.095	0.921	0.949	1.252	0.117
433_23	0.775	0.991	0.844	0.890	1.163	0.091	0.846	0.882	1.332	0.172
133_31	0.779	1.012	0.857	0.886	1.391	0.184	0.855	0.895	1.387	0.183
133_32	0.807	1.012	0.861	0.901	1.397	0.181	0.875	0.910	1.326	0.158
133_33	0.763	1.023	0.867	0.906	1.397	0.176	0.847	0.891	1.459	0.205
233_31	0.777	1.020	0.856	0.896	1.397	0.180	0.856	0.897	1.415	0.190
233_32	0.778	1.027	0.851	0.902	1.397	0.178	0.859	0.901	1.435	0.194
233_33	0.813	1.028	0.876	0.917	1.394	0.175	0.884	0.920	1.361	0.164
233_34	0.833	1.040	0.896	0.929	1.378	0.160	0.901	0.937	1.354	0.154
333_31	0.771	1.012	0.858	0.891	1.281	0.125	0.850	0.891	1.404	0.190
333_32	0.778	1.020	0.867	0.909	1.282	0.122	0.857	0.898	1.414	0.189
333_33	0.793	1.020	0.875	0.911	1.292	0.118	0.867	0.906	1.378	0.175
333_34	0.798	1.036	0.865	0.912	1.321	0.123	0.876	0.916	1.417	0.182

Table F-4 Results of the Monte Carlo simulations and fitted lognormal curve (β_9 = 0.2)

			Monte Carlo simulations				Fitted lognormal curve			
Specimen	$Y_{0.001}$	$Y_{0.05}$	$Y_{0.005}$	$Y_{0.01}$	ρ_{MG}	V_{MG}	$Y_{0.005}$	$Y_{0.01}$	ρ_{MG}	V_{MG}
433_31	0.863	1.044	0.941	0.967	1.246	0.108	0.924	0.954	1.308	0.132
433_32	0.907	1.049	0.954	0.976	1.242	0.104	0.955	0.979	1.244	0.101
433_33	0.879	1.041	0.947	0.977	1.211	0.090	0.934	0.962	1.271	0.117
433_34	0.822	1.021	0.896	0.934	1.179	0.083	0.888	0.922	1.322	0.151

Table F-5 Results of the Monte Carlo simulations and fitted lognormal curve (β_9 = 0.4)

			Monte Carlo simulations				Fitted lognormal curve			
Specimen	$Y_{0.001}$	$Y_{0.05}$	$Y_{0.005}$	$Y_{0.01}$	ρ_{MG}	V_{MG}	$Y_{0.005}$	$Y_{0.01}$	ρ_{MG}	V_{MG}
111_21	0.722	1.030	0.828	0.876	1.530	0.217	0.819	0.871	1.593	0.250
211_21	0.712	1.046	0.810	0.871	1.527	0.208	0.817	0.873	1.680	0.271
311_21	0.768	1.078	0.875	0.912	1.597	0.211	0.867	0.919	1.630	0.238
411_21	0.719	1.110	0.867	0.932	1.658	0.206	0.839	0.905	1.903	0.307
111_31	0.728	1.054	0.818	0.881	1.554	0.222	0.830	0.885	1.658	0.260
211_31	0.725	1.060	0.843	0.896	1.567	0.213	0.830	0.886	1.690	0.267
211_32	0.766	1.087	0.870	0.928	1.547	0.194	0.867	0.921	1.667	0.246
311_31	0.665	1.069	0.823	0.885	1.586	0.216	0.788	0.855	1.935	0.337
311_32	0.744	1.094	0.872	0.916	1.584	0.206	0.853	0.912	1.759	0.272
411_31	0.733	1.058	0.846	0.902	1.546	0.177	0.835	0.890	1.658	0.258
411_32	0.780	1.103	0.871	0.944	1.618	0.218	0.882	0.936	1.684	0.243
122_21	0.668	1.010	0.788	0.834	1.521	0.221	0.774	0.831	1.685	0.292
222_21	0.707	1.032	0.816	0.862	1.527	0.214	0.809	0.863	1.642	0.266
222_22	0.736	1.060	0.860	0.900	1.528	0.199	0.838	0.892	1.659	0.257
322_21	0.772	1.055	0.848	0.888	1.555	0.209	0.863	0.910	1.542	0.219
322_22	0.734	1.098	0.872	0.926	1.580	0.206	0.847	0.908	1.805	0.284
422_21	0.660	1.043	0.816	0.860	1.490	0.164	0.776	0.840	1.847	0.325
422_22	0.758	1.104	0.885	0.927	1.643	0.204	0.866	0.925	1.752	0.265
122_31	0.745	1.026	0.819	0.873	1.556	0.221	0.835	0.882	1.513	0.224
122_32	0.703	1.044	0.814	0.864	1.553	0.218	0.809	0.866	1.701	0.279
222_31	0.721	1.050	0.815	0.876	1.554	0.217	0.824	0.880	1.665	0.264
222_32	0.727	1.060	0.821	0.900	1.556	0.213	0.831	0.887	1.683	0.265
222_33	0.735	1.074	0.824	0.913	1.550	0.202	0.841	0.898	1.713	0.267
322_31	0.730	1.047	0.806	0.875	1.560	0.212	0.830	0.883	1.631	0.254
322_32	0.730	1.060	0.843	0.908	1.573	0.210	0.834	0.889	1.678	0.263
322_33	0.769	1.094	0.854	0.912	1.575	0.206	0.872	0.927	1.682	0.247

Table F-5 Results of the Monte Carlo simulations and fitted lognormal curve (β_9 = 0.4)

			Monte Carlo simulations				Fitted lognormal curve			
Specimen	$Y_{0.001}$	$Y_{0.05}$	$Y_{0.005}$	$Y_{0.01}$	ρ_{MG}	V_{MG}	$Y_{0.005}$	$Y_{0.01}$	ρ_{MG}	V_{MG}
322_34	0.816	1.097	0.893	0.939	1.552	0.195	0.907	0.954	1.567	0.207
422_31	0.681	1.038	0.798	0.861	1.481	0.162	0.791	0.851	1.751	0.298
422_32	0.718	1.079	0.815	0.875	1.536	0.168	0.830	0.890	1.787	0.288
422_33	0.800	1.090	0.874	0.929	1.599	0.203	0.893	0.942	1.588	0.217
422_34	0.753	1.087	0.871	0.924	1.555	0.205	0.858	0.914	1.703	0.258
133_21	0.721	1.026	0.814	0.856	1.530	0.224	0.817	0.869	1.581	0.248
133_22	0.743	1.039	0.833	0.878	1.525	0.210	0.837	0.887	1.562	0.235
233_21	0.693	1.019	0.801	0.853	1.531	0.223	0.795	0.850	1.639	0.272
233_22	0.743	1.043	0.823	0.890	1.531	0.208	0.838	0.889	1.576	0.238
333_21	0.690	1.049	0.816	0.872	1.544	0.208	0.801	0.861	1.764	0.296
333_22	0.685	1.072	0.829	0.879	1.573	0.211	0.803	0.868	1.871	0.317
333_23	0.770	1.088	0.873	0.937	1.577	0.208	0.871	0.924	1.658	0.243
433_21	0.674	1.036	0.798	0.856	1.449	0.155	0.786	0.846	1.765	0.304
433_22	0.677	1.063	0.819	0.873	1.541	0.173	0.795	0.859	1.866	0.320
433_23	0.758	1.096	0.871	0.929	1.623	0.222	0.864	0.921	1.721	0.259
133_31	0.716	1.047	0.822	0.866	1.553	0.221	0.820	0.875	1.670	0.267
133_32	0.706	1.044	0.815	0.878	1.557	0.219	0.811	0.868	1.691	0.276
133_33	0.706	1.046	0.827	0.884	1.556	0.213	0.812	0.869	1.699	0.277
233_31	0.692	1.058	0.828	0.887	1.555	0.215	0.805	0.866	1.790	0.300
233_32	0.679	1.062	0.803	0.886	1.566	0.219	0.796	0.860	1.852	0.317
233_33	0.723	1.056	0.837	0.896	1.553	0.208	0.828	0.884	1.683	0.267
233_34	0.752	1.070	0.845	0.911	1.546	0.201	0.853	0.906	1.647	0.248
333_31	0.663	1.040	0.814	0.894	1.553	0.209	0.778	0.841	1.826	0.320
333_32	0.690	1.060	0.831	0.870	1.572	0.211	0.804	0.866	1.808	0.304
333_33	0.722	1.062	0.845	0.898	1.573	0.211	0.828	0.885	1.708	0.272
333_34	0.769	1.076	0.886	0.920	1.571	0.206	0.867	0.919	1.620	0.235

Table F-5 Results of the Monte Carlo simulations and fitted lognormal curve (β_9 = 0.4)

			Monte Carlo simulations				Fitted lognormal curve			
Specimen	$Y_{0.001}$	$Y_{0.05}$	$Y_{0.005}$	$Y_{0.01}$	ρ_{MG}	V_{MG}	$Y_{0.005}$	$Y_{0.01}$	ρ_{MG}	V_{MG}
433_31	0.690	1.052	0.831	0.876	1.465	0.157	0.801	0.862	1.775	0.298
433_32	0.704	1.060	0.803	0.876	1.497	0.160	0.815	0.874	1.755	0.288
433_33	0.729	1.086	0.857	0.923	1.556	0.174	0.840	0.900	1.776	0.281
433_34	0.731	1.090	0.886	0.926	1.592	0.206	0.843	0.903	1.786	0.282